



Universidad de Oviedo

**Departamento de Energía**

***Analysis of availability, functional integration  
and remote maintenance for the design of  
critical components and systems in nuclear  
fusion technology***

Autor: Iván Fernández Berceruelo

Director: Luis A. Sedano Miguel

Co-director: Jorge Xiberta Bernat

**Tesis Doctoral**





Vicerrectorado de Internacionalización  
y Postgrado  
Universidad de Oviedo



**SR. DIRECTOR DE DEPARTAMENTO**

---

DE \_\_\_\_\_ /  
SR. PRESIDENTE DE LA COMISIÓN ACADÉMICA DEL PROGRAMA DE DOCTORADO EN \_\_\_\_\_



## Justificación

La tecnología del reactor de fusión nuclear es uno de los retos científico- técnicos más complejos de la actualidad. De hecho hace más de 50 años que las grandes potencias científico – económicas están trabajando en ello y muchos dudan que en este siglo se llegue a desarrollar un reactor de fusión nuclear económicamente viable. Pero hay que trabajar en ello para avanzar lo que se pueda y de paso se desarrollan tecnologías en paralelo que son útiles para otros asuntos.

En la hoja de ruta trazada por los órganos de la Comisión Europea para el desarrollo de la energía de fusión, se contemplan dos opciones de diseño para DEMO: DEMO 1 y DEMO 2.

DEMO 1 está basado en una línea de diseño conservadora. Es un concepto que puede desarrollarse a corto-medio plazo, basado en la experiencia de ITER. DEMO 1 es el concepto elegido para la primera generación de reactores, mientras que DEMO 2, requiere desarrollos más evolucionados. DEMO 1 podría actuar como 'instalación de evaluación de componentes', mientras se genera una base de datos que permitan diseñar un blanket y un divertor más avanzados

Los conceptos de mantenimiento deben validarse tanto mediante modelización avanzada y simulación, como mediante la explotación de instalaciones de demostración a escala real o reducida.

El presente trabajo describe diversos desarrollos producidos en el marco de las actividades de programa del Laboratorio Nacional de Fusión, integrado en el CIEMAT, y encaminados hacia la consecución de los objetivos de disponibilidad para los futuros reactores de demostración y centrales de producción de energía eléctrica por fusión. El texto incluye desarrollos relacionados con varios de los puntos clave mencionados: diseño de componentes, integración de diseños complejos y demostración física de conceptos de mantenimiento y manipulación remota.

En el Capítulo I se definen varios conceptos de RAMI y se discute su papel en la hoja de ruta de fusión planeada por la Comisión Europea.

El Capítulo II desarrolla el concepto de una instalación de demostración de la capacidad integral de manipulación remota en ITER. Se describen los procesos y el equipamiento y se comparan con los conceptos planteados para DEMO.

El Capítulo III ofrece una perspectiva de los sistemas de conversión de potencia estudiados para DEMO. Se presenta un estudio de balance para un reactor DEMO de corto plazo, refrigerado por helio y usa ciclos Brayton de CO<sub>2</sub> supercrítico en el secundario.

El Capítulo IV se trata la importancia de la modelización y la simulación en la integración de componentes y sistemas complejos, en ITER.

El Capítulo V introduce estrategias para la conexión y desconexión de tuberías en DEMO, como alternativas a las actuales. También se analiza el estado del arte de diferentes tecnologías para la inspección remota no destructiva de uniones soldadas.

**El Capítulo VI recoge las conclusiones generales de la tesis y propuestas para un desarrollo más profundo de los conceptos expuestos**

Analizado el trabajo, tiene la actualidad y la calidad científico-técnica necesaria para este tipo de trabajos, por lo que procede su presentación y defensa

Oviedo, 18 de mayo de 2015

Fdo.: Juan Carlos Luengo García  
Director del Departamento ENERGIA

Contra la presente resolución podrá interponer recurso de alzada ante el Excmo. Sr. Rector Magfco. de esta Universidad en el plazo de un mes a contar desde el siguiente a la recepción de la presente resolución, de acuerdo con lo previsto en el artículo 114 de la Ley 30/92, de 26 de noviembre, del Régimen Jurídico de las Administraciones Públicas y Procedimiento Administrativo Común (B.O.E. de 27 de noviembre), modificada por la Ley 4/1999, de 13 de enero (B.O.E. de 14 de enero)

**SRA. PRESIDENTA DEL CENTRO INTERNACIONAL DE POSTGRADO  
SRES. DIRECTOR/A DE LA TESIS DOCTORAL  
SR. D. IVAN FERNANDEZ BERCERUELO**



## RESUMEN DEL CONTENIDO DE TESIS DOCTORAL

1.- Título de la Tesis	
Español/Otro Idioma: Análisis de disponibilidad, integración funcional y mantenimiento remoto para el diseño de componentes y sistemas críticos en tecnología nuclear de fusión	Inglés: Analysis of availability, functional integration and remote maintenance for the design of critical components and systems in nuclear fusion technology
2.- Autor	
Nombre: Iván Fernández Berceruelo	DNI/Pasaporte/NIE:
Programa de Doctorado: Tecnología, diversificación, calidad y ahorro energético	
Órgano responsable: Departamento de Energía	

### RESUMEN (en español)

Junto a las conocidas ventajas de la Fusión Nuclear frente a otras tecnologías energéticas: seguridad inherente por principio físico, gestión del impacto ambiental y disponibilidad a largo plazo de combustibles primarios (deuterio, litio), la competitividad de la energía generada por fusión determinará su capacidad de penetración en el mercado. Para lograrla será necesario revisar rigurosamente las opciones de diseño existentes, de modo que se justifique sólidamente la elección de una solución de diseño para los primeros reactores demostradores (DEMO). DEMO constituirá la etapa intermedia entre ITER y las centrales de producción de energía eléctrica por fusión (FPP) y deberá demostrar, probablemente a través de más de una generación de dispositivos, el funcionamiento integrado de las tecnologías necesarias para la producción de potencia neta, a nivel pre-comercial.

El proceso consistirá en el análisis sistemático del coste desglosado del ciclo de vida para determinar el compromiso óptimo entre coste y robustez de diseño.

Los factores que incidirán directamente sobre el tamaño y el coste de inversión de las centrales de fusión están claramente identificados: configuraciones de plasma que permitan regímenes estacionarios o con tiempos globales de operación extendidos, bobinas magnéticas superconductoras de alta temperatura, sistemas para reducir la carga térmica en el divertor, sistemas de calentamiento y generación de corriente de alta eficiencia, materiales avanzados que permitan alargar la vida operativa de los componentes de los reactores y recurrir a ciclos de conversión de potencia de alta eficiencia y el empleo de métodos de fabricación simples para los componentes de mayor tamaño.

Junto a esas medidas, que permitirán reducir los costes anuales de adquisición de equipos, operación y mantenimiento, combustible, etc., el otro factor clave que afectará directamente al coste de la energía generada será la disponibilidad del reactor (*availability*, "A"). Ésta depende intrínsecamente de tres cualidades de la planta que vienen determinados por el diseño y las opciones tecnológicas: el tiempo de operación, el tiempo de paradas planificadas y el tiempo de paradas no planificadas. A su vez, estos tiempos están relacionados con tres conceptos de esencial importancia, vinculados de manera transversal a la integración del diseño: la fiabilidad (*reliability*, "R"), la mantenibilidad (*maintainability*, "M") y la inspeccionabilidad (*inspectability*, "I"). La primera afecta al tiempo de paradas no planificadas, mientras que la segunda y la tercera repercuten tanto sobre el tiempo de paradas planificadas como sobre el tiempo de paradas no planificadas.

Estos cuatro conceptos: disponibilidad, fiabilidad, mantenibilidad e inspeccionabilidad se reúnen en una disciplina denominada RAMI (Reliability, Availability, Maintainability,



Inspectability), que se identifica con una metodología para afrontar un problema de ingeniería de sistemas, por lo cual no puede considerarse de forma aislada. También podemos calificarlo como una herramienta de gestión establecida al más alto nivel. Es más, aunque es diferente a un sistema de gestión de calidad, puede decirse que idealmente es su herramienta complementaria.

El proceso de desarrollo y diseño de un reactor DEMO habrá de integrar estrechamente un programa formal de RAMI, con sus procesos, herramientas y métodos asociados. Debe partirse de una visión global de la disponibilidad desde el principio y constituirse un proceso iterativo a lo largo de la toda las fases del desarrollo y operación del reactor: diseño pre-conceptual y conceptual, diseño de ingeniería y desarrollo de planta, ensamblaje, puesta en marcha, operación y soporte.

El RAMI ha de levantarse sobre el conocimiento disponible a partir de programas de fusión previos (JET, Tore Supra, ITER, IFMIF, etc.) y sobre la experiencia de otros campos de la tecnología. Debe responder a los desafíos ligados a la transición entre las instalaciones experimentales y las plantas de producción de energía eléctrica, a través del escalado tecnológico y de la introducción de equipos primeros en su especie.

Esta condición es crítica para la fiabilidad inicial de un componente o sistema, ya que depende en gran medida de lo novedoso que sea su diseño. Es decir, cuanto más novedoso, mayor es la incertidumbre inicial y la probabilidad de que aparezcan modos de fallo inesperados, lo cual conduce a una fiabilidad inicial menor. La forma de mejorar la fiabilidad es adquirir experiencia y conocimiento sobre el comportamiento del sistema, lo cual puede conseguirse a través de programas de evaluación y ciclos de operación, gracias a la corrección de las deficiencias en el diseño, los procesos de fabricación y las interacciones con el entorno operativo, que se manifiestan en forma de anomalías y fallos.

Así, cada generación de un diseño hace disminuir el número de fallos debidos a un conocimiento limitado del sistema. Según madura el diseño, los fallos 'basados en el conocimiento' prácticamente se eliminan y ceden su lugar a los fallos 'basados en el proceso', es decir, fallos aleatorios debidos a variaciones inherentes a la fabricación, el mantenimiento, los procesos de operación y las características del entorno. La fiabilidad de un diseño maduro depende considerablemente de la complejidad del diseño, de modo que un diseño simple favorece que se reduzcan los fallos basados en el proceso, mientras que un diseño complejo origina incertidumbres en la fabricación, el montaje y la operación de los componentes, en sus interacciones a nivel de sistema y en la interacción del sistema con el entorno. Por ello, dada la complejidad de los diseños de equipos para DEMO, muchos de los cuales serán primeros en su especie, las reglas de diseño, entre las que se incluyen códigos de diseño, como ASME o RCC-MR, bases de datos de propiedades de materiales y códigos de prácticas, junto con la estandarización de elementos de diseño, constituyen una herramienta imprescindible para garantizar que no aparezcan fallos por deterioro hasta un tiempo suficientemente largo tras el fin de la vida operativa concebida.

No obstante, y aunque, como se ha dicho, la primera fuente de datos de fiabilidad y disponibilidad (especialmente para tecnología de fusión) sea la experiencia operativa, la extrapolación desde ITER y el resto de dispositivos experimentales hasta DEMO/FPP resulta difícil, por varias razones:

- Hay diferencias significativas en los esquemas de operación y mantenimiento con respecto a DEMO/FPP. Las instalaciones experimentales operan en series de campañas experimentales de varias semanas, separadas por periodos de parada en los que se analizan los resultados, se modifican los sistemas (ej. diagnósticos), se llevan a cabo tareas de mantenimiento, reparaciones y mejoras, etc., mientras que DEMO y FPP estarán orientados a un esquema de operación más industrial.
- Los datos y resultados de disponibilidad vienen expresados como disponibilidad inherente sobre el tiempo de operación experimental.



- En general, las condiciones de operación (niveles de fluencia neutrónica, daño en materiales, flujos térmicos, etc.) no son *DEMO relevant*.

Una cuestión importante es qué objetivo de disponibilidad debería esperarse para un DEMO o una FPP. En principio, la indisponibilidad programada puede considerarse similar a la de las centrales de fisión (habría paradas más largas para reemplazar los componentes del interior de la cámara de vacío pero el tiempo de operación entre paradas planificadas sería mayor).

Debido a la complejidad de diseño, puede suponerse que la tasa de paradas de un reactor de fusión sea mayor, dado que el número de penetraciones en la cámara de vacío y su segmentación toroidal conlleva el sellado de un gran número de medios y espacios bajo condiciones mucho más exigentes que en los reactores de fisión, en cuanto a vacío, radiación, confinamiento de tritio, manipulación remota y criogenia.

Por lo tanto, se requiere que la calidad de los componentes sea superior a la de los componentes de los reactores de fisión. Sin embargo, como resulta difícil que la calidad de los elementos básicos de diseño (tuberías, uniones, etc.) sea mejor en un dispositivo de fusión que en un reactor de fisión, es la configuración de tales elementos (ej. diseño del componente) la que debe lograr que, en caso de fallo, las consecuencias sean lo menos severas posibles.

En los análisis RAMI de los primeros estudios conceptuales europeos para reactores de potencia (PPCS) se definió un objetivo de disponibilidad (referido al suministro de electricidad a la red) del 75%, teniendo en cuenta tanto paradas planificadas como no planificadas, debidas a fallos en los componentes del interior de la cámara de vacío (in-vessel) y a eventos no planeados surgidos durante el mantenimiento. También se asumía que todas las operaciones de mantenimiento ex-vessel se llevarán a cabo en paralelo con las operaciones planificadas in-vessel.

En la hoja de ruta trazada por los órganos de la Comisión Europea para el desarrollo de la energía de fusión, semejante a las consideradas por otros socios internacionales, se contemplan dos opciones de diseño para DEMO: DEMO 1 y DEMO 2. DEMO 1 está basado en una línea de diseño conservadora. Es un concepto que puede desarrollarse a corto-medio plazo, basado en la experiencia de ITER y con mejoras razonables en diversos aspectos científicos y tecnológicos.

DEMO 1 es el concepto elegido para la primera generación de reactores demostradores, mientras que DEMO 2, que asume mayores desafíos, requiere desarrollos más evolucionados (ej. escenario de plasma avanzado con alta densidad de potencia y materiales capaces de aguantar una elevada carga térmica y fluencia neutrónica). Es decir, DEMO 1 podría actuar como 'instalación de evaluación de componentes', mientras se genera una base de datos de ingeniería que permitan diseñar y fabricar un blanket y un divertor más avanzados.

Los análisis RAMI sugieren que, si se opera directamente en los escenarios pulsados asumidos para la primera fase de DEMO, la disponibilidad máxima del reactor estaría limitada al 83% (en el caso de pulsos de 4 horas) o al 75% (en el caso de pulsos de 2 horas). Por supuesto, sin tener en cuenta los periodos de parada necesarios para el mantenimiento.

Si además consideramos que la primera fase de operación estará caracterizada por una estrategia de puesta en marcha y por el dominio del mantenimiento no planificado, como consecuencia de fallos aleatorios y la consiguiente investigación y rectificación de dichos fallos, un objetivo razonable para la disponibilidad sería el 30%. Realmente, este objetivo está expresado como disponibilidad inherente, sin tener en cuenta los correspondientes retrasos por mantenimiento in-vessel (y su contribución a la indisponibilidad). Para las siguientes fases de DEMO o FPP, en el que se contemplan vidas operativas de 3,9-5,5 años (a plena potencia) para los componentes in-vessel, el objetivo de disponibilidad debería ser superior al 80%.

En cualquier caso, las distintas evaluaciones llevadas a cabo desde los primeros programas de



PPCS coinciden en que tal objetivo podría conseguirse a través de la optimización del esquema de mantenimiento, dado que se estima que las mayores fuentes de indisponibilidad estarán provocadas, además de por el fallo de componentes, por el tiempo de reemplazo de los grandes componentes in-vessel (segmentos del blanket y cassettes del divertor), así como por tareas de mantenimiento de corta duración y procesos de inspección.

Los conceptos de mantenimiento deben validarse tanto mediante modelización avanzada y simulación como mediante la explotación de instalaciones de demostración a escala real o reducida.

En los últimos años se han producido grandes avances en modelización y simulación de estructuras y organizaciones complejas, y el desarrollo continúa de forma imparable. Por ejemplo, hoy en día es habitual utilizar software de CAD para la validación dimensional y la integración de componentes y sistemas complejos. El uso extensivo de herramientas de diseño gráfico y herramientas de modelización y simulación de sistemas dinámicos permitirá acortar significativamente el tiempo de diseño de conceptos de mantenimiento y ayudará a optimizar el equipamiento y los procesos.

Sin embargo, la validación final requerirá el uso de equipamiento de hardware e instalaciones de demostración, no disponibles hoy en día, que puedan reproducir las condiciones representativas de un DEMO/FPP. Esto se enmarcaría dentro del diseño y la ejecución de un programa ambicioso de I+D, con ITER, IFMIF y components test facilities como pilares fundamentales, que permita alcanzar un grado elevado de confianza en la operación, la vida operativa y la fiabilidad de los componentes y sistemas nucleares para los futuros reactores de fusión. La posibilidad de licenciar este tipo de instalaciones dependerá en buena medida de nuestra capacidad para predecir y garantizar su funcionamiento seguro. DEMO jugará un papel clave, tanto como receptor de todo el conocimiento previo como suministrador de datos reproducibles para los reactores de potencia, de acuerdo con la definición de las hojas de ruta.

El presente trabajo describe diversos desarrollos producidos en el marco de las actividades de programa del Laboratorio Nacional de Fusión, integrado en el CIEMAT, y encaminados hacia la consecución de los objetivos de disponibilidad para los futuros reactores de demostración y centrales de producción de energía eléctrica por fusión señalados en los párrafos anteriores. El texto incluye desarrollos relacionados con varios de los puntos clave mencionados: diseño de componentes primeros en su especie, estrategias de integración de diseños complejos y demostración física de conceptos de mantenimiento y manipulación remota.

En el Capítulo I se definen varios conceptos de RAMI y se discute su papel en la hoja de ruta de fusión planeada por la Comisión Europea.

El Capítulo II desarrolla el concepto de una instalación de demostración de la capacidad integral de manipulación remota del Test Blanket System en ITER. Se describen los procesos y el equipamiento y se comparan con los conceptos planteados para DEMO en relación a la disponibilidad operativa de los dispositivos.

En el Capítulo III se ofrece una perspectiva de los sistemas de conversión de potencia estudiados para DEMO. Se presenta un estudio de balance de planta para un reactor DEMO de corto plazo basado en un blanket refrigerado por helio y en el uso de ciclos de Brayton de dióxido de carbono supercrítico en el secundario. Además, tras un breve resumen del Programa Consolider TecnoFus, se describe el diseño innovador de un intercambiador de calor PbLi eutéctico/CO<sub>2</sub> supercrítico desarrollado en el marco de este Programa.

En el Capítulo IV se trata la importancia de la modelización y la simulación en la integración de componentes y sistemas complejos, en particular para los casos del Test Blanket System y el Divertor System en ITER.

El Capítulo V introduce diversas estrategias para la conexión y desconexión de tuberías de



componentes in-vessel en DEMO, como alternativas a las técnicas actuales. Los diseños propuestos se basan en bridas y sellos vacío, sistemas de desconexión rápida y conectores por brazing. También se analiza el estado del arte de diferentes tecnologías para la inspección remota no destructiva de uniones soldadas.

Finalmente, el Capítulo VI recoge las conclusiones generales de la tesis y propuestas para un desarrollo más profundo de los conceptos expuestos.

### RESUMEN (en Inglés)

Together with the well-known advantages of nuclear fusion over other energy technologies: inherent safety by physical principle, environmental impact management and long term availability of primary fuels (deuterium, lithium), the competitiveness of fusion energy will determine its capability to penetrate into market. A rigorous review of existing design options will be necessary to achieve that goal, so that the choice of the design solution for the first demonstrator reactors (DEMO) is solidly justified. DEMO will constitute the intermediate step between ITER and the fusion power plants (FPP) and shall demonstrate, probably through more than one generation of devices, the integrated operation of technologies that are necessary for net power production at pre-commercial level.

The process will consist on the systematic analysis of detailed lifecycle cost to determine the optimum compromise between cost and design robustness.

The factors directly having an impact over power plants size and investment cost are clearly identified: plasma configurations allowing steady-state regimes or with extended operation global times, high temperature superconducting magnets, high efficiency divertor heat exhaust systems, high efficiency heating and current drive systems, advanced materials which allow increasing reactor components lifetime and using high efficiency power conversion cycles, as well as the use of simple manufacturing methods for the largest components.

Together with those measures which will allow reducing annual costs of equipment acquisition, operation and maintenance, fuel, etc., the other key factor which will directly affect the cost of generated power will be the reactor availability (A). This one depends intrinsically on three plant features which are determined by design and technology options: operation time, scheduled downtime and unscheduled downtime. These times are in turn related to three essential concepts linked to design integration in a transversal way: reliability (R), maintainability (M) and inspectability (I). The first one affects unscheduled downtime, whereas the second and the third concepts have an effect on both unscheduled and scheduled downtimes.

These four concepts: availability, reliability, maintainability and inspectability gather in a discipline called RAMI, which is identified with a methodology to face an engineering systems problem, for which it must not be considered in isolation. It can be also described as a management tool established at the highest level. Further, although it is different to a quality management system, it can be said that it is ideally its complementary tool.

The design and development process of a DEMO reactor shall closely integrate a formal RAMI



program, with its associated processes, tools and methods. It is needed to start from a global view of availability since the beginning and to constitute an iterative process along every reactor development and operation stage: pre-conceptual and conceptual design, engineering design and plant development, assembly, commissioning, operation and support.

RAMI must be built on the knowledge available from previous fusion programs (JET, Tore Supra, ITER, IFMIF, etc.) and experience achieved in other technology fields. It must give answer to challenges related to transition between experimental facilities and power plants, through technology scale up and first-of-its-kind plant introduction.

This condition is critical for the initial availability of a component or system, since it strongly depends on the novelty of its design. That is, the more novel, the larger the initial uncertainty and less likely occurrence of unexpected failure modes, which leads to smaller initial reliability. The way to improve reliability is gaining experience and knowledge about the system performance, which can be achieved through evaluation programs and operation cycles, by correcting deficiencies in design, manufacturing processes and interactions with the operation environment, which are revealed by defects and failures.

Thus, each design generation decreases the number of failures due to limited knowledge of the system. As the design matures, 'knowledge-based' failures are practically eliminated and outweighed by 'process-based' failures, that is, random failures due to variations inherent to manufacturing, operation processes and environment characteristics. Mature design reliability considerably depends on design complexity, so that a simple design favours reduction of process-based failures, whereas a complex design originates uncertainties in components manufacturing, assembly and operation, in its interactions at system level and in the interaction between system and environment. For this reason, considering the complexity of DEMO equipment designs, many of them first-of-its-kind, design rules, including design codes like ASME or RCC-MR, material properties databases and codes of practices, together with design elements standardization, constitute an indispensable tool to ensure that wear-out failures can be expected to occur only after times sufficiently longer than the envisaged operation times.

Nevertheless, although the first reliability and availability data source (specially for fusion technology) is operational experience, as mentioned, extrapolation from ITER and the rest of experimental devices to DEMO/FPP is difficult for several reasons:

- There are significant differences in operation and maintenance schemes with respect to DEMO/FPP. Experimental facilities operate in series of experimental campaigns of few weeks spaced by shutdown periods for results analysis, systems modifications (e.g. diagnostics), maintenance, repair and upgrades, etc., while DEMO/FPP will be oriented to a more industrial operation scheme.
- Availability data and results are given as inherent availability over the experimental operation time.
- In general, the environmental conditions (levels of neutron fluence, damage in materials, thermal fluxes, etc.) are not DEMO relevant.

An important point is what availability goal should be expected for DEMO or FPP. In principle, unscheduled unavailability can be considered similar to the fission power plants one (there would be longer shutdown periods to replace in-vessel components but after longer operation periods).

Due to the design complexity, the outage rate of a fusion reactor might be expected to be higher, since the number of penetrations into the vacuum vessel and the toroidal segmentation involve sealing more media and spaces under much more stringent conditions with respect to vacuum, radiation, tritium, remote handling and cryogenics in comparison with fission reactors.

Therefore the component quality is required to be higher than that of fission reactor components. As the quality of single design elements, for instance pipes or pipe joints, can



hardly be better in a fusion machine than in a fission reactor, it is the arrangement of such elements (e.g. the design of the component) which has to be such that their failing has acceptably benign consequences.

An availability goal (referred to electricity supply to the grid) of 75% was defined in the RAMI analyses carried out in the framework of the first European Power Plant Conceptual Studies (PPCS), taking into account both scheduled outages and unplanned outages, due to in-vessel components failures and unplanned events during maintenance. It was also assumed that all the ex-vessel maintenance operations are performed in parallel with in-vessel scheduled operations.

Two design options for DEMO are considered in the Fusion Roadmap plotted by the European Commission, which is similar to the ones managed by other international partners: DEMO 1 and DEMO 2. DEMO 1 is based on a conservative design line. It is a concept which can be developed in short-medium term, based on the experience gained in ITER and with reasonable upgrades in different scientific and technological aspects.

DEMO 1 is the concept chosen for the first generation of demonstration reactors, whereas DEMO 2, which assumes larger challenges, requires further development (e.g. advanced plasma scenario with high power density and materials capable to withstand high thermal loads and neutron fluence). That is, DEMO 1 could serve as 'components test facility' while an engineering database which allows designing more advanced blanket and divertor is generated.

RAMI analyses suggest that, if a reactor is directly operated in the pulsed scenarios assumed for the first DEMO stage, the maximum reactor availability would be limited to 83% (in the case of 4 h pulses) or 75% (in the case of 2 h pulses). This is without taking into account any maintenance shutdown periods that will, of course, be necessary.

If we also consider the first operation stage will be characterized by a commissioning strategy and dominated by unscheduled maintenance, as a consequence of random failures and the subsequent investigation and rectification of such failures, a reasonable availability goal would be 30%. This is really for "kind of" inherent availability, without taking into account the corresponding delays for scheduled in-vessel maintenance (and its contribution to unavailability).

For the next DEMO/FPP stages, when lifetimes of 3.9-5.5 fpy for in-vessel components, the availability goal should be higher than 80%.

Anyway, the different evaluations carried out from the first PPCS agree about such target could be met through the optimization of the maintenance scheme, since it is estimated that the biggest unavailability sources will be caused, apart from components failures, by replacement of large in-vessel components (blanket segments and divertor cassettes), as well as by short maintenance tasks and inspection processes.

Maintenance concepts must be validated by both advanced modelling and simulation and exploitation of real or reduced scale test facilities.

Important advances in modelling and simulation of complex structures and organizations have been produced in last years, and development continues non-stop. For example, today is common using CAD for dimensional validation and integration of complex components and systems. Extensive use of graphic design tools and dynamic systems modelling and simulation tools will allow significantly reduce maintenance concepts design time and will help to optimize equipment and processes.

Nevertheless, final validation will require using hardware equipment and test facilities, not available today, which are able to reproduce DEMO/FPP representative conditions. This would be part of the design and execution of an ambitious R&D program having ITER, IFMIF and



components test facilities as fundamental pillars, which allows reaching high confidence in operation, lifetime and reliability of nuclear components and systems for future fusion reactors. The possibility of licensing this kind of facilities will strongly depend on our ability to predict and guarantee their safe operation. DEMO will play a key role, both as receptor of the whole previous knowledge and as supplier of data reproducible for power plants, as defined in roadmaps.

The present work describes different developments carried out in the framework of the Fusion National Laboratory activities (integrated into CIEMAT), which are focused on the achievement of previously mentioned availability goals for future demonstration reactors and fusion power plants. The text includes developments related to several of the referred key points: design of first-of-its-kind plants, complex design integration strategies and physical demonstration of maintenance and remote handling concepts.

In Chapter I several RAMI concepts are defined and their role on the fusion roadmap plotted by the European Commission is discussed.

Chapter II explains the concept of a test facility to demonstrate the integral remote handling capability of the ITER Test Blanket System. The processes and the equipment are described and compared to those concepts planned for DEMO regarding devices operational availability.

A perspective of power conversion systems which are being studied for DEMO is offered in Chapter III. An assessment of the balance of plant of a near term DEMO reactor based on a helium-cooled blanket using supercritical carbon dioxide Brayton cycles for the secondary side is presented. Furthermore, after a short summary of the Consolider TecnoFus Programme, the innovative design of lead-lithium/supercritical CO<sub>2</sub> heat exchanger which has been developed in the framework of this program is described.

The importance of modelling and simulation in the integration of complex components and system is treated in Chapter IV, in particular for the cases of the ITER Test Blanket System and the Divertor System.

Chapter V introduces different strategies to connect and disconnect DEMO in-vessel components pipes, as alternative to current techniques. The proposed designs are based on flanges, quick disconnection systems and brazing connectors. Additionally, the state-of-the-art of different technologies for non-destructive inspection of welded joints is analysed.

Finally, Chapter VI collects the general conclusions of the thesis and some proposals for the further development of the exposed concepts.

# Acknowledgements / Agradecimientos

A mi director, Luis Sedano, y a mi co-director y tutor, Jorge Xiberta, por su ayuda y apoyo durante estos años.

A todos los compañeros y colegas que, de algún modo u otro, han participado en esta tesis. En orden alfabético: José Manuel Arroyo, Alexis Cantizano, Oliver Crofts, Carlos Fernández Robles, Carlos Fernández Vecilla, Antonio García, Ismael García, Andrés Gómez, Luis Enrique Herranz, Jesús Juanas, José Ignacio Linares, Álvaro Marqueta, Rafael Martínez-Oña, Beatriz Yolanda Moratilla, Carlos Moreno, Iole Palermo, Luis Ríos, Raquel Rodríguez, Elena Rosa, Ana Ruiz de Assín, Antonio Terribile, Santiago Terrón y Gerardo Veredas.



# Contents

## Abstract

## Chapter I: Introduction

<b>List of figures</b> .....	<b>1</b>
<b>1.1. Introduction</b> .....	<b>3</b>
<b>1.2. RAMI general concepts</b> .....	<b>3</b>
1.2.1. <i>MTBF and MDT/MTTR</i> .....	4
1.2.2. <i>Reliability</i> .....	4
1.2.3. <i>Availability</i> .....	5
1.2.4. <i>Maintainability</i> .....	6
1.2.5. <i>Inspectability</i> .....	6
<b>1.3. RAMI design guidelines</b> .....	<b>7</b>
1.3.1. <i>Increasing the reliability of components and systems</i> .....	7
1.3.1.1. <i>Redundancy</i> .....	7
1.3.1.2. <i>Internal compensation</i> .....	8
1.3.1.3. <i>Derating</i> .....	8
1.3.1.4. <i>Preventive Maintenance</i> .....	9
1.3.2. <i>Specific approach. Fusion reliability components</i> .....	10
1.3.2.1. <i>Constituents of mechanical components in First Wall and Breeding Blanket</i> .....	10
1.3.2.2. <i>Constituents of fusion specific process systems: Heating Systems, Tritium Processing Systems and Cryogenic Process Systems</i> .....	10
1.3.2.3. <i>Reliability data: information management, FRDB, data and uncertainties</i> .....	11
1.3.3. <i>Increasing maintainability of systems and components</i> .....	11
1.3.3.1. <i>Maximizing SSC Maintainability</i> .....	11
1.3.3.2. <i>Minimizing MDT from preventive maintenance requirements</i> .....	12
1.3.3.3. <i>Minimizing MDT from curative maintenance activities</i> .....	12
1.3.3.4. <i>Specific approach. Maintainability in fusion facilities</i> .....	13
1.3.4. <i>Detection and inspectability</i> .....	13
1.3.4.1. <i>Detection</i> .....	13
1.3.4.2. <i>Inspectability</i> .....	14
<b>1.4. Availability in fusion power plants</b> .....	<b>15</b>
1.4.1. <i>Reliability of components and QA</i> .....	15
1.4.2. <i>Design codes and standardization</i> .....	17
1.4.3. <i>Modelling plant availability</i> .....	17
<b>1.5. The EU fusion roadmap</b> .....	<b>19</b>
1.5.1. <i>Demo challenges in technology and physics</i> .....	20
1.5.1.1. <i>Technology challenges</i> .....	20
1.5.1.2. <i>Physics challenges</i> .....	20
1.5.2. <i>DEMO design options and approach</i> .....	21
1.5.2.1. <i>Key design drivers</i> .....	22
<b>1.6. Scope of this work</b> .....	<b>23</b>
<b>1.7. References</b> .....	<b>24</b>

## Chapter II: ITER Test Blanket System integration studies. Conceptual design of a remote handling test facility

<b>List of figures</b> .....	<b>25</b>
<b>List of tables</b> .....	<b>28</b>
<b>2.1. Introduction</b> .....	<b>31</b>
<b>2.2. The ITER Project</b> .....	<b>31</b>
2.2.1. <i>Main features of ITER</i> .....	33
<b>2.3. ITER Remote Maintenance System</b> .....	<b>42</b>
2.3.1. <i>Blanket Remote Handling System</i> .....	43
2.3.2. <i>Divertor Remote Handling System</i> .....	44
2.3.3. <i>Cask and Plug Remote Handling System</i> .....	45
2.3.4. <i>In-Vessel Viewing System</i> .....	45
2.3.5. <i>Neutral Beam Cell Remote Handling</i> .....	46
2.3.6. <i>Hot Cell Remote Handling System</i> .....	47
<b>2.4. ITER Test Blanket System</b> .....	<b>48</b>

2.4.1.	<i>TBM testing strategy and planning</i> .....	49
2.4.2.	<i>Breeding blanket concepts to be tested in ITER</i> .....	50
2.4.2.1.	HCLL TBS .....	50
2.4.2.2.	HCPB TBS.....	50
2.4.2.3.	WCCB TBS.....	51
2.4.2.4.	HCCR TBS .....	51
2.4.2.5.	HCCB TBS .....	51
2.4.2.6.	LLCB TBS.....	52
2.4.3.	<i>TBS ancillary systems and supplies</i> .....	52
<b>2.5.</b>	<b>Conceptual design of a TBM remote handling test facility</b> .....	<b>53</b>
2.5.1.	<i>Overall description of the EU TBS RH System</i> .....	54
2.5.1.1.	Integration of the TBS in the Equatorial Port Cell .....	54
2.5.1.2.	TBM port plug replacement strategy.....	55
2.5.2.	<i>Objectives of the TBM RH Test Facility</i> .....	56
2.5.3.	<i>Design methodology</i> .....	57
2.5.4.	<i>Requirements of the RH Test Facility</i> .....	58
2.5.4.1.	Transfer of the port plug with the TBM & shield assemblies from the transfer cask to a tool inside the Hot Cell (operation #1).....	59
2.5.4.2.	Movement of the TBM & shield and port plug assembly within the Hot Cell on rails (operation #2) .....	61
2.5.4.3.	Cleaning of dust from the port plug in order to reduce the dose rate (operation #3).....	61
2.5.4.4.	Disconnection of water pipes of the TBM & shield assembly from the main water system of the port plug and the vacuum vessel (operation #4) .....	62
2.5.4.5.	Removal of the sealing features and mechanical attachments between the port plug and the TBM & shield assemblies (operation #5).....	64
2.5.4.6.	Vertical extraction of the TBM & shield assembly from the PP frame (operation #6).....	65
2.5.4.7.	Cleaning of dust from the TBM & shield assembly (operation #7) .....	67
2.5.4.8.	Separation of the TBM from the shield (operation #8) .....	69
2.5.4.9.	TBM splitting and packing into transport casks to be shipped (operation #9) .....	73
2.5.4.10.	Introduction of the TBM & shield assembly into the port plug frame (operation #10).....	76
2.5.4.11.	Joining of the TBM & shield assembly to the port plug frame (operation #11).....	78
2.5.4.12.	Connection of the water pipes of the TBM & shield assembly from the main water system of the port plug and the vacuum vessel (operation #12) .....	79
2.5.4.13.	Checking of vacuum sealing between the port plug and the TBM shield (operation #13).....	81
2.5.4.14.	Checking of the water loop (operation #14).....	82
2.5.4.15.	Transfer of the Pipe Forest & Bioshield Door assembly between the Storage Area and the Port Cell (operation #15) .....	84
2.5.4.16.	Installation/removal of the Pipe Forest & Bioshield Door in/from the Interspace (operation #16) .....	86
2.5.4.17.	Transfer of the RH Platform Unit between the Storage Area and the Port Cell (operation #17).....	90
2.5.4.18.	Welding of pipes in IF2a (operation #18).....	91
2.5.4.19.	Inspection of weld beads in IF2a (operation #19) .....	94
2.5.4.20.	Installation and removal of thermal insulations at IF2a (operation #20).....	96
2.5.4.21.	Constriction/unconstriction of pipes at IF2a (operation #21).....	97
2.5.4.22.	Cut of pipes in IF2a (operation #22) .....	99
2.5.4.23.	Installation/removal of the AEU in/from the Port Cell (operation #23).....	101
2.5.4.24.	Installation/removal of the Port Plug in/from the Port (operation #24) .....	103
2.5.4.25.	Vacuum sealing of the Port Plug – Port interface (operation #25) .....	107
2.5.5.	<i>Hosting building description and space layout in the TBM RH facility</i> .....	109
2.5.5.1.	Operations Hall.....	110
2.5.5.2.	TBM Port Cell RH operations area .....	113
2.5.5.3.	Hot Cell RH operations area.....	114
2.5.5.4.	Storage area.....	115
2.5.5.5.	Unloading and Parking zone.....	116
2.5.5.6.	Office and auxiliary systems building.....	116
2.5.5.7.	Ground floor.....	117
2.5.5.8.	First floor.....	118
2.5.6.	<i>Conceptual design of equipment, structures and fixed mock-ups</i> .....	120
2.5.6.1.	Ancillary Equipment Unit (AEU) mock-up .....	121
2.5.6.2.	Pipe forest & bioshield door assembly mock-up .....	124
2.5.6.3.	Port plug mock-up .....	128

2.5.6.4.	TBM & shield mock-ups.....	129
2.5.6.5.	Air transfer system (ATS) .....	134
2.5.6.6.	Band sawing machine .....	137
2.5.6.7.	Drums and shipping basket mock-up .....	138
2.5.6.8.	Plasma cutting tool .....	141
2.5.6.9.	Gasket flange maintenance equipment .....	141
2.5.6.10.	Hot Cell manipulator .....	143
2.5.6.11.	Welds inspection tool.....	144
2.5.6.12.	Thermal insulating modules.....	146
2.5.6.13.	Laser cutting tool .....	146
2.5.6.14.	Lifting tool for TBM & shield.....	149
2.5.6.15.	20 ton overhead rotating crane.....	150
2.5.6.16.	Palletising system and storage shelves.....	153
2.5.6.17.	Port Cell robotic arm and RH Platform Unit.....	156
2.5.6.18.	Polisher.....	159
2.5.6.19.	Test stand.....	159
2.5.6.20.	Screwer .....	162
2.5.6.21.	Transfer cask.....	163
2.5.6.22.	Vertical positioning tool.....	166
2.5.6.23.	Welding tool for the PC robotic arm.....	170
2.5.6.24.	50 ton overhead crane.....	172
2.5.6.25.	Bench for dust cleaning and separation of TBM from shield.....	173
2.5.6.26.	Hot Cell door for the vertical positioning tool .....	174
2.5.6.27.	Hot Cell door for the test stand .....	176
2.5.6.28.	Port Cell mock-up.....	178
2.5.6.29.	Port mock-up .....	180
2.5.6.30.	Supporting bench for new TBM & shield assemblies. Storage container .....	183
2.5.7.	<i>Auxiliary systems</i> .....	184
2.5.7.1.	Remote Handling Control System .....	185
2.5.7.2.	Electric system .....	191
2.5.7.3.	Water supply system .....	192
2.5.7.4.	Heating, ventilating and air conditioning system (HVAC) .....	194
2.5.7.5.	Vacuum system .....	194
2.5.7.6.	Compressed air system.....	196
2.5.7.7.	Helium System .....	197
2.6.	<b>Comparison between DEMO blanket and ITER TBS maintenance schemes.....</b>	<b>199</b>
2.6.1.	<i>Vertical maintenance</i> .....	200
2.6.2.	<i>Decay heat</i> .....	203
2.6.3.	<i>Occupational radiation exposure</i> .....	205
2.6.4.	<i>Processes automation</i> .....	205
2.6.5.	<i>Hot cell activities</i> .....	206
2.6.6.	<i>Ex-vessel transport</i> .....	207
2.6.7.	<i>Spare components and redundancy</i> .....	207
2.6.8.	<i>Operation time</i> .....	208
2.7.	<b>References .....</b>	<b>210</b>

## Chapter III: Power conversion systems for DEMO

List of figures .....	215
List of tables .....	216
3.1. Introduction .....	217
3.2. The role of power conversion cycle in the competitiveness of fusion .....	217
3.3. Integration of the primary heat transfer system and the power conversion cycle .....	219
3.4. Power conversion cycles studies for DEMO in EU .....	221
3.4.1. PPCS and early DEMO .....	221
3.4.2. EFDA PPPT WP12-13 studies: Helium-cooled blanket/water steam DEMO BoP (WP12).....	223
3.4.2.1. Introduction.....	223
3.4.2.2. Helium-cooled blanket/water steam BoP .....	224
3.4.3. Water-cooled blanket/water steam DEMO BoP (WP13).....	224
3.4.3.1. Introduction.....	224
3.4.3.2. Water-cooled blanket/water steam BoP .....	225
3.4.4. Helium-cooled blanket/water steam DEMO BoP (WP13).....	226
3.4.5. Helium-cooled blanket/supercritical CO <sub>2</sub> DEMO BoP (WP13).....	227

3.4.5.1.	Introduction.....	227
3.4.5.2.	Literature survey on S-CO <sub>2</sub> Brayton cycles .....	227
3.4.5.3.	Thermal specification of the DEMO1 reactor .....	230
3.4.5.4.	Methodology .....	231
3.4.5.5.	Results.....	235
3.4.5.6.	Sensitivity analysis .....	237
3.4.5.7.	Conclusions .....	242
3.4.6.	<i>The issue of pulsed-operation</i> .....	242
3.4.6.1.	Steam turbines .....	242
3.4.6.2.	S-CO <sub>2</sub> turbines .....	244
<b>3.5.</b>	<b>TecnoFus Programme .....</b>	<b>245</b>
3.5.1.	<i>Introduction</i> .....	245
3.5.2.	<i>Brief summary of TecnoFus achievements</i> .....	245
3.5.2.1.	Integrated design .....	245
3.5.2.2.	Neutronics .....	250
3.5.2.3.	Thermomechanics .....	250
3.5.2.4.	Thermal-hydraulics and magnetohydrodynamics .....	251
3.5.2.5.	Production and characterization of breeding blanket functional and structural materials.....	253
3.5.2.6.	Plant systems and technologies .....	254
3.5.2.7.	Environmental issues .....	256
3.5.2.8.	DEMO specifications & systems codes .....	256
3.5.3.	<i>Power conversion system</i> .....	256
3.5.4.	<i>Design of the lead-lithium/supercritical CO<sub>2</sub> heat exchanger</i> .....	260
3.5.4.1.	Introduction.....	260
3.5.4.2.	Design of the PCHE .....	261
3.5.4.3.	1-D heat transfer model.....	267
3.5.4.4.	3-D CFD model.....	268
3.5.4.5.	Tritium transport model.....	271
3.5.4.6.	The issue of blockage.....	272
3.5.4.7.	Conclusions .....	272
<b>3.6.</b>	<b>References .....</b>	<b>272</b>

## Chapter IV: The value of CAD & graphic design tools and virtual reality in the integration of complex systems

<b>List of figures .....</b>	<b>279</b>
<b>4.1. Introduction .....</b>	<b>281</b>
<b>4.2. CAD kinematics simulation and virtual reality .....</b>	<b>281</b>
4.2.1. <i>Dynamic effects</i> .....	283
4.2.2. <i>Web-based virtual reality environments</i> .....	283
4.2.3. <i>Virtual reality for hands-on maintenance</i> .....	284
4.2.4. <i>Reliability in remote handling software</i> .....	284
<b>4.3. Application case 1: ITER Test Blanket System RH system.....</b>	<b>285</b>
4.3.1. <i>Tools and methodology</i> .....	285
4.3.2. <i>Description of the sequences and influence on the design</i> .....	288
4.3.2.1. Extraction of a TBM & shield assembly from the port plug .....	288
4.3.2.2. Split of the TBM & shield .....	291
4.3.2.3. Insertion of the TBM & shield assembly inside the port plug .....	298
4.3.2.4. Consequences of the simulation process .....	303
4.3.2.5. Installation and removal of the Pipe Forest & Bioshield Door assembly .....	304
4.3.2.6. Connection and disconnection of pipes at Interface 2a .....	312
4.3.2.7. Installation and removal of the Ancillary Equipment Unit.....	318
4.3.2.8. Consequences of the simulation process .....	321
<b>4.4. Application case 2: ITER Divertor RH system .....</b>	<b>322</b>
4.4.1. <i>Introduction</i> .....	322
4.4.2. <i>Design of the CTM cable guide</i> .....	323
4.4.3. <i>Tools and methodology</i> .....	327
4.4.4. <i>Description of the sequences and influence on the design</i> .....	329
4.4.4.1. Performance of the cable guide during the toroidal movement of the CTM .....	329
4.4.4.2. Plugging of the multi-pin connector by the CMM MAM .....	335
4.4.4.3. Consequences of the simulation process .....	338
<b>4.5. References .....</b>	<b>339</b>

## Chapter V: Alternative piping connection systems for DEMO and non-destructive testing technologies

List of figures .....	343
List of tables .....	344
<b>5.1. Introduction .....</b>	<b>345</b>
<b>5.2. General piping assumptions.....</b>	<b>345</b>
<b>5.3. Design of a QDS-compatible flange jacket for DEMO blanket pipes.....</b>	<b>346</b>
5.3.1. Description of the design.....	347
5.3.1.1. Flange.....	349
5.3.1.2. Gasket (Helicoflex HNR-229) .....	349
5.3.1.3. Materials.....	352
5.3.1.4. Surface finish.....	353
5.3.1.5. Calculation of the minimum seating load and the flange groove dimensions .....	354
5.3.1.6. Design of the Quick Disconnect System (v-clamp).....	356
5.3.2. Remote handling operations to install/uninstall the flange connector .....	360
5.3.3. Summary of results and conclusions .....	366
<b>5.4. Design of a brazing connector for DEMO blanket pipes .....</b>	<b>367</b>
5.4.1. Preliminary selection of materials.....	367
5.4.1.1. Filler metals .....	368
5.4.1.2. Protective atmospheres.....	369
5.4.1.3. The case of EUROFER .....	369
5.4.2. Design description.....	369
5.4.2.1. Main design features .....	369
5.4.2.2. Filler metals pre-placement .....	372
5.4.2.3. Adaptability to flow direction .....	373
5.4.2.4. Brazing processes.....	373
5.4.2.5. Brazing atmosphere and inspection system .....	374
5.4.3. Induction heating assessment.....	375
5.4.3.1. New electromagnetic-thermal analysis .....	379
5.4.3.2. Thermomechanical analyses .....	380
5.4.4. Modelling of capillary flow.....	382
5.4.4.1. Governing equations: .....	383
5.4.4.2. Simulation results .....	384
5.4.5. Transmutation assessment .....	386
5.4.6. Tritium permeation assessment .....	388
5.4.7. Remote handling implementation .....	390
5.4.7.1. Positioning and alignment system. Disconnection sequence (bolted union option) .....	390
5.4.7.2. Hanford Purex clamping concept.....	394
5.4.7.3. Quick geared triple hook concept .....	397
5.4.8. Mechanical properties of the brazed joint and alternative filler metals .....	399
<b>5.5. State of the art of non-destructive testing technologies.....</b>	<b>399</b>
5.5.1. Introduction.....	399
5.5.2. Peltier cooled cameras for visual inspection.....	401
5.5.2.1. Thermoelectric cooling .....	401
5.5.2.2. CCD/CMOS cameras in DEMO radiation environment .....	402
5.5.2.3. CID cameras.....	404
5.5.3. Electromagnetic-acoustic transducers.....	407
5.5.3.1. Advantages and limitations of EMATs .....	407
5.5.3.2. EMATs for weld inspection in DEMO pipes .....	408
5.5.4. Laser ultrasonic transducers .....	409
<b>5.6. References .....</b>	<b>411</b>

## Chapter VI: General conclusions and proposals for further development

6.1. Introduction .....	415
6.2. ITER Test Blanket System integration studies. Conceptual design of a remote handling test facility .....	415
6.3. Power conversion systems for DEMO .....	416
6.4. The value of CAD & graphic design tools and virtual reality in the integration of complex systems .....	418
6.5. Alternative piping connection systems for DEMO and non-destructive testing technologies .....	418

**Annex I: Objetivos**

**Annex II: Capítulo VI**

**Annex III: Related publications**

**Annex IV: Abbreviations**

# Abstract

Together with the well-known advantages of nuclear fusion over other energy technologies: inherent safety by physical principle, environmental impact management and long term availability of primary fuels (deuterium, lithium), the competitiveness of fusion energy will determine its capability to penetrate into market. A rigorous review of existing design options will be necessary to achieve that goal, so that the choice of the design solution for the first demonstrator reactors (DEMO) is solidly justified. DEMO will constitute the intermediate step between ITER and the fusion power plants (FPP) and shall demonstrate, probably through more than one generation of devices, the integrated operation of technologies that are necessary for net power production at pre-commercial level.

The process will consist on the systematic analysis of detailed lifecycle cost to determine the optimum compromise between cost and design robustness.

The factors directly having an impact over power plants size and investment cost are clearly identified: plasma configurations allowing steady-state regimes or with extended operation global times, high temperature superconducting magnets, high efficiency divertor heat exhaust systems, high efficiency heating and current drive systems, advanced materials which allow increasing reactor components lifetime and using high efficiency power conversion cycles, as well as the use of simple manufacturing methods for the largest components.

Together with those measures which will allow reducing annual costs of equipment acquisition, operation and maintenance, fuel, etc., the other key factor which will directly affect the cost of generated power will be the reactor *availability (A)*. This one depends intrinsically on three plant features which are determined by design and technology options: operation time, scheduled downtime and unscheduled downtime. These times are in turn related to three essential concepts linked to design integration in a transversal way: *reliability (R)*, *maintainability (M)* and *inspectability (I)*. The first one affects unscheduled downtime, whereas the second and the third concepts have an effect on both unscheduled and scheduled downtimes.

These four concepts: availability, reliability, maintainability and inspectability gather in a discipline called *RAMI*, which is identified with a methodology to face an engineering systems problem, for which it must not be considered in isolation. It can be also described as a management tool established at the highest level. Further, although it is different to a quality management system, it can be said that it is ideally its complementary tool.

The design and development process of a DEMO reactor shall closely integrate a formal RAMI program, with its associated processes, tools and methods. It is needed to start from a global view of availability since the beginning and to constitute an iterative process along every reactor development and operation stage: pre-conceptual and conceptual design, engineering design and plant development, assembly, commissioning, operation and support.

RAMI must be built on the knowledge available from previous fusion programs (JET, Tore Supra, ITER, IFMIF, etc.) and experience achieved in other technology fields. It must give answer to challenges related to transition between experimental facilities and power plants, through technology scale up and first-of-its-kind plant introduction.

This condition is critical for the initial availability of a component or system, since it strongly depends on the novelty of its design. That is, the more novel, the larger the initial uncertainty and less likely occurrence of unexpected failure modes, which leads to smaller initial reliability. The way to improve reliability is gaining experience and knowledge about the system performance, which can be achieved through evaluation programs and operation cycles, by correcting deficiencies in design, manufacturing processes and interactions with the operation environment, which are revealed by defects and failures.

Thus, each design generation decreases the number of failures due to limited knowledge of the system. As the design matures, 'knowledge-based' failures are practically eliminated and

outweighed by 'process-based' failures, that is, random failures due to variations inherent to manufacturing, operation processes and environment characteristics. Mature design reliability considerably depends on design complexity, so that a simple design favours reduction of process-based failures, whereas a complex design originates uncertainties in components manufacturing, assembly and operation, in its interactions at system level and in the interaction between system and environment. For this reason, considering the complexity of DEMO equipment designs, many of them first-of-its-kind, design rules, including design codes like ASME or RCC-MR, material properties databases and codes of practices, together with design elements standardization, constitute an indispensable tool to ensure that wear-out failures can be expected to occur only after times sufficiently longer than the envisaged operation times.

Nevertheless, although the first reliability and availability data source (specially for fusion technology) is operational experience, as mentioned, extrapolation from ITER and the rest of experimental devices to DEMO/FPP is difficult for several reasons:

- There are significant differences in operation and maintenance schemes with respect to DEMO/FPP. Experimental facilities operate in series of experimental campaigns of few weeks spaced by shutdown periods for results analysis, systems modifications (e.g. diagnostics), maintenance, repair and upgrades, etc., while DEMO/FPP will be oriented to a more industrial operation scheme.
- Availability data and results are given as inherent availability over the experimental operation time.
- In general, the environmental conditions (levels of neutron fluence, damage in materials, thermal fluxes, etc.) are not DEMO relevant.

An important point is what availability goal should be expected for DEMO or FPP. In principle, unscheduled unavailability can be considered similar to the fission power plants one (there would be longer shutdown periods to replace in-vessel components but after longer operation periods).

Due to the design complexity, the outage rate of a fusion reactor might be expected to be higher, since the number of penetrations into the vacuum vessel and the toroidal segmentation involve sealing more media and spaces under much more stringent conditions with respect to vacuum, radiation, tritium, remote handling and cryogenics in comparison with fission reactors.

Therefore the component quality is required to be higher than that of fission reactor components. As the quality of single design elements, for instance pipes or pipe joints, can hardly be better in a fusion machine than in a fission reactor, it is the arrangement of such elements (e.g. the design of the component) which has to be such that their failing has acceptably benign consequences.

An availability goal (referred to electricity supply to the grid) of 75% was defined in the RAMI analyses carried out in the framework of the first European Power Plant Conceptual Studies (PPCS), taking into account both scheduled outages and unplanned outages, due to in-vessel components failures and unplanned events during maintenance. It was also assumed that all the ex-vessel maintenance operations are performed in parallel with in-vessel scheduled operations.

Two design options for DEMO are considered in the Fusion Roadmap plotted by the European Commission, which is similar to the ones managed by other international partners: DEMO 1 and DEMO 2. DEMO 1 is based on a conservative design line. It is a concept which can be developed in short-medium term, based on the experience gained in ITER and with reasonable upgrades in different scientific and technological aspects.

DEMO 1 is the concept chosen for the first generation of demonstration reactors, whereas DEMO 2, which assumes larger challenges, requires further development (e.g. advanced plasma scenario with high power density and materials capable to withstand high thermal loads and neutron fluence). That is, DEMO 1 could serve as 'components test facility' while an engineering database which allows designing more advanced blanket and divertor is generated.

RAMI analyses suggest that, if a reactor is directly operated in the pulsed scenarios assumed for the first DEMO stage, the maximum reactor availability would be limited to 83% (in the case of 4 h pulses) or 75% (in the case of 2 h pulses). This is without taking into account any maintenance shutdown periods that will, of course, be necessary.

If we also consider the first operation stage will be characterized by a commissioning strategy and dominated by unscheduled maintenance, as a consequence of random failures and the subsequent investigation and rectification of such failures, a reasonable availability goal would be 30%. This is really for “kind of” inherent availability, without taking into account the corresponding delays for scheduled in-vessel maintenance (and its contribution to unavailability).

For the next DEMO/FPP stages, when lifetimes of 3.9-5.5 fpy for in-vessel components, the availability goal should be higher than 80%.

Anyway, the different evaluations carried out from the first PPCS agree about such target could be met through the optimization of the maintenance scheme, since it is estimated that the biggest unavailability sources will be caused, apart from components failures, by replacement of large in-vessel components (blanket segments and divertor cassettes), as well as by short maintenance tasks and inspection processes.

Maintenance concepts must be validated by both advanced modelling and simulation and exploitation of real or reduced scale test facilities.

Important advances in modelling and simulation of complex structures and organizations have been produced in last years, and development continues non-stop. For example, today is common using CAD for dimensional validation and integration of complex components and systems. Extensive use of graphic design tools and dynamic systems modelling and simulation tools will allow significantly reduce maintenance concepts design time and will help to optimize equipment and processes.

Nevertheless, final validation will require using hardware equipment and test facilities, not available today, which are able to reproduce DEMO/FPP representative conditions. This would be part of the design and execution of an ambitious R&D program having ITER, IFMIF and components test facilities as fundamental pillars, which allows reaching high confidence in operation, lifetime and reliability of nuclear components and systems for future fusion reactors. The possibility of licensing this kind of facilities will strongly depend on our ability to predict and guarantee their safe operation. DEMO will play a key role, both as receptor of the whole previous knowledge and as supplier of data reproducible for power plants, as defined in roadmaps.

The present work describes different developments carried out in the framework of the Fusion National Laboratory activities (integrated into CIEMAT), which are focused on the achievement of previously mentioned availability goals for future demonstration reactors and fusion power plants. The text includes developments related to several of the referred key points: design of first-of-its-kind plants, complex design integration strategies and physical demonstration of maintenance and remote handling concepts.

In **Chapter I** several RAMI concepts are defined and their role on the fusion roadmap plotted by the European Commission is discussed.

**Chapter II** explains the concept of a test facility to demonstrate the integral remote handling capability of the ITER Test Blanket System. The processes and the equipment are described and compared to those concepts planned for DEMO regarding devices operational availability.

A perspective of power conversion systems which are being studied for DEMO is offered in **Chapter III**. An assessment of the balance of plant of a near term DEMO reactor based on a helium-cooled blanket using supercritical carbon dioxide Brayton cycles for the secondary side is presented. Furthermore, after a short summary of the Consolider TecnoFus Programme, the

innovative design of lead-lithium/supercritical CO<sub>2</sub> heat exchanger which has been developed in the framework of this program is described.

The importance of modelling and simulation in the integration of complex components and system is treated in **Chapter IV**, in particular for the cases of the ITER Test Blanket System and Divertor System.

**Chapter V** introduces different strategies to connect and disconnect DEMO in-vessel components pipes, as alternative to current techniques. The proposed designs are based on flanges, quick disconnection systems and brazing connectors. Additionally, the state-of-the-art of different technologies for non-destructive inspection of welded joints is analysed.

Finally, **Chapter VI** collects the general conclusions of the thesis and some proposals for the further development of the exposed concepts.

# Sinopsis

Junto a las conocidas ventajas de la Fusión Nuclear frente a otras tecnologías energéticas: seguridad inherente por principio físico, gestión del impacto ambiental y disponibilidad a largo plazo de combustibles primarios (deuterio, litio), la competitividad de la energía generada por fusión determinará su capacidad de penetración en el mercado. Para lograrla será necesario revisar rigurosamente las opciones de diseño existentes, de modo que se justifique sólidamente la elección de una solución de diseño para los primeros reactores demostradores (DEMO). DEMO constituirá la etapa intermedia entre ITER y las centrales de producción de energía eléctrica por fusión (FPP) y deberá demostrar, probablemente a través de más de una generación de dispositivos, el funcionamiento integrado de las tecnologías necesarias para la producción de potencia neta, a nivel pre-comercial.

El proceso consistirá en el análisis sistemático del coste desglosado del ciclo de vida para determinar el compromiso óptimo entre coste y robustez de diseño.

Los factores que incidirán directamente sobre el tamaño y el coste de inversión de las centrales de fusión están claramente identificados: configuraciones de plasma que permitan regímenes estacionarios o con tiempos globales de operación extendidos, bobinas magnéticas superconductoras de alta temperatura, sistemas para reducir la carga térmica en el divertor, sistemas de calentamiento y generación de corriente de alta eficiencia, materiales avanzados que permitan alargar la vida operativa de los componentes de los reactores y recurrir a ciclos de conversión de potencia de alta eficiencia y el empleo de métodos de fabricación simples para los componentes de mayor tamaño.

Junto a esas medidas, que permitirán reducir los costes anuales de adquisición de equipos, operación y mantenimiento, combustible, etc., el otro factor clave que afectará directamente al coste de la energía generada será la disponibilidad del reactor (*availability*, "A"). Ésta depende intrínsecamente de tres cualidades de la planta que vienen determinados por el diseño y las opciones tecnológicas: el tiempo de operación, el tiempo de paradas planificadas y el tiempo de paradas no planificadas. A su vez, estos tiempos están relacionados con tres conceptos de esencial importancia, vinculados de manera transversal a la integración del diseño: la fiabilidad (*reliability*, "R"), la mantenibilidad (*maintainability*, "M") y la inspeccionabilidad (*inspectability*, "I"). La primera afecta al tiempo de paradas no planificadas, mientras que la segunda y la tercera repercuten tanto sobre el tiempo de paradas planificadas como sobre el tiempo de paradas no planificadas.

Estos cuatro conceptos: *disponibilidad, fiabilidad, mantenibilidad e inspeccionabilidad* se reúnen en una disciplina denominada RAMI (*Reliability, Availability, Maintainability, Inspectability*), que se identifica con una metodología para afrontar un problema de ingeniería de sistemas, por lo cual no puede considerarse de forma aislada. También podemos calificarlo como una herramienta de gestión establecida al más alto nivel. Es más, aunque es diferente a un sistema de gestión de calidad, puede decirse que idealmente es su herramienta complementaria.

El proceso de desarrollo y diseño de un reactor DEMO habrá de integrar estrechamente un programa formal de RAMI, con sus procesos, herramientas y métodos asociados. Debe partirse de una visión global de la disponibilidad desde el principio y constituirse un proceso iterativo a lo largo de la toda las fases del desarrollo y operación del reactor: diseño pre-conceptual y conceptual, diseño de ingeniería y desarrollo de planta, ensamblaje, puesta en marcha, operación y soporte.

El RAMI ha de levantarse sobre el conocimiento disponible a partir de programas de fusión previos (JET, Tore Supra, ITER, IFMIF, etc.) y sobre la experiencia de otros campos de la tecnología. Debe responder a los desafíos ligados a la transición entre las instalaciones experimentales y las plantas de producción de energía eléctrica, a través del escalado tecnológico y de la introducción de equipos *primeros en su especie*.

Esta condición es crítica para la fiabilidad inicial de un componente o sistema, ya que depende en gran medida de lo novedoso que sea su diseño. Es decir, cuanto más novedoso, mayor es la incertidumbre inicial y la probabilidad de que aparezcan modos de fallo inesperados, lo cual conduce a una fiabilidad inicial menor. La forma de mejorar la fiabilidad es adquirir experiencia y conocimiento sobre el comportamiento del sistema, lo cual puede conseguirse a través de programas de evaluación y ciclos de operación, gracias a la corrección de las deficiencias en el diseño, los procesos de fabricación y las interacciones con el entorno operativo, que se manifiestan en forma de anomalías y fallos.

Así, cada generación de un diseño hace disminuir el número de fallos debidos a un conocimiento limitado del sistema. Según madura el diseño, los fallos 'basados en el conocimiento' prácticamente se eliminan y ceden su lugar a los fallos 'basados en el proceso', es decir, fallos aleatorios debidos a variaciones inherentes a la fabricación, el mantenimiento, los procesos de operación y las características del entorno. La fiabilidad de un diseño maduro depende considerablemente de la complejidad del diseño, de modo que un diseño simple favorece que se reduzcan los fallos basados en el proceso, mientras que un diseño complejo origina incertidumbres en la fabricación, el montaje y la operación de los componentes, en sus interacciones a nivel de sistema y en la interacción del sistema con el entorno. Por ello, dada la complejidad de los diseños de equipos para DEMO, muchos de los cuales serán primeros en su especie, las reglas de diseño, entre las que se incluyen códigos de diseño, como ASME o RCC-MR, bases de datos de propiedades de materiales y códigos de prácticas, junto con la estandarización de elementos de diseño, constituyen una herramienta imprescindible para garantizar que no aparezcan fallos por deterioro hasta un tiempo suficientemente largo tras el fin de la vida operativa concebida.

No obstante, y aunque, como se ha dicho, la primera fuente de datos de fiabilidad y disponibilidad (especialmente para tecnología de fusión) sea la experiencia operativa, la extrapolación desde ITER y el resto de dispositivos experimentales hasta DEMO/FPP resulta difícil, por varias razones:

- Hay diferencias significativas en los esquemas de operación y mantenimiento con respecto a DEMO/FPP. Las instalaciones experimentales operan en series de campañas experimentales de varias semanas, separadas por periodos de parada en los que se analizan los resultados, se modifican los sistemas (ej. diagnósticos), se llevan a cabo tareas de mantenimiento, reparaciones y mejoras, etc., mientras que DEMO y FPP estarán orientados a un esquema de operación más industrial.
- Los datos y resultados de disponibilidad vienen expresados como disponibilidad inherente sobre el tiempo de operación experimental.
- En general, las condiciones de operación (niveles de fluencia neutrónica, daño en materiales, flujos térmicos, etc.) no son *DEMO relevant*.

Una cuestión importante es qué objetivo de disponibilidad debería esperarse para un DEMO o una FPP. En principio, la indisponibilidad programada puede considerarse similar a la de las centrales de fisión (habría paradas más largas para reemplazar los componentes del interior de la cámara de vacío pero el tiempo de operación entre paradas planificadas sería mayor).

Debido a la complejidad de diseño, puede suponerse que la tasa de paradas de un reactor de fusión sea mayor, dado que el número de penetraciones en la cámara de vacío y su segmentación toroidal conlleva el sellado de un gran número de medios y espacios bajo condiciones mucho más exigentes que en los reactores de fisión, en cuanto a vacío, radiación, confinamiento de tritio, manipulación remota y criogenia.

Por lo tanto, se requiere que la calidad de los componentes sea superior a la de los componentes de los reactores de fisión. Sin embargo, como resulta difícil que la calidad de los elementos básicos de diseño (tuberías, uniones, etc.) sea mejor en un dispositivo de fusión que en un reactor de fisión, es la configuración de tales elementos (ej. diseño del componente) la que debe lograr que, en caso de fallo, las consecuencias sean lo menos severas posibles.

En los análisis RAMI de los primeros estudios conceptuales europeos para reactores de potencia (PPCS) se definió un objetivo de disponibilidad (referido al suministro de electricidad a

la red) del 75%, teniendo en cuenta tanto paradas planificadas como no planificadas, debidas a fallos en los componentes del interior de la cámara de vacío (in-vessel) y a eventos no planeados surgidos durante el mantenimiento. También se asumía que todas las operaciones de mantenimiento ex-vessel se llevarán a cabo en paralelo con las operaciones planificadas in-vessel.

En la hoja de ruta trazada por los órganos de la Comisión Europea para el desarrollo de la energía de fusión, semejante a las consideradas por otros socios internacionales, se contemplan dos opciones de diseño para DEMO: DEMO 1 y DEMO 2. DEMO 1 está basado en una línea de diseño conservadora. Es un concepto que puede desarrollarse a corto-medio plazo, basado en la experiencia de ITER y con mejoras razonables en diversos aspectos científicos y tecnológicos.

DEMO 1 es el concepto elegido para la primera generación de reactores demostradores, mientras que DEMO 2, que asume mayores desafíos, requiere desarrollos más evolucionados (ej. escenario de plasma avanzado con alta densidad de potencia y materiales capaces de aguantar una elevada carga térmica y fluencia neutrónica). Es decir, DEMO 1 podría actuar como 'instalación de evaluación de componentes', mientras se genera una base de datos de ingeniería que permitan diseñar y fabricar un blanket y un divertor más avanzados.

Los análisis RAMI sugieren que, si se opera directamente en los escenarios pulsados asumidos para la primera fase de DEMO, la disponibilidad máxima del reactor estaría limitada al 83% (en el caso de pulsos de 4 horas) o al 75% (en el caso de pulsos de 2 horas). Por supuesto, sin tener en cuenta los periodos de parada necesarios para el mantenimiento.

Si además consideramos que la primera fase de operación estará caracterizada por una estrategia de puesta en marcha y por el dominio del mantenimiento no planificado, como consecuencia de fallos aleatorios y la consiguiente investigación y rectificación de dichos fallos, un objetivo razonable para la disponibilidad sería el 30%. Realmente, este objetivo está expresado como disponibilidad inherente, sin tener en cuenta los correspondientes retrasos por mantenimiento in-vessel (y su contribución a la indisponibilidad). Para las siguientes fases de DEMO o FPP, en el que se contemplan vidas operativas de 3,9-5,5 años (a plena potencia) para los componentes in-vessel, el objetivo de disponibilidad debería ser superior al 80%.

En cualquier caso, las distintas evaluaciones llevadas a cabo desde los primeros programas de PPCS coinciden en que tal objetivo podría conseguirse a través de la optimización del esquema de mantenimiento, dado que se estima que las mayores fuentes de indisponibilidad estarán provocadas, además de por el fallo de componentes, por el tiempo de reemplazo de los grandes componentes in-vessel (segmentos del blanket y cassettes del divertor), así como por tareas de mantenimiento de corta duración y procesos de inspección.

Los conceptos de mantenimiento deben validarse tanto mediante modelización avanzada y simulación como mediante la explotación de instalaciones de demostración a escala real o reducida.

En los últimos años se han producido grandes avances en modelización y simulación de estructuras y organizaciones complejas, y el desarrollo continúa de forma imparable. Por ejemplo, hoy en día es habitual utilizar software de CAD para la validación dimensional y la integración de componentes y sistemas complejos. El uso extensivo de herramientas de diseño gráfico y herramientas de modelización y simulación de sistemas dinámicos permitirá acortar significativamente el tiempo de diseño de conceptos de mantenimiento y ayudará a optimizar el equipamiento y los procesos.

Sin embargo, la validación final requerirá el uso de equipamiento de hardware e instalaciones de demostración, no disponibles hoy en día, que puedan reproducir las condiciones representativas de un DEMO/FPP. Esto se enmarcaría dentro del diseño y la ejecución de un programa ambicioso de I+D, con ITER, IFMIF y *components test facilities* como pilares fundamentales, que permita alcanzar un grado elevado de confianza en la operación, la vida operativa y la fiabilidad de los componentes y sistemas nucleares para los futuros reactores de fusión. La posibilidad de licenciar este tipo de instalaciones dependerá en buena medida de

nuestra capacidad para predecir y garantizar su funcionamiento seguro. DEMO jugará un papel clave, tanto como receptor de todo el conocimiento previo como suministrador de datos reproducibles para los reactores de potencia, de acuerdo con la definición de las hojas de ruta.

El presente trabajo describe diversos desarrollos producidos en el marco de las actividades de programa del Laboratorio Nacional de Fusión, integrado en el CIEMAT, y encaminados hacia la consecución de los objetivos de disponibilidad para los futuros reactores de demostración y centrales de producción de energía eléctrica por fusión señalados en los párrafos anteriores. El texto incluye desarrollos relacionados con varios de los puntos clave mencionados: diseño de componentes primeros en su especie, estrategias de integración de diseños complejos y demostración física de conceptos de mantenimiento y manipulación remota.

En el **Capítulo I** se definen varios conceptos de RAMI y se discute su papel en la hoja de ruta de fusión planeada por la Comisión Europea.

El **Capítulo II** desarrolla el concepto de una instalación de demostración de la capacidad integral de manipulación remota del Test Blanket System en ITER. Se describen los procesos y el equipamiento y se comparan con los conceptos planteados para DEMO en relación a la disponibilidad operativa de los dispositivos.

En el **Capítulo III** se ofrece una perspectiva de los sistemas de conversión de potencia estudiados para DEMO. Se presenta un estudio de balance de planta para un reactor DEMO de corto plazo basado en un blanket refrigerado por helio y en el uso de ciclos de Brayton de dióxido de carbono supercrítico en el secundario. Además, tras un breve resumen del Programa Consolider TecnoFus, se describe el diseño innovador de un intercambiador de calor PbLi eutéctico/CO<sub>2</sub> supercrítico desarrollado en el marco de este Programa.

En el **Capítulo IV** se trata la importancia de la modelización y la simulación en la integración de componentes y sistemas complejos, en particular para los casos del Test Blanket System y el Divertor System en ITER.

El **Capítulo V** introduce diversas estrategias para la conexión y desconexión de tuberías de componentes in-vessel en DEMO, como alternativas a las técnicas actuales. Los diseños propuestos se basan en bridas y sellos vacío, sistemas de desconexión rápida y conectores por brazing. También se analiza el estado del arte de diferentes tecnologías para la inspección remota no destructiva de uniones soldadas.

Finalmente, el **Capítulo VI** recoge las conclusiones generales de la tesis y propuestas para un desarrollo más profundo de los conceptos expuestos.

# **Chapter I**

## ***Introduction***



## List of figures

Fig. 1. RAMI elements and their interrelation [Pin 12]. .....	3
Fig. 2. Time lapses for availability estimation [Pin 12]. .....	5
Fig. 3. Part stress and part strength versus probability density of failure [Arr 12]. .....	8
Fig. 4. Contribution to SSC unavailability down time [IAEA]. .....	12
Fig. 5. Working procedure [Bue 95].....	16
Fig. 6. Variation of cost of electricity (arbitrary units) with duration of scheduled shutdowns for divertor replacement [Tay 00]. .....	18
Fig. 7. Effect of the duration of scheduled shutdowns for divertor replacement on the tokamak major radius after optimization for minimum cost of electricity [Tay 00]. .....	18
Fig. 8. Effect of the duration of scheduled shutdowns for divertor replacement on the blanket lifetime and neutron wall load after optimization for minimum cost of electricity [Tay 00]. .....	19



## 1.1. Introduction

The main concepts employed in RAMI are introduced in this Chapter. Afterwards some design guidelines and strategies to reduce unavailability sources are provided, with a specific approach to fusion components and systems. Some references to past studies about availability in fusion power plants are also given.

The main challenges for a demonstration reactor (DEMO) are summarized at the end of the Chapter, including a brief status of some of the most critical technological issues which are being studied within the European Fusion Programme. They are addressed in the framework of the current roadmap towards the achievement of electricity by fusion by the middle of this century.

## 1.2. RAMI general concepts

RAMI is an approach for technical risk management applied in engineering development projects. It introduces a structured iterative process of targets setting, analysis and assessment, evaluation, correction, monitoring and tracking. Through this process it aims to ensure that the produced system design (and implementation) fulfils the imposed system requirements regarding RAMI and does not contain features which could cause unreliable operation or insufficient unavailability of the system [Pin 12].

In order to be most effective the systematic process for RAMI needs to be initiated as early as possible in the conceptual design phase so that it can drive (or influence) the early decisions and selections made which are relevant for reliability and availability performance of the future system. Beside this, it is needed to point out those system elements of which specific RAMI aspects are most critical for the achievement of the performance targets issued for the system, and which thus need thorough monitoring and control throughout the design process [Pin 12].

RAMI management process is an iterative process in which the analyses and assessments get gradually refined as the design progresses and more and better knowledge is gained on different aspects affecting system performance. By systematically driving the efforts on design and assessments on those issues representing the highest uncertainty and risk for system failure, each design gate should result in improved confidence on achieving the reliability and availability targets set for the system [Pin 12].

RAMI management process can be extended also to the operating phase, to cover the overall lifecycle of the system. The RAMI knowledge base compiled during the design process comprises the baseline for the operating phase RAMI activities.

RAMI comprises the elements of Reliability, Availability, Maintainability and Inspectability. These elements are interrelated in specific manner as indicated in Fig. 1 and further explained in the following definitions.

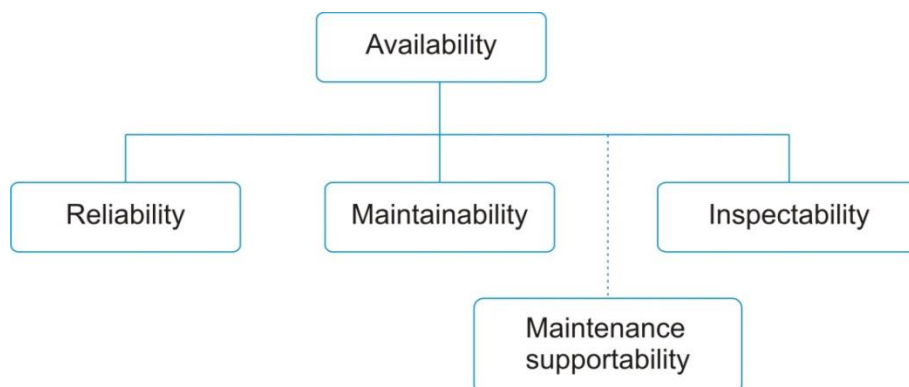


Fig. 1. RAMI elements and their interrelation [Pin 12].

### 1.2.1. MTBF and MDT/MTTR

MTBF is the Mean Time Between Failures of the system, a basic measure of reliability. For a given mission time, to achieve high reliability, a long MTBF is required [Arr 12].

MTTR is the Mean Time To Repair the system, a basic measure of maintainability. MDT represents the time the system is offline and may include the time to diagnose the failure and have access to the failed component, logistic times, shutdown and start-up times, conditioning or tuning times, etc. [Arr 12].

### 1.2.2. Reliability

Reliability is defined as the ability of a system to perform a required function under given conditions for a given time interval [IEC 99].

Reliability deals with the frequency of failures over a time interval and is a measure of the probability for failure-free operation during a given interval; e.g. it is a measure of success for a failure free operation [Arr 12]. As addressed in the definition, reliability refers to a specific expression of an awaited service. What is expected of the considered system must be specified first before it is possible to talk about its reliability. For example, whether any type of repair (provided there are redundant components and no discontinuity of function) is allowed during the time interval needs to be delineated. Also the exact time interval requested for operation must be specified [Pin 12].

The reliability function  $R(t)$  can be written as the probability  $0 \leq R(\Delta t) \leq 1$  that an item, initially working at time  $t_1=0$ , will perform failure free its intended function over a specified time interval  $\Delta t$  under given conditions. In other words,  $R(t)$  determines the probability that the item survives the time interval  $(0, t]$  and is still functioning at time  $t$ . Consequently,  $R(t)$  is also called the survivor function [Pin 12].

$$R(t) = 1 - F(t) = P(T > t) \text{ for } t > 0 \quad (1)$$

where time to failure  $T$  is a random variable distributed with probability density function  $f(t)$  and distribution function  $F(t)$  so that:

$$F(t) = P(T \leq t) = \int_0^t f(u) du \text{ for } t > 0 \quad (2)$$

Both the reliability function  $R(t)$  and the failure distribution function  $F(t)$  are uniquely determined by the failure rate function  $z(t)$ :

$$R(t) = 1 - F(t) = e^{-\int_0^t z(u) du} \text{ for } t > 0 \quad (3)$$

The above expression for  $R(t)$  assumes that the item is functioning at the beginning of the mission, i.e. at  $t=0$ .

The reliability function is often expressed in function of the MTBF when the failure rate is assumed to be constant along the component's life (in some case it could be assumed that it increases at the end of the life for example) [Arr 12]:

$$F(t) = \exp\left(-\frac{t}{MTBF}\right) = \exp(-\lambda \cdot t) \quad (4)$$

Where  $t$  is the time at which the reliability is calculated, MTBF is mean time between failures and  $\lambda$  is the failure rate (constant).  $\lambda = 1/MTBF$ .

### 1.2.3. Availability

Availability is defined as probability that a system is in a state to perform the required function for which it was designed under given conditions at a given time, assuming that the required external resources needed are provided [IEC 99].

Instantaneous availability  $A(t)$  differs from reliability in that aspect that it considers the ability of an item to deliver the required function at an instant in time  $t$  instead of on a given length of time [Pin 12]. Availability can be used as a measure of reliability of repairable items. For a repairable item, functioning at time  $t$  does not necessarily imply functioning over the overall time interval  $[0, t]$ . For a non-repairable item obviously  $A(t)=R(t)$ .

Interval or mission availability  $A_{av}(t_1, t_2)$  in time interval  $(t_1, t_2)$  is defined as the average value of the instantaneous availability  $A(t)$  over the specified time interval.

$$A_{av}(t_1, t_2) = \frac{1}{t_2 - t_1} \int_{t_1}^{t_2} A(t) dt \quad (5)$$

The average availability  $A_{av}(t_1, t_2)$  may be interpreted as the mean proportion of time in the specified interval that the item is able to function. When the time interval  $\tau$  approaches infinity, the average interval availability will approach a limit called the long-run average availability or the steady-state availability  $A_{av}$  of the item.

Considering a repairable item that is put into operation and is operating at time  $t=0$ , and which is replaced by a new identical item or repaired to an “as good as new” condition whenever the item fails. Based on the sequence of lifetimes (or up-times) ending to item failure to perform the required function, and downtimes in between to restore the item back in operation, the (long run) average availability of the item can be shown to be:

$$A_{av} = \frac{\text{Up time}}{\text{Total time}} = \frac{MTTF}{MTTF + MDT} \quad (6)$$

The mean uptime of the system is considered here to be equal to “mean time to failure” MTTF. The mean downtime MDT (or mean forced outage time) is usually significantly longer than the mean time to repair the item, denoted as MTTR, and will include in addition to the active repair time also e.g. time required to detect the failure, time to access the item and diagnose the failure, logistic delays, and time to test and start-up the item after the repair. The main time concepts are further clarified in Fig. 2, where MUT is the mean unavailability time [Pin 12].

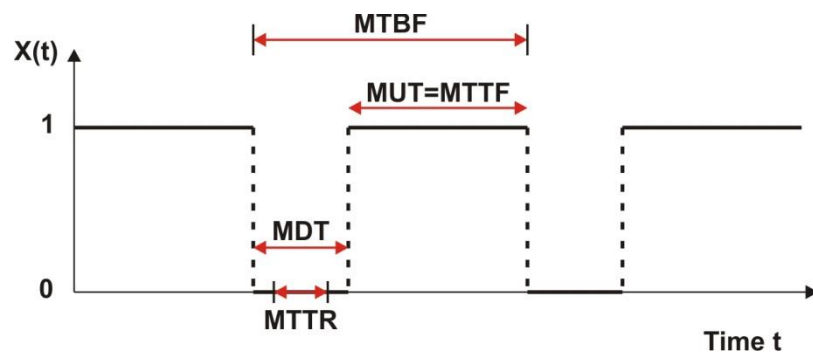


Fig. 2. Time lapses for availability estimation [Pin 12].

As indicated by the equation above, system (or item) availability is a function of system’s reliability, maintainability and maintenance support performance. A system may have low availability due to being unreliable, e.g. having short MTTF and failing frequently, or because of

long outage times caused by repairs, or inspection and maintenance actions introduced in order to avoid realization of the failures [Pin 12].

Two essentially different measures of system availability can be identified [Pin 12]:

- Inherent (average) Availability with the focus on outage times due only to failures (e.g. non-scheduled/ forced outages) and ideal repair time. Inherent availability reflects the quality of the technical design. Inherent availability of a system depends on inherent availabilities of its subsystems and can be approximated as the product of inherent availabilities of the subsystem.

$$A_i = \frac{MUT}{MUT + MDT_{NS}} = \frac{MTTF}{MTTF + MTTR} \quad (7)$$

- Operational (average) Availability takes into account the overall system outage time including also preventive maintenance activities and delays in maintenance and repair due to non-design factors, as well as all other non-operational periods of the system:

$$A_o = \frac{MUT}{MUT + MDT} \quad (8)$$

Where MDT addresses all corrective and preventive actions with down time, e.g. MDTNS and MDTs respectively, and any other times when the system is deliberately kept stopped.

#### **1.2.4. Maintainability**

Maintainability is defined as ability of a system under given conditions of use to be retained in or restored to a state in which it can perform the required function, when maintenance is performed under given conditions and using stated procedures and resources [IEC 99].

Maintainability is a measure of the ease and rapidity with which a system can be restored to operational status following a failure or a detected need for maintenance. It is a characteristic of system design and installation, availability of personnel in required skill levels, adequacy of maintenance procedures and equipment, and the physical environment under which maintenance is performed. Maintainability engineering aims at minimizing the time and resource expenditure to a) recognize, isolate and correct a malfunction, b) gain access to faulty items, c) repair or replace faulty items, and d) test and verify accuracy and adequacy of the maintenance actions [Hou 12].

Maintenance supportability is a related concept defining the ability of a maintenance organization, under given conditions, to provide upon demand, the resources required to maintain an item under a given maintenance policy [IEC 99].

#### **1.2.5. Inspectability**

Inspectability implies the characteristic of design and integration that allows in situ monitoring of equipment performance in regard to the amount of usable lifetime remaining [Hou 12].

Inspectability is related to preventive maintenance and considered essential when component reliability cannot be improved enough. Autonomous online condition monitoring systems with integrated fault detection algorithms to provide early warnings of faults to prevent major component failures are one example of implemented inspectability [Pin 12].

### 1.3. RAMI design guidelines

The objective of this Section is on one hand, to identify the main contributors to unavailability, and on the other hand to provide some design guidelines and strategies in order to reduce such unavailability contribution. The whole information has been extracted from [Arr 12].

Both general approach and specific approach are taken into account. Therefore, both generic ways of improving reliability and maintainability, and specific approach in terms of collection of specific recommendations based on previous studies are given.

Also the needs in view of future fusion power plant and DEMO, and different expected conditions with respect to experimental fusion devices are considered.

According to the RAMI general concepts explained in Section 1.2, the availability (A) can be improved mainly by both:

- Increasing the reliability of components. This reduces the number of failures. It means increasing the MTBF, which increases the value of A.
- Reducing the total shutdown time (by improving the maintenance program, using spare component, etc.). This corresponds to decreasing the value of MTTR in the formula, which also increases the value of A.

Generic and some specific approaches form improving reliability and maintainability are outlined in the following Subsections.

#### 1.3.1. Increasing the reliability of components and systems

Increasing the reliability of components cannot be achieved only by improving their performance itself. Some of the components are already at a mature stage now and thus a great increase of their MTBF due to technological improvement is not realistic. Other solutions have to be found, and the main ones are detailed below. Basically the idea is on one hand to compensate failures (redundancy, fail tolerance), and on the other hand avoid failures by derating. Performing preventive maintenance is also a way of improving reliability.

##### 1.3.1.1. Redundancy

Several types of redundancy can be used, depending on the availability target and the cost:

- Simple parallel redundancy: in a simple parallel system, at least one of the units must succeed for the system to succeed. Units in parallel are also referred to as redundant units.
- Combination of series and parallel systems: larger and more complex systems may involve both series and parallel configurations.
- K-out-of-n redundancy: This configuration is a special case of parallel redundancy. This type of configuration requires that at least k components succeed out of the total n parallel components for the system to succeed.

Regarding the readiness of the spare system, there are three basic states possible for the back-up system. Each has implication on the amount of information that must be available for the back-up system at the time of the failure:

- Hot Stand-by: this is the more complex and more expensive spare state to implement. In that case, the back-up system is designed to instantaneously take over operation when a failure happens. This requires a running duplicate of the primary system: the spare is often designed to load share with the primary system.
- Warm Stand-by: in this case, the redundant system is partially prepared. However, the system does not have all the state information that the primary system knows, for an

immediate take-over. This model is less expensive than the hot stand-by, but requires more time to perform the switching task.

- Cold Stand-by: a redundant system is cold when no state information is maintained between the backup or standby system and the system it protects. This is the less expensive model but also the one leading the higher switching time in case of failure.

### 1.3.1.2. Internal compensation

Depending on the design, the failure of a single component does not necessarily lead to a machine shutdown but could also only slightly decrease the overall performance. This happens when a system has got the intrinsic capability to tolerate failures.

### 1.3.1.3. Derating

Derating is defined as the method of assuring that stresses, either environmental or operational, are applied below rated values. Identical part numbers will not have identical operational parameters: each part will contain slight variations, even when the parts have been manufactured in the same production line.

The purpose of derating is hence to protect against those variations, by imposing a margin between the strength and the stresses of a part. It thus helps to improve the reliability of a part.

The strength of a generic part varies within a lot, from lot to lot, and from manufacturer to manufacturer. Part strength is thus a random variable that can be represented by a statistical distribution. Likewise, the stress applied to a part is random, changing with temperature, vibration, electrical transients, shock, and other factors (radiation, electromagnetic interferences...) and can also be represented by a statistical distribution.

Each statistical distribution can be represented by a probability density function. The average value is the highest point of the curve. Part strength must exceed part stress in order for a part to operate properly. However, since strength and stresses are both random, there is always a probability that stresses applied to a part will exceed the strength of the part. This is represented by the intersection (shaded area) of the graphs in Fig. 3. The larger the shaded area, the higher the probability of failure in a part becomes.

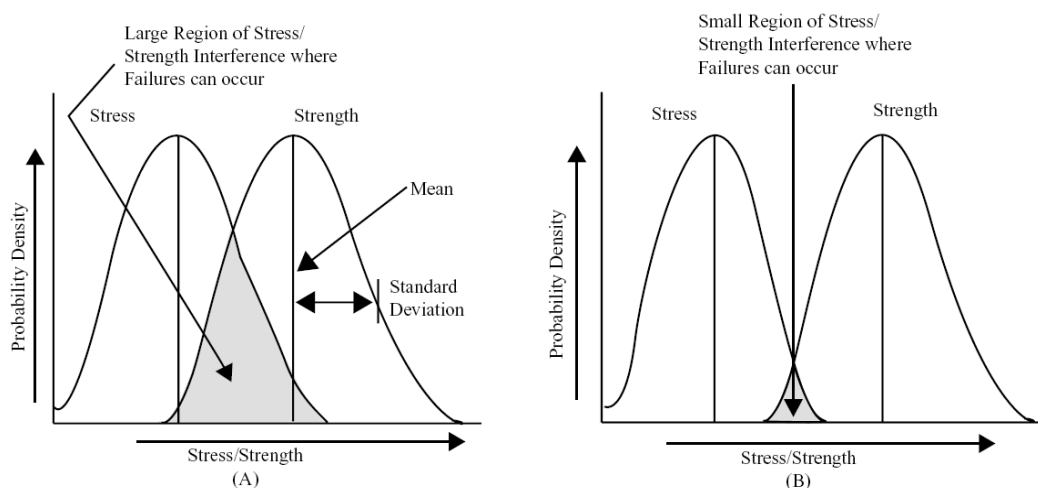


Fig. 3. Part stress and part strength versus probability density of failure [Arr 12].

The four basic stress derating approaches are:

- 1) Increase average strength: the 'when in doubt, make it stout' approach is good if increasing size and weight is not a problem.
- 2) Decrease average stress: if possible, and if it does not affect the part's capability.

- 3) Decrease stress variations: variations are usually difficult to control, but limiting them can sometimes be achieved (for example by improving the temperature control).
- 4) Decrease strength variations: this is to be done during the manufacturing process, by ensuring a better quality control (running tests to eliminate defects and tolerance differences).

The “strength” of a part is directly related to specific parameters. For instance, for electronic components: the “strength” of capacitors is primarily a function of the applied voltage at a given temperature and for most solid state electronic components the strength is simultaneously related to three different parameters: junction temperature, current and voltage. Therefore, more than one parameter must be considered before derating a part. Variations are difficult, and in most cases impossible to accurately quantify at the time of design, so engineering estimates and past experiences are often the only means available to assess the percentage of derating required.

The art lies in selecting the right amount of derating. Insufficient derating is obviously undesirable. On the other hand, excessive derating would require adding more parts (2 power supplies of 100 kW instead of one of 150 kW for example) or require higher rated parts (a power supply of 200 kW instead of one of 150 kW for instance) and would decrease the overall system availability (due to the higher complexity of the system) and increase the cost.

#### 1.3.1.4. Preventive Maintenance

Preventive maintenance is a schedule of planned maintenance actions aimed at the prevention of breakdowns and failures. The primary goal of preventive maintenance is to prevent the failure of equipment before it actually occurs. It is designed to preserve and enhance equipment reliability by replacing worn components before they actually fail.

There are multiple misconceptions about preventive maintenance. One such misconception is that it is unduly costly. This logic dictates that it would cost more for regularly scheduled downtime and maintenance than it would normally cost to operate equipment until repair is absolutely necessary. This may be true for some components; however, one should compare not only the costs but the long-term benefits and savings associated with preventive maintenance. Without preventive maintenance, for example, costs for lost production time from unscheduled equipment breakdown will be incurred. Also, preventive maintenance will result in savings due to an increase of effective system service life.

In some cases, performing maintenance only to repair the system when it is down could be less expensive than applying a preventive maintenance policy. On the short term, preventive maintenance surely increases the downtime, but on the long term it should allow a better control and a reduction of the downtime (only a number of short stops for routine maintenance instead of long stops for more important failures), and an improvement of the system reliability. This depends on each design however, a specific study must be processed to see if such actions are useful, and with which components.

Regarding when is it worth to perform preventive maintenance, it has to be noticed that preventive maintenance is a logical choice if, and only if, the following two conditions are met:

- The component in question has an increasing failure rate. In other words, the failure rate of the component increases with time, thus implying wear-out. Preventive maintenance of a component that is assumed to have an exponential distribution (which implies a constant failure rate) does not make sense.
- The overall cost of the preventive maintenance action must be less than the overall cost of a corrective action. (Note: In the overall cost for a corrective action, one should include ancillary tangible and/or intangible costs, such as downtime costs, loss of production costs, lawsuits over the failure of a safety-critical item, loss of goodwill, etc.).

If both of these conditions are met, then preventive maintenance makes sense. Additionally, based on the costs ratios, an optimum time for such action can be easily computed for a single component.

In general, components such as mechanical components with moving parts or power supplies will have this type of maintenance. Nevertheless, the usefulness of doing preventive maintenance on electronics and cables is not obvious.

### **1.3.2. Specific approach. Fusion reliability components**

Below specific recommendations and conclusions from previous studies are collected regarding the reliability of the foreseen main contributors to unavailability in view of DEMO and fusion power plant.

#### **1.3.2.1. Constituents of mechanical components in First Wall and Breeding Blanket**

Studies for NET already revealed the influence of weld and pipes on the plant availability via components in the high vacuum area: in-vessel components (divertor, first wall, blanket, limiter, shield, etc.), the vacuum vessel, and to a lesser extent the heat transport system and magnet cooling systems.

Information on failure rates and corresponding scaling factors has a broad basis so they are considered fairly robust. However, additional information from applications closer to the fusion-specific features may help to reduce the span between minimum and maximum values and provide an improved basis for the scaling factors.

Assuming that the data collected are representative of the quality achievable by industry, upgrading of the manufacturing quality is unlikely to provide the necessary improvements. Hence, if the failure rate of a certain type of design element cannot be reduced, the design has to be modified.

As leaking of welds was identified as the most frequent type of failure, the aim is to design for continued plant operation in spite of leaks. Secondary containments with an interspace connected to a low pressure system for pumping out leaking media can be effected at different levels of detail, also making use of the well-known principle of separation of functions: a structural weld required to be tight can be divided into two welds to serve separately structural and sealing functions, keeping an interspace for leakage removal; a sealing weld can be separated in an analogous way. In special cases, supply and pumping off a special separating medium, for instance helium, might be considered. This, however, would require additional interspaces. In general, each of these measures might reduce the effective failure rate by one to two orders of magnitude (depending on the capacity of pumping from the interspace) whereas the failure rate due to welds may only be about doubled.

The possibilities for applying these measures and the choice of measure depends on the design details of each weld in question such as, for instance, the location, load level, geometrical shape, requirements for inspection and repair welding at first assembly and after operation. Only stringent Quality Assurance (QA) during the design can yield the necessary improvements.

#### **1.3.2.2. Constituents of fusion specific process systems: Heating Systems, Tritium Processing Systems and Cryogenic Process Systems**

Among these, the largest improvements are required for the heating and magnet systems as well as for process engineering systems such as fuel handling and plasma vacuum pumping. For these systems, it is very important the work to improve the database for the subcomponents. This would allow more reliable identification of the largest contributors to unavailability. This is especially true for heating systems. Reliability analyses of magnet systems also have to be adjusted to recent designs and the database improved before identifying areas of further improvement; the same is true for the other systems cited.

From NET studies, only a few rough indications for design improvements can be given. The neutral beam injection system might require redundancies of subcomponents such as power

supply and ion sources. The magnet systems might require, for instance, improvement of the reliability of the current leads. In the fuel handling system, installation of redundancy in terms of adding parallel subcomponents and media storage capacity may decrease the necessity of plant shutdown due to failure.

Redundancy by oversizing the vacuum pumping capacity would allow partial compensation for the loss of capacity without plant shutdown.

### **1.3.2.3. Reliability data: information management, FRDB, data and uncertainties**

The know-how in operating experiences related to the management of systems and equipment similar to the ones applied in the DEMO plant is an indispensable need for the application of the reliability assurance programme in DEMO.

Reliability and availability data on component and equipment, as well as maintenance and inspection processes, experienced in applications relevant for DEMO, has to be identified and accumulated as a necessary base for the future RAMI analyses done in assistance to the design development.

A specific database with useful statistical data for RAMI of DEMO has to be generated, through statistical data on relevant operating plants and devices and through data collection from existing database in literature. Synergies, or eventually, integrations with the 'Fusion Component Failure Rate Database (FCFR DB)' under development by ENEA for the F4E website have to be pursued [Pin 12].

The following issues must be defined:

- Relevant data to be searched in existing facilities.
- Possible methodology to obtain statistical data.
- Procedures for the database management and updating.

Because for many DEMO components and equipment (e.g.: in-vessel components), actual operating experiences transferable to the future DEMO application do not yet exist, some testing devices simulating future DEMO applications can be required, e.g.: testing of applied type of welds or jointing features. Accordingly, components and equipment that should undergo dedicated testing programs have to be identified. Required tests and testing arrangements have to be outlined, as well as the data to be captured and the methodology to collect and statistically analyse it.

In the absence of sufficient specific data, 'generic' data should be used, assuming an appropriate confidence level. Data from nuclear power plants, chemical industry, aeronautic and military applications and off-shore platforms can be used at least to identify ranges of probabilistic data.

In case of some components or equipment having practically no experience data available, structured expert judgement methods could still be used to specify initial estimates for the reliability parameters of these components and equipment. Specific methods for aggregating expert judgements have been introduced and recommended in use for example in the fission power and aerospace sectors [Pin 12].

## **1.3.3. Increasing maintainability of systems and components**

### **1.3.3.1. Maximizing SSC Maintainability**

In addition to having a concern for the complexity or frequency of maintenance which in turn may lead to a higher than necessary maintenance error rate which has an impact on component reliability, there is also a concern for SSC (Systems, Structures and Components)

maintainability. This is the case when the SSC characterization indicates that average down time is a dominant contributor. In this case the focus shifts from examination of the impact that maintenance has on reliability, to an assessment of how to minimize the average down time, or restoration and repair time which is associated with each preventive and corrective maintenance action. The potential contributors to SSC down time are depicted in the simplified goal tree shown in Fig. 4.

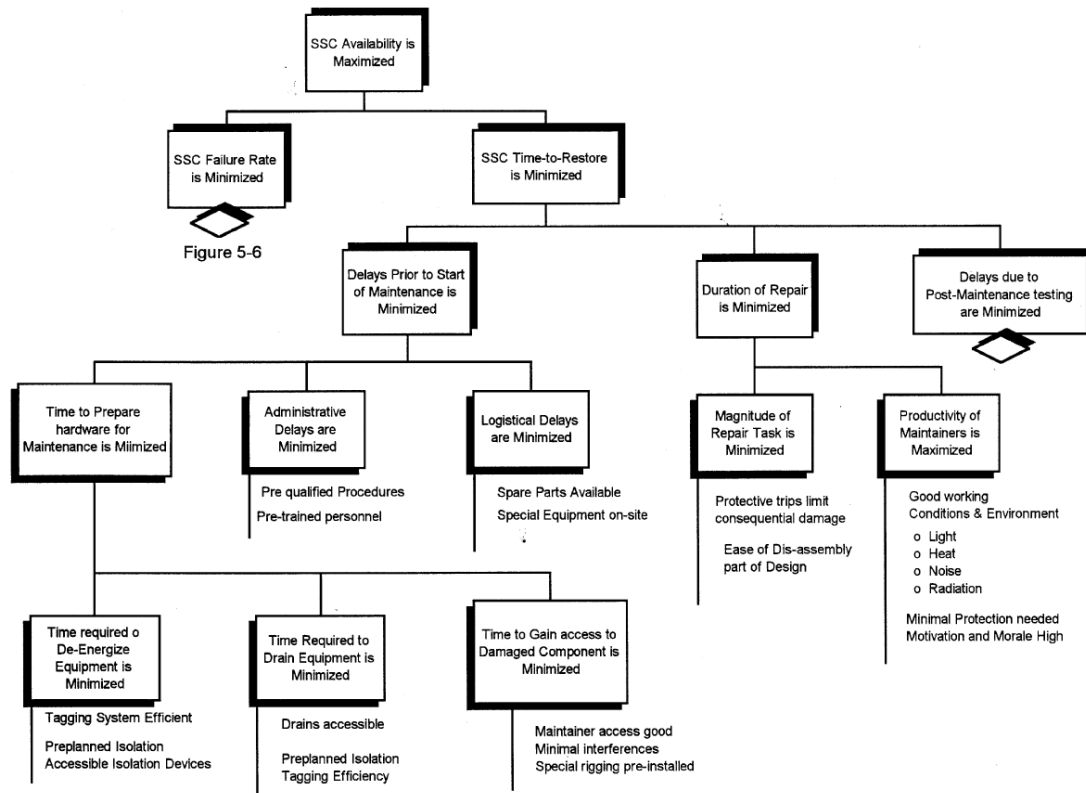


Fig. 4. Contribution to SSC unavailability down time [IAEA].

### 1.3.3.2. Minimizing MDT from preventive maintenance requirements

It must be pointed out that in industry the designer is generally unable to influence the requirements for some routine preventive maintenance activities because they are established by the equipment manufacturer, and are presumably based upon his experience with its basic design characteristics and operational experience with similar equipment. The important thing is that the SSC procurement specifications request the preventive maintenance schedule so that the costs from down time can be calculated and compared for each offering, and an evaluation of their relative magnitudes used to influence the selection process, to the point that the benefits from reduced down time are commensurate with the benefits to safety and economy.

It could well be that, later in the design phase or early in the operational phase, an effective reliability centred maintenance (RCM) programme may justify a reduction in frequency for the required maintenance or a shift from periodic to condition directed maintenance. At the time that the procurement process is initiated it is unlikely that the RCM programme will have been developed, however, if it has been, the insights it brings should be factored into the SSC specification and evaluation process [IAEA].

### 1.3.3.3. Minimizing MDT from curative maintenance activities.

Maintainability review to assess the impact of design decisions on the mean down time needed to perform corrective maintenance for important SSCs is very important because the design

team has a great deal of influence over its magnitude. Down time contributions from corrective maintenance have several generic origins, each of which is described below. Though all of the discrete contributors to down time are described for the sake of completeness, not all can be remedied by design. Some will be resolved during operation.

The broad general sources of time expended during corrective maintenance, and their individual contributing mechanisms are as follows:

- Time lost from the time that the failure occurs to the time that it is detected and remedial actions are initiated by the plant staff.
- Time lost from the time that the failure is detected until corrective actions are initiated on the SSC:
- Time required to perform the repair, following completion of all preparatory activities
- Time lost from the time that repairs are complete and the component is restored to full operational status.

When the designer is developing the specifications for an SSC whose importance is a result of its unavailability or high average mean down time, each of the issues listed above must be considered. The specifications must define the maintainability targets for the SSC. Below some basic guidelines and recommendations for reducing maintenance shutdown time are given:

- Spare components have to be available and easy to replace. A good management of the amount of spare components must guarantee the availability of a spare component when a change is needed, so that the downtime is only due to the replacement process, and not to the delay of ordering and receiving the failed component.
- Standard components must be used as much as possible. Using standard components lowers the retuning and commissioning time of the new component since standard parameters (field value, voltage, frequency...) can be applied. The easiest the components are to repair, the shorter is the maintenance time required.
- The modularity of components, which means enabling the possibility to isolate and repair separately the failed part of a component, is also an important factor to reduce the MTTR.
- Enabling the hand on maintenance every time it is possible is a key factor in reducing the shutdown time for maintenance. This is especially important for rotative (and semi-rotative) components.
- An important decrease of the components MTTR can be achieved by means of fast diagnosis by built-in computerized diagnosis and written troubleshooting procedures.

#### **1.3.3.4. Specific approach. Maintainability in fusion facilities**

Regarding specific issues about maintenance of DEMO, a revision of “schools” of thought on how to replace the inner power core components, corresponding maintenance schemes, and identified R&D needs in this field have been explained in previous sections.

Apart from power core components, fusion power plants will incorporate several individually unique technologies in one site, namely: cryogenic production plant, balance-of-plant systems for electricity production, high technology vacuum plant, state-of-the-art gas purification systems, a small gaseous fuel storage plant and so on. Many of these scientific systems have more in common with particle accelerators than fission reactor power plants. This enhances also the importance of getting feedback from particle accelerator facilities. And on the other hand, there will be a highly diverse in-plant electrical distribution system. All of this will imply the need for a large maintenance staff trained to work on this wide variety of technologies [Til 08].

### **1.3.4. Detection and inspectability**

#### **1.3.4.1. Detection**

Reliability, availability, and automatic supervision of technical processes and their control systems are important consideration in overall system design and operation. An integral

element of a highly reliable, fault tolerant system is an efficient fault detection and identification technique that can detect and isolate the sensors, actuators, or system component failures so that remedies can be undertaken. A failure is defined to be any deviation of a system from its normal or intended behaviour; diagnosis is the process of detecting an abnormality in the system behaviour and isolating the cause or the source of this abnormality. Built in test (BIT) will help diagnose healthy systems, systems that are degrading or nearing failure, and those that have failed.

Integrated System Health Management (ISHM) in an ideal implementation reduces costs directly by predicting failures and thereby converting all unscheduled maintenance actions into scheduled maintenance actions. In addition, ISHM is capable of reducing costs by improving plant availability. At present, the most advanced control systems in industry, particularly aerospace, are capable of implementing what is called Reconfigurable Control. That means that when a failure occurs, the control system is capable of detecting the failure, determining what to do with the parameters it still controls and are functional so as to achieve continued operation of the system, and, finally, is capable of acting on that determination. ISHM takes this process one step further, in that the system is now capable of monitoring trends in performance of the system, and predicting failures before they occur.

As it is said in previous section for revision of technologic status, methods for integrated control, including control automation and ISHM, are currently embryonic within the fusion energy community. This shall be adapted from other industries in future.

#### 1.3.4.2. Inspectability

Inspectability is the ability to visit a component or otherwise perform visual or other detailed examinations of a component and determine its status. Keeping the inspection time duration brief promotes high plant availability. In the fission industry, inspectability has two facets: 'testing' generally refers to active components (pumps, fans, circuit breakers, safety circuits, computers, etc.) and 'inspection' generally refers to passive components (tanks, heat exchangers, pipes). All of these tests are mandatory, for example the periodic surveillance tests of safety-related components that are defined in the fission plant's Technical Specifications as part of the plant's licensing basis. Other mandatory inspections are cited in the American Society of Mechanical Engineers (ASME) Boiler and Pressure Vessel Code (BPVC), which must be used for fission power plants (as directed in federal regulations, 10CFR50.55a). The ASME in-service inspection of welds, piping and vessels identifies cracks, material flaws, and wall thinning. Inspections typically use visual examination and radiography during fabrication, then visual examination and ultrasonic or dye penetrant techniques during the component's service life to monitor health and remaining lifetime. For example, the single-walled TFTR vessel was stress tested to Section III class 2 of the ASME BPVC, and all welds were 100% volumetrically inspected during fabrication according to Section IX of the code. After TFTR operation began the vessel welds were helium leak-tested for vacuum integrity, but they were not ultrasonic tested each 10 years as specified in the ASME BPVC. Considering that ITER has a double-walled vessel and due to ITER's size it has hundreds of meters of coolant piping in guard pipes, it is clear that fusion must develop, and defend to regulators, good methods to test large vacuum vessels, cryostats, and shrouded piping to demonstrate integrity during off-normal events [Til 08].

Appropriate testing methods for in-vessel wall modules must also be developed beyond video inspection. In general, systems must be made safe for test and inspection, the downtime must be brief or it will detract from plant availability. Efficient techniques are needed for inspectability. Some fission power plants have adopted a combined reliability-centred maintenance (RCM) and "condition monitoring" approach to good advantage; this may be very useful for fusion as well.

Inspection rules for fission reactors do not apply very well to fusion. The ITER experiment will forge new paths forward for proving device integrity to reliably contain modest amounts of tritium fuel and activation products. The DEMO facility would likely have higher radiological and chemical inventories on site and in-vessel than ITER, so system integrity carries both economic and safety concerns. Tests and inspections based on equipment condition monitoring can focus on the most likely failure mechanisms, and these will be learned during ITER operation. As

pointed out previously, if the DEMO design diverges from ITER, then new techniques or methods may need to be developed for the DEMO.

## **1.4. Availability in fusion power plants**

The economic performance of a power plant is strongly influenced by the proportion of time that the plant is available to produce full electrical power output. This plant 'availability' is a function of the frequency and duration of planned and unplanned outages, as well as anything which prevents a 100% load factor. For a fusion power plant, in which the cost of electricity generation is dominated by capital construction costs rather than operating costs, the plant availability is an even more important than in some other electricity generation technologies in which fuel costs are more significant. It is thus a factor worthy of special attention in the assessment of the economic attractiveness of conceptual fusion power plant designs.

A full assessment of plant availability requires a detailed design, with a complete taxonomy of components, and full information about the reliability of each item, the modes and frequencies of failure, and time to repair for each failure mode. At this stage in the development of fusion power, there is not only the lack of a full detailed design for a power plant, but an absence of reliability data for many of the components. Indeed, it is the novel technologies, not yet fully developed, which are likely to dominate the plant outages for maintenance.

Probably the most comprehensive analysis of the availability of a fusion plant was that of Buende [Bue 95], who assessed the reliability requirements for the Next European Torus (NET). Buende described the essentials of the reliability and availability programme, its results, and the guidelines derived for further work towards a sufficiently reliable fusion plant. These guidelines comprised two working files: improvement of the reliability database and the quality assurance (QA) to be performed at the design stage of a next step fusion machine [Bue 95].

Other relevant assessments include that by Abdou et al. [Abd 96] who, in the context of a design study for a volumetric neutron source, considered the availability requirements for a demonstration power plant (DEMO) the consequent reliability needed of blanket systems. This was to establish requirements for testing of components in the proposed neutron source, but includes some important observations about the influence of blanket lifetimes (time between failures) on plant availability. An availability goal of 60% was assumed for DEMO, a commonly accepted value, and it was found practically impossible to assure, ab initio, blanket lifetimes of sufficient duration to provide this. Instead an initial period of operation at the much lower target of 30% was assumed during which component reliabilities could be established. Values of 70-80% are needed for economically viable commercial power plants, indicating that achievement of the required blanket reliability could be a very demanding goal, although Schnauder et al. have assessed the availability of four candidate blanket designs for DEMO as being in the range 84-88% [Sch 97].

Earlier studies of fusion power plant availability [Mus 83] [Shef 86] set similar availability goals, and, achieved them only by assuming very high reliability and lifetime of some components (which might now be regarded as unrealistic) and redundancy of others, the economic penalty of which was permitted only because other assumptions (e.g. high neutron wall load) provided an acceptable overall cost of electricity.

### **1.4.1. Reliability of components and QA**

The principle of toroidal magnetic confinement features the combination of nuclear-thermal components supplied from the outside via penetrations through cryogenic-electromagnetic components. Owing to its complexity, single fusion reactor down times for repair or replacements may be longer than those of fission reactors. Thus the failure rate of the fusion reactor must be lower to achieve a similar outage risk [Bue 95].

At first glance also the outage rate of the fusion reactor might be expected to be higher. The component penetrations, together with the toroidal segmentation, are required to seal more media and spaces to seal more media and spaces from each other under more stringent conditions with respect to vacuum, radiation, tritium, remote handling and cryogenics in comparison with fission reactors. Therefore, the component quality is required to be higher than that of fission reactor components [Bue 95].

As the quality of single design elements, for instance pipes or pipe joints, can hardly be better in a fusion machine than in a fission reactor, it is the arrangement of such elements, e.g. the design of the component, which has to be such that their failing has acceptably benign consequences. Stringent quality assurance (QA) exceeding that which is usually applied for fission reactor design is therefore required during the design stage [Bue 95].

Design QA incorporates verification of proper application of specified design rules, codes, materials data and standards and implementation of development work for improving the reliability of specifically important design elements [Bue 95].

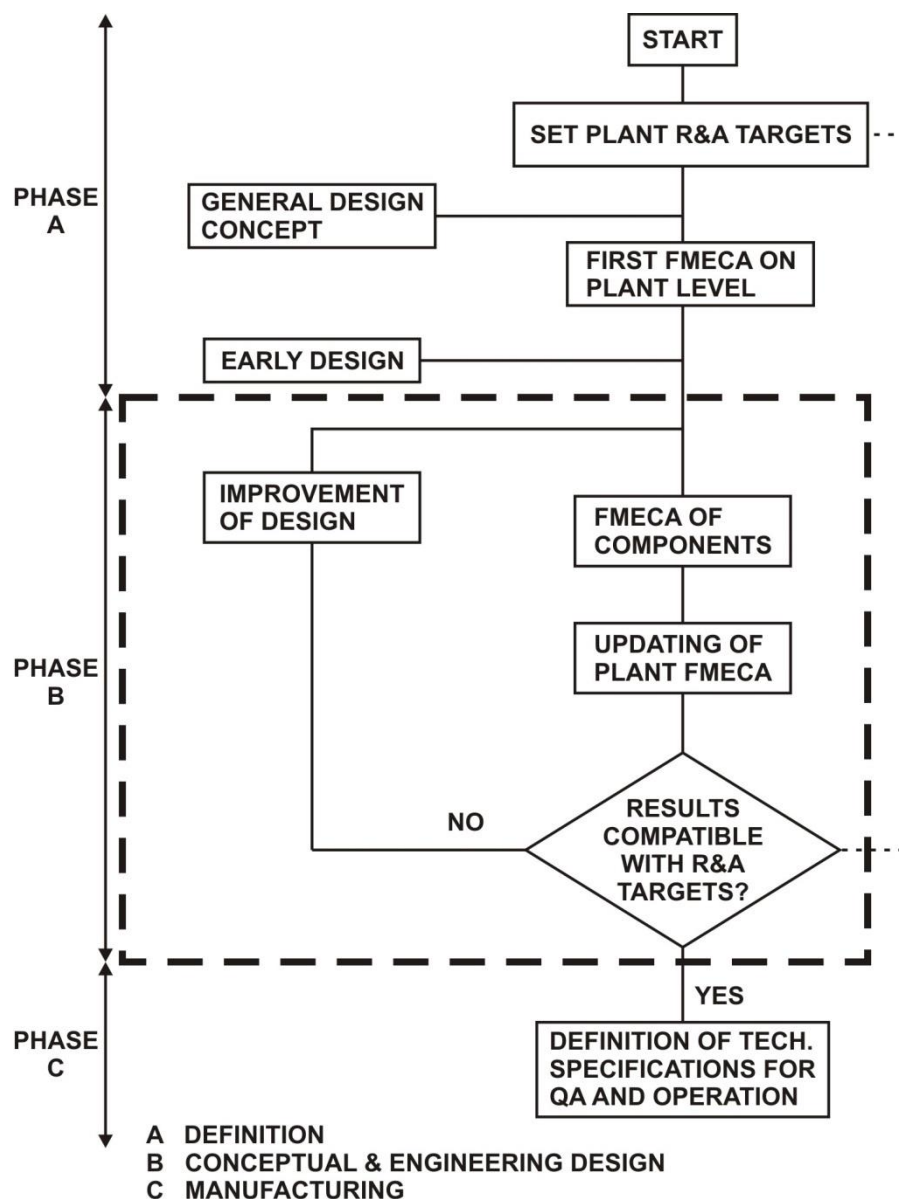


Fig. 5. Working procedure [Bue 95].

### **1.4.2. Design codes and standardization**

As part of the input to components design, design rules are necessary depending on the specific technology applied such as, for instance, the combination of heat transfer, nuclear and ultra-high vacuum technology for the vacuum vessel, in-vessel components and corresponding cooling systems, or the combination of electromagnetic and cryogenic technology for the magnet systems including cryostat and corresponding electrical and coolant supplies [Bue 95].

Such rules may include design codes, for instance ASME or RCC-MR. In combination with these design codes data on materials properties have to be prescribed. Further, codes of practice, for instance for the types and arrangements of welds under different conditions at vacuum vessel or in-vessel components, have to be provided and their correct application enforced. To follow these codes strictly will ensure that wear-out failures can be expected to occur only after times sufficiently longer than the envisaged operating times [Bue 95].

On the other hand, certain design elements like sealing & structural welds, flanges, pivots, bolts, piping, etc. will be used repeatedly in a fusion power plant, although under different conditions depending on the component and the location. They should be standardized, which requires their qualification for a set of conditions expected at application [Bue 95]. Therefore, it is mandatory to characterize the performance of such elements under representative working conditions and to update design codes according with the obtained results.

### **1.4.3. Modelling plant availability**

In a fusion plant, it is envisaged planned outages resulting from scheduled maintenance of the divertor, the blanket and other plasma-facing components (PFCs) will dominate over unplanned outages. These ones occur as a result of failure of components or systems during service. Depending on the response of the plant to such failures, the provision of redundancy and/or protective measures, the plant may be at zero or reduced power output while a repair or replacement is carried out. In a fusion power plant there is a vast array of components, each with a range of potential failure modes, every one of which has a distribution of failure rates and repair times, many of them dependent on the plant state at the time of the failure and on the sequence of events which follow the initial fault. It is apparent that a probabilistic approach is needed to model this behaviour, and that for a thorough assessment a detailed plant design is required, together with complete knowledge of component reliabilities, failure rates and repair times. At this stage such detail is unavailable; therefore a generic approach supported by engineering judgement is necessary. Taylor et al. created a Monte Carlo model to evaluate the effect on overall plant availability of component failures described by probabilistic models of their behaviour, which was implemented the PAMPAS code [Tay 00]. Using limited data [Cad 98], the overall plant availability was calculated as 61%. The down time is roughly divided between planned and unplanned outages, with unavailabilities of 18.6 and 20.3%, respectively. The contribution to unavailability from infrequent failures of major plant items is matched in some cases by the more frequent failures of minor items, typically because they are high in number. This means that to raise the predicted 61% availability to an acceptable value (such as 75%) it may be necessary to improve the overall performance of these minor plant items, as well as the major items which are commonly the focus of attention.

The same authors also incorporated a simplified global representation of plant availability into a plant systems model to allow assessing economic implications. Systems codes are used to study the influence of power plant parameters on key performance measures, typically economic indicators such as the cost of electricity (CoE). This is done with global models of the physics as well as simple representations of the plant technology, along with costing algorithms, coupled together in a way which permits optimisation in a multi-parameter space. Starting from the estimation of the divertor and blanket lifetimes from neutron fluence, Taylor et al. used the PROCESS tokamak power plant systems code to represent plant availability [Tay 00]. Assuming a value of 20% for unplanned unavailability (obtained from PAMPAS) and replacement times of 0.25 years for divertor and 0.5 years for the combination of divertor and blanket, PROCESS results show increasing the length of time taken for divertor replacement would have an important effect on the cost of electricity. For a plant with 1 GW<sub>e</sub> output,

prolonging the shutdown to replace divertor from 3 to 6 months has the effect of increasing the CoE by about 10%.

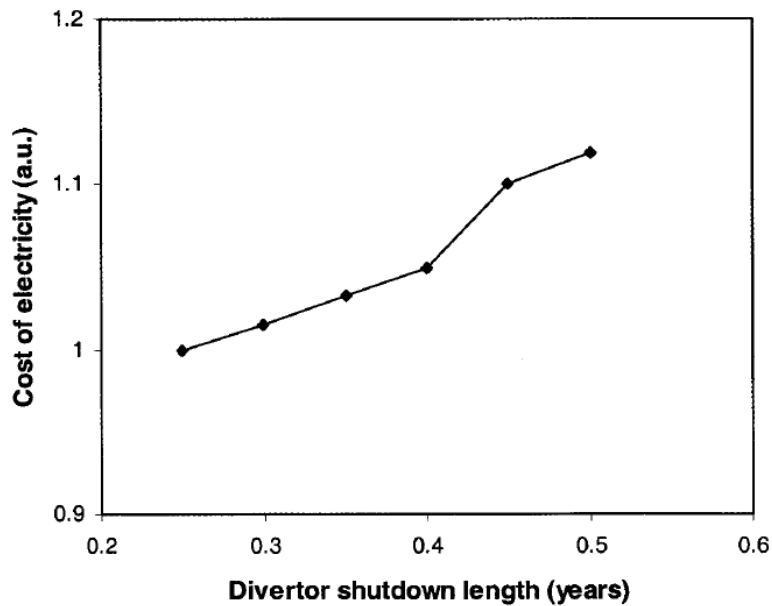


Fig. 6. Variation of cost of electricity (arbitrary units) with duration of scheduled shutdowns for divertor replacement [Tay 00].

The PROCESS CoE minimisation adjusts many plant parameters, and it is interesting to observe how these optimum parameters vary. Fig. 7 shows one of these, the torus major radius, which is seen to increase from about 8.3 to 9.6 m as the divertor shutdown time is extended from 3 to 6 months. The fact that this and other curves of this type are not entirely smooth is due to the discontinuous nature of the maintenance scheme timings, there being an integer number of divertor replacements between each blanket replacement. In these calculations the length of the combined blanket/divertor replacement shutdowns is assumed to be always double that of the divertor replacement shutdown [Tay 00].

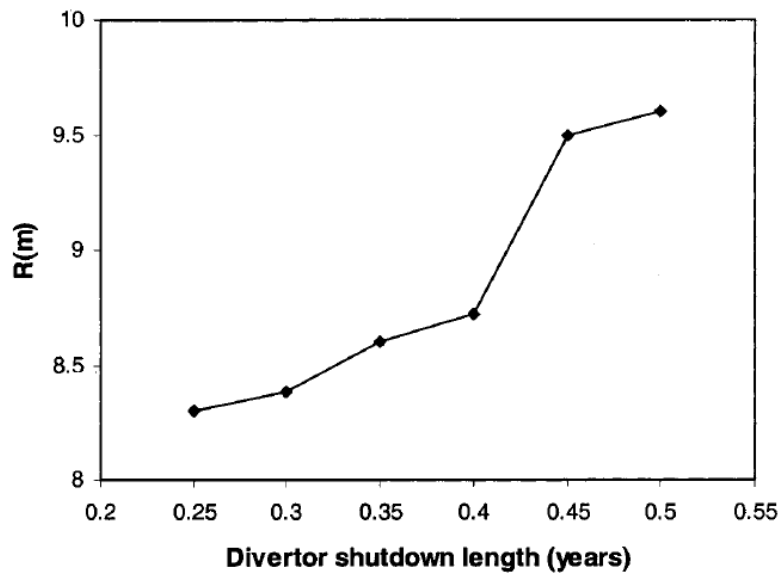


Fig. 7. Effect of the duration of scheduled shutdowns for divertor replacement on the tokamak major radius after optimization for minimum cost of electricity [Tay 00].

The effect of extending the length of shutdowns is to drive the machine design to a larger size, lower wall load machine. In order to prevent high values of unavailability, the systems code optimiser chooses a design with large major radius and high radiated power, which extends the divertor lifetime by reducing the density of power flow to the divertor [Tay 00].

Fig. 8 shows the influence of the same range of divertor replacement times on two other parameters, related to the blanket performance. These are the blanket lifetime (in terms of operational life) and the neutron wall load ( $\text{MW m}^{-2}$ ) at the first wall, after optimisation for minimum CoE. Doubling the divertor replacement shutdown time from 3 to 6 months makes it necessary to increase the blanket lifetime by about 20% to remain economically optimal [Tay 00], with a corresponding decrease in wall loading affected by the larger major radius (Fig. 7). All these results confirm the economic importance of improving plant availability.

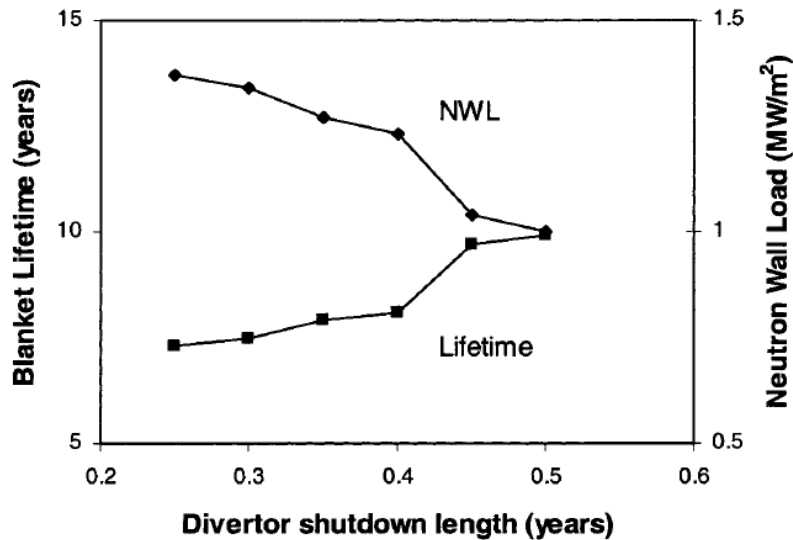


Fig. 8. Effect of the duration of scheduled shutdowns for divertor replacement on the blanket lifetime and neutron wall load after optimization for minimum cost of electricity [Tay 00].

## 1.5. The EU fusion roadmap

In 2001, The European fusion community adopted the so-called Fast Track approach to fusion energy. Since then, the European fusion roadmap has been based on three key elements [Rom 12]:

- The ITER project as the 'essential step towards energy production in a fast track' (see Chapter 2).
- A single step (DEMO) between ITER and the commercial fusion power plant designed 'as a credible prototype for a power-producing fusion reactor, although in itself not fully technically or economically optimised'.
- The International Fusion Materials Irradiation Facility (IFMIF), for material qualification under intense neutron irradiation, in parallel with ITER.

The role of these elements in the programme has been reviewed in the last years, producing a new roadmap aimed at electricity production from fusion by 2050. Specifically, the roadmap has been constructed in such a way that the only critical path is ITER, focusing on solutions that minimise the construction of large and complex test facilities and relying as far as possible on existing facilities and on access to the facilities of the international collaborators [Rom 12].

The current roadmap addresses three separate periods with distinct main objectives:

1. Horizon 2020 (2014-2020) with five overarching objectives.

- a. Construct ITER within scope, schedule and cost (currently the beginning of ITER operation is not expected before 2026 and cost has surpassed the forecast).
  - b. Secure the success of future ITER operation.
  - c. Prepare the ITER generation of scientists, engineers and operators.
  - d. Lay the foundation of the fusion power plant.
  - e. Promote innovation and EU industry competitiveness.
2. Second period (2021-2030)
    - a. Exploit ITER up to its maximum performance and prepare DEMO construction.
  3. Third period (2031-2050).
    - a. Complete the ITER exploitation; construct and operate DEMO.

Therefore, to meet the goal of fusion electricity demonstration by 2050, DEMO construction should begin in the early 2030s at the latest, to allow the start of operation in the early 2040s. Meeting such schedule will strongly depend on ITER achieves its goals, so the innovation potential is fully exploited on the more critical issues and a pragmatic approach to DEMO has been chosen [Rom 12].

Thus, beyond the goals that ITER shall achieve, crucial objectives considered for the EU DEMO, but also for other DEMO concepts, are the following [Fed 14] [Zoh 13]:

- Resolve all physics and technical issues foreseen in the plant and demonstrate reactor relevant technologies.
- Demonstrate production of several 100 MW of electricity.
- Achieve tritium self-sufficiency.
- Achieve adequate availability/reliability operation over a reasonable time span.
- Allow the assessment of the economic prospects of a fusion power plant.

### **1.5.1. Demo challenges in technology and physics**

The list of main challenges in technology and physics for DEMO has been discussed largely in the last decade. The following list has been summarized by Zohm [Zoh 13] from a work carried out by an EU group in 2010 [Bat 10].

#### **1.5.1.1. Technology challenges**

- Development of so-called 'Enabling Technologies' (remote handling, heating and current drive systems, diagnostics and control, tritium processing and superconducting magnet technology) concerning the maintenance, the efficiency requirements in terms of energy conversion and the availability that have to apply to a power plant.
- Radiation resistant materials qualification for designing components with adequate lifetime, up to many dpa for the first wall elements, while keeping the promise of low radiological burden.
- Performance and durability of in-vessel components, especially the breeding blanket necessary for the tritium self-sufficiency requirements of operation and divertor/plasma-facing systems, which will be driven by the extreme heat and neutron loads.

#### **1.5.1.2. Physics challenges**

The following are the challenges identified for a tokamak DEMO beyond those encountered for ITER:

- Steady-state tokamak operation: this includes the whole challenge of achieving an appropriate scenario, e.g. at high bootstrap fraction and the associated MHD limit(s), ITB formation and control with external knobs (H&CD systems) in an alpha-dominated plasma, etc.

- Operation at high density: due to the unfavourable scaling of Greenwald density  $n_g$  with size, it seems unavoidable to operate DEMO at or above  $n_g$ , which is worrying in terms of confinement and disruption danger.
- Power exhaust: power plant conceptual studies showed that pushing a DEMO toward economic attractiveness increases the power exhaust problem into a parameter space where either power handling of plasma-facing components and first wall components is dramatically improved or solutions are found where a very large fraction of power has to be radiated before it reaches the plates. Also, it is not clear if present tools proposed for ELM mitigation in ITER (pellet pacing, in-vessel coils) are also DEMO compatible.
- Disruptions: in DEMO, the disruption problem goes beyond machine protection because it can make the whole concept unattractive.
- Control: availability of sensors (diagnostics) and actuators (H&CD, fuelling systems) on DEMO will pose strong boundary conditions and should be treated in an integrated manner. The DEMO scenario will have to be compatible with the available sensors and actuators.

It must be noted that stellarators promise to be advantageous compared to tokamaks in the first two points and also the fourth, but of course based on a data base that is far from the maturity of that of tokamaks [Zoh 13].

On the other hand, it has been seen over time that the discussion of a single topic from e.g. the previous list leads to the formulation of requirements for another topic that may be unachievable. Therefore, it is necessary to strengthen the link between technology and physics and come to an integrated approach that applies the same level of optimism/realism for each item under discussion. This iteration can lead to a hierarchy of design decisions which then also helps to highlight where progress in a certain field would be especially helpful [Zoh 13].

### **1.5.2. DEMO design options and approach**

The task of choosing an appropriate set of design parameters and engineering technologies involves trade-offs between the attractiveness and technical risk associated with the various design options. One of the crucial points is the size of the device and the amount of power that can be reliably produced and controlled in it. Depending upon the assumptions that are made on the readiness of required advances in the previous list of challenges, two different DEMO design options are currently investigated in EU, in an attempt to identify a realistic range of possibilities [Fed 14]:

- A near-term DEMO (DEMO1) is a rather “conservative baseline design”, e.g. a DEMO concept deliverable in the short to medium term (e.g., construction possibly starting ~20 years from now), based on the expected performance of ITER ( $Q = 10$ ) with reasonable improvements in science and technology; i.e., a large, modest power density, long-pulse inductively supported plasma in a conventional plasma scenario. The design of Balance of Plant (BoP) for a near-term DEMO must also make use of mature and reliable technology.
- A more advanced, DEMO design concept (DEMO2) based around more optimistic (but “less mature”) physics assumptions, which are at the upper limit of what may be achieved in ITER phase-2, i.e., an advanced higher power density high current drive steady-state plasma scenario. It is clear that this can only be delivered on a longer term (e.g., construction to be started on a much longer time scale assuming that the required significant advances in the physics basis be demonstrated using ITER and the limited number of satellite fusion devices available in the next 10-20 years).

It is not to be inferred that two DEMOs should be built but rather that there is a need to incorporate some flexibility to mitigate the uncertainty in the design requirements for DEMO. The approach to select realistic DEMO machine parameters being followed in Europe consists on [Fed 14]: 1) defining a set of main requirements, constraints and assumptions, captured in a set of DEMO design guidelines (both for physics and technology); 2) integrating them into a coherent conceptual design through implementation in 0-D systems codes; and 3) using the results of systems codes to spin off more detailed assessments, using higher dimensional

integrated modelling codes, e.g. codes that solve the time-dependent plasma transport equations (1-D) self-consistently with the magnetic equilibrium (2-D).

Clearly, it is necessary to iterate between these steps, for instance finding that some of the assumptions lead to inconsistencies in the integrated design, or that the results of more detailed assessments lead to changes in some of the assumptions. Therefore, the definition and assessment of plasma scenarios for DEMO, an essential step for the design of the machine, requires a careful iteration of the two approaches, systems codes and specific codes modelling relevant aspects of DEMO physics with a higher level of detail [Fed 14].

### 1.5.2.1. Key design drivers

According to the list of technology challenges shown in Sub-subsection 1.5.1.1, breeding blanket technology and coolants, divertor design configuration and technology, first-wall protection and integration to the blanket, H&CD systems, remote maintenance and balance of plant are the technology areas with largest uncertainties that have a large impact on the concept definition and that require extensive development in parallel to and beyond ITER.

The issues which are more closely related to this thesis: balance of plant, remote maintenance and breeding blanket technologies are further discussed in the next Chapters.

Regarding divertor design configuration and technology, significant progress has been made during the last two decades (thanks to the ITER programme) in the development of technologies for divertor high-heat-flux-components cooled with either water or helium. Water-cooled prototypes fabricated both with carbon and tungsten have been successfully tested under cyclic loads of up to  $20 \text{ MW/m}^2$ ; whilst helium-cooled solutions have been found to withstand  $10 \text{ MW/m}^2$  for a large number of cycles. In addition, in the case of exposure under large neutron irradiation fluence, such as those expected in DEMO, the indicated power handling limits will be reduced [Fed 14].

In a tokamak power plant the loss power would be a factor 5-10 greater than in ITER, while the area of the divertor high heat flux components will probably differ by less than a factor of 2. Therefore, as anticipated in Sub-subsection 1.5.1.1, it will be probably necessary to radiate the majority of the loss power, whilst still maintaining sufficient confinement and plasma purity. At present, the most favoured approach is to use impurity seeding to establish highly radiating edge and divertor plasmas, combined with core radiation, to distribute the exhaust power over a large wall area. This would be combined with tungsten plasma-facing components, to ensure an acceptable interval between PFCs replacements [Fed 14].

In addition to developing high radiation scenarios in standard X-point configurations, it is also prudent to look into solutions using advanced magnetic configurations, where issues such as thermal stability and radiating volume may be different, or advanced plasma-facing materials targets, such as liquid metals, which could reduce the radiation requirements. Emphasis should be on the heat exhaust capability of the solutions proposed during normal conditions but also with a view to the occurrence of possible non-controlled transients. More specifically, feasibility studies aimed at objectively and rationally determining and comparing the strengths and weaknesses of the various configurations (e.g. snowflake, X-divertor, super-X divertors, etc.) are urgently needed. In particular, an analysis of the implications of the target configuration on the mechanical integration and maintenance scenarios, as well as an investigation of the design integration and engineering constraints arising from the use of large current coils in the divertor region, or of liquid metal, in the case of LM targets [Fed 14].

With respect to the first wall design and its integration with the breeding blanket, an important decision is whether or not to make the first wall (FW) hydraulically and mechanically integrated with the blanket or whether to make it, as ITER plans, separable from the blanket for replacement or repair operations. The FW and the blanket have a number of fundamentally different design requirements and functions. Also, previous design studies have predicted FW design lifetimes considerably lower than the breeding blanket [Fed 14]. The design of a FW than can be separated from the blanket represents a complex challenge. On one hand, it can relax the thermal requirements for blanket designers. On the other hand, if a larger amount of

structural material and non-breeding coolant is required, it could be necessary more radial space to compensate the loss of breeding capability, as well as access to permit simple FW removal operation (increase reactor size for a given neutron wall loading).

Finally, in a DEMO based on a long-pulse/inductive regimes of operation and not on fully steady-state operations, heating and current drive (H&CD) systems primarily need to provide heating power for H-mode access, suppression of MHD instabilities and increase of the pulse length; whereas the detailed control of the equilibrium current density profile will not be the primary requirement. This choice will reduce the risks on the DEMO H&CD systems and is in line with the pragmatic approach advocated in the EU roadmap [Fed 14]. ITER will test the potential of different heating systems (ICH, NBI and ECH, with lower Hybrid CD as a possible upgrade to be decided at a later stage) from the point of view of their application to DEMO regimes of operation. The approach is to pursue only specific developments to comply with the parameters of DEMO (e.g. higher magnetic field) and to ensure high system availability (e.g. by minimizing the need of maintenance outside the scheduled periods), reliability (e.g. by ensuring the modularity of the systems) and plant efficiency (e.g. by minimizing the re-circulating power).

## **1.6. Scope of this work**

The main objective of this thesis is to demonstrate the need of applying RAMI principles to the design of nuclear components and systems for fusion technology.

This is addressed through several technical objectives which can be summarized in the following paragraphs:

- Proposal of a conceptual design of a remote handling test facility for the ITER Test Blanket System. This facility, complementary to other components tests facilities which will be demanded in the incoming years, must provide solutions to validate design concepts, to assess equipment reliability –certainly valuable to grow and improve the databases which will be used in the design of subsequent devices- and to train future RH systems operators.
- Development of methodologies to validate integration concepts and maintenance operations by using combinations of CAD and graphical design tools. These methodologies, which are shown as very useful to minimize time, efforts and cost in technology development, are applied to study a number of remote maintenance operations related to the Test Blanket System and the Divertor System in ITER.
- The difficulty of reaching high overall plant availability in future fusion power plants and its influence on the cost of electricity can be partially counteracted by optimizing the balance of plant. This is addressed here through the design of a compact, efficient, reliable and adaptable to pulsed generation profiles power conversion cycle for a near term demonstration reactor based on supercritical carbon dioxide.
- Design of first-of-its-kind components aimed to maximize the reliability and availability of the systems they shall form part and, at the same time, to optimize their functional performance (e.g. thermal efficiency, sealing level, etc.). This comprises the design of: a) a novel liquid metal heat exchanger for the power conversion system of a mid-term DEMO; and b) quick pipe connection and disconnection systems: reliable, inspectable and remote handling compatible, which increase the availability of in-vessel components representing the most critical elements in fusion power plants.

## 1.7. References

- [Abd 96] M.A. Abdou, S.E. Berk, A. Ying, Y.K. Marting Peng et al., Results of an international study on a high-volume plasma-based neutron source for fusion blanket development, *Fusion Technology* 29 (1996) 1-57.
- [Arr 12] J.M. Arroyo, RAMI Management Process for DEMO. Final report for Task Agreement WP12-DTM02-T03, EFDA internal document (EFDA\_D\_2GE7ZV), 2012.
- [Bat 10] P. Batistoni, S. Clement Lorenzo, K. Kurzydowski, D. Maisonnier, et al., Report of the Ad hoc Group on DEMO Activities, CCE-Fu 49/6.7, 2010.
- [Bue 95] R. Buende, Reliability, availability and quality assurance considerations for fusion components, *Fusion Engineering and Design* 29 (1995) 262-285.
- [Cad 98] L.C. Cadwallader, Selected component failure rate values from fusion safety assessment tasks, Idaho National Engineering and Environmental Laboratory report INEEL/EXT-98-00892, 1998.
- [Fed 14] G. Federici, R. Kemp, D. Ward, C. Bachmann et al., Overview of EU DEMO design and R&D activities, *Fusion Engineering and Design* 89 (2014) 882-889.
- [Hou 12] D. van Houtte, K. Okayama, F. Sagot, ITER RAMI Analysis Programme, ITER internal document (ITER\_D\_28WBXD), 2012.
- [IAEA] Reliability Assurance Programme guidebook for advanced LWR, IAEA internal report (IAEA-TECDOC-1264), 2011.
- [IEC 99] International Electrotechnical Vocabulary, chapter 191 (IEC 60050-191): Dependability and quality of service, 1999.
- [Mus 83] Z. Musicki, C.W. Maynard, The availability analysis of fusion power plants as applied to MARS, *Fusion Science and Technology* 4 (1983) 284-289.
- [Pin 12] T. Pinna, R. Tuominen, M. Siuko, Outlines for the definition of RAMI guidelines for DEMO systems, final report for Task Agreement WP11-DAS-RH-08, EFDA internal document (EFDA\_D\_2KVG3G), 2012.
- [Rom 12] F. Romanelli et al., Fusion electricity: a roadmap to the realisation of fusion energy, EFDA report, 2012.
- [Sch 97] H. Schnauder, C. Nardi, M. Eid, Comparative availability analysis of the four European DEMO blanket concepts in view of the selection exercise, *Fusion Engineering and Design* 36 (1997) 343-365.
- [Shef 86] J. Sheffield, R.A. Dory, S.M. Cohn, J.G. Delene et al., Cost assessment of a generic magnetic fusion reactor, *Fusion Technology* 9 (1986) 199-249.
- [Tay 00] N.P. Taylor, P.J. Knight, D.J. Ward, A model of the availability of a fusion power plant, *Fusion Engineering and Design* 51-52 (2000) 363-369.
- [Til 08] M.S. Tillack, D. Steiner, L.M. Waganer, S. Malang et al., Issues and R&D needs for commercial fusion energy, interim report of the ARIES technical working groups, 2008.
- [Zoh 13] H. Zohm, Assessment of DEMO challenges in technology and physics, *Fusion Engineering and Design* 88 (2013) 428-433.

## **Chapter II**

***ITER Test Blanket System  
integration studies.***

***Conceptual design of a  
remote handling test  
facility***



## List of figures

Fig. 1. Layout of the different IFMIF facilities. ....	32
Fig. 2. Section view of the JT-60SA. ....	32
Fig. 3. ITER vacuum vessel. ....	34
Fig. 4. ITER small-scale prototype (1/6) of the blanket first wall [F4E 14]. ....	35
Fig. 5. ITER cryostat. ....	36
Fig. 6. ITER divertor cassette. ....	37
Fig. 7. ICRH antenna system. ....	38
Fig. 8. Model of ITER cryopump tested at the TIMO test facility. ....	39
Fig. 9. ITER cooling water system layout. ....	40
Fig. 10. ITER closed D-T fuel cycle. ....	41
Fig. 11. Test platform at Naka site for the remote positioning of the first wall panels. ....	43
Fig. 12. Divertor Test Platform (DTP 2) at Tampere University of Technology. ....	44
Fig. 13. Analysis of cask trajectories in the tokamak building port cells and corridors. ....	45
Fig. 14. Scanning probe (1: rotating head; 2: optical box; 3: connection box) [Dub 14]. ....	46
Fig. 15. Beam source equipment maintaining the beam source [Shu 14]. ....	47
Fig. 16. CEA proposal for HC tooling (ICRH antenna port plug refurbishment) [Fer 13]. ....	47
Fig. 17. General view of the Test Blanket System in the Port Cell and the Port interspace. ....	54
Fig. 18. Test Blanket System and AEU (right). ....	54
Fig. 19. Layout of EU Test Blanket System in the Tokamak Building and the Tritium Building. ....	55
Fig. 20. Design process (phases and sub-phases). ....	57
Fig. 21. Working methodology according to IMMS. ....	58
Fig. 22. Vertical positioning tool. ....	60
Fig. 23. Vacuum cleaner located on the floor of the PP maintenance area. ....	62
Fig. 24. Pipes connecting PP and shield water cooling circuits to the vacuum vessel cooling system. ....	63
Fig. 25. Unscrewing of captive bolts which joins the shield flange to the PP frame. ....	65
Fig. 26. Scheme of the extraction of a TBM & shield assembly [Bed 08]. ....	66
Fig. 27. Lifting tool extracting a TBM & shield assembly. ....	67
Fig. 28. Cleaning of dust from the TBM & shield assembly. ....	68
Fig. 29. Mechanical joints between TBM and shield at Interface 1. ....	70
Fig. 30. Possible way to pass cabling to/from the TBM through the shield. ....	70
Fig. 31. Cut of the joints between the TBM and the shield by laser. ....	71
Fig. 32. Separation of the TBM from the shield using the clamping bench and the crane. ....	71
Fig. 33. Insertion of the shield in the storage container. ....	72
Fig. 34. Placing of TBM on the band sawing machine. ....	72
Fig. 35. Cutting of TBM by band sawing machine. ....	74
Fig. 36. Introduction of a TBM piece into a drum. ....	74
Fig. 37. Introduction of a drum into the shipping cask. ....	75
Fig. 38. Space needed for the operation (in red). ....	75
Fig. 39. Polishing of the port plug flange. ....	77
Fig. 40. Insertion of a TBM & shield assembly in the port plug. ....	77
Fig. 41. Screwing of shield captive bolts to PP frame. ....	78
Fig. 42. Welding points for the inlet interface circuit between shields (left and right), port plug (centre) and vacuum vessel. ....	80
Fig. 43. Port plug inserted in test stand for vacuum sealing test. ....	81
Fig. 44. Diagram of vacuum sealing test with test stand. ....	82
Fig. 45. Checking of the water loop. ....	84
Fig. 46. Entry of Pipe Forest & Bioshield assembly in the Port Cell. ....	86
Fig. 47. Pipe Forest & Bioshield Door assembly moving on ATS rails towards the Interspace (Port Cell Structures not shown). ....	87
Fig. 48. Folding of the intermediate wheels. ....	87
Fig. 49. Pipes alignment at IF2a. ....	88
Fig. 50. Plugging of diagnostics/electric supply connectors. ....	88
Fig. 51. Screwing of captive bolts. ....	89

Fig. 52. Entry of the RH Platform Unit in the Port Cell. ....	90
Fig. 53. Bioshield window mechanism. ....	92
Fig. 54. The robotic arm goes through the Bioshield window. ....	92
Fig. 55. 1) The robotic arm takes the welding tool from the tool rack. 2) The robotic arm gains access to the IF2a. 3) Welding of a pipe at IF2a. ....	93
Fig. 56. The robot takes the inspection final effector from the tool rack. ....	94
Fig. 57. Inspection of a welding bead at IF2a. ....	95
Fig. 58. Standalone thermal insulation. ....	96
Fig. 59. Installation of an insulating module. ....	97
Fig. 60. Constricted IF2a pipes. ....	98
Fig. 61. Unconstricted IF2a pipes. ....	98
Fig. 62. Cutting head. ....	99
Fig. 63. Cut of a pipe at IF2a. ....	100
Fig. 64. Entry of the AEU in the Port Cell. ....	101
Fig. 65. Alignment of pipes at IF2b. ....	102
Fig. 66. Hands-on operations at IF2b. ....	102
Fig. 67. Transfer cask. ....	103
Fig. 68. Docking flange (blue) installed in the port. Docking flange lugs and the two pins of the TC that go into the lugs. ....	104
Fig. 69. Docking system. ....	104
Fig. 70. Helping cantilever system: rollers and rear flange pockets. ....	105
Fig. 71. Helping cantilever system in the port extension and the Transfer Cask. ....	105
Fig. 72. Insertion of the Port Plug in the Port Extension. ....	106
Fig. 73. Gasket flange sealing. ....	107
Fig. 74. Gasket flange detail. ....	107
Fig. 75. Gasket flange maintenance equipment. ....	108
Fig. 76. Polishing disc and camera [Meu 07]. ....	108
Fig. 77. Spatial layout of the TBM RH test facility hosting building. ....	110
Fig. 78. Dimensions of the TBM RH test facility site. ....	110
Fig. 79. Space allocation in the Operations Hall. ....	111
Fig. 80. Top view of the operations hall. ....	112
Fig. 81. View of the operations hall from the office and auxiliary system building. ....	112
Fig. 82. Operations hall ground view 1. ....	113
Fig. 83. Operations hall ground view 2. ....	113
Fig. 84. Port Cell RH operations area. ....	114
Fig. 85. Port Cell RH operations area. Top view. ....	114
Fig. 86. Hot Cell RH operations area. ....	115
Fig. 87. Storage area (view 1). ....	115
Fig. 88. Storage area (view 2). ....	116
Fig. 89. Truck parked at the Unloading and Parking zone, carrying a port plug mock- up. ....	116
Fig. 90. Space layout of the Office and Auxiliary Systems building ground floor. ....	117
Fig. 91. Ground floor (offices and auxiliary systems building). ....	118
Fig. 92. Space layout of the Office and Auxiliary Systems building first floor. ....	119
Fig. 93. First floor (Offices and Auxiliary Systems building). ....	119
Fig. 94. Control room. ....	120
Fig. 95. Ancillary equipment unit. ....	122
Fig. 96. AEU Platform. ....	123
Fig. 97. Pipes layout at interfaces 2b and 3. ....	123
Fig. 98. Pipe Forest. ....	125
Fig. 99. Pipe Forest wheels. ....	125
Fig. 100. PF Motor-driven wheels. ....	126
Fig. 101. Intermediate wheels. ....	126
Fig. 102. PF Bioshield. ....	127
Fig. 103. PF alignment system. ....	127
Fig. 104. Bioshield Window system. ....	128
Fig. 105. Port plug. Section. ....	129
Fig. 106. HCLL handles (HC operations). ....	130
Fig. 107. Interface between HCLL TBM and shield (HC operations). ....	131
Fig. 108. HCLL shield design proposal (HC operations). ....	132

Fig. 109. HCLL & HCPB TBM & shields. ....	133
Fig. 110. Diagnostics plugs at IF2a. ....	134
Fig. 111. ATS used to transport the equipment. ....	134
Fig. 112. Design of the ATS [Lor 07]. ....	135
Fig. 113. ATS with the pallet of the Transfer Cask. ....	135
Fig. 114. ATS under the pallet [Lor 07]. ....	136
Fig. 115. ATS ready for transport [Lor 07]. ....	136
Fig. 116. Platform dedicated for Pipe Forest. Detail. ....	137
Fig. 117. Band sawing machine. ....	137
Fig. 118. TN-MTR shipping basket [Ghi 12]. ....	138
Fig. 119. Drum. ....	139
Fig. 120. Internal dimensions of a drum. ....	139
Fig. 121. Detail of the lifting eyes of the drum coupled to the gripping interface. ....	140
Fig. 122. Shipping basket with one drum inserted. ....	140
Fig. 123. Plasma cutting tool. ....	141
Fig. 124. Gasket flange maintenance equipment. ....	142
Fig. 125. Bolting and polishing tools. ....	142
Fig. 126. Pinion-rack system. ....	143
Fig. 127. Hot Cell manipulator. ....	144
Fig. 128. Welds inspection tool. ....	144
Fig. 129. Welds inspection tool (open water sealing cover). ....	145
Fig. 130. Scheme of a weld inspection. ....	145
Fig. 131. Thermal insulating module. ....	146
Fig. 132. Laser source. ....	147
Fig. 133. Support structure. Detail of the cutting head. ....	148
Fig. 134. Laser shield. ....	148
Fig. 135. Laser cutting tool. ....	149
Fig. 136. TBM & shield lifting tool and container. ....	150
Fig. 137. View of the two trolleys integrated in the crane of 20 tons. ....	151
Fig. 138. Trolley with coupling tool (left). Zoom view of the coupling tool (right). ....	152
Fig. 139. Telescopic mast. ....	152
Fig. 140. Storage shelves and palletising system. ....	153
Fig. 141. Palletising system. ....	155
Fig. 142. PC robotic arm (KUKA KR16). ....	156
Fig. 143. KUKA KR16 mounted on a deployable carrier. ....	157
Fig. 144. RH Platform Unit. ....	158
Fig. 145. Robot, insulations container and tool rack. ....	158
Fig. 146. Polisher tool and container. ....	159
Fig. 147. Test stand. ....	160
Fig. 148. Test stand lid. ....	160
Fig. 149. Test stand flange. Front and back views. ....	161
Fig. 150. Gasket flange installed in the test stand. ....	161
Fig. 151. Section of the port plug inserted into the test stand. ....	162
Fig. 152. Screwer system. ....	163
Fig. 153. Screw driver. ....	163
Fig. 154. Pallet. ....	164
Fig. 155. Cask enclosure and double seal door. ....	165
Fig. 156. Cask enclosure frame. ....	165
Fig. 157. Cask side connector [Yao 07]. ....	166
Fig. 158. Tractor. ....	166
Fig. 159. Vertical positioning tool. ....	167
Fig. 160. Sliding frame. ....	168
Fig. 161. Rail and rack. ....	168
Fig. 162. Driving assembly. ....	169
Fig. 163. Rotating frame. ....	169
Fig. 164. Rotating system. ....	170
Fig. 165. Port plug inserted in the vertical positioning tool. ....	170
Fig. 166. Welding tool. ....	171
Fig. 167. Welding tool components. ....	171
Fig. 168. Top view of the operations hall showing the 50 ton and 20 ton cranes. ....	172

Fig. 169. View of the 50 ton crane. ....	173
Fig. 170. Cleaning and separation bench. ....	173
Fig. 171. TBM and shield assembly inserted in the cleaning and separation bench. ....	174
Fig. 172. PP transfer from the transfer cask to the vertical positioning tool. ....	175
Fig. 173. Hot Cell door for the vertical positioning tool. ....	175
Fig. 174. Test stand door. ....	176
Fig. 175. Transfer of the port plug. ....	177
Fig. 176. Assembly of the gasket flange. ....	177
Fig. 177. Dimensions of the Port Cell mock-up. ....	178
Fig. 178. Components of the Port Cell mock-up. ....	179
Fig. 179. Double floor in the Port Cell zone. ....	180
Fig. 180. Port components. ....	181
Fig. 181. Port integrated with the rest of components. ....	182
Fig. 182. Port supporting system. ....	183
Fig. 183. Shipping bench for TBM & shield assemblies. ....	184
Fig. 184. Integration of the different parts of the Remote Handling Control System. ....	185
Fig. 185. Spatial layout of the control room of JET. ....	188
Fig. 186. DTP2 control room. ....	189
Fig. 187. JET vessel simulation – GUI. ....	189
Fig. 188. Example of camera for the viewing system. ....	190
Fig. 189. Vacuum system location within the Hot Cell operations area. ....	195
Fig. 190. Vacuum system diagram. ....	196
Fig. 191. Mass spectrometer. ....	198
Fig. 192. Layout of the He system for testing operations. ....	198
Fig. 193. Layout of the test stand. ....	199
Fig. 194. Section through the port closure cask showing the fully extracted port closure plates, pipes and thermal shield plug [Col 14]. ....	202
Fig. 195. Rotation of the central outboard segment in a vertical plane during its extraction process (CoG displacement) [Ccf 14]. ....	203
Fig. 196. Vertical maintenance crane proposed for DEMO blanket MMS [Igl 13b]. Heat transfer coefficient results for natural convection (in-cask simulations). ....	204
Fig. 197. Active components storage [Igl 13b]. ....	204
Fig. 198. Processing flow chart in the AMF [Ros 14]. ....	206

## List of tables

Table 1. ITER construction and operational parameters. ....	33
Table 2. List of RH operations to be demonstrated in the Test Facility. ....	59
Table 3. Operation #1 requirements. ....	60
Table 4. Operation #2 requirements. ....	61
Table 5. Operation #3 requirements. ....	62
Table 6. Operation #4 requirements. ....	64
Table 7. Operation #5 requirements. ....	65
Table 8. Operation #6 requirements. ....	67
Table 9. Operation #7 requirements. ....	68
Table 10. Operation #8 requirements. ....	73
Table 11. Operation #9 requirements. ....	76
Table 12. Operation #10 requirements. ....	78
Table 13. Operation #11 requirements. ....	79
Table 14. Operation #12 requirements. ....	80
Table 15. Operation #13 requirements. ....	82
Table 16. Operation #14 requirements. ....	84
Table 17. Operation #15 requirements. ....	85
Table 18. Operation #16 requirements. ....	89
Table 19. Operation #17 requirements. ....	91
Table 20. Operation #18 requirements. ....	93
Table 21. Operation #19 requirements. ....	95
Table 22. Operation #20 requirements. ....	97

---

Table 23. Operation #22 requirements. ....	99
Table 24. Operation #22 requirements. ....	100
Table 25. Operation #23 requirements. ....	102
Table 26. Operation #24 requirements. ....	106
Table 27. Operation #25 requirements. ....	109
Table 28. Dimensions of the operations hall. ....	111
Table 29. Dimensions of the Office and Auxiliary Systems building rooms which are situated on the ground floor. ....	118
Table 30. Dimensions of the Office and Auxiliary Systems building rooms which are located on the first floor. ....	120
Table 31. List of equipment, structures and fixed mock-ups. ....	121
Table 32. Main location and allocated space of the auxiliary systems. ....	184
Table 33. Areas of TBM RH test facility to which the auxiliary systems provide services. ....	185
Table 34. HVAC power needs. ....	194



## **2.1. Introduction**

This chapter recovers the most important aspects of the ITER Project, and specifically the TBM Program. The studies carried out in order to elaborate a conceptual design of a test facility to demonstrate the remote handling of TBM and their ancillary systems are described below. Finally, the maintenance schemes proposed for both the ITER Test Blanket System and the DEMO breeding blanket are compared.

## **2.2. The ITER Project**

ITER is a large scale scientific experiment whose objective is to demonstrate the scientific-technologic feasibility of fusion energy. It is a transcendental step in the evolution from the first plasma physics studies to the future fusion power plants.

The Project was born in Geneva in 1985, when Gorbachov, General Secretary of the Soviet Union, proposed to USA president Reagan an international project aimed at developing fusion energy for peaceful purposes, following the discussions with President Mitterand of France and Prime Minister Thatcher of the United Kingdom [ITER 14].

The initial signatories: the former Soviet Union, the USA, the European Union (via EURATOM) and Japan, were joined by the People's Republic of China and the Republic of Korea in 2003, and by India in 2005.

Conceptual design work for the fusion project began in 1988, followed by increasingly detailed engineering design phases until the final design for ITER was approved by the Members in 2001. Further negotiations established the Joint Implementation Agreement to detail the construction, exploitation and decommissioning phases, as well as the financing, organization and staffing of the ITER Organization.

Each Member has set up a domestic agency, employing staff to manage procurements for its in-kind contributions. The ITER Members have agreed to share every aspect of the project: science, procurements, finance, staffing... with the aim that in the long run, each Member will have the know-how to produce its own fusion energy plant.

Selecting a location for ITER was a long process that was finally concluded in 2005. In Moscow, on June 28, high representatives of the ITER Members unanimously agreed on the site proposed by the European Union—the ITER installation would be built at Cadarache, near Aix-en-Provence in Southern France.

The ITER Agreement was officially signed in Paris in November 2006. This Agreement established a legal international entity to be responsible for construction, operation, and decommissioning of ITER. In October 2007, following ratification by all Members, the ITER Agreement entered into force and officially established the ITER Organization.

On the other hand, a "Broader Approach" agreement for complementary research and development was also signed in 2007 between EURATOM and the Japanese government. It established a framework for Japan to conduct R&D activities in support of ITER over a period of ten years. Within the Broader Approach the following three main projects were set into motion [F4E 14]:

The first on them is the detailed engineering design of the International Fusion Materials Irradiation Facility (IFMIF). IFMIF will allow testing and qualifying advanced materials in an environment similar to the future fusion power plants one.

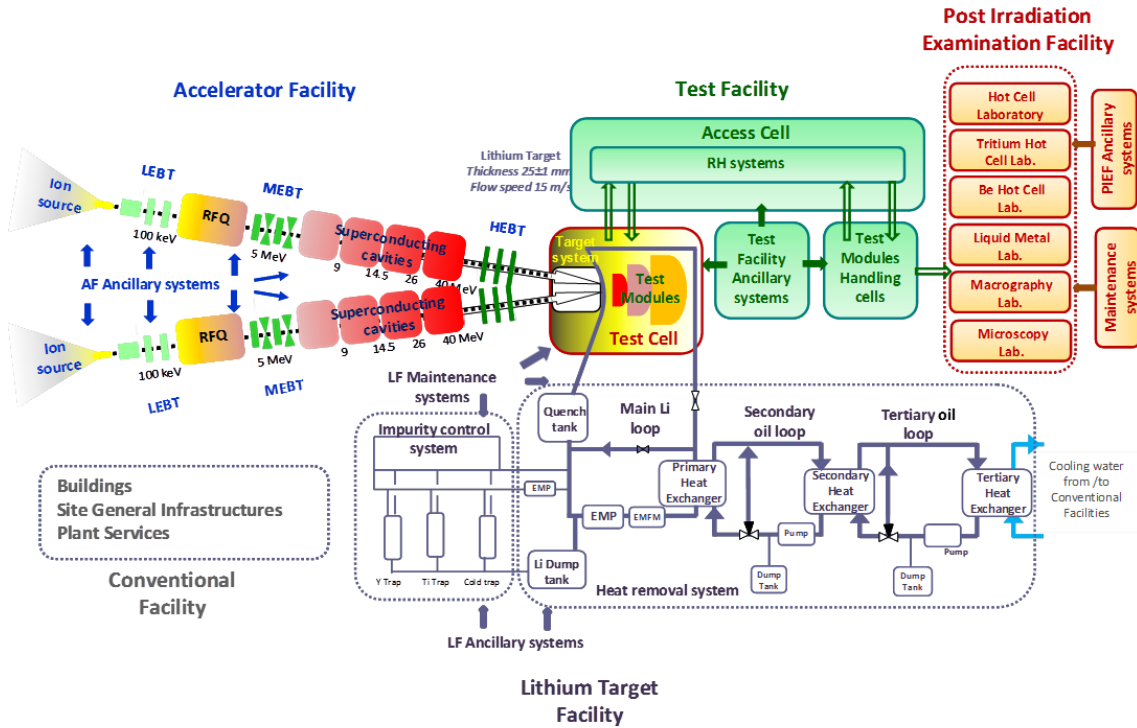


Fig. 1. Layout of the different IFMIF facilities.

The second project is the Satellite Tokamak Programme (STP), which consists in the construction and operation of an advanced superconducting tokamak (JT-60SA) which will act as ITER satellite device during its operation.

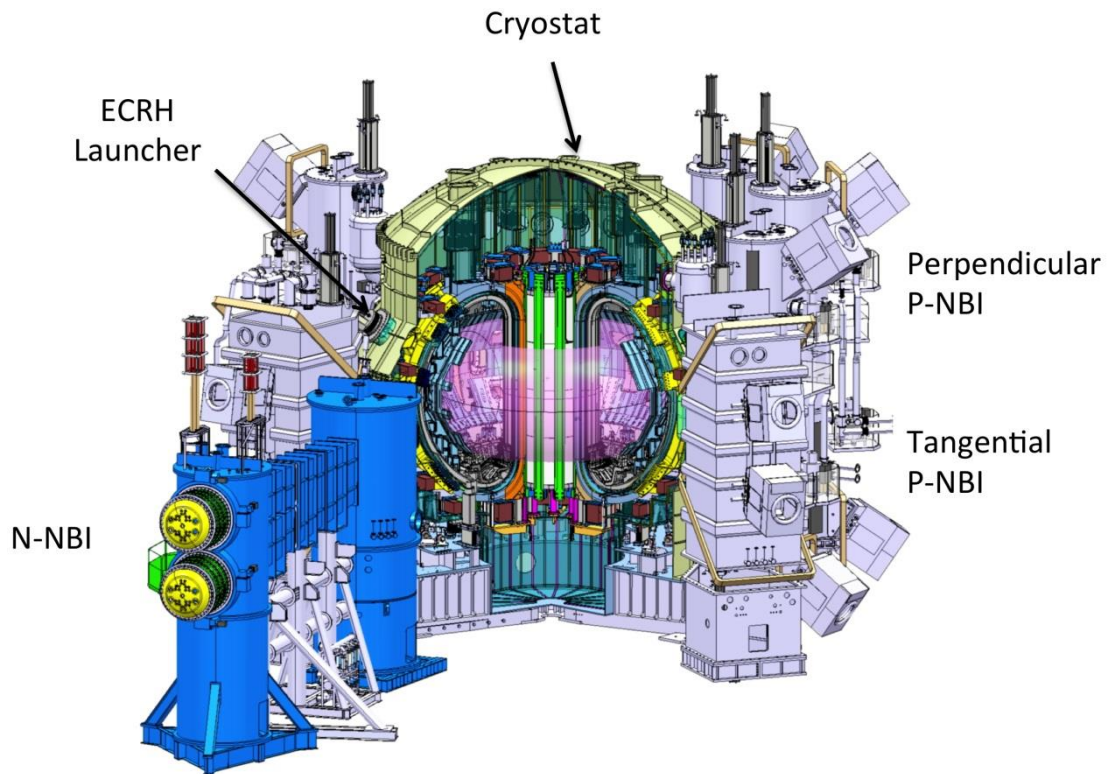


Fig. 2. Section view of the JT-60SA.

The third project is the International Fusion Energy Research Centre (IFERC), whose objectives include coordination of design and R&D activities for DEMO, large scale simulation of fusion plasmas through supercomputing and remote experimentation activities to allow a great number of scientists participating in ITER experiments.

### **2.2.1. Main features of ITER**

ITER means a fundamental contribution for establishing the technologic bases of a future demonstrator reactor. It represents a great challenge in the following fields:

- Development of large superconducting magnets able to reach high magnetic induction values.
- Development of high thermal flux components for the divertor (20 MW/m<sup>2</sup>).
- Development of remote handling systems.
- Development of deuterium-tritium fuel cycle.
- Development of plasma heating & current drive systems.
- Development of diagnostics compatible with the environment.

ITER will operate D-T plasmas to produce 500 MW of fusion power. The main construction and operational parameters are shown in Table 1.

Parameters	Value	Parameters	Value
Aspect ratio (A), R / r	6.2 m / 2.0 m	Average electron temperature (T <sub>e</sub> )	8.9 keV
Volume (V)	837 m <sup>3</sup>	Average toroidal beta (β <sub>t</sub> )	2.5
Toroidal surface area (St)	678 m <sup>2</sup>	Average poloidal beta (β <sub>p</sub> )	0.67
Plasma cross section area (Sp)	21.9 m <sup>2</sup>	Alpha power	82 MW
Toroidal field at 6.2 m radius (B <sub>t</sub> )	5.3 T	Neutral beam power	33 MW
Plasma current (I <sub>p</sub> )	15 MA	Radiofrequency power	7 MW
Elongation / 95% flux triangularity-separatrix	1.86 / 0.5 1.75 / 0.35	Radiated power	48 MW
Ellipticity (k <sub>95</sub> ) / safety factor (q <sub>95</sub> ) at 95% flux	1.6 / 3.0	Fusion power gain (Q)	10
Normalized Beta (β <sub>n</sub> )	1.77	Confinement time (τ <sub>E</sub> )	3.7 s
Average electron density (n <sub>e</sub> )	1.014x10 <sup>20</sup> m <sup>-3</sup>	Fusion power (/margin)	410 MW (/1.6)
Fraction of Greenwald limit (n/n <sub>gw</sub> )	0.85	Z effective (Z <sub>eff</sub> )	1.65
Average ion temperature (T <sub>i</sub> )	8.1 keV	Burn time	400 s

Table 1. ITER construction and operational parameters.

The ITER **magnet system** comprises 18 superconducting toroidal field and 6 poloidal field coils, a central solenoid, and a set of correction coils that magnetically confine, shape and control the plasma inside the vacuum vessel. Additional coils will be implemented to mitigate Edge Localized Modes (ELMs). The superconducting material for both the central solenoid and the toroidal field coils is designed to achieve operation at high magnetic field (13 Tesla), and is a special alloy made of niobium and tin (Nb<sub>3</sub>Sn). The poloidal field coils and the correction coils use a different, niobium-titanium (NbTi) alloy. In order to achieve superconductivity, all coils are cooled with supercritical helium in the range of 4 K.

The **vacuum vessel** (VV) houses the fusion reactions and acts as a first safety containment barrier. It is designed to provide ultra-high vacuum conditions for plasma operations, as well as to attenuate/absorb neutrons and photons energy to levels tolerated by the superconducting magnets.

The VV will be twice as large and sixteen times as heavy as any previous tokamak, with an internal diameter of 6 metres. It will measure a little over 19 m across by 11 m high, and weigh in excess of 5000 t.

It will have double stainless steel walls, with passages for cooling water to circulate between them, whereas 44 ports will provide access to the inside for remote handling operations, diagnostic systems, heating, and vacuum systems: 18 upper ports, 17 equatorial ports, and 9 lower ports.

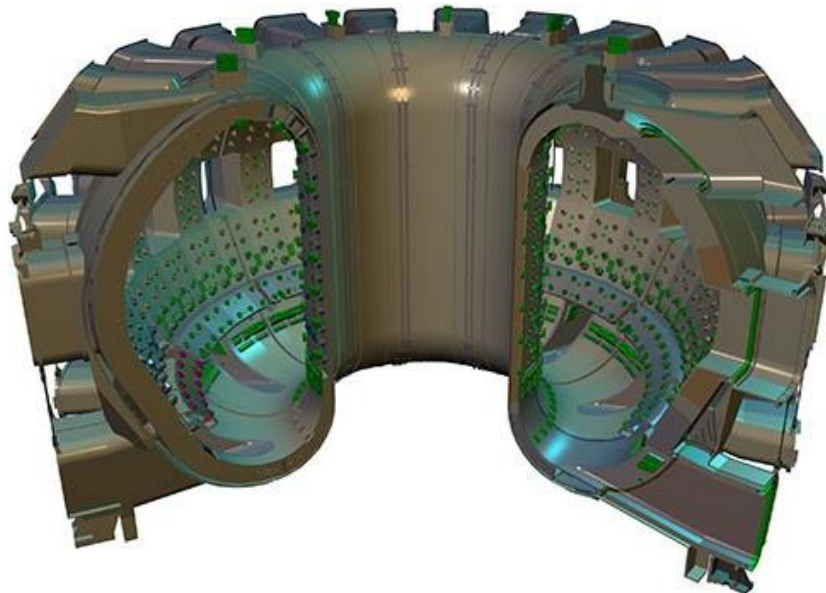


Fig. 3. ITER vacuum vessel.

The **blanket** covers the interior surfaces of the vacuum vessel, providing shielding to the vessel and the superconducting magnets from the heat and neutron fluxes of the fusion reaction. The neutrons are slowed down in the blanket where their kinetic energy is transformed into heat energy and collected by the coolants.

For purposes of maintenance on the interior of the vacuum vessel, the blanket wall is modular. It consists of 440 individual segments, each measuring 1x1.5 m and weighing up to 4.6 tons. Each segment has a detachable first wall which directly faces the plasma and removes the plasma heat load, and a semi-permanent blanket shield dedicated to the neutron shielding.

Beryllium has been chosen as the element to cover the first wall. The rest of the blanket shield will be made of high-strength copper and stainless steel.

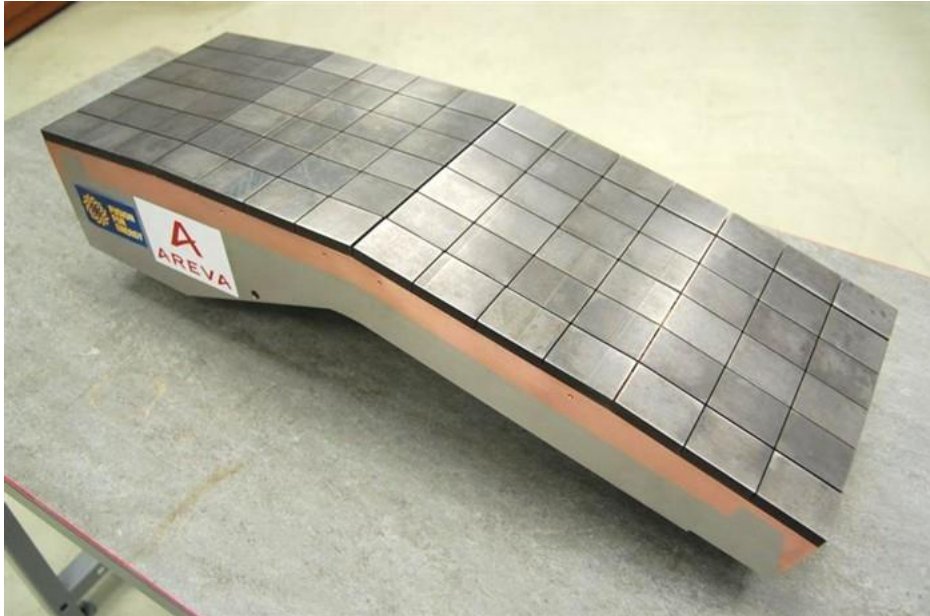


Fig. 4. ITER small-scale prototype (1/6) of the blanket first wall [F4E 14].

The vacuum vessel and the superconducting coils are surrounded by a large, stainless steel structure called **cryostat**, which provides a cool, vacuum environment. It is made of a single wall cylindrical construction, reinforced by horizontal and vertical ribs. The cryostat is 29.3 m height and 28.6 m width.

It has many openings to provide access to the vacuum vessel for cooling systems, magnet feeders, auxiliary heating, diagnostics, and the removal of blanket and divertor parts. Large bellows are used between the cryostat and the vacuum vessel to allow for thermal contraction and expansion in the structures. The cryostat is completely surrounded by a concrete layer known as the **bioshield**. Above the cryostat, the bioshield thickness is 2 m.

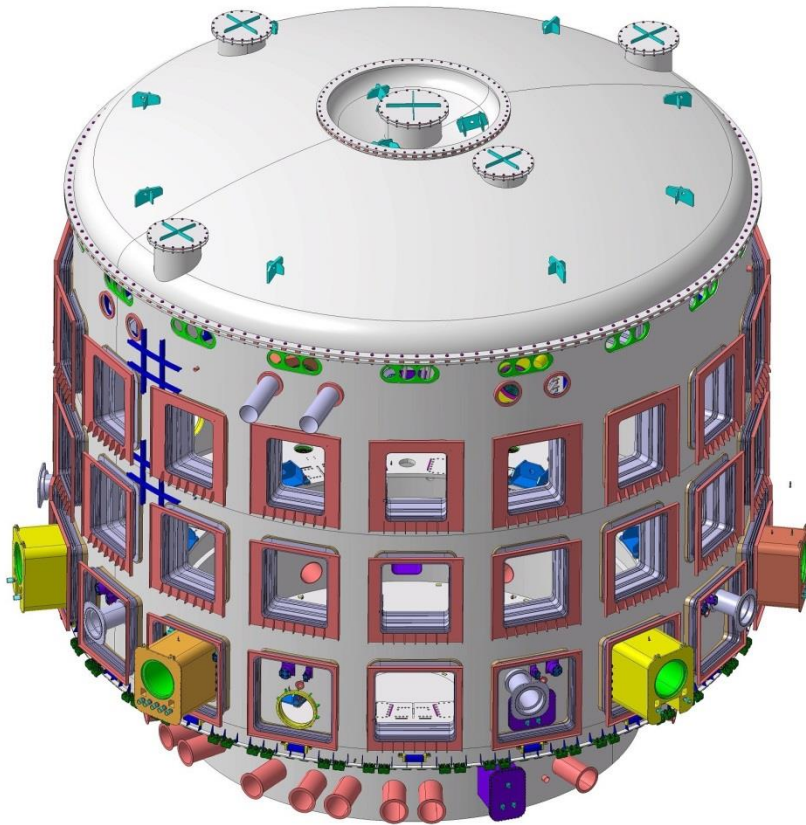


Fig. 5. ITER cryostat.

The **divertor** sets the confined plasma boundary, called the Last Closed Flux Surface (LCFS), using magnetic fields. It allows the D-shaping of the plasma, which makes H-mode plasmas easier to obtain.

The main purposes of the ITER divertor are:

- Reduce impurity content: plasma-surface interactions remote from confined plasma and particle flow prohibits impurities from entering the confined plasma.
- Removing alpha-particle power: transfer heat to the water cooling system.
- Remove helium ash: pump out helium to avoid dilution of fusion fuel.

Located at the bottom of the vacuum vessel, the ITER divertor is made up of 54 remotely-removable cassettes, each holding three plasma-facing components: dome, inner and outer vertical targets. ITER planned to begin operations with a divertor target made of carbon fibre-reinforced carbon composite (CFC) to be followed by a second divertor with tungsten targets which offer the advantage of a lower rate of erosion and longer lifetime. Currently, due to cost cutting considerations, the ITER management is investigating the feasibility of implementing tungsten right from the beginning of operations [ITER 14].

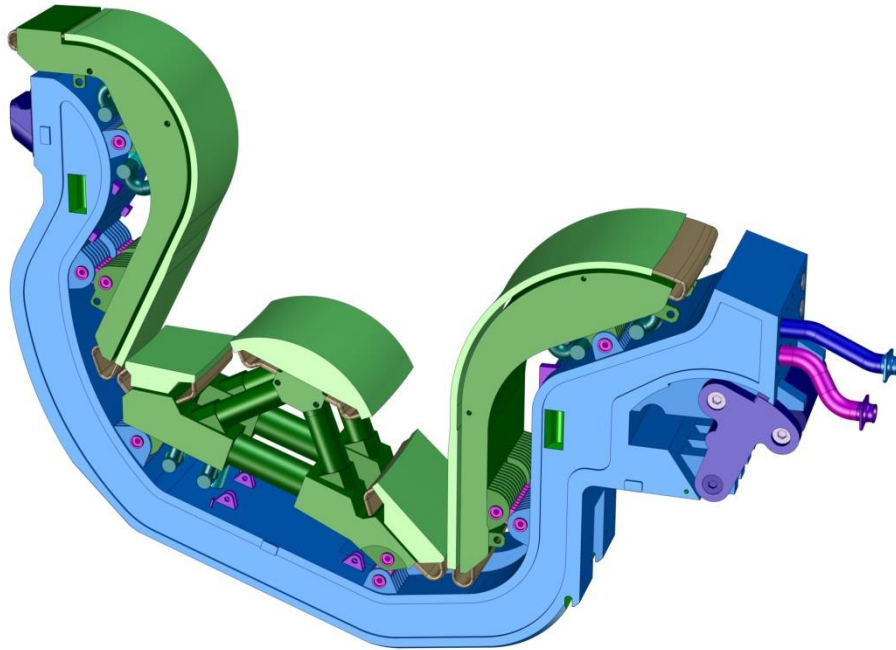


Fig. 6. ITER divertor cassette.

ITER will use three sources of **external heating** to provide the input heating power of 50 MW required to bring the plasma to the temperature necessary for fusion. These are neutral beam injection and two sources of high-frequency electromagnetic waves.

Neutral beam injectors are used to shoot uncharged high-energy particles into the plasma where, by way of collision, they transfer their energy to the plasma particles.

Before injection, deuterium atoms must be accelerated outside of the tokamak to 1 MeV. For this, electrons must be removed from neutral atoms to create a positively-charged ion. The process must then be reversed before injection into the fusion plasma; otherwise the electrically-charged ion would be deflected by the magnetic field of the plasma cage. In neutral beam injection systems, the ions pass through a cell containing gas where they recover their missing electron and can be injected as fast neutrals into the plasma. Two neutral beam injectors are currently foreseen for ITER. A third neutral beam will be used for diagnostic.

Ion and electron cyclotron heating methods use radio waves at different frequencies to bring additional heat to the plasma. In Ion Cyclotron Resonance Heating (ICRH), energy is transferred to the ions in the plasma by a high-intensity beam of electromagnetic radiation with a frequency of 40 to 55 MHz.

A generator produces high-power radio frequency waves that are carried along a transmission line to an antenna located in the vacuum vessel, sending the waves into the plasma.

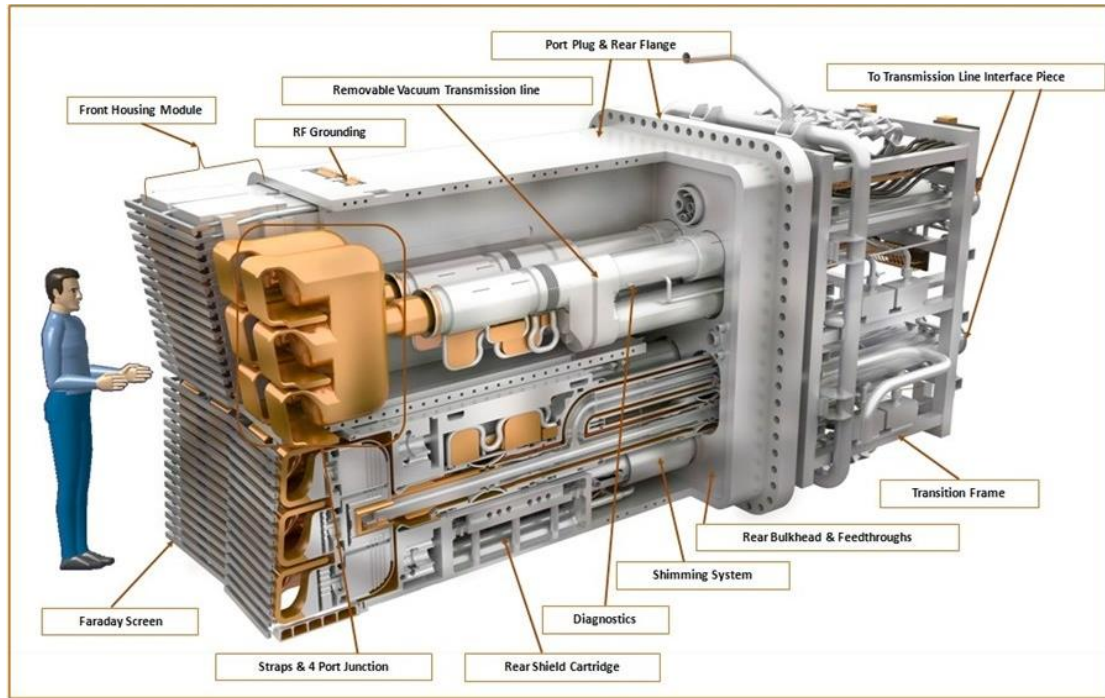


Fig. 7. ICRH antenna system.

Electron Cyclotron Resonance Heating (ECRH) heats the electrons in the plasma with a high-intensity beam of electromagnetic radiation at a frequency of 170 GHz. The electron cyclotron heating system is also used to deposit heat in very specific places in the plasma, as a mechanism to minimize the build-up of certain instabilities that lead to cooling of the plasma. In comparison to the ICRH system, the ECRH has the advantage that the beam can be transmitted through air which simplifies the design and allows the source to be far from the plasma, simplifying maintenance. Power will be provided by high-frequency gyrotrons. The ITER design includes the development of a 1 MW gyrotron operating at 170 GHz with pulse duration of more than 500 s.

An extensive **diagnostic system** will be installed on the tokamak to provide the measurements necessary to control, evaluate and optimize plasma performance in ITER and to further the understanding of plasma physics. These include measurements of temperature, density, impurity concentration, and particle and energy confinement times.

The system will comprise about 50 individual measuring systems drawn from the full range of modern plasma diagnostic techniques, including lasers, X-rays, neutron cameras, impurity monitors, particle spectrometers, radiation bolometers, pressure and gas analysis, and optical fibres.

Because of the harsh environment inside the vacuum vessel, these systems will have to cope with a range of phenomena not previously encountered in diagnostic implementation, while all the while performing with great accuracy and precision. The levels of neutral particle flux, neutron flux and fluence will be respectively about 5, 10 and 10000 times higher than the harshest experienced in today's machines.

ITER includes also a large number of **auxiliary systems**. For example, the **Control and Data Acquisition System (CODAC)** interfaces to more than 30 ITER plant systems containing actuators, sensors and local instrumentation and control (I&C). Machine protection (interlock) system and safety (personnel and environment) systems are explicitly decoupled from CODAC and act fully independently. Control System Division is also responsible for the central interlock system and central safety system.

The **vacuum system** is one of the most important auxiliary systems in ITER, taking into account that, with a volume of 1400 m<sup>3</sup> and 8500 m<sup>3</sup> respectively, the ITER vacuum vessel and cryostat range amongst the largest vacuum systems ever built.

Mechanical pumps and powerful cryogenic pumps evacuate the air out of the vessel and the cryostat until the pressure inside has dropped to one millionth of normal atmospheric pressure. Considering the previous volume, this operation will take 24 to 48 hours. The main pumping systems are 6 torus exhaust pumps, 4 cryopumps for the neutral beam injection systems used in plasma heating, and 2 cryopumps for the ITER cryostat and the contained superconducting magnets. They will be cooled with supercritical helium.

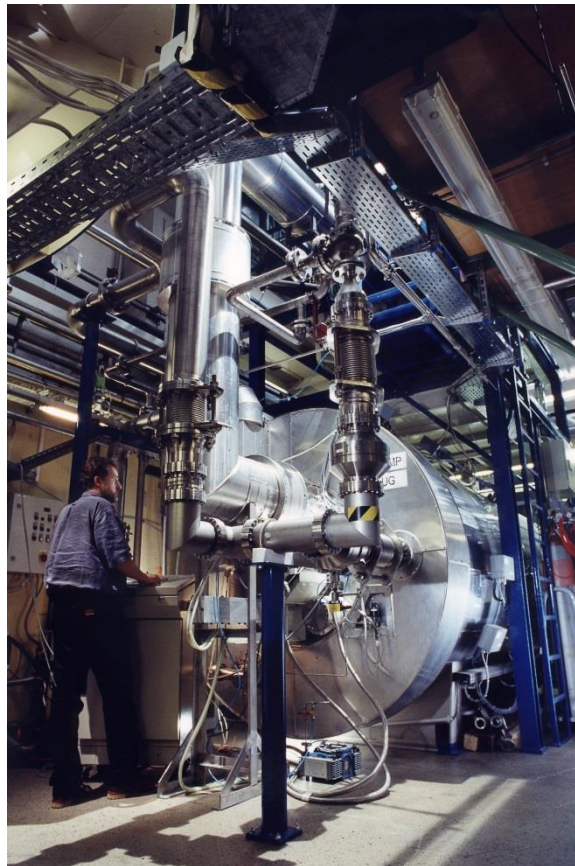


Fig. 8. Model of ITER cryopump tested at the TIMO test facility.

In fact, cryogenic technology will be extensively used at ITER to create and maintain low-temperature conditions for the magnet, vacuum pumping and some diagnostics systems. Apart from the mentioned cryopumps, the superconducting coils will be cooled with supercritical helium at 4 K in order to operate at the high magnetic fields necessary for the confinement and stabilization of the plasma. They will be surrounded by the cryostat and an actively-cooled thermal shield with a forced flow of helium at 80 K. A **cryoplant** on the ITER platform will produce the required cooling power, and distribute it through a complex system of cryolines and cold boxes that make up the cryodistribution system.

The cryoplant is composed of helium and nitrogen refrigerators combined with a 80 K helium loop. Storage and recovery of the helium inventory (25 tons) is provided in warm and cold (4 K and 80 K) gaseous helium tanks. Three helium refrigerators supply the required cooling power via an interconnection box providing the interface to the cryodistribution system. Two nitrogen refrigerators provide cooling power for the thermal shields and the 80 K pre-cooling of the helium refrigerators. The distribution of cooling power is accomplished through cryodistribution boxes with helium circulating pumps for the cooling of the magnets and cryopumps, and a complex system of cryogenic transfer lines—located both within the Tokamak Building, within the cryoplant buildings, and between the two.

**Electricity requirements** for the ITER plant and facilities will range from 110 MW to up to 620 MW for peak periods of 30 seconds during plasma operation. Power will be provided through the 400 kV circuit that already supplies the nearby CEA Cadarache site. ITER will have a steady state distribution system to supply the electricity needed to operate the entire plant, including offices and the operational facilities. The cooling water and cryogenic systems will together absorb about 80% of this supply.

A second pulsed power system will be used during plasma operation to provide the superconducting magnet coils and the heating and current drive systems with the large amount of power that they need. Electricity from the 400 kV circuit will be transformed to an intermediate level (69 kV) via 3 step-down transformers. Emergency backup power for the ITER plant and facilities will be covered by two diesel generators.

On the other hand, ITER will be equipped with a **cooling water system** to manage the heat generated during operation of the tokamak. Water will be used to remove heat from the vacuum vessel and its components, and to cool auxiliary systems such as radio frequency heating and current drive systems, the chilled water system (CHWS), the cryogenic system, and the coil power supply and distribution system. The cooling water system incorporates multiple closed heat transfer loops plus an open-loop heat rejection system (HRS). Heat generated in the plasma during the deuterium-tritium reaction will be transferred through the tokamak cooling water system (TCWS) to the intermediate component cooling water system (CCWS), and to the HRS, which will reject the heat to the environment.

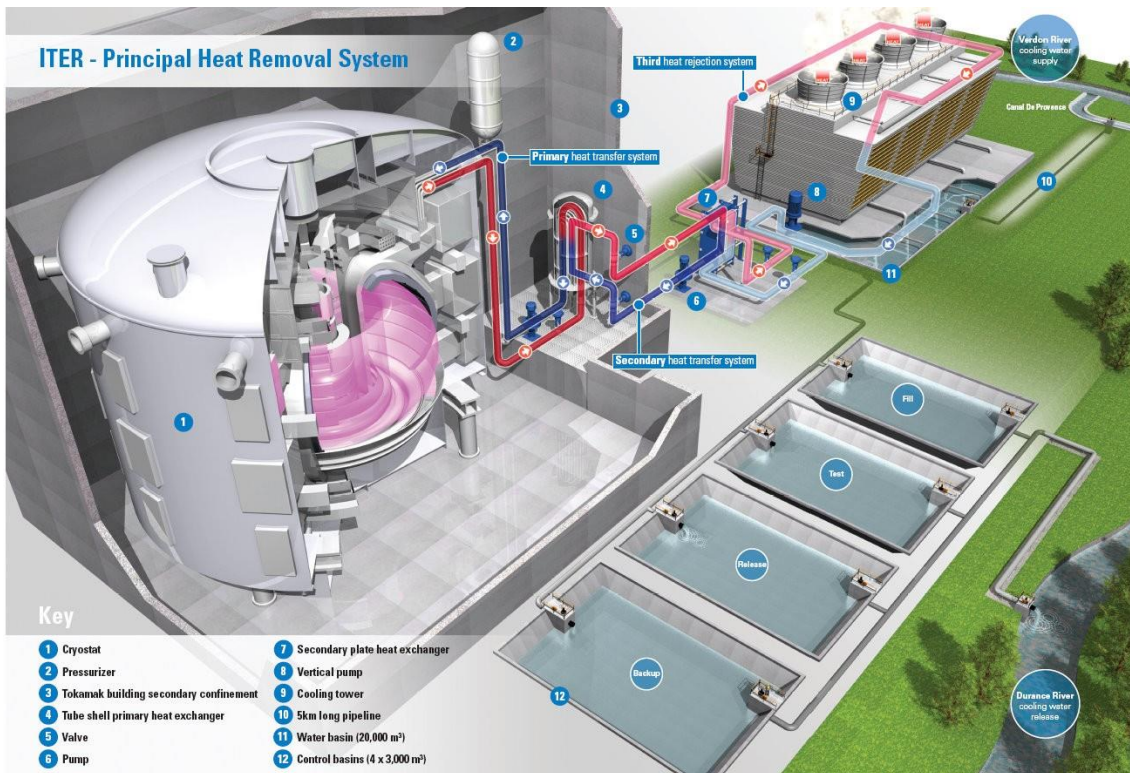


Fig. 9. ITER cooling water system layout.

The ITER Tokamak and plant auxiliary systems will produce an average of 500 MW of heat during a typical plasma pulse cycle, with a peak of more than 1100 MW during the plasma burn phase. It must be dissipated to the environment. This is accomplished by the evaporation of HRS water as it passes through the induced-draft cooling towers. The high rate of evaporation concentrates minerals in the HRS water; as a result, part of the water is continuously discharged from the system and replaced by water from the Canal de Provence. During plasma operations, the combined flow rate of all water in circulation in the cooling water system loops is approximately 33 m<sup>3</sup>/s, flowing through pipes with nominal diameters of up to 1.6 m.

The fuels used in ITER will be processed in a closed cycle. Commissioning will happen in three phases: hydrogen operation, followed by deuterium operation, and finally full deuterium-tritium operation. The first step of the ITER **fuel cycle** consists in the evacuation of air and impurities from the vacuum vessel. The superconducting coils are then turned on and the low-density gaseous fuel is introduced into the VV by a gas injection system. Once the fuel has been introduced into the vacuum chamber, an electrical current is applied to the system which causes the gas to be ionized and form a plasma.

A second fuelling system, a pellet injector, will also be used at ITER. An extruder punches out several millimetre-sized deuterium-tritium ice pellets that are propelled by a gas gun up to 3600 km/h. This is fast and cold enough to penetrate deep into the plasma core. The frozen pellets are injected through a guide tube located in the inner wall of the vacuum vessel and another guide tube for outer wall injection.

Pellet injection is the principal tool used to control plasma density and is also efficient in controlling Edge Localized Modes (ELMs). By shooting the frozen fuel pellets where they are needed, pellet injection has been shown to be effective in ELM management. Special technology is being developed to allow these pellets to fly along curved trajectories, thereby attaining specific zones within the plasmas where ELMs are particularly disruptive.

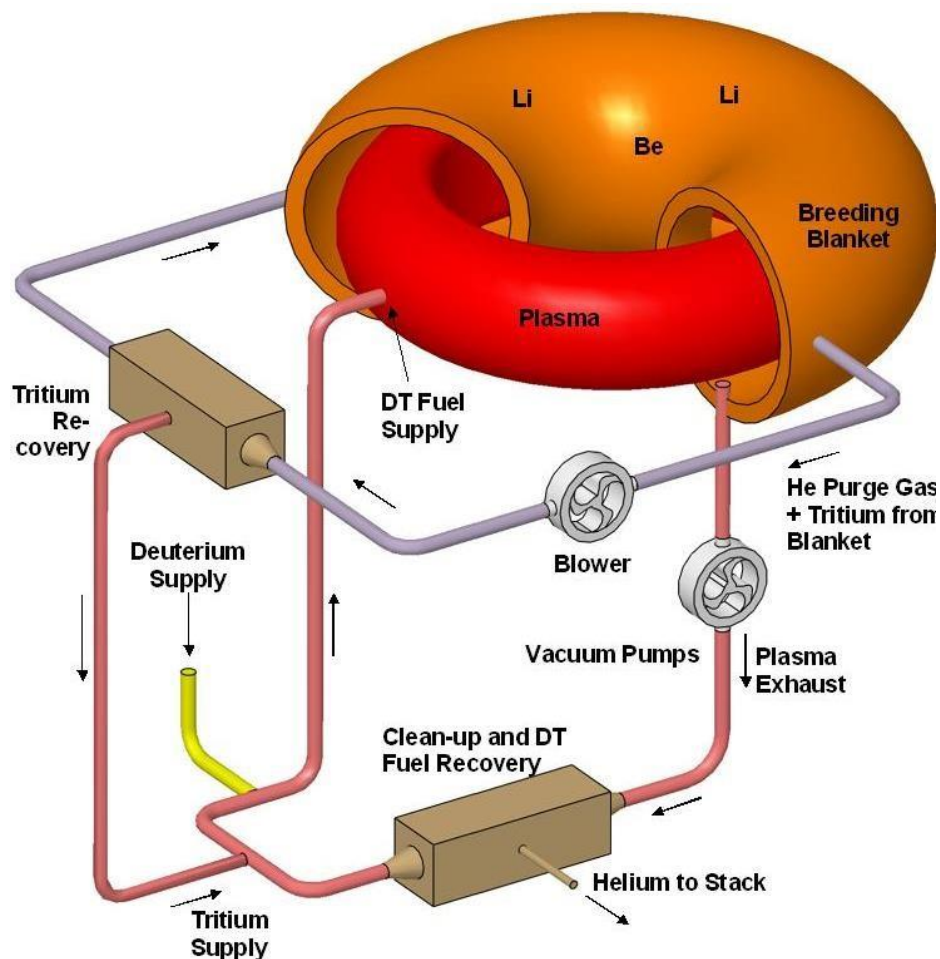


Fig. 10. ITER closed D-T fuel cycle.

Less than 1 g of fusion fuel is present in the VV at any one moment. The divertor located at the bottom of the vacuum vessel permits the recycling of any fuel that is not consumed: unburned fuel flows to the divertor, is pumped out and separated from helium produced during the fusion reaction, mixed with fresh tritium and deuterium, and re-injected into the vacuum chamber.

Next to the tokamak building, there will be a **Hot Cell Facility** to provide a secure environment for the processing, repair or refurbishment, testing, and disposal of components that have become activated by neutron exposure, as well as materials contaminated by beryllium and tungsten dust. In addition, the Hot Cell Facility will perform the removal of tritium from tritiated components and materials. This operation will be housed in a safe, confined, and shielded area containing analytical systems for tritium measurement, and a detritiation system for gaseous streams in order to minimize releases and waste.

All waste materials will be treated, packaged, and temporarily stored in the Hot Cell Facility before being handed over to the French authorities.

### **2.3. ITER Remote Maintenance System**

One of the most relevant auxiliary systems in ITER is the Remote Maintenance System, since a major objective of the Project is to demonstrate that a future fusion power plant can be maintained effectively and offer practical levels of plant availability.

During its operational lifetime, many systems of the ITER machine will require maintenance and modifications. The need for timely, safe and effective remote operations on a machine as complex as ITER and within such hostile environment represents a major challenge at every level of the ITER Project organization, engineering and technology.

In summary, the RH approach required for a fusion device like ITER is characterized by:

- a) Geometrically complex working environment.
- b) Large, heavy components with close tolerance fits.
- c) Limited access through narrow ports.
- d) Poor visibility.
- e) The RH equipment comprises combination of large transporters, specialized end-effectors (including teleoperated manipulators) and tooling.
- f) Relatively long distance between the reactor and the hot cell.
- g) Hot cell dimensions and functions.

Additionally, the environmental conditions in which the RH equipment is required to operate are:

- a) Ultra-high vacuum clean conditions.
- b) High gamma radiation.
- c) Contamination by beryllium dust, tritiated carbon dust, gaseous tritium and activated tungsten dust, among others.
- d) Some level of magnetic field.

The ITER Remote Maintenance System (IRMS) relies on the use of RH equipment and tools which will be deployed inside the vacuum vessel, in the Hot Cell and, depending on the actual radiation levels at the time, inside the cryostat. It is designed taking into account several principles which positively affect its functionality, reliability and availability:

- a) Simple and robust design of the machine components to be maintained.
- b) Simple, staged and rehearsed RH procedures for the replacement of each machine component, requiring a high level of RH equipment testing in RH relevant conditions, under normal and off-normal conditions (requires full size mock-up test facilities).
- c) Robust, reliable and proven RH equipment and tools.

The current extent of the IRMS is based on an ITER machine upgrade plan established around 2007, to be implemented during the lifetime of the machine, to accommodate the scientific and technological development of the ITER experimental program [Tes 08]. Thus, the current IRMS is the result of the progressive definition of remote handling needs and consists of the following systems [Dam 14]:

- Divertor Remote Handling.

- Blanket Remote Handling.
- Cask and Plug Remote Handling.
- In-Vessel Viewing System.
- Neutral Beam Cell Remote Handling.
- Hot Cell Equipment (including RH “hot” and “cold” test facilities).
- Multi-purpose deployment system.
- Remote Handling Supervisory system.

Most of these RH systems are briefly described in the following subsections.

### **2.3.1. Blanket Remote Handling System**

The blanket RH equipment design has been developed by the Japan Domestic Agency (JADA).

The replacement of some blanket shielding modules (BSM) is likely to be required at least once during the lifetime of ITER due to local erosion or damage. The installation and removal of the BSM will be performed by the In-Vessel Transporter (IVT) running on a passive rail self-deployed around the equatorial region. The IVT implies the use of up to four pairs of casks (main and intermediate) operating in VV port cells 3, 8, 12 and 17 for the support of the IVT rail, the deployment of the IVT vehicle/manipulator system & services plus the hosting of the BSM exchange system. The IVT also provides complementary functionalities like bolting/unbolting, cooling pipes cutting, welding & inspection and sensing/viewing. Up to 4 BSM can be transferred in the CPRHS (Cask & Plug Remote Handling System) from VV to the hot cell building (HC) for refurbishment (e.g. change of the damaged First Wall (FW) panels) and/or disposal as radwaste.

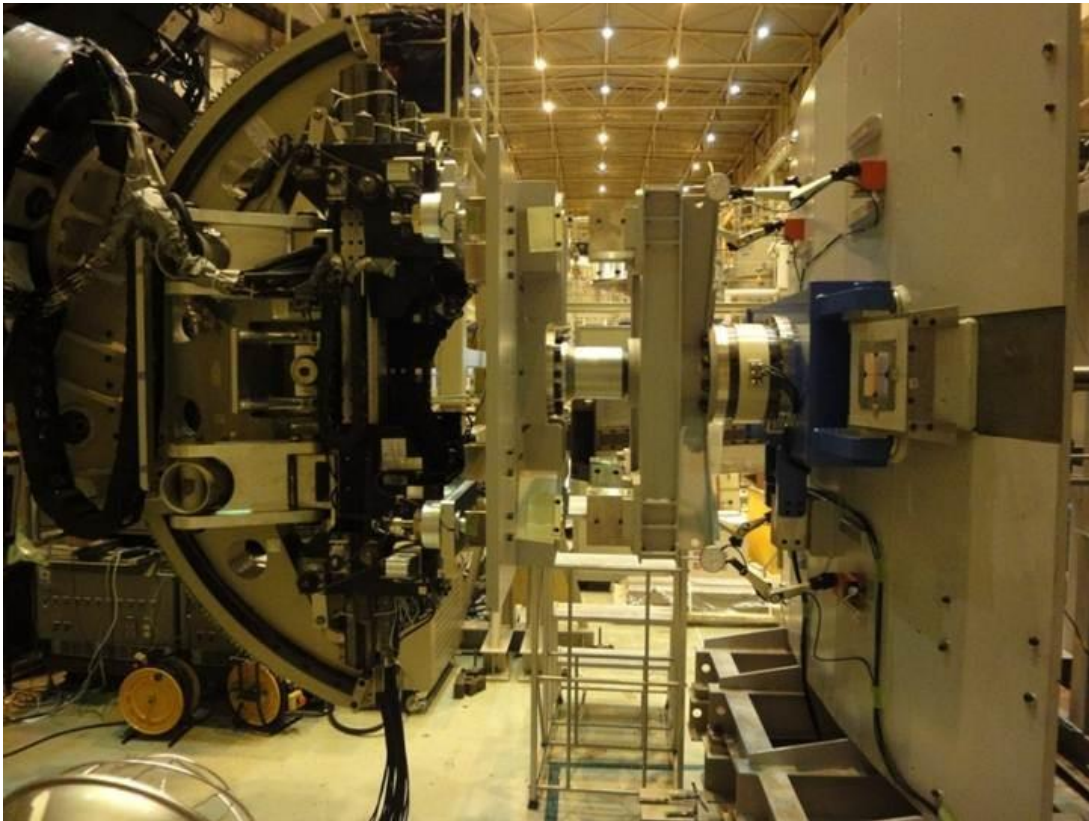


Fig. 11. Test platform at Naka site for the remote positioning of the first wall panels.

Each BSM (indicative weight around 4 t) requires remote manipulation with 5 mm accuracy between the module and the support keys in the VV. During IVT operation, connection and

disconnection of the rail joint, for rail deployment/stowage in the CPRHS, is a crucial operation. The remote installation of BSMs is carried out using sensor-based control, with a combination of distance sensors for rough positioning plus force and contact sensors for fine positioning. A camera, using a monocular vision method, provides visual information which is processed to determine the relative positioning between location keys and BSM.

During the ITER nuclear phase the decay gamma dose rates during in-vessel maintenance will be in the order of several hundreds of Gy/h, therefore, all RH systems must be tolerant to such high levels of radioactivity and to a total dose in excess of 1 MGy.

### **2.3.2. Divertor Remote Handling System**

It is expected the cumulative erosion of the plasma-facing components will require the exchange of the whole divertor three times during the first 20 years of ITER operation. The divertor remote handling system shall, therefore, provide the means for remote installation and removal of the ITER divertor and the divertor-related components.

The replacement, one by one, of the 54 divertor cassettes is performed via 3 RH ports and is based on the coordinated intervention of the so-called cassette toroidal mover (CTM), able to travel toroidally into the vessel while transporting a cassette, and the cassette multifunctional mover (CMM), able to travel radially into the RH conduits and transport either a cassette or the CTM itself (allowing to this one to start its toroidal trajectory). The movers are served by a transfer cask that hosts them, and ensures nuclear confinement during the transportation of components (a cassette cantilevered by the CMM) from the vacuum vessel to the Hot Cell. The reverse sequence is applied for cassette installation [Dam 14].



Fig. 12. Divertor Test Platform (DTP 2) at Tampere University of Technology.

Each mover is equipped with force-feedback manipulator arm, special tooling, cameras, sensors, cabling, etc. in order to carry out -in addition to cassette lifting and transportation- other complementary maintenance tasks (cassette locking/unlocking from VV, pipe cut/weld/inspection, cassette and VV dust cleaning) and is remotely controlled by operators

from a work-cell located in the RH control room by means of the high level control system (HLCS) that includes computer-based human machine interface (HMI), haptic devices, viewing monitors and virtual reality. On the other hand, isolators (i.e. glove boxes) are installed in the port cell to support the divertor pipe cutting/welding operations.

### **2.3.3. Cask and Plug Remote Handling System**

The access to the vessel and the transportation of RH devices and of components like blanket, divertor, heating and diagnostic plugs is performed by remotely controlled casks (CPRHS) able to dock to the vessel ports, move along the corridors of the tokamak and hot cell buildings, dock to the hot cell stations, whilst preserving nuclear confinement of the transported items.

A fleet of different typologies of casks is therefore the transport and confinement system that makes the reactor maintenance possible. In total, different types of casks for the following equipment are required:

- 1) Cryopump.
- 2) Divertor cassettes.
- 3) In-vessel viewing system and glow discharge cleaning system.
- 4) Blanket modules.
- 5) Equatorial heating and diagnostics plugs.
- 6) Upper heating and diagnostics plugs.

The dimensions of the largest CPRHS are 8500 x 2620 x 3680 mm (length x width x height) and the maximum weight is about 100 t (including its 50 t payload) [Dam 12].

The CPRHS requires, like the others RH packages, a powerful and reliable control system and its human-machine interface to provide operators with visual feedback and spatial awareness during remote operations. The vehicles will move semi-autonomously (powered by on-board batteries) and will be remotely controlled following prescribed trajectories defined according to the different RH maintenance operations.

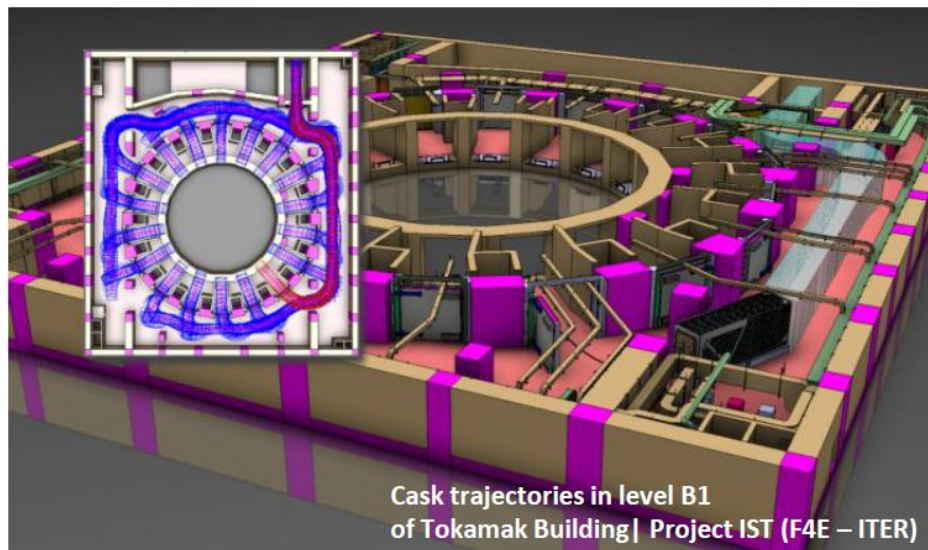


Fig. 13. Analysis of cask trajectories in the tokamak building port cells and corridors.

### **2.3.4. In-Vessel Viewing System**

The IVVS is an inspection tool, remotely operated, able to gather viewing and metrology data from inside the vessel, in order to monitor the status of first wall and plasma facing surfaces.

This allows detecting if a significant amount of damage and erosion (at the level of tenths of millimetre) has occurred on a component (e.g. a divertor cassette), in order to take a decision on its possible replacement.

Parked during plasma pulses in a VV port extension (some meters away from the plasma), the IVVS can be deployed, like an endoscope, into the main chamber a few hours after the last pulse, still under ultra-high vacuum, high magnetic field, high temperature (up to 150°C) and high gamma dose rate (~1 kGy/h).

Basically, the IVVS plug consists of: 1) the IVVS probe, i.e. the scanning head that performs the inspection; 2) the deployment system that takes the probe into the desired scanning positions; 3) B<sub>4</sub>C neutron shielding; 4) the structure that hosts the rest of IVVS components and interfaces the port extension during operation and the transfer cask during transportation. In order to ensure coverage of the whole vessel, 6 IVVS plugs, located in different toroidal positions at the tokamak lower level, are operated in parallel. The present design is based on an amplitude-modulated laser system whose proof-of-principle prototype has been extensively tested at the ENEA Frascati laboratories [Dam 14]. Being mostly utilized during ITER operation (e.g. in between plasma pulses), the IVVS remote control system is located in the ITER main control room.

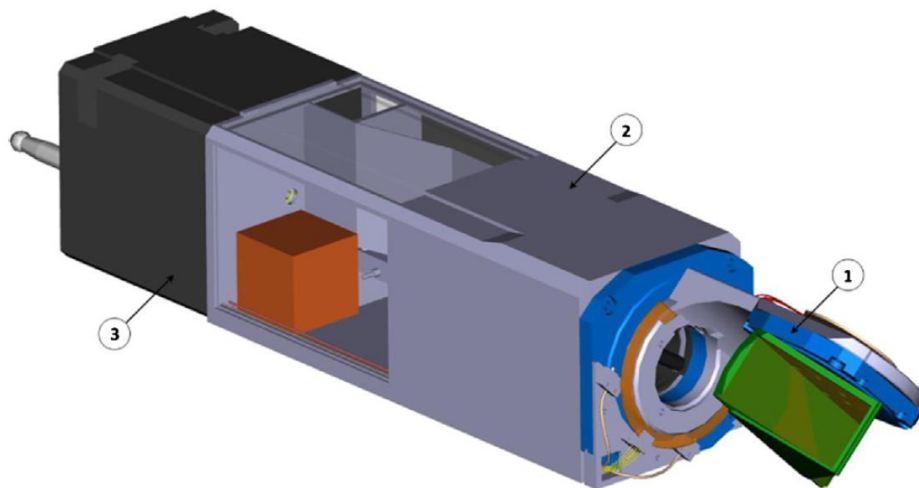


Fig. 14. Scanning probe (1: rotating head; 2: optical box; 3: connection box) [Dub 14].

### 2.3.5. Neutral Beam Cell Remote Handling

The Neutral Beam (NB) Cell located at the equatorial level hosts two heating and one diagnostic NB Injector, part of the vacuum vessel pressure suppression system, and diagnostics (e.g. the neutron flux monitor) located in an intermediate level. A complex suite of NB RH devices serves the maintenance of the cell:

- 50-ton monorail crane, and related rail system, able to lift and transport components, for example those belonging to an injector, to a transfer area near the exit of the cell (from where a cask system is able to collect it for transportation to hot cell or radwaste building).
- Force feedback manipulator arm and related tooling, able to perform tasks like component bolting/unbolting, pipe or lip-seal cut/weld/inspection, feed-trough connection/disconnection, etc. This arm can be installed in different positions and configurations.
- Beam source equipment able to remove the 30-ton NB source-accelerator from inside the injector (with the support of the mentioned arm).
- Swing rails, mast, a transfer platform, cradles, storage and lifting frames, auxiliary crane, complementing the functionalities of the devices previously described. As for the

divertor remote handling, sensors, actuators, cameras, cabling and cubicles allow remote control by the HLCS resident in a specific work cell in the control room.

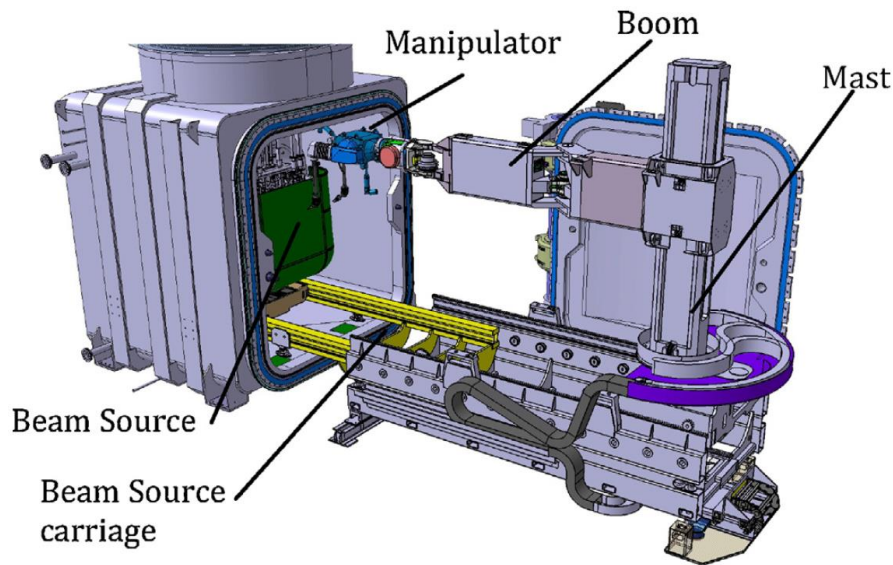


Fig. 15. Beam source equipment maintaining the beam source [Shu 14].

### **2.3.6. Hot Cell Remote Handling System**

The Hot Cell (HC) facility will provide a secure environment and handling facilities for performing two main functions:

- Repair, refurbishment and testing of components that must be returned to service.
- Radwaste processing and storage.

Such operations will be carried out with the radioactive and/or contaminated Tokamak components from the vessel and from the Neutral Beam injection system: divertor cassettes, blanket modules, heating and diagnostic plugs and tubes, cryopumps, NB components, etc. In order to carry out these operations, the HC is organized in various subsystems, each of them installed in a dedicated area with specific equipment and tools for the execution of RH tasks on the machine components and on the HC systems (e.g. lights, connectors, cables). Most of the processes will be performed by RH equipment with the support of a viewing system (cameras) for surveillance and close up monitoring.



Fig. 16. CEA proposal for HC tooling (ICRH antenna port plug refurbishment) [Fer 13].

Specialized equipment will be used to clean the machine components prior to the start of the repair/refurbishment/testing operations in order to reduce the radioactive dust inventory inside the HC and keep the HC RH tooling contamination as low as possible. The same equipment will be used for the decontamination of the IRMS to allow subsequent hands-on maintenance and inspection prior to its return to service. General purpose RH workstations will be provided to support the repair, refurbishment and radwaste processing operations. These will consist of adjustable support structures to place the machine component in the most favourable orientation relative to the RH tooling. The latter will be deployed by gantry cranes fitted with telescopic masts and manipulator(s).

## **2.4. ITER Test Blanket System**

A tritium breeding blanket (BB) ensuring tritium breeding self-sufficiency is a compulsory component for a demonstration reactor, although is not present in ITER. Mock-ups of DEMO BB, called Test Blanket Modules (TBMs), will be inserted and tested in ITER in three dedicated equatorial ports directly facing the plasma. They are the principal means by which ITER will provide the first experimental data on the performance of the BBs that is still an open issue on the path to commercial fusion power. These activities correspond to the so-called "TBM Program". A successful ITER TBM Program represents an essential step on the path to DEMO for any fusion power development plan [Gia 06].

A testing strategy has been developed for the first ten years of ITER operation. In fact, six mock-ups of six whole DEMO-BB systems will be tested in ITER, which means that the TBMs are connected with several ancillary systems, such as cooling systems, tritium extraction systems, coolant purification systems, and instrumentation and control (I&C) systems. TBMs and associated systems are called Test Blanket Systems (TBSs).

The TBSs functional characteristics are dictated by the operational conditions and requirements expected in a DEMO-BB system and, in this sense, they differ from the other ITER components that are designed in compliance with only ITER requirements. However, they must be fully integrated in ITER; therefore they must be compatible with the systems and operational procedures of ITER and the ITER operating plan. Moreover, TBS testing must not endanger ITER performances, safety and availability [Gia 12].

The TBM is expected to give answers to two main questions regarding the exploitation of fusion energy: 1) is possible to regenerate and extract tritium at the same rate as it is consumed in the reactor, taking also into account the losses by radioactive decay? and 2) is possible to extract thermal power from the reactor simultaneously with tritium breeding in temperature ranges suitable for efficient thermoelectric conversion? A fundamental difficulty is that direct testing of DEMO-BB in ITER is not possible since ITER operating conditions are different from the expected DEMO ones. However, most required data can be obtained by the testing of TBSs in ITER, provided the TBMs use the same structural and breeding materials as in the DEMO-BB and the TBMs are designed using proper engineering scaling [Gia 12]. For instance, reference neutron, thermal mechanics and thermal hydraulic codes (and their possible coupling) and tritium control modelling can be validated during these tests.

Therefore, the overall objective of the TBM Program is to acquire all relevant data and information concerning a given breeding blanket in order to validate the applied codes for the relevant analyses and to be able to design, to manufacture and to operate a BB system in DEMO and subsequent fusion power reactors, provided that data on long-term irradiation effects and failure modes are obtained in parallel in other facilities. Since several BB designs are tested simultaneously in ITER, the TBM Program could also determine the figure of merit of the various designs prior the DEMO-BB design and manufacturing. In particular, the major testing objectives are: (1) validation of the theoretical predictions of the breeding blankets structural integrity under combined and relevant thermal, mechanical and electromagnetic loads; (2) validation of tritium breeding predictions; (3) validation of tritium recovery process efficiency and tritium inventories in the different blanket materials; (4) validation of thermal predictions for strongly heterogeneous breeding blanket concepts with volumetric heat sources

and magnetic fields; and (5) demonstration of the integral performance of the BB systems [Gia 12].

### **2.4.1. TBM testing strategy and planning**

The TBMs will be installed in 3 dedicated equatorial ports of ITER (ports number 2, 18, and 16) directly facing the plasma. The TBMs First Wall is therefore acting as a plasma-facing component, although it will be recessed of 120 mm compared to the ITER shield modules FW, in order to avoid major heat loads transients which are expected in ITER but should not be present in DEMO. TBMs are inserted in a 20 cm-thick water-cooled stainless steel frames that act as the unique interface with shield modules and vacuum vessel from thermal, mechanical and neutronic point of view. Each TBM is attached to a shield block to form a TBM set. Each port can accommodate 2 TBM sets (typical dimensions of each TBM are 1.66 m (poloidal) x 48 cm (toroidal) x 50/70 cm (radial)), therefore 6 TBMs and associated independent systems can be simultaneously tested in ITER. The TBM frames also provide a separation wall between the 2 neighbouring TBM-Sets. The mechanical system formed by a TBM frame and 2 TBM sets is called the "TBM Port Plug (PP)".

The TBS testing strategy for each BB design is to test different design versions of the corresponding TBM concept, each of them adapted to the operational plan of ITER that foresees different plasma phases with very different operating conditions, from the initial H/He-pulses (without neutrons) to a high-duty D-T phase after several years of operations (long pulses up to about 3000 s and back-to-back pulses for several days), passing through the D-phase and the low-duty D-T phase.

Depending on the considered version and operating conditions, it will be possible to perform specific experiments in the different fields such as neutronics, thermo-mechanics, magnetohydrodynamics (MHD) and electromagnetic (EM), tritium control and management.

Typically, at present, up to four TBMs versions are expected for each TBS, to be used throughout the various plasma phases, corresponding to four experimental campaigns. Each campaign is connected with the ITER experimental program and its duration corresponds to the operation time between each ITER long-term maintenance shutdown (resulting in ~16 months of operations). The possibility to extend the scope of tests associated with a given version of TBM or to combine 2 TBM versions into a single one is not precluded at this stage of the planning.

It is assumed that all four TBM versions will share the same basic architecture, in particular their structural part, whose design will be qualified during the testing program in laboratory facilities before TBM commissioning and checked/monitored step-by-step during the different phases of ITER operation. This strategy ensures a relatively stable interface between the TBM and ITER during the whole operation time, facilitating the licensing aspects.

An important difference in the design of each version will concern the integration of the specific instrumentation and the design of internals; in particular of the breeding zone that could be modified for testing optimized design variants or to achieve the required testing conditions. For instance, the thickness of the breeder material could be increased to achieve DEMO-relevant temperatures, and the  $^6\text{Li}$  enrichment could be modified to obtain the desired test conditions. Therefore, different versions of the TBMs will operate at different operating conditions; however, the DEMO-relevant values will have to be reached in some time-periods of the experimental campaigns.

The TBSs are expected to be installed in ITER during the second assembly. If one (or more) TBM set is not ready for installation, it will be replaced by a dummy TBM [Mer 10].

## 2.4.2. Breeding blanket concepts to be tested in ITER

The six breeding blanket concepts which are currently considered to be tested in ITER as part of the TBM Program are the following [Sch 14]:

- Port #16: Helium Cooled Lithium Lead (HCLL) and Helium Cooled Pebble Bed (HCPB).
- Port #18: Water Cooled Ceramic Breeder (WCCB) and Helium Cooled Ceramic Reflector (HCCR).
- Port #2: Helium Cooled Ceramic Breeder (HCCB) and Lithium Lead Ceramic Breeder (LLCB).

The European Union is responsible of the HCLL and the HCPB. Japan and Korea are respectively responsible of WCCB and HCCR, whereas China and India (with support of the Russian Federation) are respectively responsible of HCCB and LLCB.

### 2.4.2.1. HCLL TBS

The DEMO HCLL-BB system uses the liquid metal Pb–15.7Li as tritium breeder and neutron multiplier and EUROFER steel as structural material. The Li is enriched at 90% in  ${}^6\text{Li}$ . The Pb–15.7Li slowly flows from the TBM to the port cell in order to extract the produced tritium in the port cell and send it to the tritium plant. It is cooled by helium at a pressure of 8 MPa and inlet/outlet temperatures of 300°C/500°C.

The corresponding HCLL-TBM features a EUROFER steel box cooled by vertical multi-passes rectangular cross section channels and closed by side cooled covers and in the rear, by 5 steel plates delimiting distributing/collecting chambers for the He coolant. Poloidal-radial and toroidal-radial He-cooled plates stiffen the TBM box in order to withstand the accidental internal pressurization at the coolant pressure. The corresponding stiffening grid forms several radial cells in which the Pb–15.7Li circulates at few mm/s for external tritium extraction purposes. In each cell are inserted various radial-toroidal cooling plates welded to a common back plate. A single He circuit is envisaged, so that helium cools first the FW and then the breeder zone.

The HCLL-TBS includes several ancillary systems, namely the helium cooling system, the Pb–15.7Li system, the tritium removal system (from Pb–15.7Li), the coolant purification system and the I&C system. Part of the components of these systems are located in the port cell #16, the remaining components are located in level 3 of the Tokamak building and in level 2 of the Tritium building.

### 2.4.2.2. HCPB TBS

The DEMO HCPB-BB uses either  $\text{Li}_4\text{SiO}_4$  or  $\text{Li}_2\text{TiO}_3$  pebble beds as tritium breeder, beryllium pebble beds as neutron multiplier and EUROFER steel as structural material. Li is enriched 30% in  ${}^6\text{Li}$  in case of  $\text{Li}_4\text{SiO}_4$  breeder and 60% in case of  $\text{Li}_2\text{TiO}_3$  breeder. Maximum temperatures are 920°C in ceramic, 650°C in Be and 550°C in steel. It is cooled by helium at a pressure of 8 MPa and with inlet/outlet temperatures of 300°C/500°C.

The HCPB-TBM consists in a He-cooled box reinforced by a He-cooled steel grid and able to withstand the full pressure of the He-coolant in accidental conditions and it features vertical cooling of the first wall with high pressure manifolds integrated in the back plate structure. Breeder units are inserted in the grid and several cooling plates ensure the heat extraction from the breeder/multiplier. Ceramic and Be pebbles are purged by a low pressure He-stream for T-extraction that flows at first in the Be beds and then through the ceramic beds from the front region to the back manifolds.

The HCPB-TBS includes several ancillary systems, namely the helium cooling system, the tritium extraction system (i.e., the purge gas system), the coolant purification system and the I&C system. Part of the components of these systems are located in the port cell #16, the remaining components are located in level 3 of the Tokamak building and in level 2 of the Tritium building.

### 2.4.2.3. WCCB TBS

The DEMO WCCB-BB uses  $\text{Li}_2\text{TiO}_3$  pebble beds as tritium breeder, beryllium pebble beds as neutron multiplier and F82H steel as structural material. Li is enriched 30% in  $^6\text{Li}$ . Maximum temperatures are 900°C in the ceramic, 600°C in the Be and 550°C in the steel. It is cooled by water at pressurized water reactor conditions ( $T_{\text{inlet/outlet}}$  are 280°C/325°C).

The WCCB-TBM is formed by 2 sub-modules having the same box structure and the same internal structure. The FW has built-in rectangular cooling channels. As for internal structure, it has multi-layer pebble beds structure similar to that of the DEMO-BB. Ceramic and beryllium pebble-beds are packed separately and divided into four layers by cooling panels. The cooling panel consists of F82H tubes and thin plates connecting adjacent tubes. The inner box structure is welded to the first wall and to the back plate. The thickness of each layer and pitches between tubes in each cooling panel have been optimized in order to feature similar levels of temperatures and possibly similar stresses to those present in a DEMO-BB. In order to reduce T-permeation from the breeder zone towards the water-coolant, the use of T-permeation barriers is envisaged.

The WCCB-TBS includes several ancillary systems, namely the water cooling system, the tritium extraction system (i.e., the purge gas system), and the I&C system. Part of the components of these systems are located in the port cell #18; the remaining components are located in level 4 and in level 2 of the tritium building.

### 2.4.2.4. HCCR TBS

The DEMO HCCR-BB uses  $\text{Li}_4\text{SiO}_4$  pebble beds as tritium breeder ( $\text{Li}_2\text{TiO}_3$  is optional), beryllium pebble bed as neutron multiplier, graphite as reflector and RAFM steel as structural material. Li is enriched 40% in  $^6\text{Li}$ . Maximum temperatures are 920°C in the breeder, 650°C in the Be and 550°C in the steel [Ahn 13].

The HCCR TBM consists of first wall (FW), breeding zone (BZ), side wall (SW) in each sub-module and common back manifolds (BM). The FW is U-shaped RAFM steel with rectangular helium cooling channels inside. The SW is used for enclosing the TBM with the FW and providing rigidity to the structure. Another main role of the SW is acting as manifold from the FW to the BZ and from the BZ to the BM. The BZ comprises seven layers: three breeder layers, three multiplier layers and one reflector layer. A thick graphite reflector is located at the back so that its nuclear efficiency can be maximized. The BM is located at back side of the TBM. It is a high pressure manifold component for helium feeding to each sub-module and gathering using RAFM plates and ribs.

The HCCR TBS includes ancillary systems such as Helium Cooling System (HCS), Tritium Extraction System (TES), Coolant Purification System (CPS) and the I&C system [Cho 14]. Part of the components of these systems are located in the port cell #18, whereas the remaining components are located in level 4 and in level 2 of the tritium building.

### 2.4.2.5. HCCB TBS

The DEMO HCCB-BB uses  $\text{Li}_4\text{SiO}_4$  pebble beds as tritium breeder, beryllium pebble beds as neutron multiplier and RAFM steel as structural material. Li is enriched 80% in  $^6\text{Li}$ . Maximum temperatures are 900°C in the breeder, 600°C in the Be, and 550°C in the steel.

The HCCB-TBM has a U-shaped plate first wall with toroidal cooling channels, reinforced by He-cooled stiffening ribs to provide required strength in off-normal operation conditions. The internal space between the first wall module and the back plate is used for breeding zone arrangement. The breeding zone contains a sequence of poloidal rows of circular coolant channels,  $\text{Li}_4\text{SiO}_4$  pebbles and Be pebbles. The  $\text{Li}_4\text{SiO}_4$  pebbles are single-size pebbles (38% porosity) while Be is used as binary pebble-bed (20% porosity) with diameters of 0.5 and 1 mm. The structure of TBM consists of the following main components: first wall, caps, grids, manifolds, attachments, cooling pipes, purge gas pipes and sub-modules.

The HCCB-TBS includes several ancillary systems, namely the helium cooling system, the tritium extraction system (i.e., the purge gas system), the coolant purification system and the control/measurement system. Part of the components of these systems are located in the port cell #02, whereas the remaining components are located in level 4 of and in level 2 of the tritium building.

#### **2.4.2.6. LLCB TBS**

The DEMO LLCB-BB system has both features of solid breeder and liquid breeder blankets. In fact, it uses  $\text{Li}_2\text{TiO}_3$  pebble beds and  $\text{Pb-15.7Li}$  as tritium breeder and RAFM steel as structural material. Li enrichment in  ${}^6\text{Li}$  is 30–60% in pebbles and 90% in  $\text{Pb-15.7Li}$ . There are two coolants: the Helium coolant for the FW and the external box structure (pressure 8 MPa,  $T_{\text{inlet/outlet}}$  300–350°C) and the PbLi coolant for ceramic breeder packed beds ( $T_{\text{inlet/outlet}}$  300–480°C). The PbLi acts also as additional breeder and neutron multiplier. To avoid too large MHD pressure drops, the PbLi is isolated from the steel walls by means of electrical insulating coatings.

The LLCB-TBM has the same features of the DEMO LLCB-B. In particular, the molten PbLi eutectic flows separately around the ceramic pebble bed compartments to extract heat produced in the ceramic and in the PbLi itself. Tritium produced in the ceramic breeder zones is extracted by low-pressure helium purge gas. The tritium produced in the PbLi circuit is extracted separately by an external detritiation system.

The LLCB-TBS includes several ancillary systems, namely the FW helium cooling system, the PbLi system, the secondary He coolant system (for PbLi), the tritium removal system (from PbLi), the tritium extraction system (i.e. the purge gas system), the coolant purification system and the I&C system. Part of the components of these systems are located in the port cell #02, the remaining components are located in level 4 and in level 2 of the tritium building.

#### **2.4.3. TBS ancillary systems and supplies**

As previously mentioned, most cooling circuit (CC) components are located in a room at level 3 of the Tokamak building for the TBS of port cell #16, and in a room at level 4 of the tritium building for the TBSs of port cells #18 and #02. To reach these locations, connecting pipes will use the corresponding port cell shaft and cross several Tokamak building rooms where other ITER systems are present. Such high temperature pipes require thermal insulation and several bends for thermal stresses release. Most of the components (including glove boxes) of the six TBS TCs are located in a room in level 2 of the tritium building. Connecting pipes are expected to be at room temperatures and run from the port cell areas to this room passing through corridors.

The main services required by each TBS are the following: 1) secondary water coolant, 2) steady-state electrical power supply, 3) helium gas distribution, 4) liquid nitrogen distribution, 5) demineralized water distribution, 6) compressed air distribution, and 7) breathing air distribution [Gia 12].

For each TBS, a secondary water coolant is required at the level of the heat exchanger for extracting the heat deposited in the TBM (about 800 kW) and for the cooling of several other TBS components (e.g., pumps, blowers).

Steady-state electrical power supply is needed for operating the various TBS components (e.g. pumps, blowers, heaters). The required power for all six TBS is about 12 MW that gives an average of 2 MW per TBS. The peak for both water flow-rate and power supply requirements occurs during the TBS operation, with strong reduction during the long-term shutdowns.

Helium supply is necessary for He-cooled TBSs to compensate helium leakages during operation and perform the initial filling of the circuits and their potential partial refilling after long-term maintenance shutdowns. Demineralized water is necessary for the initial filling of the water-cooled TBS and its possible refilling.

Compressed air is necessary to actuate the numerous valves that are necessary for all TBS ancillary systems. In particular it is needed for the isolation valves that are required to isolate, in case of accident, all the pipes feeding the TBMs since they correspond to a direct access to the vacuum vessel.

## **2.5. Conceptual design of a TBM remote handling test facility**

The TBMs are considered as Remote Handling Class 1 (scheduled maintenance) components in ITER. This implies that all RH operations associated to the installation and removal of a TBM in ITER must be physically demonstrated using mock-ups before such TBM can be accepted by the IO. In fact, physical demonstration is essential to ensure the TBS RH system reliability under long term operation and to train RH operators in order to reduce downtime duration and failures linked to remote operations, so that the whole system availability is improved.

A Remote Handling Test Facility for demonstrating the feasibility of RH handling operations involving TBMs is therefore needed. By the moment it is not clear where the demonstration of the RH operations associated to the European TBMs will take place, although Research Centre Rez (Czech Republic) –institute belonging the EU TBM Consortium of Associates, as well as CIEMAT and another 4 European institutes- has recently communicated its intention to build a TBM RH test facility financed by European Cohesion Funds.

CIEMAT interest in hosting such TBM RH test facility resulted in the launch of a series of studies about the integration of the European Test Blanket Systems in ITER by remote handling operations. These studies, developed together with IBERDROLA and funded by CDTI (Spanish Centre for the Development of Industrial Technology), began in 2008, with the review of documentation and requirements for the remote maintenance of the TBMs and their auxiliary systems. The first version of the conceptual design document was released in July 2009.

New campaigns of studies were carried out by CIEMAT and IBERDROLA in 2010-2011 to update the Test Facility conceptual design according to the evolution of the HCLL TBM and TBS designs. Since the HCLL design was then more mature than the HCPB one, it was chosen as the reference design for these studies, although some considerations were also made for the HCPB. Thus, in 2010, the demonstration of several RH operations to be performed in the ITER Hot Cell was studied in detail. In particular, operations related to the substitution of TBMs in the equatorial port plug 16 after each experimental campaign of the TBM Program, as well as their adaptation for post-irradiation exams. In 2011, all the RH operations to be performed in the ITER Port Cell and the Port Interspace were redefined, as a consequence of the development of European R&D Programmes: redistribution of Port Cell systems and establishment of new interfaces, modification of the maintenance strategy of the Ancillary Equipment Unit (remote to manual), etc. Finally, the conceptual design document was updated at the beginning of 2012.

The level of detail of the conceptual design of the TBM RH Test Facility as well as that of the equipment requiring a specific design for the Facility is relatively low, except in some specific matters, since it was only conceived as the first step for the subsequent elaboration of detailed specifications for the construction of the Facility and for the manufacture of the installation-specific equipment.

After a brief explanation of the EU Test Blanket System Remote Handling System, the following subsections describe the conceptual design of the TBM RH Test Facility, in terms of RH equipment and operations, auxiliary systems & supplies and building requirements, among others.

## 2.5.1. Overall description of the EU TBS RH System

### 2.5.1.1. Integration of the TBS in the Equatorial Port Cell

In the port 16, several pipes (e.g., He coolant, He purge gas, PbLi) and various I&C cables cross the VV boundary and the biological shield plug to reach the area of the port cell where the Ancillary Equipment Unit (AEU) is located. The corresponding bundle of pipes between the back of the PP and the biological shield (corresponding to the port interspace) is called the Pipe Forest (PF).

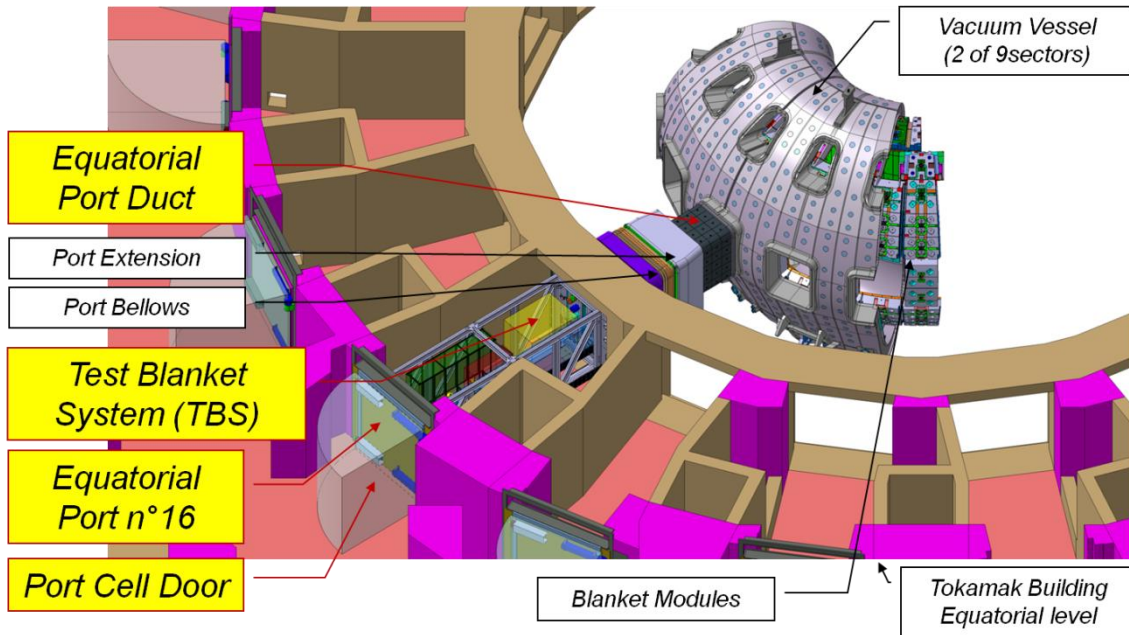


Fig. 17. General view of the Test Blanket System in the Port Cell and the Port interspace.

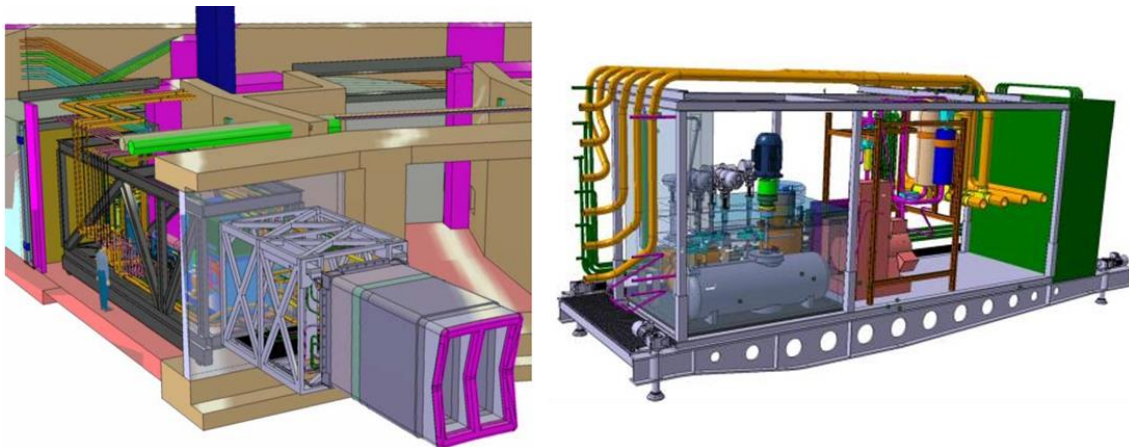


Fig. 18. Test Blanket System and AEU (right).

The PF includes all the pipes feeding the two TBMs and a cantilevered supporting structure attached to two vertical metallic beams which are themselves attached to the concrete of the bioshield. The temperature of the pipes ranges between 280 and 500°C and, therefore, pipes are surrounded by thermal insulator layers up to 14 cm-thick. Despite the insulator, the heat release in the PF area could reach about 10 kW. Each pipe has several bends in order to reduce thermal stresses. Most pipes will contain tritiated fluid and therefore could potentially release tritium through permeation.

Several interfaces are established between the TBMs, the Port Interspace/Port Cell Equipment and the rest of the TBS (Fig. 19). The union between the TBMs and their shielding modules is called Interface 1. The shielding modules meet the Pipe Forest at the Interface 2a. The Pipe Forest is connected to the AEU through the Interface 2b, whereas the Interface 3 connects AEU systems which the rest of the TBS equipment which is placed outside the Port Cell.

The AEU includes: 1) part of the tritium circuits; 2) part of the Helium Cooling System; 3) the PbLi loop of the HCLL; 4) some I&C systems; and 5) shield (as needed). The AEU (not only the European TBMs one) is expected to have a closed self-sustained structure with the same external dimensions of a Transfer Cask (2.6 m x 3.7 m x 8.5 m) and to make use of the same Transfer Cask System for the transfer to the Hot Cell Facility (HC). The AEU is supported by several pads fixed to embedded plates present in the floor. The supports have been designed taking into account the appropriate seismic loads. Several connection pipes and cables leave the AEU and pass either through the corresponding shaft or through the Tokamak corridor to reach the main helium cooling and tritium circuit components, as well as the I&C cubicles located up to 40 m far away.

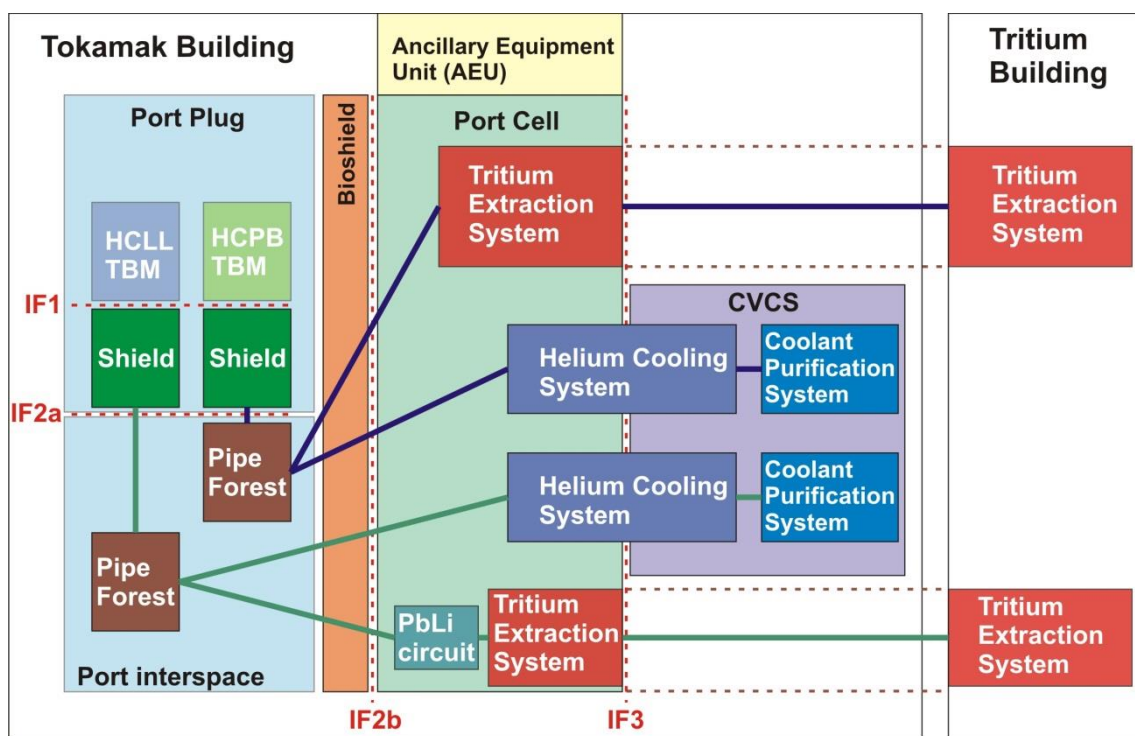


Fig. 19. Layout of EU Test Blanket System in the Tokamak Building and the Tritium Building.

The heat release from AEU will be dealt with the installation of Local Air Coolers (LAC) in some corners of the port cell taking into account that the air temperature in the port cell has to be limited to 40°C. The assessment of the countermeasures able to deal with the tritium releases is still on-going. In fact, personnel access is required in the PF area during the planned long-term shutdown (e.g., 8 months) and in the AEU area also during the short-term shutdowns (e.g., 3–4 days). To allow personnel access, the tritium concentration in the port cell air has to be controlled.

#### 2.5.1.2. TBM port plug replacement strategy

The adopted replacement strategy for the 6 TBMs is to replace the whole TBM PPs with new ones prepared and stored in advance in the Hot Cell Facility (HCF) and to perform off-line maintenance. This strategy requires the availability of six TBM-PP frames, three of them installed and operating in the TBM ports and other three ones stored in the HCF. The refurbishment of the TBMs will occur off-line.

For each TBM set, it is expected to have up to three replacements in the first ten years of ITER operation. The TBM sets will be replaced in pairs for each port; therefore, a strict coordination of the testing plan is necessary for the two TBMs located in the same port. To replace the 2 TBM sets, each TBM PP will be removed from the vacuum vessel using the ITER Equatorial Cask Transport System (ECTS) and delivered to the appropriated area of the HCF.

A new TBM PP, containing two new TBM-Sets, has to be available for immediate installation in the TBM port. TBM-PP pre-installation tests have to be performed in the PP Test Facility. Typical dimensions of a TBM PP are 2.2 m x 1.8 m x 3.6 m. In order to reuse the TBM frames, the 2 irradiated TBM sets will be remotely extracted from the PP and replaced with two new ones (off-line operations). Then each irradiated TBM set will be further remotely dismantled, the shield block will be treated as radwaste, and the TBMs will be stored in a dedicated buffer storage for specific further treatment in order to be, at least partially, packaged and shipped to the ITER Member owner for Post-Irradiation Examinations. Appropriate equipment and tools will be installed to perform these operations.

Prior to the replacement of the TBM PP, the corresponding AEU and PF will have to be disconnected and transferred in the HCF in this order. The AEU will be disconnected and transferred in a specific HCF area dedicated to AEU maintenance (using the same pathway as the ECTS). In the HCF, it will be maintained on-line and, after testing, sent back to the corresponding port cell after the installation of the new TBM PP and the new PF. The required equipment in the HCF includes: inspection equipment, preparation equipment for reinstallation in the port cell, and testing equipment. The PF (including the bio-shield plug) has also to be disconnected and transferred to the HCF where it will be treated as type-A waste. Therefore, a new Pipe Forest will have to be available for installation. This strategy will allow minimizing the dose received by the workers during the PF reinstallation.

### **2.5.2. Objectives of the TBM RH Test Facility**

The main goals of the TBM RH test facility are the following:

- Demonstrate the feasibility of the remote handling operations involving TBMs in ITER.
  - This involves in particular:
    - Demonstration of RH operations related to the installation of the TBM and auxiliary systems in Port and Port cell.
    - Demonstration of RH operations related to the replacement of the TBM in the Hot Cell.
    - Demonstration of RH operations related to the transport of the port plug between the Port Cell and the Hot Cell.
  - Vacuum leak tests will be performed only to validate the quality -in terms of vacuum tightness- of certain RH operations, such as pipe welding or vacuum sealing of the interface between TBM and PP.
- Confirm design choices for TBM RH equipment and systems (manipulators, tools, viewing, virtual reality, actuators, controllers, software, etc.).
- Validate and optimize operating procedures.
- Examine consequences of system failures and confirm pre-planned rescue procedures.
- Allow long term endurance testing to assess availability/reliability of RH systems.
- Provide a training platform for RH systems designers and operators.

The facility is non-radioactive. A parallel program to qualify components & systems under radiation is needed.

### 2.5.3. Design methodology

The method followed for the conceptual design of the TBM RH test facility has consisted of two fundamental parts:

- 1) Identification of requirements (equipment, structures, auxiliary systems and space) associated to the RH operations which must be demonstrated).
  - Many operations are not well defined in the available EU TBM RH documentation, mainly coming from the ITER on-line Document Management System (IDM) and the EU TBM Consortium of Associates (e.g. on-line SharePoint), so it has been necessary to make an important number of hypotheses to define the RH equipment and processes.
- 2) Design of the Facility considering all the requirements which were identified in the operation analysis. This comprises the conceptual design of equipment and systems, as well as the layout of equipment and systems in the facility.

The logical integration of both parts has been made according to the following scheme of phases and sub-phases:

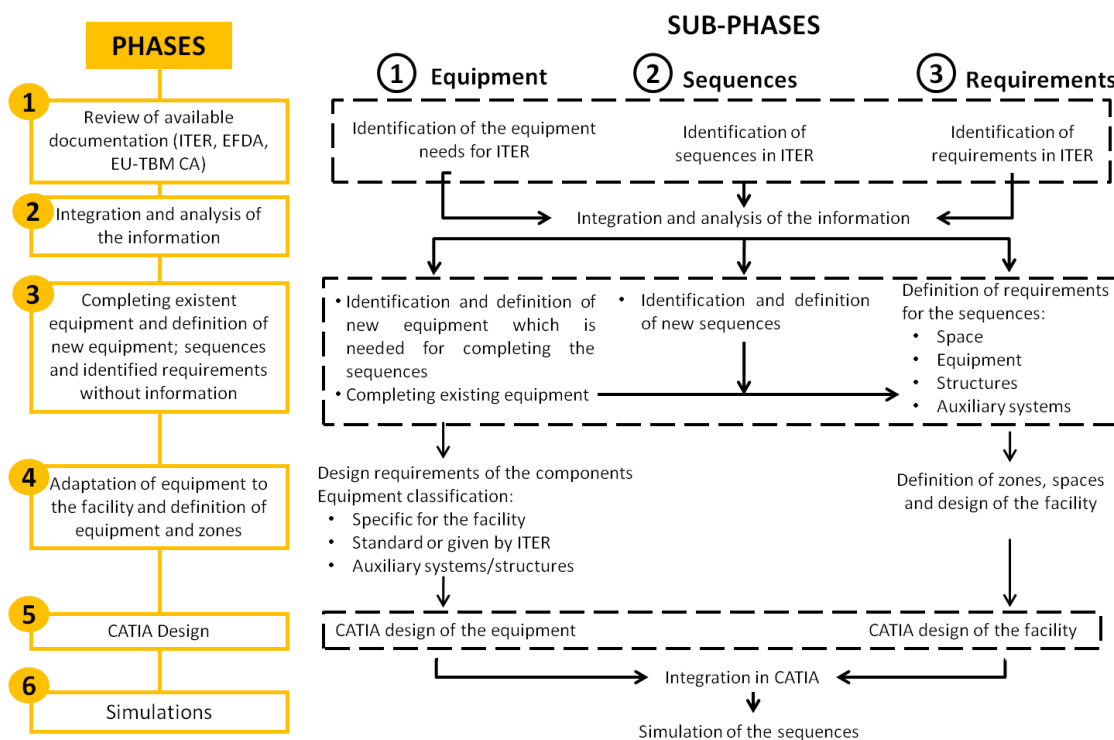


Fig. 20. Design process (phases and sub-phases).

The ITER Remote Handling Code of Practice [Raj 09] has been followed for planning activities and documentation generation.

Graphic design using CATIA v5 has been extensively used. Around 350 assemblies with a total number of ~1200 parts have been designed and/or integrated in the 3D CAD model. Graphic design has been combined with kinematic simulations, especially for the Hot Cell and Port Cell operations mentioned at the beginning of this chapter which have been studied with higher level of detail. This point will be further developed in Chapter 4.

On the other hand, the design process described in the ITER Maintenance Management System (IMMS) has been followed to study such operations with higher level of detail. This methodology to define new RH processes is composed by the following steps:

- I. Establishment of the Plant Definition Forms (PDF). The PDF are cards with the information of the equipment necessary to define the RH processes.
- II. Establishment of the Task Definition Forms (TDF). These are cards which describe the detailed list of steps of the RH operation, without explaining how it is carried out neither the needed tools. They define the requirements of the RH tasks (what to do).
- III. Establishment of the Operations Sequence Description (OSD). The RH process and the needed tools are described in detail in the RH process. In this case, the Operation Sequence Descriptions have been detailed scripts based in 3D CAD views of the RH processes which have been used for subsequent simulations. The OSD describe how each step identified in the TDF is made.
- IV. In the step III, it may appear the need of modifying the design of the equipment which is remotely handled (plant design). In such case, the PDF is modified and the TDF and OSD are redefined. The equipment design (plant design) and the RH process (RH design concept) are linked. The definition of the RH design concept is an iterative process where a change into the plant design affects the RH design concept and vice versa. As previously mentioned, the development of new tools can also be necessary, but it is preferable to use the standard tools defined in the ITER Code of Practice. In this case, standards appearing in the JET Remote Handling Manual have been also used.

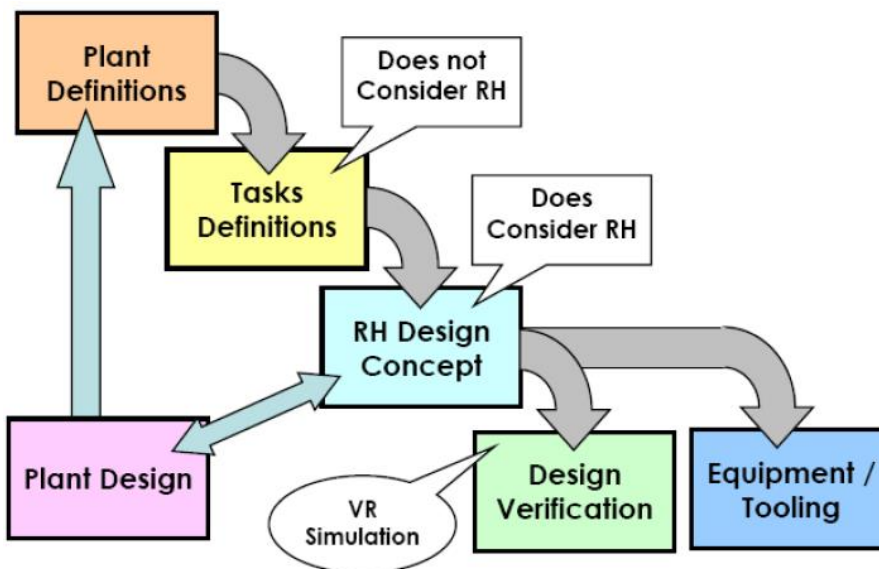


Fig. 21. Working methodology according to IMMS.

#### 2.5.4. Requirements of the RH Test Facility

This section specifies the requirements imposed by the demonstration of the TBM RH operations in the ITER Hot Cell, Port Interspace and Port Cell, as well as operations concerning the port plug installation/removal in/from the vacuum vessel equatorial port and the transport between the vacuum vessel and the Hot Cell. Such requirements are defined in terms of equipment, structures, auxiliary systems and space.

A number of 25 remote handling operations has been identified and studied. The complete list is shown in Table 2.

Area	Operation
1 HC	Transfer of the port plug with the TBM & shield assemblies from the transfer cask to a tool inside the Hot Cell (operation #1)

2	HC	Movement of the TBM & shield and port plug assembly within the Hot Cell on rails (operation #2)
3	HC	Cleaning of dust from the port plug in order to reduce the dose rate (operation #3)
4	HC	Disconnection of water pipes of the TBM & shield assembly from the main water system of the port plug and the vacuum vessel (operation #4)
5	HC	Removal of the sealing features and mechanical attachments between the port plug and the TBM & shield assemblies (operation #5)
6	HC	Vertical extraction of the TBM & shield assembly from the PP frame (operation #6)
7	HC	Cleaning of dust from the TBM & shield assembly (operation #7)
8	HC	Separation of the TBM from the shield (operation #8)
9	HC	TBM splitting and packing into transport casks to be shipped (operation #9)
10	HC	Introduction of the TBM & shield assembly into the port plug frame (operation #10)
11	HC	Joining of the TBM & shield assembly to the port plug frame (operation #11)
12	HC	Connection of the water pipes of the TBM & shield assembly from the main water system of the port plug and the vacuum vessel (operation #12)
13	HC	Checking of vacuum sealing between the port plug and the TBM shield (operation #13)
14	HC	Checking of the water loop (operation #14)
15	PC	Transfer of the Pipe Forest & Bioshield Door assembly between the Storage Area and the Port Cell (operation #15)
16	PC	Installation/removal of the Pipe Forest & Bioshield Door in/from the Interspace (operation #16)
17	PC	Transfer of the RH Platform Unit between the Storage Area and the Port Cell (operation #17)
18	PC	Welding of pipes in IF2a (operation #18)
19	PC	Inspection of weld beads in IF2a (operation #19)
20	PC	Installation and removal of thermal insulations at IF2a (operation #20)
21	PC	Constriction/unconstriction of pipes at IF2a (operation #21)
22	PC	Cut of pipes in IF2a (operation #22)
23	PC	Installation/removal of the AEU in/from the Port Cell (operation #23)
24	Port	Installation/removal of the Port Plug in/from the Port (operation #24)
25	Port	Vacuum sealing of the port plug – port interface (operation #25)

Table 2. List of RH operations to be demonstrated in the Test Facility.

The following subsections expose the requirements linked to each operation. Descriptions of the sequences and assumed hypotheses, as well as equipment, structures, auxiliary systems and space requirements (in tabular form) are included.

#### 2.5.4.1. *Transfer of the port plug with the TBM & shield assemblies from the transfer cask to a tool inside the Hot Cell (operation #1)*

The transfer cask door couples to the Hot Cell port. Then the gripper moves ahead and introduces the port plug in the vertical positioning tool frame. In ITER, the Hot Cell port will have a maintenance door as the Port Cell Port. Once the TC docks into the Hot Cell port both the TC door and the maintenance door are lifted together to the upper part of the TC. In the TBM RH test facility the Hot Cell port does not have a maintenance door. Only the TC door is lifted to allow the insertion of the PP into the vertical positioning tool.

##### Sequence

Once the transfer cask is docked to the HC port, the transfer cask door and the HC port are linked face to face. The TC door is lifted to the upper part of the TC. Then the gripper starts moving along the rails until it goes beyond the Hot Cell door and introduces the port plug in the

vertical positioning tool frame, which has moved to the Hot Cell port and is arranged in horizontal position. Once the PP is completely inserted in the vertical positioning tool frame, the gripper uncouples and returns to its initial position.

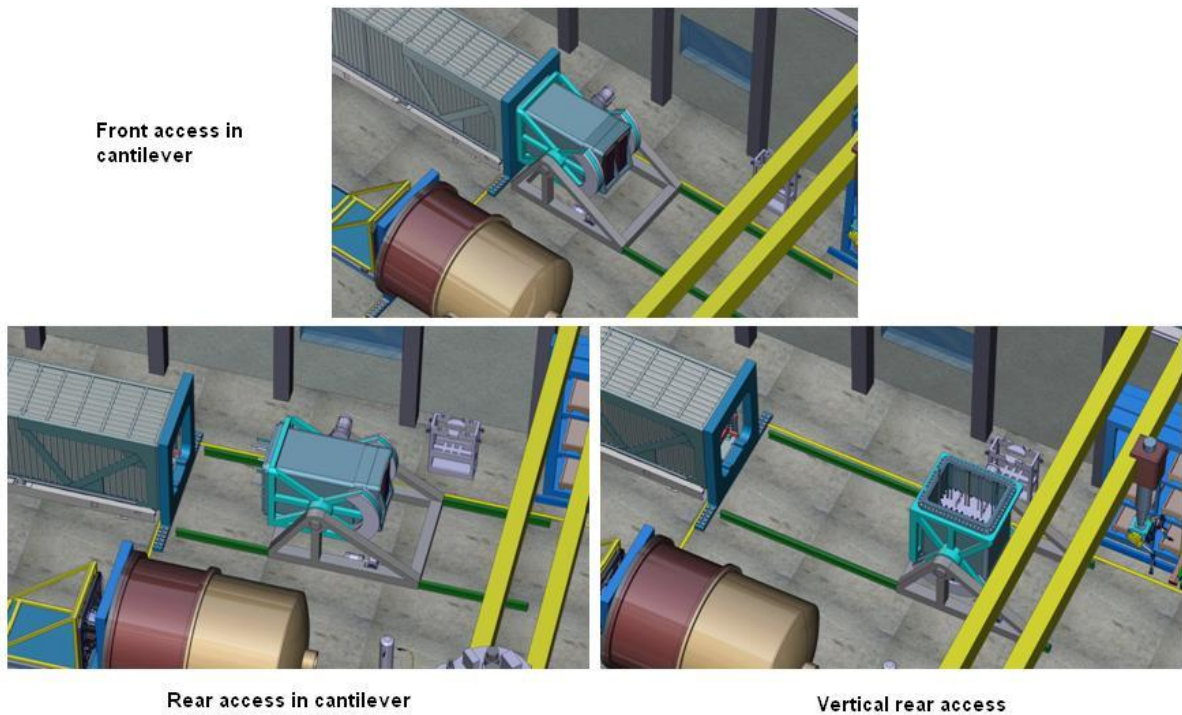


Fig. 22. Vertical positioning tool.

Space requirements

~50 m<sup>2</sup> (3.5 m x 11 m) x 5 m (height). This space has been determined from [Ben 08], [Bed 08], and the known dimensions of the Port Plug (length 3.64 m, height 2.33 m, width 1.66 m). 3.5 m is the width of the vertical positioning tool proposed in [Bed 08]. 11 m is the distance which covers the vertical positioning tool on the rails (also obtained from [Bed 08]). This space sizing has been supported by subsequent simulations. 5 m (height) is the distance between the rear part of the Port Plug and the floor when the Port Plug is in vertical position.

RH operation	TBM RH test facility requirements				
	Equipment		Structures	Auxiliary systems	Space
	Not requiring a specific design	Requiring a specific design			
Transfer of TBM & shield and port plug assembly from transfer cask to a tool inside the Hot Cell	- Transfer cask. - Vertical positioning tool.	- Port plug mock-up.	- HC door. - Rails. - Rack.	- Electric supply.	3.5 m x 11 m x 5 m

Table 3. Operation #1 requirements.

Hypotheses

- The existence of the PP vertical positioning tool proposed in [Bed 08] in the ITER Hot Cell is assumed. Its displacement on rails into the Hot Cell is also assumed.

### 2.5.4.2. Movement of the TBM & shield and port plug assembly within the Hot Cell on rails (operation #2)

Once the PP (including the TBMs with their shielding modules) is coupled to the vertical positioning tool [Bed 08], this set moves along horizontally by means of a pinion-rack system. The rack is fixed to the floor and the pinion is part of the vertical positioning tool. The pinion is moved by an electrical motor. This concept is analogous to the one used in the transfer cask to move the gripper with the port plug. Besides, a set of rollers slide through rails (one in each side, the rails have a double T contour) making easier the movement. After the vertical positioning tool reaches the refurbishment zone, the port plug is rotated for refurbishment operations, adopting a vertical position (previously it was horizontal). Finally a brake is set to fix the position.

#### Space requirements

This operation has the same space requirements as operation #1: 3.5m x 11 m x 5 m (W, L, H).

RH Operation	TBM RH test facility requirements				
	Equipment		Structures	Auxiliary systems	Space
	Not requiring a specific design	Requiring a specific design			
Movement of TBM & shield and port plug assembly within Hot Cell on rails	- Vertical positioning tool.	- PP mock-up.	- Rails. - Rack.	- Electric supply.	3.5 m x 11 m x 5 m

Table 4. Operation #2 requirements.

#### Hypotheses

- The vertical positioning tool is used as the TBM PP acceptance & movement system in the Hot Cell.

### 2.5.4.3. Cleaning of dust from the port plug in order to reduce the dose rate (operation #3)

The palletising system takes the vacuum cleaner from the shelves and leaves it in the refurbishment area. The telescopic mast moves to this area, the manipulator picks the duct of the vacuum cleaner and cleans the surface of the port plug (reachable sides and faces of the port plug and shield). Then the manipulator picks up a brush or mechanical rotating brush-like tool and cleans again the surface of the port plug. The port plug, during the operation, is fixed to the vertical positioning tool in vertical position.

Once the manipulator finishes the vacuum cleaner is removed to the shelves.

#### Space requirements

6.5 m x 5.5 m x 9 m (W, L, H). The width and the length have been obtained from the dimensions of the vertical positioning tool and the pallet which contains the vacuum cleaner, as well as the space needed for the operation of the HC manipulator. The height (9 m) has been obtained from [Bed 08]. This height is the free operation space. It does not take into account the space taken by the crane itself.

RH Operation	TBM RH test facility requirements			
	Equipment	Structures	Auxiliary systems	Space (W, L, H)

	Not requiring a specific design	Requiring a specific design			
Cleaning of dust from port plug in order to reduce the dose rate	<ul style="list-style-type: none"> <li>- Vacuum cleaner.</li> <li>- Vertical positioning tool.</li> <li>- Brushing tool.</li> <li>- Palletising system.</li> <li>- Overhead rotating crane.</li> <li>- Telescopic mast.</li> <li>- HC manipulator.</li> </ul>	<ul style="list-style-type: none"> <li>- PP mock-up.</li> </ul>	<ul style="list-style-type: none"> <li>- Pallets shelves.</li> </ul>	<ul style="list-style-type: none"> <li>- Electric supply.</li> </ul>	6.5 m x 5.5 m x 9 m

Table 5. Operation #3 requirements.

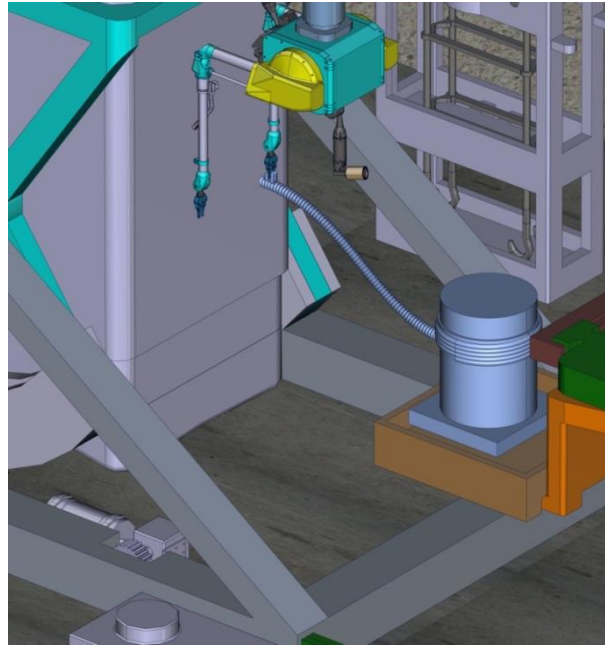


Fig. 23. Vacuum cleaner located on the floor of the PP maintenance area.

#### Hypotheses

- The cleaning is done with a vacuum cleaner operated by a manipulator. The references for the involvement of such equipment –as well as the palletising system, the telescopic mast and the HC manipulator- are [Tes 08b] and [San 08].
- We assume the hypothesis that vacuum cleaning is not enough and that brushing is necessary.

#### 2.5.4.4. Disconnection of water pipes of the TBM & shield assembly from the main water system of the port plug and the vacuum vessel (operation #4)

The operation is carried out with the PP inserted in the PP vertical positioning tool. The back of the PP is facing up.

We assume the hypothesis that the vacuum vessel cooling circuit feeds in parallel the PP and shielding module cooling circuits through a common interface circuit. There would be an inlet (lower) and an outlet interface circuit (upper). Another possibility would be having the shield cooling circuit fed by the PP cooling circuit and having the PP cooling circuit fed by the vacuum vessel cooling circuit.

### Sequence

The Hot Cell manipulator takes the cutting tool located in a pallet placed left on the floor by the palletising system. Then it approaches one of points to cut the interface circuits. The interface circuit is cut at the points where these circuits are connected by welding to the PP and shield cooling circuits. It is assumed that despite all the pipes coming out of the back of the shield there is clearance for the hot cell manipulator to carry out the cutting operations. The cutting operation is repeated in all cutting points. After the cutting operations the HC manipulator helps in connecting the crane hooks to the lifting eyes or lifting interfaces of one interface circuit. Then the crane lifts up the interface circuit. It is assumed that the interface circuits are designed with lifting eyes or some kind of lifting interface. The lifting operation is repeated for the second interface circuit.

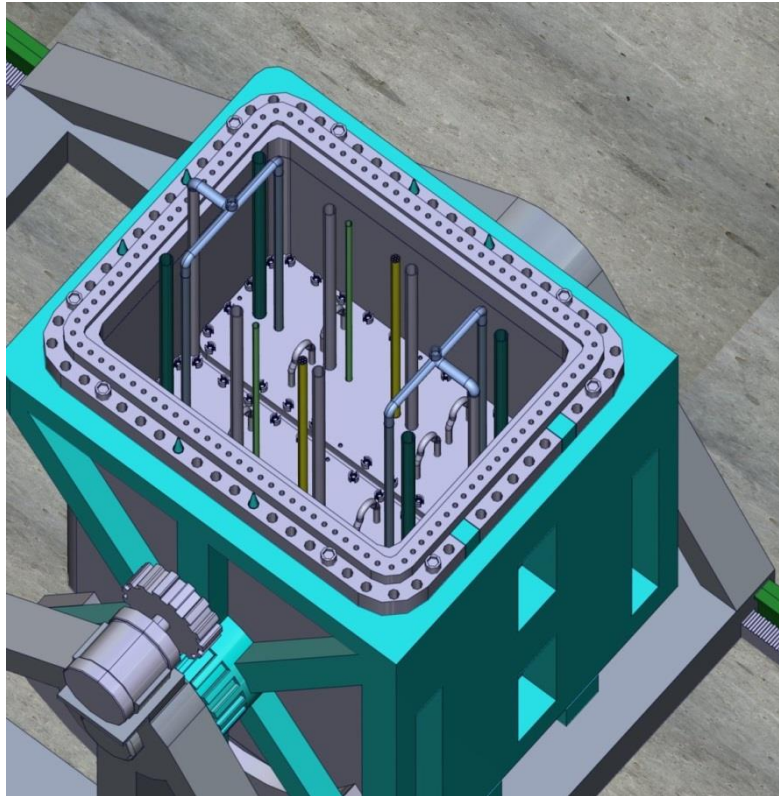


Fig. 24. Pipes connecting PP and shield water cooling circuits to the vacuum vessel cooling system.

### Space requirements

6.5 m x 5.5 m x 9 m (W, L, H). The width and the length have been obtained from the dimensions of the vertical positioning tool and the pallet for the cutting tool, as well as the space needed for the operation of the HC manipulator. The height (9 m) has been obtained from [Bed 08]. This height is the free operation space. It does not take into account the space taken by the crane itself.

RH Operation	TBM RH test facility requirements				
	Equipment		Structures	Auxiliary systems.	Space (W, L, H)
	Not requiring a specific design	Requiring a specific design			
Disconnection of water pipes of TBM & shield assembly from	<ul style="list-style-type: none"> <li>- Vertical positioning tool.</li> <li>- Cutting tool for HC manipulator.</li> <li>- Gripping tool for coupling</li> </ul>	<ul style="list-style-type: none"> <li>- PP mock-up.</li> <li>- TBM &amp; shield mock-ups.</li> </ul>	<ul style="list-style-type: none"> <li>- Pallet shelves.</li> </ul>	<ul style="list-style-type: none"> <li>- Electric supply.</li> </ul>	6.5 m x 5.5 m x 9 m

main water system of port plug and vacuum vessel	tool. - Palletising system. - Overhead rotating crane. - Telescopic mast. - HC manipulator.				
--	---	--	--	--	--

Table 6. Operation #4 requirements.

Hypotheses

- It is assumed that the First Wall/Blanket Primary Heat Transfer System feeds water in parallel to the PP and shield cooling circuits through a common interface circuit.
- The hypothesis of the geometry for the interface circuits is similar to the one shown in Fig. 24 is assumed. The hypothesis that it is possible to successively align and weld the pipes of each interface circuit to the pipes of the PP and shield cooling circuits is assumed.
- It is assumed that the main detritiation of the PP and shield cooling circuits has been carried out in the Port Cell (standard ITER procedure for port plugs).
- It is assumed that the manipulator has access to the cutting points despite the set of pipes coming out of the back of the shield.
- It is assumed that the interface circuit has design features (lifting eyes or other) allowing the crane to lift it.

2.5.4.5. Removal of the sealing features and mechanical attachments between the port plug and the TBM & shield assemblies (operation #5)

Before the extraction of each TBM & shield assembly from the port plug, it is needed to remove the sealing and joining features between both [Meu 07] [Tes 07].

Sequence

The Hot Cell manipulator (moved by the crane and the telescopic mast) grips the hydraulically driven screwer from the storage shelves and places it on each captive bolt of the shield flange. It unscrews the bolts and leaves the screwer in the pallet [Rio 10].

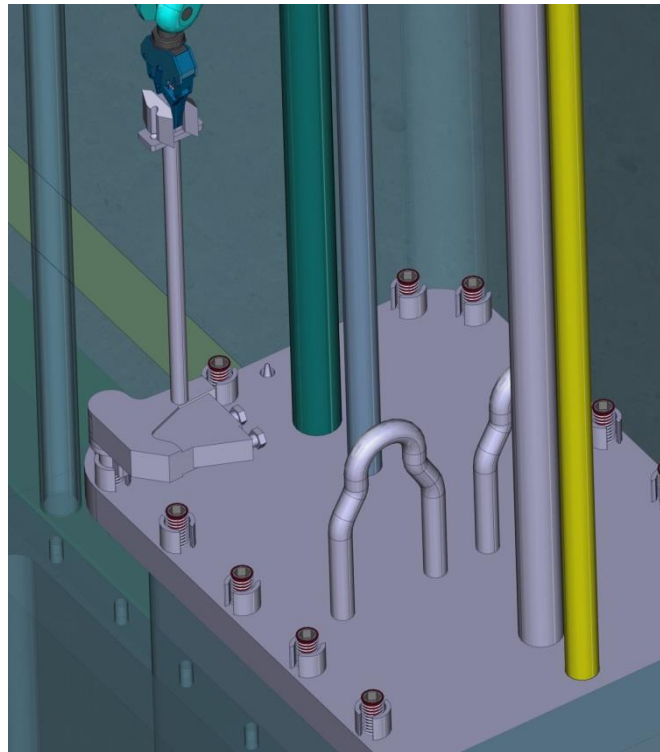


Fig. 25. Unscrewing of captive bolts which joins the shield flange to the PP frame.

#### Space requirements

6.5 m x 5.5 m x 9 m (W, L, H). The width and the length have been obtained from the dimensions of the vertical positioning tool and the pallet for the screwer, as well as the space needed for the operation of the HC manipulator. The height (9 m) has been obtained from [Bed 08]. This height is the free operation space. It does not take into account the space taken by the crane itself.

RH Operation	TBM RH test facility requirements				
	Equipment		Structures	Auxiliary systems.	Space (W, L, H)
	Not requiring a specific design	Requiring a specific design			
Removal of sealing features and mechanical attachments between port plug and TBM & shield assembly	<ul style="list-style-type: none"> <li>- Vertical positioning tool.</li> <li>- HC manipulator.</li> <li>- Telescopic mast.</li> <li>- Overhead rotating crane.</li> <li>- Palletising system.</li> <li>- Screwer.</li> </ul>	<ul style="list-style-type: none"> <li>- PP mock-up.</li> <li>- TBM &amp; shield mock-ups.</li> </ul>	<ul style="list-style-type: none"> <li>- Pallet shelves.</li> </ul>	<ul style="list-style-type: none"> <li>- Hydraulic supply.</li> <li>- Electric supply.</li> </ul>	6.5 m x 5.5 m x 9 m

Table 7. Operation #5 requirements.

#### Hypotheses

- Two vacuum seals (Helicoflex metal gasket) are integrated in the shield flange.
- TBM & shield assemblies are joined to the PP frame by captive bolts.
- A hydraulically driven screwer is used to unscrew captive bolts.

#### 2.5.4.6. Vertical extraction of the TBM & shield assembly from the PP frame (operation #6)

The overhead travelling crane must extract the TBM & shield assembly from the PP frame.

It is assumed that the shield has hoisting features (lifting eyes) allowing its extraction from the PP frame.

Sequence

The shield lifting tool attached to the 20 t overhead travelling crane coupling tool hooks the lifting eyes in the back of the shield. Then the crane lifts the TBM & shield assembly and leaves it in a bench for cleaning and separation. Finally a movement of the crane disconnects the shield lifting tool from the lifting eyes on the back of the shield [Rio 10].

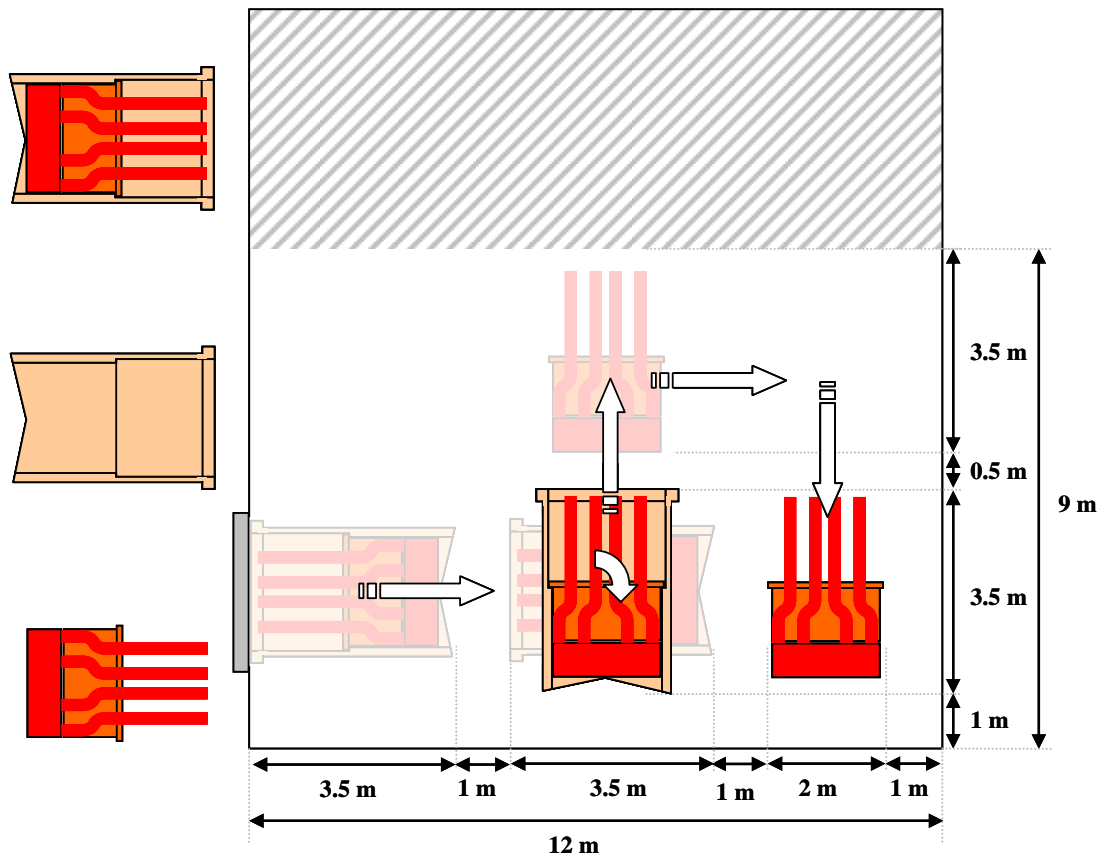


Fig. 26. Scheme of the extraction of a TBM & shield assembly [Bed 08].

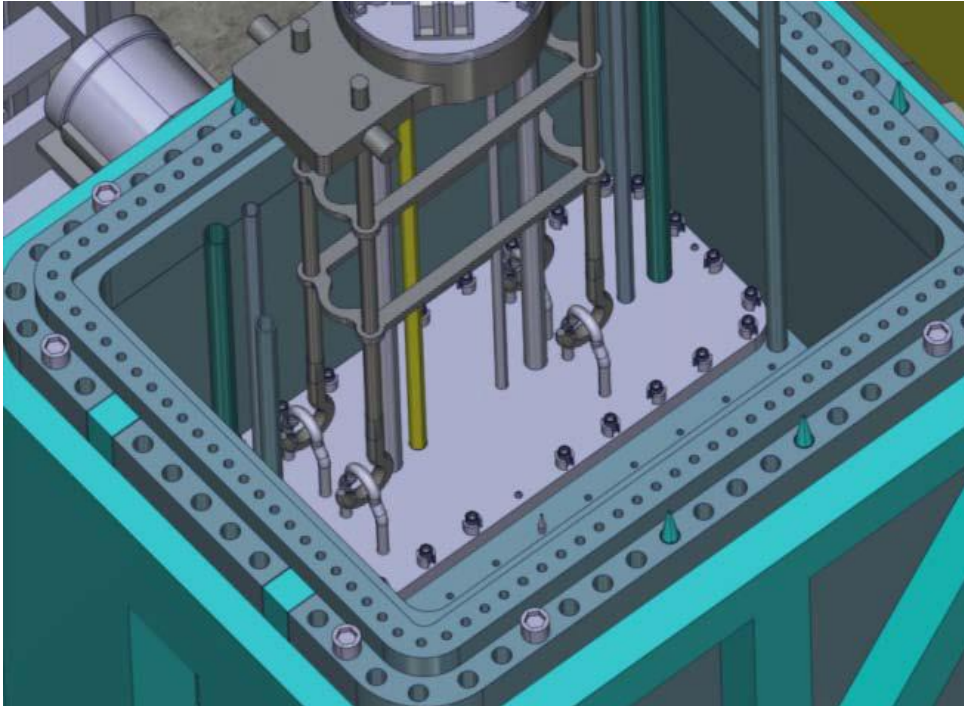


Fig. 27. Lifting tool extracting a TBM & shield assembly.

#### Space requirements

5 m x 3.5 m x 9 m (W, L, H). The width and the length have been obtained from the dimensions of the vertical positioning tool. The height (9 m) has been obtained from [Bed 08]. This height is the free operation space. It does not take into account the space taken by the crane itself.

RH Operation	TBM RH test facility requirements				
	Equipment		Structures	Auxiliary systems.	Space (W, L, H)
	Not requiring a specific design	Requiring a specific design			
Vertical extraction of the TBM & shield assembly from the PP frame	<ul style="list-style-type: none"> <li>- Vertical positioning tool.</li> <li>- Overhead rotating crane.</li> <li>- Lifting tool for TBM &amp; shield.</li> </ul>	<ul style="list-style-type: none"> <li>- PP mock-up.</li> <li>- TBM &amp; shield mock-ups.</li> </ul>	<ul style="list-style-type: none"> <li>- Bench for TBM &amp; shield assembly cleaning and separation.</li> </ul>	<ul style="list-style-type: none"> <li>- Electric supply.</li> </ul>	5 m x 3.5 m x 9 m

Table 8. Operation #6 requirements.

#### Hypotheses

- It is assumed that the back of the shield has lifting eyes.
- It is assumed that the crane will lift the TBM and shield assembly by using a “shield lifting tool” as the one shown in Fig. 27.
- It is assumed that the TBM & shield assembly is left on a bench for cleaning and separation. The design of the bench is hypothetical.

#### 2.5.4.7. Cleaning of dust from the TBM & shield assembly (operation #7)

The dust accumulated on the surface of the TBM & shield assembly is removed by means of the HC manipulator and the HC vacuum cleaner.

Operation sequence

The TBM & shield assembly starts on a special bench for cleaning and separation after having been extracted from the PP. The palletising system leaves on the floor next to the bench a pallet with the vacuum cleaner tool and brushing tool. The HC manipulator (suspended from the crane through the telescopic mast) picks the vacuum cleaning tool and proceeds to clean the TBM & shield assembly. Then it leaves the vacuum cleaning tool on the pallet, takes the brushing tool and cleans again the TBM & shield assembly with the brushing tool. Once the cleaning is finished the palletising system takes the pallet with the vacuum cleaner and brushing tool back to the pallet shelves.

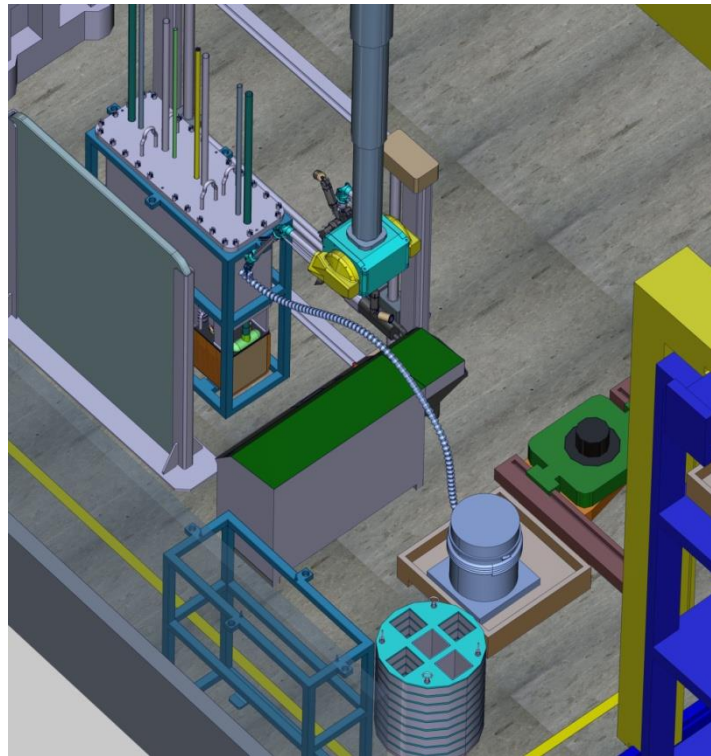


Fig. 28. Cleaning of dust from the TBM & shield assembly.

Space requirements

8.2 m x 2.5 m x 9 m (W, L, H). The width and length has been estimated from TBM dimensions and the features of the HC manipulator, the palletising system and the vacuum cleaner [Tes 08b] [Rio 10]. The height (9 m) has been obtained from [Bed 08]. This height is the free operation space. It does not take into account the space taken by the crane itself.

RH Operation	TBM RH test facility requirements				
	Equipment		Structures	Auxiliary systems.	Space
	Not requiring a specific design	Requiring a specific design			
Cleaning of dust from TBM & shield assembly	<ul style="list-style-type: none"> <li>- Vacuum cleaner.</li> <li>- Brushing tool.</li> <li>- Palletising system.</li> <li>- Overhead rotating crane.</li> <li>- Telescopic mast.</li> <li>- HC manipulator.</li> </ul>	<ul style="list-style-type: none"> <li>- TBM &amp; shield mock-ups.</li> <li>-</li> </ul>	<ul style="list-style-type: none"> <li>- Bench for TBM &amp; shield assembly cleaning and separation.</li> <li>- Pallet shelves.</li> </ul>	<ul style="list-style-type: none"> <li>- Electric supply.</li> </ul>	8.2 m x 2.5 m x 9 m

Table 9. Operation #7 requirements.

### Hypotheses

- It is assumed that there is a specific bench in the HC for the separation of the TBM and the shield and cleaning operations.
- It is assumed that the dust is removed with a vacuum cleaner as shown in the Oxford Technologies video about divertor refurbishment in the Hot Cell [San 08].
- It is assumed that the vacuum cleaning is not enough to remove the dust and that brushing is necessary.

#### 2.5.4.8. Separation of the TBM from the shield (operation #8)

In this operation the connections between TBM and shield (Interface 1) must be removed. These connections include:

- Mechanical joints.
- Helium and lithium lead pipes connections.
- Electrical connections (CODAC).

Once separated, TBM and shield must be placed in the band sawing machine [Bai 09] and the storage container, respectively.

### Operation sequence

The operation starts with the TBM and shield assembly inside the separation bench. The lifting tool is above the shield, the laser cutting tool is in front of the bench and the laser shielding structure is behind the bench.

The laser cutting tool is activated and makes a first horizontal sweep to cut the first row of union plates and the interface piping, without cutting the lifting eyes and the shear keys. After this, the laser cutting tool makes a second horizontal sweep cutting the second row of union plates. Then, the four hooks of the lifting tool attached to the 20 t crane coupling tool takes the shield through its four lifting handles. The lifting tool is lifted up and extracts the shield from the bench [Rio 10].

Once extracted, the shield is transported horizontally and introduced in a storage container to be treated as waste. The lifting tool is disengaged from the shield, lifted up again and moved back to the separation bench.

This extraction sequence is repeated for the TBM, but here the lifting tool must place it on the roller conveyor of the band sawing machine.

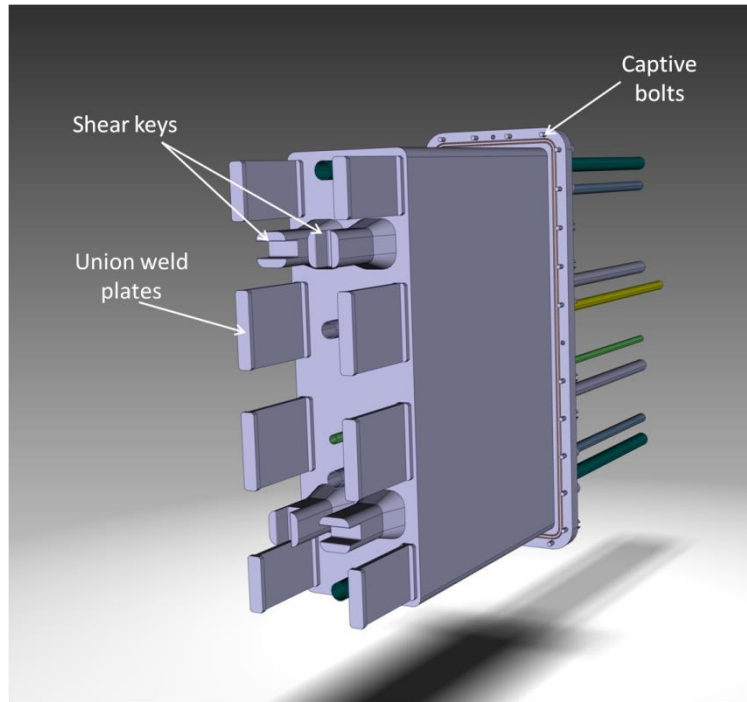


Fig. 29. Mechanical joints between TBM and shield at Interface 1.

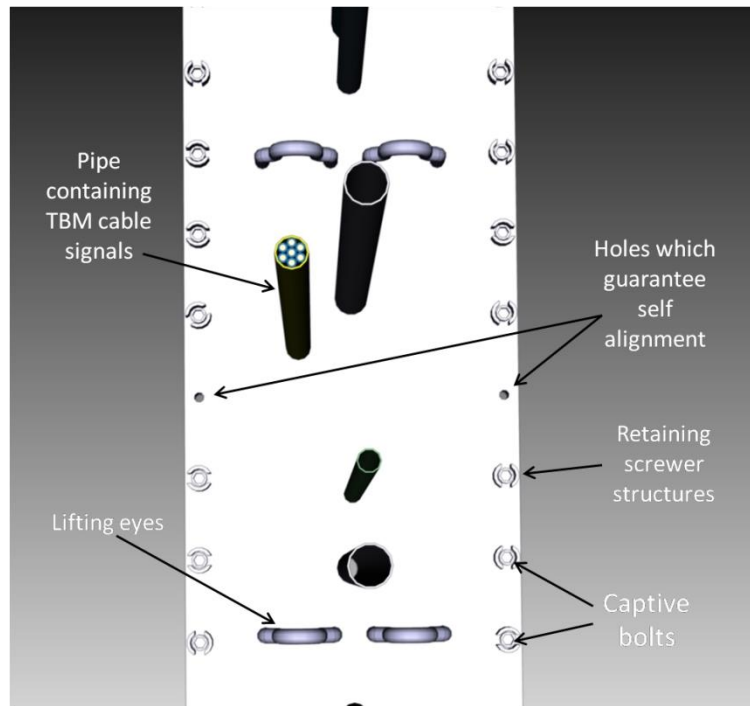


Fig. 30. Possible way to pass cabling to/from the TBM through the shield.

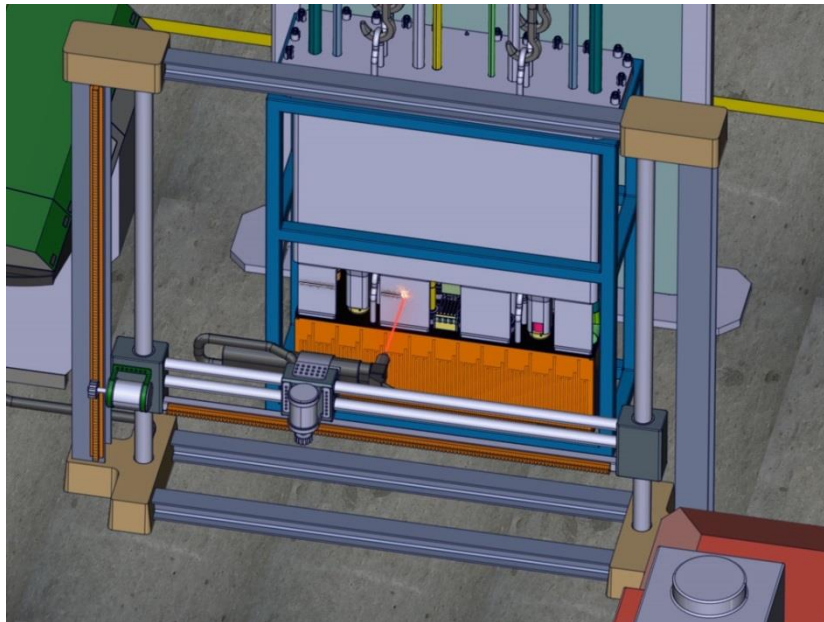


Fig. 31. Cut of the joints between the TBM and the shield by laser.

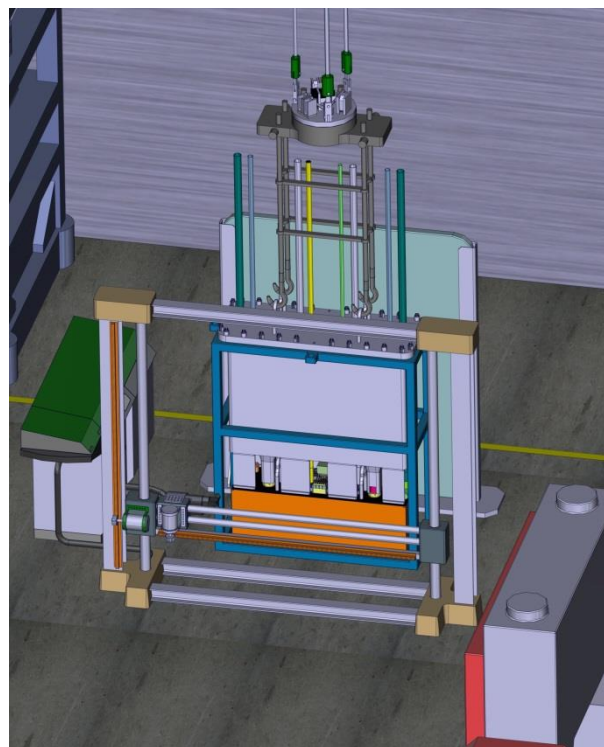


Fig. 32. Separation of the TBM from the shield using the clamping bench and the crane.

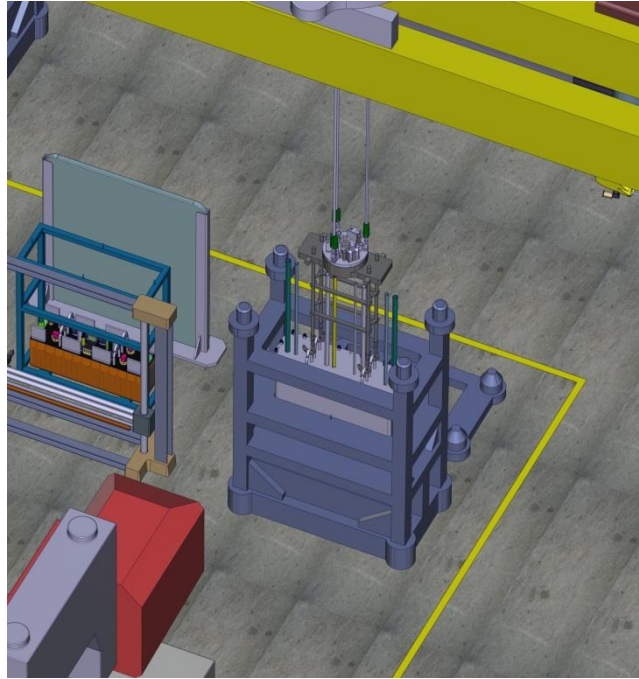


Fig. 33. Insertion of the shield in the storage container.

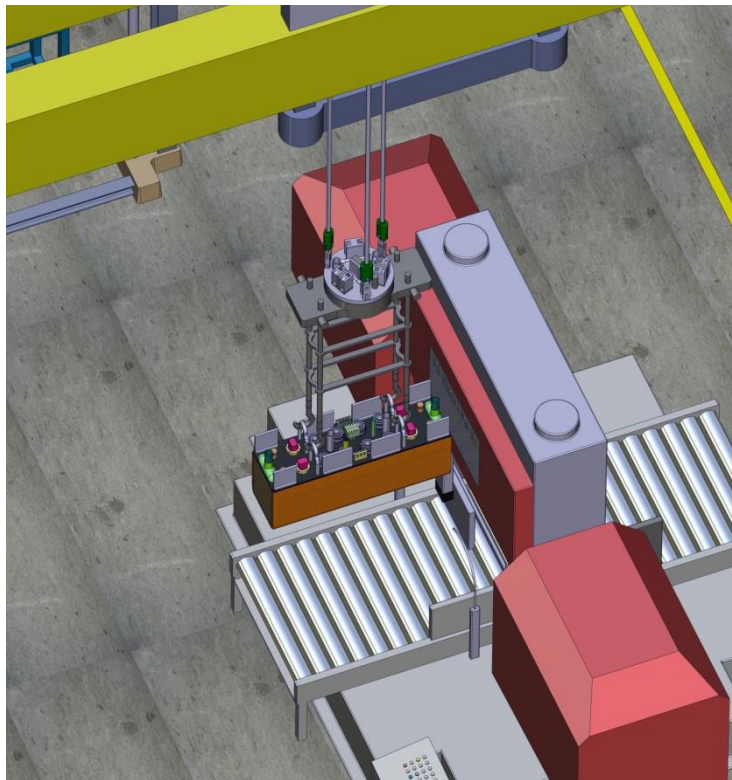


Fig. 34. Placing of TBM on the band sawing machine.

### Space requirements

12 m x 11 m x 9 m (W, L, H). The width and the length are taken from the dimensions of the separation bench and the band sawing machine. The height (9 m) has been obtained from [Bed 08]. This height is the free operation space. It does not take into account the space taken by the crane itself.

RH Operation	TBM RH test facility requirements				
	Equipment		Structures	Auxiliary systems.	Space
	Not requiring a specific design	Requiring a specific design			
Separation of TBM from shield	<ul style="list-style-type: none"> <li>- Laser cutting tool.</li> <li>- Lifting tool for TBM &amp; shield.</li> <li>- Overhead rotating crane.</li> </ul>	<ul style="list-style-type: none"> <li>- TBM &amp; shield mock-ups.</li> </ul>	<ul style="list-style-type: none"> <li>- Bench for TBM &amp; shield assembly cleaning and separation.</li> <li>- Storage container.</li> </ul>	<ul style="list-style-type: none"> <li>- Electric supply.</li> </ul>	12 m x 11 m x 9 m

Table 10. Operation #8 requirements.

### Hypotheses

- It is assumed that the joint between the TBM and the shield is achieved through welded plates and shear keys [Mad 09].
- It is assumed that two sweeps of laser are necessary to cut the TBM/shield interface.
- It is not necessary to cut the pipes of the rear side of the shield.
- It is assumed that there is a specific bench in the HC for TBM & shield separation and cleaning operations.
- It is assumed that there are lifting eyes or other type of lifting interface allowing the lifting and transportation to the separation bench by the crane through the use of winch hooks.
- It is assumed that there is enough clearance between the TBM and the shield for the HC manipulator and cutting tool to reach He and PbLi pipes linking them.

### 2.5.4.9. TBM splitting and packing into transport casks to be shipped (operation #9)

After visual and metric inspections, the TBM is cut in smaller elements which are introduced in transport casks and then shipped to the post irradiation exams facilities.

### Sequence

The TBM is located in a band sawing table. The tool cuts up the TBM into pieces which are introduced in drums by the HC manipulator. These drums are in turn introduced by the crane in shipping casks for irradiated material. The use of TN-MTR commercial shipping casks is considered here [Ghi 12]. In ITER, these casks would be carried by cranes and lifts in the Hot Cell to a level where they would be loaded on trucks to be shipped to the analysis facilities. The introduction of the TBM pieces into the drums and the introduction of the drums into the shipping cask will be the only operations to be made in the test facility.

Whether the cutting process (in the HCPB case) respects the breeder units or a hole is done in it to suck the ceramic pebbles is not defined. We assume as hypothesis that the cutting process respects the HCPB breeder units.

The collection of the pieces process is not defined (auxiliary tools, manipulator and crane roles, etc.).

We assume operations like visual and metric inspections before cutting have not to be demonstrated in the test facility.

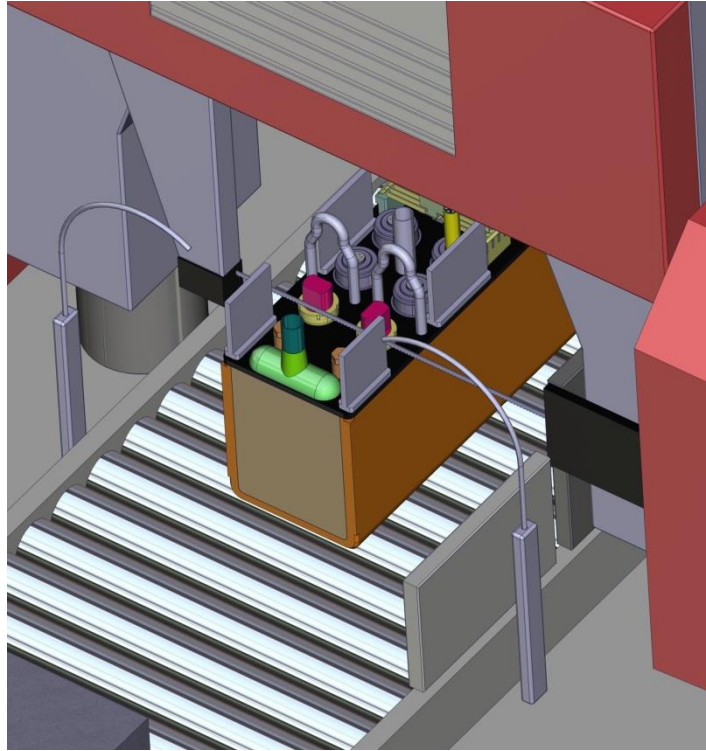


Fig. 35. Cutting of TBM by band sawing machine.

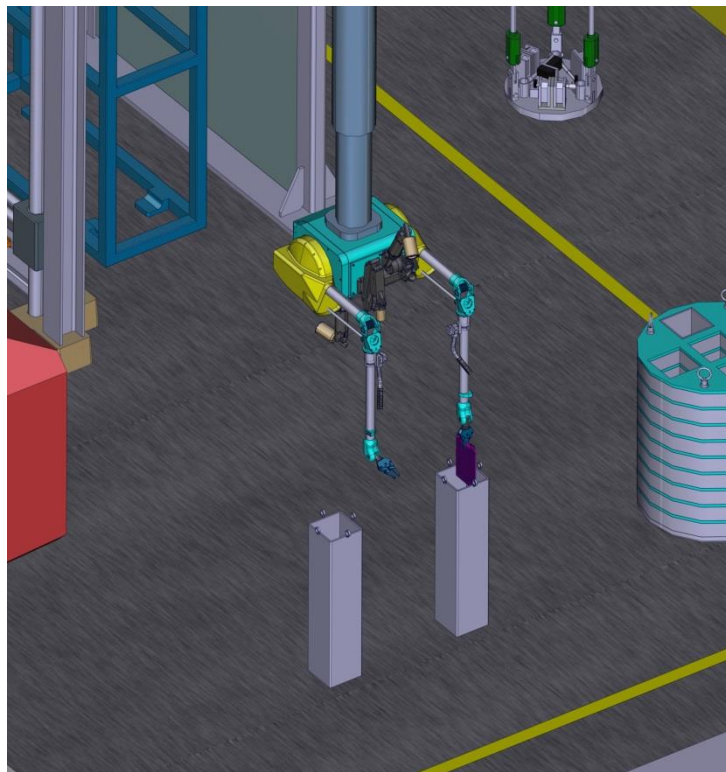


Fig. 36. Introduction of a TBM piece into a drum.

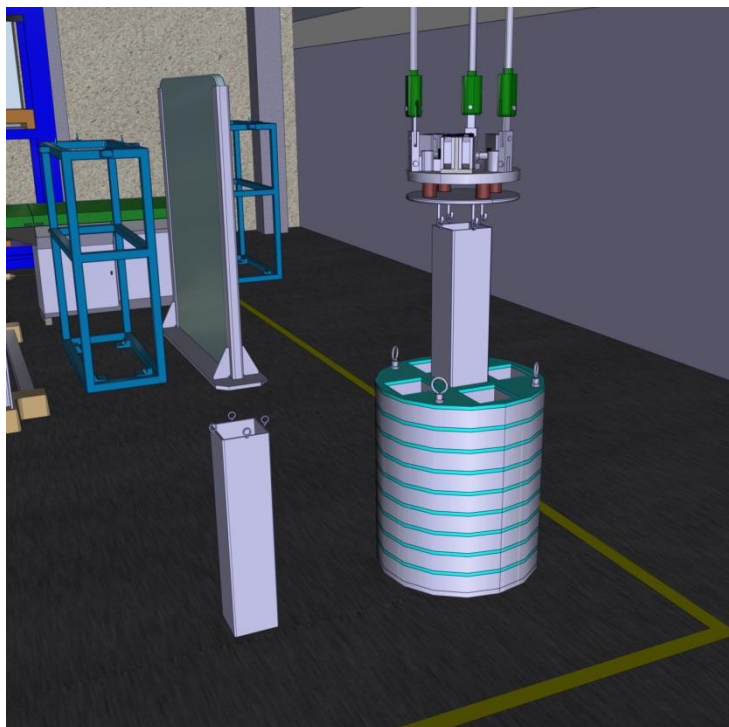


Fig. 37. Introduction of a drum into the shipping cask.

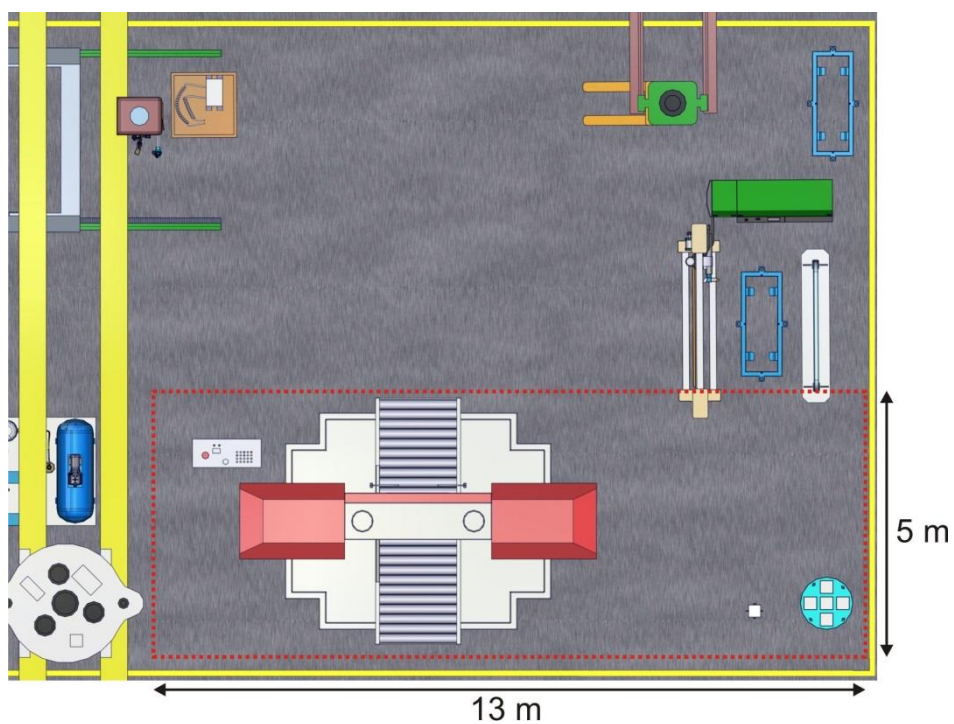


Fig. 38. Space needed for the operation (in red).

#### Space requirements

5 m x 13 m x 9 m (W, L, H). The space requirements are obtained from the dimensions of the band sawing machine, the drums and the shipping cask, as well as the space required for the

HC manipulator operation. The previous figure shows the space occupied by the equipment which takes part in the operation.

RH operation	TBM RH test facility requirements				
	Equipment		Structures	Auxiliary systems	Space (w, L, H)
	Not requiring a specific design	Requiring a specific design			
TBM splitting and packing into transport casks to be shipped	<ul style="list-style-type: none"> <li>- Band sawing machine.</li> <li>- Drums.</li> <li>- Clamping bench for drums.</li> <li>- Shipping cask.</li> <li>- Overhead rotating crane.</li> <li>- Telescopic mast.</li> <li>- HC manipulator.</li> </ul>	<ul style="list-style-type: none"> <li>- TBM mock-ups.</li> </ul>		<ul style="list-style-type: none"> <li>- Electric supply.</li> </ul>	5 m x 13 m x 9 m

Table 11. Operation #9 requirements.

### Hypotheses

- We assume the use of a band sawing machine as cutting tool [Bai 09].
- We assume the cutting process respects the breeder units. The breeder units will not be holed to suck the ceramic pebbles, as [Bai 09] proposes.
- We assume the use of the HC manipulator for moving the TBM pieces from the band sawing machine to the drums. We also assume the use of a gripping tool joined to the overhead travelling crane for introducing the drums into the shipping cask. The details of this process are not defined.
- We assume visual and metric inspections before cutting are not operations to be demonstrated in the test facility.

### 2.5.4.10. Introduction of the TBM & shield assembly into the port plug frame (operation #10)

The objective of this operation is to prepare the surface of the port plug flange and insert a new TBM & shield assembly into the port plug.

#### Operation sequence

The palletizing system places the polisher and its transfer box near the vertical positioning tool. The robotic manipulator grips the polisher and moves inside the PP. Once the polisher is positioned in the PP, the robotic manipulator moves it along the PP frame and removes the rests left of the O-ring. At the end, the robotic manipulator moves outside of the PP and leaves the polisher in its transfer box, which is put in the storage shelves by the palletizing system.

Then the overhead travelling crane coupling tool takes the lifting tool and moves to the new TBM & shield assembly shipping bench. The lifting tool picks the assembly up and introduces it into the port plug frame. After the lifting tool hooks uncouple from the shield lifting eyes, the tool moves out of the port plug.

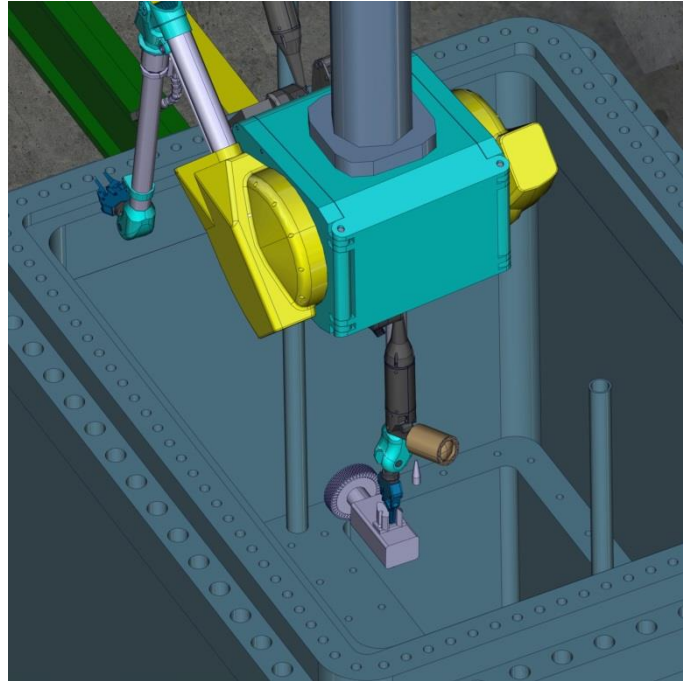


Fig. 39. Polishing of the port plug flange.

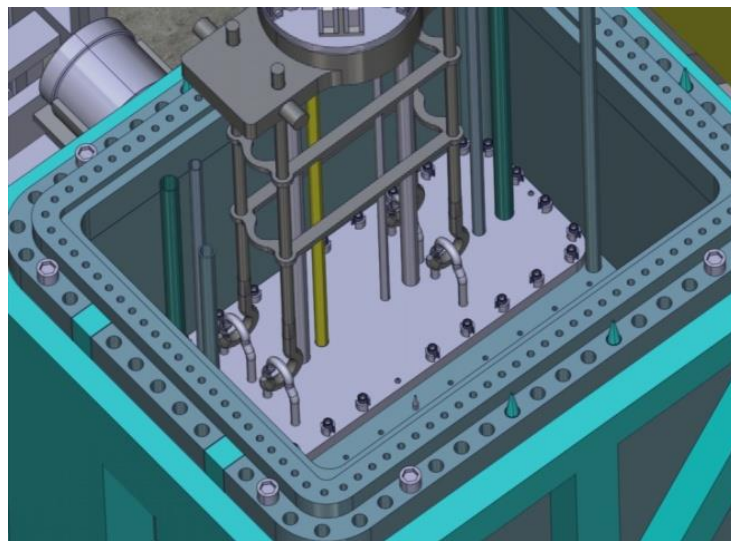


Fig. 40. Insertion of a TBM & shield assembly in the port plug.

### Space requirements

5 m x 3.5 m x 9 m (W, L, H). The width and the length have been obtained from the dimensions of the vertical positioning tool. The height (9 m) has been obtained from [Bed 08]. This height is the free operation space. It does not take into account the space taken by the crane itself.

RH Operation	TBM RH test facility requirements				
	Equipment		Structures	Auxiliary systems.	Space
	Not requiring a specific design	Requiring a specific design			

Introduction of TBM & shield assembly into the PP frame	<ul style="list-style-type: none"> <li>- Vertical positioning tool.</li> <li>- Lifting tool for TBM &amp; shield.</li> <li>- Polisher.</li> <li>- Overhead rotating crane.</li> <li>- Palletising system.</li> </ul>	<ul style="list-style-type: none"> <li>- TBM &amp; shield mock-ups.</li> <li>- PP mock-up.</li> </ul>	<ul style="list-style-type: none"> <li>- Supporting bench for new TBM &amp; shield assemblies.</li> <li>- Pallet shelves.</li> </ul>	<ul style="list-style-type: none"> <li>- Electric supply.</li> </ul>	5 m x 3.5 m x 9m
---	--	---	--	--	------------------

Table 12. Operation #10 requirements.

### Hypotheses

- The new TBM & shield assembly is supposed to come from factory inside a bench. This bench will be placed in the Hot Cell area. The bench is the same as the one used for the shield long term storage.
- It is assumed that the crane can rotate the TBM & shield assembly in order to achieve the correct orientation for insertion.
- It is assumed that the accurate alignment of the shield is achieved in the final phase of the insertion operation. It is allowed by several dowels integrated in the port plug flange. It is assumed that 4 dowels (one for each side of the flange) are enough to warrant the correct alignment of the captive bolts in the shield flange and the screwed holes in the PP flange.

### 2.5.4.11. Joining of the TBM & shield assembly to the port plug frame (operation #11)

After the insertion of the new TBM & shield assembly into the port plug, it must be joined to the PP to ensure an ultra-high vacuum sealing.

### Sequence

The palletizing system takes the pallet which contains the screwer from the storage shelves. It leaves it near the vertical positioning tool. The robotic manipulator takes the screwer from the pallet and moves inside the port plug, where screws the entire captive bolts of the shield flange to the port plug flange. Finally the robotic manipulator moves out of the PP and leaves the tool on its transfer box.

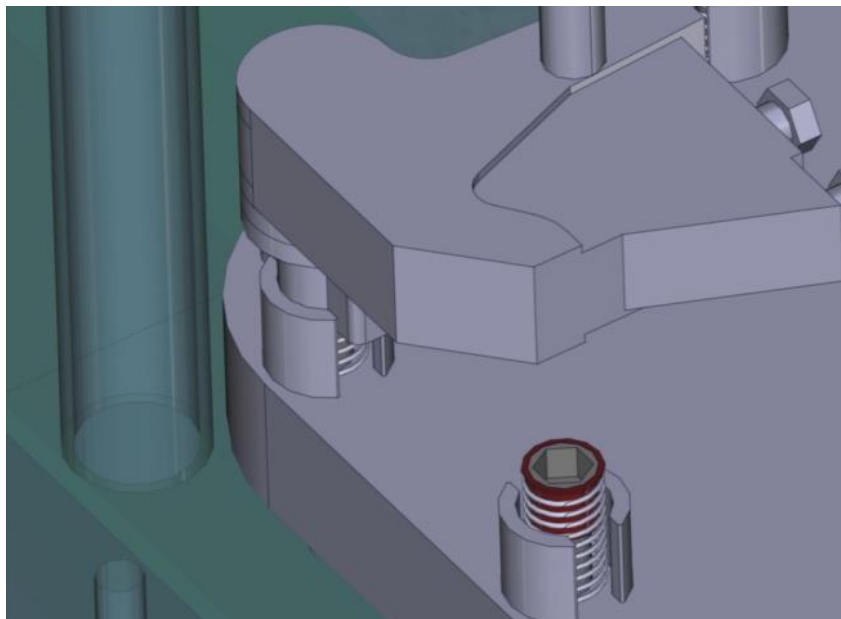


Fig. 41. Screwing of shield captive bolts to PP frame.

### Space requirements

6.5 m x 5.5 m x 9 m (W, L, H). The width and the length have been obtained from the dimensions of the vertical positioning tool and the pallet for the screwer, as well as the space needed for the operation of the HC manipulator. The height (9 m) has been obtained from [Bed 08]. This height is the free operation space. It does not take into account the space taken by the crane itself.

RH Operation	TBM RH test facility requirements				
	Equipment		Structures	Auxiliary systems.	Space
	Not requiring a specific design	Requiring a specific design			
Joining of TBM & shield assembly to port plug frame	<ul style="list-style-type: none"> <li>- Screwer.</li> <li>- Vertical positioning tool.</li> <li>- Palletising system.</li> <li>- Overhead rotating crane.</li> <li>- Telescopic mast.</li> <li>- HC manipulator.</li> </ul>	<ul style="list-style-type: none"> <li>- TBM &amp; shield mock-ups.</li> <li>- PP mock-up.</li> </ul>	<ul style="list-style-type: none"> <li>- Pallet shelves.</li> </ul>	<ul style="list-style-type: none"> <li>- Hydraulic supply.</li> <li>- Electric supply.</li> </ul>	6.5 m x 5.5 m x 9 m

Table 13. Operation #11 requirements.

### Hypotheses

- It is assumed that the shield flange and vacuum flange have captive bolts enabling their connection to the PP frame flange.
- It is assumed that the vacuum sealing in the shield to PP frame interface is achieved through two vacuum seals (Helicoflex metal gasket) which are integrated in the shield flange [Meu 07].
- It is assumed that a hydraulically driven screwer is used to unscrew captive bolts [Rio 10].

#### 2.5.4.12. Connection of the water pipes of the TBM & shield assembly from the main water system of the port plug and the vacuum vessel (operation #12)

Like operation #4, this operation is carried out with the PP inserted in the PP vertical positioning tool. The back of the PP is facing up.

### Sequence

Due to the lack of definition about how the interface circuit is welded to the PP and shield cooling circuits, we assume that the interface circuit is positioned in place by the crane. A guiding system could maybe be used to leave the interface circuit in position before the HC manipulator proceeds to align and weld the pipes in the connection points. Following the welding some kind of inspection would have to be carried out. It is assumed that water is not allowed in the Hot Cell and that this inspection method would not involve the use of water.

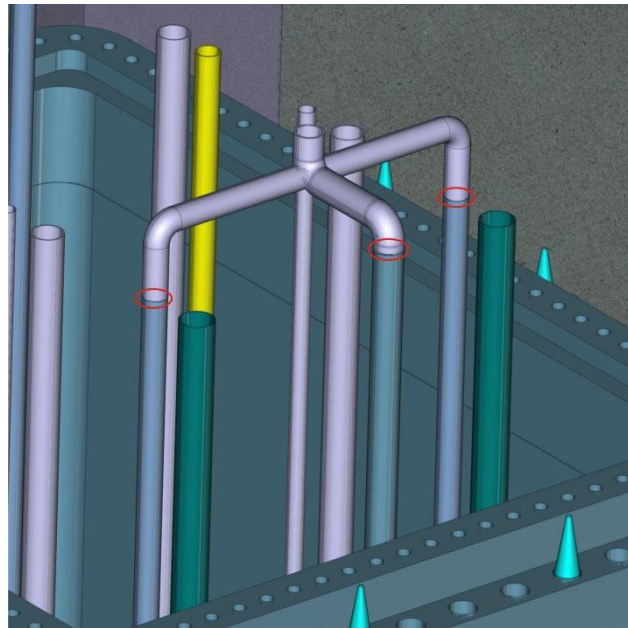


Fig. 42. Welding points for the inlet interface circuit between shields (left and right), port plug (centre) and vacuum vessel.

Space requirements

6.5 m x 5.5 m x 9 m (W, L, H). The width and the length have been obtained from the dimensions of the vertical positioning tool and the pallet for the welding tool, as well as the space needed for the operation of the HC manipulator. The height (9 m) has been obtained from [Bed 08]. This height is the free operation space. It does not take into account the space taken by the crane itself.

RH Operation	TBM RH test facility requirements				
	Equipment		Structures	Auxiliary systems	Space (W, L, H)
	Not requiring a specific design	Requiring a specific design			
Connection of water pipes of TBM & shield assembly from main water system of port plug and vacuum vessel	<ul style="list-style-type: none"> <li>- Vertical positioning tool.</li> <li>- Welding tool for HC manipulator.</li> <li>- Gripping tool for coupling tool.</li> <li>- Palletising system.</li> <li>- Overhead rotating crane.</li> <li>- Telescopic mast.</li> <li>- HC manipulator.</li> </ul>	<ul style="list-style-type: none"> <li>- PP mock-up.</li> <li>- TBM &amp; shield mock-ups.</li> </ul>	<ul style="list-style-type: none"> <li>- Pallet shelves.</li> </ul>	<ul style="list-style-type: none"> <li>- Electric supply.</li> </ul>	6.5 m x 5.5 m x 9 m

Table 14. Operation #12 requirements.

Hypotheses

- It is assumed that the First Wall/Blanket Primary Heat Transfer System feeds water in parallel to the PP and shield cooling circuits through a common interface circuit.
- The hypothesis of a geometry for the interface circuits similar as the one shown in Fig. 42 is assumed. The hypothesis that it is possible to successively align and weld the pipes of each interface circuit to the pipes of the PP and shield cooling circuits is assumed.
- It is assumed that the main PP and shield cooling circuits detritiation process has been carried out in the Port Cell (standard ITER procedure for port plugs).
- It is assumed that the manipulator has access to the cutting points despite the pipe forest coming out of the back of the shield.
- It is assumed that the interface circuit has design features (lifting eyes or other) allowing the crane to lift it.

### 2.5.4.13. Checking of vacuum sealing between the port plug and the TBM shield (operation #13)

It is not yet defined how the vacuum sealing of the PP to shield interface will be tested. This vacuum sealing test is necessary in order to assess the quality of the vacuum sealing operation performed by remote handling.

We assume that the vacuum sealing test is carried out by inserting the TBM PP in a test stand in which vacuum is created. In the ITER Hot Cell the test stands are only accessible from outside the Hot Cell. The PP can only be inserted in the test stand from the outside by means of a transfer cask and PP gripper. Within the RH TBM test facility the operation sequence would be as follows:

#### Operation sequence

Once the TBM is joined to the PP frame, the PP is transferred from the vertical positioning tool to the transfer cask. The PP is then transported to the test stand and inserted into it. We assume that the PP bolting to the test stand flange, the placing of the metallic gaskets and the vacuum flange is performed following the procedure described in operations #24 and #25 (use of gasket flange maintenance equipment). Then vacuum is created in the test stand and helium is blown (manually or by means of a He blowing tool installed in the test stand or handled by the HC manipulator) in the zone of the PP-shield vacuum seal. A helium detector connected to the test stand detects any He leak through the vacuum seal.

#### Space requirements

5 m x 21 m x 5 m (W, L, H). These space requirements have been obtained from the test stand dimensions (L = 5.9 m, W= 3.42 m, H = 3.42 m [Bea 08]) and the space occupied by the auxiliary systems of the test stand (vacuum system in our case) and the gasket flange maintenance equipment. In [Bar 08] an example of space occupied by a test stand and its auxiliary systems is shown. In the TBM RH test facility there will be no baking tests performed in the test stand so the surface occupied by the auxiliary systems will be smaller. These auxiliary systems could also be placed away from the test stand in dedicated rooms and connected to it through pipes. As a more conservative hypothesis we assume that they are placed next to the test stand. We assume that the space occupied by the vacuum system (pumps, He bottle, testing equipment) is 2 m x 2 m. We assume that the auxiliary systems are placed next to the test stand along its axis.

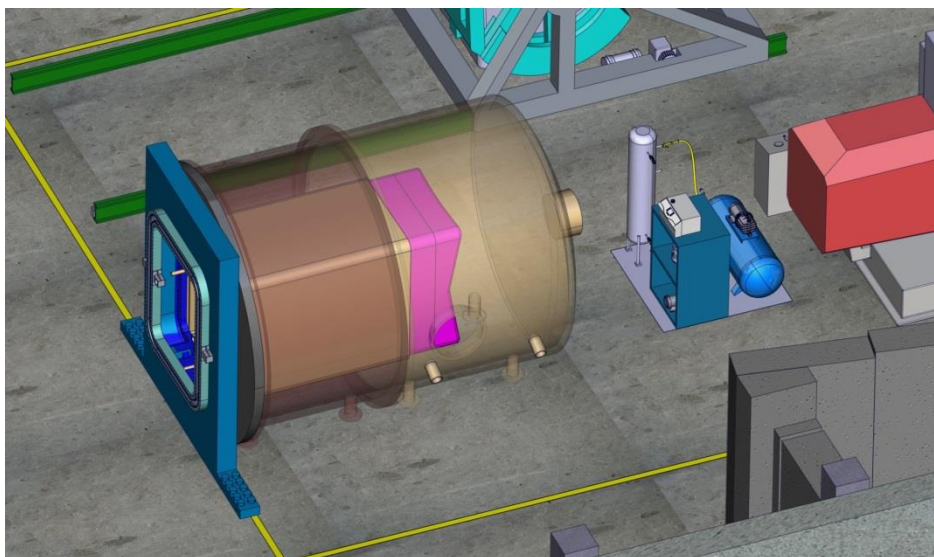


Fig. 43. Port plug inserted in test stand for vacuum sealing test.

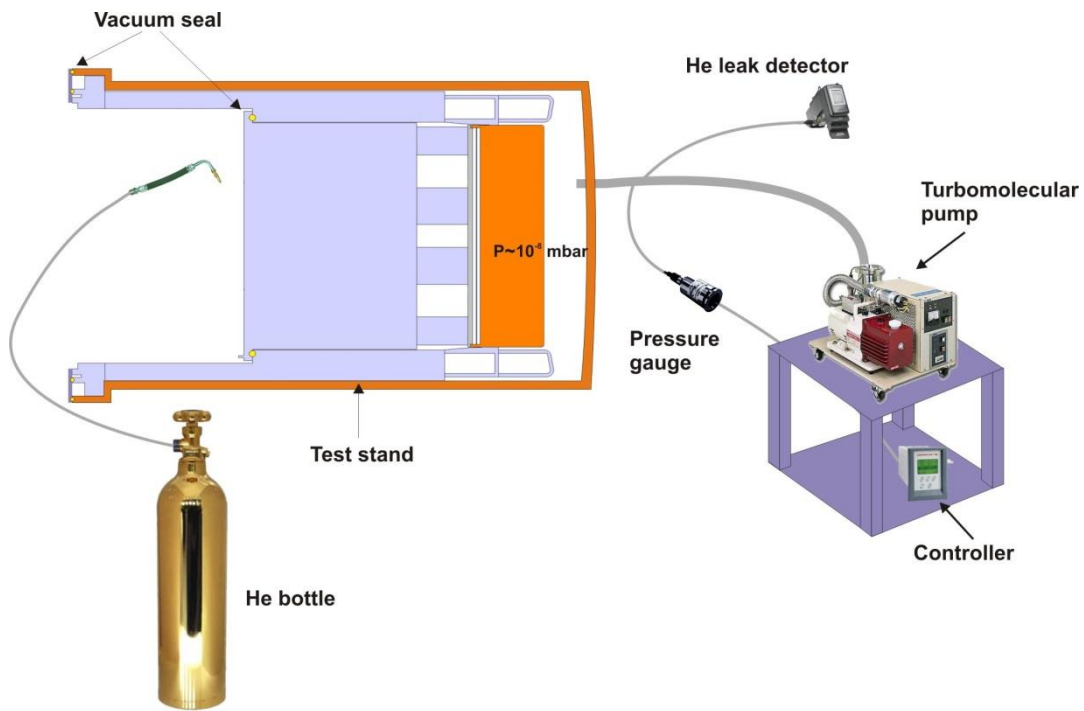


Fig. 44. Diagram of vacuum sealing test with test stand.

RH Operation	TBM RH test facility requirements				
	Equipment		Structures	Auxiliary systems	Space (W, L, H)
	Not requiring a specific design	Requiring a specific design			
Checking of vacuum sealing between port plug and shield	<ul style="list-style-type: none"> <li>- PP test stand.</li> <li>- Transfer cask.</li> <li>- Docking flange.</li> <li>- Gasket flange.</li> <li>- Vertical positioning tool.</li> <li>- Gasket flange maintenance equipment.</li> </ul>	<ul style="list-style-type: none"> <li>- TBM &amp; shield mock-ups.</li> <li>- PP mock-up.</li> </ul>	<ul style="list-style-type: none"> <li>- HC door.</li> </ul>	<ul style="list-style-type: none"> <li>- Vacuum testing system.</li> <li>- Gas supply.</li> <li>- Electric supply.</li> </ul>	5 m x 21 m x 5 m

Table 15. Operation #13 requirements.

Hypotheses

- It is assumed that the ITER vacuum test stand is used to test the vacuum sealing of the PP to shield interface [Bar 08].
- It is assumed that the test stand is only accessible from the outside of the Hot Cell (the PP needs to be inserted in the test stand from outside the Hot Cell).
- The vacuum sealing of the joint between the port plug and the test stand is achieved in the same way (metallic gasket and vacuum flange) as in the PP-port structures joint.

2.5.4.14. Checking of the water loop (operation #14)

**Vacuum leak test of welds**

It is necessary to carry out a vacuum leak test of the welds joining the PP cooling circuit and the shield cooling circuit to the interface circuit (see operation #12).

We assume the hypothesis that this vacuum leak test will be done by creating vacuum inside the whole PP, shield and interface cooling circuits and blowing He from outside the welds. A helium detector integrated in the vacuum system will detect any He leak over its threshold value. In order to carry out this test, the interface circuit should be designed with connection points for the vacuum system and valves for closing the open ends during the vacuum test.

A different option would consist in blowing He inside the cooling circuits and detecting a leak from inside to outside by sweeping the welds with a He sniffer. The assumed option is preferred over this one because it allows detecting smaller leaks and makes leak detection simpler as it does not involve looking for the leak point by sweeping the weld surface with the sniffer. In addition the same vacuum system used for testing the vacuum sealing of the PP to shield interface could be used.

### Operation sequence

At the beginning of the operation the PP is inserted in the vertical positioning tool. The interface circuit is already welded to the PP and shield cooling circuits. The HC manipulator, aided by some to be defined gripping device or feature, connects the vacuum system pipes (we assume they are flexible) to the connection points in the interface circuit. Then vacuum is created in the whole circuit. The HC manipulator takes a He blowing tool and brings it to each weld of the circuit. Helium is blown on welds, so any eventual leak is detected by the He detector integrated in the vacuum circuit.

### **Welds pressure test**

In addition to the vacuum leak test it will be necessary to carry out a weld pressure test by blowing gas inside the cooling circuits. During normal plasma operation, in the first wall/blanket primary heat transfer system, the water pressure is  $3 \text{ MPa} \pm 0.2 \text{ MPa}$  [Cor 11]. We assume a test pressure of 4.5 MPa. The use of water in the ITER HC is avoided in order to prevent tritium substitution in the water molecules. The goal of this test is to check the mechanical resistance of the welds. When the pressure test is finished a new leak test is necessary.

The operation sequence would be similar to that of the leak tests. In this case the interface circuit would be connected to the compressed inert gas system instead of the vacuum system.

### Space requirements

8.6 m x 5 m x 9 m. The width and length correspond to the dimensions of the vertical positioning tool and the vacuum system, as well as the distance between them. The height (9 m) has been obtained from [Bed 08]. This height is the free operation space. It does not take into account the space taken by the crane itself.

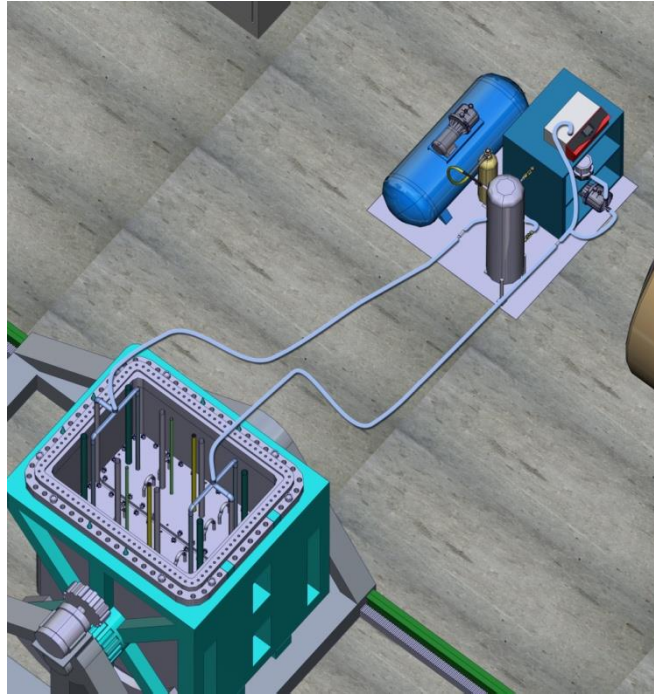


Fig. 45. Checking of the water loop.

RH Operation	TBM RH test facility requirements				
	Equipment		Structures	Auxiliary systems	Space (W, L, H)
	Not requiring a specific design	Requiring a specific design			
Checking of water loop	<ul style="list-style-type: none"> <li>- Vertical positioning tool.</li> <li>- He insufflating tool for HC manipulator.</li> <li>- Overhead rotating crane.</li> <li>- Telescopic mast.</li> <li>- HC manipulator.</li> </ul>	<ul style="list-style-type: none"> <li>- TBM &amp; shield mock-ups.</li> <li>- PP mock-up.</li> </ul>		<ul style="list-style-type: none"> <li>- Vacuum testing system.</li> <li>- Pneumatic supply.</li> <li>- Electric supply.</li> </ul>	8.6 m x 5 m x 9 m

Table 16. Operation #14 requirements.

### Hypotheses

- It is assumed that there is an interface circuit joining the PP and shield cooling circuits. This interface circuit would be welded later to the ITER First Wall/Blanket Primary Heat Transfer System.
- It is assumed that in ITER the vacuum leak tests and pressure tests of the welds joining the (hypothetical) interface circuit to the PP and shield cooling circuits will be done in the HC by RH.
- It is assumed that the interface circuit has design features (such as connection points allowing its connection to the vacuum system) allowing the leak tests to be performed.
- It is assumed that the leak vacuum test is performed by creating vacuum inside the PP, shield and interface circuits and blowing helium on the welded surfaces from the outside.
- It is assumed that the welds pressure test will be done in the HC by blowing compressed air at a pressure around 4.5 MPa.

#### 2.5.4.15. Transfer of the Pipe Forest & Bioshield Door assembly between the Storage Area and the Port Cell (operation #15)

The Pipe Forest & Bioshield Door assembly must be carried from the Storage Area and positioned in the Port Cell, previously to its installation in the Interspace. After removing the assembly from the Interspace, it must be placed again in the Storage Area.

### Operation sequence

The Air Transfer System takes the Pipe Forest & Bioshield Door assembly in the Storage Area and carries it to the Port Cell Area. After the Port Cell door opens, the ATS with the Pipe Forest & Bioshield Door assembly enters in the Port Cell. The ATS is positioned opposite the Bioshield Wall step by means of the viewing system.

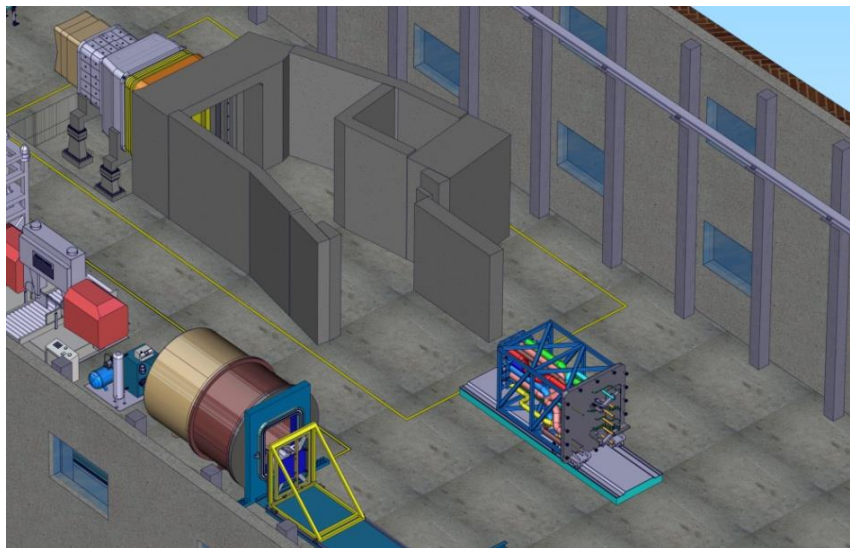
After removal of the Pipe Forest & Bioshield Door assembly from the Interspace, it is returned to the Storage Area by the ATS, following the reverse path of the previous sequence.

### Space requirements

25 m x 50 m x 6 m (W, H, L). The width and the length represent the maximum area occupied by the assembly during its transport between the Storage Area and the Port Cell. The height is taken from the dimensions of the Port Cell Structures and the Port Supports.

RH Operation	TBM RH test facility requirements				
	Equipment		Structures	Auxiliary systems	Space (W, L, H)
	Not requiring a specific design	Requiring a specific design			
Transfer of the Pipe Forest & Bioshield Door assembly between the Storage Area and the Port Cell.	- Air Transfer System.	- Pipe Forest & Bioshield Door assembly mock-up.	- Port Cell Structures.		25 m x 50 m x 6 m

Table 17. Operation #15 requirements.



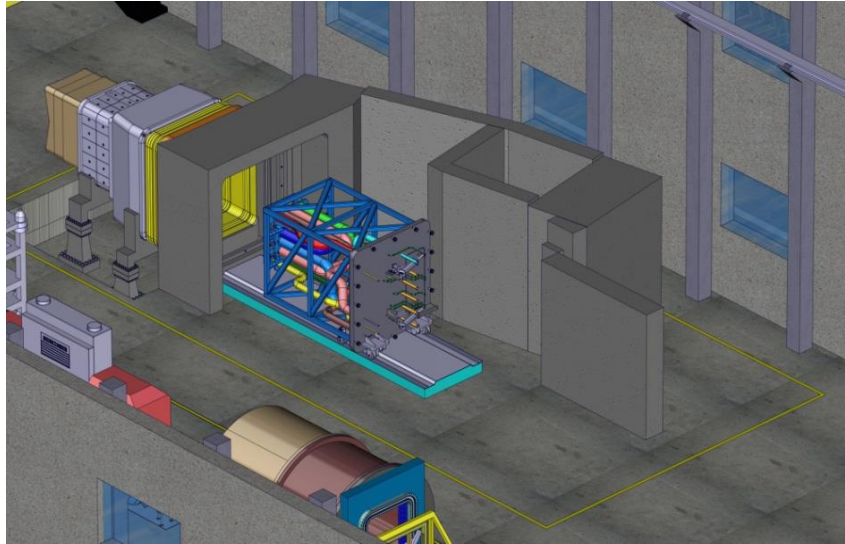


Fig. 46. Entry of Pipe Forest & Bioshield assembly in the Port Cell.

#### Hypotheses

- The Pipe Forest & Bioshield Door assembly is transported between the Storage Area and the Port Cell by means of the Air Transfer System [Gar 12].

#### 2.5.4.16. Installation/removal of the Pipe Forest & Bioshield Door in/from the Interspace (operation #16)

The Pipe Forest & Bioshield Door assembly is introduced in the Interspace. Through this operation, the pipes arising from the port plug and the Pipe Forest are aligned at Interface 2a. At the end, diagnostics/electric supply connectors are plugged at this point.

In ITER, the Bioshield is a concrete wall which acts as radiological shield. For that reason, it must be closed during the operation of the tokamak. Once fitted to the fixed wall, the moveable Bioshield Door must be joined by means of captive bolts.

The removal operation, which is the reverse of the installation operation, must be also demonstrated in the Test Facility.

#### Operation sequence

The Air Transfer System is correctly placed on the Port Cell floor. The assembly begins to move on the ATS rails by means of its rear wheels. Later, the front wheels of the Pipe Forest assembly reach the connecting duct rails. The intermediate wheels of the Pipe Forest assembly are folded when Bioshield doorstep is reached.

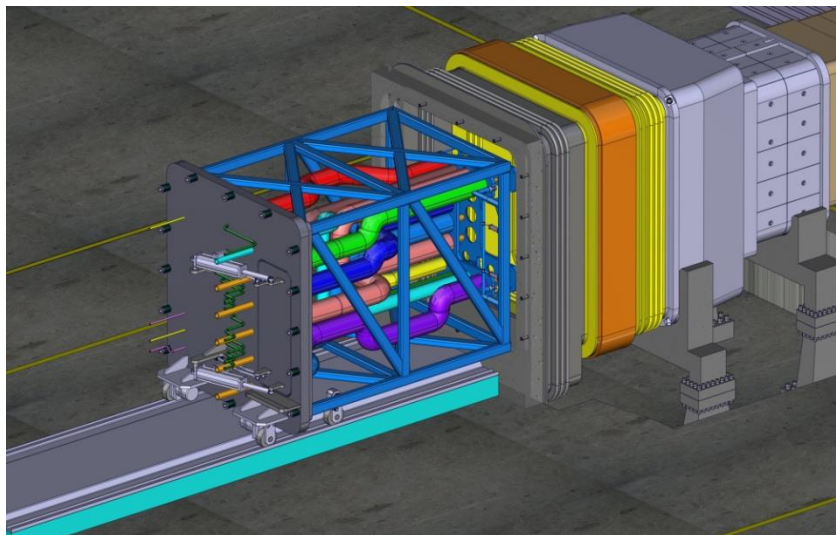


Fig. 47. Pipe Forest & Bioshield Door assembly moving on ATS rails towards the Interspace (Port Cell Structures not shown).

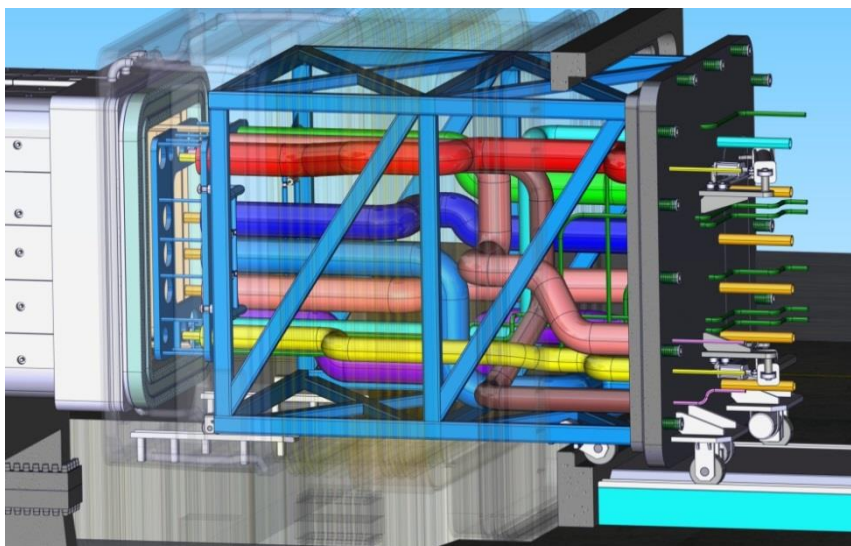


Fig. 48. Folding of the intermediate wheels.

The Bioshield Door fits in the Bioshield Wall and the diagnostics/electric supply connectors are connected. At the same time, pipes are aligned by the alignment system at IF2a.

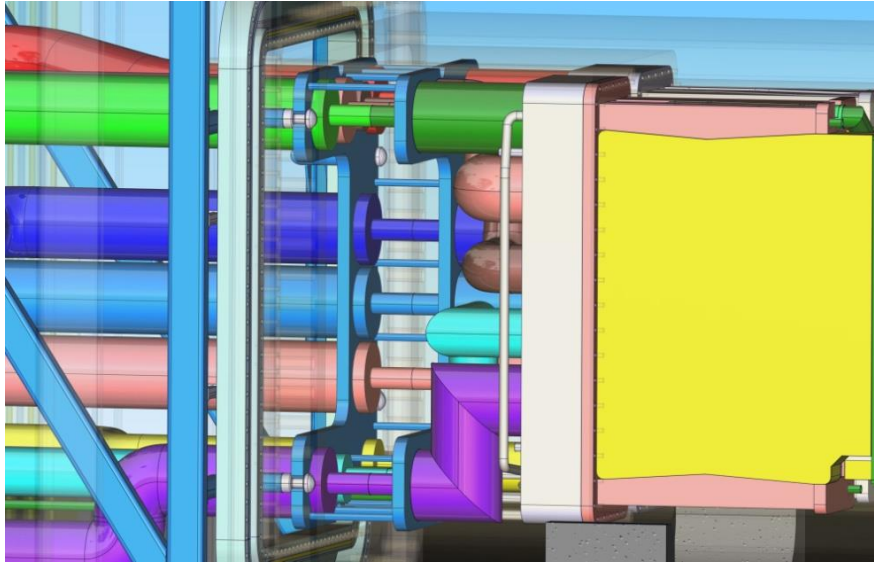


Fig. 49. Pipes alignment at IF2a.

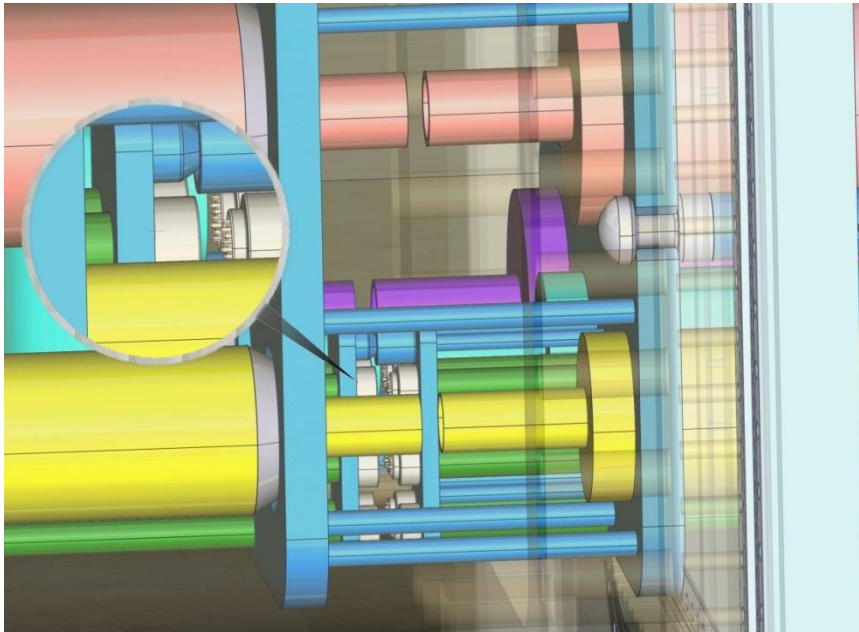


Fig. 50. Plugging of diagnostics/electric supply connectors.

The Bioshield Door is fitted to the Bioshield Wall. Captive bolts are screwed/unscrewed by hands on (the used tool is not defined yet).

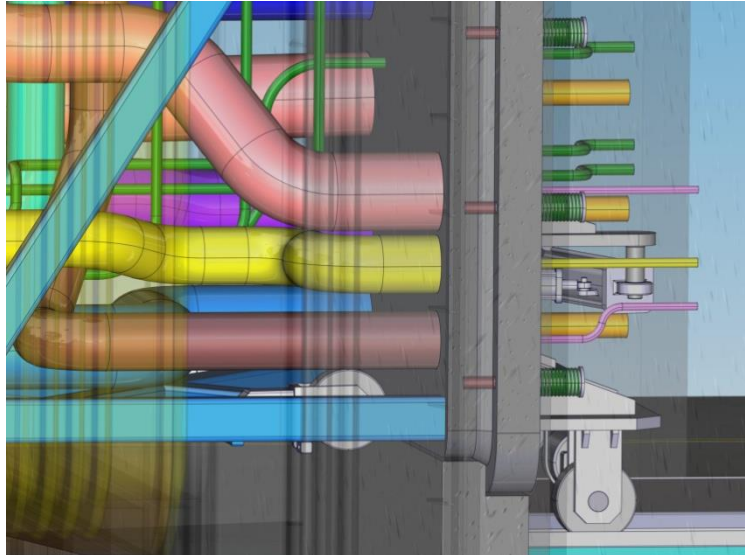


Fig. 51. Screwing of captive bolts.

During the removal of the Pipe Forest & Bioshield assembly, the followed operations sequence is the reverse of the previous one.

#### Space requirements

10.5 m x 24 m x 6 m (W, H, L). The width and the length represent the dimensions of the Port Cell Area. The height is taken from the dimensions of the Port Cell Structures and the Port Supports.

RH Operation	TBM RH test facility requirements				
	Equipment		Structures	Auxiliary systems	Space (W, L, H)
	Not requiring a specific design	Requiring a specific design			
Installation/removal of the Pipe Forest & Bioshield Door in/from the Interspace	- Air Transfer System.	- Pipe Forest & Bioshield Door assembly mock-up.	- Port structures. - Port Cell structures.		10.5 m x 24 m x 6 m

Table 18. Operation #16 requirements.

#### Hypotheses

- The Pipe Forest is introduced in the Interspace by means of a 6-wheel system. Some of the wheels are motor-driven, which are located behind the Bioshield Door [Gar 12].
- The wheels are guided by rails located on both the ATS and the Port Structures, without interfering with the Bellows.
- The two front wheels are placed at a higher level than the four rear ones, avoiding height discontinuity between ATS base and Port base, in such a way that before the Pipe Forest arrives to the port, it is supported only on the rear wheels.
- The intermediate wheels are collapsible, so that when they reach the height of the Bioshield Door they fold back and remain in that position by small hydraulic cylinders. At this point, the front wheels have already been supported on the Port Structures rails so the Pipe Forest can continue to its final position.
- To ensure the piping alignment of the Pipe Forest with both TBMs (HCPB and HCLL) on the Interface 2a, the Pipe Forest has an alignment system based on two plates joined together by rigid joints. The first plate has circular holes in which are inserted the pipes of the Pipe Forest. The second plate, which is located nearer the Port Plug, has tapered holes to achieve the correct coupling of the TBM pipes.

- Some elements with the same taper as in the previous plate are installed in each TBM pipe, providing the self-alignment of the TBM pipes with those of the Pipe Forest.
- The gap between the first and second plate on the alignment system is enough to allow the robotic arm to gain access to all the pipes and perform the IF2a maintenance operations.
- It is assumed that captive bolts are used to join the Bioshield Door to the Bioshield Wall.
- It is assumed that human access to the rear part of the Bioshield Door (once fitted to the fixed wall) is allowed to carry out the screwing/unscrewing of the captive bolts.

#### 2.5.4.17. Transfer of the RH Platform Unit between the Storage Area and the Port Cell (operation #17)

The RH Platform Unit is a mobile equipment designed to allow the remote handling equipment in charge of performing maintenance operations at IF2a (cutting, welding and inspection of pipes; installation/removal of thermal insulations), gaining access to such interface.

The RH Platform Unit must be transferred from the Storage Area to the Port Cell after the installation of the Pipe Forest & Bioshield assembly, and placed next to it, for the subsequent movement of the deployable carrier through the Bioshield window and the Pipe Forest corridor.

##### Operation sequence

The Air Transfer System takes the RH Platform Unit in the Storage Area and carries it to the Port Cell Area. After Port Cell door opens, the ATS with the RH Platform Unit entries in the Port Cell. Finally, the ATS positions in front of the Bioshield Door, with the deployable carrier opposite the Bioshield Window, and leaves the RH Platform Unit on the Port Cell floor.

After carrying out installation operations at IF2a, it must be removed by the ATS to allow the installation of the Ancillary Equipment Unit. The sequence is repeated during the removal of the TBS equipment from the Port Cell and the Interspace.

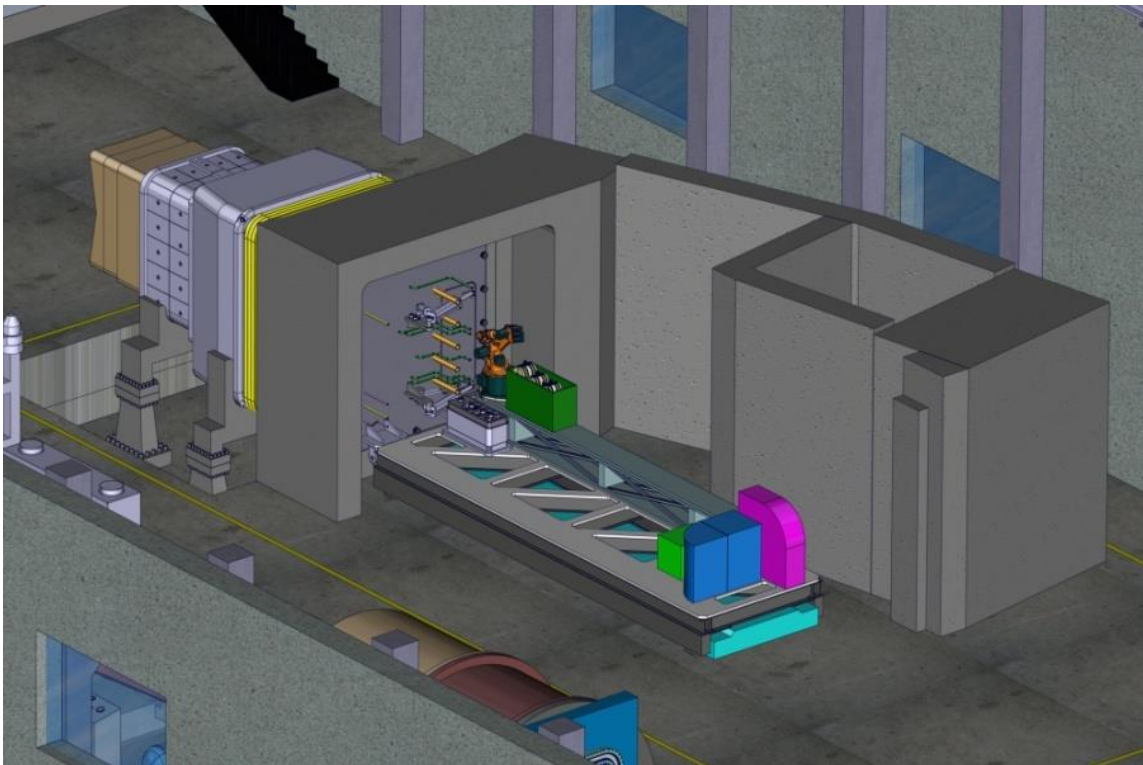


Fig. 52. Entry of the RH Platform Unit in the Port Cell.

### Space requirements

25 m x 50 m x 6 m (W, H, L). The width and the length represent the maximum area occupied by the RH Platform Unit during its transport between the Storage Area and the Port Cell. The height is taken from the dimensions of the Port Cell Structures and the Port Supports.

RH Operation	TBM RH test facility requirements				
	Equipment		Structures	Auxiliary systems	Space (W, L, H)
	Not requiring a specific design	Requiring a specific design			
Transfer of the RH Platform Unit between the Storage Area and the Port Cell	- Air Transfer System. - RH Platform Unit.	- Pipe Forest & Bioshield Door assembly mock-up.	- Port Cell structures.		25 m x 50 m x 6 m

Table 19. Operation #17 requirements.

### Hypotheses

- The RH Platform Unit contains all the remote handling equipment which is needed to carry out the maintenance operations at Interface 2a [Gar 12].
- The RH Platform Unit is transported between the Storage Area and the Port Cell by means of the Air Transfer System [Gar 12].

#### 2.5.4.18. Welding of pipes in IF2a (operation #18)

The welding process in IF2a requires the alignment of the pipe lines. The orbital welding technology proposed to weld the pipes requires strict tolerances between the relative positions of the ends of the pipe lines, a prerequisite for ensuring the quality of the weld seams made.

According to [Bed 07] the welds would be done by a sophisticated welding tool attached to the Port Cell robotic arm by means of the interface standard tool. This welding tool is able to hold the ends of the tubes to be welded, using two clamps and weld them using an orbital welding device (OWT, orbital welding technology). Both mechanisms, clamps and OWT, are available as a compact single head for the robotic arm.

This tool is used to weld the interface 2a pipes by orbital TIG (tungsten inert gas). The tube welding tool is water-cooled and includes weaving function and automatic arc length control (by controlling the arc voltage).

The radial positioning is based on two gripping jaws forced with springs. The geometry of the jaws is created to adapt to the different tube diameters. The axial positioning is provided by strong springs, which are opened with pneumatic cylinders.

### Operation sequence

The RH Platform Unit is placed on the Port Cell floor, next to the Bioshield Door. When the Bioshield window opens, the robotic arm takes the welding end effector from the tool rack and gains access to the IF2a through the Pipe Forest corridor by means of the deployable carrier. Here, the welding end effector welds all the pipes. Finally, the deployable carrier returns the robotic arm returns to the rear part of the RH Platform Unit, where it leaves the welding end effector in the tool rack.

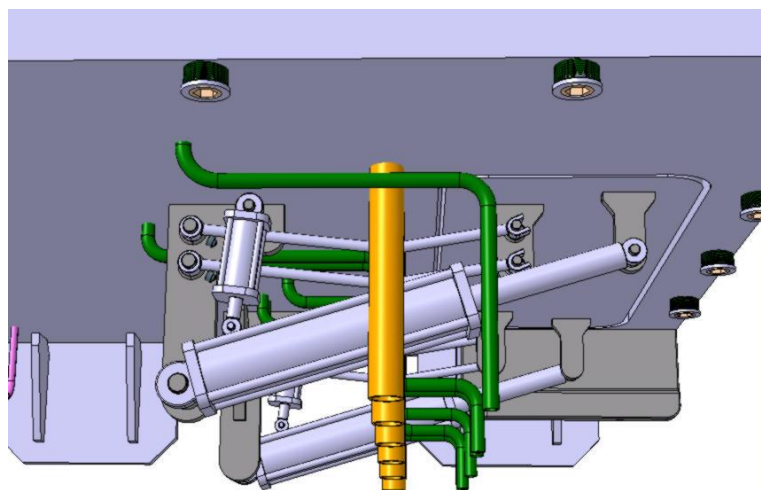


Fig. 53. Bioshield window mechanism.

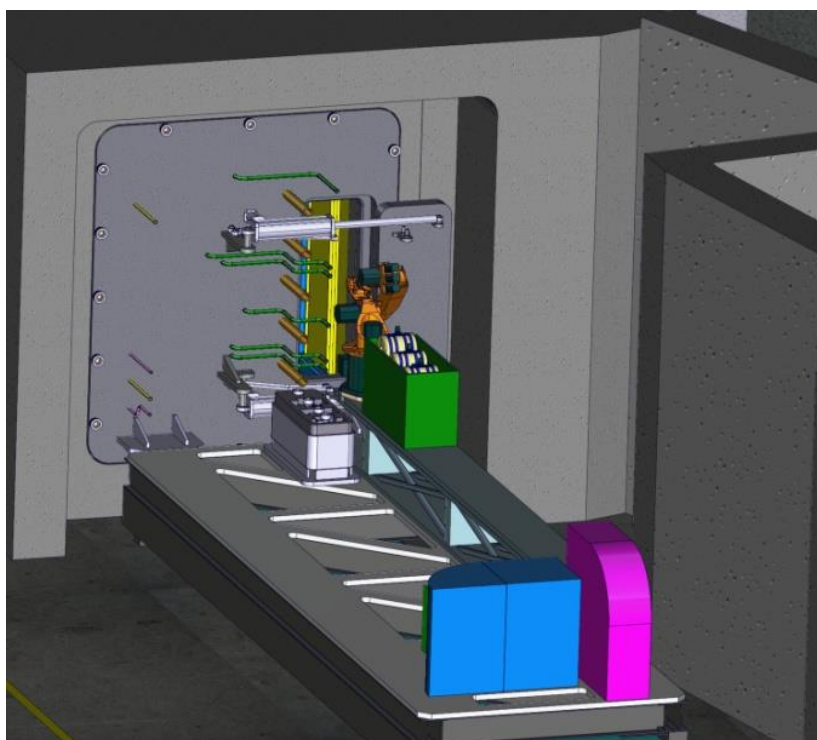


Fig. 54. The robotic arm goes through the Bioshield window.

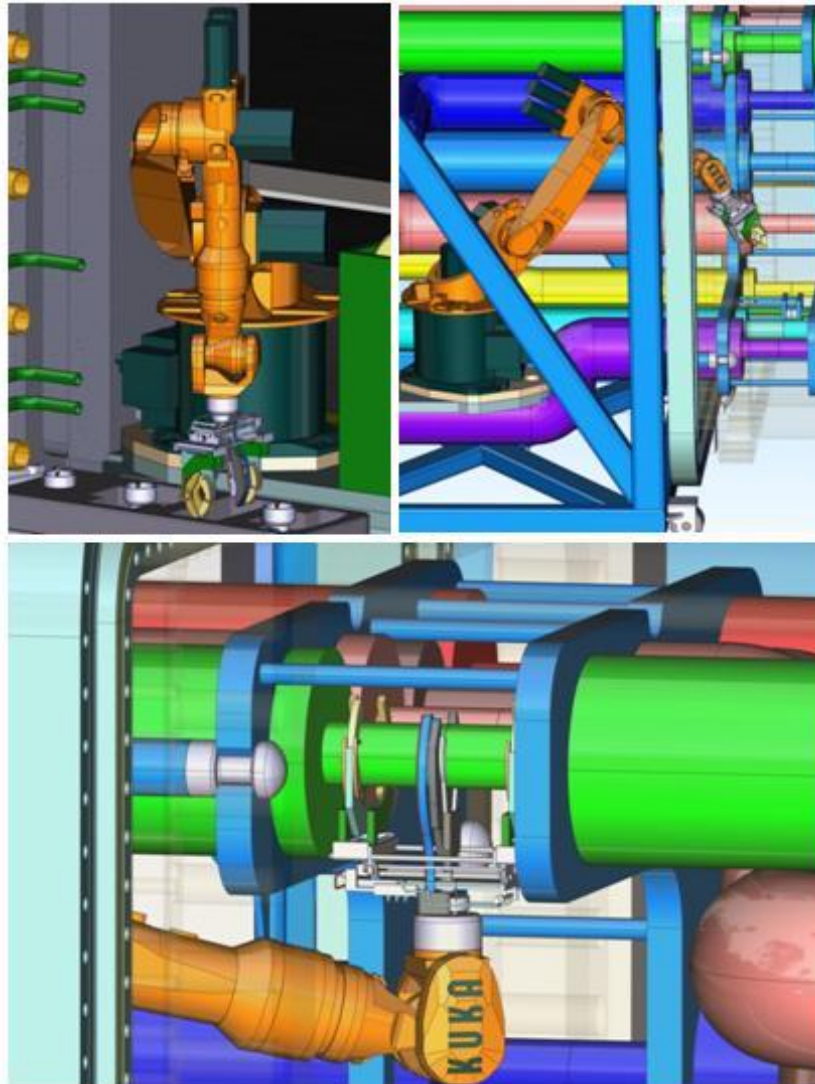


Fig. 55. 1) The robotic arm takes the welding tool from the tool rack. 2) The robotic arm gains access to the IF2a. 3) Welding of a pipe at IF2a.

#### Space requirements

10.5 m x 24 m x 6 m (W, H, L). The width and the length represent the dimensions of the Port Cell Area. The height is taken from the dimensions of the Port Cell Structures and the Port Supports.

RH Operation	TBM RH test facility requirements				
	Equipment		Structures	Auxiliary systems	Space
	Not requiring a specific design	Requiring a specific design			
Welding of pipes at interface 2a	<ul style="list-style-type: none"> <li>- PC robotic arm.</li> <li>- RH platform unit.</li> <li>- Welding tool for PC robotic arm.</li> </ul>	<ul style="list-style-type: none"> <li>- TBM &amp; shield mock-ups.</li> <li>- PP mock-up.</li> <li>- Pipe Forest &amp; Bioshield Door assembly mock-up.</li> </ul>	<ul style="list-style-type: none"> <li>- Port structures.</li> <li>- Port Cell structures.</li> </ul>	<ul style="list-style-type: none"> <li>- Electric supply.</li> <li>- Pneumatic supply.</li> <li>- Gas supply.</li> </ul>	10.5 m x 24 m x 6 m

Table 20. Operation #18 requirements.

Hypotheses

- The conceptual design of the welding tool is taken from [Bed 07].
- The robotic arm can access to the IF2a through a window in the Bioshield Door and a corridor in the Pipe Forest [Bed 07].
- The welding material is inside a cartridge attached to the welding tool. Otherwise it would be necessary to provide a system that would run along the robotic arm. The only advantage of this option would be to avoid changes of the cartridges caused by the depletion of the available content on the cartridge.
- The welding operations are restricted by the available space around each space. It is assumed that the welding tool is capable of welding pipes with different diameters.

**2.5.4.19. Inspection of weld beads in IF2a (operation #19)**

The inspection of the weld beads made in IF2a is necessary to avoid possible failures in service, which would cause unscheduled stops in ITER.

The inspection method is based on the technology of ultrasonic inspection (phased-array technology). This technique is optimal for quick and reliable inspections in a short space of time, as in a single inspection it is capable to detect any defect, regardless of its orientation.

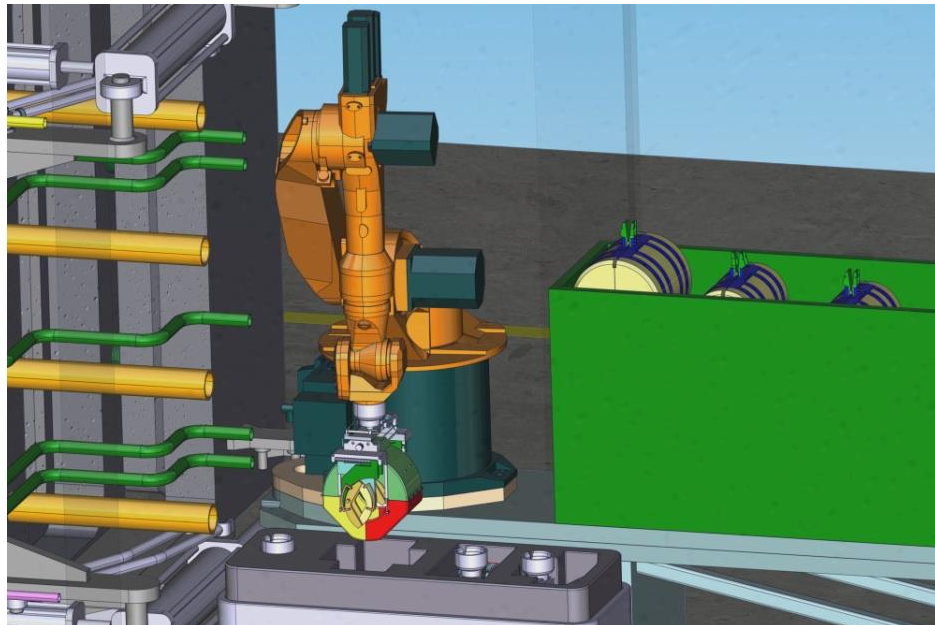


Fig. 56. The robot takes the inspection final effector from the tool rack.

The strategy used in the inspection operation is similar to that used for other operations in IF2a: using a head specifically designed for this function. This head is coupled to the robotic arm through the interface tool. The arm must guarantee the access of the head to the different beads, place it in the position to perform the task and provide the necessary supplies for operation.

In particular, this head has an orbital mechanism with two multi-element probes, arranged so that it can inspect the full length of the entire string with a 180 degree turn. Since it is planned that the probes perform the operation submerged in water (for better contact and emission-reception of the signal), the rest of the system consists in a water-sealing cover so that the orbital tool can act submerged in water. The arm should therefore provide water to this volume and air for the sweep after the inspection. The design it is not yet defined in detail.

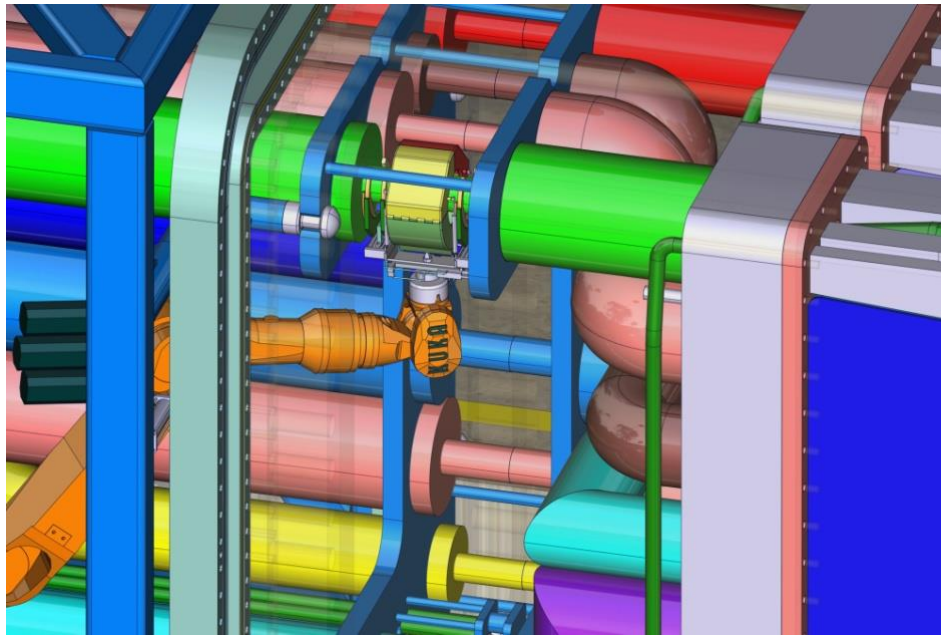


Fig. 57. Inspection of a welding bead at IF2a.

Before performing ultrasonic leak inspections in all the welds in IF2a, it is necessary to check their tightness. At present, the procedure is not established. It can be done in a similar way as the weld pressure tests for the PP water loop (operation #14), by blowing gas inside the PbLi and He circuits.

#### Operation sequence

The robotic arm takes the inspection end effector from the tool rack in the RH Platform Unit. The robotic arm goes through the Bioshield window and the Pipe Forest corridor by means of the deployable carrier and reaches IF2a, where it proceeds to check the welds. Finally, the robotic arm returns to the Port Cell and leaves the inspection tool in the tool rack.

#### Space requirements

10.5 m x 24 m x 6 m (W, H, L). The width and the length represent the dimensions of the Port Cell Area. The height is taken from the dimensions of the Port Cell Structures and the Port Supports.

RH Operation	TBM RH test facility requirements				
	Equipment		Structures	Auxiliary systems	Space
	Not requiring a specific design	Requiring a specific design			
Inspection of welding beads in IF2a	<ul style="list-style-type: none"> <li>- PC robotic arm.</li> <li>- RH platform unit.</li> <li>- Inspection tool.</li> </ul>	<ul style="list-style-type: none"> <li>- TBM &amp; shield mock-ups.</li> <li>- PP mock-up.</li> <li>- Pipe Forest &amp; Bioshield Door assembly mock-up.</li> </ul>	<ul style="list-style-type: none"> <li>- Port structures.</li> <li>- Port Cell structures.</li> </ul>	<ul style="list-style-type: none"> <li>- Electric supply.</li> <li>- Water supply.</li> <li>- Pneumatic supply.</li> <li>- Vacuum testing system.</li> </ul>	10.5 m x 24 m x 6 m

Table 21. Operation #19 requirements.

#### Hypotheses

- It is assumed the method and tool for ultrasonic inspection of welds which is proposed in [Bed 07].

- The robotic arm is capable of providing water supply to the head required for the operation of the ultrasound probe through the interface tool. If not, the arm should have an alternative water supply or may be necessary to use a specific arm for this task.
- The description of the cover that contains the volume of water for the inspection tool is not defined with big detail. It is assumed that this does not imply any change to the installation.
- It is assumed that it is necessary to test the tightness of welded joints of the He and PbLi circuits before proceeding with the ultrasonic inspection of the beads.
- It is assumed that the tightness tests shall be conducted by introducing pressurized helium inside the PbLi and He circuits. The connection points of the pneumatic supply are not established.

#### 2.5.4.20. Installation and removal of thermal insulations at IF2a (operation #20)

The IF2a pipes must be thermally insulated during the TBM operation. Therefore the use of remotely installable/removable thermal insulations is proposed [Bed 07]. In respect to Interfaces 2b and 3, which are placed outside the Bioshield, the installation/removal of the insulations is made by hands-on.

As the operation in IF2a has to be performed by remote handling, the installation/removal of the insulations must be as easy as possible. A clip made by 2 insulated jaws which is kept closed around the pipes thanks to a torsion spring is proposed. A RH compatible claw enables to open the clip, with a simple pneumatic parallel gripper. When the clip is opened the arm can remove it, and store it in a specific container.

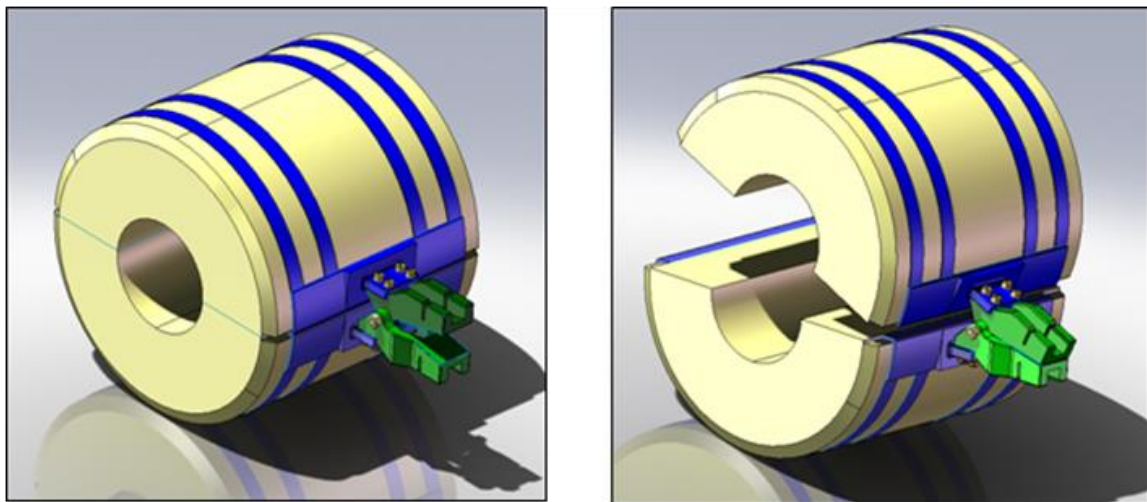


Fig. 58. Standalone thermal insulation.

#### Operation sequence

The robotic manipulator takes the claw end effector from the tool rack. The deployable carrier positions the robotic manipulator and the insulations container next to IF2a. The robotic manipulator takes each insulating module and installs it in the correct pipe.

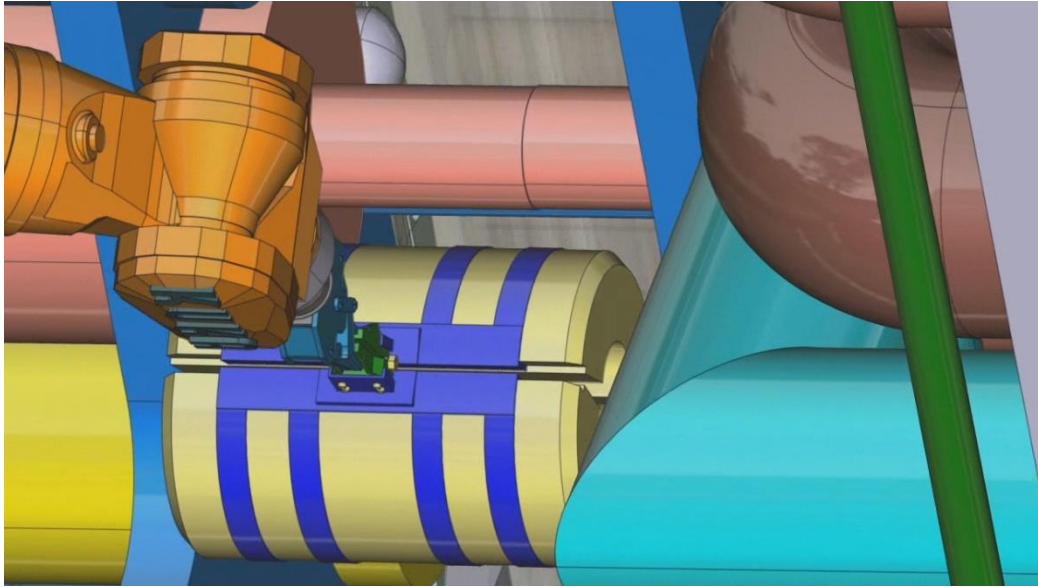


Fig. 59. Installation of an insulating module.

The removal sequence is the reverse of the installation sequence.

#### Space requirements

10.5 m x 24 m x 6 m (W, H, L). The width and the length represent the dimensions of the Port Cell Area. The height is taken from the dimensions of the Port Cell Structures and the Port Supports.

Operation	TBM RH test facility requirements				
	Equipment		Structures	Auxiliary systems	Space
	Not requiring a specific design	Requiring a specific design			
Installation and removal of the IF2a pipes thermal insulations	<ul style="list-style-type: none"> <li>- PC robotic arm.</li> <li>- Insulating modules.</li> <li>- RH Platform Unit.</li> </ul>	<ul style="list-style-type: none"> <li>- TBM &amp; shield mock-ups.</li> <li>- PP mock-up.</li> <li>- Pipe Forest &amp; Bioshield Door assembly mock-up.</li> </ul>	<ul style="list-style-type: none"> <li>- Port structures.</li> <li>- Port Cell structures.</li> <li>- Insulating modules container.</li> </ul>	<ul style="list-style-type: none"> <li>- Electric supply.</li> </ul>	10.5 m x 24 m x 6 m

Table 22. Operation #20 requirements.

#### Hypotheses

- The conceptual design of the thermal insulators has been adapted from the one proposed in [Kel 10].
- There is a specific container to store the insulating modules, which is placed on the deployable carrier, behind the robotic manipulator.

#### 2.5.4.21. Constriction/unconstriction of pipes at IF2a (operation #21)

The rear plate of the Pipe Forest alignment system –hence the Pipe Forest pipes- is fixed to the Pipe Forest frame by several bars which fit in plate slots. This position is maintained to perform maintenance operations at IF2a. The fixing bars can be extracted from the plate slots by means of hydraulic cylinders, in a way that the plate is maintained only by the rigidity of the pipes. In ITER, this state is required to accommodate the displacement of the Vacuum Vessel and the thermal expansion of pipes.

Operation sequence

*Constriction*

The four hydraulic cylinders which drive the fixing bars of the Pipe Forest frame expand, so the ends of the bars fit in the plate slots. In this position, maintenance operations at IF2a can be carried out.

*Unconstriction*

The cylinders compress so that the ends of the fixing bars leave the plate slots, so the plate is only supported by the pipes rigidity. In ITER, this state is required to accommodate the displacement of the Vacuum Vessel and the thermal expansion of pipes.

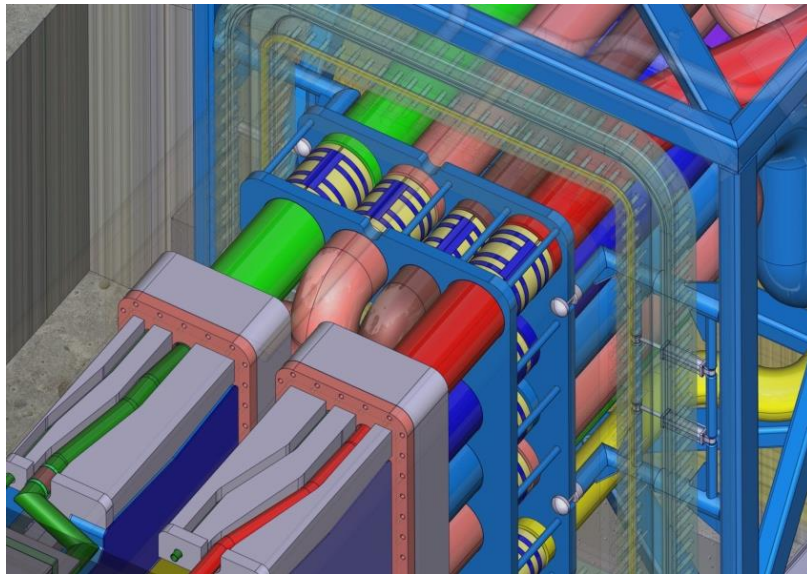


Fig. 60. Constricted IF2a pipes.

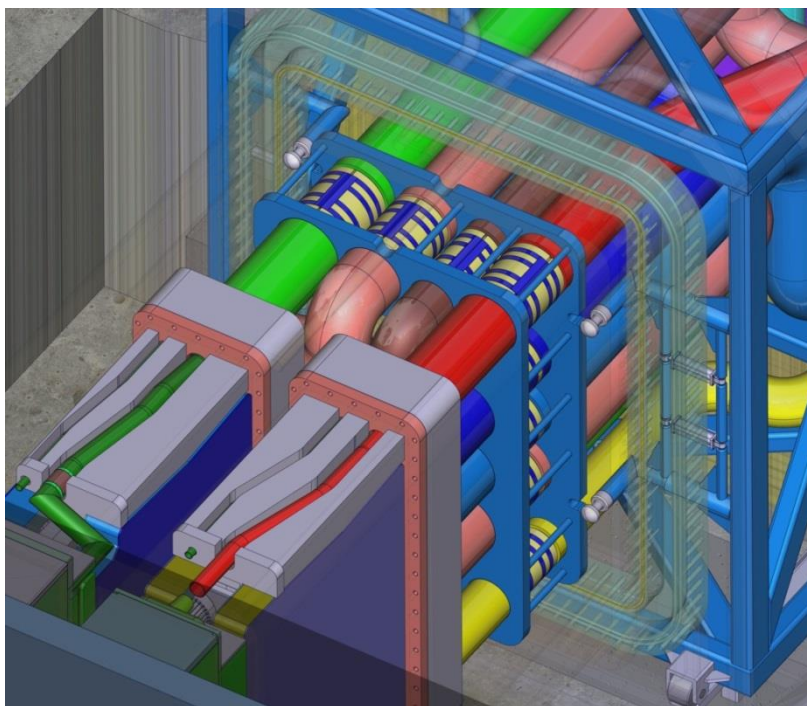


Fig. 61. Unconstricted IF2a pipes.

### Space requirements

10.5 m x 24 m x 6 m (W, H, L). The width and the length represent the dimensions of the Port Cell Area. The height is taken from the dimensions of the Port Cell Structures and the Port Supports.

Operation	TBM RH test facility requirements				
	Equipment		Structures	Auxiliary systems	Space
	Not requiring a specific design	Requiring a specific design			
Constriction/unconstriction of pipes at IF2a		<ul style="list-style-type: none"> <li>- TBM &amp; shield mock-ups.</li> <li>- PP mock-up.</li> <li>- Pipe Forest &amp; Bioshield Door assembly mock-up.</li> </ul>	<ul style="list-style-type: none"> <li>- Port structures.</li> <li>- Port Cell structures.</li> </ul>	<ul style="list-style-type: none"> <li>- Electric supply.</li> </ul>	10.5 m x 24 m x 6 m

Table 23. Operation #22 requirements.

### Hypotheses

- The need of a system to constrict/unconstrict the pipes at IF2a is assumed [Gar 12].

#### 2.5.4.22. *Cut of pipes in IF2a (operation #22)*

In this operation, the pipes in IF2a (previously welded for normal operation) that join the Pipe Forest to the port plug are cut.

The technology selected for this task is plasma cutting. According to [Bed 07], the advantages of this method are versatility, speed and limited thermal involvement of the material to be cut. The tool design consists of an interchangeable head with two components, a clamp and an orbital tool which houses two plasma torches. This configuration allows positioning and cutting around the pipe diameter in a 180 degree turn of the orbital tool.

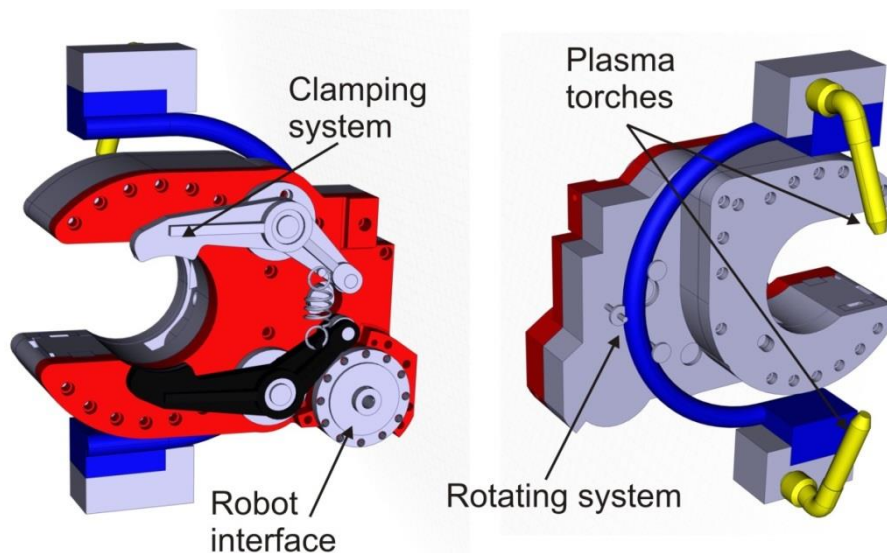


Fig. 62. Cutting head.

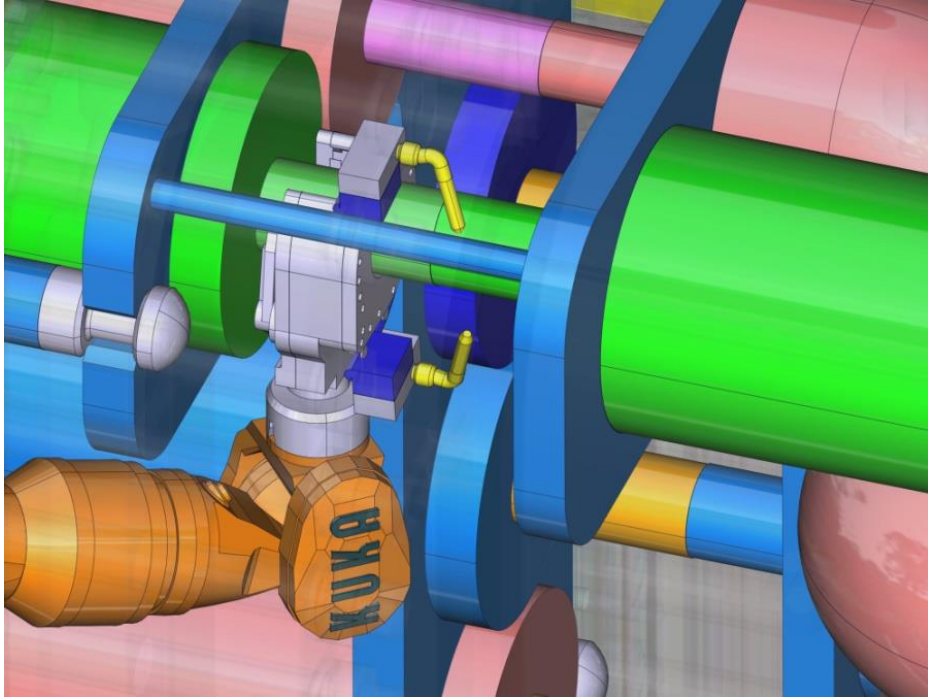


Fig. 63. Cut of a pipe at IF2a.

The demonstration of this operation should consist in the sequential access to all the pipes of interface 2a and their cut. The change of the torches should also be part of the demonstration of the operation. The different diameters of the pipes of interface 2a suggest a possible need to change the torches in order to avoid possible overheating of the pipe if the plasma torch is bigger than required.

#### Space requirements

10.5 m x 24 m x 6 m (W, H, L). The width and the length represent the dimensions of the Port Cell Area. The height is taken from the dimensions of the Port Cell Structures and the Port Supports.

RH Operation	TBM RH test facility requirements				
	Equipment		Structures	Auxiliary systems	Space
	Not requiring a specific design	Requiring a specific design			
Cut of pipes in IF2a	- PC robotic arm. - Cutting tool	- TBM & shield mock-ups. - PP mock-up. - Pipe Forest & Bioshield assembly mock-up.	- Port structures.	- Electric supply. - Gas supply. - Vacuum system for dust extraction.	10.5 m x 24 m x 6 m

Table 24. Operation #22 requirements.

#### Hypotheses

- It is assumed plasma cutting is chosen as cutting method, as is it proposed in [Bed 07].
- It is assumed that there is no need for a system to collect particles generated during cutting. It is assumed that the plasma torch only generates vaporized waste. However, it is possible that such a system will eventually be necessary because there will be a layer of solidified PbLi inside the pipes where liquid metal circulates which could generate a release of tritium in the PC during cutting.

#### 2.5.4.23. Installation/removal of the AEU in/from the Port Cell (operation #23)

As previously mentioned in this Chapter, the Ancillary Equipment Unit (AEU) is a mobile device which contains several components of the Test Blanket System, in a way that allows the fast integration of these components by reducing the installation processes. The AEU must be installed in the Port Cell after the installation of the Pipe Forest & Bioshield Door assembly, which includes transporting from the Storage Area, placing and alignment in the Port Cell, and joining the AEU systems to the Pipe Forest (Interface 2b) and the rest of the TBS equipment which is placed outside the Port Cell (Interface 3).

The task finishes with the removal of the AEU and its transport back to the Storage Area, to allow the subsequent removal of the Pipe Forest & Bioshield Door assembly.

Joining and disjoining operations will be carried out by hands-on, so they do not need to be demonstrated in the Test Facility. Therefore a mock-up of Interface 3 pipes should not be included in the Facility.

##### Operation sequence

The Air Transfer System takes the AEU in the Storage Area and carries it to the Port Cell. The ATS places the AEU opposite the Bioshield Door, such that AEU pipes are aligned with the rest of the Port Cell pipes with enough accuracy. Once the alignment is achieved, the ATS leaves the AEU on the Port Cell floor and returns to the Storage Area. The installation of the AEU finishes with the welding of pipes at Interface 2b, the inspection of the welds and the setting up of thermal insulations, which are carried out by hands-on (not demonstrated in the Test Facility).

The removal sequence includes the removal of thermal insulations, the cut of pipes at Interface 2b (hands-on: not demonstrated in the Test Facility) and the transport of the AEU to the Storage Area by the ATS.

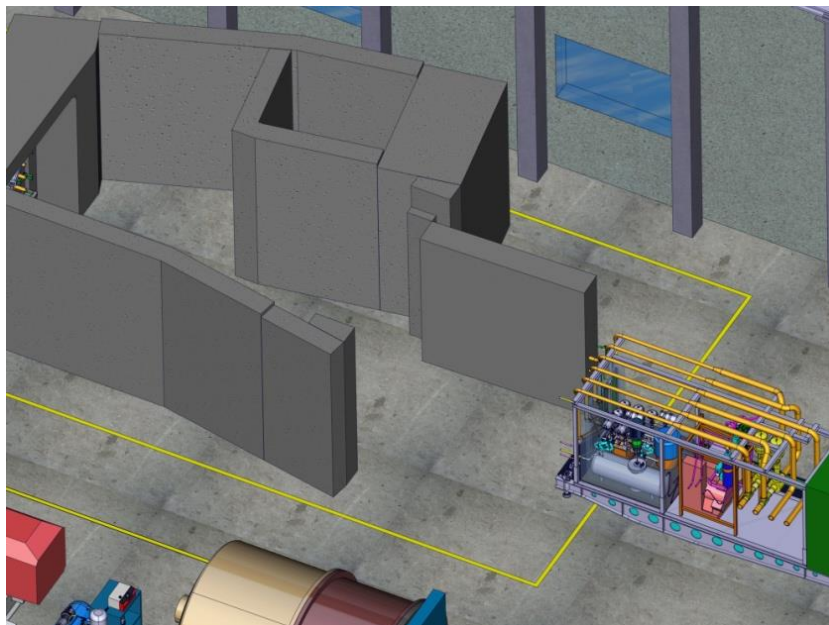


Fig. 64. Entry of the AEU in the Port Cell.

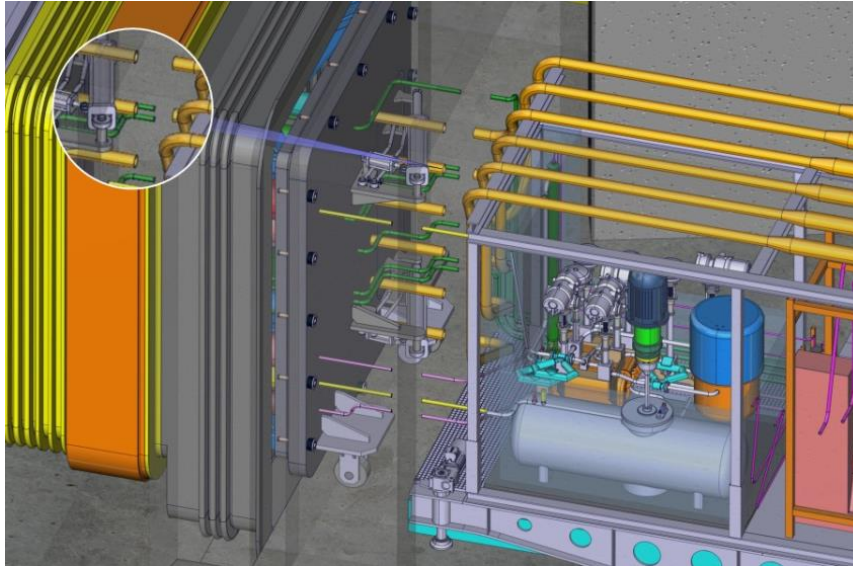


Fig. 65. Alignment of pipes at IF2b.

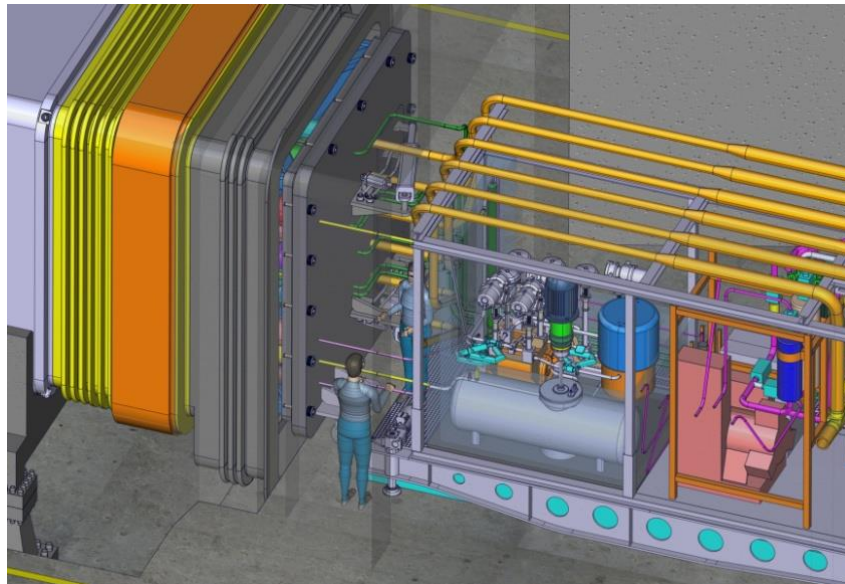


Fig. 66. Hands-on operations at IF2b.

Space requirements

25 m x 50 m x 6 m (W, H, L). The width and the length represent the maximum area occupied by the AEU during its transport between the Storage Area and the Port Cell. The height is taken from the dimensions of the Port Cell Structures and the Port Supports.

RH operation	TBM RH test facility requirements				
	Equipment		Structures	Auxiliary systems	Space
	Not requiring a specific design	Requiring a specific design			
Installation/removal of the AEU in/from the Port Cell	- Air transfer system.	- AEU mock-up. - Pipe Forest & Bioshield Door assembly mock-up.	- Port Cell structures.	- Electric supply. - Water supply. - Gas supply.	25 m x 50 m x 6 m

Table 25. Operation #23 requirements.

### Hypotheses

- The Air Transfer System (ATS) must be able to align the AEU pipes to the Pipe Forest and Port Cell pipes with enough accuracy to allow carrying out the pipe maintenance operations by hands-on.
- There is no Interface 3 pipes mock-up in the Facility.

#### 2.5.4.24. Installation/removal of the Port Plug in/from the Port (operation #24)

It must be noted that the demonstration of the installation of the Port Plug is not part of the objectives of the TBM RH test facility. The demonstration of this operation is not the responsibility of Domestic Agencies, but of ITER Organization. However this operation needs to be performed in the test facility if the same PP and TBM mock-ups are going to be used in the Port Cell and Hot Cell operation areas. Therefore the requirements arising from the performing of this operation are listed.

The Port Plug installation sequence starts with the following conditions:

- 1) The Interspace and the Port Cell are clear (without AEU, Pipe Forest & Bioshield Door assembly or any other components).
- 2) The Docking Flange is placed around the Port Extension flange.
- 3) The Maintenance Door is closing the Port.

The installation process begins with the arrival of the Transfer Cask (TC) to the PC.

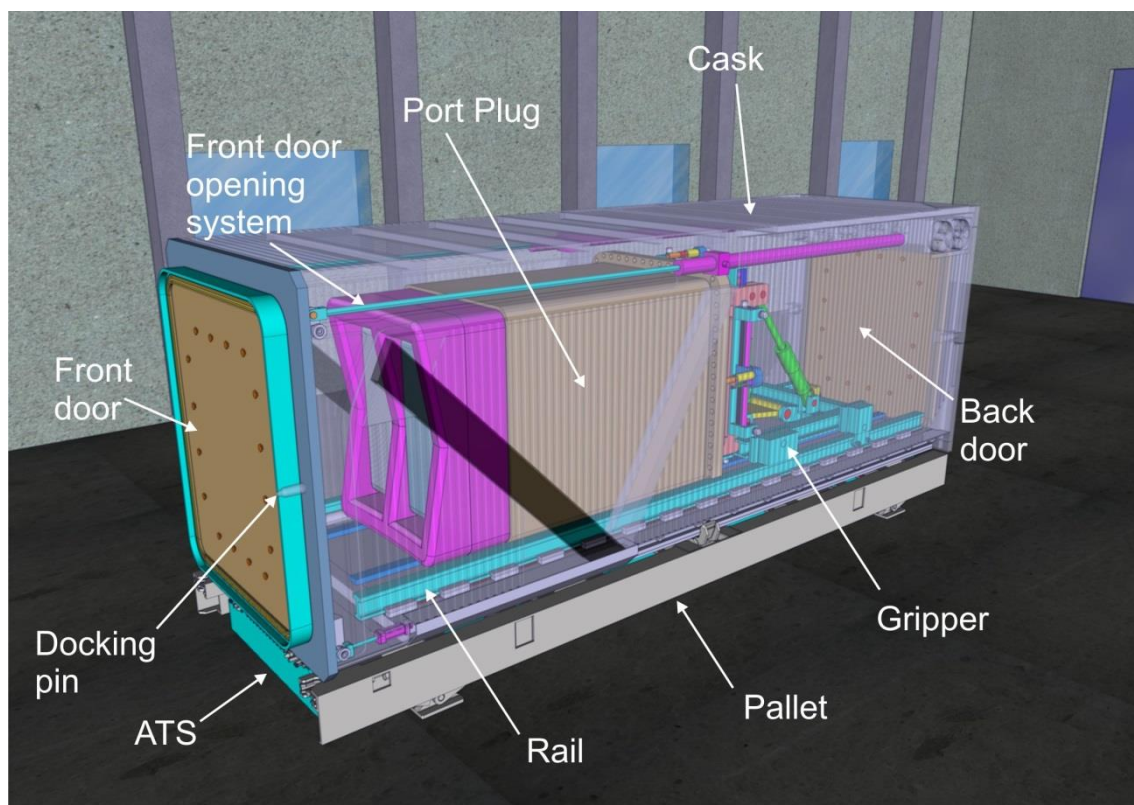


Fig. 67. Transfer cask.

The first step of this process is the docking of the transfer cask. The positioning system for the docking of the TC is formed by two fixed positioning supports (docking pins), two forks and the docking flange. The fixed positioning supports (docking pins) are two slender vertical cylinders, about 0.5 m high, located on the PC, close to the Vacuum Vessel, while the forks are two devices on the front of the TC that grasp the docking pins. The docking flange is a removable piece that is placed around the flange of the extension of the port and serves as a limit for the

positioning of the container of the TC. It has two lugs placed on its sides where the TC inserts two projecting cylinders situated in the front of the container.

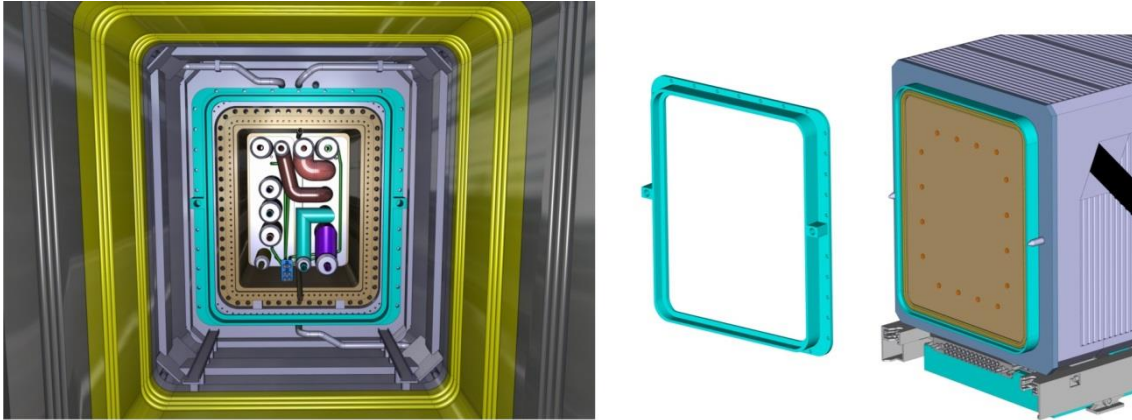


Fig. 68. Docking flange (blue) installed in the port. Docking flange lugs and the two pins of the TC that go into the lugs.

The coupling of the forks to the docking pins guarantees the relative position between TC and PC with enough precision to make possible the electrical connection between them through the port service connector.

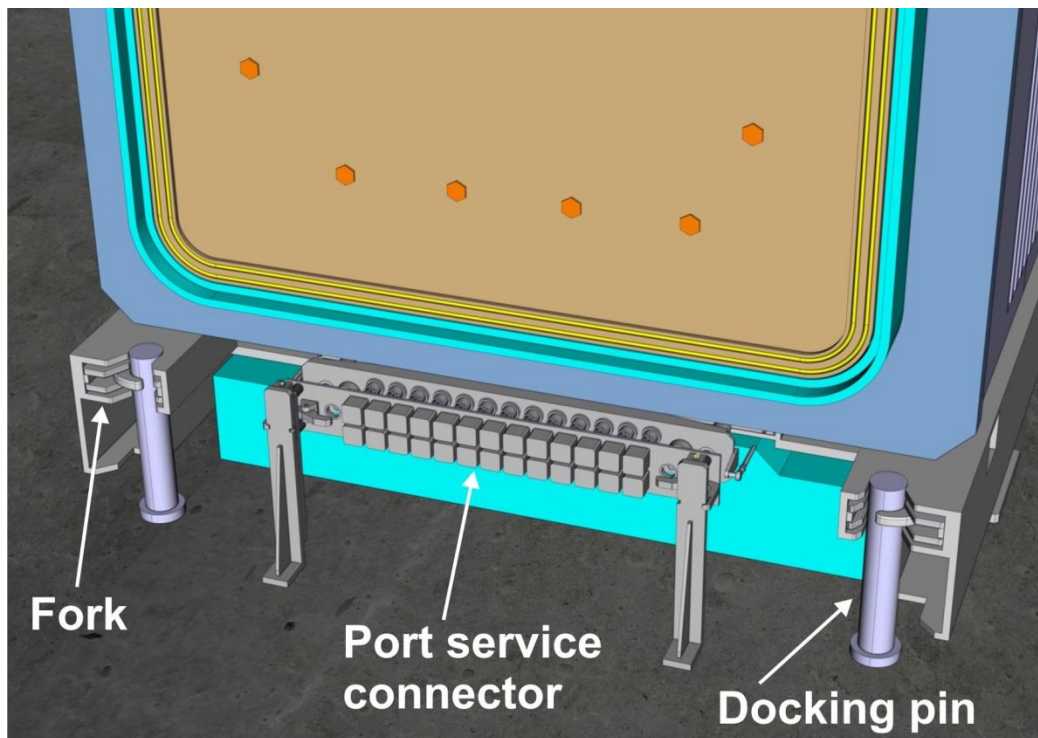


Fig. 69. Docking system.

The ATS system allows more precise movements to finalise the alignment of the TC. Once the ATS is connected to the port service connector, the four supports of the pallet lower down, supporting the weight of the entire TC. The inclination of the TC can be adjusted if necessary to align it with the port.

Once the pallet is correctly aligned, the cask moves through the biological shield, the cryostat and the bellows, sliding on the pallet. The front of the cask reaches the docking flange and the

projecting cylinders are inserted into the lugs. This sliding movement is driven by means of an electric motor, a rack-pinion system and a set of rails and rollers.

Once the cask is deployed and coupled to the docking flange, both the maintenance door (door in the Port) and the TC door are lifted at the same time and put in the upper part of the cask. The maintenance door and TC door set is called “double seal door”.

The rails of the TC (where the Port Plug wheels slide on) move until they contact with the rails of the Port Extension flange. When this operation is finished, the gripper holding the port plug slides along the rails and installs the Port Plug. The movement is aided by the Helping Cantilever System in order to guarantee the stability of the set (TC+PP). The helping cantilever system assures that the PP is supported once it leaves the TC. It consists of two rollers in the PP and two rails in the Port Extension. At the end of these rails there are two notches to house the rollers, leaving 20 mm space between the port plug and the port extension. The Helping Cantilever System is a proposal of CEA in [9].

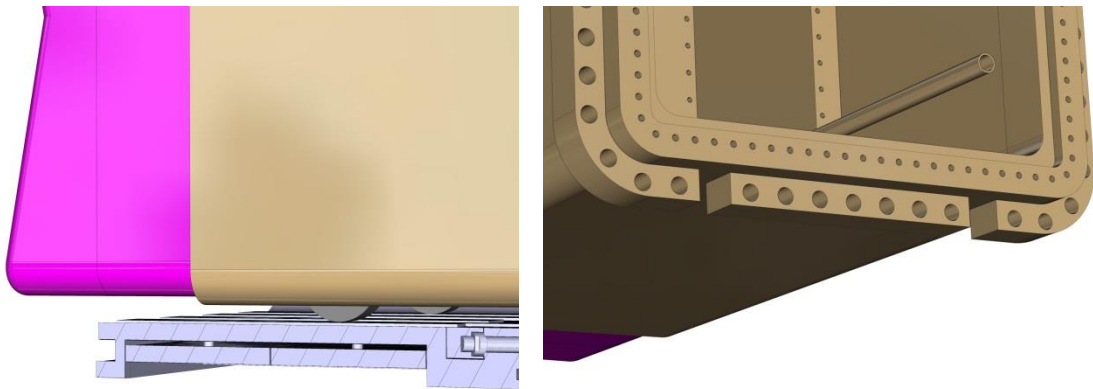


Fig. 70. Helping cantilever system: rollers and rear flange pockets.

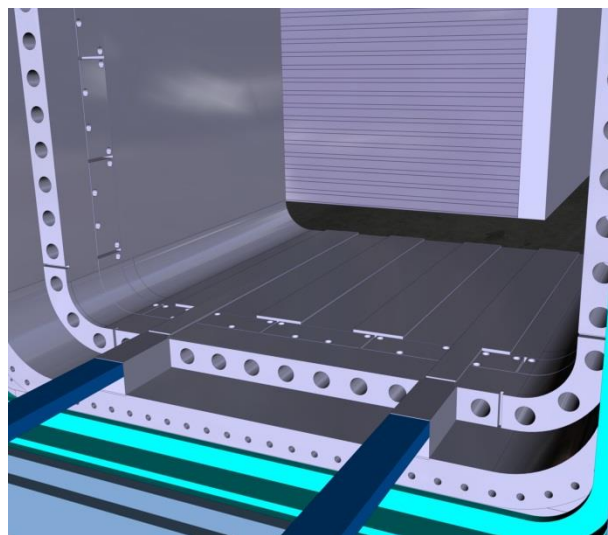


Fig. 71. Helping cantilever system in the port extension and the Transfer Cask.

The operation ends with the screwing of the screws which join the Port Extension flange with the Port Plug rear flange. It could be performed by a tool integrated in the TC gripper (similar to the one used in the Gasket Flange Maintenance Equipment).

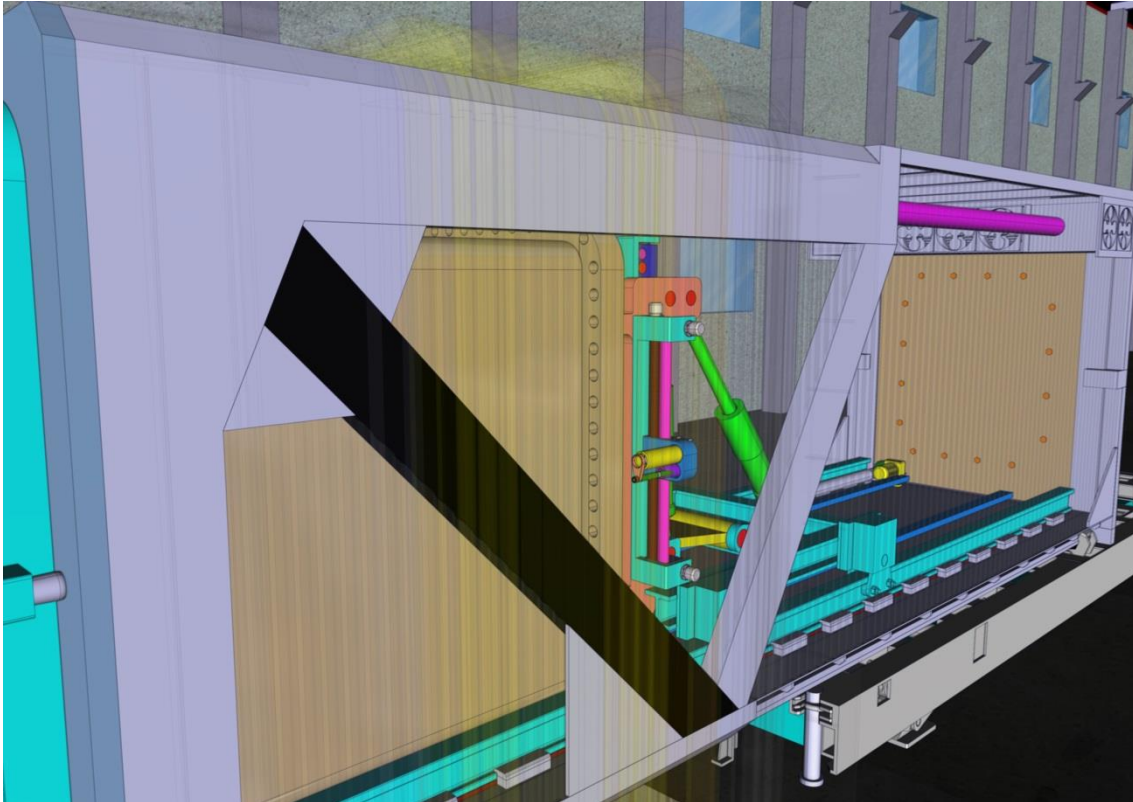


Fig. 72. Insertion of the Port Plug in the Port Extension.

The operation of removal is thought to be the other way round, with the same steps.

Space requirements

25 m x 50 m x 6 m (W, H, L). The width and the length represent the maximum area occupied by the PP and the TC during its transport between the Storage Area and the Port Cell. The height is taken from the dimensions of the Port Cell Structures and the Port Supports.

RH Operation	TBM RH test facility requirements				
	Equipment		Structures	Auxiliary systems	Space
	Not requiring a specific design	Requiring a specific design			
Installation/ removal of the port plug in/from the Port	- Docking flange. - Transfer cask. - Air transfer system.	- TBM & shield mock-ups. - PP mock-up.	- Port structures. - Port Cell structures.	- Electric supply.	25 m x 50 m x 6 m

Table 26. Operation #24 requirements.

Hypotheses

- The precision of ATS movements is enough for the docking of the TC. The pallet positioning system and the gripper ensure the accurate insertion of the Port Plug.
- We consider that the system of double doors does not require specific RH equipment apart from the one included in the TC.
- It is not established the procedure to install/remove the docking flange in/from the Port structures.

- The port plug is joined to the Port Extension flange by means of a screwing tool integrated in the TC gripper [Meu 07].

#### 2.5.4.25. Vacuum sealing of the Port Plug – Port interface (operation #25)

In ITER, the ultra-high vacuum sealing between the Port Plugs and their Ports must be ensured by the installation of a gasket flange. This operation is a responsibility of ITER Organization, but it would be interesting to test the required equipment by performing it in the TBM RH test facility.

The gasket flange consists of two coronas. The inner corona is screwed to the PP flange and the outer corona is screwed to the Port Extension flange. The Helicoflex metallic gaskets are placed in slots between the PP rear flange and the gasket flange and between the Port Extension flange and the gasket flange.

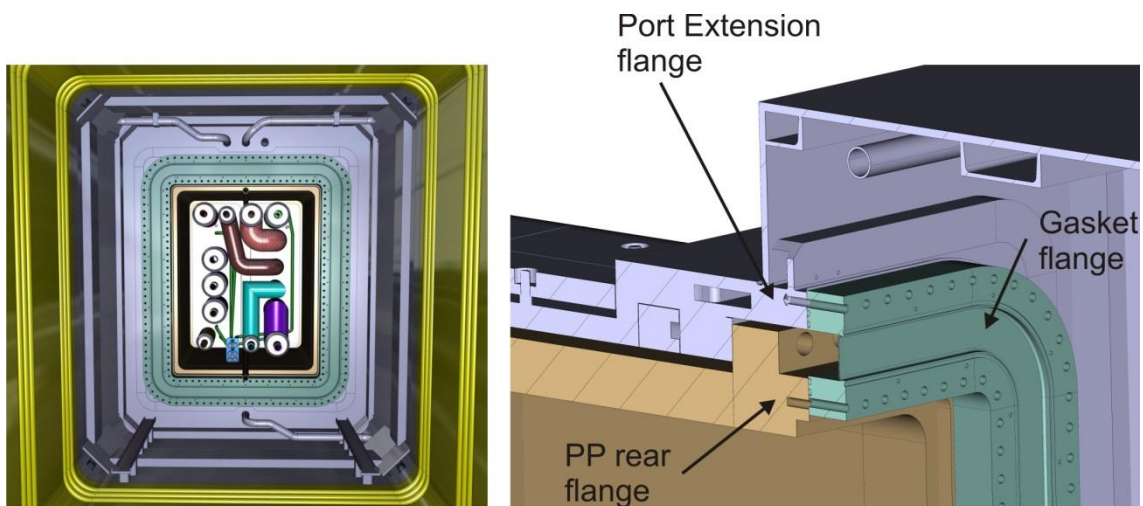


Fig. 73. Gasket flange sealing.

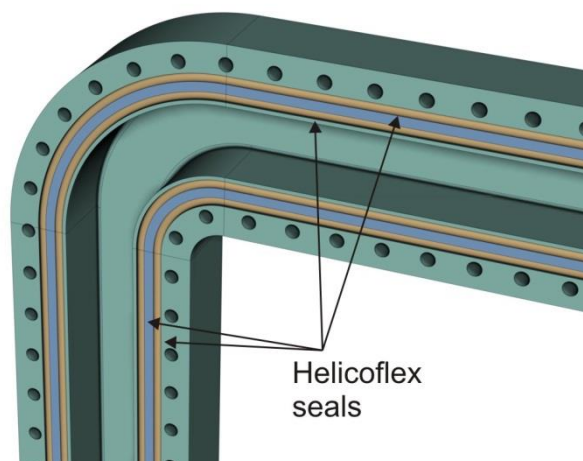


Fig. 74. Gasket flange detail.

The sealing surface must be carefully treated in order to avoid any marks that could compromise the vacuum tightness. A light temporary frame could be mounted instead of the gasket flange during maintenance operations.

A special device called Gasket Flange Maintenance Equipment is needed to install and remove the gasket flange. This equipment consists of a special tool and a transport system. The

transport system is similar to the ATS. The maintenance tool has 6 degrees of freedom, allowing it to place correctly the gasket flange. It is equipped with four small trolleys (one per side). The different tools (screwing tools, polishing discs...) required for the different operations are located in each of the trolleys.

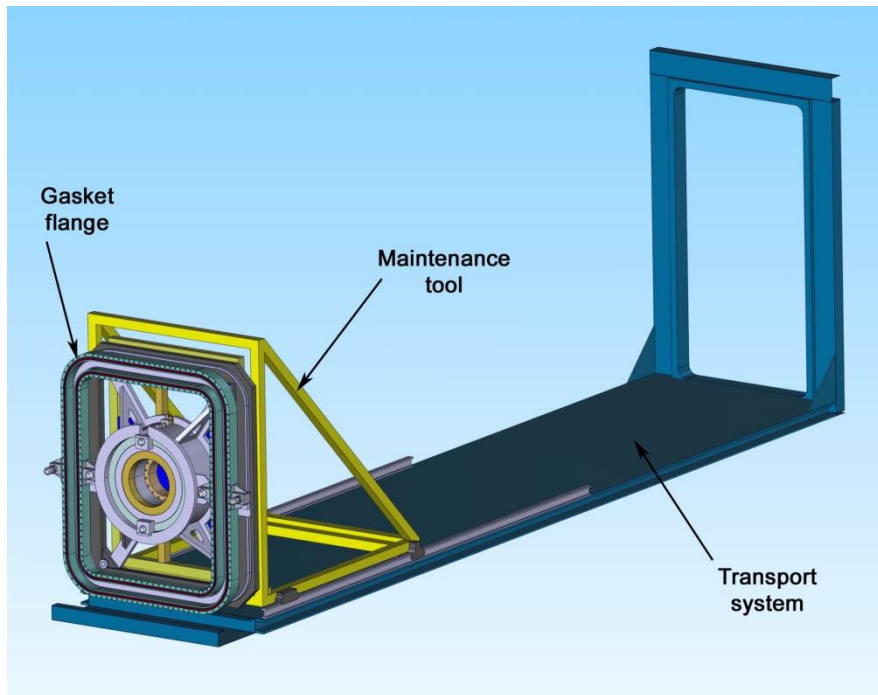


Fig. 75. Gasket flange maintenance equipment.

The first step is to polish the surface where the HELICOFLEX metallic gaskets will be housed. This is done by means of polishing discs and cameras attached to the trolleys.

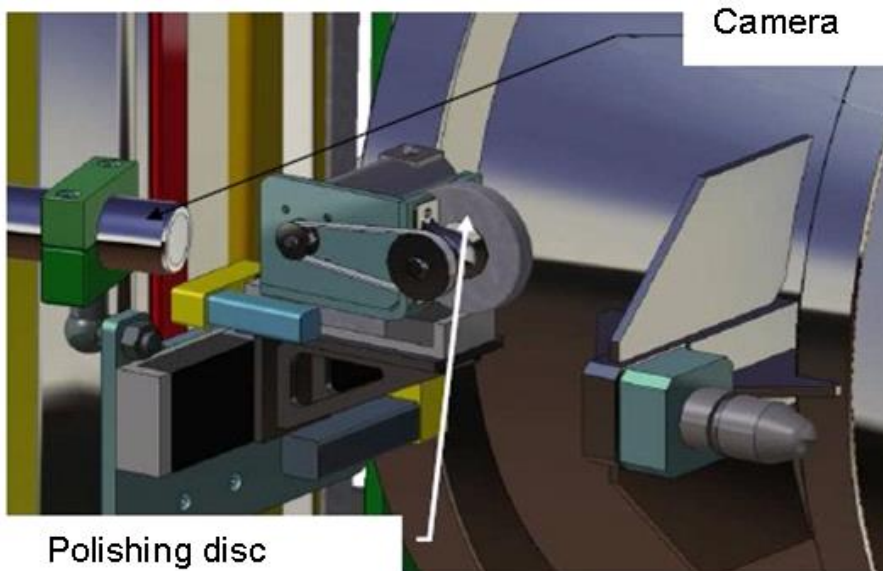


Fig. 76. Polishing disc and camera [Meu 07].

After polishing, the Helicoflex metallic gasket is installed (it is not defined how). Then the gasket flange maintenance equipment installs the gasket flange in the port and screws all the screws in both coronas.

The gasket flange maintenance equipment includes a leak detection equipment to test the joint sealing quality by hands-on.

#### Space requirements

10.5 m x 24 m x 6 m (W, H, L). The width and the length represent the dimensions of the Port Cell Area. The height is taken from the dimensions of the Port Cell Structures and the Port Supports.

RH Operation	TBM RH test facility requirements				
	Equipment		Structures	Auxiliary systems	Space (W, L, H)
	Not requiring a specific design	Requiring a specific design			
Vacuum sealing of the PP-port interface.	<ul style="list-style-type: none"> <li>- Gasket flange.</li> <li>- Gasket flange maintenance equipment.</li> <li>- Light temporary frames.</li> </ul>	<ul style="list-style-type: none"> <li>- TBM &amp; shield mock-ups.</li> <li>- PP mock-up.</li> </ul>	<ul style="list-style-type: none"> <li>- Port structures.</li> <li>- Port Cell structures.</li> </ul>	<ul style="list-style-type: none"> <li>- Vacuum testing system.</li> <li>- Electric supply.</li> </ul>	10.5 m x 24m x 6 m

Table 27. Operation #25 requirements.

#### Hypotheses

- The use of the sealing method and equipment described in [Meu 07] is assumed.

### **2.5.5. Hosting building description and space layout in the TBM RH facility**

The proposed host building of the TBM RH test facility is a standard industrial building with pre-manufactured metallic walls and gable roof. The empty hosting building hall is 85 m (length) per 30 m (width). The minimum height of the hall is 12 m. This guarantees enough free height below the crane (9 m), as specified in the operations requirements section, once the height occupied by the crane structure and hook has been taken into account. Inside the hall a 25 m (length) per 30 m (width) area is occupied by a pre-manufactured building hosting the control room, offices, the workshop, the warehouse and the auxiliary systems. This pre-manufactured building is called “*Office and Auxiliary Systems building*” here. The rest of the hall is dedicated to the actual test facilities for the demonstration of the RH operations in the Hot Cell and the Port Cell. This part of the hosting building is called “*Operations Hall*”.

There are two entrances into the facility, marked with an arrow in Fig. 78. The entrance into the operation hall is used for trucks for loading and unloading equipment. The entrance into the office and auxiliary system building is used by people.

Fig. 77 and Fig. 78 show the proposed dimensions of the TBM RH test facility site. These are important because land cost is a significant part of the total cost of the TBM RH test facility.

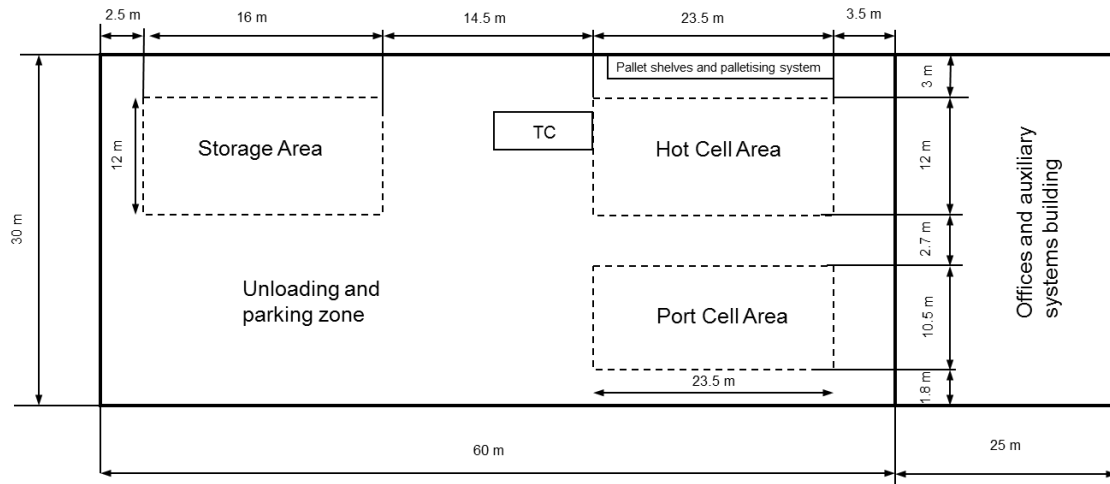


Fig. 77. Spatial layout of the TBM RH test facility hosting building.

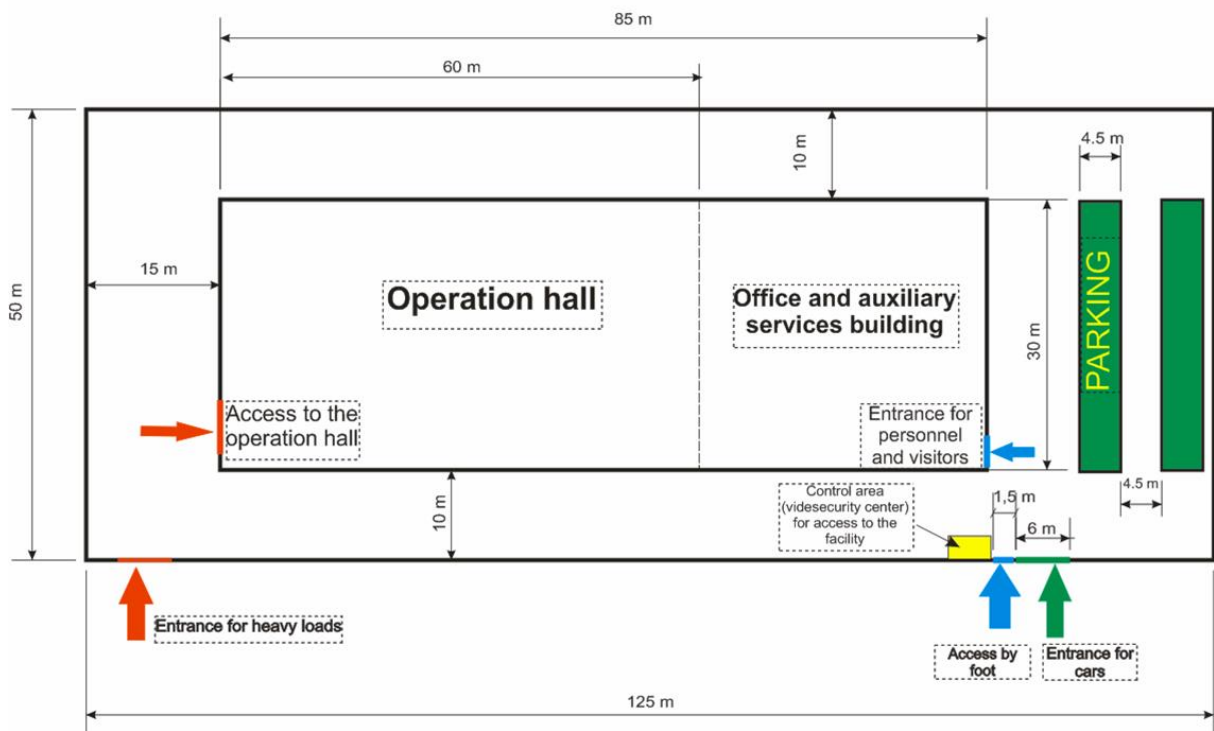


Fig. 78. Dimensions of the TBM RH test facility site.

### 2.5.5.1. Operations Hall

The space requirements for the demonstration of the RH operations in the Hot Cell and Port Cell have been summarized in 2.5.4. From these requirements four areas within the operations hall have been defined:

- Hot Cell RH operations area.
- Port Cell RH operations area.
- Storage area.
- Unloading and parking zone.

Fig. 79 shows the layout of these areas within the operations hall.

There is a 2.7 m (width) corridor between the HC RH operations area and the PC RH operations area. This corridor allows movement of equipment into and out of the workshop and warehouse area.

Between the HC RH operations area and the Storage area there is a 14.5 m gap allowing the manoeuvring of the ATS.

A 20 ton rotating crane with a telescopic mast and a robotic manipulator is used to perform RH operations in the Hot Cell area.

A 50 ton standard industrial crane is used for lifting heavy loads during the installation and commissioning phase of the test facility (e.g. installation of the port plug in vertical positioning tool, installation of the port structures mock-up, etc.).

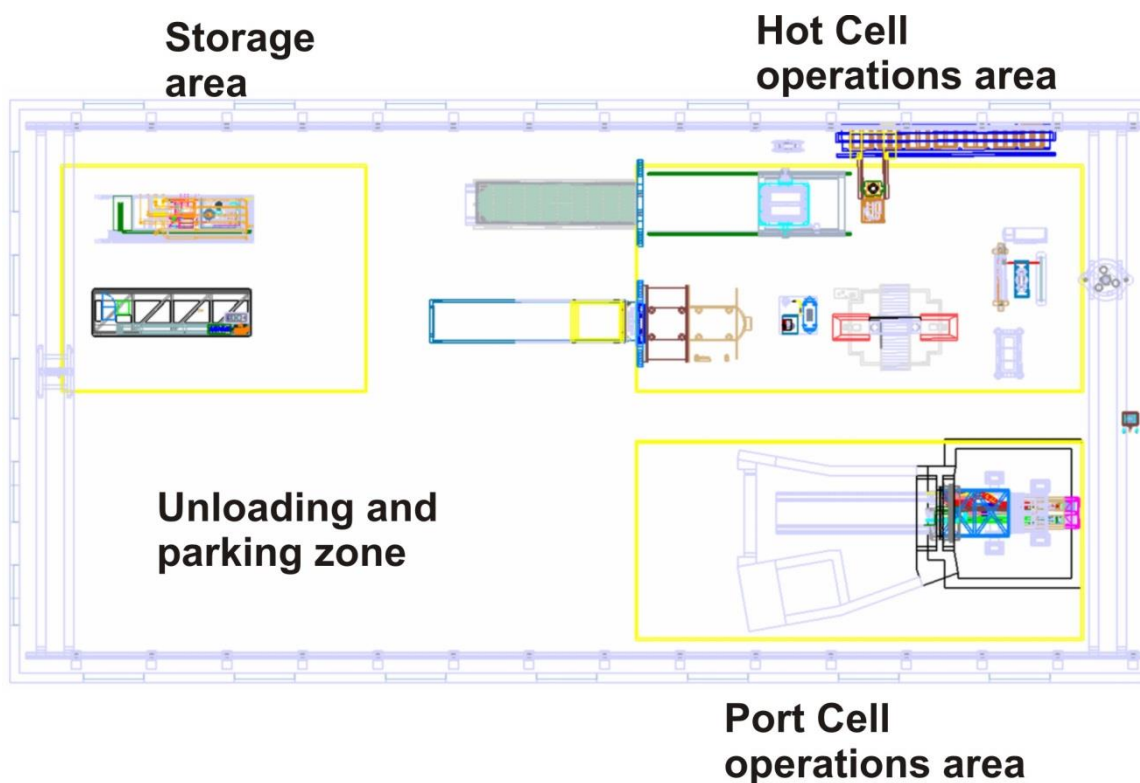


Fig. 79. Space allocation in the Operations Hall.

	Length	Width	Area (m <sup>2</sup> )
<b>Dimensions of the Operations Hall</b>	60	30	1800
<b>Hot Cell RH operations area</b>	23.5	12	282
<b>Port Cell RH operations area</b>	23.5	10.5	246.75
<b>Storage area</b>	16	12	192
<b>Unloading and Parking zone</b>	25	14	350
<b>Corridors and free space in the operations hall</b>			729.25

Table 28. Dimensions of the operations hall.

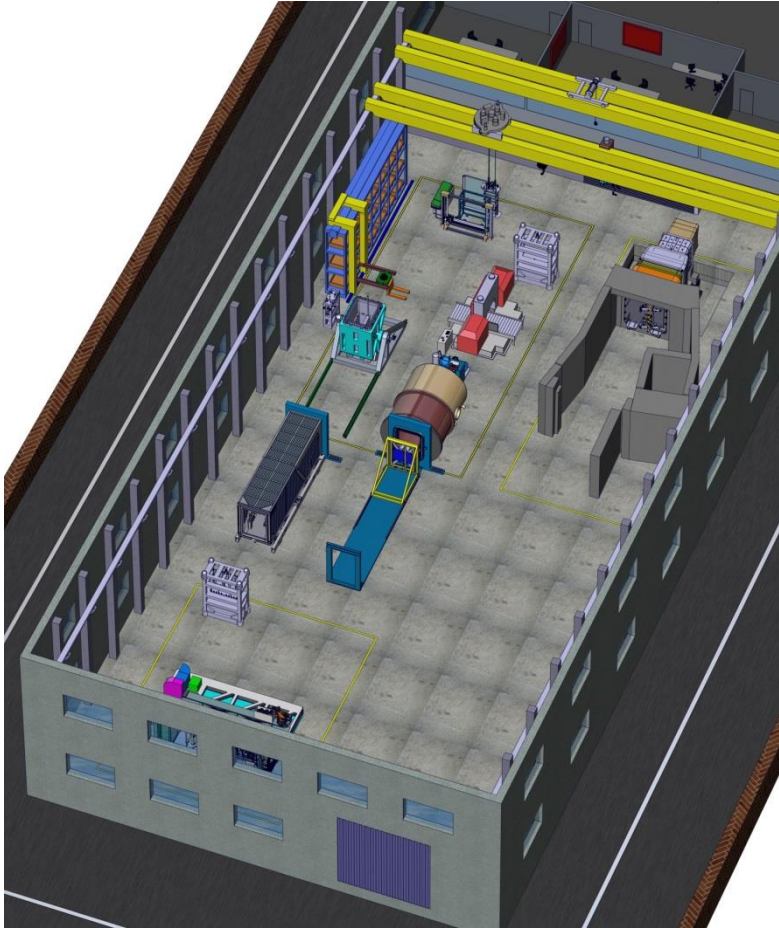


Fig. 80. Top view of the operations hall.

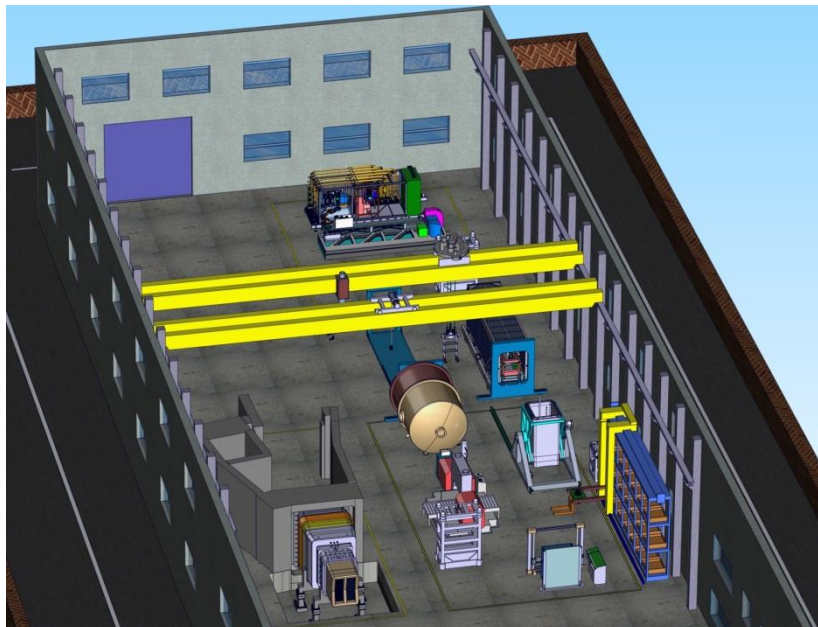


Fig. 81. View of the operations hall from the office and auxiliary system building.

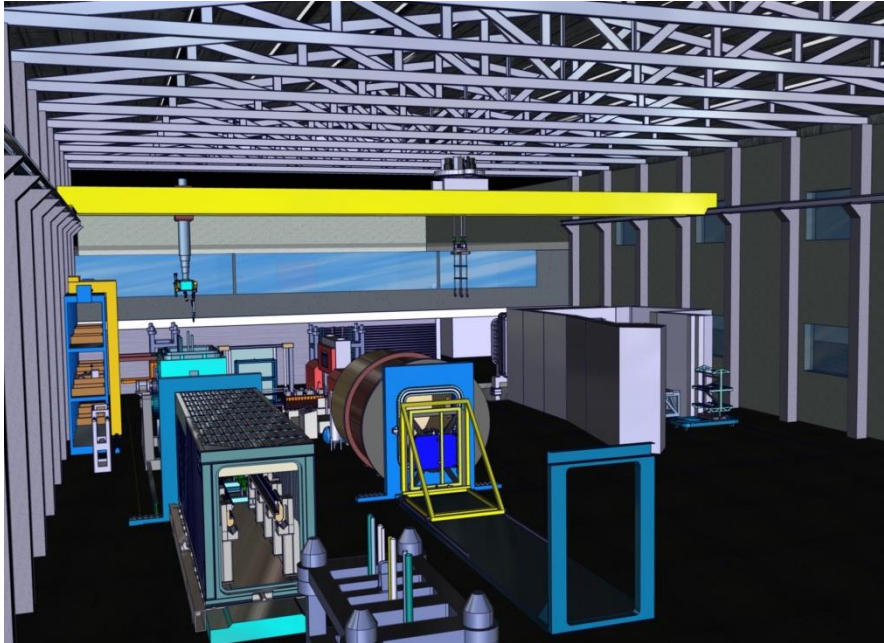


Fig. 82. Operations hall ground view 1.

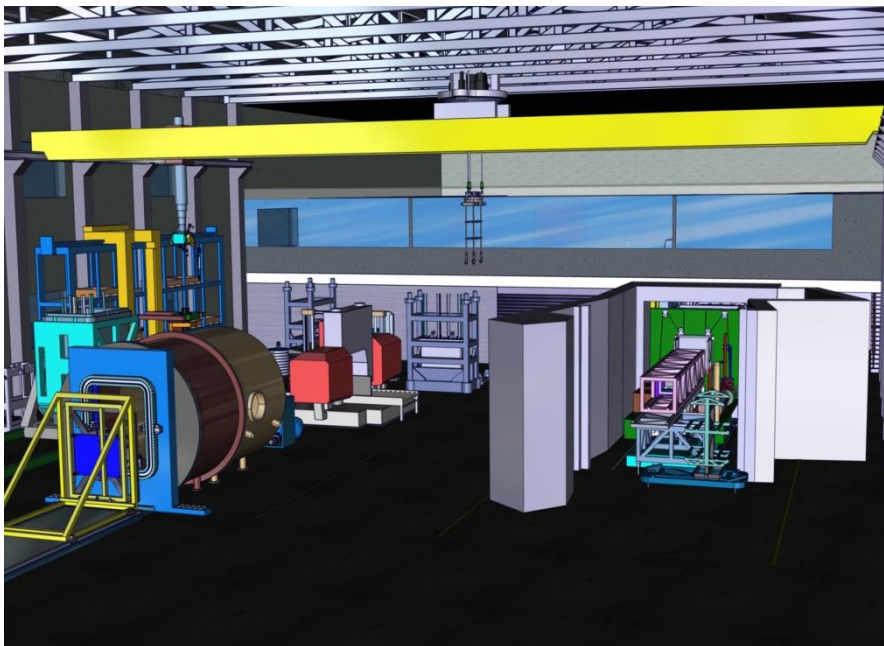


Fig. 83. Operations hall ground view 2.

#### 2.5.5.2. TBM Port Cell RH operations area

The TBM Port Cell RH operations area occupies 246.75 m<sup>2</sup>. It has a double floor within the area where the Port Structures mock-up is held by means of two supporting structures. The Port Cell structures are modular walls that can be installed and removed as desired.

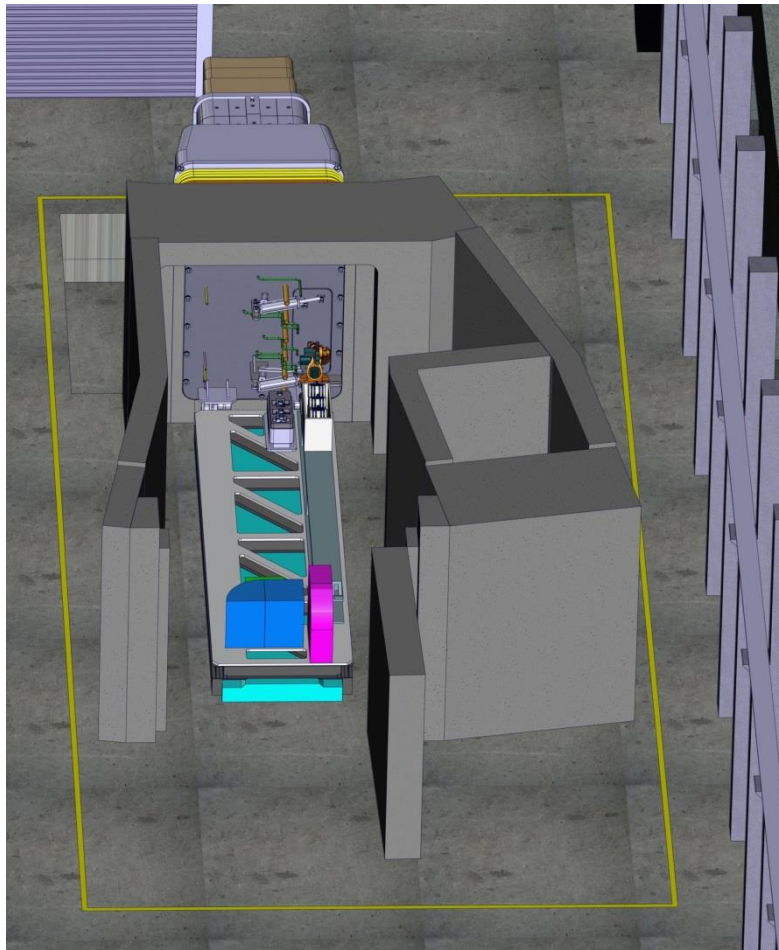


Fig. 84. Port Cell RH operations area.

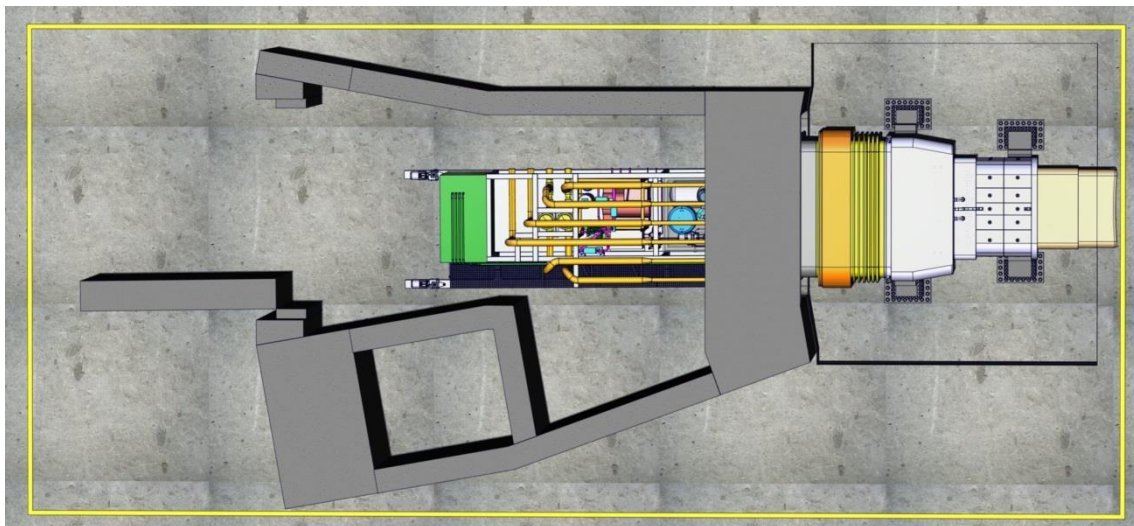


Fig. 85. Port Cell RH operations area. Top view.

### 2.5.5.3. Hot Cell RH operations area

The HC RH operations area occupies 282 m<sup>2</sup>. The space layout and the equipment in this area are shown in the following figure.

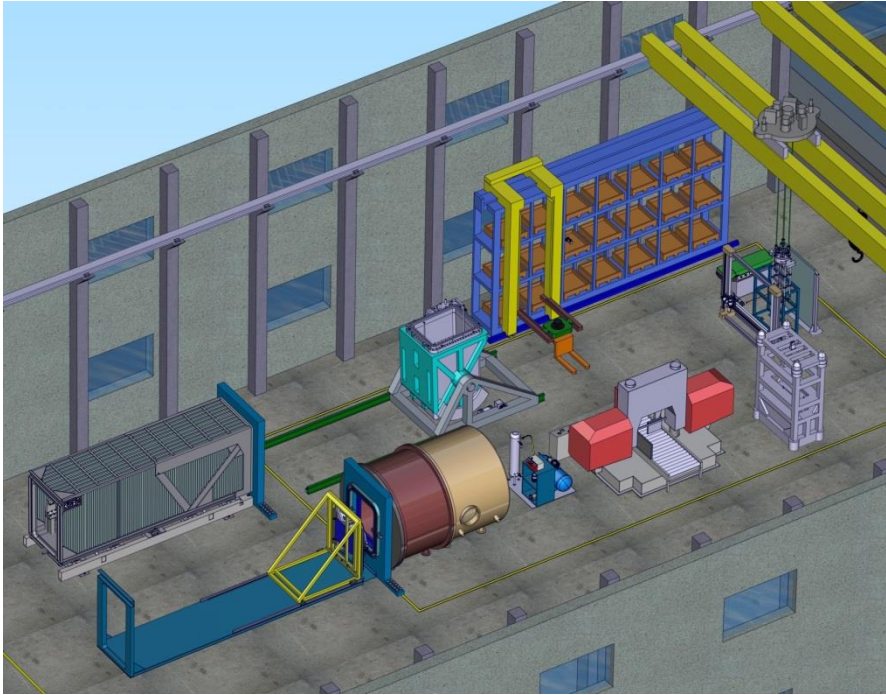


Fig. 86. Hot Cell RH operations area.

#### 2.5.5.4. Storage area

This area (192 m<sup>2</sup>) is destined to the storage of equipment and individual components. There are neither shelves nor palletising system in this zone. The tools are stored in the Hot Cell operations area shelves.

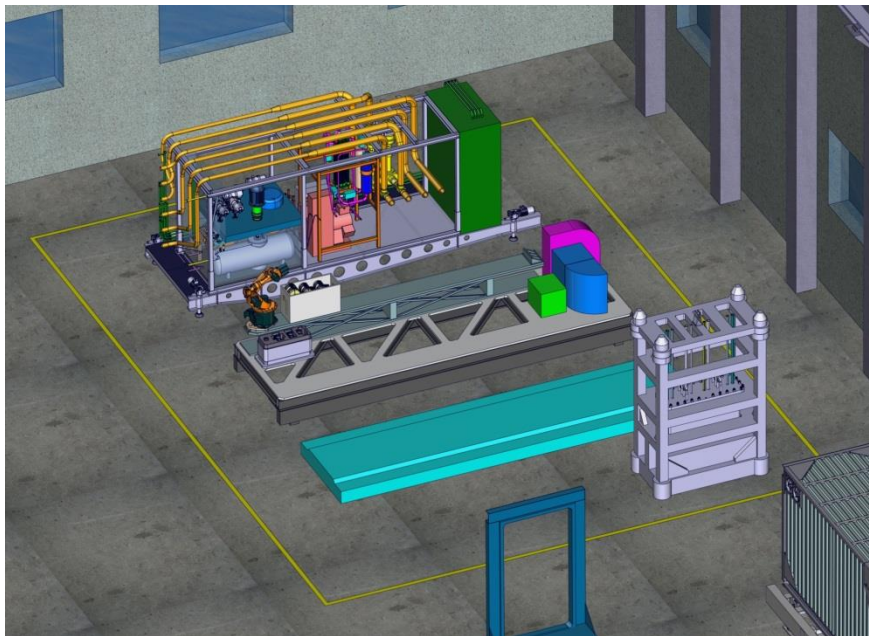


Fig. 87. Storage area (view 1).

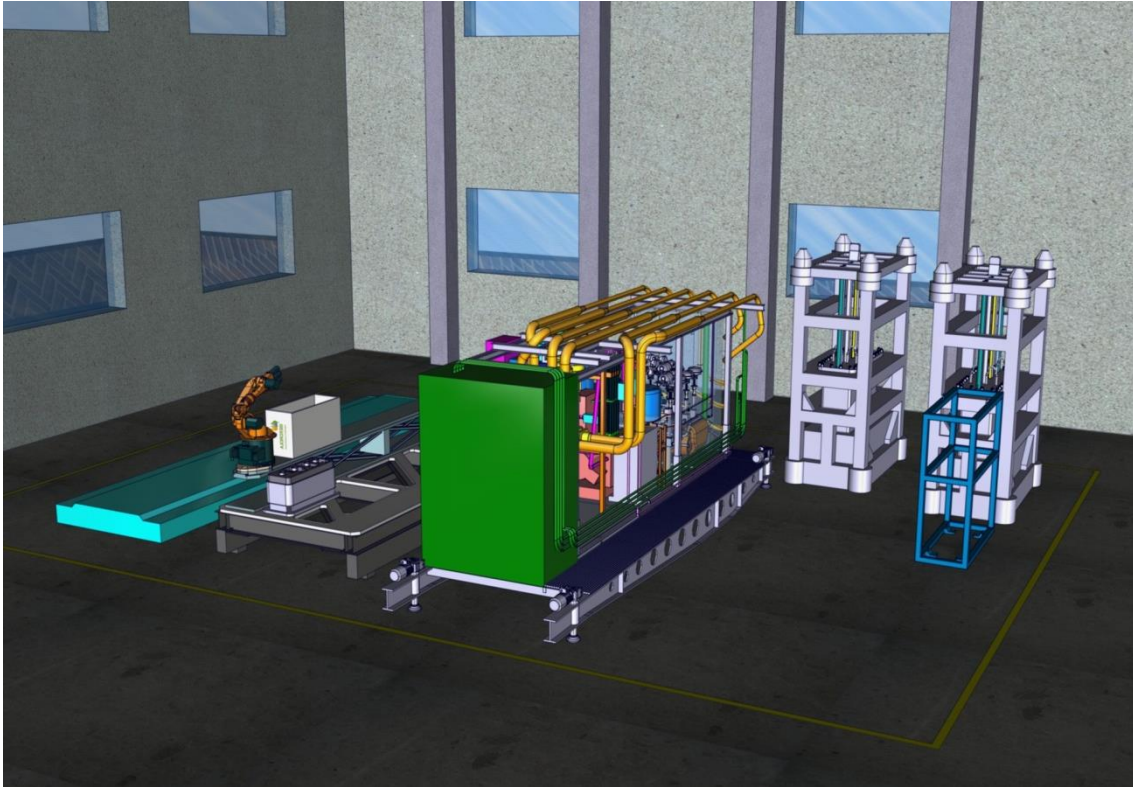


Fig. 88. Storage area (view 2).

#### 2.5.5.5. Unloading and Parking zone

The Unloading and Parking zone is used by external transports as parking, as well as temporary storage area. It is used also for loading and unloading of equipment. Equipment like the RH Platform Unit, Air Transfer System, Transfer Cask and the AEU mock-up could be parked in this area when they are not used. The removable wall modules of the Port Cell structures mock-up could be stored in this area if necessary. The Unloading and Parking zone occupies 350 m<sup>2</sup>. It is placed next to the large front door to facilitate loading and unloading operations.

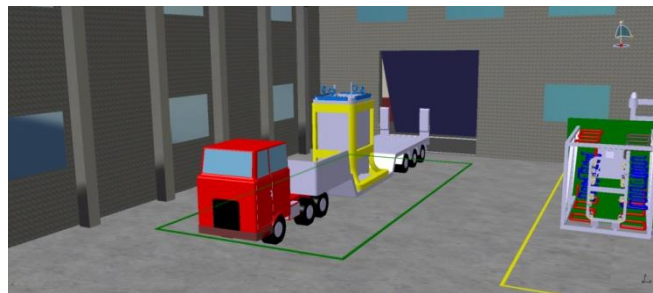


Fig. 89. Truck parked at the Unloading and Parking zone, carrying a port plug mock-up.

#### 2.5.5.6. Office and auxiliary systems building

The Office and Auxiliary Systems building is made of pre-manufactured construction elements and it is located next to the Operations Hall. It occupies an area of 25 m x 30 m, with a height of 7 m. The ground level height is 4 m, whereas the first level height is 3 m.

### 2.5.5.7. Ground floor

The workshop, the warehouse and the auxiliary systems (HVAC, electric panels, pneumatic supply, etc.) are located on the ground floor. A sliding door allows entering from the Operations Hall into the warehouse and the workshop and vice versa.

The air conditioning system provides conditioned air to the offices located on the first floor (370 m<sup>2</sup>). The heating system provides hot water (not air) to the operations hall. The dimensions of both the air conditioning system room and the heating system room have been calculated taking into account the dimensions of the office area and the Operations Hall.

A 4 m length corridor has been included in order to allow for the eventual replacement of equipment from the auxiliary systems. This corridor allows for large equipment to be taken from the operation hall into the different rooms and vice versa.

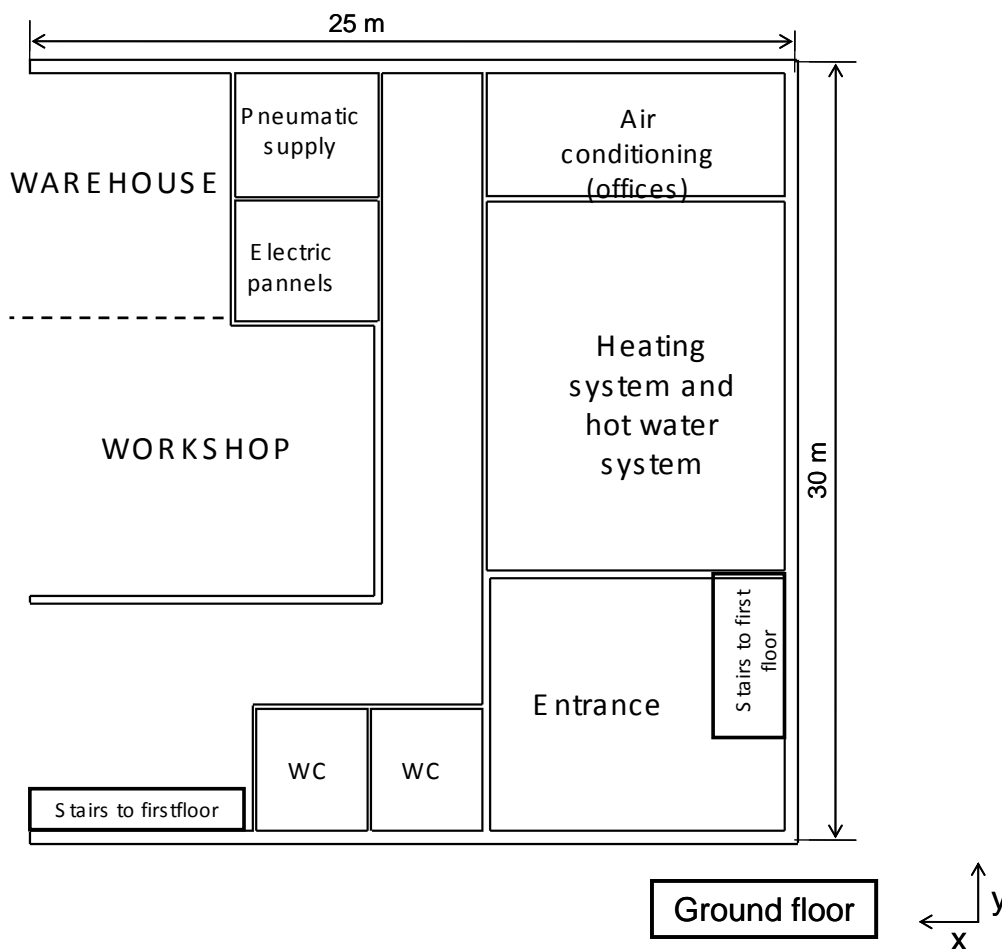


Fig. 90. Space layout of the Office and Auxiliary Systems building ground floor.

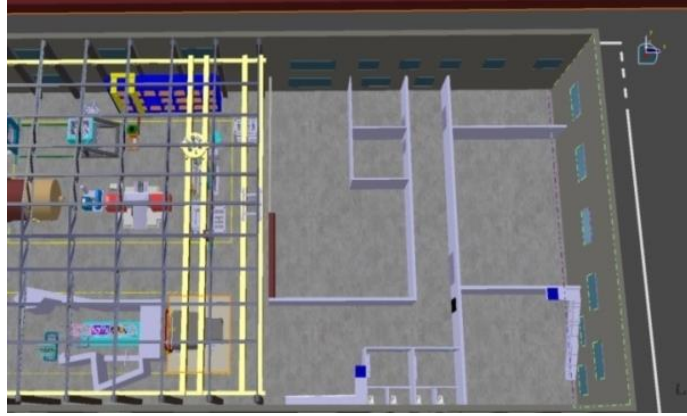


Fig. 91. Ground floor (offices and auxiliary systems building).

The dimensions of each room on the ground floor of the Office and Auxiliary Systems building are shown in the table below.

	x (m)	y (m)	Area (m <sup>2</sup> )
Stairs 1 (Entrance)	4.00	2.00	8.00
Stairs 2 (near workshop)	1.50	4.00	6.00
<b>Area occupied by stairs</b>			<b>14.00</b>
Air conditioning	11.85	4.90	58.07
Heating system + hot water system	11.85	14.60	173.01
Warehouse	8.00	10.00	80.00
Workshop	13.70	10.70	146.59
Electric panels	5.70	4.93	28.07
Pneumatic system	5.70	4.93	28.07
WC and wardrobe	4.43	4.85	21.46
WC and wardrobe	4.43	4.85	21.46
Entry	11.70	10.00	117.00
<b>Area occupied by rooms</b>			<b>673.73</b>
<b>Walls and corridors</b>			<b>62.27</b>
<b>Total area in the ground floor</b>	<b>25.00</b>	<b>30.00</b>	<b>750.00</b>

Table 29. Dimensions of the Office and Auxiliary Systems building rooms which are situated on the ground floor.

#### 2.5.5.8. First floor

The offices, control room and meeting rooms are on the first floor. The personnel requirements of the TBM RH test facility have been estimated at 10 people maximum during operation (including engineers and technicians). During the construction and commissioning phases the number of people working on the TBM RH test facility could triple. The offices located on the first floor have been dimensioned to accommodate 10 people plus temporary visitors to the facility (less than 5).

A glass window in the control room allows direct visual contact with the different operation areas. The size of the control room is sufficient to host the required equipment (screens, manipulators control devices, etc.), the RH equipment operators and all other personnel in the facility who would want to follow the operations from it.

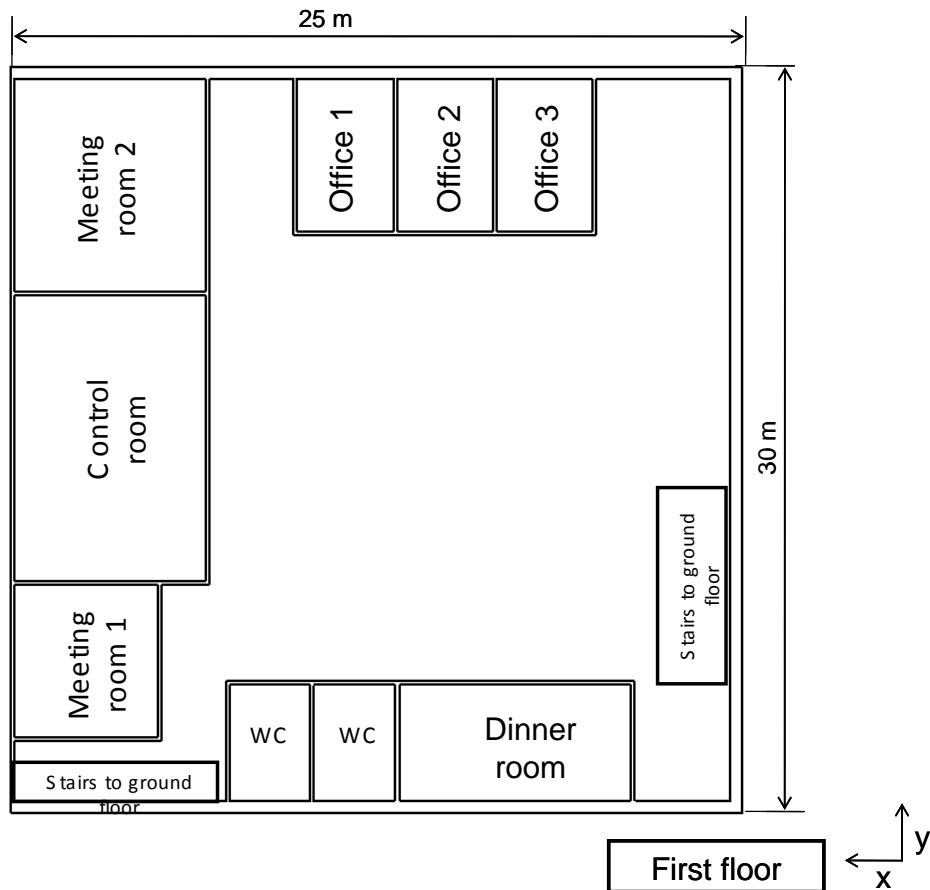


Fig. 92. Space layout of the Office and Auxiliary Systems building first floor.



Fig. 93. First floor (Offices and Auxiliary Systems building).

	x (m)	y (m)	Area (m <sup>2</sup> )
Stairs 1 (Entrance)	4.00	2.00	8.00
Stairs 2 (near workshop)	1.50	4.00	6.00
<b>Area occupied by stairs</b>			<b>14.00</b>
Meeting room 1	8.00	8.85	70.80
Meeting room 2	6.00	6.50	39.00
Control room	8.00	11.85	94.80
WC	3.35	5.00	16.75

WC	3.35	5.00	16.75
Dinner room	9.65	4.85	46.80
Office 1	4.23	6.35	26.83
Office 2	4.23	6.35	26.83
Office 3	4.23	6.35	26.83
<b>Area occupied by rooms</b>			<b>365.39</b>
<b>Walls, corridors and free space</b>			<b>370.61</b>
<b>Total area in the first floor</b>	25.00	30.00	<b>750.00</b>

Table 30. Dimensions of the Office and Auxiliary Systems building rooms which are located on the first floor.



Fig. 94. Control room.

### 2.5.6. Conceptual design of equipment, structures and fixed mock-ups

The equipment needed for the facility can be classified in two groups. The first group corresponds to the equipment which requires a specific design for the TBM RH test facility. The second group corresponds to standard commercial equipment or equipment identical to the one used in ITER.

For the equipment requiring a specific design a list of functional requirements and a conceptual design proposal is included. For the standard and ITER identical equipment a short informative description about the most important parts is given. The list of the whole equipment, structures and fixed mock-ups is shown in Table 31.

<b>Equipment requiring a specific design for the TBM RH test facility</b>
Ancillary Equipment Unit (AEU) mock-up
Pipe forest & bioshield door assembly mock-up
Port plug mock-up
TBM & shield mock-ups
<b>Equipment non requiring a specific design for the TBM RH test facility</b>
Air transfer system
Band sawing machine

Drum and shipping basket mock up
Plasma cutting tool
Gasket flange maintenance equipment.
Hot Cell manipulator
Welds inspection tool
Thermal insulating modules
Laser cutting tool
Lifting tool for TBM & shield
20 ton overhead rotating crane
Palletising system and storage shelves
Port Cell robotic arm and RH platform unit
Polisher
Test stand
Screwer
Transfer cask
Vertical positioning tool
Welding tool for PC robotic arm
50 ton overhead crane
<b>Structures and fixed mock-ups</b>
Bench for dust cleaning and separation of TBM from shield
Hot Cell door for vertical positioning tool
Hot Cell door for test stand
Port Cell mock up
Port mock up
Supporting bench for new TBM & shield assemblies. Storage container

Table 31. List of equipment, structures and fixed mock-ups.

### 2.5.6.1. Ancillary Equipment Unit (AEU) mock-up

#### Functional requirements

- It must allow its transference from the Storage area to the Port Cell area by means of the automated air cushion transporter, which will be adopted in ITER.
- It must have equal mass and dimensions to those of the real AEU to check the AEU transport and manipulation by the ATS.
- It must include equipment which simulates the external geometry of the real AEU system and allows the RH demonstration operations.
- It must contain all He and PbLi pipes in IF2b.
- It must be the structural support for the Test Blanket System pipes.
- It must allow the RH system to gain access to IF2a through a 700 mm wide corridor, so the necessary RH operations can be carried out.

## Conceptual design proposal

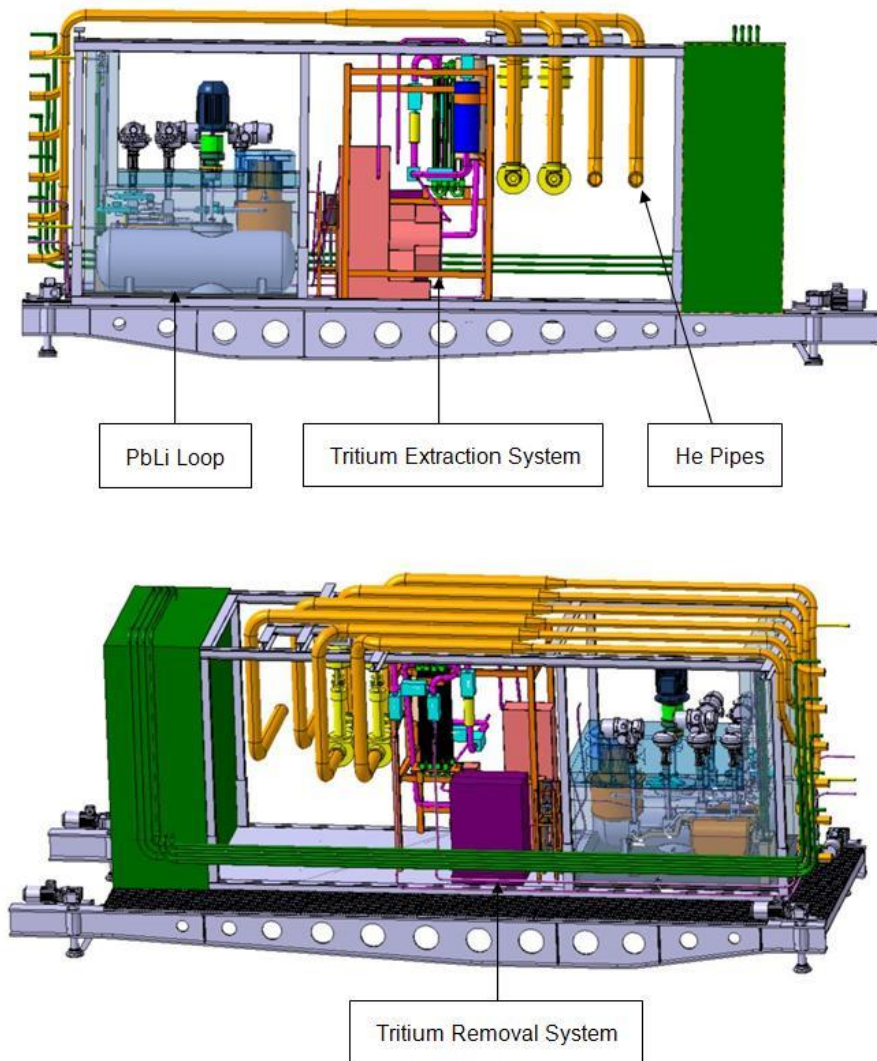


Fig. 95. Ancillary equipment unit.

The Ancillary Equipment Unit (AEU) is basically a steel structure which contains those parts of the Test Blanket System which are placed in the Port Cell.

The AEU consists of a useful space for the integration of all the equipment (diagnostics, PbLi loop, valves, etc.) and supply pipes with the proper support.

The AEU is a movable component which can be transported, installed and refurbished as one unit. Its maximum size is limited by the Equatorial Transfer Cask System in order to be possible to move it through the corridors and lifts of the Tokamak Building and the Hot Cell Building which are designed taking into account the TCS features.

AEU contains five TBM ancillary loops, here below listed:

- Part of the HCS (Helium Cooling System) for the HCPB TBM. The remaining part is located in the TCWS.
- Part of the HCS for the HCLL TBM. The remaining part is located in the TCWS.
- The whole PbLi loop for the HCLL TBM.
- Part of the TES (Tritium Extraction System) for the HCPB TBM. The remaining part is located in the Tritium Building.

- Part of the TRS (Tritium Recovery System) for the HCLL TBM. The remaining part is located in the Tritium Building.

The AEU is connected to the Pipe Forest through the Interface 2b, whereas the Interface 3 connects the AEU systems which the rest of the TBS equipment placed outside the Port Cell.

The AEU mock-up must include only those systems whose geometry or weight is relevant for the demonstration of the RH operations: transport of AEU between the Storage and Port Cell areas and positioning in the Port Cell, installation/removal of the AEU in/from the Port Cell and maintenance operations at IF2a.



Fig. 96. AEU Platform.

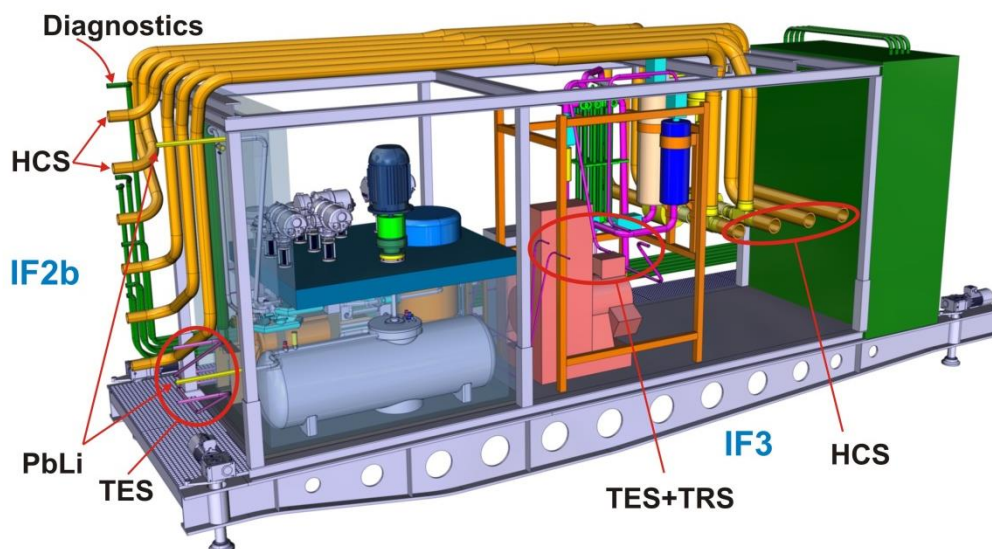


Fig. 97. Pipes layout at interfaces 2b and 3.

### 2.5.6.2. Pipe forest & bioshield door assembly mock-up

#### Functional requirements

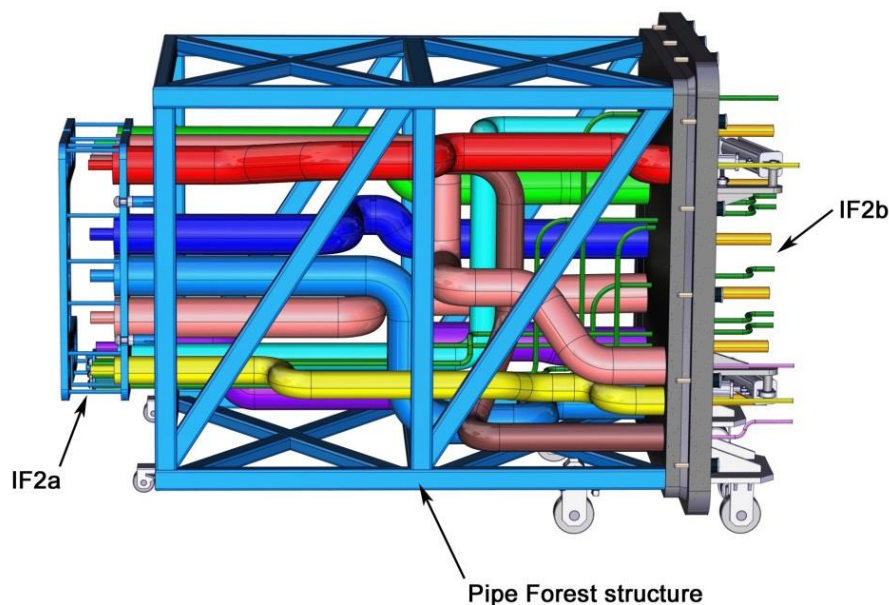
- It must allow its transference from the Storage area to the Port Cell area by means of the automated air cushion transporter, which will be adopted in ITER.
- There is a pipe grid connecting both TBMs (HCLL and HCPB) with the AEU systems.
- The bioshield door works as radiological shield.
- It must have wheels to allow its movement to the bioshield wall. These wheels should be compatible with the rails installed in the ATS.
- It must be the structural support for the Test Blanket System pipes.
- It must allow access to interface 2a by the RH system (robot and supporting structure) so that it can perform the necessary RH operations (cutting, preparing, welding, inspection of weld seams, etc.)
- It must allow switching the mechanical behaviour of IF2a pipes from rigid to flexible and vice versa (pneumatic cylinders and plates system).
- It must contain a wall which simulates the bioshield part, which includes a window to allow the RH tool to access IF2a.
- It must have equal mass and dimensions to those of the real PF to evaluate the PF transport and manipulation by the ATS.
- It must be equipped with a positioning and aligning system, equivalent to the real PF one.
- The interface 2a pipes will have the same flexibility as the real PF ones, in such a way that the aligning, welding and cutting operations can be correctly simulated.

#### Conceptual design proposal

The Pipe Forest is a pipe grid which is installed in the Interspace and connects both Test Blanket Modules (HCLL and HCPB) with the AEU systems at Interfaces 2a and 2b.

In ITER, it allows to accommodate the displacement of the Vacuum Vessel and the thermal expansion of pipes, as well as to avoid neutron streaming through the TBS pipes.

The Pipe Forest consists of a steel frame in charge of supporting pipes. The Bioshield Door is a reinforced concrete wall which acts as radiological shield. It is joined to the Pipe Forest frame and the fixed Bioshield structure, whereas the pipes of the Pipe Forest go through it.



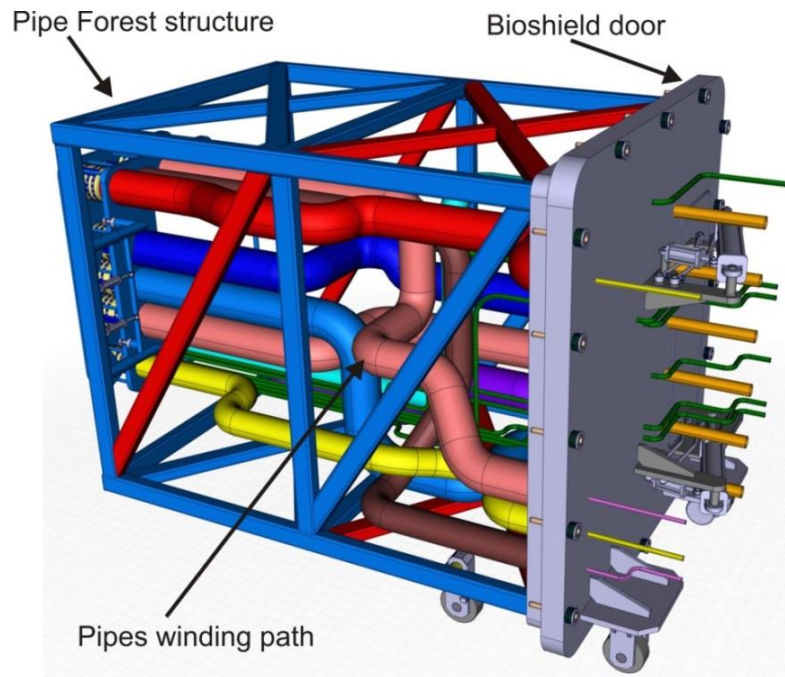


Fig. 98. Pipe Forest.

The geometry of the assembly allows its transport between the Hot Cell and the Port Cell areas by means of the Air Transfer System, whereas it has an autonomous drive system for movements in the Interspace. This system is based on 6 wheels which are guided by rails located on both the ATS and the Port Connecting Duct, without interfering with the Bellows.

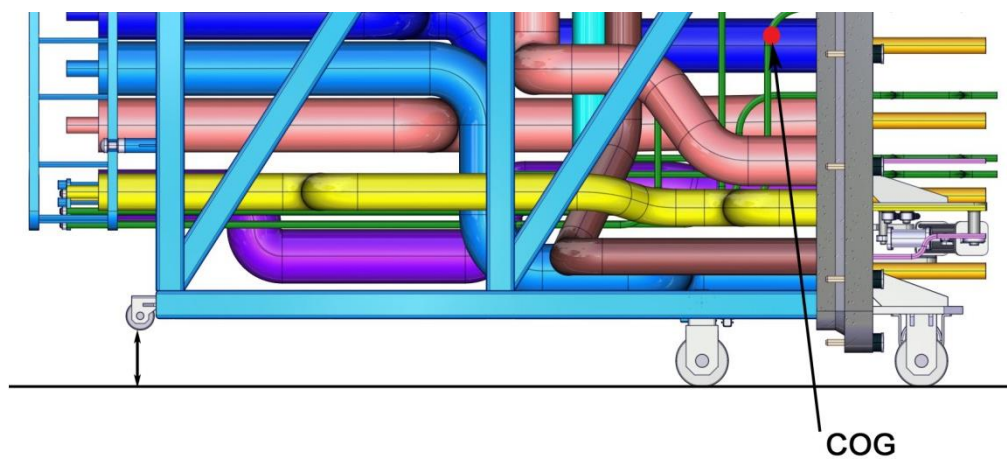


Fig. 99. Pipe Forest wheels.

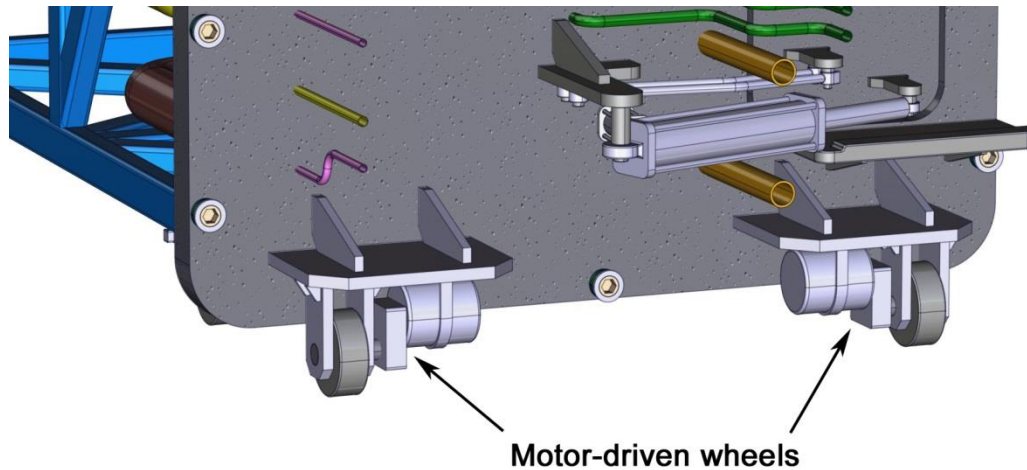


Fig. 100. PF Motor-driven wheels.

There are three rows of two wheels. The rear pair, located behind the Bioshield Door, is driven by electric motors. The intermediate wheels are collapsible, so when they reach the step of the Bioshield Wall, they fold back and remain in that position by means of small hydraulic cylinders. The two front wheels are smaller than the previous four, and are located at a higher level, avoiding height discontinuity between the ATS base and the Port base. Before the Pipe Forest arrives to the port, it is supported only on the four rear wheels (the centre of gravity of the assembly is located between the intermediate wheels and the rear ones). When the intermediate wheels fold back, the front wheels rest on the Connecting Duct rails, so the Pipe Forest can continue to its final position.

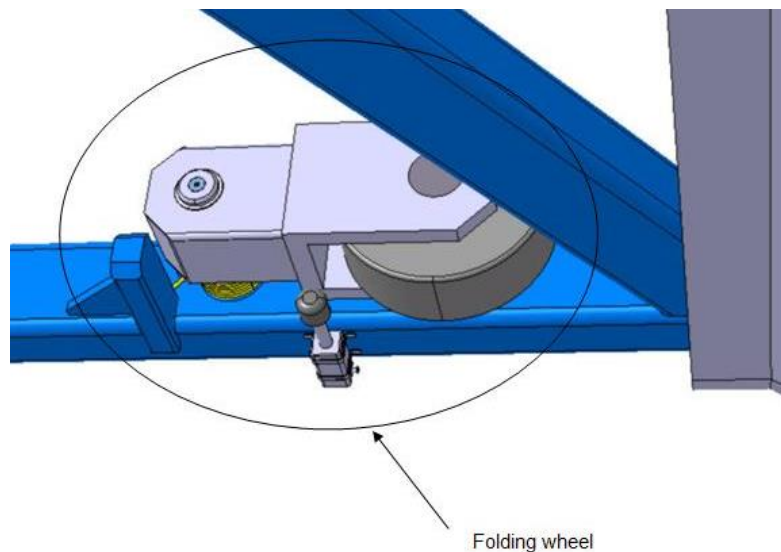


Fig. 101. Intermediate wheels.

The Pipe Forest includes a system to ensure the piping alignment at IF2a. It consists of two plates joined by rigid bars. The rear plate has circular holes where the Pipe Forest pipes are fitted. The front plate has tapered holes to guide the ends of the TBMs pipes (also tapered) as the Pipe Forest moves forward in the Interspace. The diagnostic pipes are aligned by the same system, although in this case the pipes end in plugs.

The gap between both plates is enough to allow the robotic arm gaining access to all the pipes to perform maintenance operations (cutting, welding and inspection of pipes and installation/removal of insulating modules).

The rear plate –hence the Pipe Forest pipes- is fixed to the Pipe Forest frame by several bars which fit in plate slots. This position is maintained to perform maintenance operations at IF2a. The fixing bars are extracted from the plate slots by means of hydraulic cylinders and the plate is only maintained by pipes rigidity. In ITER, this state is required to accommodate the displacement of the Vacuum Vessel and the thermal expansion of pipes during the tokamak operation.

The Bioshield Door includes an alignment system based on conical elements. It also includes a set of captive bolts around its perimeter to secure the anchor.

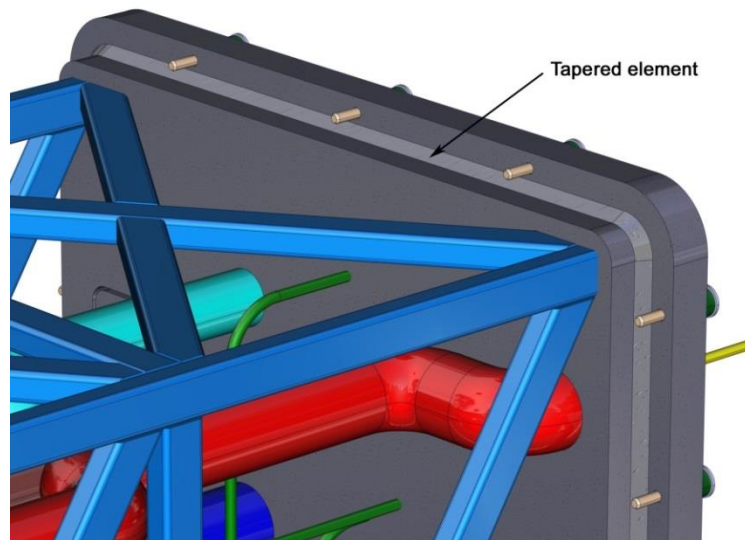


Fig. 102. PF Bioshield.

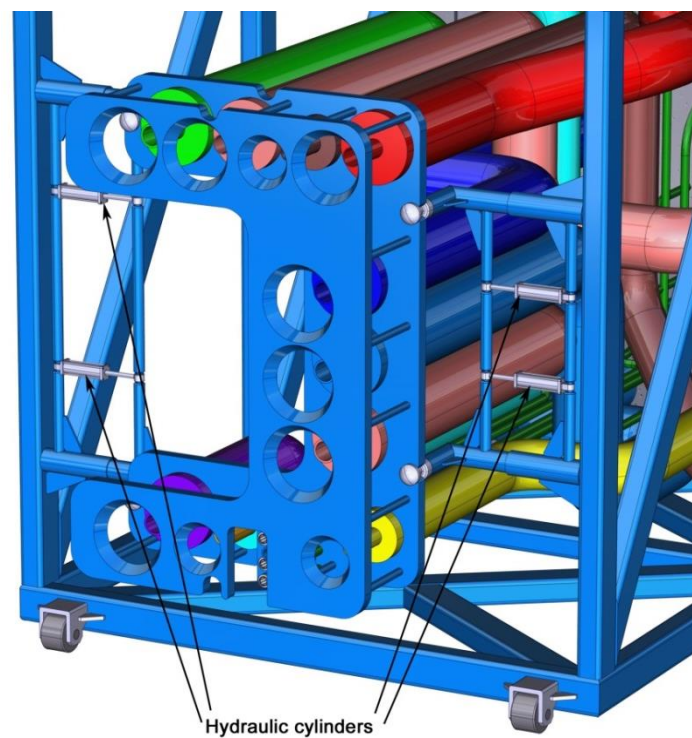


Fig. 103. PF alignment system.

The Pipe Forest includes a pipe-free corridor allowing access to the robotic arm to IF2a. The robotic arm must go through the Bioshield Door to gain access to the corridor, so a window has been included. It is opened and closed by means of a system based on a quadrilateral mechanism of parallel bars and powered by four hydraulic cylinders. They allow the window moving back and, in a second stage, moving laterally to the right of the Bioshield Door.

The window has a wheel in its underside which rides on a platform, holding on most of the weight and decreasing forces in bars and cylinders.

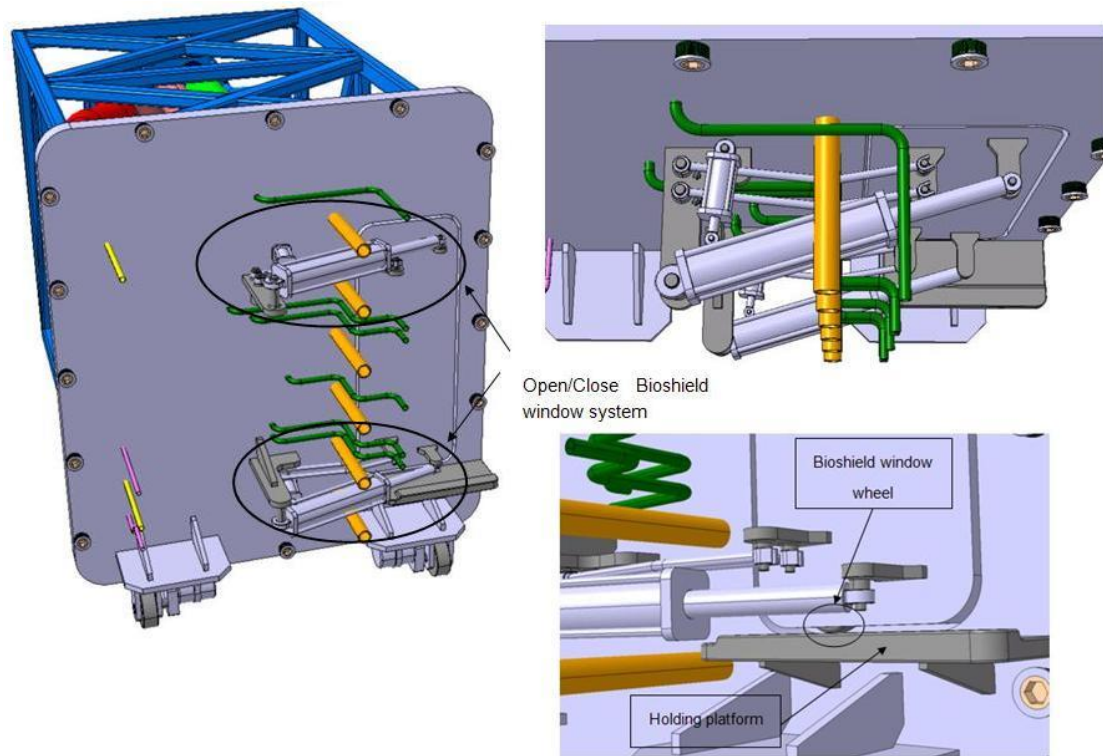


Fig. 104. Bioshield Window system.

### 2.5.6.3. Port plug mock-up

#### Functional requirements

- It must reproduce the external shape of the real port plug.
- The weight and the position of the centre of gravity must be equal to those of the real port plug.
- It must allow the vacuum sealing of the external flange used for attaching the PP to the port extension, as well as the vacuum sealing and vacuum testing of the internal flanges used for attaching the TBM & shield assembly to the PP frame.
- It must allow its manipulation during transport, in-port installation and maintenance operations in the Hot Cell.
- It must allow the welding of the pipes which connect the port plug cooling circuit with the TBM shield and the vacuum vessel cooling circuits.
- It must allow leak testing and pressure testing of the port plug and shield cooling circuits.
- It must withstand the mechanical stresses occurring during its manipulation.

#### Conceptual design proposal

In ITER, the equatorial port plug houses several systems and closes the equatorial ports, to ensure ultra-high vacuum conditions inside the Vacuum Vessel. The port plug is also the component in which the two EU TBM & shield assemblies are inserted. It is composed by a

central shield body, two windows for the TBMs first wall, a rear flange to be connected to the tokamak port and two internal flanges for fixing the shield modules.

It includes a guiding system for introducing the TBM & shield assemblies, which consists of 8 dowels (4 for each assembly) with conical head and cylindrical base which are placed on the shield fixing flanges –instead of the corresponding screw holes.

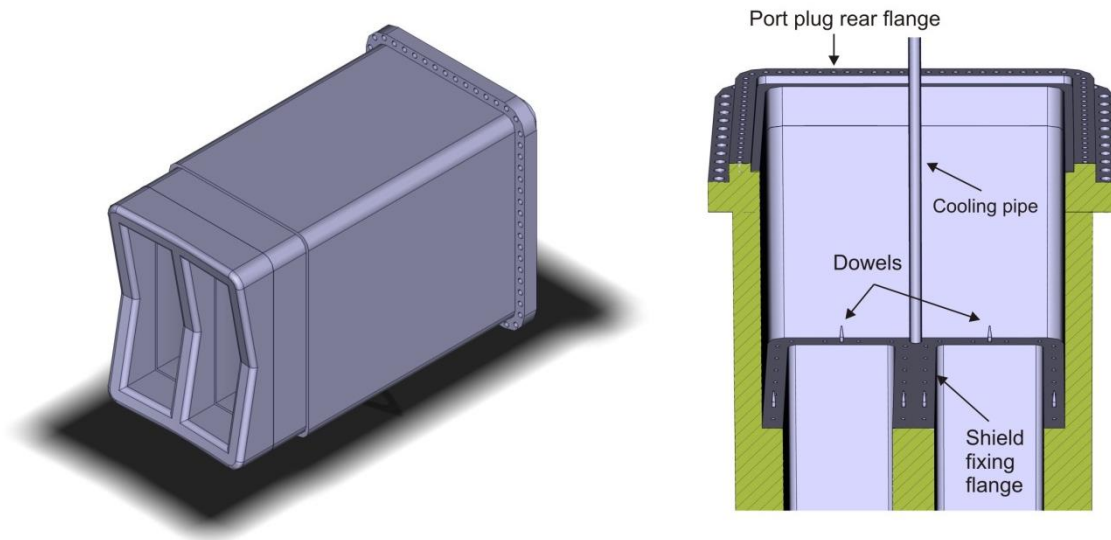


Fig. 105. Port plug. Section.

It also includes a helping cantilever system to make easier its movement inside the transfer cask and its transference between the transfer cask and the port or the vertical positioning tool. The lower side of the shield body has two wheels which move over the rails situated in the interior of the transfer cask. Given the port plug mass, its physical configuration and the design of the transfer cask gripper system, these wheels are needed during the transfer operation from the TC to the port extension in order to prevent the TC and PP set from tipping when the PP is held outside of the TC by the gripper in cantilever. This requires two hollows in the rear flange to allow the rails pass.

#### 2.5.6.4. TBM & shield mock-ups

##### Functional requirements

- The TBM mock-ups design must be such that the cutting operations for PIE (post irradiation examination) performed on it are equivalent in terms of difficulty to the ones performed on the real TBM.
  - It will include internal structural elements of the real TBMs. It will be also made of a material with similar behaviour regarding cutting.
- The TBM mock-ups design must be such that it is equivalent to the real TBMs one with regard to the remote handling operations to be demonstrated.
  - To ensure this the mock-ups will have the same total mass and a mass distribution that will give them an equivalent dynamic response to moments and vibration. They will also have the same external geometry (dimensions and shapes).
  - The connecting elements (pipes, mechanical and electrical connections, etc.) with the shield must be accurately reproduced so that they are equivalent in terms of RH features.
  - The pipes connecting the TBM and the shield must be such that the RH cutting operations are carried out in conditions equivalent to the real case ones.
- As long as the two previous requirements are respected, the internal circuits (cooling, regeneration, CODAC) of the TBM mock-ups may be removed.
- The TBM mock-ups must withstand the mechanical stresses occurring during their manipulation (separation from the port plug, separation from the shield, etc.).

- The shielding module mock-ups design must be such that it is equivalent to the real shielding modules with regard to the remote handling operations to be demonstrated. To ensure this:
  - They will have also the same external geometry (dimensions and shapes).
  - The shielding module mock-ups will have the same total mass and their mass distribution will give them equivalent dynamic response to moments and vibration.
  - The connecting elements with the TBM must be accurately reproduced so that they are equivalent in terms of RH. For example the flexibility of the mechanical connections and pipes should be the same as in the real shielding module.
  - The connecting pipes with the AEU must be accurately reproduced so that they are equivalent in terms of RH. For example the flexibility of the mechanical connections and pipes should be the same as in the real shielding module.
  - The shielding modules design must allow testing the vacuum seal quality between the shielding modules and the port plug.
  - The design must be such that the handling and separation (TBM-shield) operations are equivalent to the ones with the real shielding module.
  - They must withstand the mechanical stresses produced during their manipulation.
  - They must withstand the pressure applied to the cooling circuits during tests.

#### Conceptual design proposal

The design of the HCLL and HCPB Test Blanket Modules, as well as their shielding modules, evolved along the development of this conceptual design (2009-2012). Most of the RH operations, especially those related to the Hot Cell, were studied according to the reference HCLL model in 2009-2010, when the model of HCPB was no available and the models of the shielding modules were not well established. As previously mentioned, in 2011-2012, all the RH operations in the Port Cell and the Interspace were redefined, considering the modifications arising from the development of the European Programmes, which include new designs of the HCLL and HCPB TBMs and shields. As the RH operations in the Hot Cell were studied taking into account the HCLL TBM & shield design available in 2010, both the previous and the current TBM & shield models are described below.

#### **Hot Cell RH operations TBM & shield (2009-2010)**

The internal structure of the HCLL TBM mock-up is a simplification of the real component design, since it is not necessary to reproduce it exactly for the demonstration of the RH operations. Here only integration features and a design proposal for the interface between the TBM and the shield are shown.

#### *Handling features*

There are 4 special remote handling handles in the back part of the TBM in order to allow insertion of the lifting tool hooks. These handles are equivalent to the ones in the shield. There is a pipe for instrumentation cables that comes out of the back of the TBM through the inside of a stiffening rod.

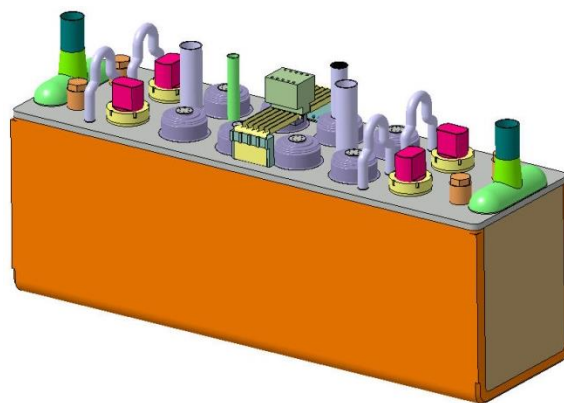


Fig. 106. HCLL handles (HC operations).

There are also other pipes that come out of the back of the shield that may need to be cut.

#### *TBM & shield interface*

The function of the interface between the TBM and the shield is to provide a rigid and stable connection between both parts. The joining of the TBM and the shield is achieved through 2 components:

- *Shear keys*: 4 shear keys are placed forming a rectangle at the back of the TBM. Their function is to resist the shear forces in horizontal and vertical directions. Therefore 2 shear keys are horizontally oriented and the other ones are vertically oriented.

Each shear key is composed of 2 parts: one welded to the TBM and the other one in contact with a shield extension that fits into it. During the cutting operation it is not necessary to cut the shear keys.

- *Union weld plates*: the function of these plates is to hold the TBM and the shield together. They are placed inside the TBM perimeter in order to not interfere with the port plug.

These plates are welded to the TBM and the shield and need to be cut to separate both components.

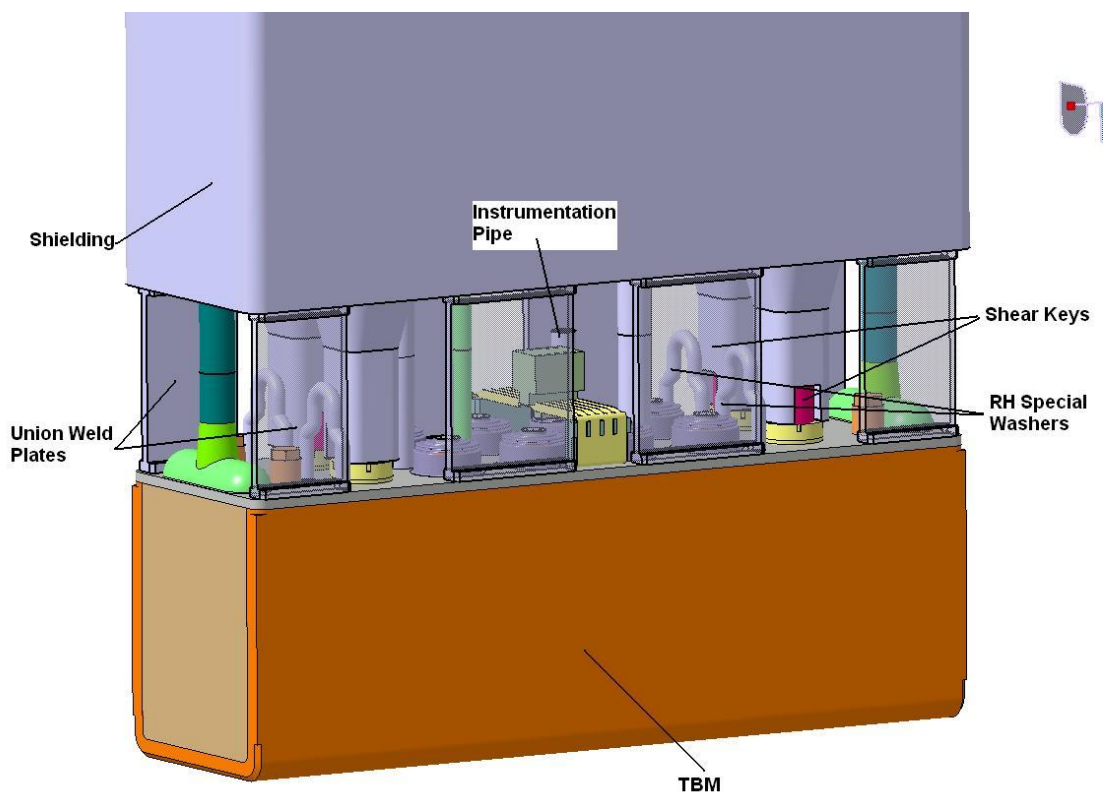


Fig. 107. Interface between HCLL TBM and shield (HC operations).

#### *HCLL shield design*

Since the TBM shield does not need to carry out a shielding function in the test facility, a simplified design of the real component can be used for the demonstration of the RH operations. At the moment of the development of this design, the real component design was still under discussion and thereby a hypothetical design is assumed here.

The pipe layout on the back of the shield is that of a HCLL TBM shield (2009-2010). The HCPB shield has a slightly different pipe layout. However, the RH relevant design features (lifting eyes, alignment dowels & holes and integrated O-ring gasket) and the RH operations would be the same in both shielding modules.

In order to perform the extraction or installation of the TBM & shield assembly in the port plug it is assumed that four lifting eyes are located at the top of the shield. The lifting eyes are wider in its base to make easier the engagement of the lifting tool hooks.

At the top of the shield and along the shield flange some captive bolts are placed. Surrounding each captive bolt there is a structure used for holding the screwer while torque is applied on the captive bolts.

There are four holes in the lower part of the shield flange in order to guarantee the self-alignment of the shield flange with the PP flange during the insertion of the TBM & shield assembly into the PP. The geometry of these holes matches that of the alignment dowels in the PP flange. Together, the dowels and holes guarantee the self-alignment function during insertion. In the lower part of the shield flange there are two slots which house the O-ring sealing gaskets.

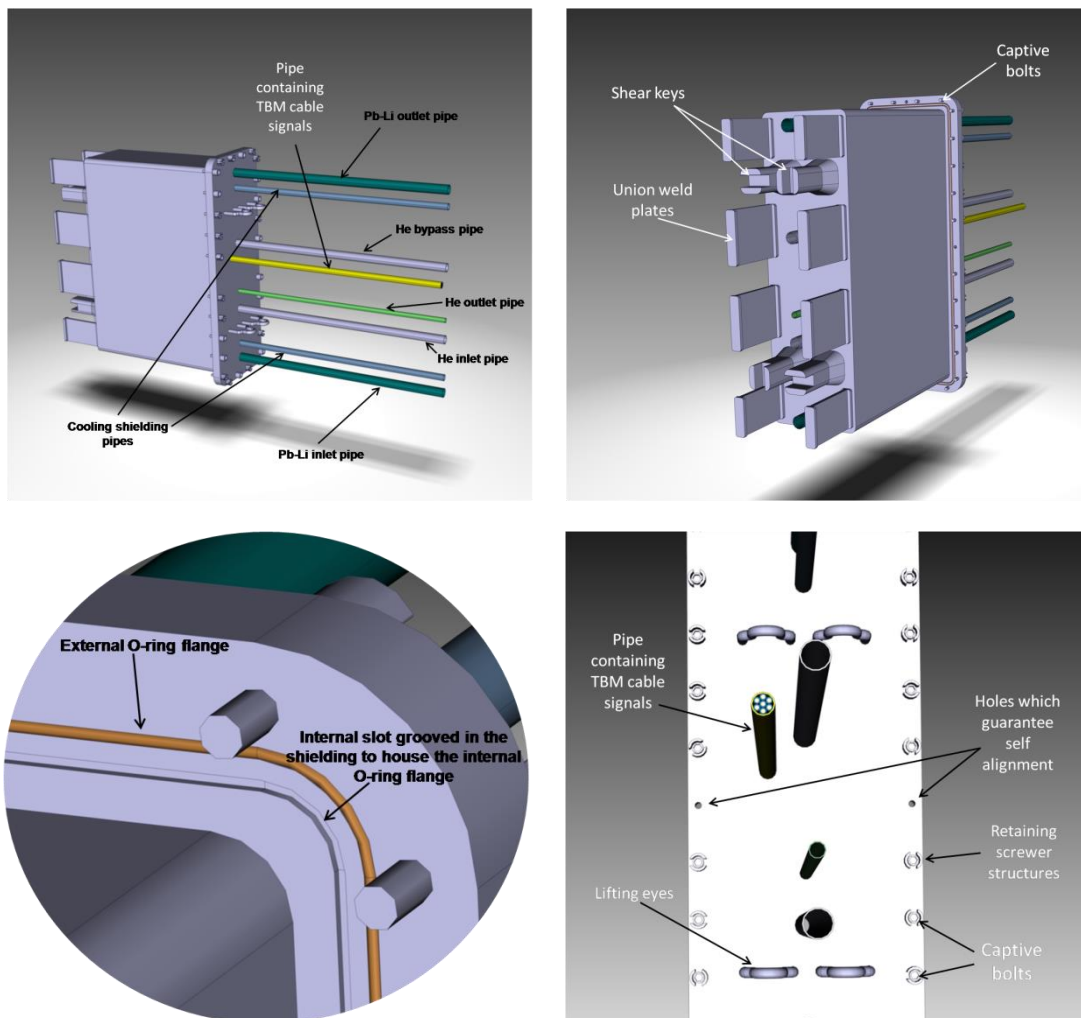
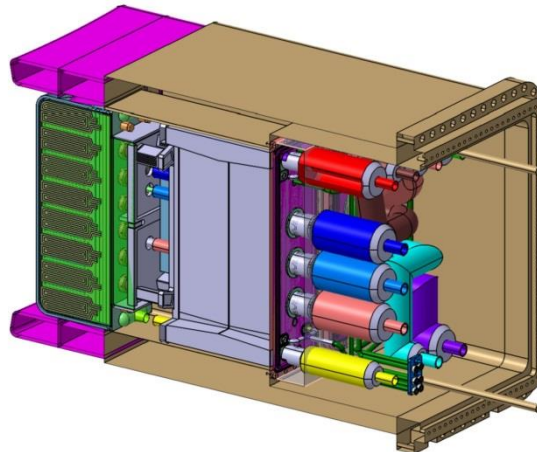


Fig. 108. HCLL shield design proposal (HC operations).

**Port Cell RH operations TBM & shield (2011-2012)**

The design of the shield available in 2011-2012 consists of two plates machined with the shape of the TBS pipes, which are joined at the central vertical plane. There are two other pieces at

the top and the bottom, also machined, that confer to the set a double T profile. These pieces are crossed by the water cooling pipes and by the inlet/outlet PbLi pipes (HCLL).



Port Plug with TBM Sets inserted. Cross section

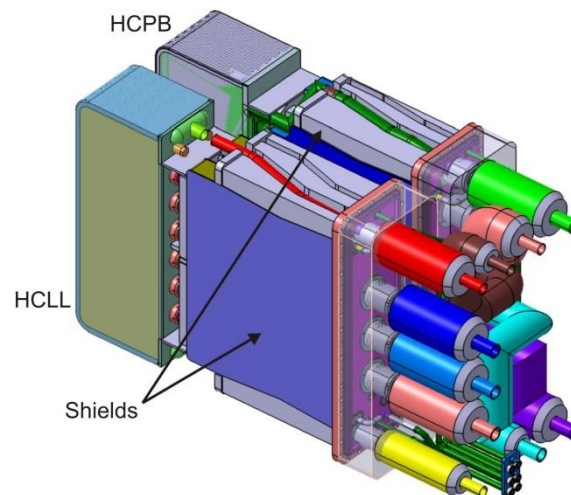


Fig. 109. HCLL & HCPB TBM & shields.

The shield plates/water tanks are placed in the lateral spaces that are among the four previous pieces and reach the IF1 coupling plate, on the TBM side (HCPB). There is an additional plate joined to the shield by means of stiffening rods in the HCLL. It is also connected to the TBM through flexible joints that arise from the plate welded to the rear side of this one.

Regarding to the HCPB, the main difference is based on the additional plate which is directly welded to the shield, without stiffening rods.

The pipes are inserted in the shield with joint looseness, which demands the use of deformable elements (bellows) built in a plate placed at the interface, on the rear side of the flange, in order to aid its adjustment (HCPB).

The TBM & shield sets pipes are welded or plugged to the Pipe Forest trough the interface IF2a. The opposite pipes must be aligned before connection can proceed.

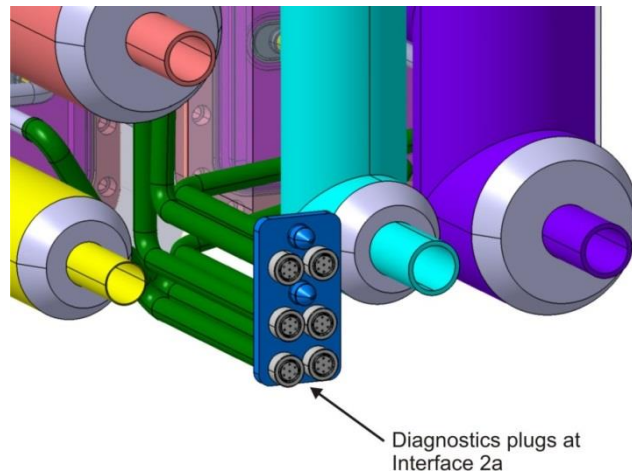


Fig. 110. Diagnostics plugs at IF2a.

### 2.5.6.5. Air transfer system (ATS)

#### Introduction

The ATS main function is to move the AEU, the Pipe Forest, the RH Platform Unit and the Transfer Cask from the Port Cell to the Hot Cell and vice versa. The ATS model used in the test facility will be the same as the one used in ITER. Since the ATS for the AEU is the same as the ATS for the TC, PF and RH Platform Unit, only one is needed in the facility. In this way the total cost is lowered.

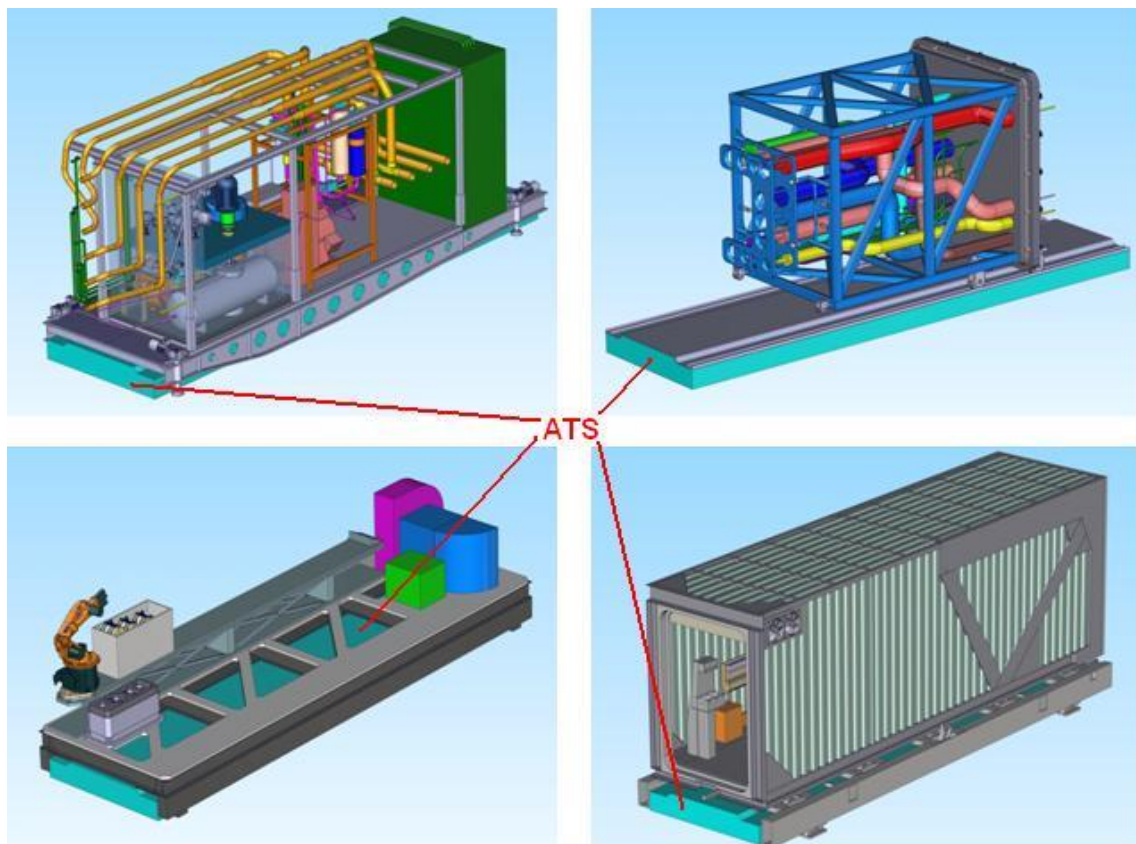


Fig. 111. ATS used to transport the equipment.

### Description

As previously mentioned, the Air Transfer System (ATS) is a transport system based on air bearings, which is used to move the Pipe Forest, AEU, RH Platform Unit and the Transfer Cask from the Port Cell to the Hot Cell and vice versa.

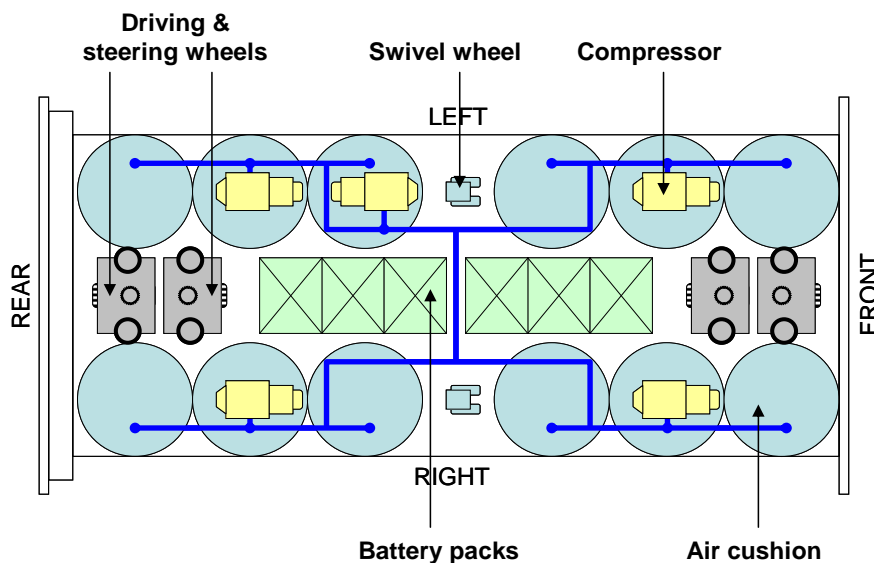


Fig. 112. Design of the ATS [Lor 07].

In normal operating conditions, it has no driver and it is remotely controlled by an operator.

The ATS uses 4 wheels (2 steering wheels and 2 laterally arranged traction wheels) to move while it is not loaded. Once the ATS is loaded, either with the AEU, the RH Platform Unit or the Transfer Cask, the air castors inflate with compressed air. These castors support the weight of the load. The wheels allow the movement and the steering of the ATS. There are some requirements concerning the absence of obstacles or the existence of too wide or deep gaps on the floor for effective movement of the ATS.

The ATS footprint dimensions are similar to those of the AEU and the Transfer Cask System.

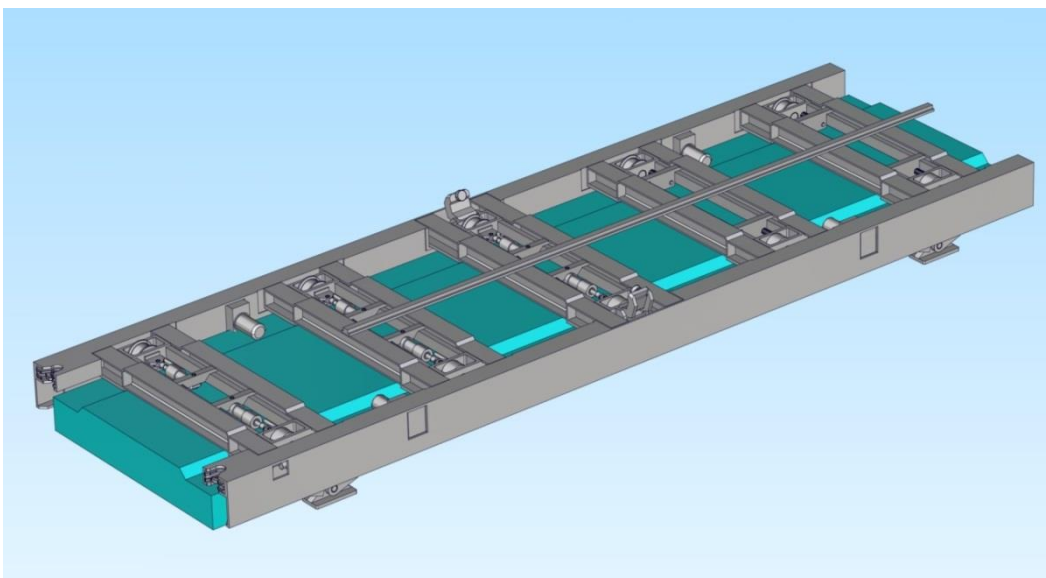


Fig. 113. ATS with the pallet of the Transfer Cask.

When the ATS is under the transfer cask pallet, the pallet legs are in contact with the ground.

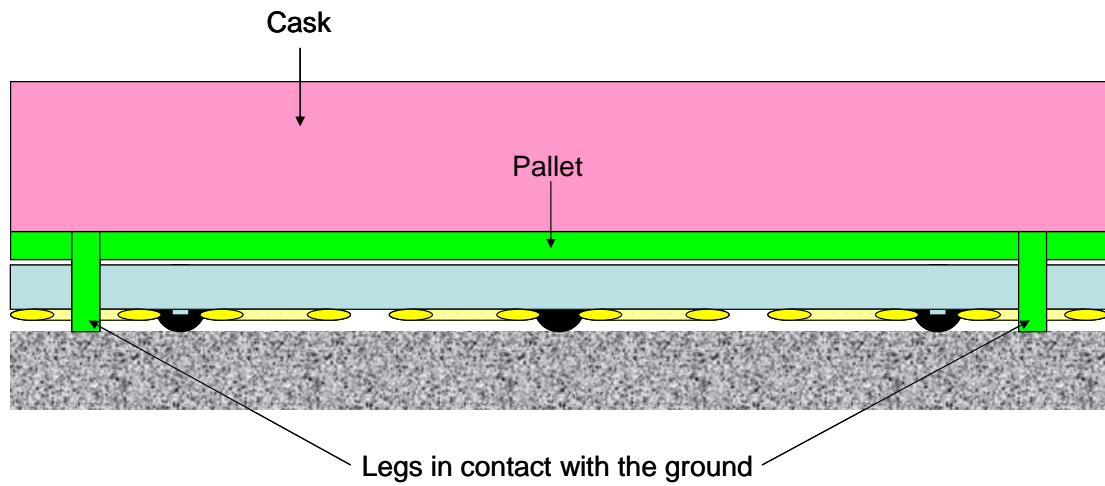


Fig. 114. ATS under the pallet [Lor 07].

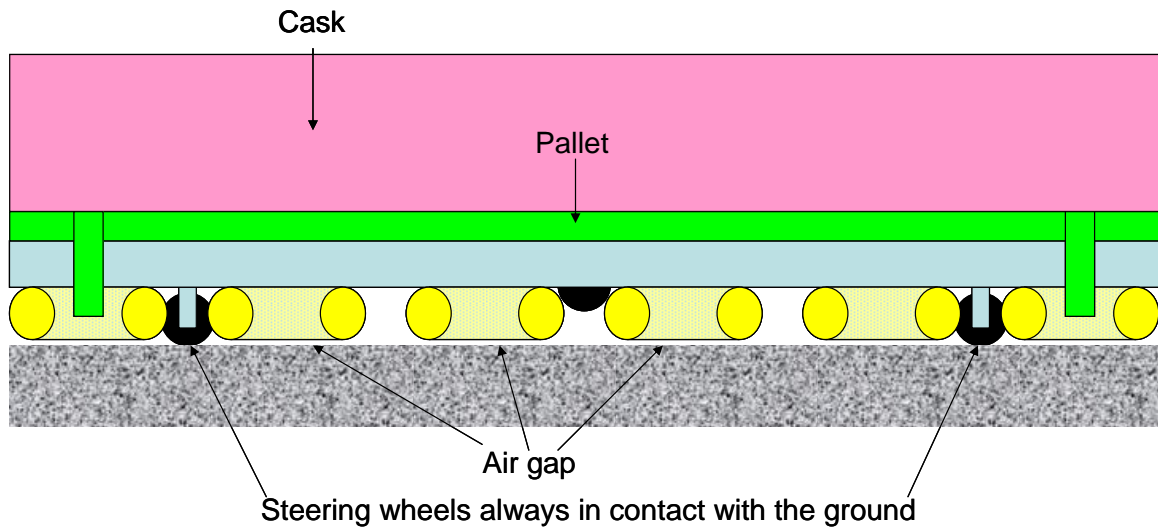


Fig. 115. ATS ready for transport [Lor 07].

Then the air cushions are inflated and produce a thin (~5 mm) air gap, so the ATS can drive the cask by means of its steering wheels.

A special platform with rails has been designed to be placed on the ATS for supporting and guiding the Pipe Forest & Bioshield Door assembly during its installation and removal.

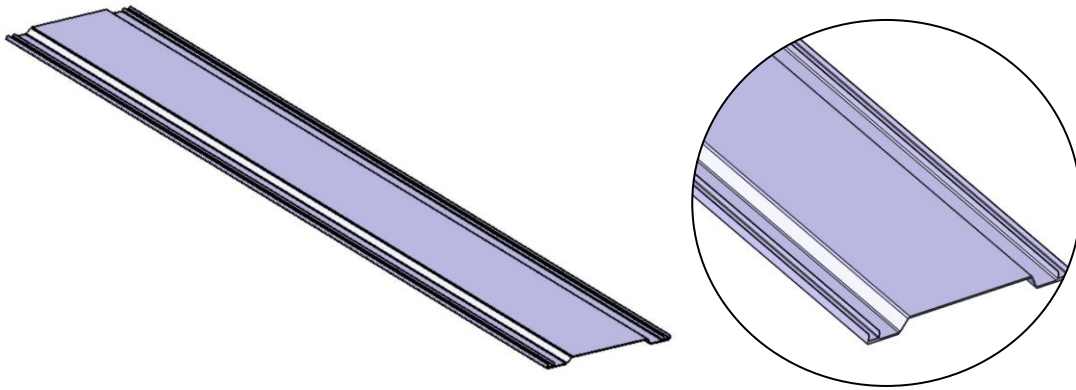


Fig. 116. Platform dedicated for Pipe Forest. Detail.

#### 2.5.6.6. Band sawing machine

##### Description

This machine allows cutting the TBM into pieces. The band sawing method is the only one that can cut very big components without limit on thickness. Moreover it does not need to follow the shape and it can cut a number of different materials. Furthermore dry-cutting is possible (no tooling fluid would be necessary) as the cutting speed is not high and the surface condition is not important [Bai 09].

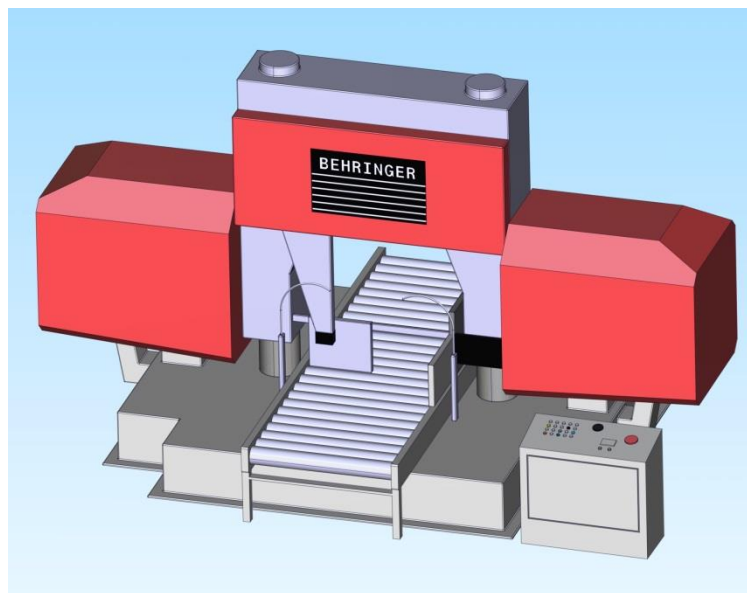


Fig. 117. Band sawing machine.

The Hot Cell manipulator and the overhead travelling crane are needed to handle the components and arrange them on the cutting table. Then a band driven by two wheels rotating in the same plane cuts the component, which slides over roller conveyors.

The machine includes hydraulic blade tensioning, a hydraulically-powered guide arm and computer numeric control (CNC).

The estimated space needs for the band saw is 4 m x 6 m x 5 m.

### 2.5.6.7. Drums and shipping basket mock-up

#### Introduction

The TN-MTR shipping basket has been proposed to be used in the ITER Hot Cell [Ghi 12]. There are different models depending on the capacity. Depending on the dimensions of the TBM pieces that will be packed and sent to the owners, the dimensions of the drums and the shipping basket will vary.

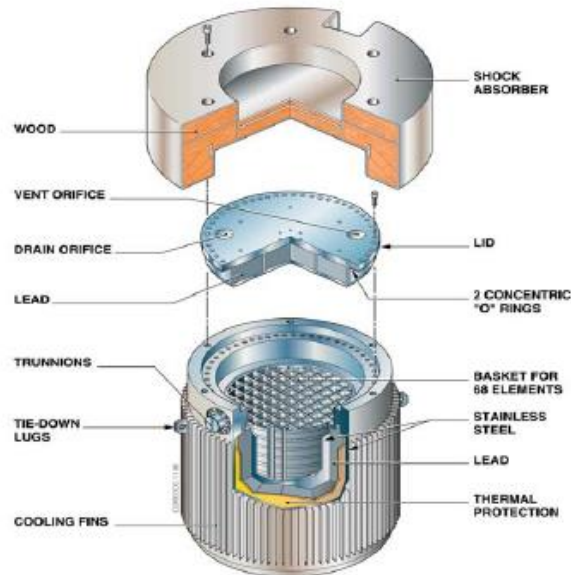


Fig. 118. TN-MTR shipping basket [Ghi 12].

#### Functional requirements

- The geometry of the shipping basket and drums mock-up must be such that the simulated RH operations consisting on the introduction of the TBM pieces into the drums and the subsequent introduction of the drums into the shipping baskets are representative of the same RH operations in ITER. For instance:
  - The inner dimensions of the drum mock-up should be the same as those of the ITER drums. The clearance between the drum and the hole where it fits in the shipping basket should be the same with the mock-ups than with the real ITER components.
  - The lifting features (if any) in the baskets and drums should be the same as in ITER.
- The construction of the drums and shipping basket should be robust enough to withstand the loads occurring during manipulation by RH.

Drum mock-up conceptual design proposal

Fig. 119. Drum.

The irradiated sample pieces are taken from the band sawing machine and introduced into the drums. Afterwards the drums are inserted into the shipping basket.

The dimensions of the drum vary according to the irradiated pieces. As no final information is available of which pieces are packed or not, the inner dimensions of the drums are still open. The inner dimensions of the drum suggested here are those that allow packing cooling plates from HCLL breeder units.

4 lifting eyes have been included in the conceptual design proposal.

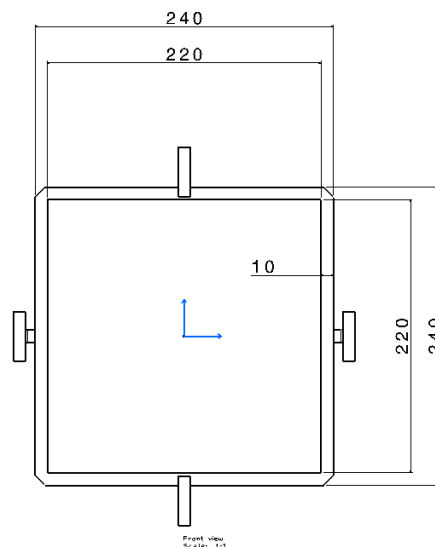


Fig. 120. Internal dimensions of a drum.

The maximum height of the drums is 1.08 m. This maximum height is imposed by the TN-MTR shipping basket dimensions. As shown in Fig. 121, the lifting eyes of the drums allow their manipulation by the crane. The design shown is hypothetical. The final shape and size of the drums must be the same as the ones adopted in ITER.

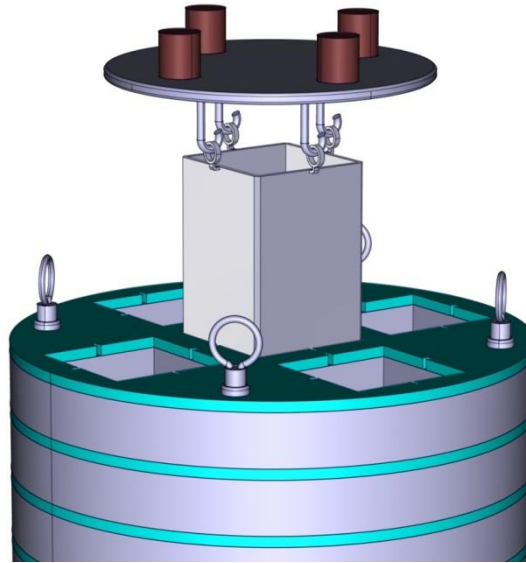


Fig. 121. Detail of the lifting eyes of the drum coupled to the gripping interface.

#### Shipping basket mock-up conceptual design proposal

The outer dimensions of the shipping basket are the ones of the TN-MTR packaging [Ghi 12]:

- Diameter of the cavity: 960 mm.
- Height of the cavity: 1080 mm.
- Weight of the empty basket: 2000 kg.

In this shipping basket conceptual design proposal there are four cavities where the drums can be introduced.

It has been assumed that placing and closing the lid are not TBM RH operations to be demonstrated in the test facility so the shipping basket does not include the shielding and lid parts of the TN-MTR container.



Fig. 122. Shipping basket with one drum inserted.

### 2.5.6.8. Plasma cutting tool

#### Description

This tool has a plasma torches rotating mechanism to cut the pipes at the Interface 2a. The plasma is produced from pressurized air (4-6 bar) [Bed 07].

It has a clamping system for positioning itself in radial direction around the pipe with high accuracy, whereas the axial accuracy requirement is achievable by the robot arm. The clamping force comes from spherical springs and the opening movement is acted by compressed air with pneumatic cylinders.

The tool operates with two plasma torches located against each other. The two torches operates together, thus a rotation angle of 180° is enough to completely cut a pipe.

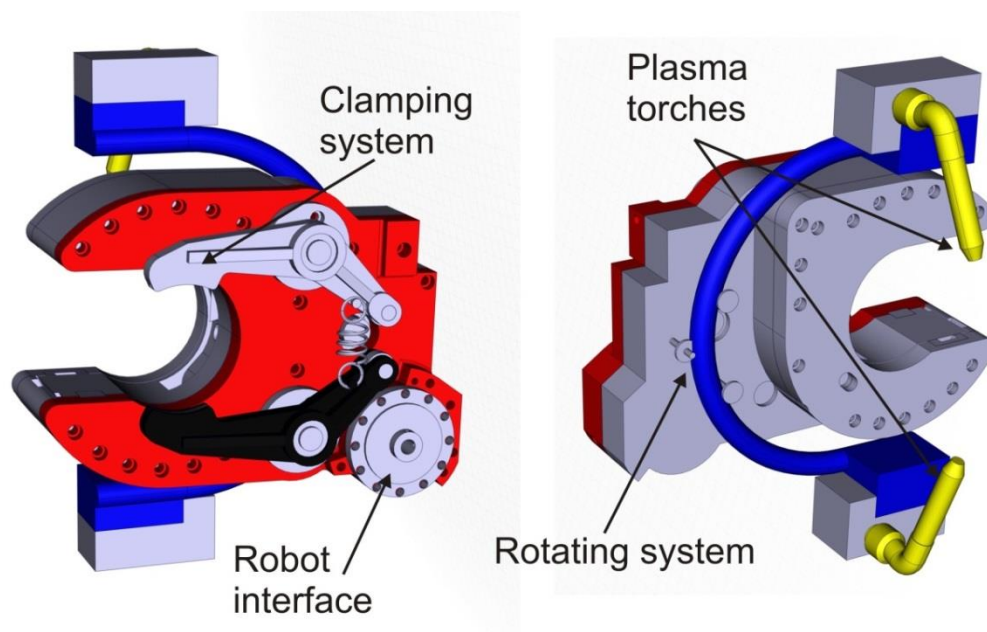


Fig. 123. Plasma cutting tool.

### 2.5.6.9. Gasket flange maintenance equipment

#### Description

This tool has been proposed in [Meu 07] to perform all operations related to the installation and removal of gasket flanges in ITER.

In the TBM RH test facility the gasket flange maintenance equipment is needed to install and remove the gasket flange from the Test Stand and the Port.

A very brief description of the gasket maintenance equipment can be found below. More details can be found in [Meu 07].

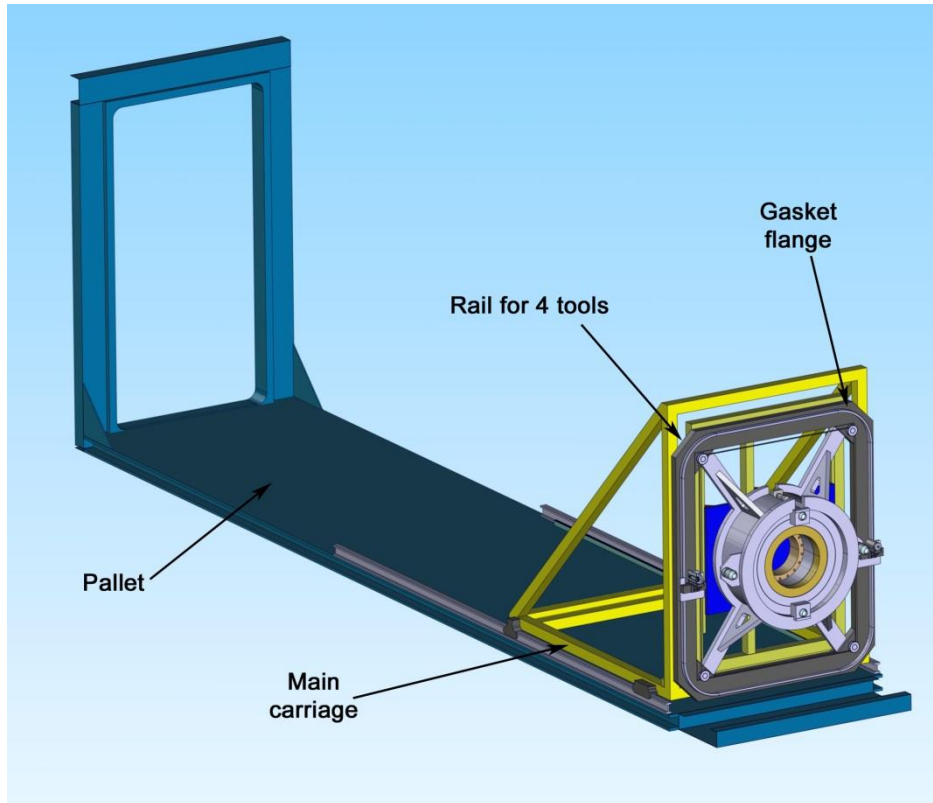


Fig. 124. Gasket flange maintenance equipment.

The gasket flange maintenance equipment consists in a pallet and a main carriage. The carriage can move along the pallet by means of a pinion-rack system. The carriage contains a rectangular rail along which different tools can move. These tools include a bolting/unbolting tool, an inspection tool (cameras) and a polishing tool. These tools would be replaced by hand.

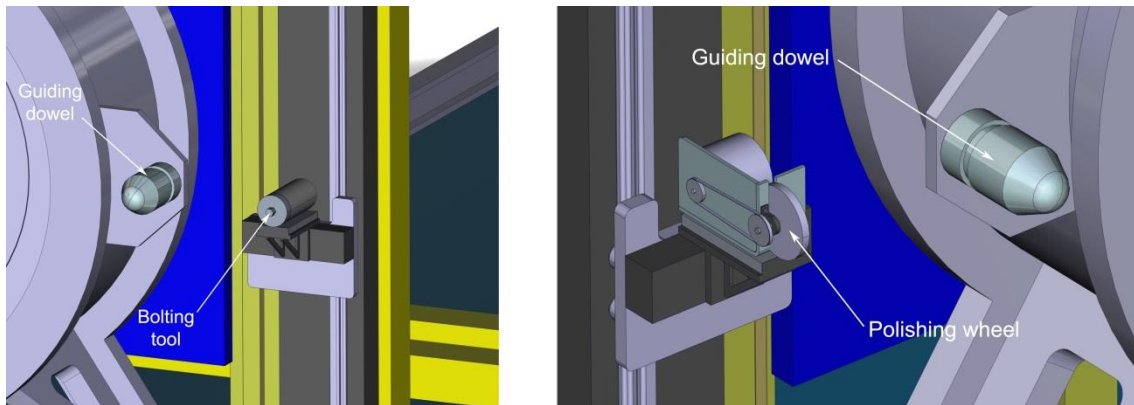


Fig. 125. Bolting and polishing tools.

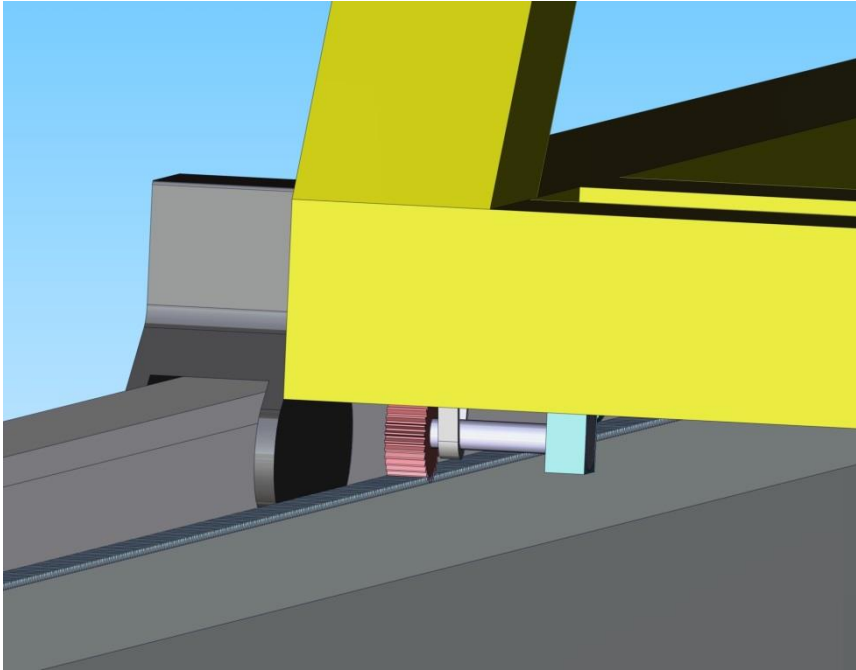


Fig. 126. Pinion-rack system.

#### 2.5.6.10. Hot Cell manipulator

##### Description

This design is the same as that of the MASCOT manipulator used in JET. It allows manipulating objects and tools like a bolt runner or a polishing tool. The manipulated tools have a gripping interface for the manipulator clamps.

Its dimensions are: 1860 mm (length of the arms – although the limits of the mechanisms do not make possible to reach all the length of the arms-); 540 mm (width of the central box) x 548 mm (length of the central box) x 420mm (height of the central box).

Each arm has seven degrees of freedom and the maximum payload by arm is 5 kg.

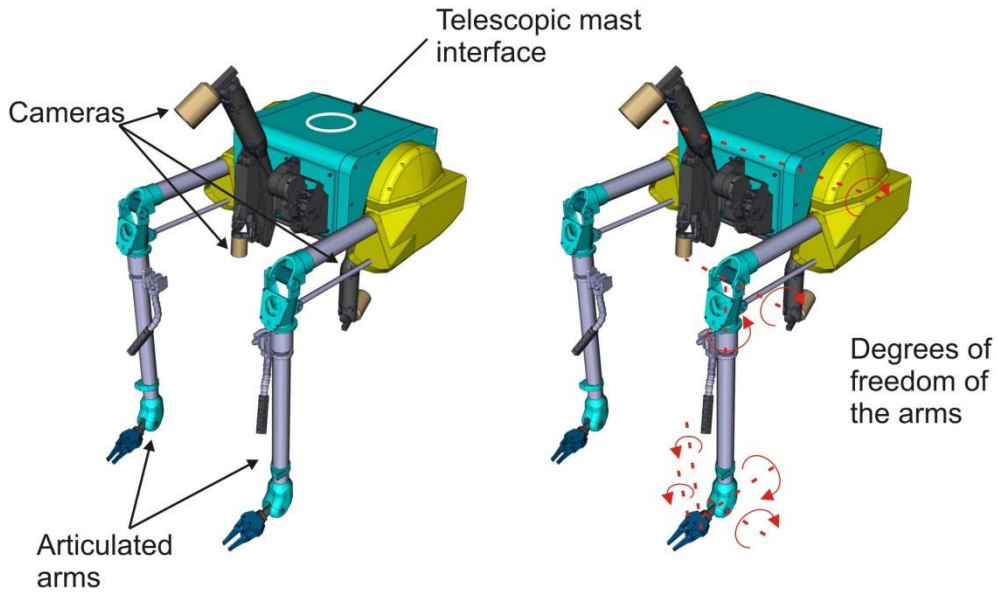


Fig. 127. Hot Cell manipulator.

The manipulator is joined to a telescopic mast which can slide along an overhead travelling crane.

#### 2.5.6.11. Welds inspection tool

##### Description

This tool is used to inspect the weld seams on the Interface 2a pipes [Bed 07]. It is based on the phased array ultrasonic technology, which allows generating an ultrasonic beam with the possibility of setting the beam parameters such as angle, focal distance and focal point size through software. Furthermore, this beam can be multiplexed over a large array.

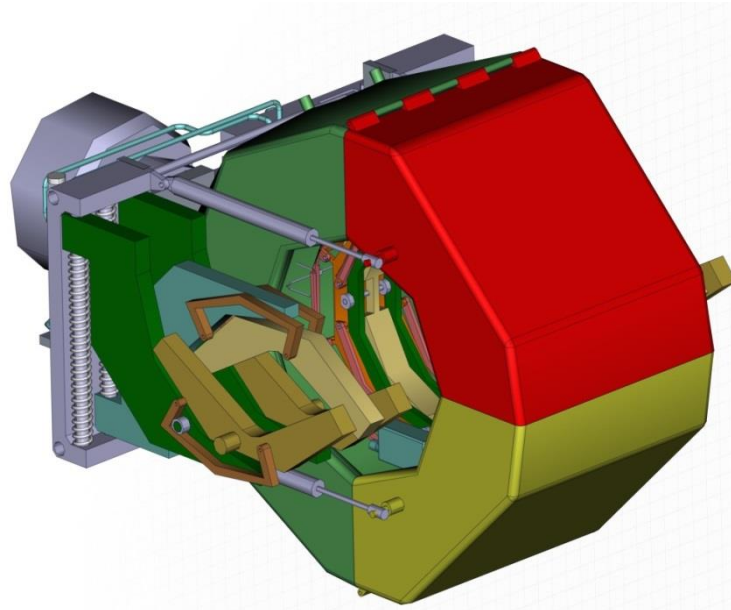


Fig. 128. Welds inspection tool.

The tool uses 4 heads to make the inspection faster. The heads are installed in pairs at the two sides of the weld seams. Two pairs are located at opposite sides of the weld seam (with 180° shift). The heads inspect the weld seams with angle.

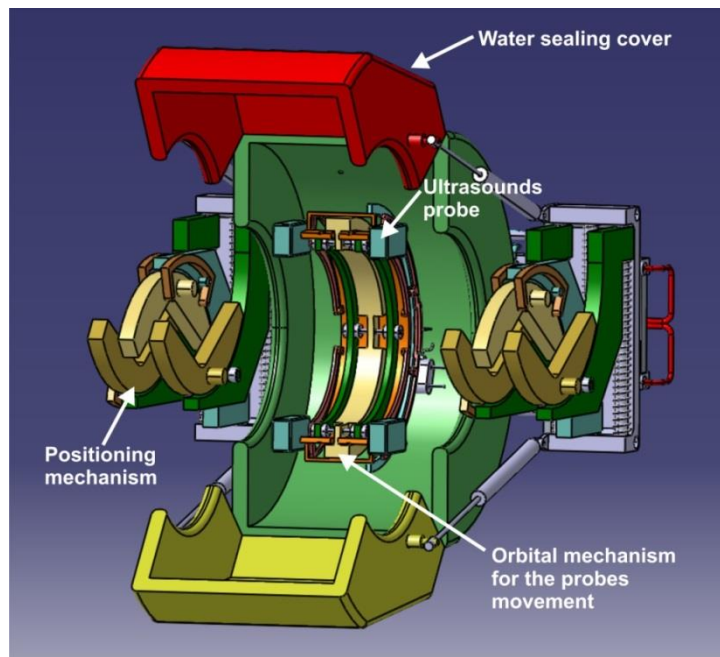


Fig. 129. Welds inspection tool (open water sealing cover).

The robot places the tool on the inspected weld seam. It is positioned by clamps driven by pneumatic cylinders. The heads rotate around the weld seam by 180°. A spring is used to provide the required force to connect the heads to the pipe surface.

The tool is filled with water to provide the proper contact medium between the inspection heads and the weld surface.

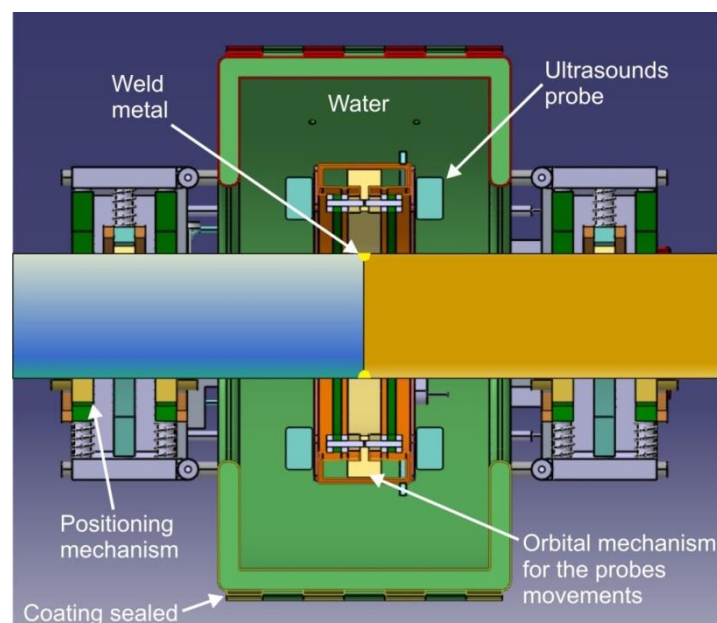


Fig. 130. Scheme of a weld inspection.

### 2.5.6.12. Thermal insulating modules

#### Description

Helium and lead lithium at high temperature are circulating through the Test Blanket System pipes between the TBMs and the AEU systems. The pipes in the zone of the Pipe Forest can be permanently insulated, but near the Interface 2a pipes must be reachable for assembly/disassembly operations during maintenance periods. Therefore, to install removable thermal insulations in this area is needed.

The proposed module design consists of a clip made by 2 insulated jaws, which is kept closed around the pipes thanks to a torsion spring [Kel 10]. A RH compatible claw enables to open the clip, with a simple pneumatic parallel gripper. When the clip is opened the robotic arm can remove it, and store it in a specific container.

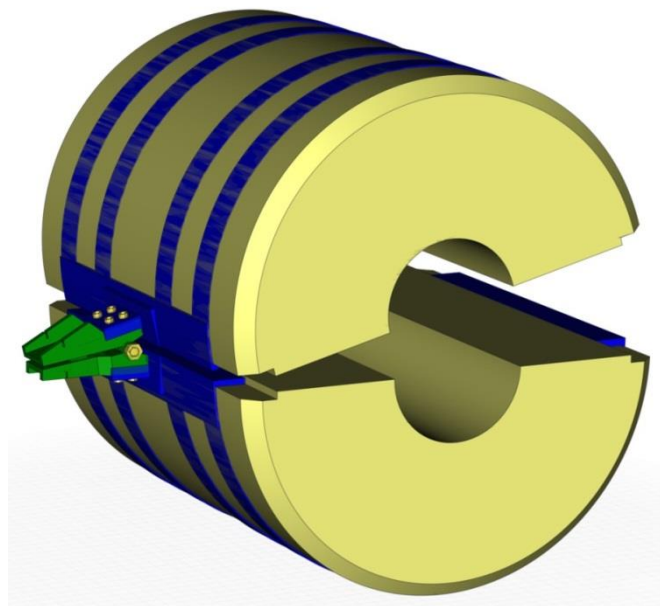


Fig. 131. Thermal insulating module.

### 2.5.6.13. Laser cutting tool

#### Description

In order to cut the interface between TBM and shield (IF1) a laser cutting system is proposed. It is attached to a special support structure and a shielding structure.

#### *Laser source features and specifications*

Laser FLS N-Series; Pulsed Nd: YAG lasers (CO<sub>2</sub>); 300 to 600 W output.

Company: LASAG Industrial Laser (Swatch Group).

Main advantages: modular design and high flexibility.

Cuts up to 20 mm thickness / oxide-free cut surface.

Materials suitable for machining: steel and stainless steel.

Sources available:

Laser type: Pulsed Nd: YAG-solid-state laser

Wavelength: 1064 nm

Pulse length: 0.1 - 20 ms  
Pulse repetition rate: 0.1 - 1000 Hz  
Pulse Energy: 60 - 150 J  
Peak power at 1 ms max.: 5 - 50 kW  
Average power max.: 300 - 600 W  
Line power:  
Configuration: 3-phase + ground,  $\pm 10\%$   
Multitap transformer for: 3x208 V, 230 V, 300 V, 400 V, 440 V, 480 V  
Power consumption: 14 - 28 kVA  
Line frequency: 50 Hz or 60 Hz  
Ambient conditions:  
Ambient temperature: 10 - 35 °C  
Relative humidity max.: 80%  
Emissions:  
Heat dissipation approx.: 0.4 kW  
Noise at 1mm, idle: 65 dBA



Fig. 132. Laser source.

#### *Support Structure and cutting head*

The Support Structure has been specially designed to support the laser head and to drive it during the cutting operation at IF1. The TBM & shield assembly is located inside a specific cutting bench. The laser support structure is located in front of the cutting bench.

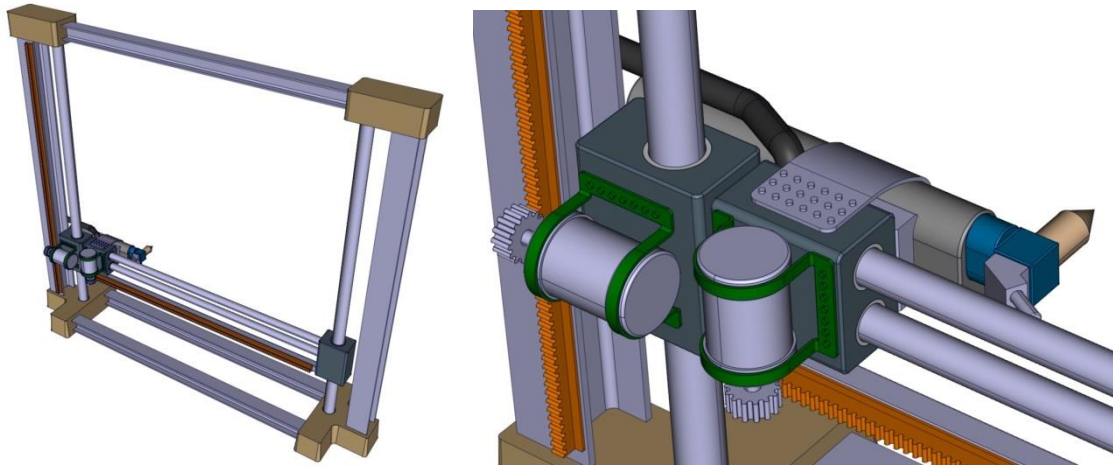


Fig. 133. Support structure. Detail of the cutting head.

The structure is composed of horizontal and vertical guides. The movement of the laser is achieved through rack-pinion systems which are powered by electric motors.

#### *Shielding structure*

The function of the shielding structure is stopping the laser beam: It is located behind the cutting bench. It is composed of a steel structure in order to contain the shielding plate.

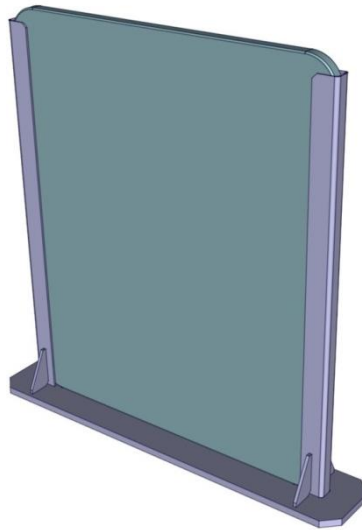


Fig. 134. Laser shield.

A refractory material such as silicon carbide can be used for the shielding plate.

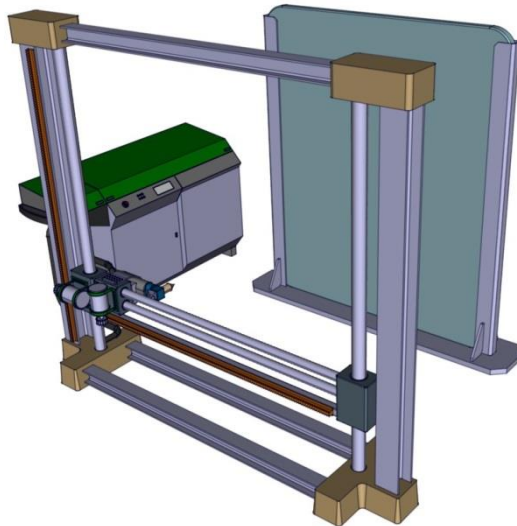


Fig. 135. Laser cutting tool.

#### 2.5.6.14. Lifting tool for TBM & shield

##### Description

The function of the lifting tool is to hold the TBM & shield assembly during the following remote handling operations in the Hot Cell:

- Extraction of the TBM & shield assembly from the port plug and insertion into the separation bench.
- Extraction of the shield from the separation bench and insertion into the supporting bench.
- Extraction of the TBM from the separation bench and insertion into the band sawing machine.
- Extraction of a new TBM & shield assembly from the supporting bench and insertion into the port plug.

The design concept of the tool is hypothetical and not formally approved by the ITER RH Group.

The shield lifting tool has four arms. Each arm ends in a hook. All the arms are coupled at the top, whereas the top interfaces with the 20 tons crane by means of four coupling pins that can be gripped by the crane. Additionally, the top of the lifting tool has four cylinders on its sides (2 per side) in order to be used as supporting points when the tool is left in the rest bench (container).

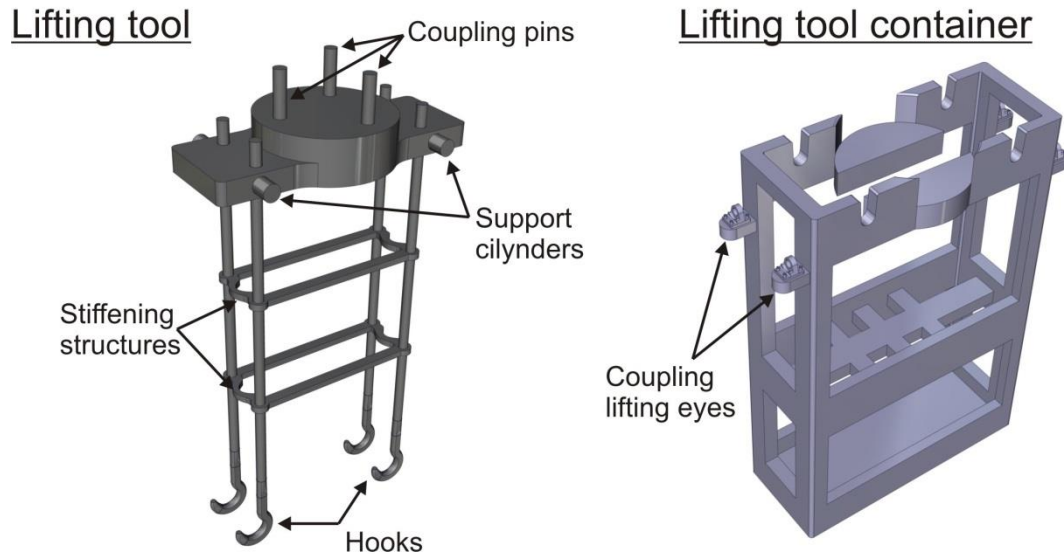


Fig. 136. TBM & shield lifting tool and container.

There are also two structures which interconnect the arms in order to stiffen them. These structures are adapted to the geometry of the shield backside pipes.

#### 2.5.6.15. 20 ton overhead rotating crane

The main function of the 20 t overhead rotating crane is to lift and rotate equipment during the demonstration of RH operations. It includes a robotic manipulator suspended from a telescopic mast, which is used in the demonstration of a number of Hot Cell TBM RH operations. The design of the rotating crane and manipulator should be the same as that of the crane and manipulator in the ITER Hot Cell. Since these are not currently defined, for the TBM RH Test facility the following conceptual design is proposed.

##### Functional requirements

- The crane must be able to reach anywhere in the operation hall area. It covers the whole width of the operation hall.
- The free space between the floor and the crane when the coupling tool and the manipulator are in their uppermost position must be in accordance with the vertical space requirements of the TBM RH operations (9 m).
- The crane must have a trolley with a rotating coupling tool suspended by cables for lifting and rotating equipment in RH operations.
- The coupling tool has a locking mechanism allowing it to remotely grip and release different lifting tools.
- The crane has a trolley with a telescopic mast and a two handed manipulator controllable from the control room.
- It must be possible to control the crane either from the operation zone or from the control room.
- The load capacity of the crane must be enough to lift any piece of equipment during the RH operations (20 tons).

##### Conceptual design proposal

The overhead crane has an electrical motor which allows it moving along the guide girders (rail beams) of its supporting structure. The crane has two independent trolleys:

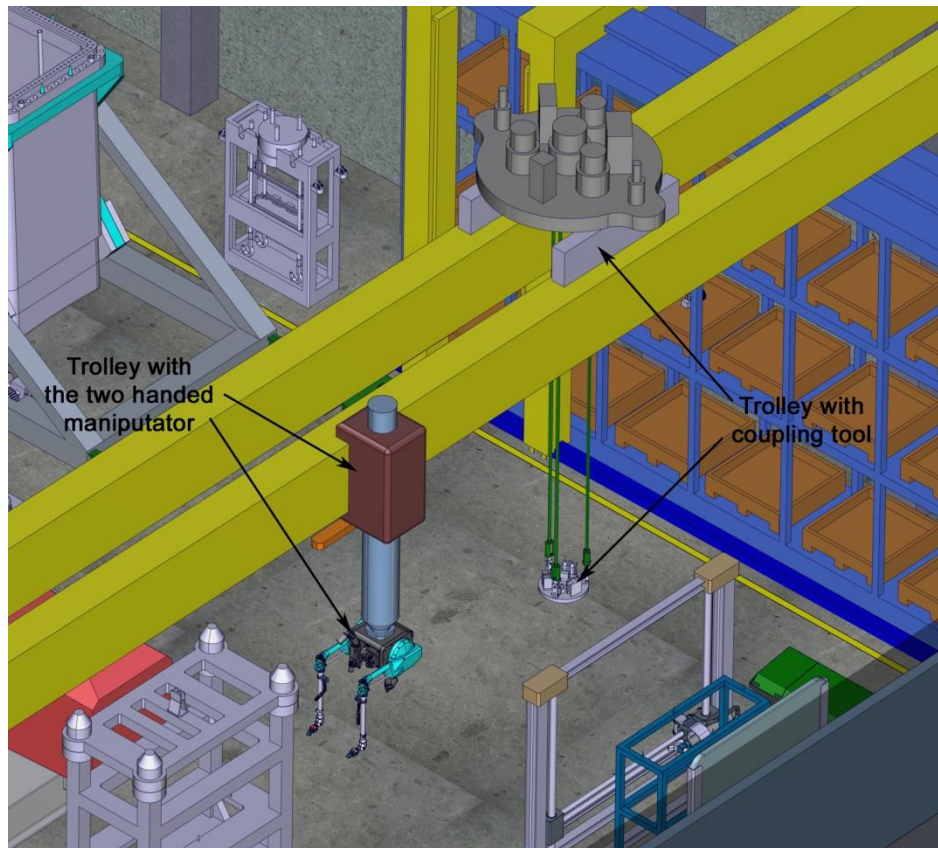


Fig. 137. View of the two trolleys integrated in the crane of 20 tons.

#### *Trolley with coupling tool*

The trolley has a motor to move it along the transversal direction. The trolley also allows rotating the coupling tool. The coupling tool design shown is inspired from the one used in the DTP facility (Divertor Test Platform, ENEA Brasimone), named PFCT (Plasma-facing Components Transporter) [Mic 07]. The coupling mechanism for the different lifting tools and pieces could be similar to the one used in the DTP coupling tool (e.g. winch mechanisms and locking actuators). The coupling tool in the TBM RH test facility can only be rotated, but it cannot be tilted. The trolley assembly holds the coupling tool by means of three cables. It has a lifting capacity of 20 tons and allows coupling tools for handling payloads at very low joint velocities with good positional accuracy.

This trolley performs the following functions:

#### *A. Removal or installation of components in RH operations*

Examples of these tasks are the removal of the TBM from the port plug or the insertion of the TBM into the port plug. Lifting some components may need special lifting tools.

#### *B. Supporting of heavy tools during RH operations for the manipulator*

The crane can be used to support heavy tools that the manipulator might not be able to hold by itself during RH operations. A special supporting interface would be needed.

#### *C. Lifting of equipment during non RH demonstration operations*

The crane could be used to move equipment around the operation hall (e.g. Port Cell wall modules), when it is not used for demonstration of RH operations.

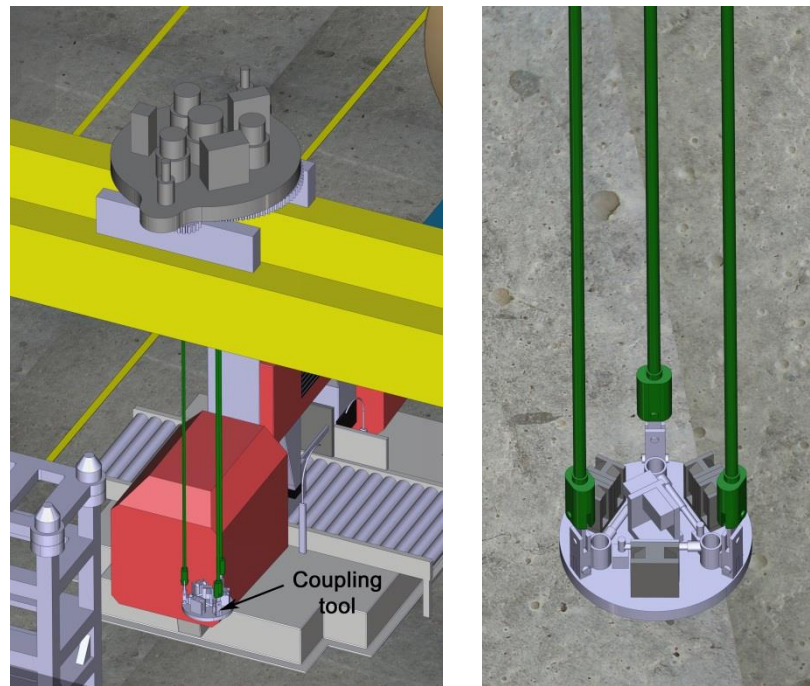


Fig. 138. Trolley with coupling tool (left). Zoom view of the coupling tool (right).

*Telescopic mast*

The telescopic mast serves as support for the robotic manipulator and gives it 3 degrees of freedom to reach its objectives.

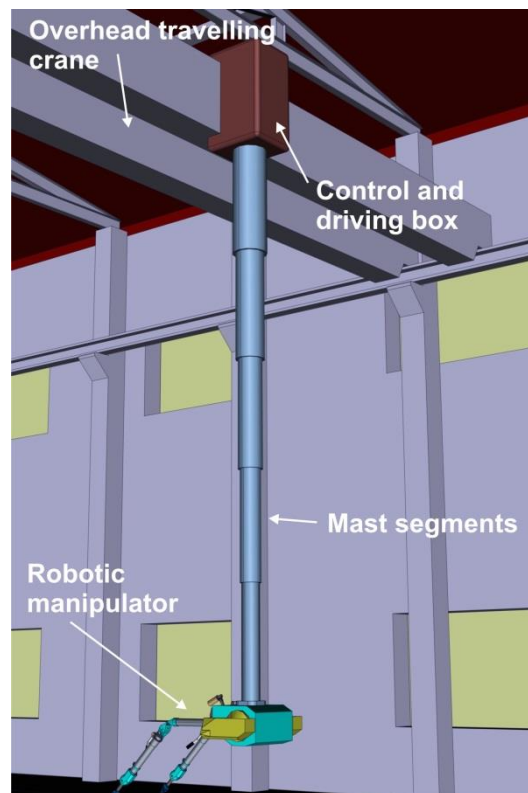


Fig. 139. Telescopic mast.

It has a hydraulic system to allow the relative vertical displacement between several concentric segments. One of the segments can also rotate around its axis, while the upper box can slide along the overhead travelling crane beam, so the combined action between the telescopic mast and the overhead travelling crane allows the manipulator reaching a large range of positions in the operation area.

#### *Control and operation of the overhead travelling crane*

The crane can be controlled either from the operations hall or from the control room. Each trolley can be independently controlled. The crane and manipulator have cameras to help the operators who are located in the control room. The amount and quality of video information should be equivalent to that of the ITER Hot Cell.

The manipulator is controlled by means of a master haptic arm situated in the control room.

#### **2.5.6.16. Palletising system and storage shelves**

##### Functional requirements

- The storage shelves must support their own weight, the weight of the palletising system and the weight of the pallets and tools.
- The palletising system must be designed in such a way that it can access all parts of the storage shelves where pallets are stored without any clash. The system must allow movement along the axis parallel to the guiding rail, along the axis perpendicular to the storage shelves and along the vertical axis. It must also allow rotation around the vertical axis.
- The storage shelves must have enough space to house all tools and pallets needed for the demonstration of the TBM RH operations in the Hot Cell.
- The storage shelves and the palletising system must be designed in such a way that pallets with tools can be left on the floor next to the areas where the RH demonstration operations are being carried out.

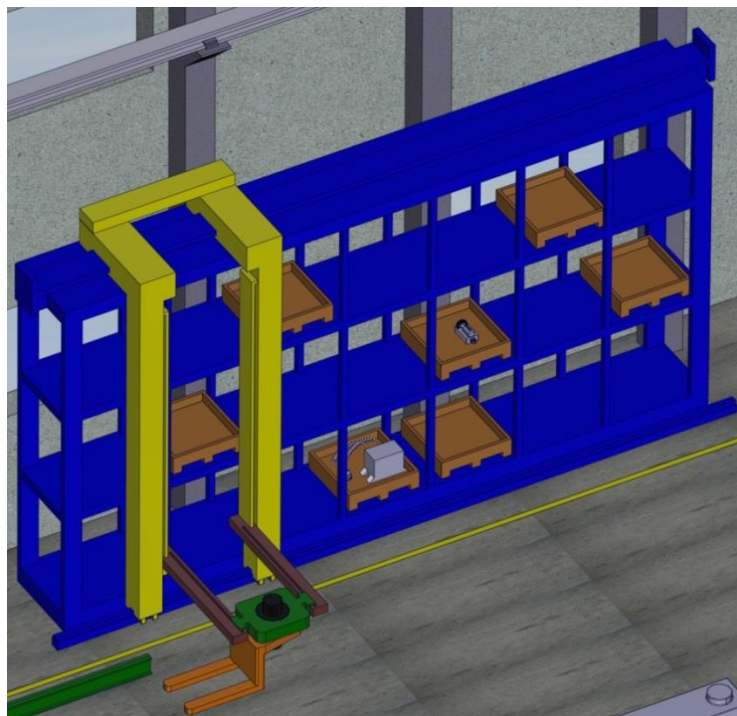


Fig. 140. Storage shelves and palletising system.

### Storage shelves conceptual design proposal

The provisional dimensions are 19.4 m x 1.4 m x 6 m. Besides, in the upper part a rail is welded with a height of 90 mm. This dimension is only for guidance; it should be modified depending on the needs within the HC. The storage shelves would be made of steel.

The palletising system moves uniaxially along the upper and lower rails. In both extremes of the shelves a non-useful space is left so that the palletising system can reach the modules located at the ends of the storage shelves.

In total there are three levels of shelves. The distance between the first level of the storage shelves and the floor could be bigger than the distance between the other levels of the storage shelves in order to house the biggest and weightiest tools, so that the requirement of these is as easier as possible. It is the case of e.g. the vacuum cleaner.

In each level there would be 12 modules. Therefore 36 modules would be available to house the tools needed for the RH demonstration operations.

The distance between the test facility floor and the bottom level of the storage shelves must be at least the height of the floor rail, so that the palletising system can reach the bottom pallets.

The factors determining the size of each module are the following:

- Width of the shelf (distance between poles): it depends on the width of the pallet. Although the tools are located on the pallets, the width of the pallet is bigger than the tools. A safety margin of 10 cm has been considered between the pallets and the poles on each side. In total the distance between poles is 1.4 m.
- Length of the storage shelves (depth): depends and the pallet dimensions as well. A safety margin of 10 cm has been considered between the pallets and the front and rear ends of the storage shelves. The depth is 1.4 m.
- The height between levels of the storage shelves is determined by the height of the tools plus the height of the pallet. As the tools needed are determined, their dimensions will be used in the definition of the height between levels of shelves. A distance of 1.6 m is assumed between the floor and the first level of shelves. This distance can be modified in order to satisfy the requirements of accessibility of the heaviest and biggest tools. The distance between the rest of levels is 2 m.

### Palletising system conceptual design

The palletising system is composed of 5 components. These are:

- Y-guide arm (left and right).
- Floor rail.
- Z-guide arm (left and right).
- X-support cylinder piece.
- Z-cylinder.
- Pins.

These components guarantee all the needed movements.

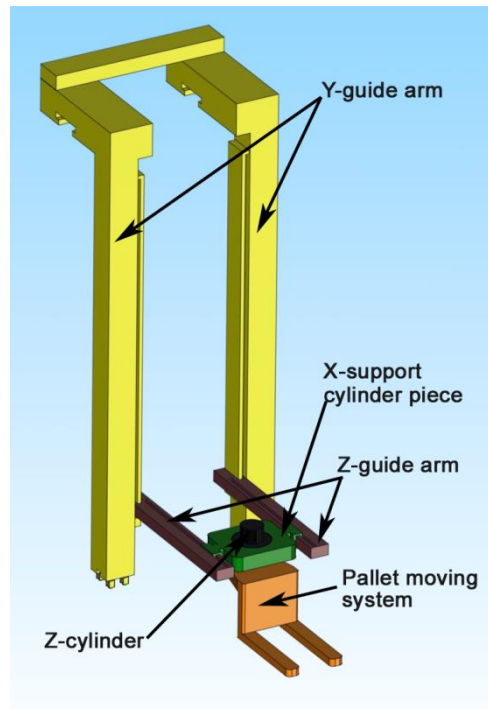


Fig. 141. Palletising system.

The movements of the palletising system are provided by electrical servo-motors.

#### *Y-guide arm*

Through the upper rail, welded to the storage shelves and the rail in the floor, this arm assures the translation along the Y axis. In the upper part this translation is provided by a rack-pinion system. The pinion would be attached to the Y-guide arm and the rack would be the upper guide rail.

The lower rail is used to support part of the weight of the Y-guide arm so that it is not supported only by the storage shelf. In the lower part of the arm, a 4 wheel system is attached in order to reduce the friction losses. Along the vertical (Z) axis the Z-axis a guide is made so that the Z-guide arm can move.

A two Y-guide design is proposed for the palletising system, although other variations would be also possible, e.g. a design with one-guide arm.

#### *Floor rail*

The length of the floor rail is the same as the upper rail. The shape of the rail is also the same as the upper rail one, although the dimensions are different.

#### *Z-guide arm*

This part assures the movement along the Z axis. The movement is proposed to be provided by a chain-pinion system. The movement is limited by the height of the shelves. There are two guiding slots made in the Z-guide arm so that the X-support cylinder piece can move along them.

Two Z-guide arms are included in the palletising system.

#### *X-support cylinder piece*

As its name indicates this piece holds the cylinder. At the same time moves through the guiding slots in the Z-guide arm assuring the movement along the X axis. The movement of this part with respect to the Z-guide arm is done through a rack-pinion system. The pinion would be located in the X-support cylinder, while the rack would be in the Z-guide arm.

#### *Z-cylinder*

It is placed in the X-support cylinder. It holds the pins. The movement is achieved through a servo-motor which would provide a rotation around the Z axis.

#### *Pallet moving system*

The pallet moving system is held by the Z-cylinder. The distance between pins, as well as their height and width are conditioned by the pallets used in the HC. The shape and dimensions of the cylinder and the pins are for guidance.

### 2.5.6.17. Port Cell robotic arm and RH Platform Unit

#### Description

The limitations of human access to IF2a require the development of a remote handling system to access the interface located inside the Port Cell Interspace between the bioshield and the port plug rear side. Additionally the RH system has to be able to implement all the required operations for connecting the TBMs to their subsystems including welds inspection and installation of thermal insulators. It is assumed that an industrial arm will be used in ITER to perform such operations. The robot used in the TBM RH test facility must be the same as the one used in ITER.

Industrial arms generations are replaced every 5-10 years depending on the company, so the arm which will be operating on the TBM may not yet exist. KUKA KR16 is one of the present proposals, since its capability to carry out the tasks [Kel 10].

The KUKA KR16 is a 6-axes electric robot. It allows manipulating several final effectors for operating in the Interface 2a.

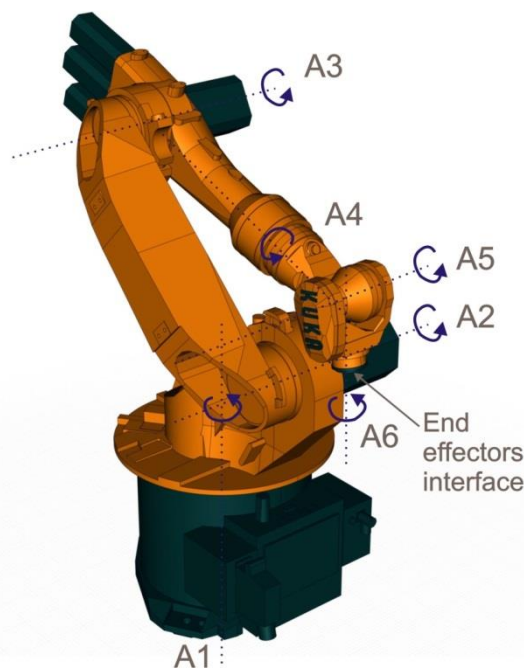


Fig. 142. PC robotic arm (KUKA KR16).

The general features of KUKA KR16 are shown below:

- Architecture: 6 axes, classic industrial arm architecture.
- Actuators: electric.
- Payload: 16 kg.
- Supplementary load: 10 kg.
- Range: 1610 mm.
- Weight : 235 Kg.
- Repeatability:  $< \pm 0.05$  mm.
- Mounting positions: Floor and vertical disposal.
- Axes maximum speed: 156°/s for A1, A2 and A3, 330°/s for A4 and A5, and 615°/s for A6.

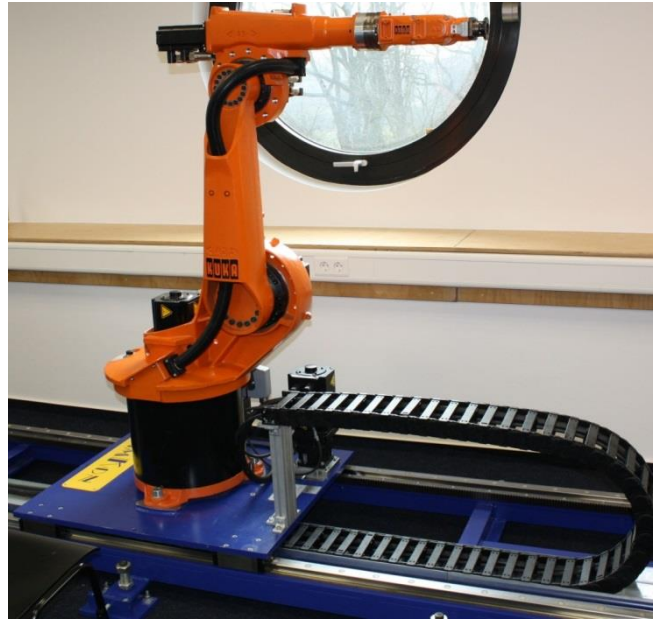


Fig. 143. KUKA KR16 mounted on a deployable carrier.

The PC robotic arm will be mounted on a deployable carrier integrated in a component named RH Platform Unit.

The RH Platform Unit contains the robotic arm and its controller, a deployable carrier to move the robotic arm between the Port Cell and the Interspace, a container to store the insulating modules, a rack for the RH final effectors, ancillary equipment (e.g. plasma source, pumps, etc.), supply lines (electrical, hydraulic, etc.) and a reel for cables.

The parts of the system are shown in the following picture:

1. Robotic arm.
2. Deployable carrier.
3. Tool rack.
4. Insulation container.
5. Cable reel.
6. Controller.
7. Ancillary equipment (e.g.: plasma torch source).
8. Standard frame.

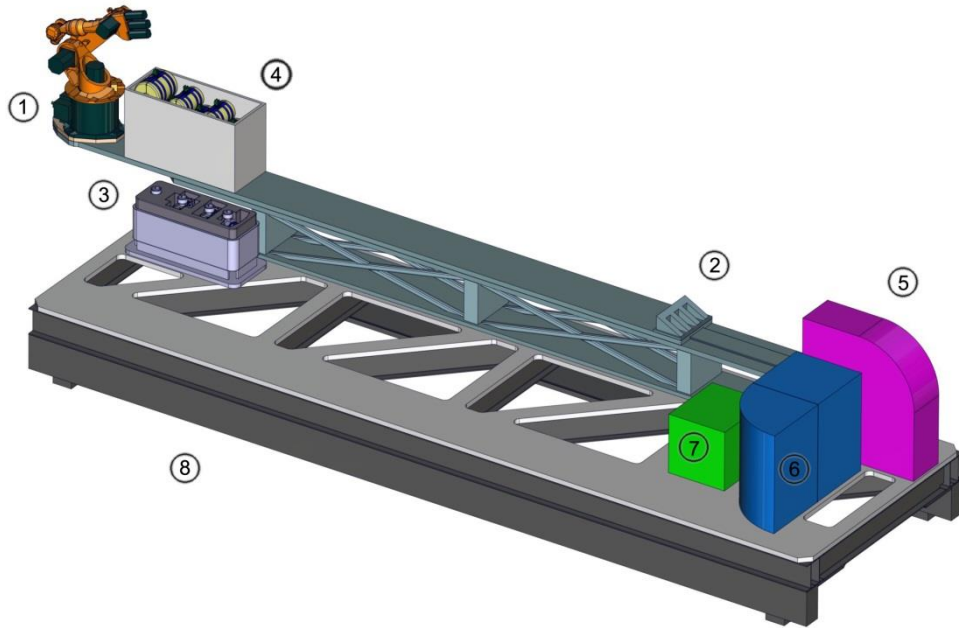


Fig. 144. RH Platform Unit.

The platform dimensions and design are similar to those of the AEU, although it is lighter. It is also compatible with the ATS, since it must be transported between the Hot Cell area and the Port Cell area depending on the maintenance sequence stage.

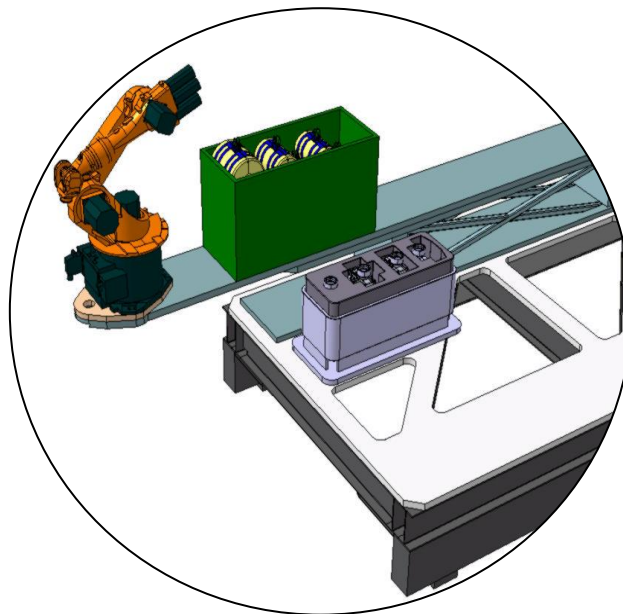


Fig. 145. Robot, insulations container and tool rack.

### 2.5.6.18. Polisher

#### Conceptual design

This tool performs the unique maintenance operation on the surface of the PP frame. It is in charge of cleaning the rests of the two O-ring flanges left after the extraction of the TBM & shield assemblies from the PP.

The tool has a polisher head formed by multiple polishing hairs, one gripping interface, one battery connector and two guides.

The width of the abrasive disc is the same as the width of the PP frame, thereby only one pass is needed to eliminate the rests.

The gripping interface is set at the top of the polisher body. The switch on/off can be controlled by radiofrequency.

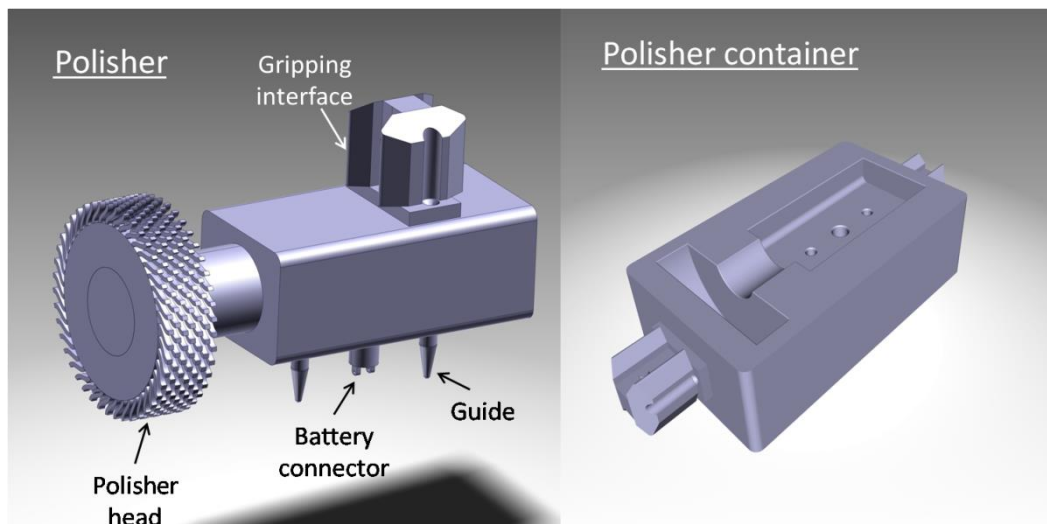


Fig. 146. Polisher tool and container.

The tool contains a connector to recharge the batteries. While the tool is not used it is left in the polisher container. When the battery is uncharged the manipulator takes the polisher and places it in the battery recharger. A correct positioning within the battery recharger is achieved by means of the two guides situated at the same face as the battery connector.

### 2.5.6.19. Test stand

#### Introduction

In the TBM RH test facility, this equipment allows checking the vacuum sealing between the port plug and the TBM shield.

The test stand used in the test facility must be the same as the one used in the ITER HC. The test stand is described in ITER documents [Bar 08]. The following is a brief description of the test stand for informative purposes.

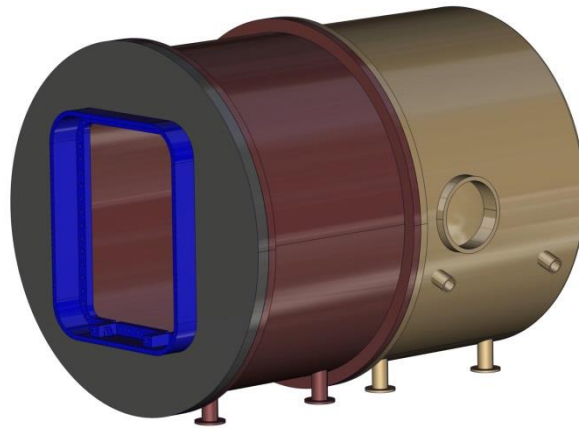


Fig. 147. Test stand.

Description of the test stand

Its design includes a two-body tank and a lid. The bodies which compose the tank are joined by welding. The lid (grey in the following figure) is also welded to the tank.

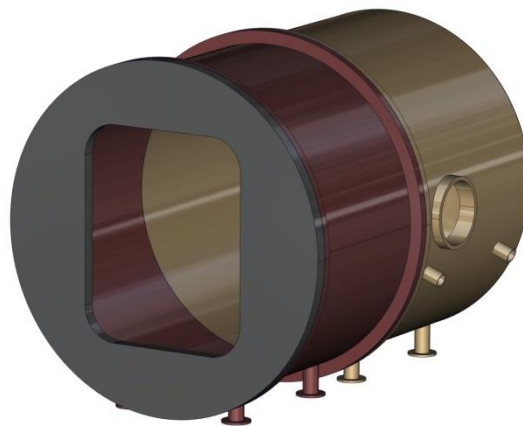


Fig. 148. Test stand lid.

As it is shown in Fig. 148, the lid has a hole in its central part to insert the port flange. The hole has the shape of the test stand flange. It is assumed that this flange, which is welded to the lid at its lateral sides, is the same as the ITER port extension flange.

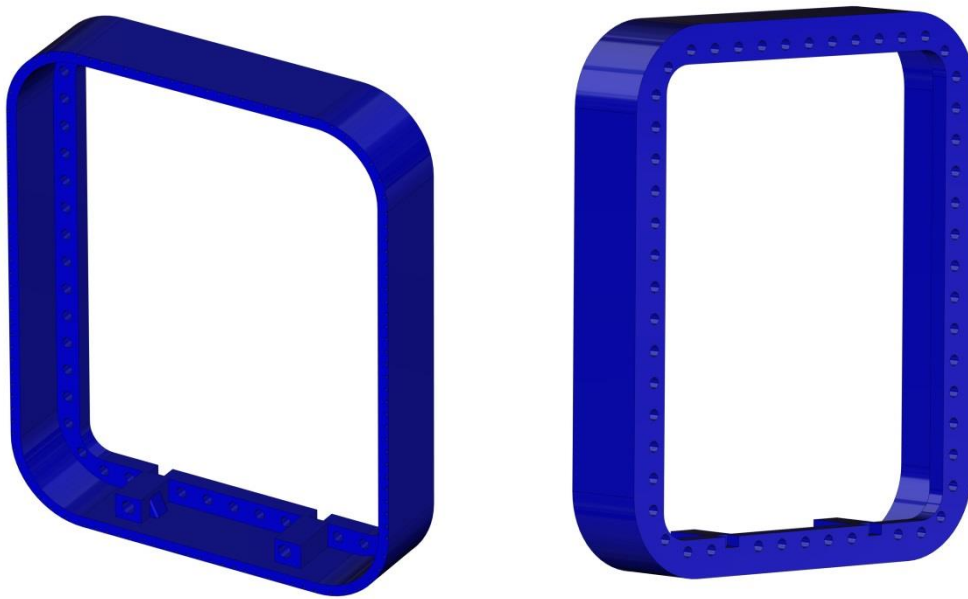


Fig. 149. Test stand flange. Front and back views.

It is also assumed that the high vacuum seal installed in the test stand is the same as that of ITER equatorial ports [Mar 09]. The steps to carry out the vacuum test are the following:

1. The port plug is inserted in the test stand and bolted to the test stand flange.
2. The Helicoflex gasket is placed in a previously polished slot by the gasket flange maintenance equipment.
3. The gasket flange is placed and bolted to the port plug flange and the test stand flange, by the gasket flange maintenance equipment.

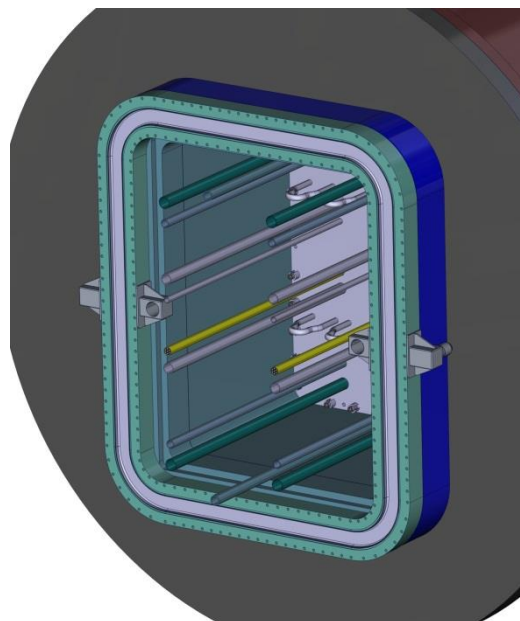


Fig. 150. Gasket flange installed in the test stand.

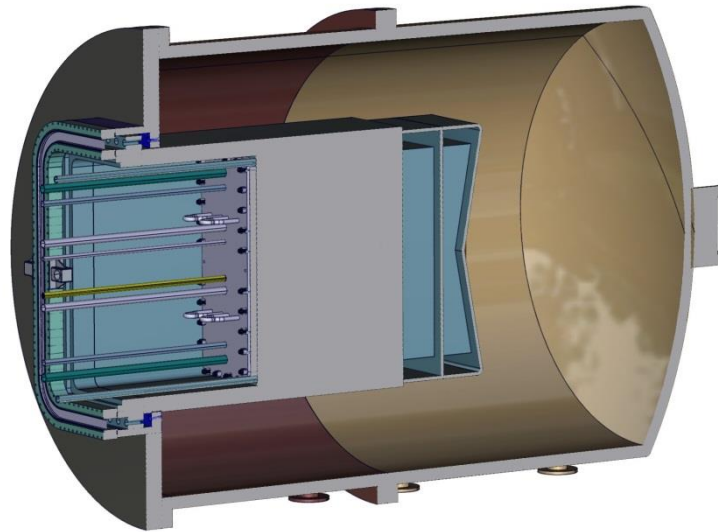


Fig. 151. Section of the port plug inserted into the test stand.

#### 2.5.6.20. Screw

##### Conceptual design

The hydraulic screwing tool is used in two operations:

- Unscrewing of the bolts of the TBM shield (first step of the TBM extraction operation).
- Screwing of the bolts of the TBM shield (last step of the TBM extraction operation).

The tool is inspired in one described in the ITER RH Code of Practice [Raj 09].

The screw system is composed by the following elements:

- *Tank*: the fluid tank and the pump are located inside. This last one pumps the fluid through the pipes and the screw driver to create the demanded momentum. The fluid is not defined yet and shall satisfy the requirements of the materials used within the Hot Cell.
- *Pipes*: elastic pipes, easy to manipulate.
- *Screw driver*: up to date, there are models used in the nuclear field similar to this one. The screwing/unscrewing is carried out by means of an Allen key coupled to the screw driver and inserted into the screw head. The screw driver includes a wing nut shape ledge to make easier the accurate positioning and to avoid the screw driver must counteract the high torque (several hundreds of Nm). The ledge is inserted into the corresponding ledges of the shield, so they can absorb the torque.
- *Extension rod*: this rod is used because the space inside the port plug is limited. The length of the manipulator arm is not enough to perform the operation inside the PP when both TBM & shield assemblies are inserted. This rod makes the operation possible. The cables which connect the gripper interface to the screw driver are located inside the rod.
- *Gripping interface*: Standard interface compatible with the HC manipulator clamps.

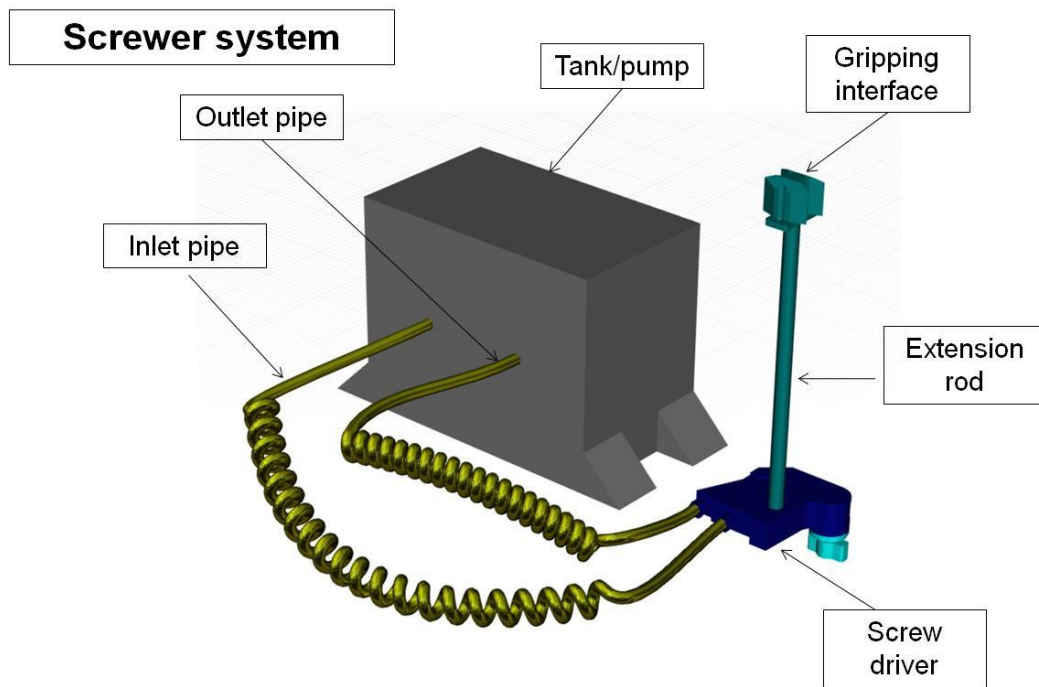


Fig. 152. Screwer system.

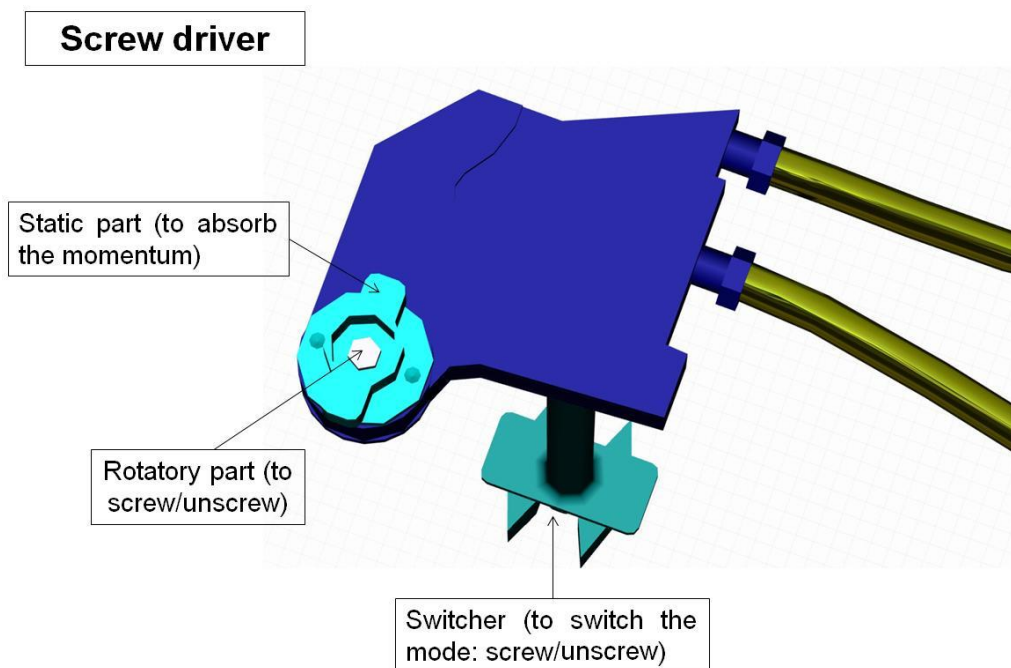


Fig. 153. Screw driver.

### 2.5.6.21. Transfer cask

#### Introduction

The transfer cask is used to move the port plug from the Port Cell to the Hot Cell and vice versa. In the facility only one will be needed, whose design must be the same as the ITER one.

The following is a brief description of the transfer cask system for informational purposes. More information can be found in [Yao 07].

Description of the transfer cask system

The transfer cask system consists of:

- Cask transporter.
- Cask enclosure.
- Cask side connector.
- Double seal door.
- Tractor system.

The dimensions of the Transfer cask are the following:

- Width (mm): 2620.
- Length (mm): 8500.
- Height (mm): 3094.

The total weight is estimated to be 27800 kg.

*Cask transporter*

The cask transporter consists of two components: the automated air cushion transporter (ATS) and the pallet, which is the interface between the transporter and the cask envelope. The ATS places itself beneath the pallet, inflates the air bearings and transports the Transfer Cask to the Port Cell guided by two steering wheels, where two notched plates at the front of the pallet engage the vertical pins, which are permanently installed on the building floor. The cask movements are remotely controlled from the control room.

Then the pallet (with the cask) is lowered by switching off the air bearings. The pallet is left on the ground resting on four vertical legs and the ATS is removed.

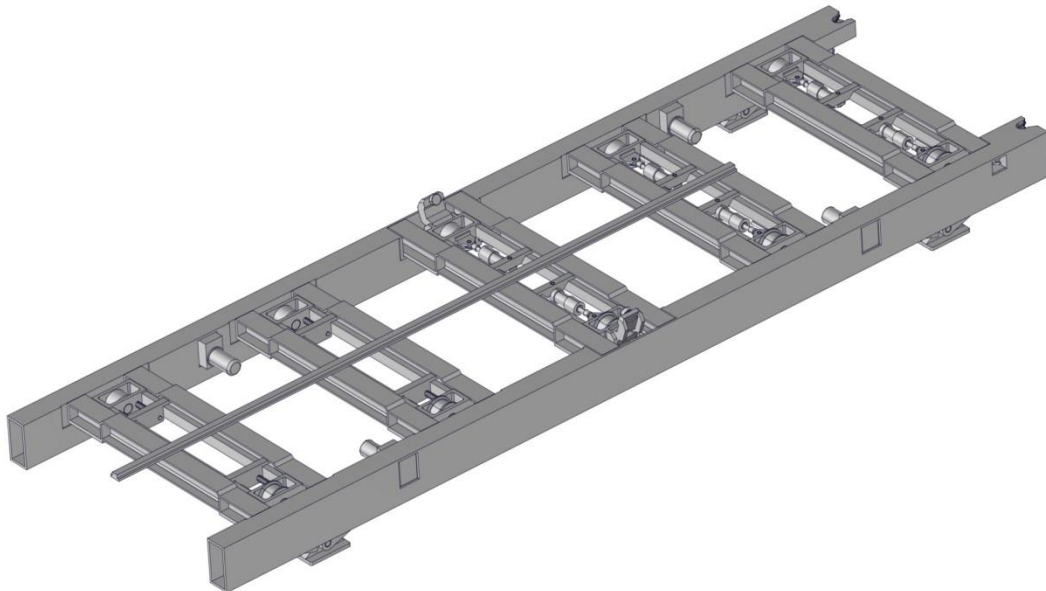


Fig. 154. Pallet.

The pallet can do fine adjustments to ensure the cask is correctly aligned with the port. The pallet can lift up the cask to the required height by using four support legs. The horizontal

adjustment will be performed by means of two inclinometers. 5 rollers integrated in the pallet ensure the lateral guiding of the cask.

#### *Cask enclosure*

The cask enclosure is attached to the pallet at its bottom. It holds the double seal door and the mechanical system to remove the double seal door, the cooling system and the tractor.

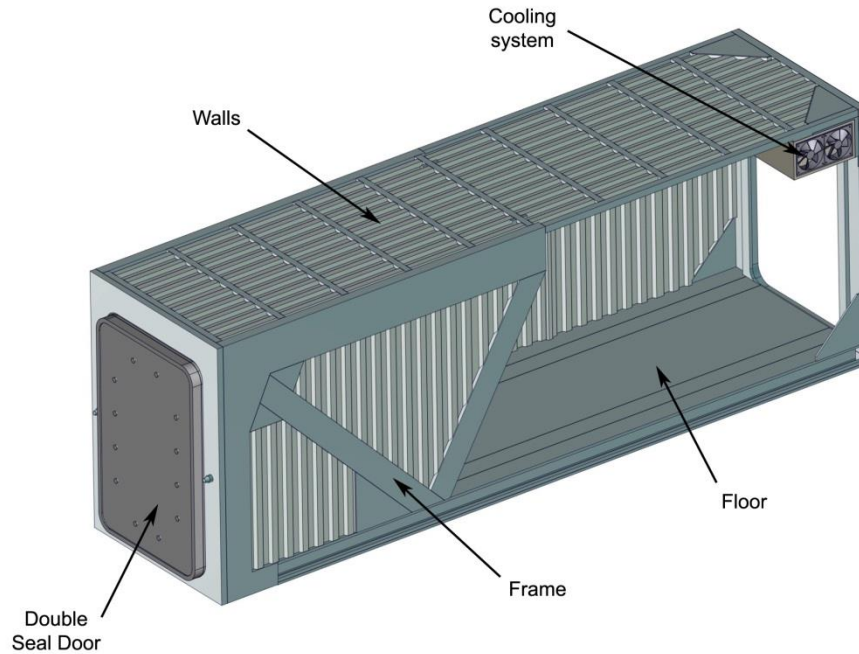


Fig. 155. Cask enclosure and double seal door.

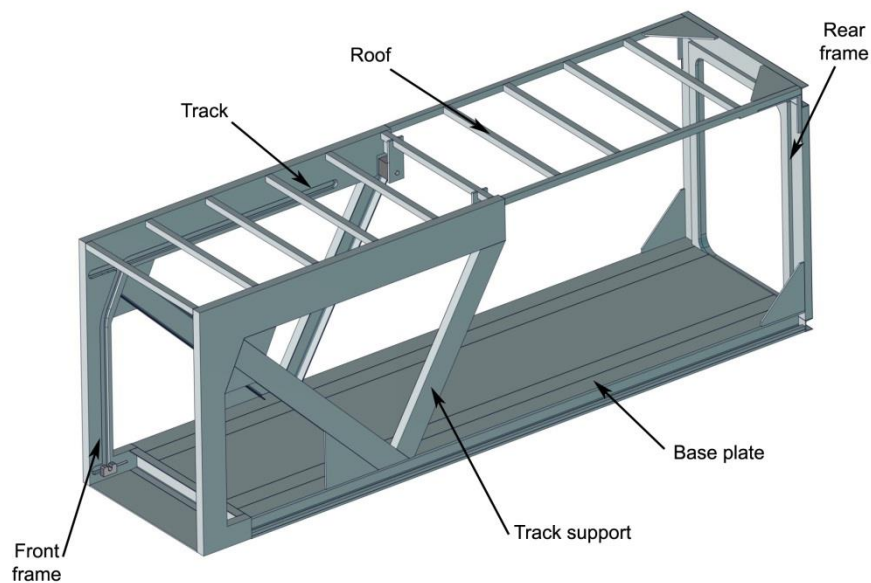


Fig. 156. Cask enclosure frame.

### *Cask side connector*

The main function of cask side connector is to connect the cask to the port service connector so that the transfer cask is connected to the building service lines (including hydraulic, pneumatic, electric power and other services).

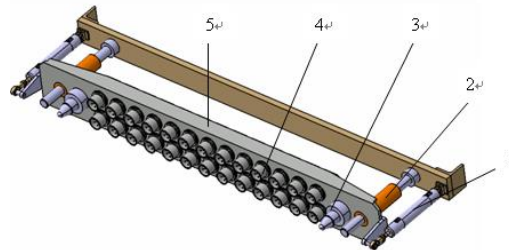


Fig. 157. Cask side connector [Yao 07].

The cask side connector is attached to the pallet.

### *Double seal door*

Once the transfer cask reaches the port docking flange, the double seal door opens and the tractor extracts the port plug. Afterwards the double seal door closes and the external door is left in the port to seal the space which was previously occupied by the port plug. At the same time the internal door of the double seal door closes the transfer cask.

### *Tractor*

The tractor system is used to insert/remove the port plug into/from the port. The gripper is attached to a base which moves along two rails. These rails are fixed to the floor of the transfer cask. The gripper has a hydraulic positioning system to place it correctly in order to insert or remove the port plug.

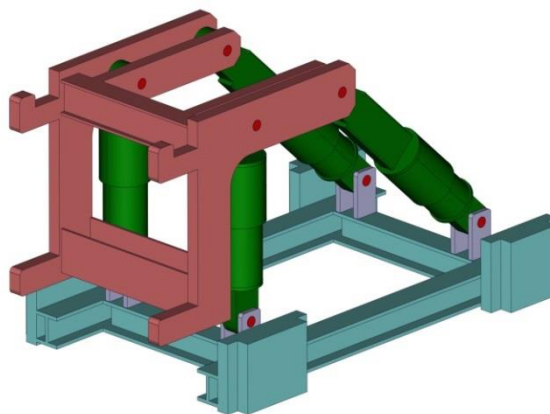


Fig. 158. Tractor.

## 2.5.6.22. Vertical positioning tool

### Introduction

There will be a tool in ITER to move the port plug from the transfer cask to the maintenance area inside the Hot Cell. It shall also allow putting the port plug in vertical position to

extract/introduce the TBM & shield assemblies with an overhead travelling crane, as well as to carry out other PP maintenance operations.

The vertical positioning tool used in the test facility must be the same as the one used in the ITER HC. The following is the description of a hypothetical design for the vertical positioning tool proposed within this work.

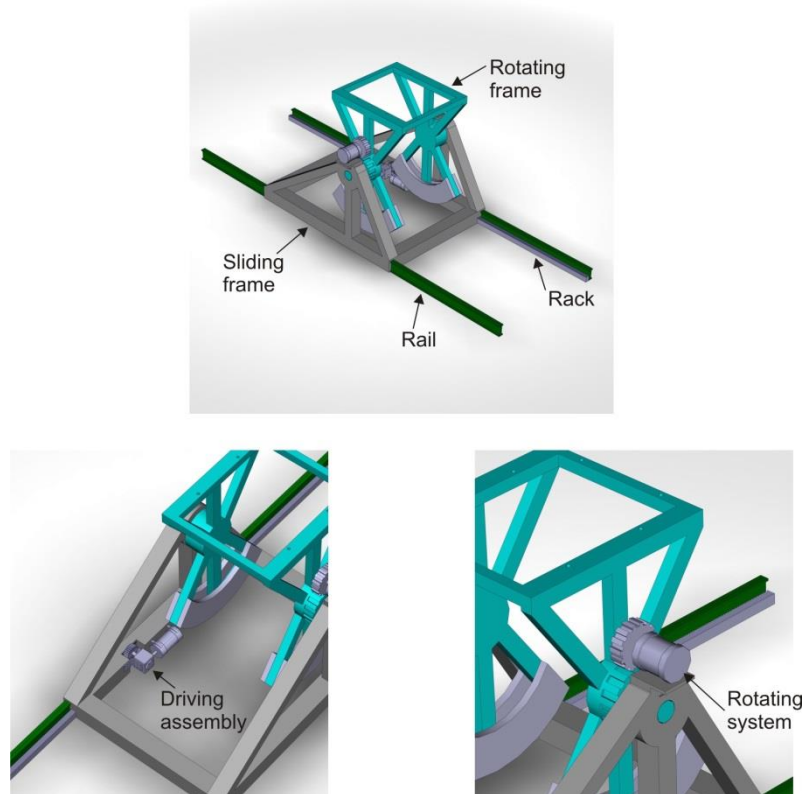


Fig. 159. Vertical positioning tool.

#### Description of the vertical positioning tool

The vertical positioning tool assembly includes two rails, a sliding frame, a rotating frame in which the port plug is inserted, a traveling system providing the sliding movement function and a rotation system providing the rotation function.

#### *Travelling system*

The frame slides along the rails by means of several roller bearings. It is driven by a pinion-rack system.



Fig. 160. Sliding frame.

It is designed for being inserted in the rails and it has to be capable of withstanding the port plug weight and inertia stresses during rotation. It has also a bedplate for supporting the rotating system motor.

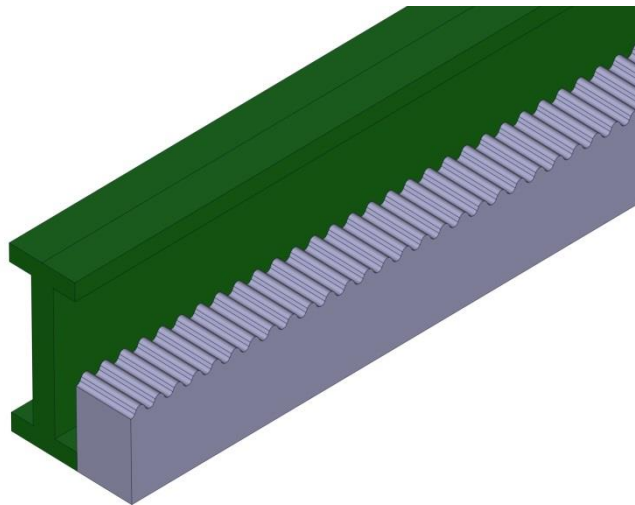


Fig. 161. Rail and rack.

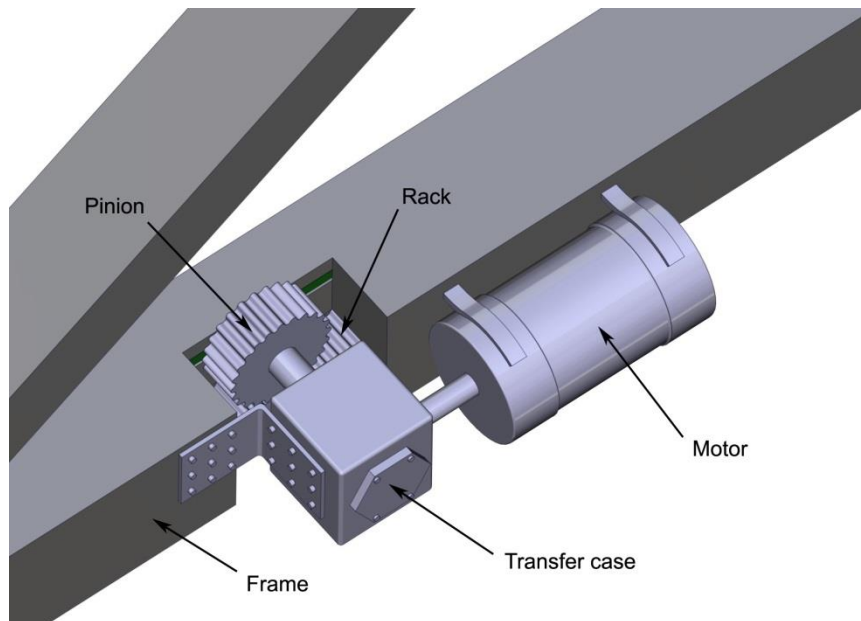


Fig. 162. Driving assembly.

The driving assembly includes an electric motor, a transfer case and a pinion.

#### *Rotating system*

It is composed of a rotating frame, an electric motor which gears to the rotating frame, two roller bearings for allowing the relative turn between the rotating frame and the sliding frame, a brake and two bodies which are used as counterweights that help minimizing the torque needed for turning.

The rotating frame supports the port plug by its flange. It is assumed that the port plug flange is bolted to the rotating frame by 6 M52, as it is proposed in [Bed 08].

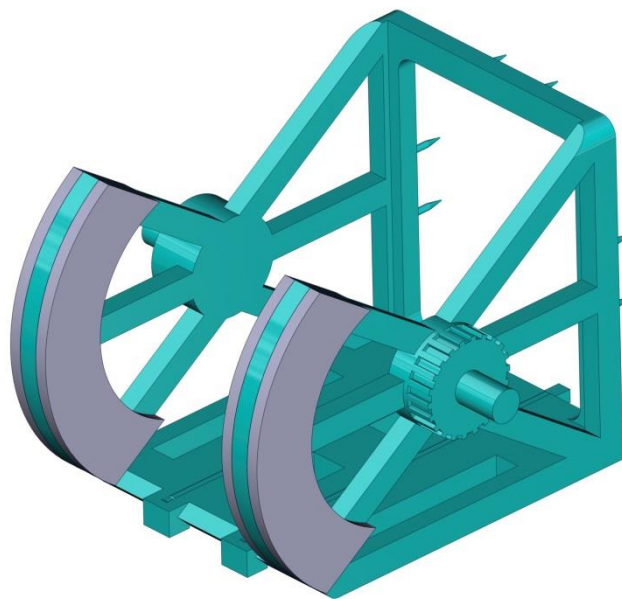


Fig. 163. Rotating frame.

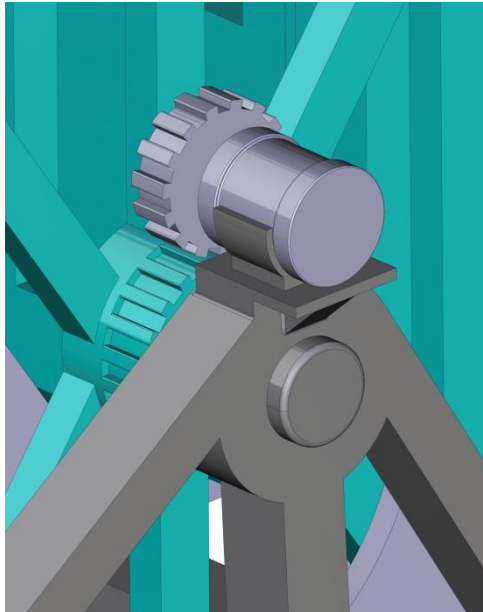


Fig. 164. Rotating system.

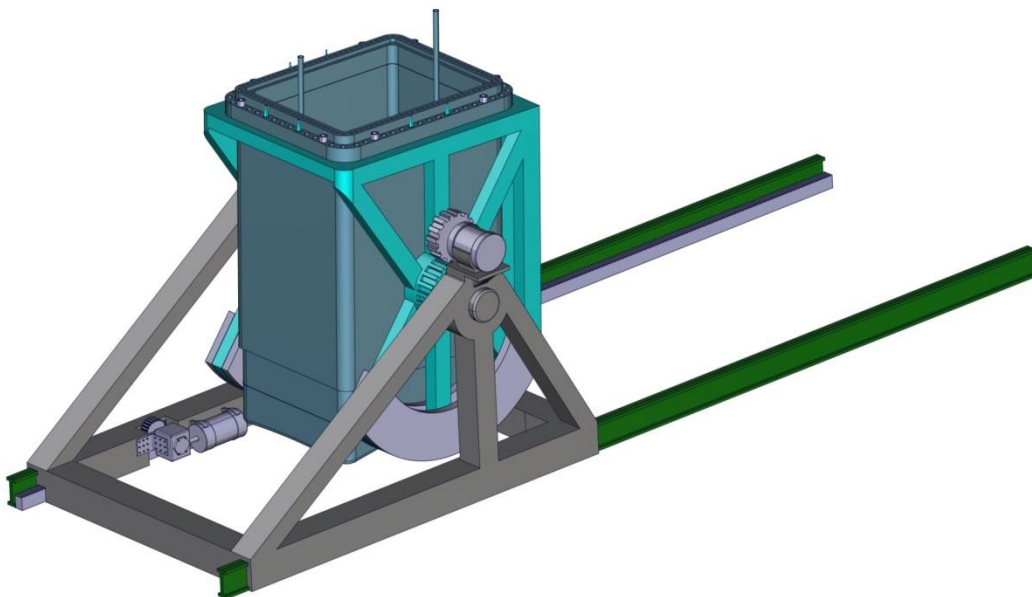


Fig. 165. Port plug inserted in the vertical positioning tool.

### 2.5.6.23. Welding tool for the PC robotic arm

#### Description

The pipes at the IF2a will be connected by welding. The chosen welding procedure is the orbital TIG (tungsten inert gas) welding. Such procedure is implemented in a specific RH tool where the welding parameters are fully controlled during operation. The pipe welding tool is water-cooled and includes weaving function and automatic arc length control (by controlling the arc

voltage). A possibility is using the ESAB A21 PRC 60-170 welding tool [Bed 07], which is capable of welding pipes with different diameters with small modifications.

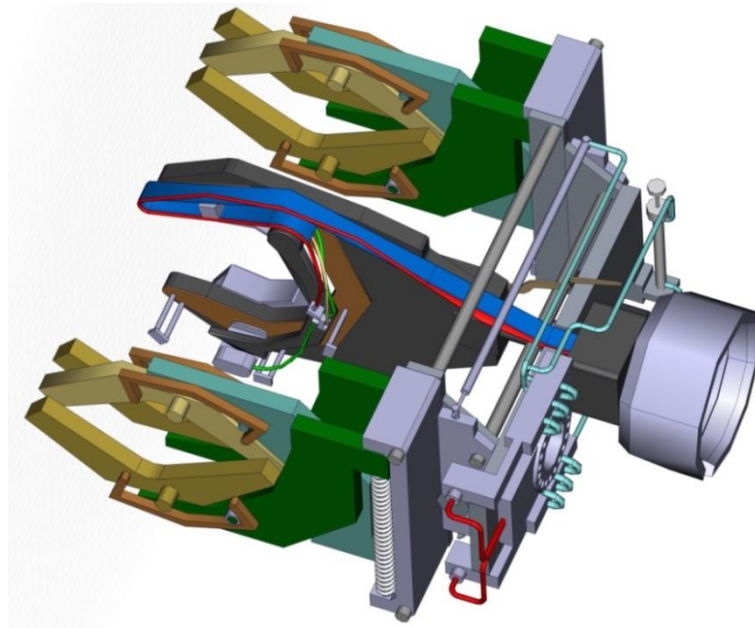


Fig. 166. Welding tool.

The proposed filler wire feed unit (ESAB MEI 21) also needs some modifications to be adapted to the RH system.

A special mounting mechanism ensures the accurate radial and axial position of the welding tool. The radial positioning system is based on two gripping jaws. These components, forced with springs, clamp on the pipe. The geometry of the jaws is designed to be adapted to the different tube diameters.

The axial positioning is provided by strong springs, which open/close by means of pneumatic cylinders. The spring force provides the accurate positioning even on failure of air supply.

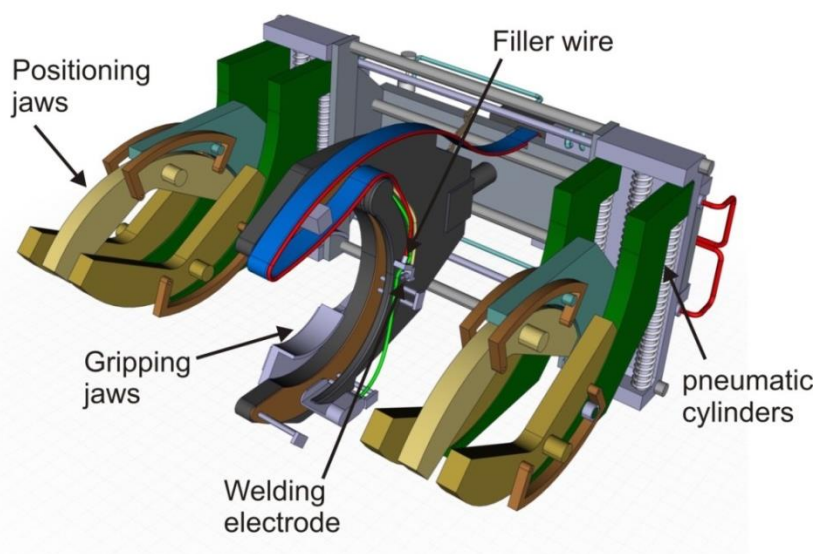


Fig. 167. Welding tool components.

### 2.5.6.24. 50 ton overhead crane

#### Introduction

This crane ensures the transport, installation, removal and positioning of heavy equipment in the operation zone, e.g. installation of the port mock-up (weight around 30 t) and placing of the port plug mock-up with two TBM & shield assemblies (45 tons) in the vertical positioning tool in the Hot Cell area. The design load assures the removal of components in case of accident (e.g. fall of the port plug with 2 TBM & shield assemblies).

This crane will not be used during normal operations (demonstration of TBM RH operations).

#### Description

The crane is supported by guide girders (rail beams), themselves supported by the hall building supporting structure (not on the walls). The crane moves along the guide girders. These guide girders are also used by the 20 ton crane.

The 50 ton crane used in the facility should be a standard commercial crane. There should be 9 m of free space between the crane and the floor. The crane covers the width of the hall (30 meters).

The 50 ton crane should have a trolley with two motors, one for transversal and one for vertical movement. No load rotation function is needed (contrary to the 20 ton crane).

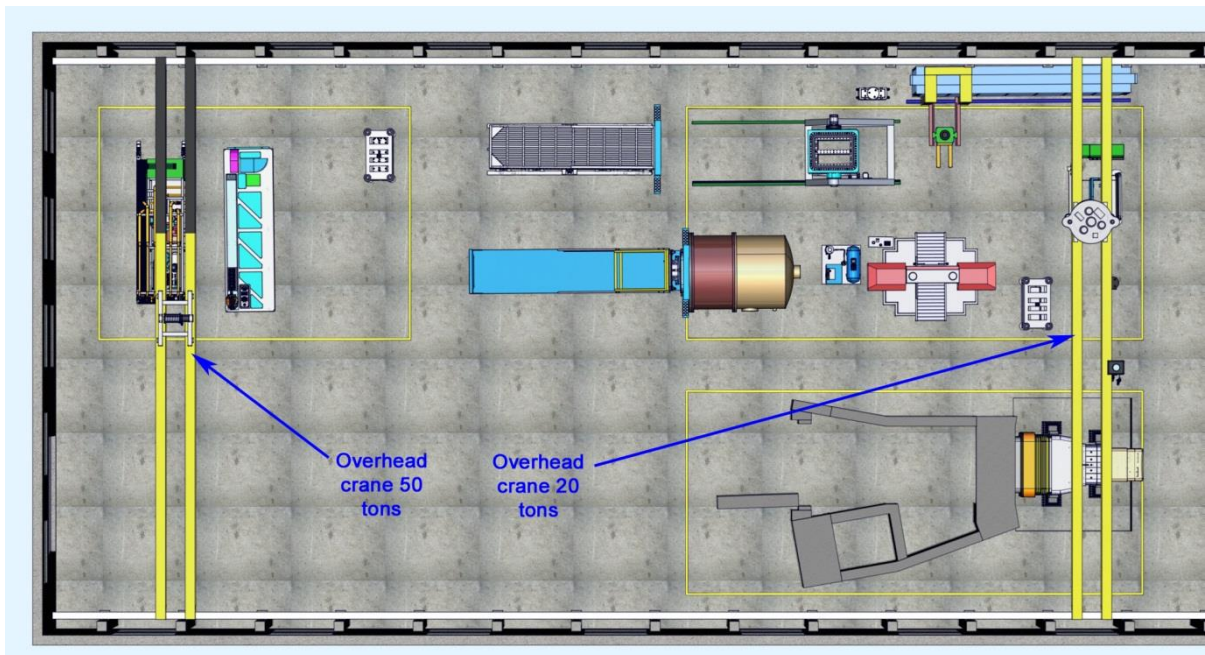


Fig. 168. Top view of the operations hall showing the 50 ton and 20 ton cranes.

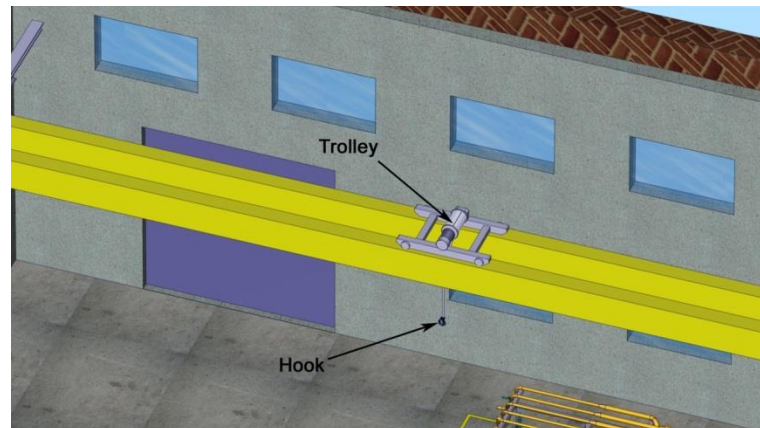


Fig. 169. View of the 50 ton crane.

#### Control and operation

The crane can be controlled either from the control room or from the operation zone. All the control is carried out through cables (no remote control). No cameras are needed on the crane to operate it.

#### 2.5.6.25. Bench for dust cleaning and separation of TBM from shield

##### Introduction

It is assumed that in the ITER HC there will be a separation bench with the function of holding the TBM while an overhead crane pulls up from the shield in order to separate it from the TBM. It is assumed that this bench will also have the function of holding the TBM and shield set while they are cleaned by means of a vacuum cleaner.

The TBM separation bench used in the test facility must be the same as the one used in the ITER HC. The following is a brief description of a hypothetical design concept for the separation bench proposed within this work, so it is very likely that the real TBM separation bench design will be different from this one.

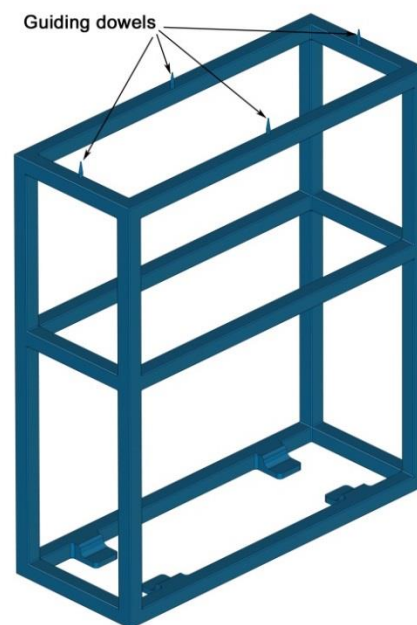


Fig. 170. Cleaning and separation bench.

### Functional requirements

This fixed structure will be the same as in ITER and it does not need to be specifically designed for the TBM RH Test facility. However, the following functional requirements are proposed.

- The separation bench mock-up must be able to hold the TBM mock-up while the overhead crane pulls from the shield module mock-up.
- The separation bench mock-up must reproduce this holding action on the TBM mock-up in the same way as the real bench in ITER.
- The separation bench mock-up must allow the vacuum cleaner gaining access to the TBM and shield surface.

### Description of the separation and cleaning bench

The TBM separation bench would include a structure in which the TBM & shield assembly is inserted. It is assumed that the shield is held by the overhead travelling crane during the operation. The shielding module would be held by the crane from its back.

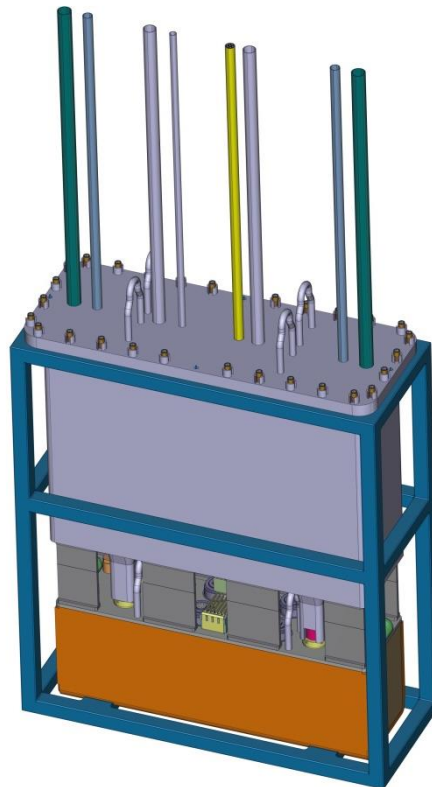


Fig. 171. TBM and shield assembly inserted in the cleaning and separation bench.

The bench must be fixed to the test facility floor to perform the separation and the dust cleaning.

### 2.5.6.26. Hot Cell door for the vertical positioning tool

This structure is needed to reproduce the geometrical constraints involved in the transfer of the port plug from the TC to the vertical positioning tool.

### Functional requirements

- It must allow the transfer of the port plug between the transfer cask and the vertical positioning tool like it will be done in ITER.

- It must allow docking the transfer cask.
- It must allow docking the ATS to a cask service connector and docking pins, in the same way as in ITER.
- It must provide (through the service connector) electrical and pneumatic supply to the transfer cask and the ATS.
- It must withstand the mechanical stresses due to the transfer cask docking and the sliding of the port plug (the transfer cask gripper goes into the Hot Cell door until the rear flange reaches the vertical positioning tool flange; then the rear flange is bolted to the vertical positioning tool and the gripper leaves).

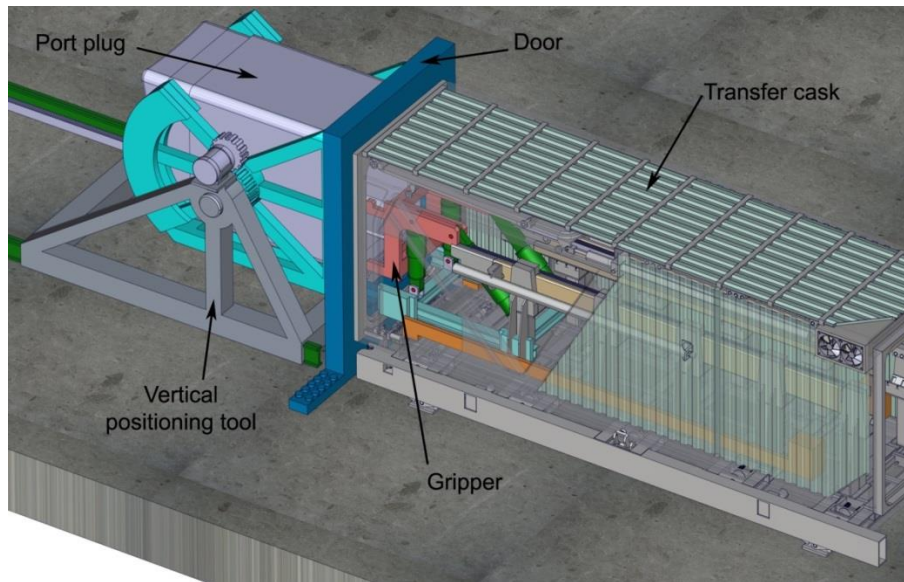


Fig. 172. PP transfer from the transfer cask to the vertical positioning tool.

#### Conceptual design of the Hot Cell door for vertical positioning tool

The Hot Cell door for vertical positioning tool consists in a concrete block with a hole allowing the introduction of the PP and its attachment to the vertical positioning tool. It is fixed to the floor by bolts. Its external dimensions are 4000 mm (height) x 2800 mm (width) x 300 mm (thickness). It includes two holes for the transfer cask docking and two ribs to allow the sliding of the port plug flange and the movement of the helping cantilever system wheels [Meu 07]. A cask service connector and two docking pins are also included. They are fixed to the floor.

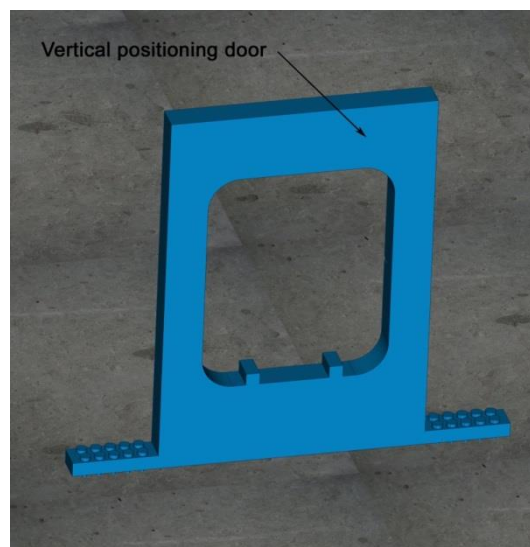


Fig. 173. Hot Cell door for the vertical positioning tool.

### 2.5.6.27. Hot Cell door for the test stand

It is assumed that the test stand is inside the HC but can only be accessed from outside the Hot Cell. There is therefore a HC door that separates the Test stand from the outside of the Hot Cell.

#### Functional requirements

- It must reproduce the ITER geometrical constraints for the attachment of the port plug to the test stand flange
- It must reproduce the ITER geometrical constraints for the attachment of the gasket flange to the PP and test stand flanges
- The Hot Cell test stand door must allow the docking of the transfer cask.
- It must allow the docking of the ATS to a cask service connector and docking pins, in the same way as in ITER.
- It must provide (through the service connector) electrical and pneumatic supply to the transfer cask and the ATS.
- It must withstand the mechanical stresses occurring during the docking of the transfer cask and the port plug and gasket flange manipulation and attachment.

#### Conceptual design proposal for the Hot Cell door for the test stand

The design of the HC door for the test stand is identical to that of the HC door for the vertical positioning tool, except for a larger hole allowing the insertion and attachment of the PP, the test stand flange and the gasket flange.

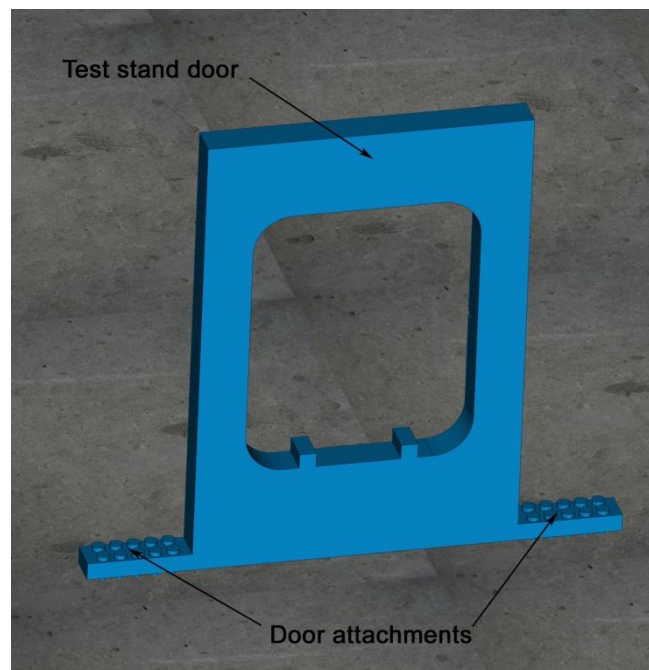


Fig. 174. Test stand door.

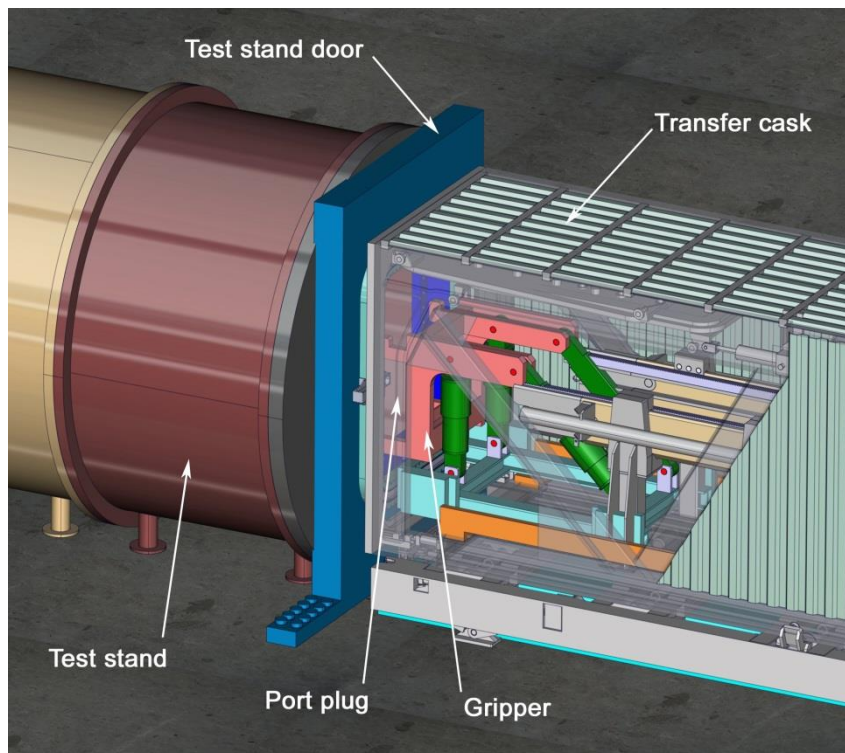


Fig. 175. Transfer of the port plug.

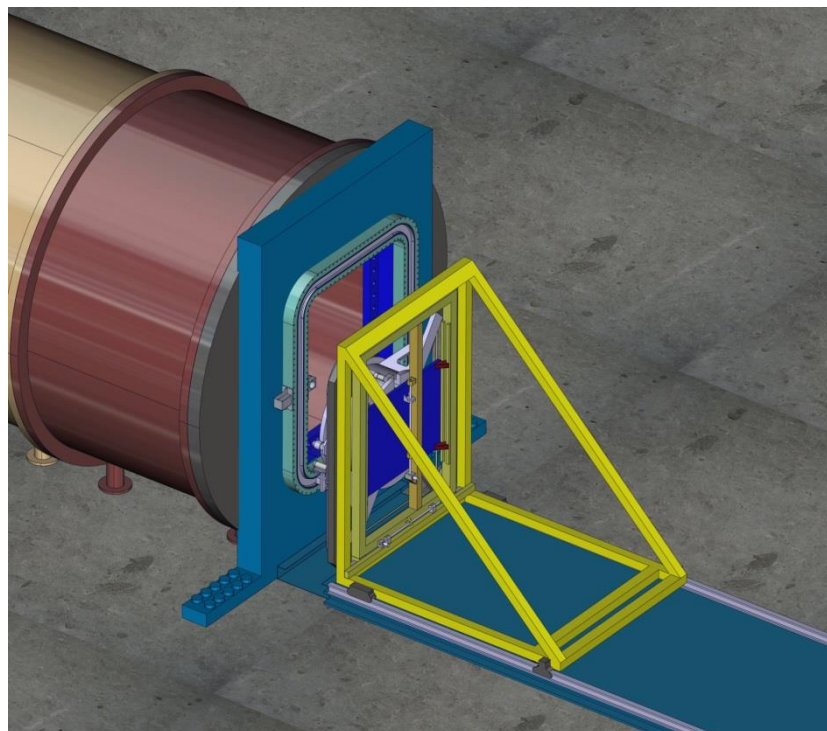


Fig. 176. Assembly of the gasket flange.

### 2.5.6.28. Port Cell mock-up

#### Functional requirements

- The test facility Port Cell must have the internal dimensions of the ITER Port Cell.
- The ceiling of the Port Cell is not needed, since the height of the walls is higher than any moving component (transfer cask, AEU, Pipe Forest + ATS).
- The wall of the Port Cell is composed of removable wall panels. These will be fixed to supporting frames to guarantee their stability. It will be possible to remove them in order to see clearly the ordinary operations inside the Port Cell, such as the AEU and pipe forest installation or the processes where the robotic arm is involved.
- The PC mock-up design should allow the ATS with transfer cask to enter the port cell in order to install the port plug. The PC mock-up design should allow the ATS entering and installing the AEU and the Pipe Forest & Bioshield Door assembly. The PC mock-up should have the features of the real PC allowing docking the ATS.
- The PC must provide electric and pneumatic supplies to the Transfer Cask through the port service connector after docking the ATS. The electric and pneumatic systems (cables and other devices) must be integrated in such a way that do not interfere with the RH demonstration operations.
- A second level floor should be built so that the operations of installing the Port extensions into the Port Cell are possible. Furthermore the supports of the Port would be placed in this floor.

#### Description

The dimensions shown here for the PC mock-up conceptual design are for guidance.

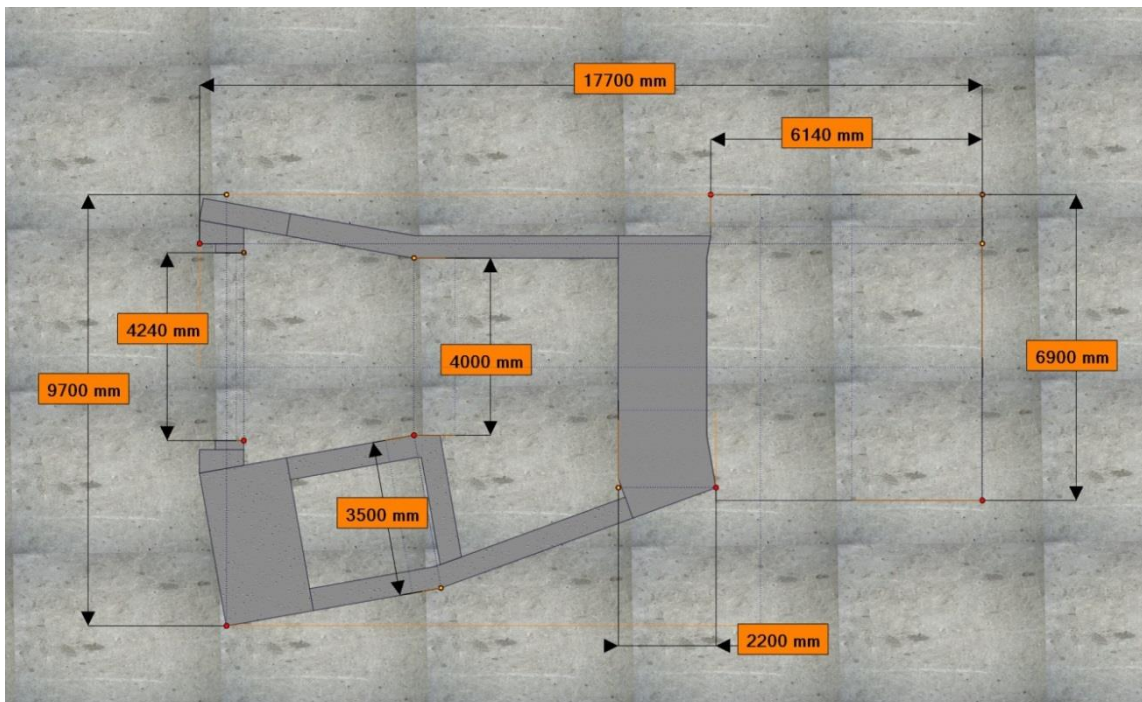


Fig. 177. Dimensions of the Port Cell mock-up.

The modules which form the wall of the Port Cell are shown in Fig. 178.

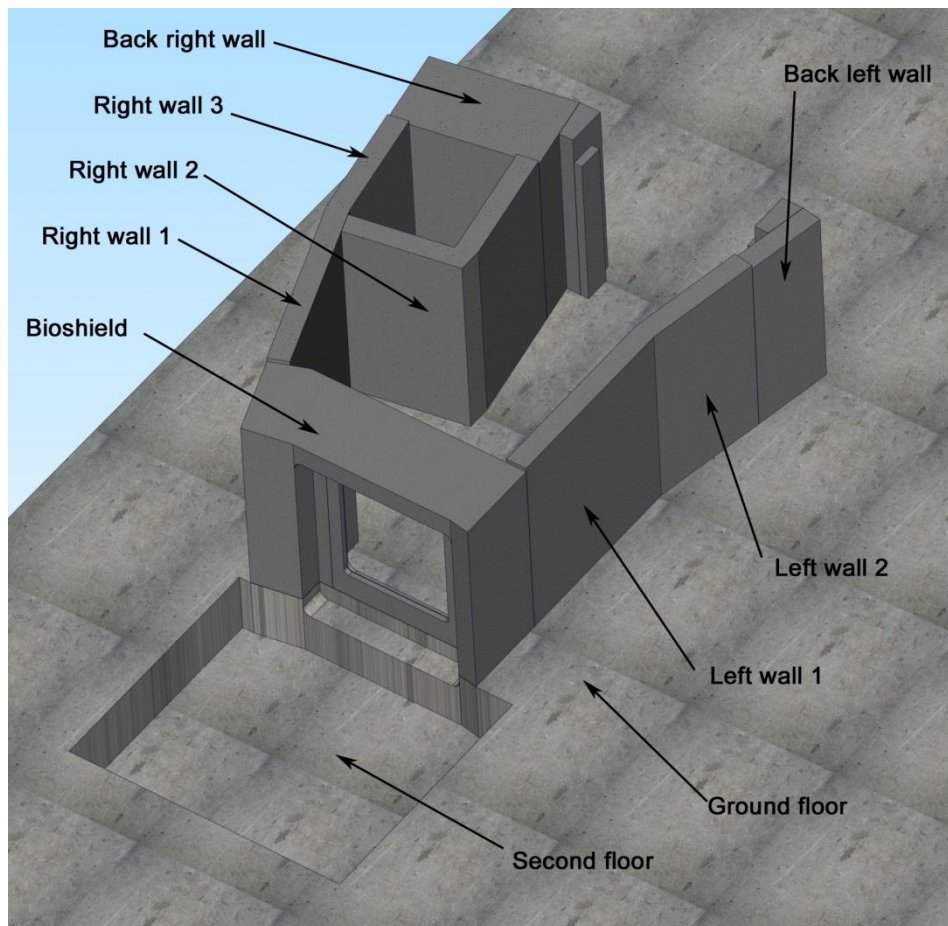


Fig. 178. Components of the Port Cell mock-up.

The thickness of the wall modules is different from that of the PC walls in ITER. It can be smaller to reduce costs. The only requirement is the conservation of the inner dimension of the complex. The modules materials can be also different in order to reduce costs.

The solution adopted here is a system of dismountable modules. The modules would consist in a metallic frame with panels attached to its sides. It should be possible to remove any wall module by crane in order to have a better view of the RH operations. The modules are attached to the PC floor (for example bolted) in a way that guarantees their stability.

The design of the Bioshield is similar to the ITER one, allowing the connections between the Port Cell and the Port.

A second floor is needed to adapt the port. The distance between the first and the second floor is given by the dimensions of the ports and of the port supports. A dimension of 1.5 m is assumed. It is also assumed that no vacuum vessel sector mock-up is needed.

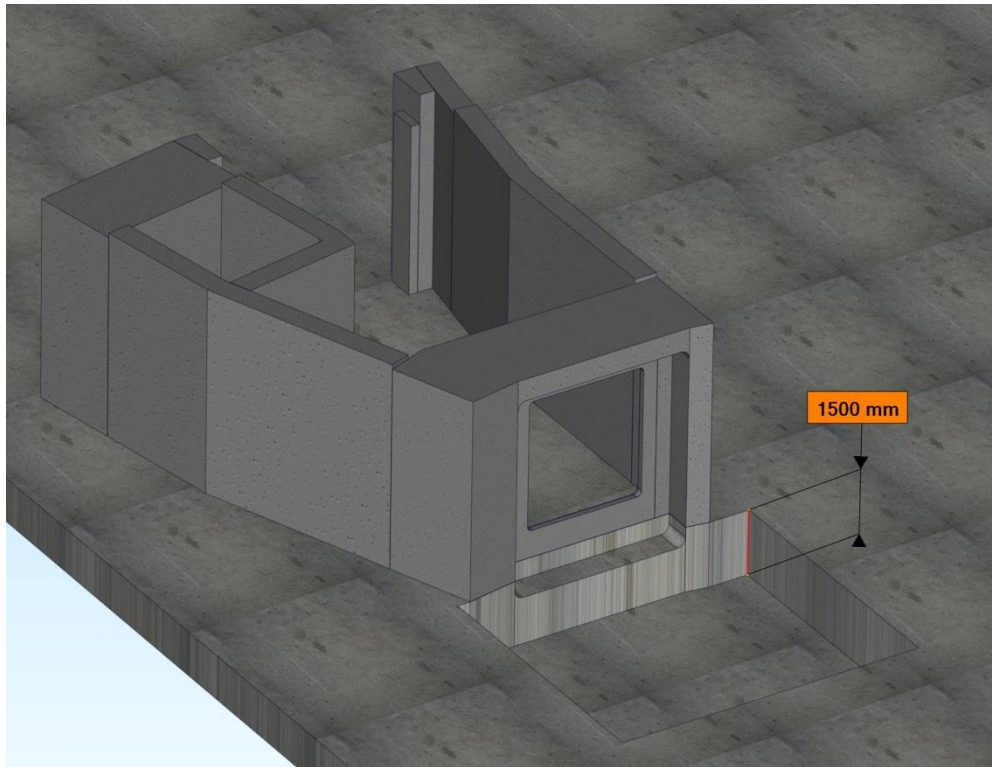


Fig. 179. Double floor in the Port Cell zone.

#### 2.5.6.29. Port mock-up

##### Functional requirements

- The Port mock-up must have the same internal dimensions and design as the ITER port. In this way the Port simulates the spatial limitations for the installation and removal of the port plug and the AEU as well as for robotic arm operations. The rails of the port plug helping cantilever system must be integrated inside the Port Extension.
- The Port mock-up must allow the insertion and bolting of the port plug.
- The Port mock-up must be able to withstand the loads appearing when the port plug (around 45 tons with TBMs and shields) is inserted.
- The Port mock-up will transfer its weight (and that of the inserted PP with TBMs and shields) to the test facility floor. Its weight will not be supported by the Port Cell structure.
- The holding frames must be dismantled so that possible future operations within the Port are possible, e.g. maintenance of the Port in a different zone of the Port Cell.

##### Port mock-up description.

The Port structures mock-up reproduces the geometry of equatorial port n. 16 in ITER. It includes the following parts:

- Bioshield Bellow.
- Cryostat.
- Connecting Duct Bellow.
- Connecting Duct.
- Port Extension.
- Supports.

The Bioshield and the Connecting Duct bellows are flexible elements which join the Cryostat with the Bioshield and the Connecting Duct. They have not any structural function, but they are only used to characterize the space and visibility restrictions in the ITER port n. 16.

The Connecting Duct contains the rails for supporting the front wheels of the Pipe Forest.

The Port flange is located in the rear side of the Port Extension, next to the Connecting Duct. The port plug, as well as the gasket flange, is bolted to this flange. The docking flange, which is used by the transfer cask to carry out the insertion/removal of the port plug, is also bolted to the port flange.

The Port Extension houses the port plug. The interior of the port extension has two rails that extend along the lower internal surface to help supporting the port plug.

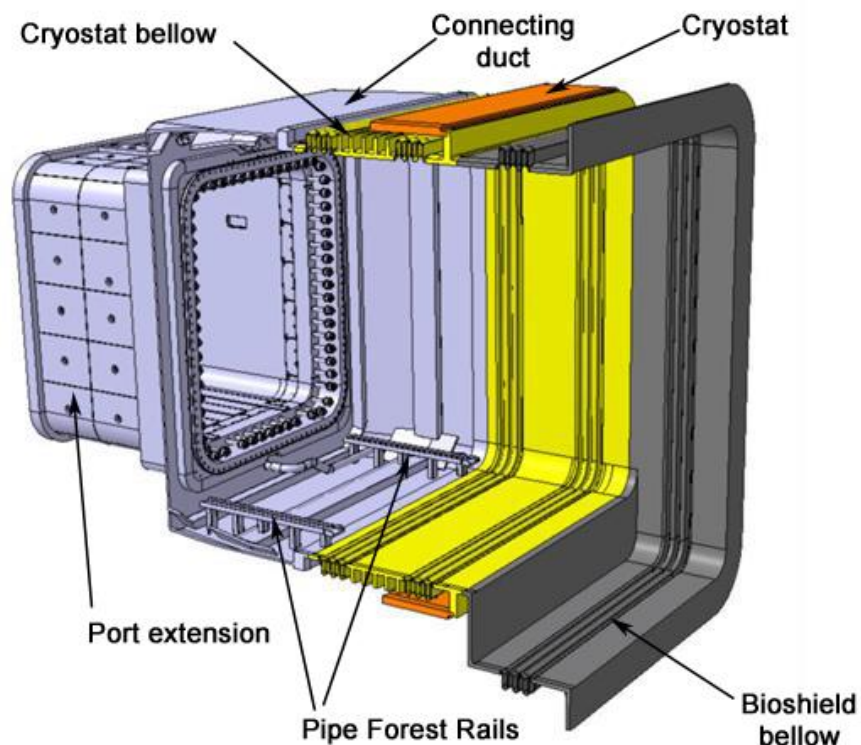


Fig. 180. Port components.

The port can be brought in one piece in order to avoid assembling operations in the TBM RH test facility. With the help of the 50 tons crane and the port supporting system, it can be placed in the correct relative position with regard to the Bioshield (Port Cell mock-up structure).

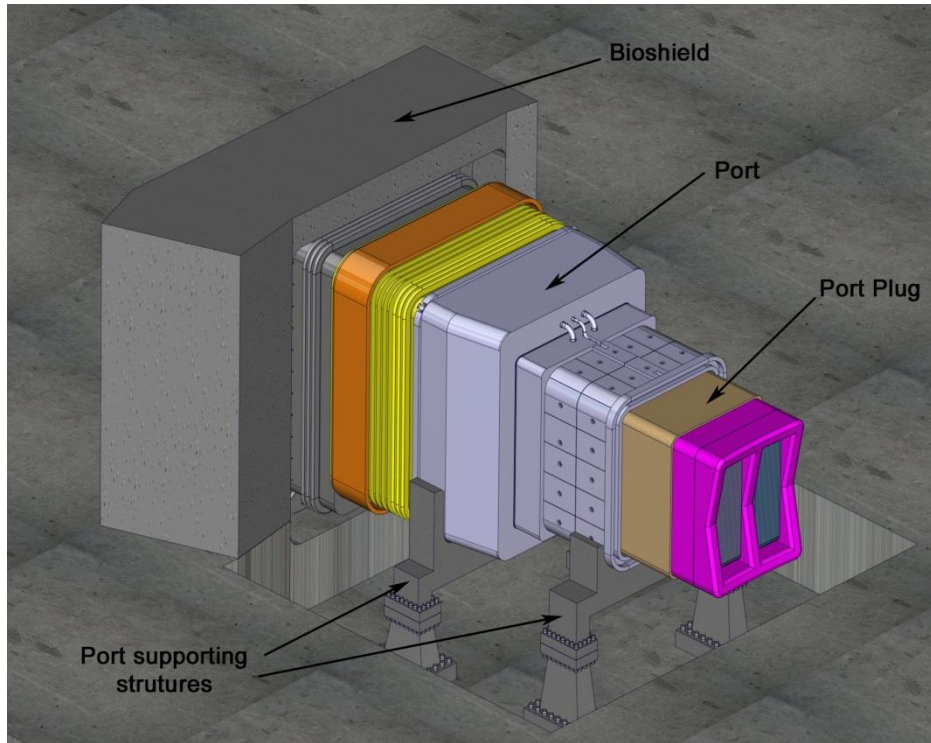


Fig. 181. Port integrated with the rest of components.

#### Port supporting system

The Port supporting system is composed of two holding frames which support the weight of the Port structures and the port plug.

One of them is placed under the Connecting Duct, while the other one is placed under the Port Extension. The design of each support is different since the outer dimensions of the Port Extension and the Connecting Duct are different.

The holding frames can be removed since they are fixed to the floor by bolts.

Fig. 182 shows the two types of holding frames and their positions relative to the ground and the second floor. As previously mentioned, the height difference between both floors is 1.5 m.

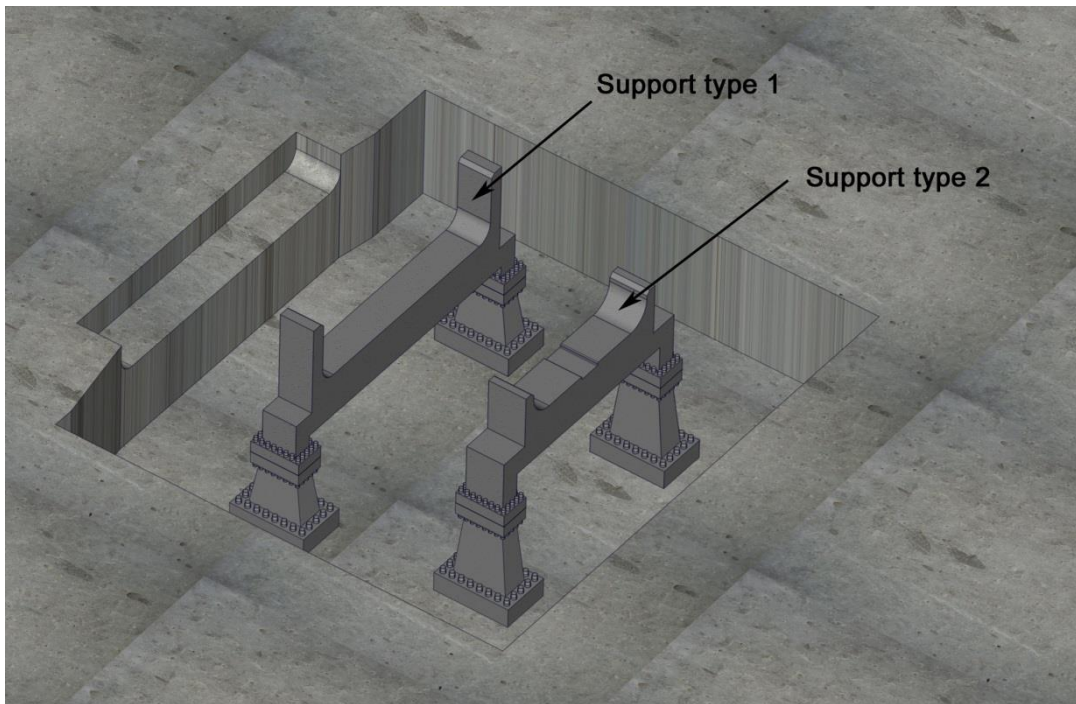


Fig. 182. Port supporting system.

#### 2.5.6.30. Supporting bench for new TBM & shield assemblies. Storage container

##### Description

In ITER, after the separation of the shield from the TBM, the shield has to be inserted into a bench to move it from the port plug maintenance area to an area where it is stored until the radioactive material decays to a required level.

The design of the shield shipping bench is still unknown; therefore the following hypotheses have been made:

- The shipping bench is used to house only one shield. The shape and size of the shipping bench have been decided considering that the shield pipes are not cut by the laser cutting tool.
- A lifting eye at the cover of the bench is placed in order to move the shipping bench along the facility.
- The shipping bench is lifted by a hook joined to the 50 tons crane through a cable.
- There must be the possibility to exchange the shipping bench for another bench in an easy way in the case that it is damaged.

Taking into account these hypotheses, the present design includes a cover with a lifting eye which couples to the bench by means of four dowels placed on top. They allow the translation of the bench between the maintenance area and the storage area, as well as benches piling in the storage area.

The bench has also four docking pins to make easier the insertion of the shield.

The bench is also used to ship the new TBM & shield assemblies to the RH test facility. In this case, the assembly is held by the TBM, which is fit to the bottom of the bench, whereas the shield flange is free.

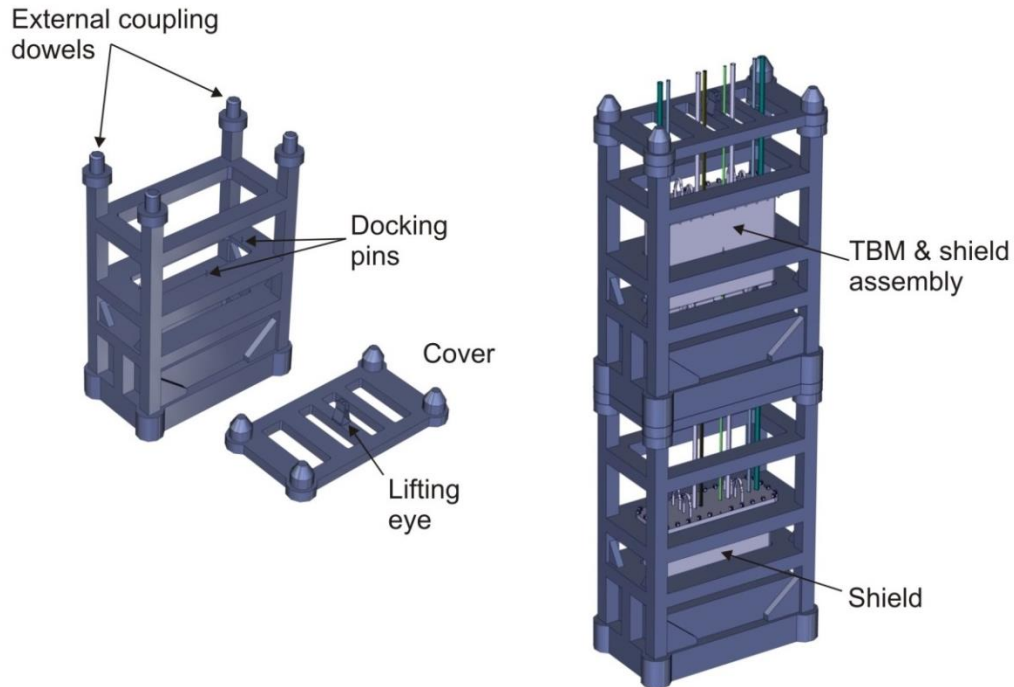


Fig. 183. Shipping bench for TBM & shield assemblies.

### 2.5.7. Auxiliary systems

The following auxiliary systems, with the exception of heating and air conditioning, have been identified in the subsection 2.5.4 (requirements of the RH Test Facility).

- RH control and visualization system.
- Electric system.
- Water supply system.
- Heating and air conditioning system.
- Vacuum system.
- Pneumatic supply system.
- Helium supply system.

The heating and air conditioning system is needed to provide comfortable working conditions for personnel working in the office area and the operations hall

The location of the different systems in the facility and their space requirements are given in the following table:

	Main location	Allocated space (m <sup>2</sup> )
RH control and visualization system	Control room	96
Electrical system	Ground floor of auxiliary systems building	25
Water supply system	Ground floor of auxiliary systems building	400
Heating system	Ground floor of auxiliary systems building	500
Vacuum system	TBM HC RH operations area	20
Pneumatic supply system	Ground floor of auxiliary systems building	30
Helium supply system	TBM HC RH operations area	30

Table 32. Main location and allocated space of the auxiliary systems.

The following table shows the correspondence between the auxiliary systems and the areas in the test facility to which they provide services:

		Area of TBM RH test facility needing services from auxiliary system.				
		PC RH operation area	TBM HC RH operations area	Storage Area	Workshop	Offices, control room and auxiliary system rooms
Auxiliary system	RH control and visualization system					
	Electrical system					
	Water supply system					
	Heating and air condition system					
	Vacuum system					
	Pneumatic supply system					
	He supply system					

Table 33. Areas of TBM RH test facility to which the auxiliary systems provide services.

### 2.5.7.1. Remote Handling Control System

The Remote Handling Control System (RHCS) integrates the different RH equipment into a RH System that allows planning and executing RH operations in an efficient and safe way.

The RHCS interfaces with the RH equipment through controllers. Sensors provide positioning signals of the different RH components. This information is used to update the virtual reality system which allows the operators controlling the RH equipment from the Control Room. They also take advantage of the information provided by the visual system (cameras in the facility plus cameras mounted on the RH equipment).

A flow diagram of the RH control system is given in the figure below.

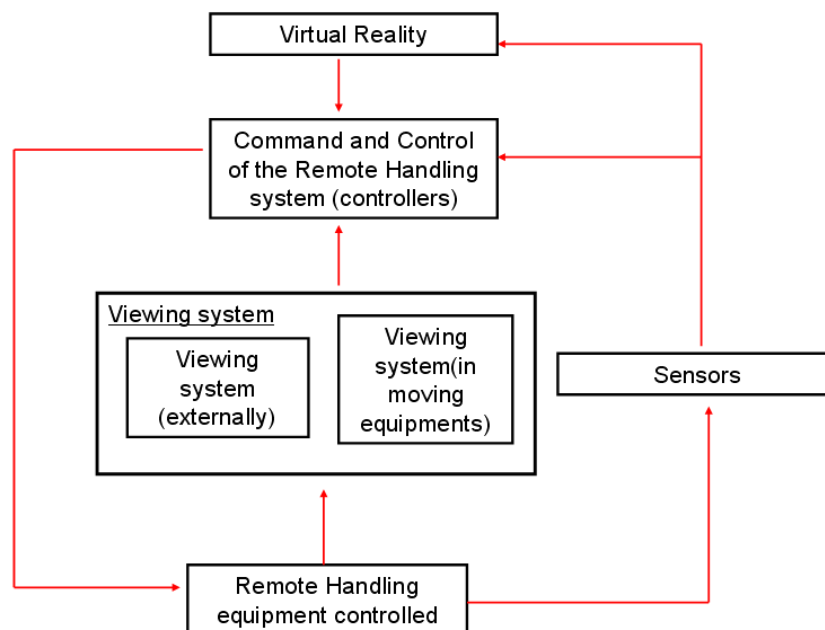


Fig. 184. Integration of the different parts of the Remote Handling Control System.

### Functional requirements

The RHCS in the TBM RH test facility shall allow operating the RH equipment in the same way as in ITER. The difficulty or ease in operating the RH equipment should be equivalent to that in ITER. Therefore, the RHCS TBM RH test facility requirements are inspired by the ITER RHCS requirements [Ham 08]. Thus, the RH control system shall provide the following main functions:

- Operator command and control of the remote handling equipment.
- Selection and control of remote viewing.
- Monitoring of the RH equipment operations in the remote environment.
- Development, control, and logging of the remote handling operations.
- Fault reporting during mock-up and actual operations.
- Remote operation simulation capabilities for procedure planning.

These RH control system functional requirements are described below with higher level of detail:

#### *General functional requirements of the RHCS*

- The RHCS shall have a real-time communication link between control devices (such as joysticks, haptic devices, and master telemanipulators) and equipment controllers, so that the control devices can be easily switched to drive the required manipulators.
- The RH Control System shall connect the equipment controller signals to connectors at the locations where the RH equipment will operate.
- The RHCS shall allow performing RH operations in a virtual environment with virtual mock ups for training and preparation purposes.
- The RHCS shall provide a system for creating and storing remote operation procedures.
- The RHCS shall provide a procedure management system for playing back the operation procedures that were developed off-line for the required tasks.
- The RHCS shall provide an intuitive, easy-to-use interface for operating the RH equipment.
- The RHCS shall optimize the remote environment sensing (viewing) and provide mechanisms for selecting and controlling the sensing of the remote environment.
- The RHCS shall support parallel operations (e.g. performing RH operations at the same time in the Hot Cell and the Port Cell).
- The RHCS shall provide a database for recording RH components reliability data.
- The RHCS shall have a collision detection system which continuously monitors for potential collisions between the RH equipment and the environment.
- The RH operators shall have hard-wired emergency stops within arms range.
- The RHCS shall look to make the best use of available technologies to enhance the operator view of the remote environment.

#### *Specific functional requirements of the command and control system*

- The Command and Control system shall allow the operators connecting to whichever pieces of RH equipment they need to control.
- The Command and Control system shall have a minimum status refresh rate of 4 Hz to ensure the operators have updated information.
- The Command and Control system shall be able to provide equipment position updates to the virtual reality system.
- The Command and Control of the equipment shall be responsive (average time to reply < 0.25 s).
- The Command and Control system shall clearly present on a graphical user interface (GUI) the important equipment status information (system states, sensor data, fault messages, etc.) taking into account accepted human factor conventions (such as colour coding).
- The Command and Control system GUI shall provide quick access to commands (single click for safety related and most frequently used commands) and intuitive use of GUI controls.

- The Command and Control system GUI shall interface with the operations management system, receiving operation command steps, and providing confirmation of command execution.
- Also, it shall be possible to use the Command and Control system for off-line planning activities.
- The Command and Control system shall be able to operate in an off-line simulation mode, having all the same features as for on-line operation.
- In off-line simulation mode, the Command and Control system shall link to an accurate off-line simulation of the equipment behaviour.

#### *Specific functional requirements of the controllers*

- The RH controllers shall implement a 'safe' state where power is isolated from the RH equipment.
- The RH controllers shall trip into the 'safe' state on detection of faults.
- The RH equipment and their associated controllers will be the same as those used in ITER.

#### *Functional requirements of the virtual reality (VR) system*

- The VR system shall deliver good graphical performance with the facility model.
- During remote and mixed-mode operations, the VR models shall closely reflect the status of the real environment.
- The VR system shall provide live tracking of RH equipment in the remote environment.
- The VR system shall provide live tracking of RH operations (movements of tools and components).
- The VR system shall provide accuracy levels better than 10 mm between the virtual environment and the real environment. This is a requirement on the whole process of establishing the VR system (such as as-built models, model simplification, registration of the RH equipment in the remote environment, accurate modelling of the RH equipment dynamics, etc.).
- The VR system shall assist in collision avoidance by monitoring projected collisions between dynamic items (RH tools and components) and between the fixed environment and dynamic items.
- The VR system shall provide look-ahead visualization of RH operations. This requires that the Command and Control system provides the VR with data on the equipment motion target positions.

For off-line simulations the VR system will be the same as for on-line simulations. For virtual trials:

- This VR system shall support the driving of simulated equipment using input devices.
- This VR system shall provide reflection of contact forces back to the operator through haptic devices at a rate of at least 100 Hz.
- This VR system shall provide simulation of physical behaviours and interactions between geometries.

#### *Functional requirements of the viewing system*

- The viewing quality properties of the cameras in the facility will be the same as in ITER.
- The viewing sensor signals (generally cameras) shall be assignable to any monitor in the RH control room, and controlled via the Command and Control system.

#### *Data storage and remote access*

- The RHCS shall store all the data obtained from the different operations. This data will be saved in hosts and must be locally or remotely accessible.
- It shall be possible to give on-line access to live information coming from the simulation of particular operations.

Conceptual design proposal for the control room

The following are some components of the control room which are needed to control the RH demonstration operations, as well as to carry out RH training.

- Computer workstations.
- Control input devices (emergency stops, joysticks, haptic arms, etc.).
- TV monitors.
- Large screen projectors.
- Audio and video link between the control room and the operations hall.
- Software.

Specifically, the following components are proposed to be installed:

- Two control stations with one supervisor.
- One haptic master telemanipulator for the TBM Hot Cell RH operations.
- One haptic master telemanipulator for the TBM Port Cell RH operations (depending on the features of the Port Cell robotic arm).
- Elements of the viewing system and the virtual reality system.

The proposed space for the control room is ~96 m<sup>2</sup> (8 m x 12 m). The figures below show two examples of equipment layout in the RH control room. The layout in the TBM RH test facility could be similar to the DTP2 control room. In addition, there would be a JET-like master telemanipulator for the Hot Cell RH operations (Fig. 185).

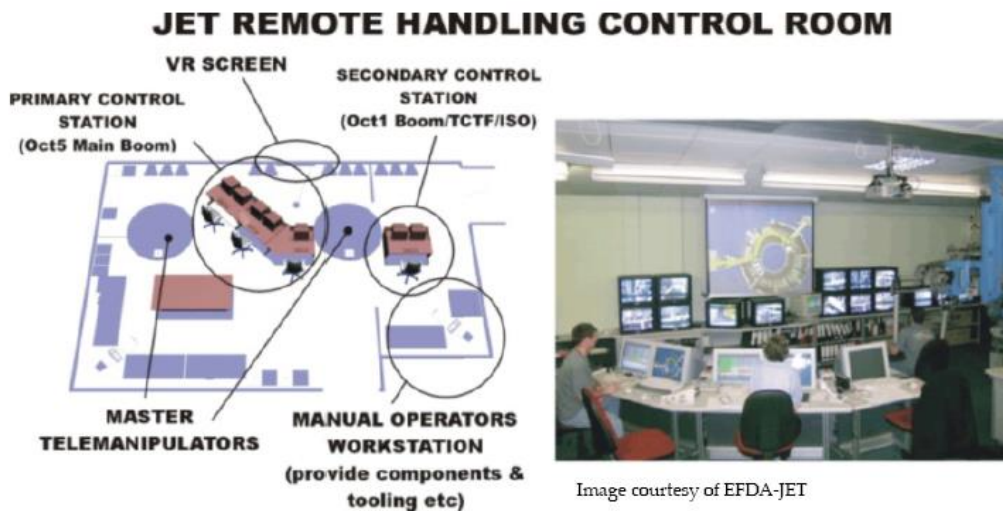


Image courtesy of EFDA-JET

Fig. 185. Spatial layout of the control room of JET.



Fig. 186. DTP2 control room.

The exchange of signals (control, position, force feedback) between the control room and the RH equipment is done by cable except for specific equipment like the ATS that is controlled via wireless remote control.

The virtual reality software used for visualization of the RH operations with virtual models of the equipment and their environment shall be the same as those used in ITER. DELMIA and VR4ROBOTS are examples of this type of software.

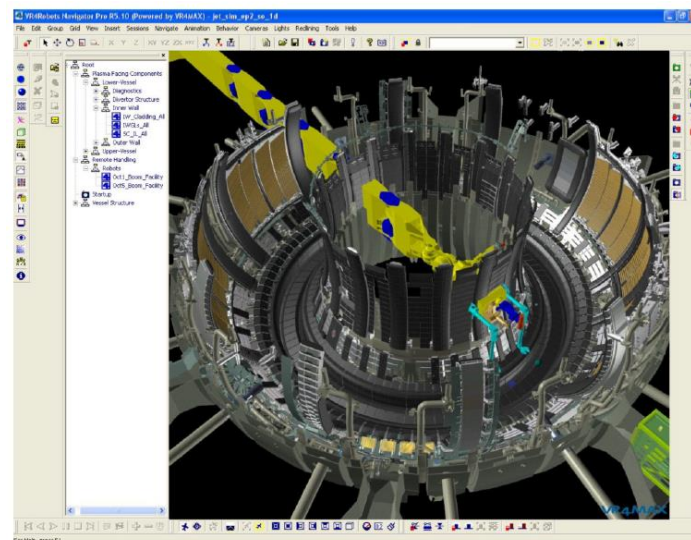


Fig. 187. JET vessel simulation – GUI.

### Cameras for the viewing system

Remote handling operations require good sensing of the environment, since operations efficiency is directly correlated to the viewing system quality.

The TBM RH Test Facility includes static or movable cameras attached to fixed elements (fixed mock ups, walls or ceilings of the building) as well as cameras integrated with the RH equipment that move with it.



Fig. 188. Example of camera for the viewing system.

Image quality involves a significant challenge in ITER due to the sensitivity of cameras to high radiation levels. Since the TBM RH Test Facility is not radioactive, problems linked to radiation are not present. However, images provided to the operators in the TBM RH test facility control room should imitate the level of quality of images provided to the operators in ITER.

#### Equipment to be controlled

A preliminary proposal of the way the control is performed in different devices of the Test Facility equipment is given in the following lines:

##### *Transfer cask*

The transfer cask system must move between the Hot Cell operation area and the Port Cell operation area. The transfer cask is controlled from the control room. The RHCS provides monitoring and control of the transfer cask internal environment. This function is performed by the ATS controllers during transfer operations and by the transfer cask controllers when it is docked and connected to the port service connector.

##### *ATS (Air transport system)*

As in ITER, the ATS shall navigate controlled from the control room with a wireless system. The ATS positions shall also be monitored using a wall mounted localization system.

##### *Gasket flange maintenance equipment*

This device can be controlled by a wireless system from the control room. Batteries can be used to supply electric power to the drive system. Several cameras are installed in the equipment to provide visual information to operators during RH operations.

##### *Port Cell robot and Hot Cell master-slave manipulator*

The Port Cell robot and the Hot Cell master slave manipulator will be controlled in the same way as in ITER (same master manipulators, same number and position of cameras, etc.).

##### *AEU*

The actuators used to constrict/unconstrict the pipes at Interface 2a will be controlled either from the Port Cell by a specific device or from the control room. In any case, the control of the AEU in the test facility must follow that chosen for ITER.

##### *Pipe Forest & Bioshield Door assembly*

The drive system can be controlled from the Control Room with a wireless system and cameras.

*RH platform unit*

The deployable carrier of the RH platform unit can be controlled from the control room with a wireless system.

*Band sawing machine, vertical positioning tool, laser cutting tool*

All this fixed equipment can be controlled by wired systems from the control room.

*Vacuum cleaner*

The vacuum cleaner can use a battery and be turned on/off by the HC manipulator. Cameras can be used to monitor the operation of the manipulator from the control room.

*PP test stand*

The vacuum system can be operated by a wired system from the control room.

*Cranes and telescopic mast*

They can be moved directly from the operations hall or from the control room.

**2.5.7.2. Electric system**

At the current stage of conceptual design the electric power supply needs of the equipment in the test facility are not well defined. However, the following functional requirements can be established based on estimates of the overall electrical power supply needs.

**Functional requirements**

- The electric system design must be in accordance with the hosting country regulations.
- The projected electric system must satisfy the worst case electrical power supply needs of the facility. The power consumption in the Test Facility is estimated around 650-700 kW, distributed in the following way:
  - Heating system for the operations hall: 280 kW.
  - Heating and air conditioning system for the office and auxiliary system building: 220 kW.
  - Lighting and equipment electric consumption: 200 kW.
- The number and distribution of points of electric supply within the facility must be defined considering the power supply needs of the equipment and systems. There will be points of electric supply close to the different RH operation areas.
- The voltage supplied in the different operation areas will be according to the equipment needs. It shall be possible to supply three phase voltage and one phase voltage to any of the demanding points.
- For the electric power needs of the facility being greater than the maximum power normally supplied by utilities on the low voltage electric grid, a transformer will be needed.
- The transformer (or set of transformers) will be placed outside the test facility building in accordance with the hosting country regulations. The power of the transformer is estimated to be 1000 kVA.
- The electric system will include a set of electric capacitors to improve the power factor.

- The electric system should be able to provide power supply during a specific time interval in case of loss of power from the electrical power grid.

#### Description of the electric system

The following is a very brief and general description of the TBM RH test facility electric system:

The electric system would consist in:

- General electric connection: it connects the power grid to the general electric distribution and control panel through the transformer.
- General electric distribution and control panel. This panel is divided into two parts: one part for the lighting of the hall and another part for power supply. Each panel has its own safety system (magneto-thermal and differential circuit breakers). The different cables to the secondary panels, consumers and the lightning system are derived from this panel.
- Cabling to electric power consumers in the remote handling system.
- Cabling to cranes.
- Cabling to secondary panels: these panels would supply the different operation areas individually (Hot Cell and Port Cell).
- Internal lighting of the facility.
- External lighting and other devices.
- An UPS (uninterrupted power supply) unit will guarantee electrical supply to RH equipment and auxiliary systems in case of loss of power from the grid. In this way the equipment can go into safe position and eventually release any loads it might be manipulating. Furthermore the UPS supplies electricity to the emergency and signalization system.

#### 2.5.7.3. Water supply system

The water supply system provides water to the points of the facility where it is needed. The functional requirements of the system and a brief and general description are given here.

#### Functional requirements

- The water supply system is divided into two independent systems: on one hand the sanitary and storm drainage system and on the other hand the plumbing system (cold and hot water).
- A system will be designed to evacuate any class of water through a unique net, up to the connection of the network of the public sewer system.
- The components that constitute the net of the sanitary and storm drainage must fulfil the hosting country regulations.
- The water supply system provides water to the Port Cell RH operation area to carry out inspection of weld seams in pipes.
- The water supply system provides water to the Hot Cell RH operation area.
- The plumbing installation is designed to supply the pressure and volume of flow required in each supply point inside the facility.
- A water heater & accumulator heats cold water and provides hot water to the rooms where it is needed (e.g. bathrooms).

#### Description of the water supply system

The following is a very brief and general description of the TBM RH Test Facility water supply system:

The following needs are assumed:

- A cold water supply point in the Hot Cell operation area.

- A cold water supply point in the Port Cell operation area to carry out inspection of weld seams on pipes.
- Three water supply points in the workshop area (hot and cold water) to perform maintenance operations of the different elements of the facility.
- Two toilets per floor (4 in total with cold and hot water). Showers in the changing room are also considered.
- Supply for the water emergency system to extinguish fires (cold water).

To comply with the specifications and the regulations two subsystems are included:

- Sanitary and storm drainage.
- Plumbing installation (cold and hot water supply and the firefighting system).

#### *Sanitary and storm drainage*

The function of this system is the evacuation of sewage water coming from industrial and human consumption as well as sewage water coming from the storm drainage.

A drip box is situated outside of the facility. It connects the sanitary and storm evacuation drainage with the public sewer system.

#### *Plumbing installation*

The water supply system of the facility is connected to the general water distribution network of the area where the facility is located.

From this connection two lines come out:

- Water supply for general needs (operation zone, maintenance room, toilets, etc.).
- Water supply for the firefighting system.

The connection is placed outside of the Facility. The water supply for general needs is divided into cold and hot water.

The distribution inside the facility is conventional. Inside the operation zone the water pipes are underground. In the PC the supply point will be the same as in ITER. In the operation areas the water supply points will not interfere with the tasks performed in such areas.

#### *Cold water system*

It provides cold water to the installation (to be used as cold water or to be heated).

A pump or set of pumps will be needed to supply the water circuit and satisfy the pressure and mass flow requirements in each point where water is needed.

#### *Hot water*

Water is heated with a conventional gas or gas oil boiler or with electric heaters. Depending on the hosting state regulation it may be required to pre-heat water with solar panels.

#### *Firefighting system*

There shall be in the facility different fireplugs according to the Test Facility hosting state regulation. A hose would be connected to each fireplug. Fire extinguishers shall be distributed around the test facility in the transformer according to regulations.

#### 2.5.7.4. Heating, ventilating and air conditioning system (HVAC)

Although the HVAC needs of the TBM RH Test Facility are unknown at present, some general considerations about functional requirements and a basic description can be given.

##### Functional requirements

- The HVAC system must be conceived to satisfy the hosting country regulation.
- Thermal quality of the environment shall be achieved through the design and dimensioning of the thermal installation by keeping the parameters which define the thermal comfort (air temperature, relative humidity, average air velocity, turbulence intensity) within the specified values.
  - Thermal stability and uniformity are not needed. Temperatures can vary  $\pm 3^{\circ}\text{C}$  and stratification is allowed.

##### Description of the HVAC system

###### *Conventional energy*

- Heat pump system for cooling (cooling units + fan-coils).
- Gas/gas oil boilers or electric heaters for heating and sanitary hot water.

###### *Non-conventional energy*

- Solar collectors for heating and sanitary hot water (may be required by hosting state regulation).

###### *Heating and cooling power*

Two arbitrary locations in Spain (Madrid and Barcelona) have been chosen to do a preliminary estimation of the heating and cooling needs. The worst orientation cases for winter and summer have been assumed in order to do a preliminary estimation of the HVAC system power needs. The heating power, considering that it is provided by gas boilers and solar energy, is shown in thermal kilowatts ( $\text{kW}_{\text{th}}$ ), whereas the cooling power –provided by heat pumps– is shown in electrical kilowatts ( $\text{kW}_{\text{e}}$ ) in Table 34.

Location	Heating power ( $\text{kW}_{\text{t}}$ )	Cooling power ( $\text{kW}_{\text{e}}$ )
<b>Operation hall</b>	220	
<b>Offices and auxiliary system building</b>	29	59

Table 34. HVAC power needs.

###### *Space needs*

Air cooling equipment:  $67 \text{ m}^2$  (offices).

Hot and cool water production equipment:  $207 \text{ m}^2$ .

Solar collectors and connecting pipes:  $250 \text{ m}^2$ .

#### 2.5.7.5. Vacuum system

The function of the vacuum system in the TBM RH test facility is to provide vacuum in order to carry out the checking of vacuum sealing between the port plug and the TBM shield, as well as the leak test of the welds connecting the intermediate water circuit with the PP and shield cooling circuits.

The sealing test is performed in the test stand, whereas the cooling circuit leak-proof is carried out while the PP is inserted in the vertical positioning tool. The fixed components of the vacuum system (rotary pumps, turbomolecular pumps) can be placed close to the test stand and the vertical positioning tool, as it is shown in the next figure.

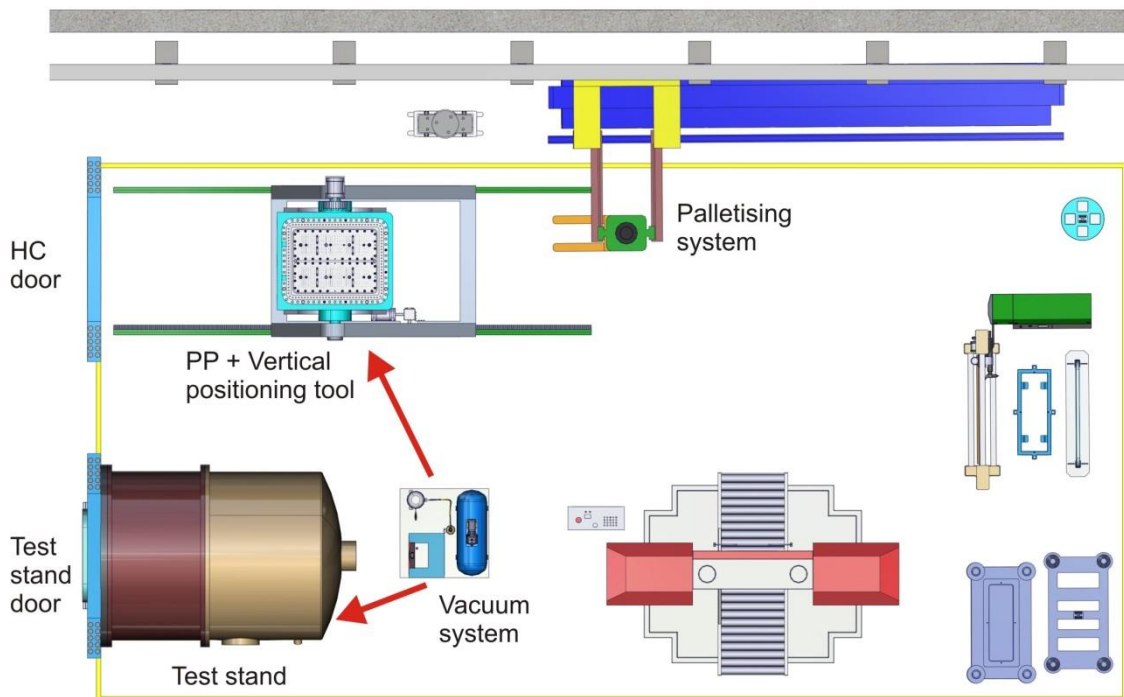


Fig. 189. Vacuum system location within the Hot Cell operations area.

#### Functional requirements

- The vacuum system must be able to create vacuum inside the test stand equivalent to that of the vacuum vessel in ITER.
- The vacuum system must be able to create vacuum inside the cooling circuit of the PP and shield in order to perform leak tests on the welds with helium.

#### Conceptual design proposal for the vacuum system

The following information is a very brief and general description of the TBM RH test facility vacuum system.

An area of 4 m<sup>2</sup> has been assumed for the fixed components of the vacuum system.

The connections between the vacuum pumps and the test stand are fixed. The vacuum system and the distribution circuit must be connected and disconnected before and after the leak testing operation.

The following list includes the required equipment (instrumentation, pipes...) for the system:

- Rough pumping (scroll pumps, piston pumps).
- Turbomolecular pumps.
- Helium leak detector.
- Data acquisition unit.
- Cables.
- Computer + software.
- Fittings.
- Flanges.
- Stainless steel low diameter pipes.

- Ultra high-vacuum valves.
- Metallic gaskets.
- Special braces for metallic gaskets.
- High pressure sensors (e.g. piezoresistive, pirani).
- Low pressure sensors (e.g. cold cathode).
- Thermocouples.
- Quick-connects for instrumentation and pipes.
- Pipes fixing elements.

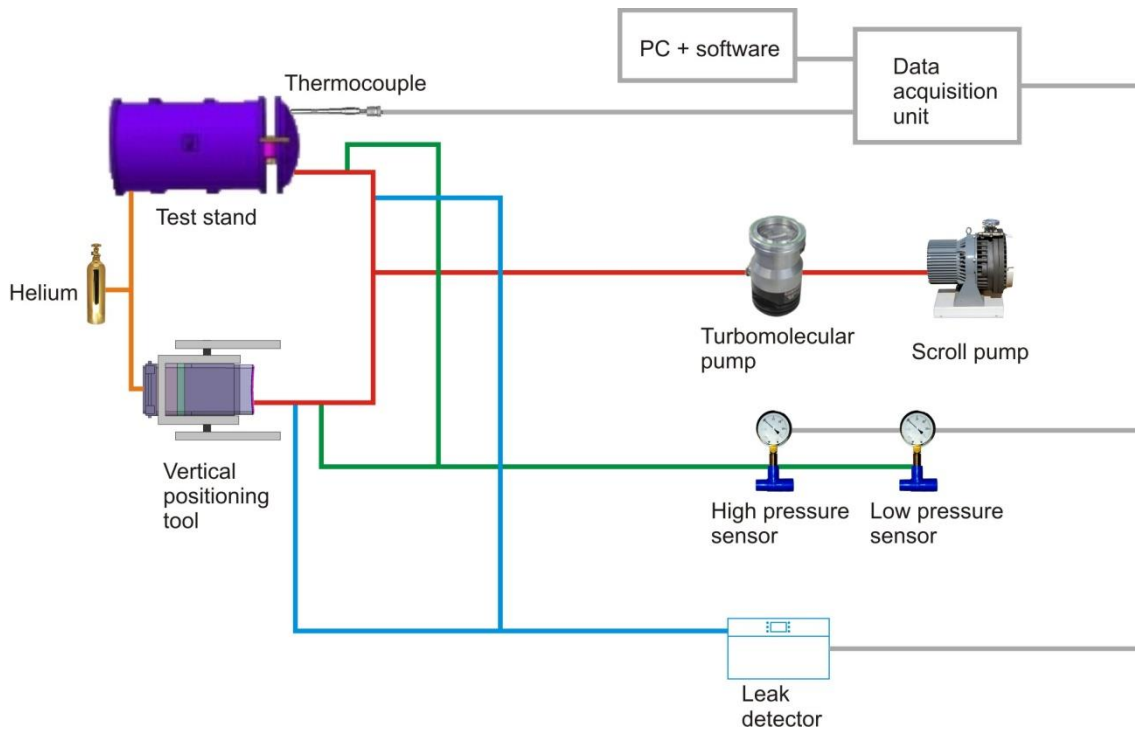


Fig. 190. Vacuum system diagram.

The combination of rough and fine pumping is needed for reaching a high vacuum level in two steps: first the rough pump works until the pressure is low enough; then the turbomolecular pump starts working to reach the required high vacuum level.

At least two pressure sensors are needed because of the accuracy of the measure, which is different for each pressure range, depending on the functioning principle of the sensor. Fittings, valves, flanges, gaskets, brace are the vacuum piping elements which compose the vacuum circuit. Quick-connects allows fast assembly/disassembly of the circuit.

Several components of the vacuum system CODAC sub-system (data acquisition unit, computer, software) would be placed in the test facility control room. Therefore, laying cables between the operation area and the control room would be needed.

The vacuum system needs low voltage electric supply and helium supply.

### 2.5.7.6. Compressed air system

#### Functional requirements

- The compressed air system must provide compressed air at 4.5 MPa (1.5 times the nominal water pressure in the PP cooling circuit) for carrying out a pressure test on the welds joining the shield and PP cooling circuits with an interface cooling circuit. Compressed air at 4.5 MPa will be introduced inside the cooling circuit instead of water because it is assumed that water is not allowed in the Hot Cell.

- The compressed air system must provide compressed air for certain tools and equipment (e.g. tools in the workshop, tools for the Port Cell manipulator).

#### Conceptual design proposal for the compressed air system

The following is a very brief and general description of the TBM RH test facility compressed air system.

The compressed air system includes the following sub-systems:

- Compressing equipment and deposit.
- Distribution pipes.
- Accessories.
- Control equipment.

The compressing equipment consists of one or several stationary compressors, depending on the pneumatic supply needs. The compressors features are to be defined, but it would be interesting that they include variable-speed-drive (VSD) technology. It would allow adapting the performance of the compressor and save energy by controlling the frequency of the current which feeds the AC motor. The equipment is completed with a dryer to dry, filter and cool compressed air. It could also include VSD technology.

Such equipment is placed in a room located in the auxiliary systems zone. A space of 30 m<sup>2</sup> can be needed if two compressors and a dryer are considered.

The distribution of the compressed air is done by an overhead system. The pipes must have a downward inclination in order to allow the natural movement of the water and make easier the drainage through blow-off valves. Independent catchers come out from the main pipe to supply compressed air where needed. The catchers come out from the upper part of the main pipe for taking the driest air (the wettest air flows through the lower part of the pipes).

The accessories to the pneumatic supply system are listed below:

- Elbows.
- Clamps.
- Butterfly valves.
- Gate valves.
- Blow-off valves.
- Siphons.

The pneumatic system is controlled from the test facility control room. The control subsystem includes pressure sensors, flow-meters, a PC and software connected to the compressors central control.

#### 2.5.7.7. Helium System

##### Functional requirements

- The Helium system must provide helium for carrying out vacuum leak tests on welds and the interface shield-port plug. Two functions must be accomplished by the system:
  - It must allow insufflating He along weld seams between the shield and PP cooling circuits and the interface circuit. It must allow insufflating He in the interface between the shield and the PP frame.
  - It must be able to detect He leaks into a space where vacuum has been created (e.g. test stand and inside of PP and shield cooling circuit during leak test).

##### Conceptual design proposal for the helium system

The following is a very brief and general description of the system.

The helium system is integrated by the following items:

- He bottle: commercial bottle of 20 or 50 litres.
- He pistol.
- Regulator of the He pistol: it provides the desired pressure and mass flow.
- Flexible pipes: they connect the test stand or the TBM shield cooling pipes to the mass spectrometer.
- Mass spectrometer: Some commercial models incorporate a vacuum pump and can be remotely operated.

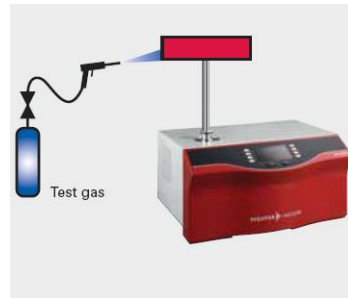


Fig. 191. Mass spectrometer.

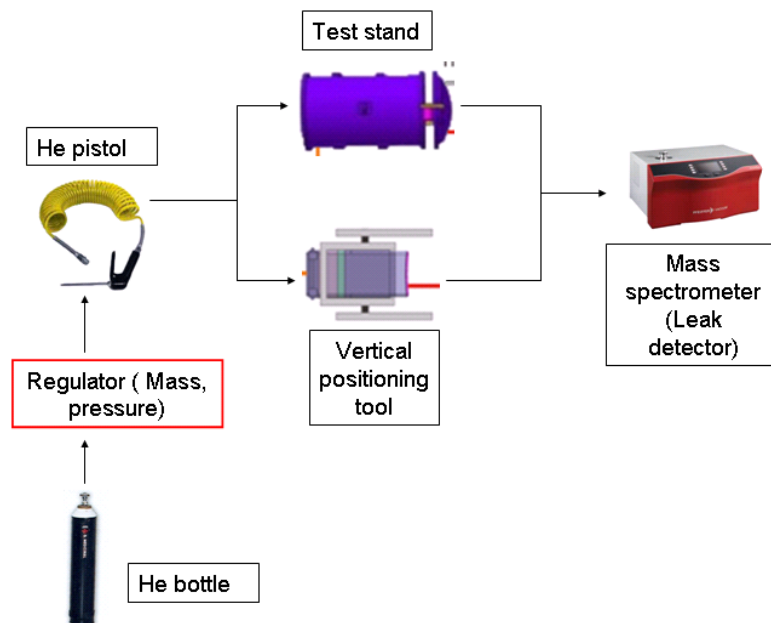


Fig. 192. Layout of the He system for testing operations.

RH operations in TBM RH test facility where helium system is involved

As previously mentioned, there are two RH operations where the He system is involved:

- Vacuum leak test of weld seams between the shield and PP cooling circuits and the interface circuit.
- Checking of vacuum seal between the PP and TBM shield.

*Check of the weld seams between the cooling circuit pipes and the PP wall*

In Subsection 2.5.4 the operation sequence is described and the welds where helium needs to be insufflated to check the weld vacuum tightness are shown. It is assumed that the HC manipulator holds the He pistol to insufflate He in the weld seams.

*Checking of the vacuum seal between the PP and the TBM shield*

Fig. 193 shows where helium needs to be insufflated to check the vacuum sealing between the PP frame and the TBM shield. In Subsection 2.5.4 the operation sequence is described.

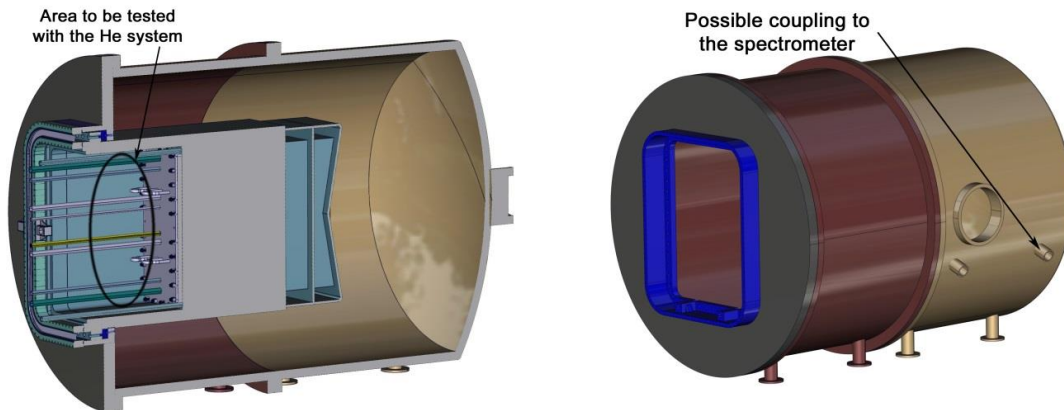


Fig. 193. Layout of the test stand.

## **2.6. Comparison between DEMO blanket and ITER TBS maintenance schemes**

Once seen the features of the maintenance procedures considered for the ITER EU TBS, mainly through the requirements, processes and equipment assumed for the TBM RH test facility, it is interesting to compare them with the maintenance schemes what are being assessed in Europe for an early DEMO. Previously, it is advisable to explain some issues about safety and mainly hydrogen isotopes handling in ITER, remarking anticipated sources of unavailability which can affect the DEMO blanket system design.

First, a fundamental difference between ITER and DEMO concerns scheduled maintenance shutdowns. In ITER they are planned in order to exchange the TBMs according to the 4 different experimental campaigns which will be carried out along the 4 plasma operation phases, as explained in Section 2.4, whereas in DEMO they are based on blanket reliability and operational lifetime. Thus, the necessary scientific approach makes ITER operation will not able to provide full operational availability demonstration for the future fusion reactors. ITER is designed and will be operated to fully optimize the available time for experiments, while DEMO shall demonstrate operational availability values which validates systems designs and procedures to be applied in commercial fusion power plants. Nevertheless, one of the main challenges for ITER will be to demonstrate the feasibility of keeping an operating rhythm under a nuclear environment with sufficient high key performance indicators [Hou 11].

In ITER, there is an availability decrease between the H phase and the D–T phase mainly coming from one function which is a key point for DEMO: tritium fuelling and recycling. This is due to an availability of 80% in the utilities group which is not considered in the H phase [Hou 11]. In fact, the inherent availability required for the level 2 function “to manage H isotope” (tritium in D-T Phase) in the Functional Breakdown Structure is the lowest one, together with the functions “to supply and distribute pulsed electrical power” and “to produce, transport and

distribute cryogenics to SSCs (systems, structures and components)” [Hou 12]. They strongly impact the availability of the overall level 1 function “to provide utilities”.

Such availability in the utilities group leads to drastically decrease the inherent availability of the overall machine operation from 60% in H phase down to 51.8% in D–T phase [Hou 11]. By introducing the scheduled downtime for maintenance and upgrades as defined in the project requirements the operational availability in D–T phase is 26.9% for the machine operation and 21.5% for the physics program, taking into account the availabilities of heating & current drive and control (diagnostics and actuators) systems [Hou 11].

Those estimations reflect the importance of the tritium plant in ITER availability and how it can have influence on DEMO performance, taking also into account that the tritium plant in DEMO will probably include an important number of first-of-its-kind components and systems, in the same way as for ITER. Relevant additional information about this issue can be obtained from experience in JET, the first fusion device in the world to achieve a significant production of controlled fusion power (nearly 2 MW) with a D-T experiment. Operation experience data regarding the Activated Gas Handling System (AGHS) in JET obtained along 11 years were analysed in order to establish a database of components reliability [Pin 10], showing the largest number of failures/malfunctions concerned ‘external leaks’ and ‘fail to operate’ of air-actuated valves and solenoid valves. Important in terms of amount of malfunctions were also ‘Erratic/No Output’ of instrumentation and electronic components. Other failures concerned scroll vacuum pumps, rotary vane and turbomolecular vacuum pumps, blowers, metal bellows, radiation monitors, no-return and pressure regulator valves, power supply systems, etc. The failure rates and the failure probabilities on demand evaluated were in very good agreement with the corresponding ones existing in literature for similar applications (e.g. CANDU fission power plants), and they could be very useful to evaluate reliability parameters in support of safety assessment and for availability/reliability analyses of fusion machines/power plants and tritium laboratories.

On the other hand, there is an important point which affects the integration of in-vessel & ex-vessel systems in ITER, and will do in DEMO, which visibly plays a role in the definition of maintenance schemes: the strategy for confinement of radioactive material. In ITER, every significant inventory is protected by two confinement systems, each comprising one or more physical or functional barriers. Broadly, the first confinement system prevents mobilization within the facility, and thereby protects workers, and the second confinement system prevents release to the environment in the event that the first confinement has failed [Tay 14]. In ITER, the first confinement barrier is the vacuum vessel and its extensions (45 ports + hundreds of penetrations for cooling systems, H&CD systems, diagnostics, etc.). The situation is complicated with the policy of not crediting any in-vessel component with a safety function. This is essential in ITER because the experimental nature of in-vessel components (e.g. TBMs) involves their reliability in accidental situations is not guaranteed. This means that, for example, the ex-vessel part of the water cooling system is part of the first confinement system and must be reliably leak-free in all situations including earthquakes. The result is a first confinement barrier that comprises many tens of km of pipework, ducts, waveguides etc. and hundreds of isolation valves and windows including non-metallic windows for which a qualification is needed. In DEMO, in-vessel components as breeding blanket must be highly reliable and some parts inside the VV could be credited with a confinement function in order to avoid the extensive and complex ex-vessel parts that complicate the first confinement barrier in ITER. This would have a clear impact on the design of both in-vessel and ex-vessel components and, in consequence, on the maintenance procedures.

The following Subsections show an analysis of the differences between the maintenance of the ITER TBS and the DEMO breeding blanket in several aspects: main schemes, processes automation and hot cell activities, among others.

### **2.6.1. Vertical maintenance**

Vertical maintenance has been the reference for EU DEMO and power plant conceptual design studies, from NET to the present EUROfusion WPRM. Only during the PPCS an ITER-like

system ('large modules') has been used as basis for the comparison of the different reactor models [Boc 12]. These studies were based only on RH considerations, but a subsequent analysis of reactor requirements (e.g. re-weldability in hydraulic connections, thermal compensation of in-vessel components, etc.) showed the questionability of the ITER-like maintenance system for a power plant.

Horizontal sector transport maintenance based on large ports has been the reference concept in the majority of American and Japanese power plant studies (DREAM, ARIES, SlimCS, etc.). In the case of vertical maintenance schemes, inter-coil structures against turnover forces in TF coils could be adopted like in ITER, but not in the case of horizontal maintenance, causing the maximum TF coil deflection in toroidal direction is considerably higher than in the case of vertical maintenance. On the other hand, the presence of upper ports for vertical maintenance involves forbidden areas for the PF coils to form upper elongation and triangularity in order to achieve MHD equilibrium in plasma. However, it is possible to obtain PF coil configurations compatible with vertical maintenance whose maximum PF coils current is lower than in the horizontal sector transport maintenance scheme [Uto 12]. There are other merits to the vertical maintenance scheme over large port maintenance schemes, as smaller vacuum vessel closure plates and reduced size and scope of containment cask handling and hot cell activity [Col 14]. In general, we can say this scheme is less invasive and its impact on other tokamak systems is lower.

Thus, the assumption of vertical maintenance architecture in DEMO implies a number of differences in the remote handling system with respect to ITER. The first one is the bigger productivity because of the use of MMS -or even banana-shape single segments- instead of the larger number of modules in an ITER-like concept.

The common implementation of a VMS foresees a segmentation of the blanket system in 5 segments per sector: 2 inboard segments (IB) and 3 outboard segments (OB). Each sector includes an upper port through which the vertical maintenance of the 5 segments is done.

The basic RH sequence for the replacement of blanket MMS consists of the following steps [Boc 12]:

- 1) Opening of the vertical port.
- 2) Cutting the pipes coming from the segments and free the port duct for the successive operations.
- 3) Extract vertically the key OB segment with a crane.
- 4) Extract the lateral OB segments; in this operation each segment should be moved toroidally to reach the opening of the vertical port to allow vertical extraction.
- 5) The IB segments must be moved first radially and toroidally to reach a position under the vertical port opening to allow a successive vertical extraction.

The main differences with the in-vessel maintenance scheme of the ITER shielding blanket, but also with the TBMs ones, in which we will focus on since they are directly connected to DEMO/FPP breeding blanket in terms of functional requirements, arise from this list of operations. As in the case of the ITER TBS, the equipment in charge of opening the port and introducing/extracting the blanket segments is housed in casks with double-doors which dock onto features in the bioshield or the vacuum vessel ensuring that contamination from the in-vessel environment is not spread to the cryostat and bioshield interspace or to the exterior of the bioshield. Furthermore, there is a port closure cask proposed for DEMO whose function is similar to the gasket flange maintenance equipment in ITER, that is, to break and re-make the port vacuum seal through a bolting/unbolting tool. There is also another cask (pipe joint cask) carrying the necessary tools for cutting, welding, making heat treatment and performing non-destructive testing (including helium leak test) in the blanket pipes, which would be the equivalent system to the RH platform unit plus the Port Cell robotic arm that we have proposed to perform such operations at the TBS interface 2a. However, there is an important difference which determines the nature and sequence of RH operations: the blanket segments in DEMO are not allocated inside port plugs, but they are directly supported by features belonging to the vacuum vessel. This implies the vacuum port flange is not a frame like in ITER equatorial ports, but it is a solid piece through which blanket service pipes pass. In consequence, bellows for

these pipes are required at the connection to the vacuum flange to compensate for thermal expansion effects of the MMS and the pipes themselves. The whole assembly of pipes segments, bellows and vacuum flange is removed like a single element. On the other hand, in the case of the ITER TBS, the pipes at interfaces 2a and 2b must be removed –as part of the pipe forest & bioshield door assembly, as described in Section 2.5- previously to the removal of the vacuum seal. However, in the case of the interface 2a pipes, neutron fluence at the beginning of the different maintenance campaigns is not high enough to be replaced for new ones, but DEMO blanket pipes must be replaced because of re-weldability requirements.

In DEMO, the use of bellows at the joining between pipes and the vacuum flange causes there is little space available for large diameter connection features (e.g. flanges, brazed connections or orbital welding). Thus, in-bore welding is considered necessary for the majority of the joints in the vertical port [Col 14], whereas orbital welding is the chosen joining technique for the IF2a in ITER TBS. Because of availability requirements in DEMO, the current approach is minimizing the number of hydraulic connections between blanket segments and their auxiliary systems, so that there is only one inlet and one outlet for the whole set of modules belonging one MMS. Only in the case of liquid breeder blanket concepts (HCLL, DCLL) an additional draining pipe or the PbLi outlet pipe itself is envisaged to be allocated at the bottom part of the segment because of safety/operational requirements. Nevertheless, this issue is not defined yet in the present EUROfusion Program 2014-2018. On the other hand, the number of pipes which communicate the EU TBMs and the rest of the TBS is considerably higher (10 He and PbLi pipes), mainly taking into account the ratio blanket segment volume/TBM volume. Another important difference in DEMO is that no diagnostics pipes are envisaged by the moment, since results obtained from the exploitation of data collected in ITER will allow DEMO having much less diagnostics because they are not necessary (e.g. findings about the thermomechanical and neutronic performance of the TBMs will be used during the engineering design of DEMO blanket: reliability growth). 3 diagnostics pipes for the HCLL TBM and another 3 ones for the HCPB TBM are proposed.

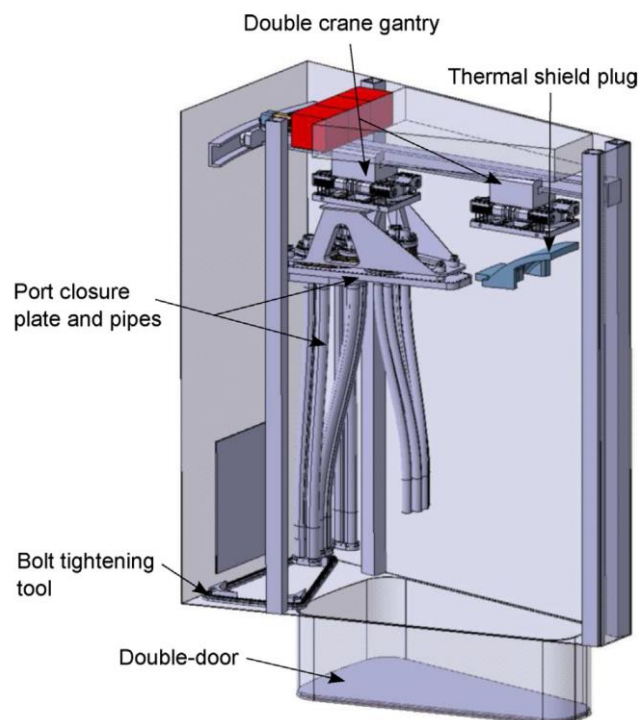


Fig. 194. Section through the port closure cask showing the fully extracted port closure plates, pipes and thermal shield plug [Col 14].

Weight is an important issue for a vertical maintenance scheme. In ITER, the pipe forest and the AEU are removed/installed by an air transfer system which slides over the building floor. In the same way, a tractor inside the transfer cask horizontally extracts/introduces the TBM port

plug from/in the corresponding equatorial port, using a helping cantilever system who guarantees its stability. But in the case of vertical extraction/insertion in DEMO, a robust crane must cope with the whole weight of in-vessel components which are significantly bigger than TBMs. For example, the weight of the EUROFER structure of a central outboard DCLL blanket segment can exceed 37 t, whereas the lateral outboard segments can exceed 54 t and the inboard segments could be around 25 t [Rap 14]. Thus, the vertical maintenance crane, which consists of a cask-housed, rigid, telescopic frame which carries a crane mounted transporter (CMT) arm and gantry, must handle all of the lifting loads, including the off-centre CoG moment. Effectively, the removal/installation of the 5 heavy blanket segments corresponding to each sector involves a combination of relatively complex movements because of the limited size of the upper ports.

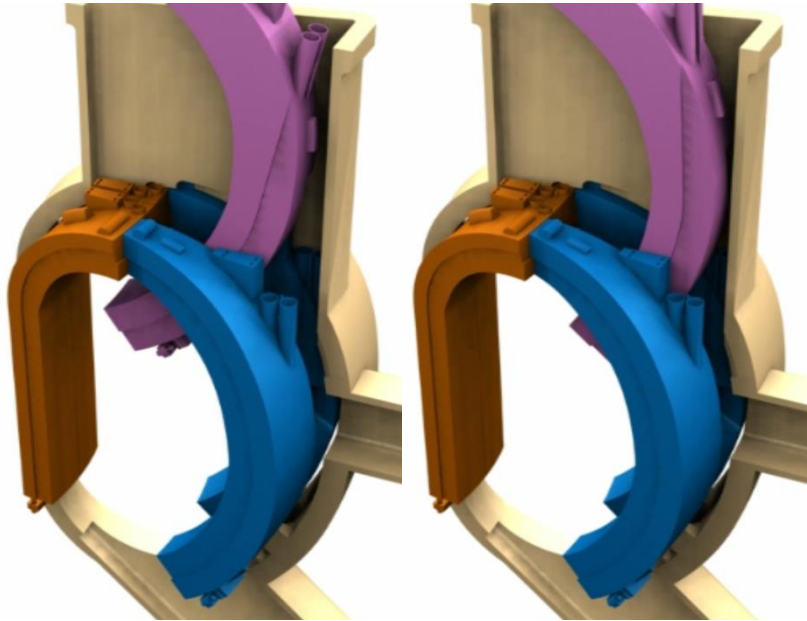


Fig. 195. Rotation of the central outboard segment in a vertical plane during its extraction process (CoG displacement) [Ccf 14].

The CMT has 5 degrees of freedom which provide the necessary movements on the horizontal plane without clashing to the frame. However, another device is required to complete the points 3, 4 and 5 of the stated RH sequence: the in-vessel mover (IVM) detaches the base of the MMS from the in-vessel supports and assists the Vertical Maintenance Crane (VMC) in disengaging the segments from the VV/thermal shield wall [CoI 14]. It is installed through the divertor port and moves toroidally on in-vessel rails, in a similar way to the ITER divertor maintenance system. This implies another two important differences with the ITER TBS RH system. First, there is not any device belonging to the TBS RH system which operates inside the vacuum vessel -apart from the equatorial port-; and second, the divertor sections in that sector must have been previously removed. This requires the blanket scheduled maintenance campaigns must be simultaneous with the divertor ones. Therefore, ensuring in-vessel components high reliability is mandatory in DEMO to avoid losing excessive time in non-scheduled maintenance and hence achieving the foreseen values of operational availability.

### **2.6.2. Decay heat**

Decay heat removal could mean another significant difference between ITER and DEMO maintenance. The low activation materials (e.g. EUROFER) that may be used for plasma facing components in DEMO would produce lower decay heat than the 316 stainless steel ITER VV, but the higher plasma power and much higher duty cycle can involve decay heat power in DEMO is one order of magnitude higher than in ITER. This may be enough to make decay heat a potential hazard in its own right, and its removal a safety function (ref. Taylor 2014).

As a consequence, the DEMO breeding blanket is expected to be about 200°C after a month of cool down and the inside of the pipes through convection and radiation will also be at a similar temperature [Igl 13]. Although this must be confirmed, if temperatures of 200°C are assumed for the pipes cutting process the RH tool will require active cooling for deployment. This is a very substantial difference with the tools operating at IF2a and IF2b in the ITER Test Blanket System, whose working temperature is much lower and do not require active cooling. During DEMO blanket pipes welding the temperature will be greatly reduced to approximately 70°C as new components are installed.

Relevant implications are also derived for ex-vessel transport and storage. Air forced ventilation could be needed in the cask which contains the vertical maintenance crane and envelops blanket segments along their transfer from inside the vacuum vessel to the Active Maintenance Facility.

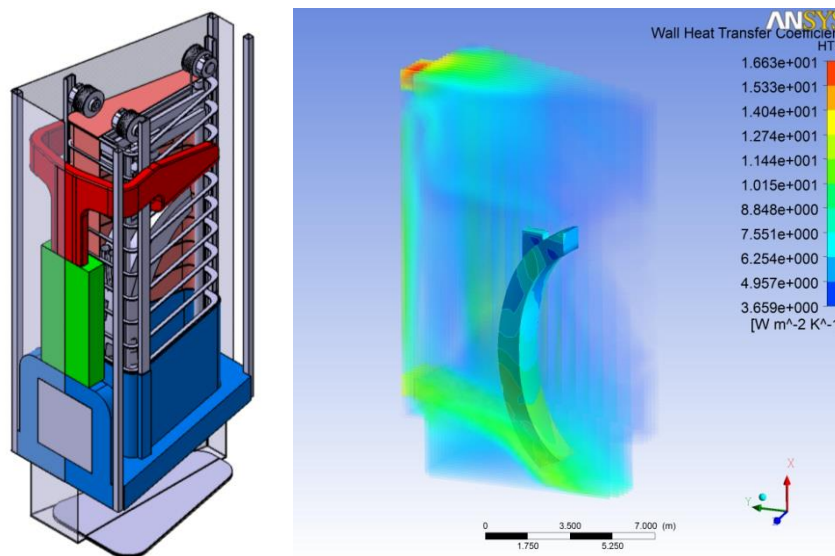


Fig. 196. Vertical maintenance crane proposed for DEMO blanket MMS [Igl 13b]. Heat transfer coefficient results for natural convection (in-cask simulations).

A similar scenario could occur regarding the storage of MMS in the Active Maintenance Facility. No decay heat removal systems are expected in the ITER Hot Cell during the refurbishment/dismantling of TBS components as AEU, port plug, TBMs and shields.

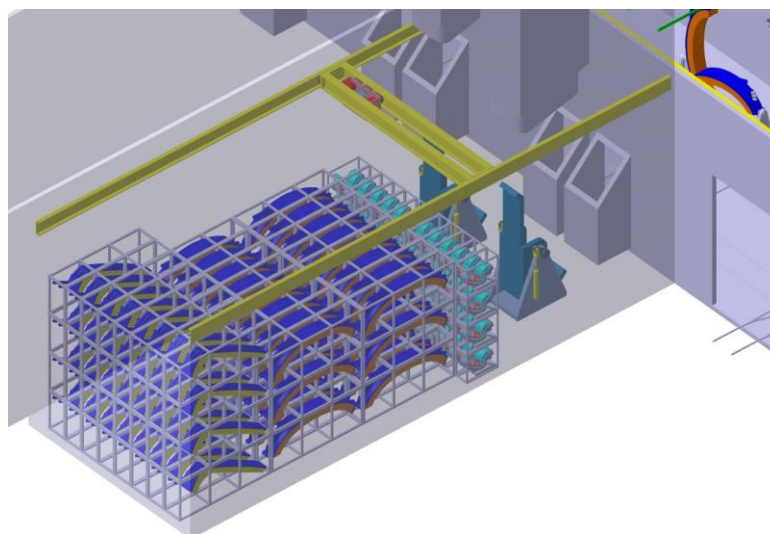


Fig. 197. Active components storage [Igl 13b].

### **2.6.3. Occupational radiation exposure**

During ITER plasma operation, access to rooms including parts of the primary water cooling circuit is prohibited due to intense high-energy gamma radiation from the decay of  $^{16}\text{N}$ , which is generated in water by the reaction  $^{16}\text{O}(n,p)^{16}\text{N}$ , and therefore unavoidable. This problem can be excluded in DEMO by choosing a coolant different than water, but other facts must be considered regarding human access to locations situated close to the cryostat.

### **2.6.4. Processes automation**

The in-vessel mover in DEMO shall function largely automatically, since sensing instrumentation like cameras and resolvers are not able to operate under the expected radiation conditions. This fact rules out man-in-the-loop operation. In general, we can anticipate fusion power plants maintenance system shall be much more automated than current remote handling systems to improve their availability. The idea is to go towards semi-automated processes and to use human operators only to confirm certain key positions before running the next automated step [Syk 13]. The extensive use of radiation hardened motion control instruments like limit switches and designs with on behaviour-shaping constraints (poka yoke) will drive the transition between human and semi-automated control. This tendency is currently followed in the design of the ITER RH system as, for example, some proposals for the control of the Cassette Toroidal Mover (CTM) (divertor RH system) [Fern 13] [Amb 13].

In a comparison between the estimated remote handling in-vessel durations and those actually achieved to install the ILW beryllium sliced wall during the Enhanced Performance stage shutdown of JET, a ratio of 1:2.3 was found for the installation of the poloidal limiter tile carriers and a ratio of 1:2.5 was found for the installation of the inner wall protection tiles [Coll 13]. Complex tele-operated devices as the BOOM (articulated structure deployed inside the JET vacuum vessel) and the MASCOT (two arms master-slave manipulator) were used in these operations. Results show that tasks duration decreases as the number of repetitions increases, showing that reading and absorbing the operational procedures is an important factor for the differential. Thus, once absorbed and understood, these actions need to be portrayed to the appropriate operators within the RH team, taking into account that the higher the complexity of the procedure the greater the impact on the duration. Another important factor is the time lost in re-orienting the cameras for the servo manipulator operator, since failures providing the best possible views will result in very poor productivity from the manipulator operator. These issues clearly support the need of automating RH procedures, but analysis of JET data shows there are other delays, often caused by the difficulty to accommodate all of the remote handling requirements in the design of components, which are not linked to human manipulation.

Man-in-the-loop control can still be required for more dexterous operations and where maintenance sequences vary; for example, if weld failures are produced at unknown locations. Another example is helium or water leak remote localization. Ongoing R&D programs for ITER are based on the use of poly-articulated robots to guide sensors for helium or water detection inside the vacuum vessel [Dur 13]. Remote interventions can be prepared and performed in a few days, which represent a short delay in comparison with the 6 months necessary to replace the blanket and the divertor in DEMO. In fact, an articulated multi-purpose deployer (MPD) is proposed to be installed in DEMO to drive a dexterous manipulator or several kinds of end-effectors [Igl 13] for cleaning or testing plasma facing components or vacuum vessel elements, so that the man-in-the-loop approach is held for non-programmed operations.

In the case of the Active Maintenance Facility, an important objective for DEMO is to automate components processing as much as possible, going one step further than the ITER HC, by accurately fixing and controlling the geometrical position of components and RH equipment in the different maintenance rooms, as well as standardizing operations (refurbishment, dismantling, recycling, disposal, transport, etc.).

### 2.6.5. Hot cell activities

Like in the ITER Hot Cell, it is foreseen that all handling operations associated with used in-vessel components in the Active Maintenance Facility (AMF) must be carried out using remote handling techniques. It has been already said that, since neutron fluence in DEMO is higher than in ITER, higher gamma dose rates and decay heating due to activation are expected, which will involve important challenges for the RH equipment. Furthermore, the storage areas would need to be actively cooled until the level of decay heating has reduced to a more manageable level [Tho 14].

A key point in the design of the AMF is parallel work. Using a number of ports at the same time for the same operations the highest continuous productivity rate can be achieved, although it requires the largest amount of RH equipment. For example, a maintenance strategy based on 8 parallel ports for in-vessel components could require handling a major component every 7 h [Tho 14]. In terms of volume, the AMF (737000 m<sup>3</sup>) would be six times larger than the ITER Hot Cell (119000 m<sup>3</sup>), taking into account just operational areas of the AMF (plant and services are not considered) [Tho 14]. Blanket processing in the AMF is anticipated to be quite similar to TBM processing in the ITER HC. First, segments are decontaminated in order to: 1) reduce the dose level in the maintenance facility; 2) minimize the potential for spreading contamination during further manipulation and 3) reduce the contamination of components to such levels that may be disposed in a lower category (lower cost) or recycled.

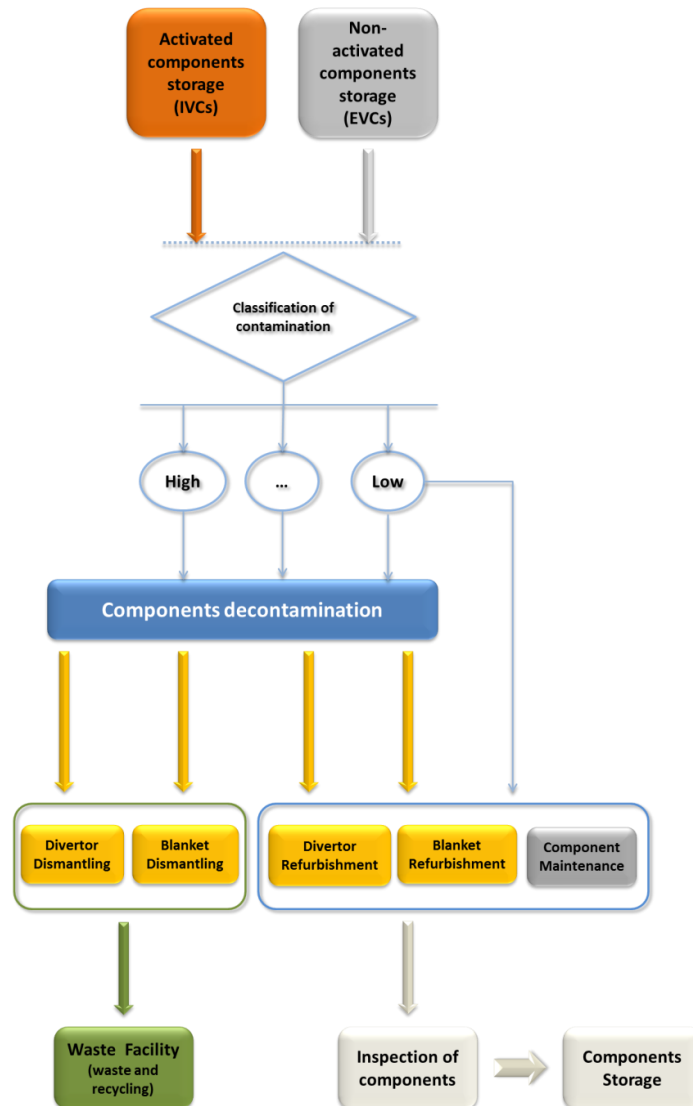


Fig. 198. Processing flow chart in the AMF [Ros 14].

Then, blanket processing in the dismantling bays consists in disassembling of the MMS in parts to disconnect all the modules from the back support structure and the pipes. Such smaller parts are separated by materials to be transferred to the Waste and Recycling Facility.

The operations in the maintenance bays are similar to the operations in the dismantling bays, although in this case the objective is to identify and replace the MMS parts having failed. The MMS could be repaired using refurbished or new parts. An important point is the fact that maintenance of modules inner parts will require accurate and time consuming operations. In consequence, the complete replacement of failed modules by new modules will be preferable to repair in many cases.

Finally, all the smallest constituting parts of the MMS and the secondary wastes coming from the component decontamination and processing (dust, tritiated water, shavings and gasses) are collected in the Waste and Recycling Facility, where they are further decontaminated, separated and classified according to their waste category for their subsequent disposal or recycling. Here an important difference with ITER underlies, since in DEMO a fundamental principle is recycling as much material as possible, with only the bare minimum going to waste.

### **2.6.6. Ex-vessel transport**

Due to the larger size of in-vessel components, shielding and possibly active cooling needs, the weight of transport casks will be considerably larger in DEMO. For example, a weight of 450 t is estimated for blanket segments handling [Tho 14], whereas the weight of the heaviest component of the Test Blanket System in ITER –The AEU, which is really located ex-vessel- is estimated around 100 t.

Several cask transport concepts and transfer solutions are being assessed for DEMO. Considering the vertical maintenance scheme, the blanket casks are expected to be handled by an overhead crane, whose trolley can move also on overhead tracks (seamless connections) which communicate the reactor hall and the AMF [Gro 13]. This can be also the main transport system inside the AMF for the blanket segments.

However, ‘on-floor’ transport concepts are considered for components whose maintenance is thought to be done through the equatorial and lower ports (H&CD systems port plugs, divertor cassettes), which are clearly more similar to the TBS components transport. In particular, wheel-rail-systems or automated guided vehicles have been proposed, together with the use of traction elevators or scissor-lifts to position the cask transporter at floor level [Gro 13]. For example, some proposals for the bioshield removal and storage are fairly similar to the concept for removing the pipe forest & bioshield assembly (ITER TBS) proposed in Section 2.5.

### **2.6.7. Spare components and redundancy**

The disposal of spare parts has been one of the main corrective actions influencing availability of present fusion devices (JET, JT-60, Tore Supra, etc.) along years, as well as design and system diagnosis improvement, operational procedures, renewing, quality assurance and quality control during modifications, preparation and management of experimental sessions, staff training and RH procedures testing & validation [Pin 10b]. Spare components have to be available and easy to replace. A good management of the amount of spare components must guarantee the availability of a spare component when a change is needed, so that the downtime is only due to the replacement process, and not to the delay of ordering and receiving the failed component [Arr 12]. For example, procuring of components in the previously mentioned maintenance of the AGHS in JET sometimes took months [Pin 10]; a suitable strategy of spare parties could have highly reduced the time spent for this issue.

For that reason, to keep spares on-site is one important protective risk-mitigation action in ITER. Further, ITER RAMI requirements include standardization of common parts used in great number in the project in order to ensure inter-changeability of spares in the design of systems [Hou 10]. This allows shortening maintenance operations (replacement of consumables, repairs

of failed components) and reducing the downtime of the systems and the severity ratings in the FMECA, reducing in consequence the risk level and allowing for more availability of ITER for the experimental program.

On the other hand, redundancy is used together with fail tolerance to compensate failures and to increase the reliability and availability of systems, since using very reliable components is often very expensive. Implementing redundancy is one of the preventive risk-mitigation actions considered in ITER to reduce the risk of losing the function [Hou 10]. For example, taking into account the relevancy of diagnostics for the experimental program, but also for monitoring and control, redundancy of critical sensors is required.

Specifically referring to the ITER Test Blanket System, however, redundancy and spare parts policy is different. In the case of failure (or delayed delivery), TBMs will be replaced by dummy TBMs whose functions are only closing and sealing the port plug. This is due to the fact of TBM is a transversal program in ITER and cannot interfere with the main scientific program.

On the other hand, to guarantee the compliance of the breeding blanket functional requirements with high availability is essential in DEMO. Therefore, certain level of redundancy within each blanket circuit could be needed in order to follow the criterion of assuring that a single active component failure (e.g. pump) would not force the reactor to shutdown [Arr 13].

Redundancy and spare systems are also fundamental pillars for the availability of the RH system in DEMO. Taking into account its complexity, the availability values estimated in the framework of EFDA WP studies are so high (~80%) because of the assumption of redundant or spare systems being provided wherever possible, as well as for the relatively high assumed reliability for the highly developed and tested system and because it is assumed that replacement casks are available on demand from the Active Maintenance Facility to replace failed equipment thereby allowing rapid recovery and return to operations [Lov 14] [Cro 14].

Redundancy is also envisaged for other critical path RH operations as MMS ex-vessel transport, including the AMF. For example, the reliability of the transport casks cooling system could be improved by the installation of redundant (parallel) cooling pumps [Gro 13]. In the AMF, one or two spare casks would be needed to ensure minimal delays in the event of a failure [Tho 14].

### **2.6.8. Operation time**

The preliminary schedule of the initial installation operations of the EU TBS equipment (AEU, pipe forest, TBM port plug and TBM & shield sets) estimates a maintenance period of 132 days from the reception to the end of the acceptance tests, and 77 days in the port cell itself [Nev 14]. In the case of the Shielding Blanket System, it is required to replace all the blanket modules (440) in less than 24 months, and under 2 months in the case of up to 3 modules [Tak 14]. In general, 16 months plasma operation periods in ITER will be followed by 8 months periods for maintenance and upgrades.

On the other hand, blanket and divertor complete replacement during long term maintenance periods in DEMO is expected to be done in 6 months [Cro 14], as a consequence of the foreseen higher productivity and reliability, as well as the optimized design of the in-vessel components and the RH system (use of MMS, parallel operations, spare components availability, etc.), among other reasons. As previously mentioned, the divertor cassettes must be removed to allow the in-vessel mover to be deployed during MMS blanket removal, but since the blanket life is likely to be higher than the divertor life this will not add to the number of times the divertor is removed [Cro 14]. Furthermore, it is expected that a 1 month cooling period is needed before remote handling operations begins. In the case of ITER, waiting 12 days after shutdown can be enough to begin the maintenance of the TBS beyond the bioshield.

The duration of in-vessel components replacement in DEMO has been estimated during last 2 years in the framework of European pre-conceptual studies [Cro 14] [Cau 13]. Such estimations are based on and extrapolated from recorded times and from operational experiences at JET

and other nuclear facilities. A two shift operation pattern was adopted as the most likely option because it provides 16 h operation per day compared to only 8 for a single shift. It is also easier to implement and more efficient in terms of the shift teams required using 3 shift teams rather than 5. The least productive hours in the middle of the night are also not used for remote operations but can be used for housekeeping operations as required.

It must be underlined that a productivity factor for human tasks is considered in this estimation. We have previously said that, at JET, productivity varies considerably depending on the task. However, a figure of about 70% is assumed, since it is considered suitable for well-developed procedures with man-in-the-loop control [Cro 14]. These procedures include the tool deployment operations considered for DEMO. On the other hand, it is estimated that the automatic procedures would have a productivity of about 90% [Cro 14]. These procedures include removal and replacement of the MMS blanket segments and divertor cassettes and the docking of casks; that is, the most time-consuming tasks.

Between other assumptions, the Active Maintenance Facility would be capable of supplying and receiving casks without delaying the critical path remote handling operations and would have a suitable number of spares to account for all likely failure scenarios. As previously said, redundancy is applied to drives and systems and spares tools are provided wherever possible [Cro 14]. Finally, TIG welding is used as the pipe joining technology due to its well characterized performance with a triple weld head employed on large bore pipes to reduce weld duration [Cro 14]. This is an important difference with welding operations at the ITER TBS Interface 2a, since only one TIG orbital welding head is used to weld a larger number of pipes. Nevertheless, since pipe connection operations (both cutting and welding) comprise a large proportion of the total process time (51% for the upper port [Cau 13]), the use of alternative joining methods (brazing, mechanical joints, etc.) shall be considered.

An essential point to estimate the duration of replacement is the number of remote handling systems working in parallel. For example, the required time for the whole replacement with a single remote handling system would be about 22 months. Doubling the number of systems operating in parallel almost halves the maintenance duration so that four systems could complete the maintenance in 6.3 months (190 days) [Cau 13]. This may be acceptable if we consider the 6 months objective, but it is important to state that additional time periods are required before and after remote maintenance can begin. These periods are for processes such as bringing the vacuum vessel up to atmospheric pressure, decreasing the levels of tritium contamination, and allowing the decay heating and gamma dose rate in the vessel to reduce. Having 8 RH systems operating in parallel easily meets the 6 month downtime requirement, with the total elapsed time being approximately 3.5 months (104 days) [Cau 13]. However, the cost increase associated with the increasing number of systems operating in parallel is significant, although it is important to consider factors as the cost reduction per RH system with increasing numbers of units. Anyway, 4 remote handling systems would be required to operate in parallel to be close to the 75% availability target [Cro 14]. This does not take into account unplanned maintenance or any other planned maintenance that might arise that cannot be undertaken in parallel with the replacement of the plasma facing components. For example, the average time to replace a single segment for unplanned maintenance is estimated in 66 days, if 2 systems are operating simultaneously [Cau 13]. Comparing this value with the duration of the whole blanket replacement for long term scheduled maintenance (190 days) reflects the importance of ensuring high reliability of blanket and divertor to minimize occurrence of unscheduled maintenance. Although, as a consequence of some uncertainty as the re-weldability of the blanket pipes, for the current estimate it has been assumed that if one blanket segment in a sector fails, all of the blanket segments in that port have to be replaced because to remove one segment the pipes to all segments must be removed [Cau 13]. This would be the worst case scenario and the time will improve if the pipes can be re-welded under any circumstances.

In the case of the Active Maintenance Facility activities, blanket segment processing time has been estimated [Ros 14] in order to assess AMF logistics, considering the influence of the capacity of the installations and the capacity of the RH equipment in each bay or the Waste and Recycling Facility. For example, assuming sequential dismantling operations (one after another) in the case of a 8-modules blanket MMS, the estimated processing times in the

decontamination bay, the dismantling bay and the Waste and Recycling Facility are respectively 69 h, 1270 h and 3915 h, resulting a total AMF processing time of 5254 h.

This preliminary assessment predicts the Waste Recycling Facility (WRF) and the processes of detritiation and tritium sampling and measurement could be a bottleneck in the AMF, interfering with in-vessel operations and ex-vessel transport logistics. For this reason, these processes shall be carried out considering the cycle of life of the different materials after leaving the AMF.

## **2.7. References**

[Ahn 13] M-Y Ahn, S. Cho, D. W. Lee et al., Design change of Korean HCCR TBM to vertical configuration, *Fusion Engineering and Design* 88 (2013) 2284– 2288.

[Amb 13] F. Ambi, A. Bagnasco, Radiation sensitive components: trade-off analysis, technical report for the Business Case of F4E-OMF-340 Lot 1 (Deliverable 1), Consortium led by Azbil Telstar Technologies S.L.U., 2013.

[Arr 12] J. M. Arroyo, RAMI Management Process for DEMO, final report for Task Agreement WP12-DTM02-T03, EFDA internal document (EFDA\_D\_2GE7ZV), 2012.

[Arr 13] J. M. Arroyo, Contribution to DEMO Plant Availability Simulation, RBD Model Decomposition & RAMI Design Requirements. Preliminary RAMI analysis of WCLL blanket and breeder systems, final report for Task Agreement WP13-DTM02-T01, EFDA internal document (EFDA\_D\_2MD5UY), 2013.

[Bai 09] Y. Bai, Conceptual study for TBM-related activities in ITER Hot Cell Facility before TBM shipment back to owner, ITER internal document (ITER\_D\_2F5UQD), 2009.

[Bar 08] R. Barnsley, Direct Investment review. Port Plug Test Stands, ITER internal document (ITER\_D\_2E44RV v1.1), 2008.

[Bea 08] B. Beaumont, News on Plug Test Stand, ITER internal document (ITER\_D\_2FF7HK), 2008.

[Bed 07] O. Bede, I. G. Kiss, A. Piros, J. Recski, Detailed analysis of the HCPB TBM maintenance sequence at interface 2 and 3, report of EFDA Subtask TW6-TTBB-001-D4, ITER internal document (ITER\_D\_27T6BS\_v1.0), 2007.

[Bed 08] O. Bede, S. Madeleine, J-P Martins, H. Neuberger, Impact of TBM maintenance process on Hot Cell Building layout, TBM Interface action items - Deliverable D1, internal report of the EU TBM Consortium of Associates, 2008.

[Ben 08] M. Benchikhoun, Hot Cell option A latest optimized version, ITER internal document (ITER\_D\_2DQX7K\_v1), 2008.

[Boc 12] L. V. Boccaccini, D. Nagy, F. Cismondi, The vertical maintenance system, Final report for Task Agreement WP11-DAS-RH02, EFDA internal document (EFDA\_D\_2LHX95), 2012.

[Cau 13] J. Caumont, Assessment of DEMO Remote Maintenance Operations, Sequence, Timing and Logistics, final report for Task Agreement WP13-DAS97-T03, EFDA internal document (EFDA\_D\_2MGFDZ), 2013.

[Ccf 14] CCFE Remote Handling Unit, Animation of DEMO blanket segments extraction kinematics, EFDA internal document (EFDA\_D\_2L3HPZ), 2014.

[Cho 14] S. Cho, M-Y Ahn, D. W. Lee et al., Design and R&D progress of Korean HCCR TBM, *Fusion Engineering and Design* 89 (2014) 1137-1143.

[Col 14] M. Coleman, N. Sykes, D. Cooper, D. Iglesias et al., Concept for a vertical maintenance remote handling system for multi module blanket segments in DEMO, Fusion Engineering and Design 89 (2014) 2347-2351.

[Coll 13] S. Collins, G. Matthews, J. Thomas, G. Hermon, Factors affecting remote handling productivity during installation of the ITER-like wall at JET, Fusion Engineering and Design 88 (2013) 2128-2132.

[Cor 11] P. Corti, Thermal-hydraulic analysis of the vacuum vessel regular equatorial port, ITER internal document (ITER\_D\_4LEEGL\_v1.4), 2011.

[Cro 14] O. Crofts, J. Harman, Maintenance duration estimate for a DEMO fusion power plant, based on the EFDA WP12 pre-conceptual studies, Fusion Engineering and Design 89 (2014), 2383-2397.

[Dam 12] C. Damiani, C. González, The European in-kind contribution to the ITER Remote Maintenance System, Fusion for Energy internal document, F4E\_D\_23GW4X, 2012.

[Dam 14] C. Damiani, C. Annino, S. Balagué et al., The European contribution to the ITER Remote Maintenance, Fusion Engineering and Design 89 (2014) 2251-2256.

[Dub 14] G. Dubus, A. Puiu, P. Bates et al., Progress in the design and R&D of the ITER In-Vessel Viewing and Metrology System (IVVS), Fusion Engineering and Design 89 (2014) 2398-2403.

[Dur 13] A. Durocher, V. Bruno, M. Chantant, L. Gargiulo et al., Remote leak localization approach for fusion machines, Fusion Engineering and Design 88 (2013) 1390-1394.

[F4E 14] <http://fusionforenergy.europa.eu>

[Fer 13] F. Ferlay, J. M. Bernard, C. Dechelle, First analysis of remote handling maintenance procedure in the hot cell for the ITER ICH&CD antenna – RVTL replacement, Fusion Engineering and Design 88 (2013) 1924-1928.

[Fern 13] I. Fernández, Conceptual design of the CTM instrumentation, technical report for the Business Case of F4E-OMF-340 Lot 1 (Deliverable 10), Consortium led by Azbil Telstar Technologies S.L.U., 2013.

[Gar 12] A. García, I. García, A. Marqueta, I. Fernández, Definition of TBS assembly and disassembly operations in Port Cell, CIEMAT internal document (IN-TBM-RHTF-06), 2012.

[Ghi 12] N. Ghirelli, Geometrical approach for TBM cask path within the HCF, ITER internal document (ITER\_D\_6XKEJL), 2012.

[Gia 06] L.M. Giancarli, V.A. Chuyanov, M. Abdou et al., Breeding blanket modules testing in ITER: an International Program on the Way to DEMO, Fusion Engineering and Design 81 (2006) 393–405.

[Gia 12] L.M. Giancarli, M. Abdou, D.J. Campbell et al., Overview of the ITER TBM Program, Fusion Engineering and Design 87 (2012) 395-402.

[Gro 13] G. Grossetti, D. Eilert, R. Geßner, M. Kubaschewski et al., Ex-vessel remote maintenance system pre-concept study, final report for Task Agreement WP13-DAS07-T07, EFDA internal document (EFDA\_D\_2LDKPX), 2013.

[Ham 08] D. Hamilton, System Requirement Document (SRD), Remote Handling Control System PBS 23-07, ITER internal document (ITER\_D\_2DRWQ6\_v2.1), 2008.

[Hou 10] D. van Houtte, K. Okayama, F. Sagot, RAMI Approach for ITER, Fusion Engineering and Design 85 (2010) 1220–1224.

[Hou 11] D. van Houtte, K. Okayama, F. Sagot, ITER operational availability and fluence objectives, Fusion Engineering and Design 86 (2011) 680-683.

[Hou 12] D. van Houtte, F. Sagot, K. Okayama, K. Blackler, A functional approach for managing ITER operations, fusion Engineering and Design 87 (2012) 652-656.

[Igl 13] D. Iglesias, D. Cooper, K. Keogh, D. Middleton-Gear, Blanket Segment Remote Maintenance, Final report for Task Agreement WP13-DAS07-T05, EFDA internal document (EFDA\_D\_2L8NHG), 2013.

[Igl 13b] D. Iglesias, Assessment of Decay Heating implications on RMS, Final report for Task Agreement WP13-DAS07-T04, EFDA internal document (EFDA\_D\_2M5PEZ), 2013.

[ITER 14] [www.iter.org](http://www.iter.org)

[Kel 10] D. Keller, Robot access feasibility study in Port Cell and preliminary location of connection/disconnection interfaces, EU TBM CA internal document (05.6\_TBMCA.2010.D4SI.0003\_f1.0), 2010.

[Lor 07] T. Lorblanches, E. Fassy, Air Transfer System control & command: preliminary ATS CC architecture, EFDA internal document (ITER-RH-T-04-004), 2007.

[Lov 14] A. Loving, O. Crofts, N. Sykes, D. Iglesias et al., Pre-conceptual design assessment of DEMO remote maintenance, Fusion Engineering and Design 89 (2014) 2246-2250.

[Mad 09] S. Madeleine, A. Saille, J-P Martins, J-F Salavy et al., Engineering studies for integration of the test blanket module (TBM) systems inside an ITER equatorial port plug, Fusion Engineering and Design 84 (2009) 1233-1237.

[Mar 09] J. P. Martins, C. Dechelle, B. Soler, J. Wagrez, ITER Port sealing tooling – Conceptual design and cost estimate, ITER internal document (ITER\_D\_2LRNK8), 2009.

[Mer 10] M. Merola, D. Loesser, A. Martin et al., ITER plasma-facing components, Fusion Engineering and Design 85 (2010) 2312–2322.

[Meu 07] L. Meunier, L. Doceul, J-P Martins, F. Julien, Engineering assessment of diagnostic port integration on ITER, ITER internal document (ITER\_D\_29NY7T), 2007.

[Mic 07] G. Micciché, M. Irving, L. Lorenzelli, L. Muro, The plasma-facing components transporter (PFCT): A prototype system for PFC replacement on the new ITER 2001 cassette mock-up, Fusion Engineering and Design 82 (2007) 2055-2061.

[Nev 14] J. C. Nevier, Maintenance Operations for TBM Port Plugs and Port Cell Equipment - Preliminary Schedule and Duration, ITER internal document (ITER\_D\_7MVVLU), 2014.

[Pin 10] T. Pinna, G. Cambi, S. Knipe, JET operating experience: Global analysis of tritium plant failure, Fusion Engineering and Design 85 (2010) 1396-1400.

[Pin 10b] T. Pinna, L. C. Cadwallader, G. Cambi, S. Ciattaglia et al., Operating experiences from existing fusion facilities in view of ITER safety and reliability, Fusion Engineering and Design 85 (2010) 1410-1415.

[Raj 09] S. Rajendran, J. Palmer, ITER Remote Handling Code of Practice, ITER internal document (ITER\_D\_2E7BC5), 2009.

[Rap 14] D. Rapisarda, I. Fernández, F. Martín-Fuertes, Magnetic material amount and distribution in blanket zone, WPBB-DEL-D-411-05, Eurofusion internal document (EFDA\_D\_2MB9T8), 2014.

[Rio 10] L. Ríos, I. Fernández, C. Fernández, J. Juanas, A. García, Definición de las operaciones de extracción, corte e inserción del TBM en la Hot Cell de ITER, CIEMAT internal document (IN-TBM-RHTF-003), 2010.

[Ros 14] E. Rosa, I. Fernández, Component processing in the Active Maintenance Facility, final report for Task Agreement WP13-DAS07-T08, EFDA internal document (EFDA\_D\_2L54GX), 2014.

[San 08] S. Sanders, animation of the cleaning operation of a divertor cassette in the Hot Cell, ITER internal document (ITER\_D\_2FDQSG v1.0), 2008.

[Sch 14] I. Schneiderova, List of PBS-56 Maintenance and RH Compatibility Documentation and Status Monitoring, ITER internal document (ITER\_D\_PU9KWY), 2014.

[Shu 14] R. Shuff, M. Van Uffelen, C. Damiani et al., Progress in the design of the ITER Neutral Beam cell Remote Handling System, Fusion Engineering and Design 89 (2014) 2378-2382.

[Syk 13] N. Sykes, M. Coleman, D. Iglesias, Development of vertical MMS blanket remote maintenance concepts, final report for Task Agreement WP12-DAS06-T04, EFDA internal document (EFDA\_D\_2LLTXY), 2013.

[Tak 14] N. Takeda, Design Description –PA 2.3.P1.JA.01- Blanket RH System, ITER internal document (ITER\_D\_9CQ2DW), 2014.

[Tay 14] N. Taylor, P. Cortes, Lessons learnt from ITER safety & licensing for DEMO and future nuclear fusion facilities, Fusion Engineering and Design 89 (2014) 1995-2000.

[Tes 07] A. Tesini, Basic ITER strategy for TBMs RH/HC replacement & refurbishment, ITER internal presentation (ITER\_D\_27T6DT\_v1\_0), 2007.

[Tes 08] A. Tesini, J. Palmer, The ITER Remote Maintenance System, Fusion Engineering and Design 83 (2008) 810–816.

[Tes 08b] A. Tesini, ITER Hot Cell maintenance & support facilities. Impact of the maintenance / upgrade plan on Remote Handling, ITER internal presentation (ITER\_D\_2EVSTF\_v1\_0), 2008.

[Tho 14] J. Thomas, A. Loving, O. Crofts, R. Morgan, J. Harman, DEMO Active Maintenance Facility concept progress 2012, Fusion Engineering and Design 89 (2014) 2393-2397.

[Uto 12] H. Utoh, K. Tobita, Y. Someya, H. Takase, Conceptual study of vertical sector transport maintenance for DEMO fusion reactor, Fusion Engineering and Design 87 (2012) 1409-1413.

[Yao 07] D. M. Yao, ITER transfer cask, ITER internal document (ITER\_D\_27Z6B2), 2007.



# **Chapter III**

***Power conversion systems for  
DEMO***



## List of figures

Fig. 1. Power balance in a fusion power plant [Kov 13].	218
Fig. 2. Trade-off between net electrical power and pulse length for different values of $\eta\gamma$ (product of H&CD wall-plug efficiency and current-drive efficiency) [Fed 14].	219
Fig. 3. Systems involved in the balance of plant.	230
Fig. 4. Classical re-compression supercritical CO <sub>2</sub> Brayton cycle. This arrangement constitutes the Layout 0 (baseline case) in this work.	232
Fig. 5. Temperature vs. Heat Power exchanged at LTR (a) and HTR (b) in Layout 0.	233
Fig. 6. Sketch of the different layouts considered.	234
Fig. 7. Arrangement of components in the selected Layout C.	235
Fig. 8. T-s diagram at the design point (Layout C).	236
Fig. 9. Sensitivity of gross power to 1% of change in key variables.	238
Fig. 10. T-Q profile at LTR.	239
Fig. 11. T-Q profile at HTR.	239
Fig. 12. Entropy generation at both recuperators depending on the pinch point at LTR.	240
Fig. 13. Entropy generation at both recuperators depending on the pinch point at HTR.	240
Fig. 14. Thermal energy storage system for a helium-cooled fusion reactor with an intermediate molten salt loop and water steam Rankine as power conversion cycle [Kov 13b].	243
Fig. 15. Electric power generated during the pulsed operation of DEMO [Bub 13].	244
Fig. 16. Reactor general view.	246
Fig. 17. Vacuum vessel and cryostat (toroidal cut).	247
Fig. 18. General view of an outboard blanket segment. Detail of PbLi inlet & outlet.	247
Fig. 19. PbLi channels and FCI (green). Helium distribution channels in the shielding module.	248
Fig. 20. Design of the structure from the PbLi channels shape [San 13].	249
Fig. 21. Helium circuit layout [San 13].	249
Fig. 22. Flowchart of the methodology followed in this activity [San 13].	250
Fig. 23. Single He cooling circuit (left) and double He cooling circuit (right) for 3D analysis.	251
Fig. 24. Temperature map using 15 m/s as helium inlet velocity and 1 m/s as PbLi inlet velocity.	251
Fig. 25. Temperature (T) and velocity (U <sub>r</sub> ) map in the PbLi channels for the given distribution of volumetric heat deposition (S) [San 13].	253
Fig. 26. Electrical conductivity of SiC samples with coating. Hollow symbols: before irradiation. Solid symbols: after irradiation.	254
Fig. 27. Permeator against vacuum prototype (left). Partial assembly of the PbLi loop (right) [Sac 14].	255
Fig. 28. He-based Brayton cycle showing all devices used analysed layouts [Lin 11].	257
Fig. 29. S-CO <sub>2</sub> cycle (coupling to a Rankine indicated) [Lin 11].	258
Fig. 30. REC2 and REC3 layouts [San 13].	260
Fig. 31. Heatric PCHE plate (left) and set of diffusion-bonded plates (right).	261
Fig. 32. Plate CAD model.	262
Fig. 33. Stack of hot and cold plates (CAD model).	262
Fig. 34. Rendered view of the interior of a channel.	263
Fig. 35. Pressure distribution over an airfoil (L: lift force, D: drag force, R: resultant force, N: normal force, A: axial force, $\alpha$ : angle of attack, $v_\infty$ : velocity) [Mey 13].	263
Fig. 36. NACA4415 profile.	265
Fig. 37. NACA0010 profile.	266
Fig. 38. Comparison of pressure distribution in NACA0010 with $\alpha>0$ (top) and $\alpha=0$ (bottom).	266
Fig. 39. Coefficient of pressure in the upper and lower surfaces of NACA0010 for $\alpha=2.8^\circ$ .	266
Fig. 40. Scheme of the 1-D heat transfer model.	267
Fig. 41. Top view of the channel configuration (scaled model).	268
Fig. 42. Temperature distribution near inlet on an intermediate plane in the PbLi channel.	269
Fig. 43. Comparison of temperature profiles in both streams for 1-D and 3-D models.	270

Fig. 44. Pressure drop in the hot and the cold streams. ....	270
Fig. 45. Process flow diagram for tritium transport.....	271
Fig. 46. Diffusive flux to the CO <sub>2</sub> stream. ....	272

## List of tables

Table 1. Main parameters of the PPCS models [Mai 05]. ....	222
Table 2. PHTS parameters for HCLL model AB [Med 07]. ....	223
Table 3. DEMO1 input parameters for the EFDA activity WP12-DAS08-T01 [Har 12]. ....	224
Table 4. DEMO1 input parameters for WP13-DAS08-T02 with water-cooled blanket [Har 13]. ....	225
Table 5. DEMO1 input parameters for WP13-DAS08-T02 with helium-cooled blanket [Har 13]. ....	227
Table 6. Consumptions and state points at the cooling loops. ....	231
Table 7. Destination of the heat released by the thermal sources in each layout. ....	234
Table 8. Electric power and efficiency with the investigated layouts. ....	235
Table 9. State points of selected layout C (notation according to Fig. 7). ....	236
Table 10. Performance of turbomachines in Layout C. ....	236
Table 11. Performance of the heat exchangers and pumping power consumption in Layout C. ....	237
Table 12. Sizes of the heat exchangers at the design point. ....	237
Table 13. Power and efficiencies in Layout C. ....	237
Table 14. Key parameters of Layout C-ECO scenario. ....	240
Table 15. Performance of turbomachines in Layout C-ECO. ....	241
Table 16. Performance of the heat exchangers and pumping power consumption in Layout C-ECO. ....	241
Table 17. Size of the heat exchangers at the economic point. ....	241
Table 18. Power and efficiencies in Layout C-ECO. ....	241
Table 19. Thermal sources [Lin 11]. ....	257
Table 20. He-based Brayton cycles performances [Lin 11]. ....	258
Table 21. S-CO <sub>2</sub> cycles performances [Lin 11]. ....	258
Table 22. Hot and Cold streams inlet conditions. ....	261
Table 23. Comparison of results for different values of pitch X. ....	269

### **3.1. Introduction**

In this Chapter, the relationship between the power conversion cycle and the fusion competitiveness is discussed. The features of thermodynamic cycles based on water steam, helium and supercritical carbon dioxide as secondary coolant, as candidates for Balance of Plant (BoP) for future reactors studied within different EU R&D programmes, are described. Furthermore, after a brief description of the TecnoFus Programme, the design of a PbLi/supercritical CO<sub>2</sub> heat exchanger developed within this program is described.

### **3.2. The role of power conversion cycle in the competitiveness of fusion**

As previously said, ITER shall demonstrate the technological feasibility of fusion energy by producing net energy (the ratio between net electricity to heating and current drive energy supply greater or equal to ten) and by testing key technologies for the following steps towards commercial fusion power plants. However, it does not include the goal of thermoelectric conversion, among other reasons because parameters of the thermal sources like temperature and mass flow are not relevant enough. DEMO will be the first fusion device which will include a power conversion system. In fact, the two central requirements for DEMO lie in its capability to generate several 100 MW of net electricity to the grid and to operate with a closed fuel-cycle.

There is a consensus about the efficiency of the power conversion cycle is one of the main factors affecting the cost of fusion energy. In fact, cost estimations carried out within different power plant conceptual studies, from EU PPCS to ARIES, notably agree in concluding that, in these early generation plant models (assumed to be 10<sup>th</sup> of a kind plants), the fusion capital will be quite strongly diluted by the cost of conventional items such as site, buildings, turbines, electrical plant, etc. This has the effect of reducing the impact of uncertainties in the fusion costs, which will be dominated by a small number of key items (magnets, vacuum vessel, blanket, etc.), which tend to have reasonably well known [Han 09]. What is not proven, of course, is that the assumed power levels, conversion efficiencies, and most notably the plant availability, can be achieved in practice.

Fig. 1 shows the power balance in a fusion power plant. Deuterium-tritium fusion reaction power (17.6 MeV) is distributed between high energy neutrons (80%) and alpha particles (20%). Alpha power is absorbed by plasma, whilst neutrons interact with materials surrounding the plasma and neutron power is multiplied at the blanket first wall by (n,2n) reactions. Plasma energy losses are produced by conduction, power transported by first orbit NBI particles and unthermalized alphas, and mainly by radiation (synchrotron radiation, line radiation and bremsstrahlung). Primary coolant/s (for blanket, divertor and vacuum vessel) extract/s most of neutron power -and radiation power deposited in the first wall-, as well as gamma power due to activation of structural and functional materials. In such a way, in steady-state regime, nearly the whole reactor thermal power ( $P_{th}$ ) is converted into gross electric power (except release to environment), whereas in pulsed regimes, a fraction of  $P_{th}$  is used to feed the thermal storage system ensuring electric power generation during the dwell period.

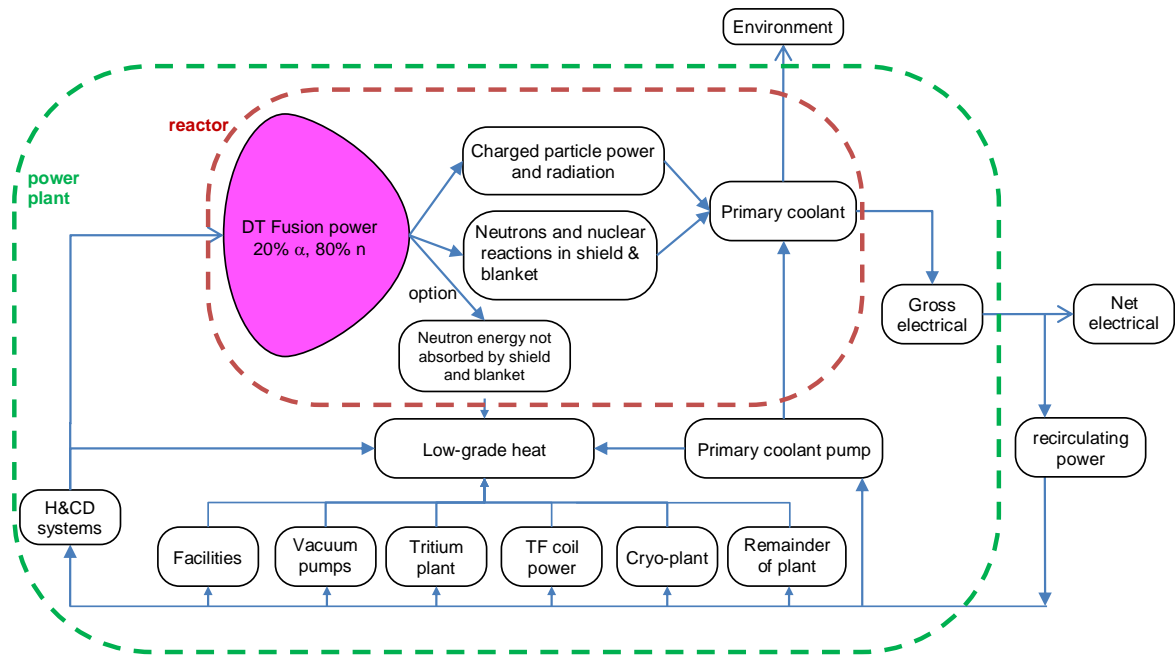


Fig. 1. Power balance in a fusion power plant [Kov 13].

The net electric power ( $P_e$ ) is obtained by subtracting different power consumptions to the gross electric power: electric power for heating and current drive, coolant pumps, cryogenic system (magnet coils cooling) and the rest of auxiliary systems (magnets, tritium plant, facilities, etc.).

$$P_e = P_{GROSS} - P_{H\&CD} - P_{PUMP} - P_{CRYO} - P_{AUX} \quad (1) \quad [\text{Zol 11}]$$

The difference between gross and net electric power is called recirculating power. Therefore, acting upon these factors opens up different ways to reduce the recirculating power factor and in consequence to maximize the net electric power.

Let's see the following example: the specifications for DEMO 1A (short-term demonstration reactor) used in EFDA WP13 include power consumptions of 50 MW and 135 MW for auxiliary systems and H&CD, respectively [Har 13]. Both represent 37% of the net electrical power defined as objective for DEMO1A in such activity (500 MW<sub>e</sub>). According to results obtained with the systems code PROCESS, Fig. 2 shows that if we design a device to generate a net electric power of 500 MW with a minimum pulse duration of 2 h and then extend the purely inductive pulse duration by auxiliary H&CD systems to be installed at a later stage, we may become over-constrained because any attempt to expand the pulse length will be off-set by the need to increase the recirculation power and therefore reduce net electricity output [Fed 14]. However, this strongly depends on the ultimate efficiency of the H&CD systems, which appears as one of the most critical challenges for commercial fusion power plants. It would be also useful to maximize current drive efficiency and minimize the requirements on externally driven current I<sub>CD</sub>, which can be achieved by maximizing the plasma normalized pressure [Pam 09].

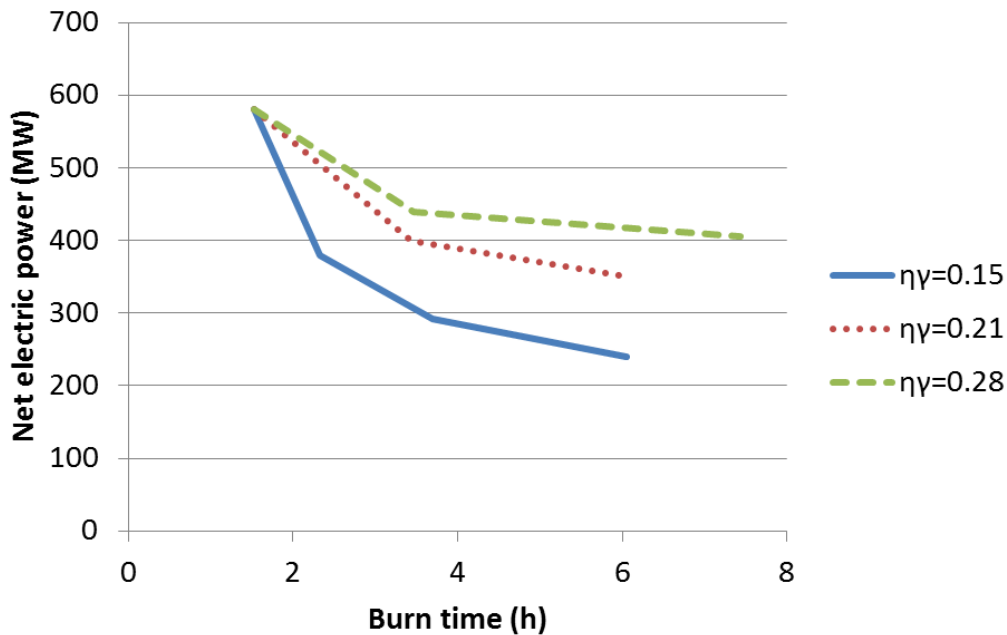


Fig. 2. Trade-off between net electrical power and pulse length for different values of  $\eta\gamma$  (product of H&CD wall-plug efficiency and current-drive efficiency) [Fed 14].

Other possibilities include, as long-term goal, to develop high temperature superconductors (HTS), allowing a magnet technology compatible with liquid nitrogen cooling. At the plant level, this would result in major simplifications and increased reliability [Pam 09]. The impact on cost cannot be assessed at the present stage of development, but replacing liquid helium with liquid nitrogen would result in a modest reduction of the power requirements (about 10-20 MW<sub>e</sub>).

Nevertheless, in spite of the importance of minimizing the recirculating power, the most significant approach to maximize the net electric power is to maximize the gross electric power. Two main plant systems are behind this goal: the primary heat transfer system (PHTS) and the secondary power conversion system (PCS). The primary heat transfer system is used to remove the thermal energy deposited on the blanket, the divertor and the vacuum vessel by plasma radiation and neutron volumetric heating, as well as decay heat due to neutron activation. On the other hand, the power conversion system transfers the thermal energy from the PHTS coolant/s to a secondary coolant and carries out thermal-electric conversion through turbomachinery and an alternator.

### **3.3. Integration of the primary heat transfer system and the power conversion cycle**

The design of the breeding blanket, which represents the main thermal source for power conversion, and the balance of plant have strong interdependencies. In fact, the performances of the breeding blanket itself in parameters as maximum power density, achievable lifetime, thermal efficiency, tritium breeding ratio and availability are not independent from each other. For instance, the tritium breeding ratio depends on the choices of tritium breeding materials and neutron multiplier materials, and the structural design of the blanket, the piping design of coolant and so on [Sak 14]. Analogue interdependencies can be established for some functions of the divertor and the first wall –and its integration with the blanket–.

On the other hand, it is possible (though not essential) that a fusion power plant will be required to operate at a range of power rather than a single operating point. There are a number of ways in which the plasma operating point can be adjusted to produce a different power output, apart from the evident influence of pulsed operation. However, they are not all equivalent in the impact they have on other aspects of the operation. Such impact in the operation and

performance of the breeding blanket and the divertor, and hence the power conversion cycle, is a powerful reason for which the operating point/s should be selected on the basis of resilience [Ward 15]; that is minimizing the sensitivity of one or more key parameters to variation in other variables.

The replacement of blanket or divertor cannot be accompanied by a complete change of the Balance of Plant, as this is clearly unfeasible. Thus, the series of blanket concepts and divertor concepts must each assume the same coolant for the entire lifetime (although the divertor and blanket coolants could, in principle, be different) [Fed 14].

In specific terms of thermal efficiency, there are some limitations in the performance of blanket designs which have important consequences on the reactor gross thermal power and the recirculating power, through the integrated operation of the primary heat transfer system and the power conversion cycle. We will feature the related main issues of the 4 blanket concepts currently developed in the framework of EUROfusion Power Plant Physics & Technology Programme (2014-2018): HCPB, HCLL, WCLL and DCLL, with an additional reference to the SCLL.

The Helium Cooled Pebble Bed blanket (HCPB), already described briefly in Chapter 2, uses high pressure helium (8 MPa) as coolant and low pressure helium (0.1-0.2 MPa) as tritium carrier (purge gas), lithiated ceramics as breeder and beryllium pebbles as neutron multiplier. The upper limit temperature of a solid breeder like  $\text{Li}_4\text{SO}_4$  is 920°C, and 650°C for Be pebbles, but the use of EUROFER (reduced-activation ferritic-martensitic steel) as structural material imposes a narrow operating thermal window: EUROFER must operate over 300 °C to avoid embrittlement because the increase of the Ductile-Brittle Transition Temperature (DBTT) with neutron irradiation. It must also operate under 550°C to avoid creep. Therefore, the limited coolant outlet temperature and its restricted difference with the inlet stream temperature (300-500°C) prevent electric efficiencies higher than 33% [Lin 15] [Lat 13] [Bub 13].

On the other hand, ceramic breeders are very sensitive to thermal stresses and would not allow the use of pebbles for high power applications [Mal 99]. Furthermore, the purge gas includes water in low concentration to promote isotopic exchange in the breeder and then facilitate the release of tritium. This produces HT and HTO and significantly complicates the fuel cycle processing (isotopic separation system), which subtracts attractiveness to this blanket concept.

Regarding liquid breeder blanket concepts, both the HCLL (Helium Cooled Lithium Lead) and the WCLL (Water Cooled Lithium Lead), the first also mentioned in Chapter 2, employ quasi stagnant Pb-15.7Li as breeder, neutron multiplier and tritium carrier, whereas pressurized helium or water are respectively used as coolant. As in the case of HCPB, both concepts consider the use of EUROFER as structural material. Apart from the mentioned maximum and minimum operation temperatures of EUROFER (300-550°C), one important limitation is the steel/liquid metal interface temperature must be kept under 500°C to avoid excessive corrosion rates. ODS steels or vanadium alloys could be subjected to the same limits, because their resistance to corrosion is similar to the EUROFER one [Mal 99]. Furthermore, the reactivity between water and lithium lead eutectic alloy still remains as one of the biggest safety concerns for this concept of blanket. Tritium permeation from the breeder to the coolant is also a main issue, with similar consequences as the pointed out for the HCPB. Another issue for the current EU WCLL design (MMS concept) and DEMO specifications is the difficulty to achieve suitable values of Tritium Breeding Ratio (TBR) [Per 15].

The achievable efficiency of the HCLL power conversion cycle is the same as the HCPB one, since it uses the same coolant with the same inlet-outlet temperatures (300-500°C). The WCLL one is very similar to the PWRs one. In consequence, there is not much margin to increase the thermal efficiency of the power conversion system beyond the 35% because this would require much higher coolant pressure and temperatures (above the critical point) [Mal 99].

Self-Cooled Lithium Lead (SCLL) is a long-term promising blanket concept to achieve higher thermal efficiency. As in the case of HCLL and WCLL, eutectic PbLi acts as neutron multiplier and tritium carrier, but it flows at much higher velocity, allowing self-cooling. The use of  $\text{SiC}_f/\text{SiC}$  as structural material allows the PbLi outlet temperature can reach 1100°C, without exceeding

the limit of 1000°C for silicon carbide composites. This would permit achieving an efficiency of ~61% in the power conversion system [Gia 03].

Dual coolant Lithium Lead blanket (DCLL) is a more conservative option to achieve high thermal efficiency in the mid-term. As in the case of SCLL, eutectic PbLi flows at relatively high velocity and it is self-cooled. However, EUROFER is used here as structural material, so pressurized helium (8 MPa) must cool the first wall and the rest of the structure walls to keep EUROFER temperature under 550°C. The inclusion of SiC<sub>f</sub>/SiC Flow Channel Inserts (FCI) to electrically insulate the liquid metal ducts and then mitigate magnetohydrodynamics phenomena provides also thermal insulation and allows the PbLi outlet temperature can reach 700°C. This makes possible thermal efficiencies around 45% in the power conversion cycle. A low temperature MMS DCLL blanket for a short-term DEMO is being developed at present within EUROfusion [Mar 14]. EUROFER-Al<sub>2</sub>O<sub>3</sub>-EUROFER 'sandwich' is currently proposed as an alternative to SiC<sub>f</sub>/SiC FCIs due to manufacturing issues. This fact, together with corrosion requirements, involves the need of reducing the PbLi outlet temperature to 500°C, whose consequence is the achievable efficiency in the power conversion system is quite similar to the HCLL and HCPB ones. However, it presents some advantages in other issues; for example, the lower tritium partial pressure considerably reduces the problem of permeation to the helium coolant.

An additional issue of helium cooled blankets (HCPB, HCLL and DCLL to a lesser degree) is the insufficient knowledge about long-term availability of helium. Besides, a common risk for every kind of blanket is the possibility of future military-political restrictions on supply of Li<sup>6</sup> enriched breeding material, associated with extremely high costs.

In summary, the use of EUROFER and helium puts temperature limits to exploit the advantage of Brayton cycles or even reach the upper limits of a Rankine cycle. Studies of BoP using the helium temperature limits arising from EUROFER indicate that the thermodynamic efficiency of Rankine or Brayton cycles limited to 500°C is insufficient to reach the net electricity generation target for DEMO when the high installed pumping power for the helium circulation (~150 MW) is subtracted [Fed 14]. This entails a further high-impact risk to the DEMO mission and highlights the need of a strong materials R&D program to solve this issue. In mid-term, two lines of R&D are recommended in EU [Sto 14]:

- Adapting developments outside fusion for high-temperature ferritic-martensitic (HT FM) steels with improved high temperature creep strength (up to 600-650°C) achieved using thermomechanical treatment (TMT), or thermal treatment to improve the microstructure and density of radiation defect recombination centres.
- Pursuing the development of oxide dispersion strengthened (ODS) alloys, subject of fusion R&D for a decade, but still without industrialization. These have good high temperature tensile strength and creep resistance.

## **3.4. Power conversion cycles studies for DEMO in EU**

### **3.4.1. PPCS and early DEMO**

From 1990 to 2000 a series of studies within the European Fusion Programme examined the safety, environmental and economic potential of fusion power. During that time, substantial advances in the understanding of fusion plasma physics and the development of more favourable plasma operating regimes were made, as well as progress in the development of materials and technology [Mai 05]. Afterwards, a European Power Plant Conceptual Study (PPCS) was carried out (2001-2004), where 4 models of commercial fusion power plants were analysed. Such models, named PPCS A to PPCS D are illustrative of a wider spectrum of possibilities, from relatively near-term concepts to more advanced conceptions. All 4 PPCS plant models differ substantially in their plasma physics, electrical output, blanket and divertor technology, economic performance, safety and environmental impacts.

	Model A	Model B	Model C	Model D
<b>Unit Size (GWe)</b>	1.55	1.33	1.45	1.53
<b>Fusion power (GW)</b>	5.00	3.60	3.41	2.53
<b>Aspect ratio</b>	3.0	3.0	3.0	3.0
<b>Elongation (95% flux)</b>	1.7	1.7	1.9	1.9
<b>Major radius (m)</b>	0.25	0.25	0.47	0.47
<b>TF on axis (T)</b>	7.0	6.9	6.0	5.6
<b>Plasma current (MA)</b>	30.5	28.0	20.1	14.1
<b><math>\beta_N</math> (thermal, total)</b>	2.8, 3.5	2.7, 3.4	3.4, 4.0	3.7, 4.5
<b>Bootstrap fraction</b>	0.45	0.43	0.63	0.76
<b><math>P_{add}</math> (MW)</b>	246	270	112	71
<b><math>n/n_g</math></b>	1.2	1.2	1.5	1.5
<b>Average neutron wall load</b>	2.2	2.0	2.2	2.4
<b>Divertor peak load (MW m<sup>-2</sup>)</b>	15	10	10	5
<b>H&amp;CD efficiency</b>	0.6	0.6	0.7	0.7
<b>Plant efficiency</b>	0.31	0.37	0.42	0.6
<b>Coolant blanket</b>	Water	Helium	PbLi/He	PbLi
<b><math>T_{in}/T_{out}</math> (°C)</b>	285/325	300/500	480/700 300/480	700/1100
<b>Coolant divertor</b>	Water	Helium	Helium	PbLi
<b><math>T_{in}/T_{out}</math> (°C)</b>	140/167	540/720	540/720	600/990
<b>Power conversion cycle</b>	Rankine	Rankine	Brayton	Brayton

Table 1. Main parameters of the PPCS models [Mai 05].

Rankine cycles were considered for the more conservative models A and B, respectively based on WCLL and HCPB/HCLL blankets and water or helium cooled divertor (low-temperature or medium-temperature divertor). On the other hand, Brayton cycles were studied for the more advanced models C and D to take advantage of the higher coolant temperatures coming from the use of DCLL or SCLL blanket and medium or high-temperature divertor.

Subsequently, different power conversion cycles were assessed in the framework of EFDA DEMO scoping studies to provide technical information focused on the selection of DEMO parameters. Thus, following the PPCS results, advanced cycles were analysed in order to get an improvement on the thermodynamic efficiency of a near-term demonstration reactor based on He-cooled blanket concepts (HCLL, HCPB) and He-cooled divertor. The parameters of an HCLL model AB were used in [Med 07] to analyse the gross and net efficiencies of alternative cycles to the standard Rankine cycle: 1) supercritical steam Rankine, 2) supercritical CO<sub>2</sub> indirect Brayton and 3) independent cycles for the blanket and the divertor.

Parameters	HCLL model AB
Fusion power (MW)	4290
Thermal power to PHTS (MW)	5145
Total thermal power (MW)	5509
<b>Blanket</b>	
Thermal power from blanket (MW)	4218.76
Thermal power from blowers (MW)	273

Helium flow (kg/s)	4070
Coolant temperature, inlet/outlet to HEX (°C)	500/287
<b>Divertor</b>	
Thermal power from divertor (MW)	926.07
Thermal power from blowers (MW)	91
Helium flow (kg/s)	1010
Coolant temperature, inlet/outlet to HEX (°C)	717/522

Table 2. PHTS parameters for HCLL model AB [Med 07].

According to this HCLL model AB, blanket extracts 82% of the total thermal power with a moderate coolant temperature (300-500°C) and the divertor, with a more respectable coolant temperature (540-717°C) delivers 18% of the thermal power. Additionally, the helium blowers raise the coolant temperature: on the one hand this increases the thermal energy available in the helium; on the other, it forces the helium outlet temperature in the blanket heat exchanger to be accordingly, lower than 300°C. These features of the heat sources together with the low inlet temperature of the blanket coolant limit the gross efficiency obtained with the cycle [Med 07].

Dramatic improvements in power plant performance can be achieved by raising inlet steam conditions in supercritical (SC) Rankine cycles. They also constitute highly regenerative cycles as the external thermal sources are at very high temperature. On the contrary, high pressure implies more pumping power, fact that is compensated by the bigger power density in the steam. Different SC cycles were studied in [Med 07]: 1) SC superheat cycle, 2) SC reheat cycle and 3) SC improved cycle. Gross efficiencies of 47.31, 46.67 and 49.88% were respectively obtained in the face of the standard Rankine cycle one (45.74%). However, only the SC improved cycle has a clear advantage on the cycle net efficiency (31.68%) over the standard Rankine (28.34%) because of the low feedwater & condensate pumping power (less steam mass flow) in comparison with the gross power.

Supercritical CO<sub>2</sub> indirect Brayton cycles were also studied in [Med 07], due to their potential for high efficiency at low temperatures due to the low compression work near the critical point (7.38 MPa, 31 °C). The analysis of a simple recuperated cycle with a single compression stage showed a very low efficiency compared to the fission reactors with a similar configuration. The main reason is the low outlet temperature of helium in the blanket HEX (287°C), that requires a maximum CO<sub>2</sub> inlet temperature of 262°C. This fact limits the amount of thermal energy than can be recovered in the recuperators and the use of an auxiliary compressor [Med 07]. A re-compression cycle allows improving the efficiency by reducing the heat rejection from the cycle by introducing an auxiliary compressor, bypassing the main cooler, the main compressor and the low temperature recuperator. A net efficiency of 26.01% was calculated for this cycle (lower than any of the Rankine options), concluding that the thermal power from the blanket and the divertor integrated into a sole re-compression cycle conducts to a non-optimal use of the available divertor exergy. For that reason, two combinations of two independent cycles for the blanket and the divertor were assessed: 1) standard Rankine (blanket) + SC CO<sub>2</sub> Brayton (divertor) and 2) Independent SC CO<sub>2</sub> Brayton (blanket and divertor). The dual cycles (2 SC CO<sub>2</sub> re-compression independent cycles) yield net efficiencies comparable to the SC 'improved' Rankine cycle [Med 07].

### **3.4.2. EFDA PPPT WP12-13 studies: Helium-cooled blanket/water steam DEMO BoP (WP12)**

#### **3.4.2.1. Introduction**

Coinciding with the end of the Seventh Framework Programme (2007-2011) of the European Atomic Energy Community (EURATOM), EFDA launched in 2011 a Work Programme which was prolonged by two years, until the end of 2013. The activities carried out within the Department of Power Plant Physics and Technology were aimed at: 1) checking assumptions

used in fusion systems design codes and to the preliminary analysis of different DEMO design options (e.g. inductive/steady state); 2) defining the strategy of the divertor R&D; 3) revisiting the rationale and technology development assumptions that have led to the selection of some design choices in the past (e.g. in the frame of the Power Plant Conceptual Study) [Efd 11].

### 3.4.2.2. Helium-cooled blanket/water steam BoP

In 2012, the Work Programme included a dedicated activity for the assessment of helium-cooled balance of plant technologies that could be relevant for a DEMO fusion power plant. With the exception of the similar blanket inlet and outlet temperatures, the considered parameters for the PHTS (characteristic of near term DEMO 1) were very different to the ones considered in [Med 07], with a much lower thermal power and a low-temperature water-cooled divertor.

Parameter	Value
Total thermal power to blanket (MW)	1781
Total thermal power to divertor (MW)	250
He mass flow rate (kg/s)	2314
Overall He pumping power (MW)	50
Blanket He inlet/outlet temperature (°C)	300/500
Divertor He inlet/outlet temperature (°C)	100/150
Net electrical output to grid (MW)	>500

Table 3. DEMO1 input parameters for the EFDA activity WP12-DAS08-T01 [Har 12].

Water steam Rankine cycles and helium Brayton cycles were analysed by CCFE and Rolls Royce [Lat 12]. Results indicated Rankine cycles were able to meet the required net efficiency target ( $\eta_{\text{overall}}=500/(1781+250)\cdot 100=24.6\%$ ) via incorporation of the divertor heat in the cycle with reheat and feed heating. The most efficient one is a supercritical cycle with feed heating and use of the divertor heat, which reaches an overall efficiency of 28.7% (40.4% cycle efficiency).

By contrast, Brayton cycles offer very low plant efficiencies and cannot meet the electrical output target. The most efficient proposed cycle –reheated and intercooled- barely reaches a cycle efficiency of 29% and an overall efficiency of 14.5% [Lat 12].

According to [Lat 12], the key advantages of steam cycles are that all heat is rejected at the lowest temperature in the cycle and the pump work is very low. Both of these effects help to increase the fundamental efficiency of a steam cycle. Steam also improves on the helium cycle in the sense that it can make good use of the divertor heat because water exits the pump at a temperature which is typically much lower than the of divertor heat source meaning the divertor can be used to pre-heat the flow entering the steam generator.

### 3.4.3. Water-cooled blanket/water steam DEMO BoP (WP13)

#### 3.4.3.1. Introduction

More ambitious objectives were set for the Work Programme 2013 regarding Balance of Plant. Design, modelling and analysis of primary heat transfer and BoP options for DEMO continued the work developed in the previous year, with a different reactor specification and different thermal sources (blanket, divertor and vacuum vessel) or secondary coolants: 1) Rankine cycles for water-cooled blanket, 2) Rankine cycles for helium-cooled blanket (following WP12) and 3) supercritical CO<sub>2</sub> Brayton cycles.

Furthermore, modelling of the time-variant behaviour of a pulsed DEMO and a design assessment of pulsed power profiles were also carried out. That is, since DEMO is likely to be a

pulsed machine, this will have implications for the PHTS and BoP in terms of thermal transients and fatigue due to cyclic loading. In order to prove the principle of connection of a pulsed energy system to the grid, it may be necessary to introduce a Thermal Energy Store to buffer the thermal transients and reduce the cyclic loading effect however which would further increase cost and complexity of the BoP [Har 13].

The WP13 activities were already aligned with the view of the EU Fusion roadmap assumed for the subsequent EUROfusion Programme (2014-2018), where the involvement of industry and the development of appropriate engineering tools are major targets, as well as the addressing of challenging issues like tritium control in heat exchangers, response to cyclic operation and BoP components failure modes.

### 3.4.3.2. Water-cooled blanket/water steam BoP

CCFE and Rolls Royce continued its collaboration begun in 2012 looking at the system design of the secondary plant and the top level design of key components [Lat 13]. For this work, a water-cooled blanket (WCLL) and a water-cooled divertor were assumed, so that the reactor is matched to a Pressurised Water Reactor (PWR) type balance of plant system used extensively in nuclear fission plants. The total thermal power of this PHTS model is quite similar to the WP 2012 one, although here the power to the divertor is lower. In spite of the specification shown in Table 4, the vacuum vessel is not included as thermal source in [Lat 13]. The difficulty to reach the net electrical power target is higher than in the case of the WP 2012 specification, since the recirculating power (auxiliaries + H&CD) is larger (185 MW vs. 50 MW) [Har 13].

Parameter	Blanket	Divertor	Vacuum vessel	Overall
Thermal power (MW)	1835	149	34.56	
Water inlet temperature (°C)	290	150	95	
Water outlet temperature (°C)	320	250	105	
Water outlet pressure (bar)	150	65	11	
Water pressure drop (bar)	3	2	1	
Power to auxiliaries (MW)				135
Power for H&CD (MW)				50
Net electrical power (MW)				≥ 500

Table 4. DEMO1 input parameters for WP13-DAS08-T02 with water-cooled blanket [Har 13].

A base case cycle and a modified version of such cycle were assessed by Rolls Royce in [Lat 13]. The first one has three high pressure turbine stages and three low pressure turbine stages. Feed heating is employed in a typical manner with low pressure turbine bleeds being used as part of a low pressure feed heating train and high pressure turbine bleeds being used as part of a high pressure feed heating train. As is common for PWR cycles a moisture separator and reheater are used in between the high pressure and low pressure turbines to dry out and increase the temperature of the flow going through the low pressure turbine. This helps to ensure that the low pressure turbine exit flow is not too wet.

The layout of the modified base case cycle adds the blanket and divertor primary circuits (including multiple steam generators). It also adds the divertor heat to the main cycle, which is used to replace the second low pressure feed heater. Another differences are the addition of a deaerator, a seal steam evaporator and gland steam systems. On the other hand, a 700 MW seven stage turbine is proposed (4 low pressure stages). In all other respects, the cycle is very similar to the base case cycle.

The power and efficiency of the cycle were calculated, resulting in gross electric efficiency of 34.9%, net electric power (whole plant) of 656.9 MW and net electric efficiency (whole plant) of 33.11% [Lat 13], which is quite close to the practical limit of 35% mentioned in Subsection 3.3.

The following expressions have been used to calculate the gross electric efficiency and the net electric efficiency, respectively:

$$\text{Gross electric efficiency} = \frac{\text{Turbine work out at generator terminals}}{\text{Total heat in}} \quad (2)$$

$$\text{Net electric efficiency} = \frac{\text{Work out at power plant terminals}}{\text{Total heat in}} \quad (3)$$

[Lat 13] does not seem to include the value of power consumed by auxiliaries and H&CD specified in [Har 13]. In such case, the net electric efficiency would be reduced to 25.11%.

On the other hand, CCFE modelled a similar cycle, with a basic version (B4) and an improved case (B5), resulting in a net power output of 740 MW. As an extension to model B5, a cycle called C1 incorporating the vacuum vessel heat was included, so that the output power increases to 746 MW, but it has been questioned whether the extra 6 MW would justify the additional feedheater and therefore model B5 has been proposed as the reference cycle for further investigation. B5 includes reheat, 4 extractions, 3 stages of feedheat and divertor heat, achieving a gross efficiency of 37.3% and a net efficiency of 36.9% (using the same terminology than in the previous case). Actually, different codes have been used by CCFE (Modelica + COFE) and Rolls Royce (Thermoflow) to model the cycles. Therefore differences between the models, like the shift of the divertor feedheater from an optimal position in model B5 to a much lower temperature point in the cycle in the Thermoflow model, can justify such differences in the results of the simulations. In fact, CCFE requested Rolls Royce and KIT using model B5 as benchmark case, with the codes Modelica, Pro-II and EBSILON, respectively. The results show a good agreement.

Anyway, since the Thermoflow model is a practical cycle from an engineering perspective, it is considered significantly more realistic and it was therefore proposed as the reference low temperature Rankine cycle for DEMO. However, the interest of this cycle remains subjected to the overcoming of the clear drawbacks of water-cooled breeding blanket concepts (e.g. safety issues related to the compatibility between PbLi and H<sub>2</sub>O in the WCLL, tritium permeation to water, etc.) and the issue of tritium permeation in the steam generator.

### 3.4.4. Helium-cooled blanket/water steam DEMO BoP (WP13)

KIT studied the balance of plant on the secondary of a DEMO reactor based on a helium-cooled blanket (HCPB/HCLL) and a water-cooled divertor [Bub 13]. The input parameters are the same as in the case of the CCFE/Rolls Royce studies, with the exception of those affecting the blanket cooling.

Parameter	Blanket	Divertor	Vacuum vessel	Overall
Thermal power (MW)	1835	149	34.56	
Helium inlet temperature (°C)	300			
Helium outlet temperature (°C)	500			
Helium outlet pressure (bar)	80			
Helium pressure drop (bar)	4.35			
Water inlet temperature (°C)		150	95	
Water outlet temperature (°C)		250	105	
Water outlet pressure (bar)		65	11	
Water pressure drop (bar)		2	1	
Power to auxiliaries (MW)				135
Power for H&CD (MW)				50
Net electrical power (MW)				≥ 500

Table 5. DEMO1 input parameters for WP13-DAS08-T02 with helium-cooled blanket [Har 13].

Most of models developed by KIT within this activity were aimed to perform static and transient calculations of the pulsed DEMO operation for different BoP configurations, including an intermediate heat storage loop. However, an assessment of Rankine cycles for steady state operation, as in the case of the studies described in 3.4.3 and 3.4.5, was also included.

The three available thermal sources (blanket, divertor, vacuum vessel) were integrated in the power conversion cycle. 14 heat exchangers between the primary side of the BoP scheme (helium) and the secondary one (water/steam) were considered. For sensitivity analyses, the pressure of the secondary side coolant was varied between 78 and 65 bar. In its back, water is heated up using heat coming from the vacuum vessel cooling circuit, and later from the divertor cooling circuit. This water is then heated up by the heat coming from the blanket up to the saturated steam parameters and transported back to the steam turbine.

Results from code EBSILON simulations showed the maximum gross electrical power (701.68 MW) is achieved with a steam pressure at turbine inlet of 78 bar, which implies a cycle efficiency of 27%. If the steam pressure at turbine inlet is 65 bar, both the gross electrical power (689.99 MW) and cycle efficiency (26.5%) decrease. The cycle efficiency was calculated as follows:

$$\text{cycle efficiency} = \frac{\text{Gross electric power} - \text{All coolant(s) pumping power}}{\text{Blanket power} + \text{Divertor power} + \text{Vessel power}} \quad (4)$$

### **3.4.5. Helium-cooled blanket/supercritical CO<sub>2</sub> DEMO BoP (WP13)**

#### **3.4.5.1. Introduction**

Like KIT, CIEMAT and the University of Comillas studied the balance of plant of a near term DEMO reactor based on a helium-cooled blanket (specifically a HCLL), but using supercritical carbon dioxide Brayton cycles (S-CO<sub>2</sub>) for the secondary side. The outcome was collected and discussed in the Final Report for this Task WP13-DAS08-T02 [Lin 13]. In this work, a survey of open literature on the matter to identify advantages and potential issues of S-CO<sub>2</sub> has been made. Right after several cycle layouts using high thermal sources (blanket) and low ones (divertor and vacuum vessel) integrated in a S-CO<sub>2</sub> power cycle have been proposed and analysed, searching the maximization of the electricity production. A realistic estimate of the electrical efficiency has been derived by accounting the pumping power demanded by the heating and cooling loops feeding the power cycle and even the self-consumptions of the plant. Once an optimum layout has been selected based on electricity production, the study has been completed by a sensitivity study on key cycle variables and by the optimization of the heat exchangers, so that a trade-off between heat exchangers size and power production has been proposed.

From the previous work, a paper was written and published in Applied Thermal Engineering [Lin 15]. The following information is extracted from this paper.

#### **3.4.5.2. Literature survey on S-CO<sub>2</sub> Brayton cycles**

The Brayton cycle is a very attractive solution for DEMO power conversion system due to its relative simplicity and compactness. However, as anticipated in Section 3.3, the use of a very light gas as helium taxes thermal efficiency because of the necessary compression before absorbing heat from the thermal source. This might be partially compensated by using thermal recuperation and by reaching very high temperatures. A good example for these two strategies is the so called VHTRs fission reactors [Her 09], in which temperatures as high as 900-1000°C are postulated. Unfortunately, fusion reactors do not reach so high levels, even at high temperature divertors [Lin 11]. In the particular case of supercritical carbon dioxide Brayton cycles overcome the high demand of compression power by entering the compression stage at

pressure slightly higher than the critical one, so that specific volume is not as large as if it was an ideal gas. Dostal compiled the fundamentals of the cycle and deepened in its performance, including heat exchanger designs, economy and turbomachinery [Dos 04]. The most outstanding feature of S-CO<sub>2</sub> cycles with respect to Rankine ones is probably their remarkable compactness. Other characteristics, though, are less favourable. Precooling for instance, is rather complex. If the cycle low pressure is near the critical one (typically 75 bar), CO<sub>2</sub> specific heat experiences a very sharp peak at low temperatures that makes heat transfer intricate. Additionally, such low pressures mean heat rejection at very low temperature differences, which requires high water flow rates (e.g. much pumping power) at the secondary side of the heat exchanger.

Most papers on S-CO<sub>2</sub> Brayton cycles deal with Generation IV fission plants, especially with Sodium Fast Reactors (SFR). High temperature thermal sources of SFRs [Perp 12] are comparable to those of EFDA DEMO1 with HCLL-HCPB blanket [Har 13], so some literature about this type of fission reactors has been revised. Dostal et al. [Dos 09] explored different configurations with Brayton cycles using CO<sub>2</sub>, from basic ones to re-compression cycles, pre-compression and partial cooling compression cycles. They concluded re-compression has the potential to achieve high efficiencies (higher than 46%), but the value of pressure should be over 200 bar for a significant result. A study conducted under similar conditions to the DEMO blanket ones concluded that no efficiency increase should be expected from inter-cooling and/or re-heating with respect to the re-compression cycle [Moi 09]. Second law analyses of the re-compression cycle were carried out to find out the potential effect of different parameters on the exergetic efficiency [Sar 09]. Finally, other studies focused on enhancing cycle efficiencies through using binary gas mixtures [Jeo 13].

The near term EFDA DEMO1 is well framed in the low temperature divertor family. A comparative analysis was conducted regarding both blanket coolant and power cycle configurations for a fusion reactor [Ish 08]. Helium proved to be better than pressurized or supercritical water due to its stability. Among steam Rankine, He-Brayton and S-CO<sub>2</sub> cycles, the analysis results depended on how blanket and divertor were considered. When both components were jointly considered as thermal sources, the highest efficiency was Rankine's, closely followed by S-CO<sub>2</sub>. However, if the blanket was conceived as the only thermal source, the Rankine reversed and S-CO<sub>2</sub> got the highest efficiency, closely followed by Rankine. Inclusion of the divertor was calculated to heavily tax S-CO<sub>2</sub> cycle efficiency (from 42% to 36.4%), but it allows generating further net power. Finally, a design including size of components was performed giving a gross volume of 16590 m<sup>3</sup> (87% for heat exchangers) for steam power plant against 7240 m<sup>3</sup> (83% for heat exchangers) for S-CO<sub>2</sub>.

The key of the S-CO<sub>2</sub> Brayton cycle is the situation of the main compressor suction close to the critical point, which allows achieving a low compressor consumption (already mentioned in Subsection 3.4.1 [Med 07]). The feasibility of the cycle depends on the stability of the compressor when operating close to the critical point, and even when operation conditions fall below the dome region of the saturation curve. This issue has been studied by Sandia National Laboratories. They released a report [Wri 10] explaining the test loops and showing exhaustive experimental results. These experimental results demonstrated stable and controllable operation near the critical point over a range of conditions and confirmed the performance potential of S-CO<sub>2</sub> cycles. Another issue about the operation close to critical point is the sharp variation of density of the CO<sub>2</sub>, being this topic studied by Moisseytsev and Sienicki [Moi 09]. So, when the compressor inlet temperature is below the pseudocritical temperature (the one at the peak in the specific heat occurs) the density is very high, reducing the compressor consumption. However, it is necessary to control this temperature because at pressures slightly higher than the critical one (around 74 bar) a small increase in this temperature produces a sharp drop in the density, with the associate problem in the operation of the compressor. This fact can be smoothed if the compressor inlet pressure is increased enough. With regards to turbomachinery design for CO<sub>2</sub>, Sandia synthesized in [Ful 12] some orientations. A more detailed explanation can be found in [Bah 12].

As previously mentioned in this thesis, one of the challenges of any power conversion system in a fusion power plant is to accommodate a pulsed mode operation. In order to discuss how S-CO<sub>2</sub> cycles would behave, concentrated solar plants (CSP) are taken as a reference given the

natural cycling of their power source, where a thermal energy storage system is usually proposed to extend the operating hours of the plant. An optimization study can be found in [Mar13]. Supercritical CO<sub>2</sub> power conversion systems are being proposed for CSP, especially for the central tower system. A thorough description is given in [Ma11], where it proposed molten salt as a thermal energy storage system. In [Chac11] advanced layouts based on S-CO<sub>2</sub> cycles are proposed for CSP plants, including combined cycles using organic Rankine cycles as bottoming cycles. Sunshot Project promoted by the Department of Energy of USA seeks to develop a megawatt-scale S-CO<sub>2</sub> cycle optimized for the highly transient solar power plant profile [Tur13]. Also, some tests conducted in Sandia National Laboratories concluded S-CO<sub>2</sub> cycles are well adapted to transient behaviour due to the short solar oscillations along a day and their low thermal mass, whereas a thermal energy storage system might be used to overcome longer oscillations [Ive13]. In [Sin13] the control strategies for CSP power plants (trough and tower) are discussed for daily fluctuations. In the nuclear sector, Floyd et al. [Flo13] dealt with the off-design response of S-CO<sub>2</sub> cycles when the sink temperature varies in the conversion power plant of an SFR nuclear power plant. Different control strategies for stability of the system are assessed.

The Printed Circuit Heat Exchanger (PCHE) is a rather novel heat exchanger type, formed by diffusion bonding of a stack of plates with fluid passages photo-chemically etched on one side of each plate by using a technique derived from that employed for electronic printed circuit boards –hence the name. The diffusion bonding process allows getting an interface-free joint between the plates, giving strength to the base material and very high pressure containment capability. The use of such heat exchangers has been investigated by Aquaro et al. [Aqu07] for high temperature recuperators in Brayton power plants (air and helium, not supercritical CO<sub>2</sub>) in fossil and VHTR fission power applications. They conclude that in this context (high temperature and not so high pressure) other compact heat exchangers, as plate-fin ones, or shell and tubes configuration as helically coiled counterflow heat exchanger are preferred to PCHE. However, there is high accord about the use of PCHE in S-CO<sub>2</sub> cycles for recuperators and eventually for heat sources and heat sink heat exchangers, mainly because of their good behaviour under high pressure difference, very high effectiveness (close to 99%) and high compactness. So, Argonne National Laboratory (ANL) uses them in the STAR-LM, a Generation IV reactor [Son07]; Korean Atomic Research Institute (KAERI) has selected them for KALIMER-600, another Generation IV reactor [Cha09]; and finally, a PCHE is included in other experimental helium loop developed by KAERI to test a design for a fusion reactor based on a helium-cooled molten lithium (HCML) blanket [Yum13]. A benchmarking survey with actual prototypes of reactors can be found in [Hal12], with thermal effectiveness from 92% to 98.7%; Sandia National Laboratories [Wri10b] supports their use for both recuperators, heat entry to the power cycle and heat rejection from the cycle, highlighting the benefits of PCHE compactness; Mito et al. [Mit06] draw attention to the reduced pressure drop and Gezelius [Gez04] gave ratios of 58-98 MW/m<sup>3</sup> for PCHE against 6.2 MW/m<sup>3</sup> with shell and tube heat exchangers working at the same capacity and log mean temperature difference. In [Ish08] a detailed design of a S-CO<sub>2</sub> cycle for 300 MW of mechanical power is given resulting minimum temperature approaches between 4 and 5°C for both recuperators and pre-cooler and power densities in the range of 7.7-13.4 MW/m<sup>3</sup> (the lowest at LTR and the highest at pre-cooler). In addition, many authors have investigated the characteristics of hydraulic performance of a PCHE, experimentally and numerically. Nikitin [Nik06] studied the performance of a PCHE with zigzag channels in a supercritical CO<sub>2</sub> experimental loop. Ngo et al. [Ngo06] analysed a new PCHE with an S-shaped fin by using a heat recovery test facility, confirming a promising thermal-hydraulic performance with water and CO<sub>2</sub>. And following these studies, Tsuzuki et al. [Tsu07] with a 3D model obtained a pressure drop reduction in a novel flow channel configuration with discontinuous fins with an S-shape. Then, Kim et al. [Kimd08], showed that airfoil shaped fin could suppress separation in the flow, which could improve the pressure drop reduction with respect to S-shaped fins. Other geometries have been analysed in [Kimj10], with a longitudinal corrugation flow channel, and a modified fin structure to the previous work mentioned above is proposed in Xu et al. [Xu14], which enhances flow resistance reduction. Another important issue regards the heat exchangers in fusion applications is the tritium permeation. In [Oh08] a two dimensional finite element analysis is conducted to analyse this topic in PCHE for VHTR, assessing the effective thickness for tritium permeation. In [Fern12] permeation in a new design of compact heat exchanger for a fusion reactor using a DCLL blanket is analysed, showing that

when using silicon carbide as structural material the permeation is practically non-existent. This design is described and discussed below in this PhD thesis (Subsection 3.5.4)

### 3.4.5.3. Thermal specification of the DEMO1 reactor

Fig. 3 shows a sketch of the balance of plant for DEMO1 considered in WP13-DAS08-T02. Each of the three thermal sources -blanket (BNK), divertor (DIV) and vacuum vessel (VV)-delivers different amounts of thermal power at different range of temperatures using its own cooling medium. So, blanket is cooled by helium and divertor and vacuum vessel by water in separate cooling loops. As in any power cycle there is an amount of heat released to the sink, shown in Fig. 3 by a water loop with a cooling tower. Each cooling loop requires a circulating device (circulator for helium and pump for water) which demands a pumping power from the gross electricity ( $W_{gross}$ ) produced by the electric generator. Another electric consumption ( $W_{aux}$ ) is required for both auxiliaries and H&CD systems.

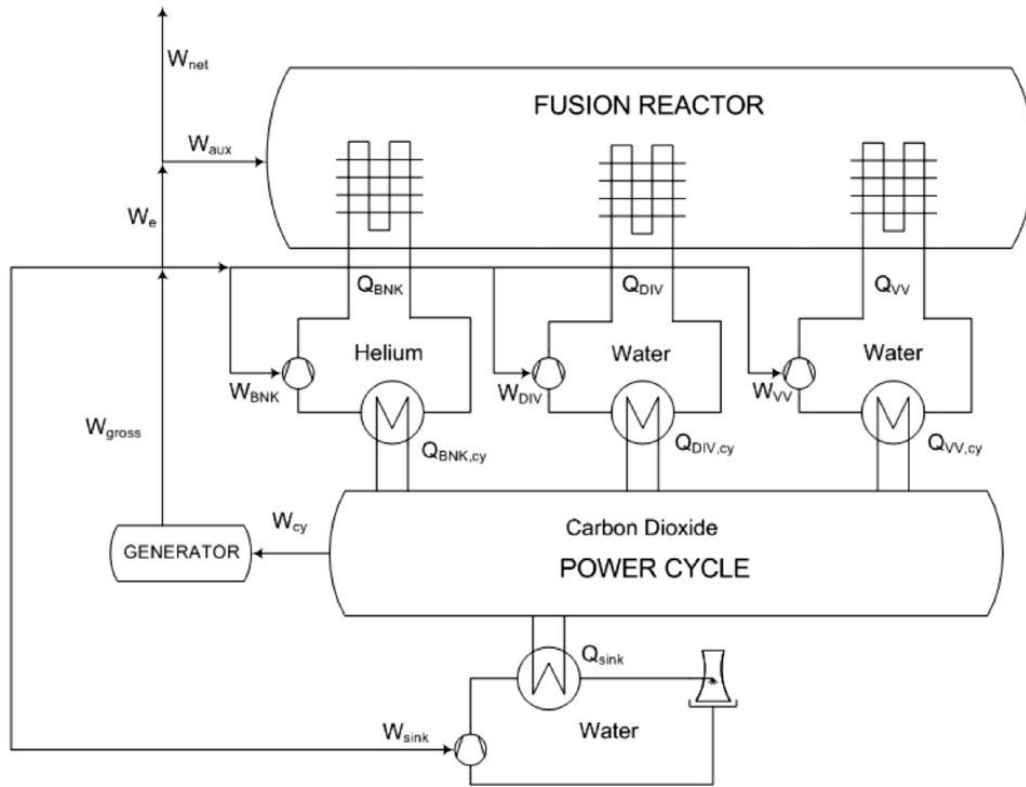


Fig. 3. Systems involved in the balance of plant.

The thermal specification used here is the same which appears in Table 5 regarding Rankine cycles (Subsection 3.4.4), including estimations for parasite power consumptions ( $W_{aux}$ ).

The thermal power given in Table 5 is the one absorbed by the cooling fluids in the reactor ( $Q_{BNK}$ ,  $Q_{DIV}$  and  $Q_{VV}$ ). To obtain the thermal power supplied to the power cycle ( $Q_{BNK,cy}$ ,  $Q_{DIV,cy}$  and  $Q_{VV,cy}$ ) is necessary to add the pumping power. Pump isentropic efficiencies have been set to 82% for the blanket (circulator) and 85% for the divertor and the vacuum vessel; pressure loss through the in-reactor heat removal has been assumed to be 1% [Por 12]. Regarding to the pumping power in the sink loop, the assumption given in Equation (5) has been done according to [Por 12]:

$$W_{sink} = Q_{sink} \cdot \left( \frac{200 \text{ kPa}}{4.18 \text{ kJ}/(\text{kg} \cdot \text{K}) \cdot 5 \text{ K} \cdot 1000 \text{ kg}/\text{m}^3} \right) \approx 0.96\% Q_{sink} \quad (5)$$

### 3.4.5.4. Methodology

The classical assessment in thermodynamic power cycles is focused on the First Law, where the efficiency of the cycle involves the mechanical power produced by the cycle ( $W_{cy}$  in Fig. 3) and the heat delivered by the thermal source to the cycle ( $Q_{x,cy}$  in Fig. 3, being 'X' BNK, DIV and/or VV, depending of the considered scenario) [Lin 11]. The present study also includes the pumping consumption in both thermal sources and sink, the efficiency of the electric generator and other parasitic consumptions devoted to maintain the plasma conditions. This type of assessment has been already performed by some authors in the steady-state operation of an SFR reactor [Perp 12] and by Floyd et al. [Flo 13] in the off-design. In both cases the heat transfer fluid in the thermal source was sodium, i.e., a liquid metal which is pumped (nearly incompressible). In the case of a fusion demonstration reactor or power plant with a HCLL blanket, the helium (compressible fluid) is responsible of the higher input of thermal power (more than 90% in Table 5) which demands a circulator to move it with a high electric demand (162 MW in Table 6). So, in feasibility studies of fusion power plants, a key issue is to take into account the pumping power. Another key issue is the consideration of auxiliaries and H&CD consumptions (185 MW in Table 5).

	Blanket	Divertor	Vacuum vessel
Heat from reactor, $Q_x$ (MW)	1835	149	34.56
Heat to cycle, $Q_{x,cy}$ (MW)	1997	149.1	34.67
Pumping consumption, $W_x$ (MW)	162	0.112	0.112
Reactor inlet temperature (°C)	300	150	95
Reactor inlet pressure (bar)	84.35	67	12
Reactor outlet temperature (°C)	500	250	105
Reactor outlet pressure (bar)	80	65	11
Pump/circulator inlet temperature (°C)	282.7	150	94.99
Pump/circulator inlet pressure (bar)	79.2	64.4	10.9

Table 6. Consumptions and state points at the cooling loops.

Fig. 3 shows the different powers produced by the balance of plant, from the cycle to the bus bar of power plant. So, the mechanical power produced by the cycle ( $W_{cy}$ : the turbine minus the compressors) is converted into gross electric power ( $W_{gross}$ ) by the electric generator through its generator efficiency (Equation 6), fixed at 97% according to [Por 12]:

$$\eta_g = \frac{W_{gross}}{W_{cy}} = 0.97 \quad (6)$$

The ratio of each power (cycle, gross, electric and net ones) to a reference input of heat defines the different efficiencies of the plant. In the case of cycle efficiency ( $\eta_{cy}$ ) only the heat of the thermal source supplied to the thermodynamic cycle is taken into account (the heat from the blanket,  $Q_{BNK,cy}$ , is always supplied to the cycle, but in some scenarios the heat from divertor,  $Q_{DIV,cy}$ , and/or the vacuum vessel,  $Q_{VV,cy}$ , are directly released to the sink). In other cases (gross efficiency,  $\eta_{gross}$ , electric efficiency,  $\eta_e$ , and net efficiency,  $\eta_{net}$ ) the reference heat is always the sum of the thermal power delivered by the reactor to each heat exchanger ( $Q_{BNK} + Q_{DIV} + Q_{VV}$ ).

Fig. 4 shows a classical S-CO<sub>2</sub> layout which takes heat from a unique thermal source, the blanket. This layout is the baseline case and is denoted as Layout 0. Using this layout it is assumed that the rest of the thermal sources release their heat power directly to the sink. S-CO<sub>2</sub> is basically a recuperative Brayton cycle where the working fluid operates always at supercritical pressure, being the lower pressure close to the critical one. This fact allows reducing the compression power due to the high density of CO<sub>2</sub> at the compressor inlet but also complicates the recuperators performance. So, at low temperatures (70-150°C), the CO<sub>2</sub> specific heat is substantially higher at high pressure than at low one, which would entail to an unbalanced heat

exchanger (the difference between the hot stream and the cold stream temperatures would not be constant) with the consequent reduction in effectiveness. This unbalance is overcome through splitting recuperation in two serial stages (Low Temperature Recuperator, LTR, for low temperature range and High Temperature Recuperator, HTR, for high temperature range), which allows that a fraction of the high pressure stream by-passes the LTR ('x' fraction in stream 6-9 in Fig. 4), introducing a new compressor (Auxiliary compressor) which compresses this by-pass 'x' fraction. The fraction 'x' is usually determined imposing the balance in the LTR heat exchanger (the same temperature difference at both extremes). This arrangement is the so called re-compression cycle (other arrangements to overcome the heat exchange drawback are feasible [Dos 09]).

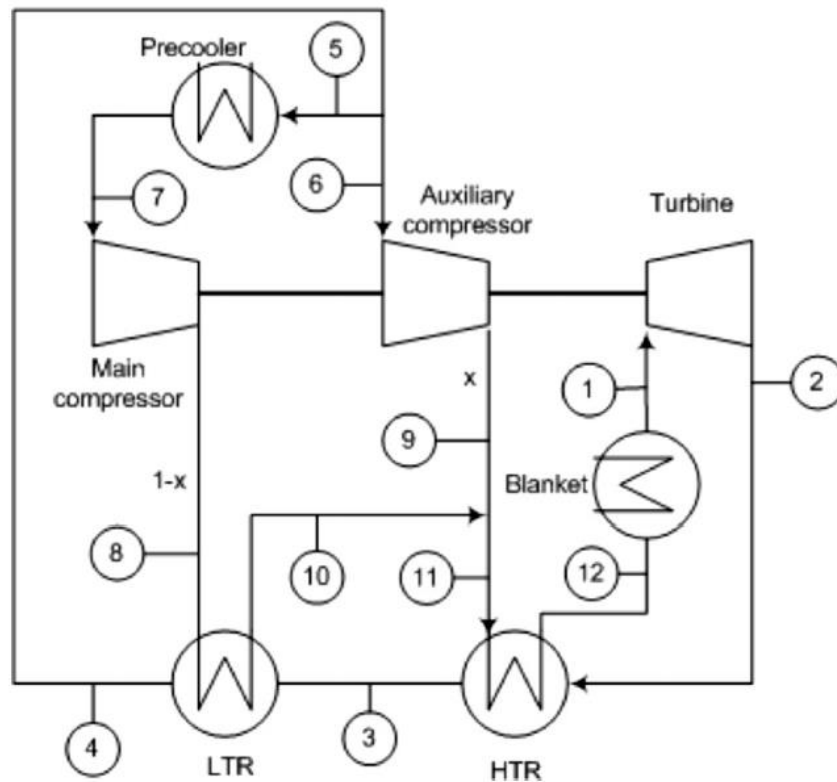


Fig. 4. Classical re-compression supercritical CO<sub>2</sub> Brayton cycle. This arrangement constitutes the Layout 0 (baseline case) in this work.

Another issue stemming from the CO<sub>2</sub> specific heat sharp changes at low temperature is that the minimum temperature difference between the two CO<sub>2</sub> streams (e.g. pinch point [Hes 01]) occurs inside the LTR (this issue can also occur in the precooler). This requires special attention when assessing LTR performance (a detailed Temperature vs. Heat Power transfer, T-Q, profile is needed for an accurate analysis). Fig. 5 shows the T-Q profiles on both recuperators of Layout 0. These have been obtained discretizing the heat exchangers and establishing an energy balance on each sub-heat exchanger. It is observed that the choice of the fraction by-passing the LTR ('x') allows achieving the balance of LTR, although the actual pinch point occurs inside the heat exchanger, being lower than the temperature difference achieved (another re-compression would be necessary) but as the values of the specific heat are nearly constant (temperatures are separated enough from the critical one) the temperature profiles are straight lines, suffering the hot stream (lower pressure, so lower specific heat) the highest temperature variation (at HTR both streams have the same mass flow rate).

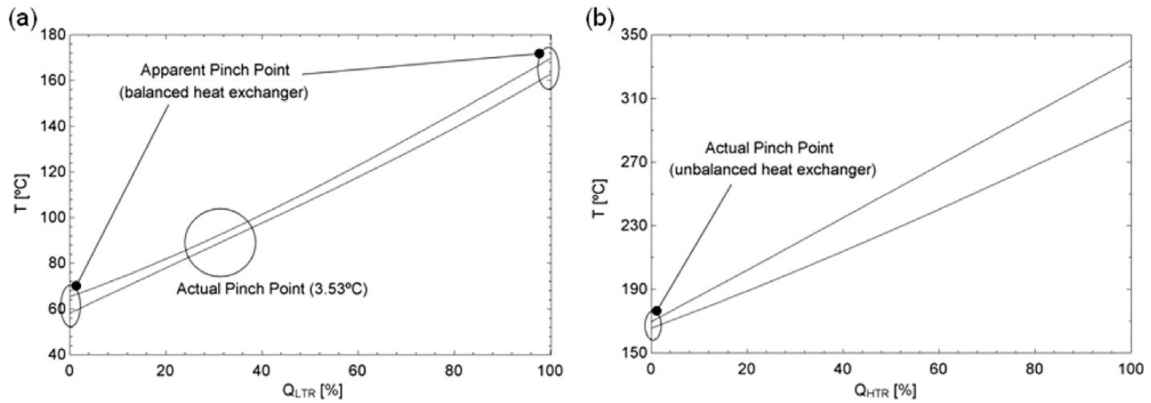


Fig. 5. Temperature vs. Heat Power exchanged at LTR (a) and HTR (b) in Layout 0.

As said above, the re-compression S-CO<sub>2</sub> power cycle has been chosen to explore its potential coupling to the HCLL DEMO reactor.

Some authors [Ish 08] analysed the convenience of the inclusion of the divertor as a thermal source. They investigated the reduction on cycle efficiency due to the low temperature of the divertor (no vacuum vessel was considered in [Ish 08]). Therefore, although the cycle efficiency decreases, the power produced by the cycle increases due to the higher power heat input. So, the analysis about the inclusion of divertor and vacuum vessel in the thermal sources, and even the study of their position in the layout to maximize the electricity production, has become a key issue. In this context, different scenarios have been considered beyond the baseline case named Layout 0 to accommodate the different thermal sources, hereafter named A, B, C and D (note that vacuum vessel is only included in scenarios C and D). Fig. 6 compiles all these layouts in a simplified manner and Table 7 shows the destination of the heat released by each thermal source in each layout. As noted, the blanket is always situated upstream the turbine, whereas the divertor and vacuum vessel locations depend on the scenario. The divertor is situated downstream the auxiliary compressor in Layout A, and by-passing the LTR in B, C and D. The vacuum vessel is upstream the divertor (at the same branch) in C and upstream the LTR in D.

At the main compressor, conditions of 85 bar and 30°C have been considered. The temperature is below the pseudo-critical point, but possible stability problems are prevented with the chosen pressure, far enough from the critical one to smooth the density-temperature curve as explained in [Moi 09]. Inlet auxiliary compressor pressure is 85.4 bar and the value at the LTR outlet is temperature dependent.

In all the layouts, except Layout A, CO<sub>2</sub> enters the turbine at 280 bar and around 447°C. This pressure matches the usual pressure ratio in S-CO<sub>2</sub> cycles (250/75) [Dos 04], with the low pressure set at 85 bar. McDonald [Mcd 14] chose 241 bar as a typical value for the inlet pressure in a steam turbine of a supercritical cycle for a fission power plant based on a combined cycle, using a VHTR reactor for topping cycle. Floyd et al. [Flo 13] stated 250 bar as a conservative value due to its compatibility with commercial pipes while Weitzel [Wei 11] fixed the present technology status (ultra-supercritical steam turbines) between 260 and 270 bar, being the limits (necessary to implement CO<sub>2</sub> capture technologies at reasonable costs of electricity) from 310 to 380 bar according to steam turbine manufacturers. So, 280 bar has been chosen as a compromise solution between well-established and medium-term technology, being closer to the former. Temperature is the maximum allowed for an acceptable value of the pinch point in the blanket heat exchanger. In Layout A, limitations from the divertor force to reduce the high pressure value to 230 bar and 417.8°C. In the literature about S-CO<sub>2</sub> cycle modelling there are well established ranges for adiabatic efficiencies of turbomachinery [Bah 12]. So, efficiency for compressors varies from 75% [Wri 10], passing by 87.5% [Cha 09] to 95.5% [Dos 04]. A value of 88% has been taken for this work. Regards to the turbine, the efficiency varies from 92.9% [Dos 04], passing by 93% [Wri 10] to 93.4% [Cha 09]. A value of 93% has been taken for the present study.

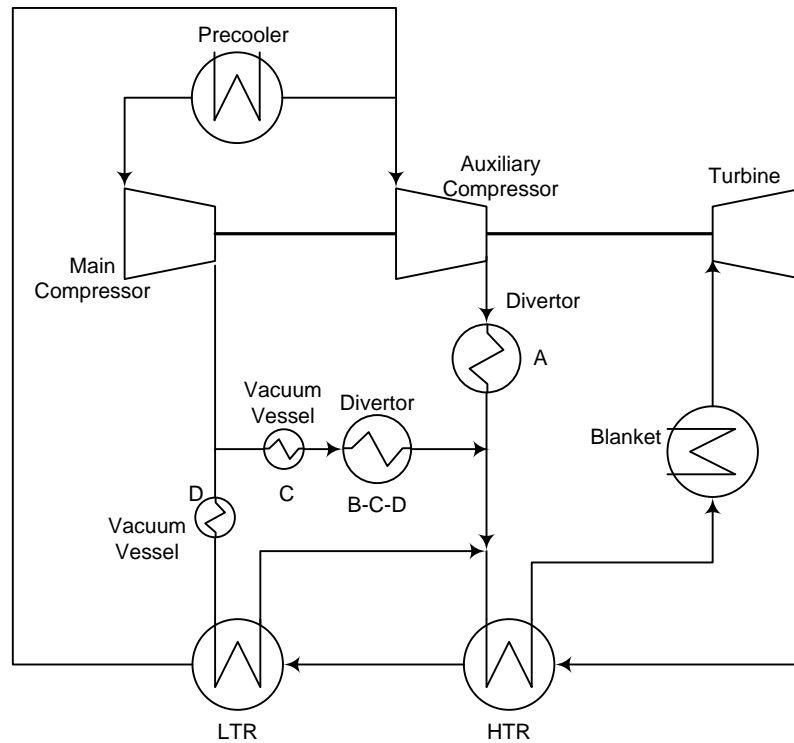


Fig. 6. Sketch of the different layouts considered.

Layout	Blanket	Divertor	Vacuum vessel
0	Power cycle	Sink	Sink
A	Power cycle	Power cycle	Sink
B	Power cycle	Power cycle	Sink
C	Power cycle	Power cycle	Power cycle
D	Power cycle	Power cycle	Power cycle

Table 7. Destination of the heat released by the thermal sources in each layout.

The entropy generation rate is used as a measurement of the internal irreversibility in the recuperators. In an adiabatic heat exchanger the general expression is given by Equation 7:

$$S_{gen.HX} = m_h \cdot (s_{ho} - s_{hi}) + m_c \cdot (s_{co} + s_{ci}) \quad (7)$$

where 'h' denotes hot stream, 'c' cold one, 'i' the input port and 'o' the output one.

In order to achieve high efficiency, low pinch points have been chosen. So, in all the cases but LTR, the range is set to 4-5°C. In LTR the minimum temperature difference (defined at the extremes of the heat exchanger) has been set to 7°C in order to achieve an actual pinch point inside the heat exchanger higher than 3°C. All these pinch point values are compatible with PCHE [Ish 08]. Pressure drops in the heat exchangers were assumed to be 40 kPa and no pressure loss is assumed along pipes and ducts [Med 07].

In all the scenarios, the heat exchangers have been discretized in sub-heat exchangers using suitable correlations [Ser 14]. Pressure drop and energy conservation equation are solved iteratively. At each time step, heat transfer coefficients are derived and, through the Log Mean Temperature Difference (LMTD) method [Hes 01], the heat exchanger length is estimated. In case the pressure drop condition is not satisfied, the number of channels is changed and the whole iterative process is initiated again. At the end of the calculation, the cross-section surface area and volume are calculated. Finally, it is verified that the number of channels and their

length per module ( $0.6 \times 0.6 \text{ m}^2$ ) do not exceed the current manufacturing capability (96000 and 1.5 m, respectively) [Ser 14].

### 3.4.5.5. Results

#### Comparison of layouts

Table 8 summarizes the electric power ( $W_e$ ) and efficiency ( $\eta_e$ ) achieved with the different layouts investigated. These parameters have been chosen because they take into account pumping consumption and leave out the auxiliaries consumption, whose power requirements are still highly uncertain at this stage of the DEMO reactor design.

Layout	Power (MW)	Efficiency (%)
0	650.1	32.20
A	662.6	32.82
B	677.6	33.57
C	684.0	33.89
D	675.8	33.48

Table 8. Electric power and efficiency with the investigated layouts.

The inclusion of the divertor in the BoP increases thermal efficiency between 2 and 4%, roughly, with respect to the basic Layout 0. The additional inclusion of the vacuum vessel entails a slightly higher improvement (between 4 and 5%, approximately). By comparing layout B (no vacuum vessel) with C and D, the significance of a right integration of thermal sources is noticeable: whereas including vacuum vessel even worsens the cycle thermal performance in case D, it is improved in case C, although in none of the cases the effect is too significant, as expected.

#### Selected layout

Table 8 highlights that layout C shows the best electrical performance and in Fig. 8 the T-s diagram of the cycle is represented, showing the state points Table 9.

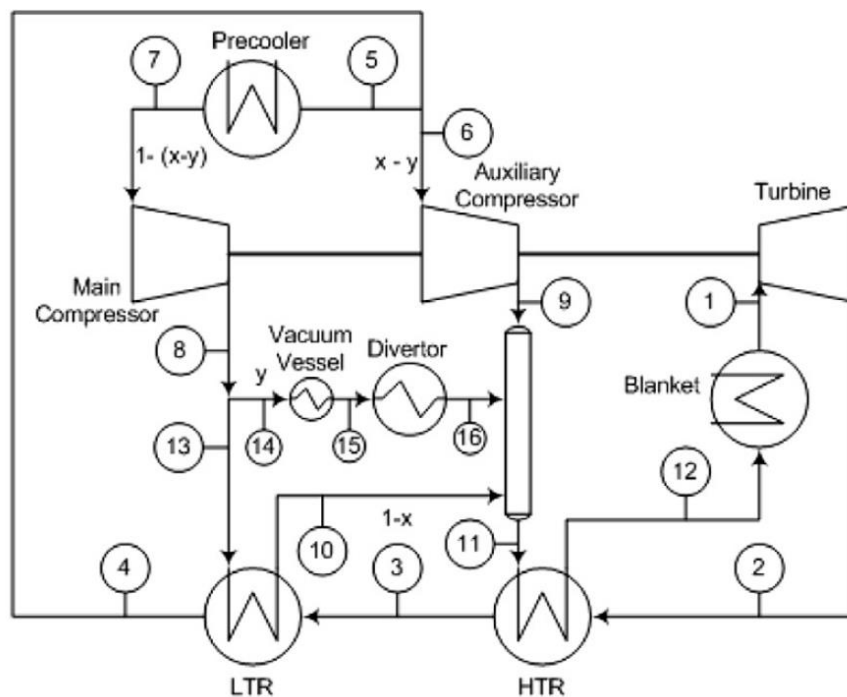


Fig. 7. Arrangement of components in the selected Layout C.

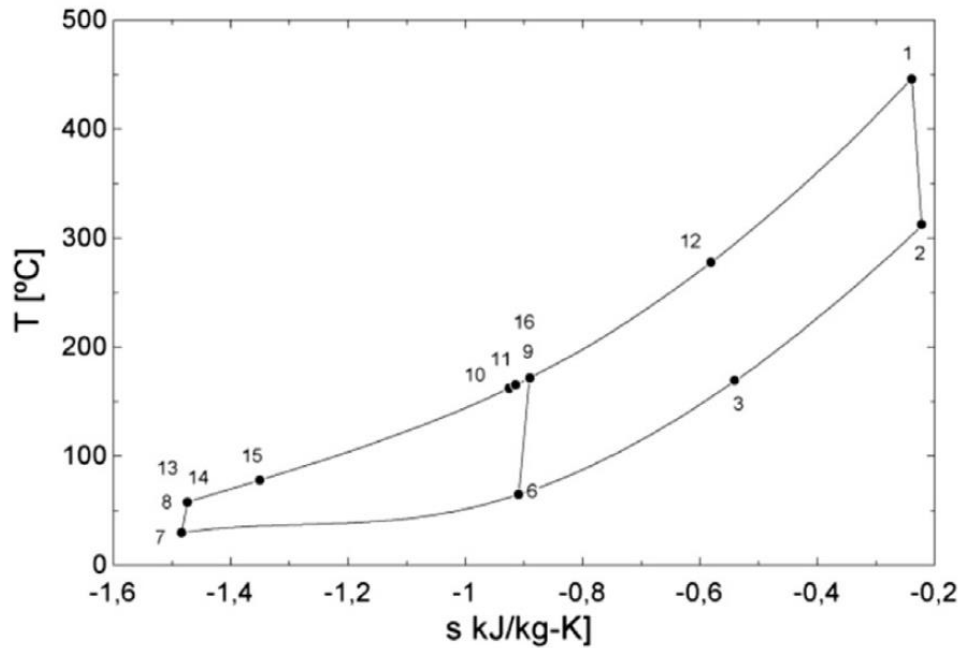


Fig. 8. T-s diagram at the design point (Layout C).

P (bar)	T (°C)	h (kJ/kg)	s (kJ/kg-K)	P (bar)	T (°C)	h (kJ/kg)	s (kJ/kg-K)
1	280.0	446.5	-0.2397	9	280.8	172.2	-0.8909
2	86.20	313.0	-0.2224	10	280.4	162.9	-0.9258
3	85.80	169.9	-0.5416	11	280.8	165.9	-0.9148
4	85.40	65.20	-0.9100	12	280.4	278.0	-0.5814
5	85.40	65.20	-0.9100	13	281.2	58.20	-1.4743
6	85.40	65.20	-0.9100	14	281.2	58.20	-1.4743
7	85	30.00	-1.4846	15	280.8	78.35	-1.3506
8	281.2	58.20	-1.4743	16	280.4	172.2	-0.8904

Table 9. State points of selected layout C (notation according to Fig. 7).

This means that when working in series with the divertor, the low flow rate (822 kg/s) of CO<sub>2</sub> heated up within the vacuum vessel heat exchanger makes the divertor more effective. As a result, the mixing of this stream and the one coming from the auxiliary compressor makes heat absorption at the HTR more efficient and also optimizes, to some extent, the thermal state of CO<sub>2</sub> at the inlet of the blanket.

Table 10 characterizes the turbomachinery performance. As expected, using CO<sub>2</sub> as the working fluid substantially reduces power consumption with respect to a classical Helium Brayton cycle. The apparently high value of power required by the auxiliary compressor, despite the low flow rate passing through (comparable to the main compressor one), is due to the higher temperature of the not-precooled CO<sub>2</sub> stream, which makes its density lower.

	Turbine	Main compressor	Auxiliary compressor
Mass flow rate (kg/s)	9271	7149	2122
Power (MW)	1238	202.9	149.9

Table 10. Performance of turbomachines in Layout C.

Table 11 compiles the heat exchangers performance and the pumping consumption. The power corresponding to blanket, divertor and vacuum vessel is the one entering the cycle (e.g. once circulator (He) or pump (water) consumptions are included). It is seen the effectiveness reaches two different set of values: higher than 93% in blanket, LTR and HTR, and lower than 95% in divertor and vacuum vessel. This fact is a consequence of the different pinch points in each of the heat exchangers (lower than 5°C in the former and higher than 26°C in the latter). So in the former group the pinch point has been set to a low value to achieve a high efficiency in the cycle, while in the latter one the pinch point is determined by the rest of imposed conditions, which avoid low values.

	Blanket	Divertor	Vacuum vessel	LTR	HTR	Sink
Power (MW)	1997	149.1	34.67	1316	1516	1296
Pinch point (°C)	4.7	71.65	26.65	3.5	4	5 <sup>a</sup>
Effectiveness (%)	97.87	58.27	43.04	93.73	97.28	-
Consumptions	162	0.112	0.112	-	-	12.4 <sup>b</sup>

<sup>a</sup> The pinch point is related to the precooler heat exchanger water/CO<sub>2</sub>

<sup>b</sup> The consumption is related to the pumping in the water loop

Table 11. Performance of the heat exchangers and pumping power consumption in Layout C.

Table 12 shows the size of all the heat exchangers used in Layout C together with their volumetric specific power. Divertor and vacuum vessel heat exchangers exhibit the highest volumetric specific power due to their high pinch point, whereas LTR has the lowest one as its pinch point is the smallest one. Blanket, precooler and HTR have similar specific power due to their similar pinch points and all of them are slightly unbalanced, although HTR requires more surface area, as both heat exchanger streams are CO<sub>2</sub> (in the other cases, water and He, which are better cooling fluids, flow through the primary side of the component).

	Frontal area (m <sup>2</sup> )	Length (m)	Volume (m <sup>3</sup> )	Specific power (MW/m <sup>3</sup> )
Blanket	64.35	1.53	98.4	20.29
Divertor	1.76	0.34	0.60	249.9
Vacuum vessel	1.96	0.16	0.31	111.6
LTR	141.5	4.26	603.2	2.18
HTR	101.3	1.48	149.8	10.1
Precooler	96.75	0.59	57.12	22.69

Table 12. Sizes of the heat exchangers at the design point.

Finally, Table 13 shows the detailed performance of Layout C. As observed, even though power cycles can reach reasonable values of thermal efficiencies and power, fusion reactors will face with two major drawbacks: the cooling power needed for blanket, divertor and vacuum vessel (gross to electric performances) and, no less important, the power demanded by all the reactor auxiliaries (electric to net performances).

	Cycle	Gross	Electric	Net
Power (MW)	885.2	858.7	684.0	499.0
Efficiency (%)	40.59	42.54	33.89	24.72

Table 13. Power and efficiencies in Layout C.

#### 3.4.5.6. Sensitivity analysis

A sensitivity analysis to explore which components affect the whole cycle configuration more strongly has been carried out. The studied variables have been: the heat exchanger size

(measured by the pinch point) and their pressure drop, also the turbine inlet pressure and the main compressor inlet temperature. In short, both heat exchangers and turbomachinery performance have been studied. The insights from this study might be valuable for cycle cost optimization.

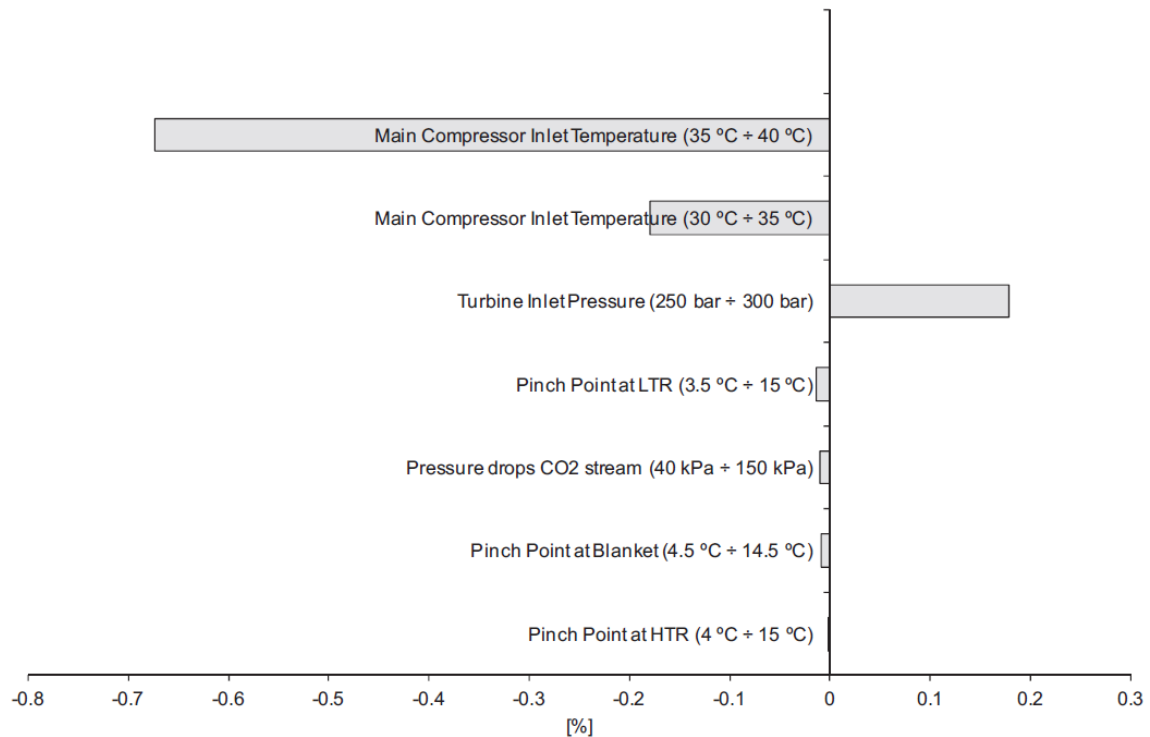


Fig. 9. Sensitivity of gross power to 1% of change in key variables.

Fig. 9 summarizes the influence of the chosen variables in gross power (e.g. no effect of pumping consumption is accounted for in the analysis) by means of the percentage variation of the gross power when each variable varies 1%. As noted in this figure, any need of pinch point increase might be compensated by raising the pressure at the turbine inlet or by reducing the inlet temperature at the main compressor. However, the latter is rejected because of the limitations imposed by the heat sink temperature.

The results indicate that the precooler is the most important heat exchanger. A high temperature at the inlet of the main compressor would burden gross power so substantially that precooler performance turns out to be instrumental for the cycle. Then, the second more important heat exchanger is the LTR, followed by the blanket. So it is necessary to set the pinch points as low as possible in order to maximize the power generation which entails to the choice of PCHE due to its excellent performance on high effectiveness (low pinch points) and relative compactness. From Fig. 9 it is also derived the low influence in the gross power of the pinch point at HTR. This result, apparently contrary to Sarkar's conclusions [Sar 09], who established that the HTR has more influence than the LTR in the efficiency of the cycle, can be better understood through a Second Law analysis.

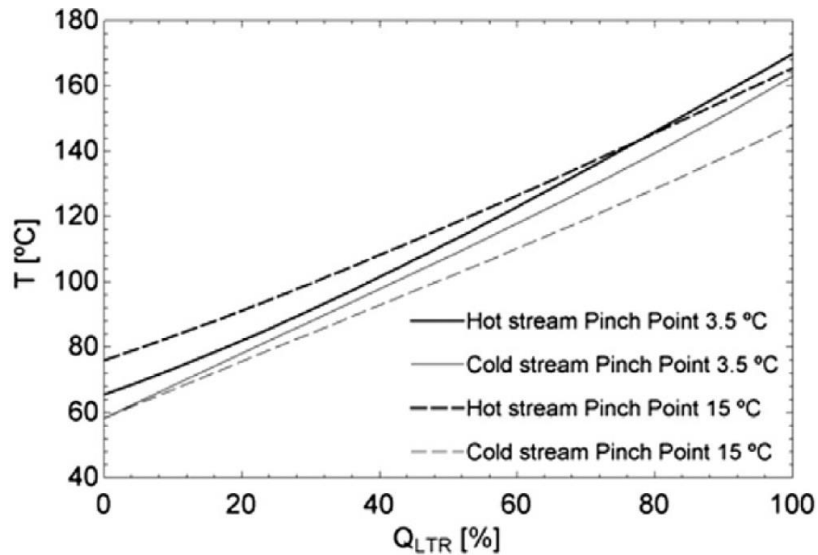


Fig. 10. T-Q profile at LTR.

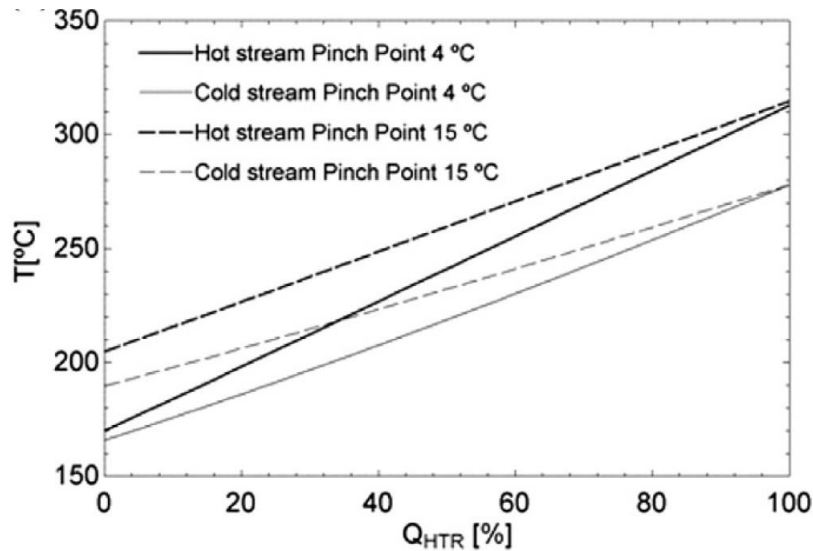


Fig. 11. T-Q profile at HTR.

Fig. 10 and Fig. 11 show the T-Q profile at LTR and HTR, respectively, depending on the pinch point considered. It is observed that the effect of increasing the pinch point is to increase the temperature difference of both streams. However, while at LTR this entails a nearly constant separation since this heat exchanger is designed to be balanced, at HTR the larger temperature difference reduces the level of unbalance of the heat exchanger, which makes gross power drop smaller. This behaviour is also revealed by the Second Law analysis shown in Fig. 12 and Fig. 13, which show higher irreversibilities at HTR than at LTR. However, the increase of the pinch point at LTR makes its irreversibilities in 239% while this is restricted to just 8.8% at HTR. On the other hand, the increase of the pinch point at HTR even reduces its irreversibilities in 6.7% while it would take the LTR to levels of around 36.4%. In short, the irreversibility in both recuperators rises to 47% when pinch point at LTR increases but only to 5.9% when is the HTR pinch point the one that increases. That is, at a given point of operation the HTR taxes more heavily the power output of the cycle than the LTR, due to its higher irreversibilities (as stated in [Sar 09]). However, the internal heat exchangers T-Q profiles make the sensitivity of the power output to the pinch point in both recuperators be much higher at LTR than at HTR.

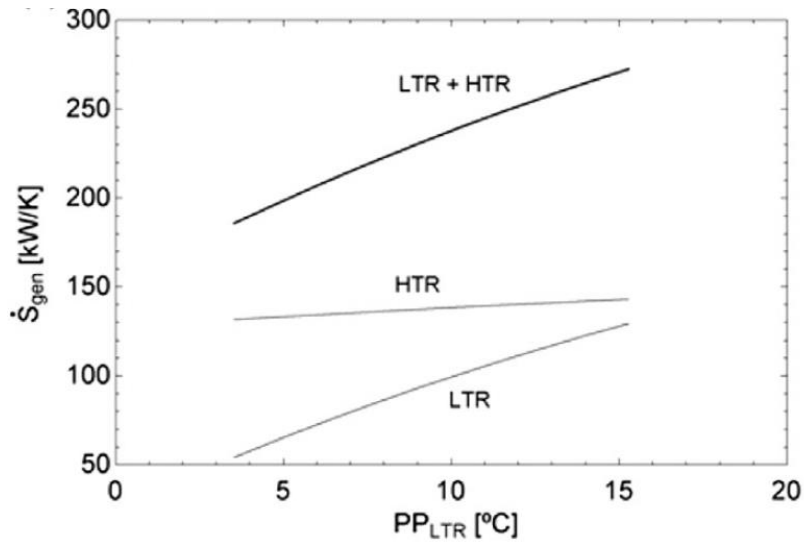


Fig. 12. Entropy generation at both recuperators depending on the pinch point at LTR.

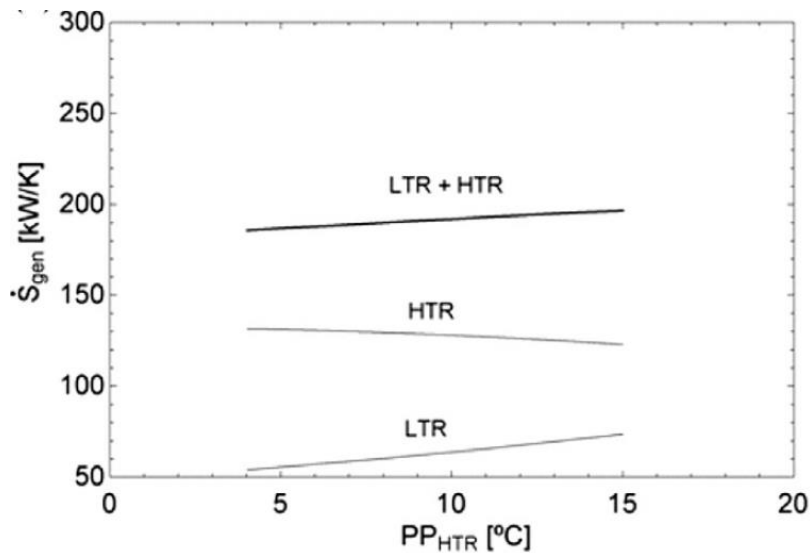


Fig. 13. Entropy generation at both recuperators depending on the pinch point at HTR.

Taking into account the results from the sensitivity analysis, Table 14 summarizes the parameters set of what has been called the Layout C-ECO. It may be noted that the main compressor inlet temperature has not been changed as it cannot be further reduced. All the pinch points have been increased (the highest increase has been set at the HTR because it hardly affects the cycle performance). Pressure drops have been also increased, so that the heat exchangers size can be reduced. And, finally the turbine inlet pressure has been increased to compensate the reduction in gross power due to the increment in pinch points.

Turbine inlet pressure (bar)	300
Main compressor inlet temperature (°C)	30
Pressure drops at CO <sub>2</sub> streams (kPa)	60
Pinch point at blanket (°C)	7.7
Pinch point at HTR (°C)	10
Pinch point at LTR (°C)	5

Table 14. Key parameters of Layout C-ECO scenario.

Table 15, Table 16 and Table 17 fully characterize this new layout C-ECO, as done above with all the other layouts explored. Table 15 gathers the performance in turbomachinery, with an increase of 1% in the turbine power and a 5% in the compressor consumption. Table 16 compiles the performance at the heat exchangers; all the effectiveness values fall except at divertor and vacuum vessel, as in these heat exchangers the pinch points were reduced as a consequence of the key parameter changes. Table 17 gives the size of the heat exchangers in the Layout C-ECO: whereas divertor and vacuum vessel increase slightly due to the reduction of their pinch points, the largest heat exchangers become smaller (19% at blanket, 32% at LTR, 57% at HTR); no significant change has been found in the precooler.

	Turbine	Main compressor	Auxiliary compressor
Mass flow rate (kg/s)	8911	6926	1985
Power (MW)	1250	216.0	155.4

Table 15. Performance of turbomachines in Layout C-ECO.

	Blanket	Divertor	Vacuum vessel	LTR	HTR	Sink
Power (MW)	1997	149.1	34.67	1494	1118	1302
Pinch point (°C)	7.7	65.55	22.79	5.64	10	5 <sup>a</sup>
Effectiveness (%)	96.56	60.93	48.85	93.82	91.68	-
Consumptions	162	0.112	0.112	-	-	12.5 <sup>b</sup>

<sup>a</sup> The pinch point is related to the precooler heat exchanger water/CO<sub>2</sub>

<sup>b</sup> The consumption is related to the pumping in the water loop

Table 16. Performance of the heat exchangers and pumping power consumption in Layout C-ECO.

	Frontal area (m <sup>2</sup> )	Length (m)	Volume (m <sup>3</sup> )	Specific power (MW/m <sup>3</sup> )
Blanket	58.95	1.35	79.8	25.02
Divertor	1.51	0.40	0.608	245.11
Vacuum vessel	2.09	0.18	0.372	93.27
LTR	108	3.78	408.4	3.69
HTR	64.57	0.98	64.57	17.25
Precooler	96.75	0.59	57.06	22.78

Table 17. Size of the heat exchangers at the economic point.

Finally, Table 18 summarizes the performance of Layout C-ECO. Compared to the original Layout C, a very slight decrease of electric efficiency charges the economic design and, in terms of net power, it hardly means a 1% reduction. Therefore, the C-ECO design would be the most promising configuration among those explored in this work, since despite having a minor effect on power cycle performance, it would mean a reduction of around 35% in the global volume of the heat exchangers, which would be likely worth.

	Cycle	Gross	Electric	Net
Power (MW)	878.86	852.49	677.77	492.8
Efficiency (%)	40.30	42.23	33.58	24.41

Table 18. Power and efficiencies in Layout C-ECO.

### **3.4.5.7. Conclusions**

Electric power and efficiency have been improved more than 5% from the baseline scenario (i.e. only blanket feeding the power cycle) matching in a proper way all the available thermal sources.

The configuration selected, with better output, is the one with vacuum vessel and divertor located in series in the bypass line of the LTR, after the main compression. This arrangement achieves 885.2 MW of cycle power and 40.6% of cycle efficiency.

The pumping power (in both thermal sources and sink) and the parasitic loads (auxiliaries + heating and current drive system consumptions) have been included in the performance assessment, entailing to high taxes due to helium is the main heat transfer fluid. So, the power produced by the electric generator is reduced a 20% after covering the pumping power and another 27% after feeding the demand for auxiliaries, heating and current drive, achieving a net efficiency of 24.7%.

On the other hand, the sensitivity study has identified the turbine inlet pressure and the main compressor inlet temperature as the key variables in the performance of the plant. Regarding the heat exchangers the pinch point at LTR and the overall pressure drop are the most influential variables. Their increase, according to their influence on electricity production, means a reduction of 1/3 of the overall volume of the heat exchangers. The turbine inlet pressure has been increased 20 bar to maintain the power losses below 1%.

Finally, as a general conclusion, the potential of S-CO<sub>2</sub> cycles as suitable converters of thermal energy to power has been demonstrated, as well as the suitable integration of all the thermal sources to maximize the electrical output. Furthermore, the key components of the layout have been identified, as a way to optimize the whole cycle performance, using a generic methodology that would be applicable to any other fusion reactor settings.

### **3.4.6. The issue of pulsed-operation**

In general, pulsed operation results in an energy generation penalty as the balance of plant system has to either run at a low efficiency off design condition or potentially be turned off completely during the dwell time. Power generation is also negatively impacted during the transitions between reduced and full power operation. In addition to this, consideration must also be given to the additional thermal cycling fatigue loads and other similar mechanisms acting over components and systems [Lat 12].

#### **3.4.6.1. Steam turbines**

If we look at the case from an operability perspective, we will see it could be particularly serious for a fusion demonstration reactor or power plant with a dwell time of 30-50 minutes, since the start-up or shutdown of a steam turbine typically takes between 10 and 30 minutes [Lat 12]. It would therefore be preferable to keep the turbine running on a low power setting throughout the dwell time if at all possible.

Start-up of steam turbines is closely linked to operation of the steam generator. In the case of a cold start, when the turbine has usually been shut down for a substantial period of time, the steam generator will usually have been turned off and must be restarted prior to turbine operation. In a hot start case, when it is expected that the turbine will not be off for very long, it is typical to continue generating steam and simply bypass the turbine sending the flow straight to the condenser until required again in the turbine. In this case, or if the steam flow through the turbine is being supplied extremely off condition, as could be necessary for a fusion reactor, the steam turbine will likely end up in a condition where a hot start of some type is required, particularly if the turbine is disconnected from the grid [Lat 13b].

In the event that one hot start is used up per every reactor cycle, the turbine life will be consumed substantially faster than a turbine operating in a steady state plant. Assuming an

operating profile of 4 hour on plus 1 hour off, and 90% of availability (1577 pulses/year), [Lat 13b] estimates the operational life of a steam turbine from the allowable number of hot starts (1500), resulting in approximately one year.

Thus, for a reliably operating fusion plant life of the steam turbine would become a key issue under the postulated scenario. A number of key systems of the turbine should be replaced, which would involve an outage of several weeks, which would dramatically impact the availability of the machine.

Both reliability and power supply continuity needs force to include a thermal energy storage system in the reactor balance of plant. The current proposal for EU DEMO studies consists on a separate closed loop using molten salt as coolant [Kov 13b]. This loop has cold and hot storage tanks and two heat exchangers; the first one serving the PHTS and the second one serving the power conversion system.

Within EFDA WP13-DAS08-T02, apart from the BoP studies for DEMO steady-state operation described in 3.4.4, KIT performed stationary and transient calculations of the proposed BoP configurations under pulsed operation, with the assumption of helium-cooled blanket and water steam Rankine cycle, as well as the mentioned thermal energy storage system. Pulses of 2 hours with 0.5 h as dwell time were also assumed, and all the thermal sources (blanket, divertor and vacuum vessel) were integrated in the cycle [Bub 13].

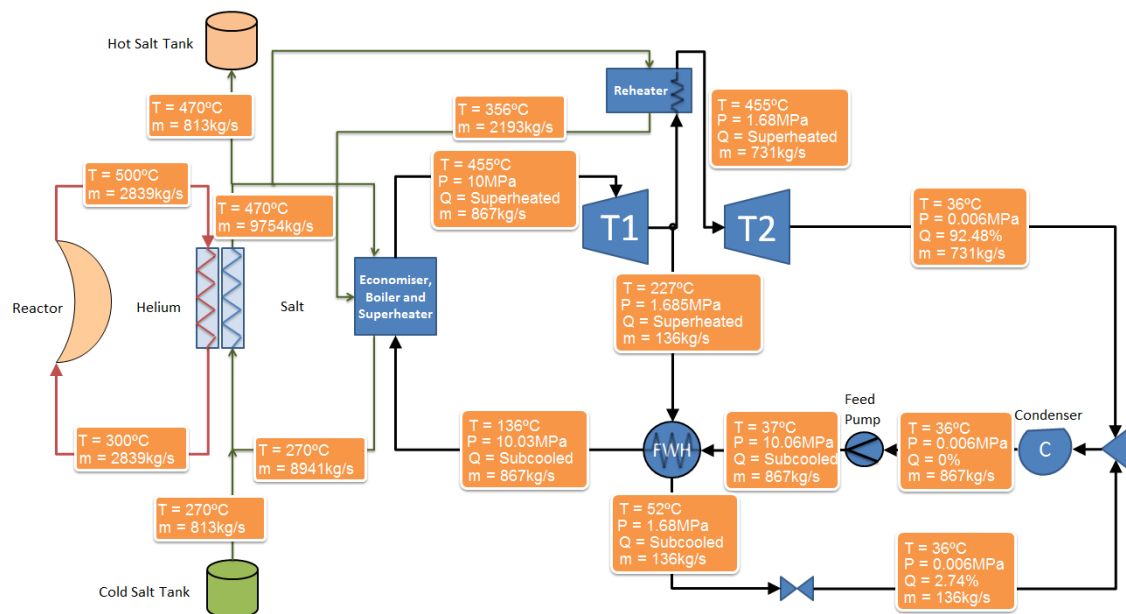


Fig. 14. Thermal energy storage system for a helium-cooled fusion cycle reactor with an intermediate molten salt loop and water steam Rankine as power conversion cycle [Kov 13b].

The stationary calculations only took into account the fraction of the operation time (~2 h) when plasma is being generated, without considering start-up and shutdown. As in the case of the steady state operation calculations, the cycle parameters were obtained for three different pressures at turbine inlet, although in this case they are lower (15.5, 33.5 and 58.5 bar) than the steady-state operation ones (65, 75 and 78 bar). The results showed a maximum gross electrical power of 675.011 MW (for the highest pressure at turbine inlet), which is 3.8% lower than the obtained for steady-state operation (701.682 MW). The cycle efficiency achieved a value of 25.6%, that is, 5.19% lower than the steady-state operation one (27.0%).

Finally, the transient calculations included the effect of start-up and shutdown. It was assumed that all coolant flowrates from the three existing heat sources (blanket, divertor and vessel) were being reduced down to zero during the shutdown period, and correspondingly all the temperatures of the coolants drop down: to 300 °C for the blanket, to 150 °C for the divertor and

to 95°C for the vessel. During that ~0.5 h time period, decay heat would be the only heat source keeping all these temperatures at the above specified values [Bub 13].

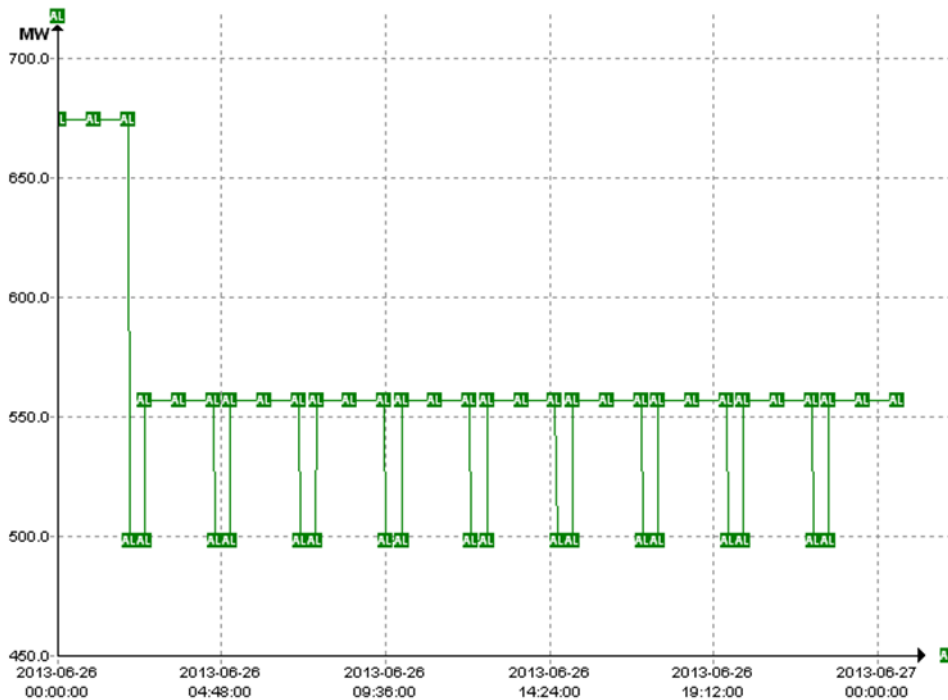


Fig. 15. Electric power generated during the pulsed operation of DEMO [Bub 13].

Results showed a maximum gross electrical power of 556.854 MW, which is 17.5% lower than the obtained in the static calculations. The maximum cycle efficiency was 19.7%, meaning a value 23% lower than the static calculations one.

In summary, pulsed generation significantly taxes both generated power and efficiency. It makes necessary to include a thermal storage system in the layout to continue producing steam during dwell, start-up and shutdown periods and running the steam turbine at a constant speed, so that electricity is continuously generated. However, the authors report usage of divertor and vacuum vessel thermal sources integrated in the power conversion cycle resulted in power fluctuations of 47-58 MW in the generated electrical power [Bub 13], as shown in Fig. 15. This could involve a problem in the connexion of the electric generator to the grid, so Bubelis et al. suggested the integration of these thermal sources should be discarded or organized in a different way.

#### 3.4.6.2. S-CO<sub>2</sub> turbines

Gas turbines are typically much quicker than steam turbines. In the particular case of supercritical CO<sub>2</sub> Brayton cycles, the lower thermal mass makes start-up and load change faster for frequent start-up/shut down operations and load adaption [Tur 13]. Sandia National Laboratories [Wri 11] has tested cold start-up processes in an experimental supercritical CO<sub>2</sub> Brayton cycle power system with start-up times compatible with the operational concept considered in DEMO BoP studies for 2 h pulses [Bub 13]. In concentrated solar plants, where important R+D activities on S-CO<sub>2</sub> power conversion systems are being developed, as commented in 3.4.5.2, Iverson et al. studied the behaviour of a PCS where thermal input to the cycle was cut by 50% and 100% for short durations. They showed that despite these fluctuations, the thermal mass in the system effectively enabled the Brayton cycle to continue to run for short periods until the thermal input could recover [Ive 13], even without an energy storage system. Finally, efforts are being also made in improving the design of turbomachinery components in terms of reliability and life cycle. For example, GE Global Research in collaboration with Southwest Research Institute is working on development of a S-CO<sub>2</sub> turbo-

expander for application to a S-CO<sub>2</sub> based power cycle for concentrated solar power (CSP) conversion [Kal 14] with a low-cycle fatigue life >10000 start and shutdown cycles.

## **3.5. TecnoFus Programme**

### **3.5.1. Introduction**

TecnoFus was an R&D programme financed by the Spanish Government (by means of a CONSOLIDER INGENIO 2010 grant) oriented towards the development of technologies associated with the breeding blanket as key component of future fusion power plants, taking as baseline the Dual Coolant Lithium Lead (DCLL) concept. 10 Spanish institutions, coordinated by CIEMAT, worked during five years (2009-2013) in different fields like neutronics, magnetohydrodynamics, basic studies on lithium lead eutectic alloy, development and characterization of structural materials similar to EUROFER, synthesis of SiC internal coatings, power conversion system and overall reactor design.

One of the main objectives of TecnoFus was generating a Spanish programme in fusion technology, based on young researchers training and mobilization of groups who had never before worked for fusion but had excellent capabilities in other areas. As a consequence of this Programme, the Spanish position on international programmes on breeding blanket technologies and other related fusion technology fields has been consolidated, from which national industry has been also benefited. Furthermore, CIEMAT coordinates at present the design activities of the DCLL breeding blanket within the EUROfusion H2020 Programme.

### **3.5.2. Brief summary of TecnoFus achievements**

#### **3.5.2.1. Integrated design**

The main characteristics of the DCLL breeding blanket have been already briefly commented in Section 3.3.

The blanket design developed in TecnoFus follows the high temperature DCLL concept proposed for the ARIES-ST reactor in 1997, where SiC<sub>f</sub>/SiC had been planned as functional material for the flow channel inserts (FCI) which would allow obtaining a PbLi outlet temperature of 700°C, therefore making easier the implementation of Brayton cycles for the power conversion system to achieve a thermal efficiency around 45%. RAFM steel is used as structural material, which is cooled by high pressure helium (8 MPa).

The approach followed for this task has been based on the generation of most of the whole reactor design with different detail level for the different components or systems (vacuum vessel, cryostat, divertor, magnet system, contention building, remote handling system, etc.), including a highly detailed design of a DCLL outboard blanket segment. Some of the designs, in particular those of systems which did not play a role in the blanket system, were made at a very preliminary level. CATIA has been used as main CAD tool.

The initial geometry was chosen following the Model C of the EU Power Plant Conceptual Study [Mai 05] and a segmentation of 12 sectors with 4 sets of auxiliary blanket systems. Each sector of the vacuum vessel includes a large upper port to allow vertical maintenance of the blanket. Each sector also includes 3 outboard and 2 inboard blanket segments with the so called 'banana' shape; that is, the segment is not subdivided in modules and follows the shape of the plasma in both outboard and inboard regions. There are two parallel circuits in toroidal direction. Each of them consists of two long ducts with rectangular cross-section which go through the segment in poloidal direction. First, the PbLi enters at the top of the segment and goes down along the back duct. Then it turns and goes up along the front side (plasma side) duct to the top of the segment, where is also located the outlet pipe. This configuration minimizes the risk of reverse flows due to flotation forces, since volumetric heat deposition is much higher in the channels situated close to the plasma, where the flow direction is upwards. Another advantage

of this configuration is the minimization of heat transfer from the main coolant (PbLi) to the minor one (helium).

The banana-shape design involves bigger challenges in e.g. manufacturing and thermomechanical behaviour with respect to the Multi-Module Segment option currently used in the EUROfusion Programme, but also has a number of advantages, like better use of the available volume and simpler path of the liquid metal stream.

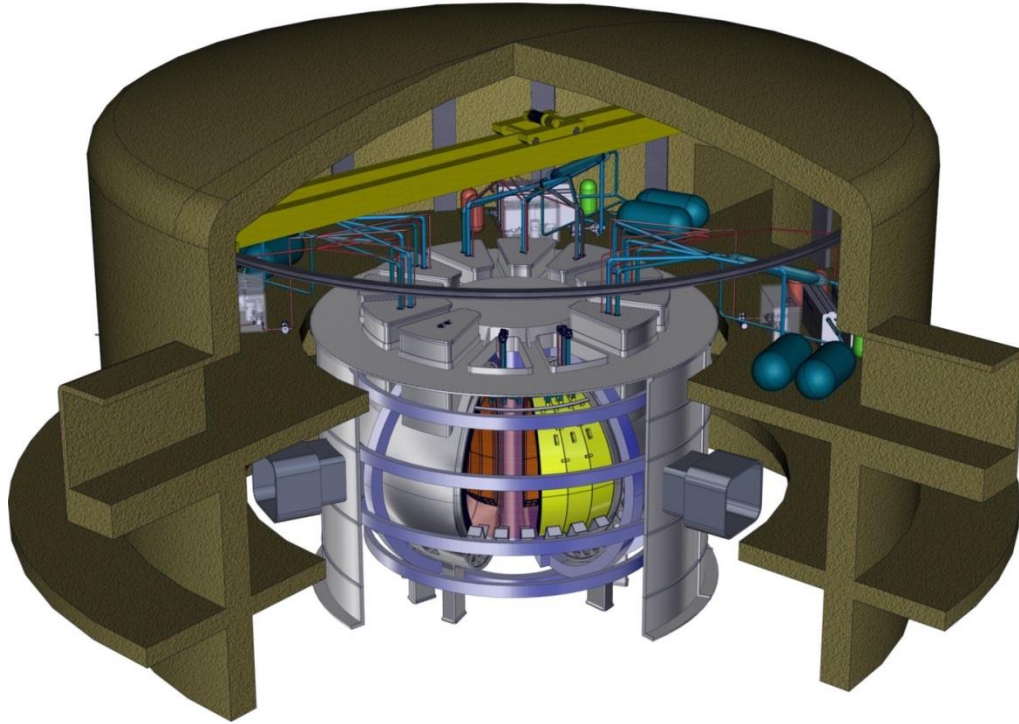


Fig. 16. Reactor general view.

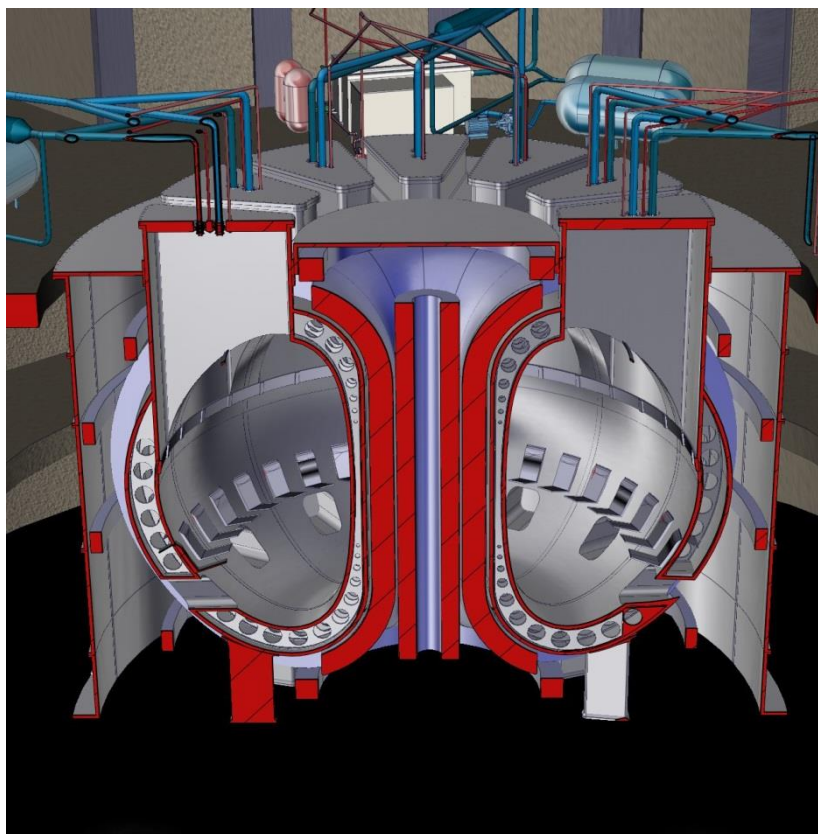


Fig. 17. Vacuum vessel and cryostat (toroidal cut).

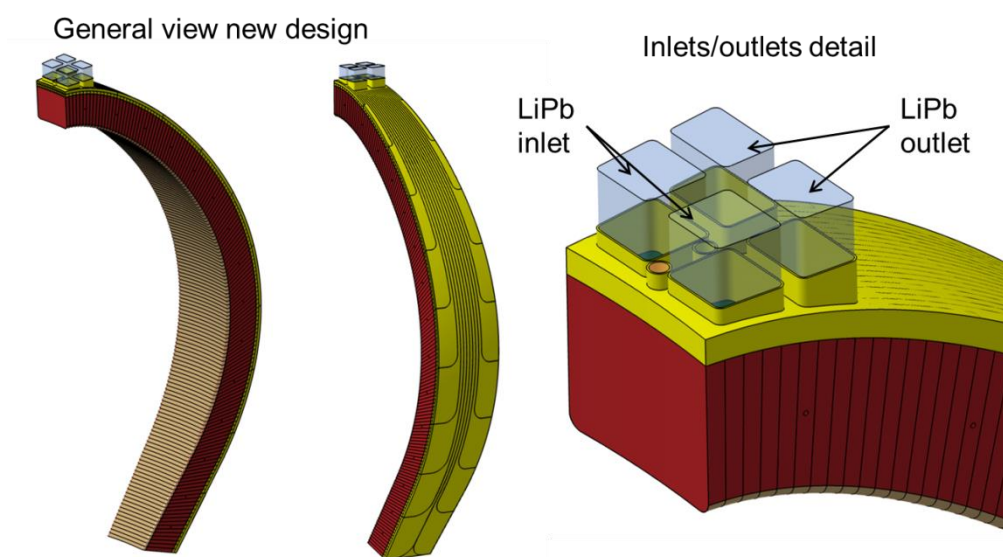


Fig. 18. General view of an outboard blanket segment. Detail of PbLi inlet & outlet.

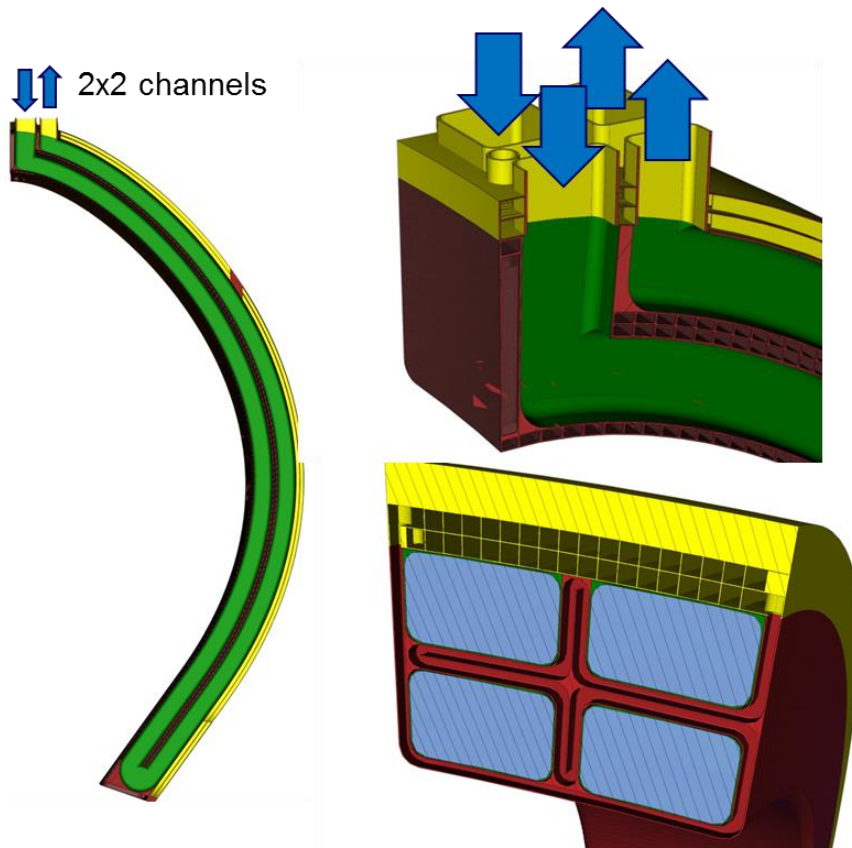


Fig. 19. PbLi channels and FCI (green). Helium distribution channels in the shielding module.

Taking into account the required shape of the PbLi channels to obtain a continuous flow along the whole segment length, the geometry of the structure which envelops the PbLi channels (defined by the flow channel inserts) is complex. Furthermore, the layout with two parallel circuits, each with two poloidal channels, complicates the cooling of all the parts of the structure. These features force to assume a topology which avoids large pressure drops in manifolds, as a consequence of the need of successive flow path divisions. This issue is solved using a double circuit plate situated at the back side of the segment which acts as distributor and collector, and welded cross-shape steel plates. This plate is also used to shield the vacuum vessel and the coils, so that the neutrons flux is maintained within the design values. On its external part it includes the He and PbLi inlet-outlet pipe connections, the supporting elements to couple to the VV and the elements for the extraction of the module by means of the remote maintenance system.

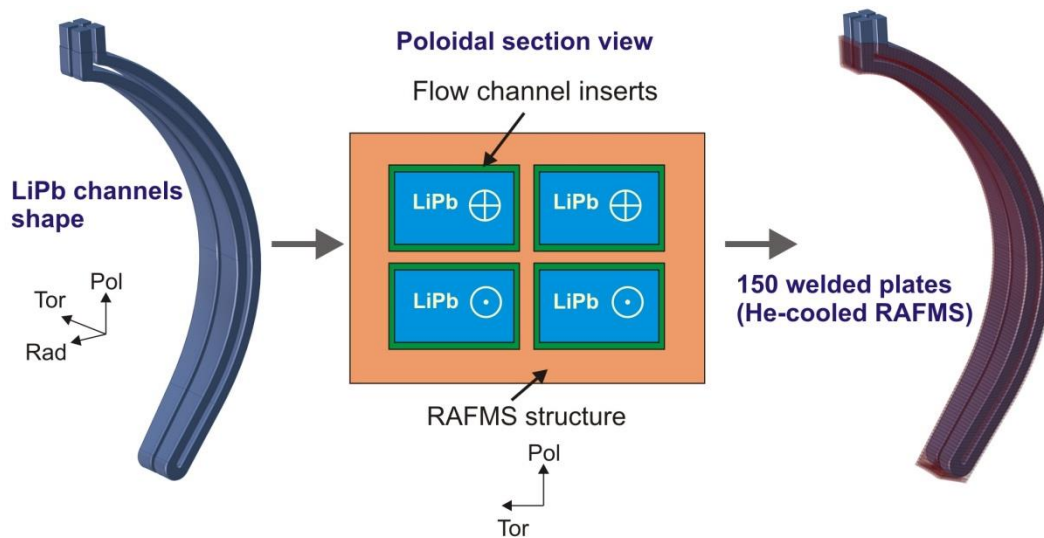


Fig. 20. Design of the structure from the PbLi channels shape [San 13].

The complete helium circuit layout is explained in Fig. 21. Helium goes into the shielding plate through a pipe located at the top. The shield is divided in two different levels along the radial direction. Helium goes down along the back level and the shield internal channels divide the flow and carry it to the channels located at the left and right sides. Then helium goes into the cross-shape plates and goes through their internal circuit, in a way that each plate is in counterflow with respect to the adjacent ones.

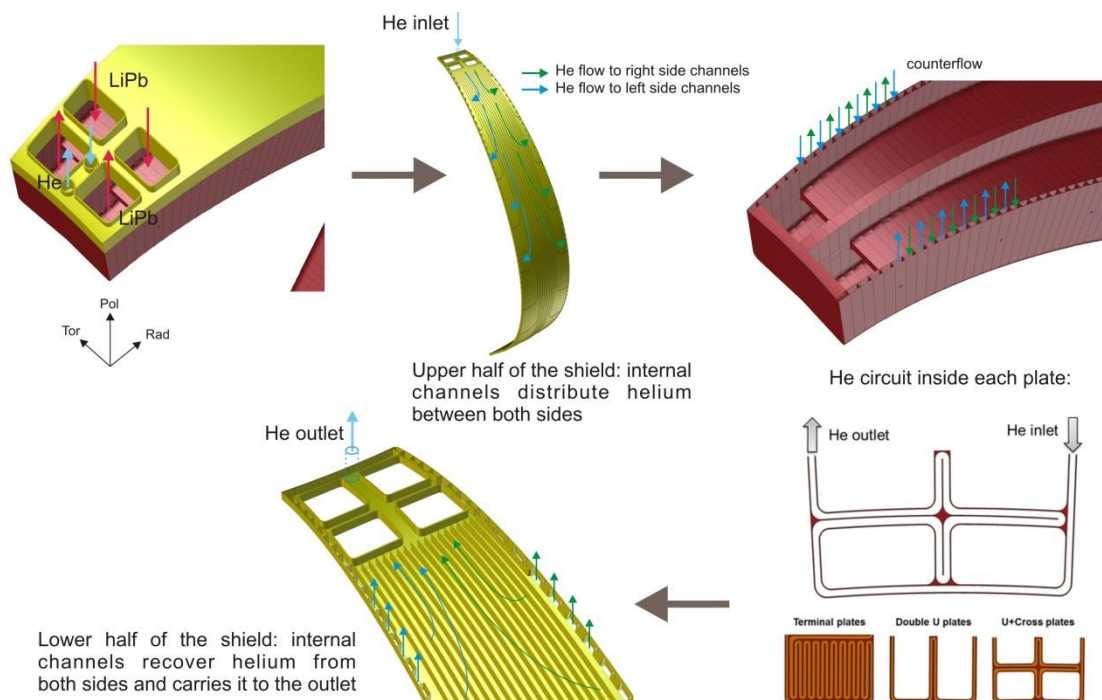


Fig. 21. Helium circuit layout [San 13].

When helium leaves the cross-shape plates goes into the front level of the shield and then goes up (lead by the internal channels) to finally reach the outlet pipe, also located at the top of the shield.

Apart from the mentioned in-vessel components, the reactor CAD design also includes ex-vessel components and systems as pipe manifolds for He and PbLi circuits (made with double-wall tube to minimize tritium losses), part of the helium and PbLi loops (heat exchangers,

coolant purification system, tritium extraction system, tanks, expansion volumes, etc.) and the pumping system.

### 3.5.2.2. *Neutronics*

A number of important 'response functions' were determined for the designs created by the CAD group: power deposition in the blanket (amplification factor), tritium breeding ratio (TBR), neutron damage calculation in the structural material (dpa, gas production, H and He), radiation loads in the superconductor coils, waste generation and activation & shutdown radiation levels.

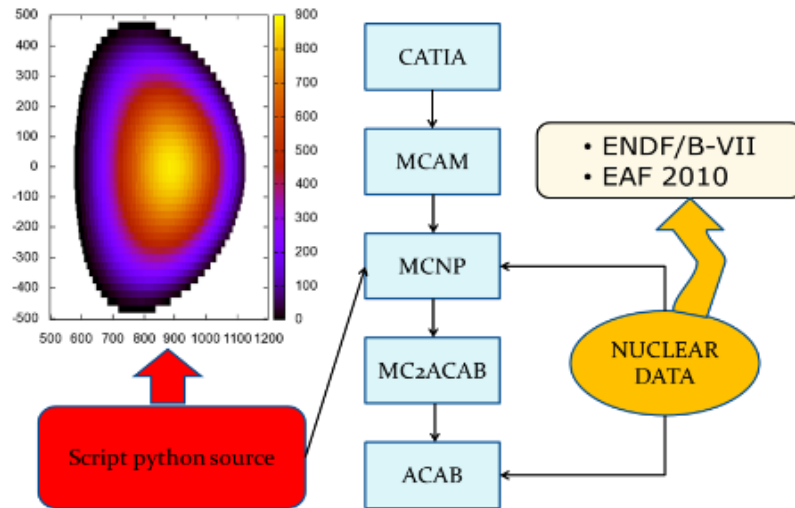


Fig. 22. Flowchart of the methodology followed in this activity [San 13].

A tool named MCAM was used by the CIEMAT-UNED team as translator between the CAD geometry generated in CATIA and the neutron transport code MCNP. The level of detail of the geometry models was increased along the activity. Moreover, the different models were iteratively modified using a CATIA macro that links the CAD models with the MCAM interface.

Once the main response functions (TBR, power deposition, etc.) were analysed and the critical issues stressed, the work focused on other key issues. For example, the radiation shielding of the toroidal field coils was optimized, and the analyses showed the best design option is dividing the shield in two parts: one that must be removed with the blanket due to neutron damage (Hot Temperature Shield or HTS) and other that can be stay inside the blanket during its whole lifetime (Low Temperature Shield or LTS) [San 13].

On the other hand, activation calculations were performed with the ACAB code, assuming an irradiation scenario of 5 full power years for the maximum neutron fluence rate in the equatorial breeding zone. The results in terms of specific activity, surface gamma dose rate and committed effective dose (CED) due to inhalation at different times were used to choose the potentially more hazardous radionuclides. The dispersion of the selected radionuclides was modelled with the HotSpot code using the gaussian plume model and two different atmospheric conditions. According to the results, fulfilling the dose requirement for no evacuation would permit to release up to 40 kg of activated PbLi, without taking into account the possible isotopic purification and detritiation systems [San 13].

### 3.5.2.3. *Thermomechanics*

Results from FEM analyses (made with a code developed by CIMNE) show the dual coolant system is an efficient way to preserve acceptable temperature levels in the RAFM structure of the outboard blanket segments. Simplified geometry models have been used (Fig. 24).

The first wall is the critical part because of the high thermal flux from the plasma. As expected, the helium circuit evacuates the thermal energy coming from the surface heat flux, whereas the PbLi cooling system is mainly used to extract the volumetric thermal energy deposited by neutrons.

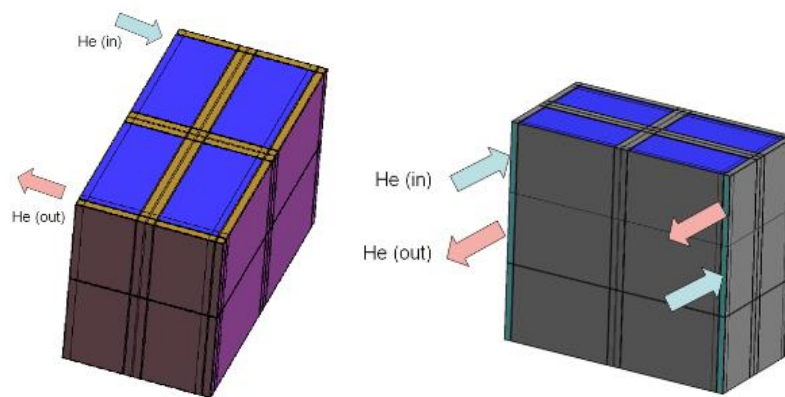


Fig. 23. Single He cooling circuit (left) and double He cooling circuit (right) for 3D analysis.

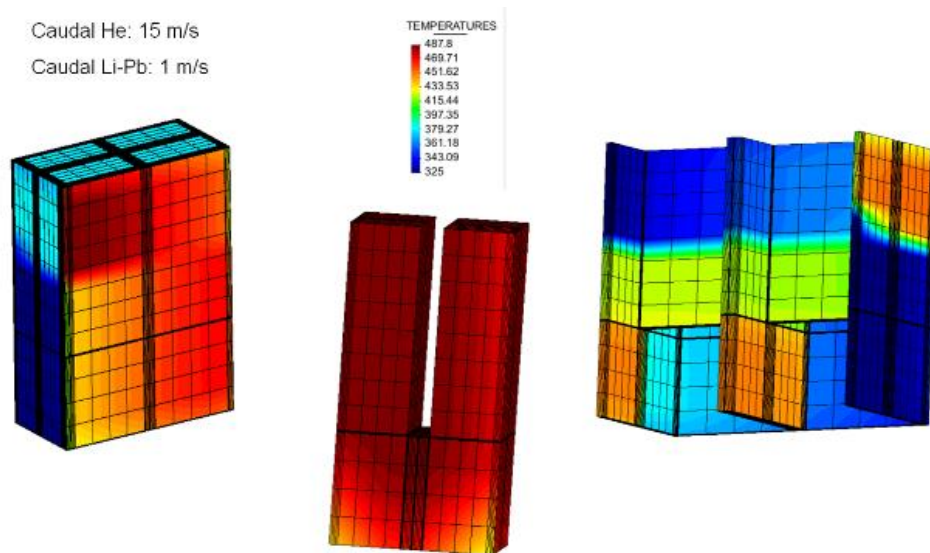


Fig. 24. Temperature map using 15 m/s as helium inlet velocity and 1 m/s as PbLi inlet velocity.

Calculations show the single helium circuit design leads to unacceptable temperature values in the first wall, in the order of 850°C; even increasing the He velocity does not help, as the temperatures stabilize for velocities above 8 m/s. The use of a double circulation of He in the RAFM structure (switching alternatively inflow and outflow) (Fig. 23, right) allows a better temperature distribution, averaging the hotter temperatures at the outflow with the cooler inflow temperature of the He. With the considered boundary conditions, it is possible to maintain temperature below 500°C in the entire structure domain [San 13].

#### 3.5.2.4. Thermal-hydraulics and magnetohydrodynamics

The UPC team developed a nucleation, growth and transport model for helium bubbles in liquid metal flows, as well as a tritium transport model in a multi-material system. These models were implemented in OpenFOAM.

Zero dimensional sensitivity calculations pointed out that the helium transport model is quite sensitive to He solubility and diffusivity in PbLi, along with the surface tension and the volume occupied by a He atom in a stable cluster. Since a large uncertainty rests on the knowledge of these parameters, it was concluded that experimental measures and molecular dynamics simulations were necessary to improve and validate the model [San 13].

The tritium transport model was coupled with the helium nucleation, growth and transport models. Results show that tritium partial pressure inside the bubbles is homogeneous, diffusive tritium transport is 1D except in the near-bubble region or bubble boundary layer, the boundary layer depth is about twice the bubble radius, and tritium mainly by-passes the bubble. Additionally, two tritium transport models were developed in order to deal with coarse meshes. A first model considers all the observations of fine mesh results and, hence, predicts accurately both the total tritium flux and the tritium partial pressure in the bubbles for all studied cases. A second and simplified model has been proposed in order to further reduce the computational cost. This simplified model presents acceptable accuracy in the total tritium flux estimation and captures the order of magnitude of the tritium partial pressure in the bubble, despite providing less accurate results [San 13].

On the other hand, a new algorithm for magneto-convective flows, with coupling of Navier-Stokes equations with Maxwell and energy equations has been developed and implemented in OpenFOAM. After defining the recommended algorithm for PbLi flows in breeding blanket channels (inductionless MHD equations implemented following a PISO-like algorithm), it has been further extended to account for fluid-solid coupling. The capabilities of the code have been also extended towards (1) the thermal coupling of the MHD modelling, based on the Boussinesq hypothesis, and (2) the transport modelling of a passive scalar, i.e. tritium [San 13].

After the full implementation and validation of the code, and after gaining some know-how on the code performance and capabilities for real design simulations, it has been applied on the prediction of the thermally coupled MHD flow inside the TecnoFus breeding blanket design. Due to the very large dimensions of the blanket along the poloidal direction (about 9 m) and considering the very extreme flow conditions (very high velocity, high magnetic field and thermal load), the 3D simulation of the entire blanket become unaffordable with the available computational resources. To overcome this issue, the MHD model was adapted to simulate 3D flows in a 2D mesh, perpendicular to the magnetic field, and accounting for the 3D features in an extra term in momentum equation. This approach allowed optimizing the flow rate and FCI thickness and thermal properties in order to maximize the thermal gain, keep the maximum EUROFER temperature below 550°C and minimize thermal stresses. It also allowed changing the liquid metal flow path, since in the original proposed it as downwards close to the first wall, allowing the possibility of reverse flows and increasing the thermal losses along the back channel. If the PbLi enters the blanket at the backward channel, the power extraction is increased by a factor of 6 [San 13].

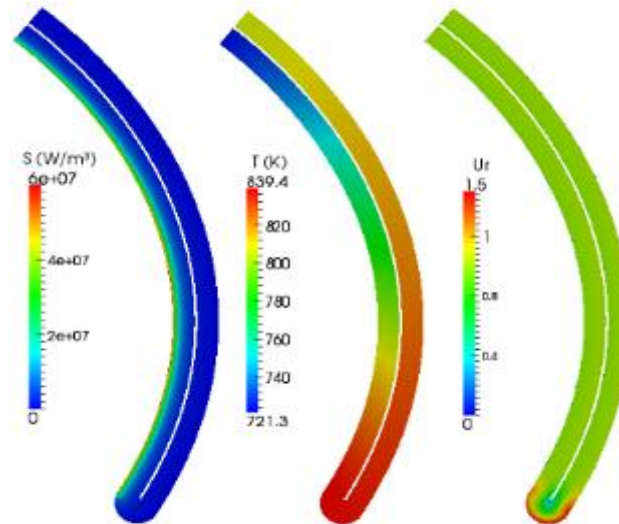


Fig. 25. Temperature ( $T$ ) and velocity ( $U_r$ ) map in the PbLi channels for the given distribution of volumetric heat deposition ( $S$ ) [San 13].

Within this task, the UPM-IFN team worked in modelling eutectic PbLi at the atomic scale in liquid phase in a wide range of concentrations, with the aim of providing a good description of the complex phenomenology and properties of the PbLi alloy. Embedded Atom Method (EAM) potentials were used and molecular dynamics simulations have been carried out using the LAMMPS code [San 13].

#### 3.5.2.5. Production and characterization of breeding blanket functional and structural materials

The ITMA-CIEMAT team worked in the production at laboratory scale of a RAFM steel, named ASTURFER, which fulfils the specification of the European reference EUROFER97. First, ITMA settled the demanding compositional requirements. Later, the process of fusion in induction furnace under protecting atmosphere was designed, elaborated and optimized. Finally the thermal treatment was applied in order to achieve the desired microstructure and the reference mechanical properties. Additional studies on thermal treatments for tenderizing, deformation in cold, thermal treatments of recrystallization and welding processes were carried out [San 13].

CIEMAT characterized 2 heats of ASTURFER alloy by testing small specimens. Microstructural examinations by optical microscope, SEM/EBSD, TEM and x-ray diffraction, as well as mechanical characterization by tensile, impact, creep and small punch tests were carried out.

Both heats showed similar tensile behaviour as EUROFER97-2, but some differences on the impact behaviour were observed, mainly due to the presence of Al-Ta oxide particles in one of the heats, and solved for the future heats production. Other relevant findings were the influence of the hot rolling temperature on the tensile and Charpy properties and the importance of the oxygen control to improve the impact properties of RAFM steels [San 13].

On the other hand, CIEMAT and UPM produced and characterized several ingots of eutectic PbLi. The obtained alloys were analysed by Differential Scanning Calorimetric (DSC) to determine the enthalpy and the transformation temperature. These studies allowed identifying the optimum process conditions involving selection of type of furnace, times, melting temperatures and composition of protective salts. Such conditions consist on the use of mixture of salt (30 mol% KCl – 70 mol% LiCl) in the presence of Ar BIP at a temperature of 450°C during 5 minutes in a crucible of SiC [San 13].

Besides, CIEMAT reviewed the existing isotope separation technologies in order to know their potential use in the production of  $^6\text{Li}$  enriched lithium for fusion breeding blankets. Among them, only two techniques appear scalable according to identified coming demands of Li batteries (the isotopic effect should be explored) and fusion technology demands. Laser isotope separation

(LIS) techniques cannot be considered scalable as a lithium enrichment technique. The scalability of electrophoretic techniques appears compromised by the ionic conductivities of the current super-ionic conductors and power consumptions of a  ${}^6\text{Li}$  production plant. High temperature distillation should be considered as scalable technique. Regarding combined methods, centrifugation assisted by thermal diffusion and high temperature distillation shows a potential exploration interest for prototyping demonstration R&D [San 13].

Finally, a combined CEIT-CIEMAT-IQS team produced and characterized SiC foams. CEIT developed a porous SiC based material with a dense CVD SiC coating (30  $\mu\text{m}$ ) for the FCI of the DCLL blanket design proposed within TecnoFus. CIEMAT measured the electrical conductivity of the obtained materials was measured after 1.8 MeV electron irradiation at 7 kGy/s up to 130 MGy and  $2 \cdot 10^{-5}$  dpa. Values of 0.4 S/m at 400°C were measured in one of the samples, whereas the curve progress indicates that values around 20 S/m may be realistic at 700°C [San 13], which would contribute to a significant reduction of the MHD pressure drop, assuming a FCI thickness of 5 mm [Smo 08].

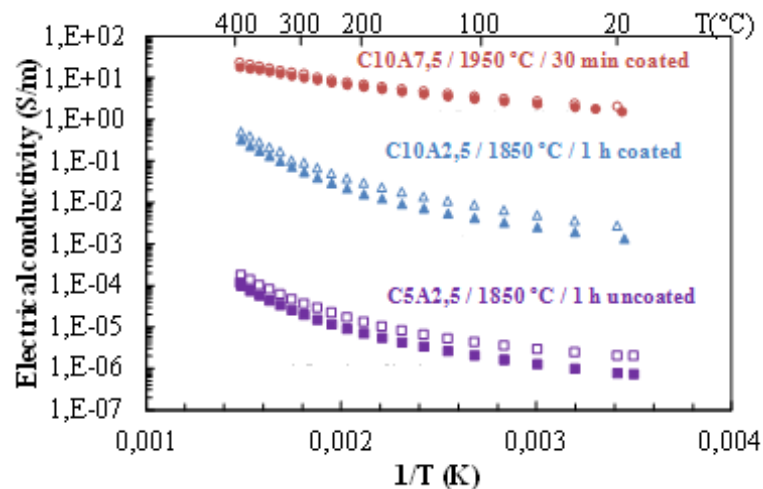


Fig. 26. Electrical conductivity of SiC samples with coating. Hollow symbols: before irradiation. Solid symbols: after irradiation.

The values of flexural strength obtained in one of the samples by three points bending tests suggest it could withstand the expected temperature difference across the FCI [San 13].

Corrosion tests of these samples in PbLi at 700°C during 1032 h were carried out by IQS, showing that a dense CVD SiC coating, despite being as thin as 30  $\mu\text{m}$ , can provide partial protection against corrosion by O-rich PbLi [San 13].

### 3.5.2.6. Plant systems and technologies

A predictive analysis of tritium transport in the blanket and the auxiliary systems was carried out, taking as reference the outboard segment design proposed within TecnoFus. EcosimPro, a tool for modelling dynamic systems including specific tritium transport libraries developed by EA and CIEMAT, was used.

A first simulation was made assuming 8 hours of continuous operation. Results show tritium permeation across SiC is negligible ( $\sim 10^5$  at/s), but there is some significant T retention in this material. The extraction system takes one day to extract 77% of generated inventory. Additionally, the model is able to obtain tritium self-sufficiency since the calculated Tritium Breeding Ratio is 1.39, the minimum tritium recovery rate allowed is 72% and the extraction rate is over 72%. Another simulation reproducing one day at fully operation shows the amount of tritium extracted is about 53% of tritium generated. Considering the same TBR, this would not allow to achieve the self-sufficiency [San 13].

In summary, the existence of FCI decreases tritium permeation because silicon carbide acts as tritium permeation barrier. This fact contributes to increase the tritium inventory in the PbLi loop and consequently the amount of extracted tritium. But a very large PbLi loop supposes a huge tritium inventory and can affect to tritium availability in the reactor, which forces to a careful study of the Tritium Extraction System (TES) efficiency and the loop parameters [San 13].

In this sense, a permeator against vacuum (PAV) was designed and manufactured by CIEMAT and SENER to evaluate its potential use as TES for DCLL blankets. This device was installed in a natural convection PbLi loop constructed ad hoc and hydrogen extraction tests under PbLi flow are being prepared at present.

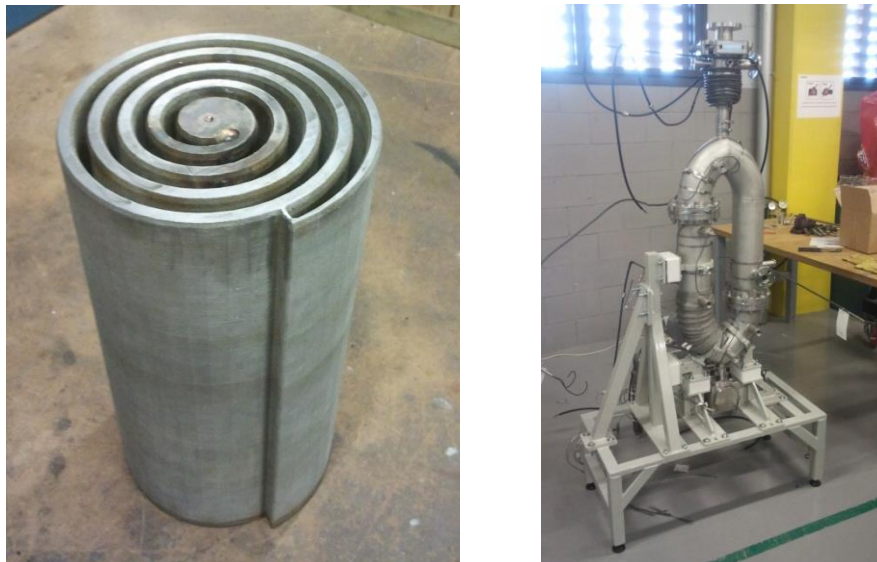


Fig. 27. Permeator against vacuum prototype (left). Partial assembly of the PbLi loop (right) [Sac 14].

The work carried out by IQS was closely linked with this facility, since they worked in the design and testing of a hydrogen sensor for determining hydrogen isotopes concentration in liquid PbLi. Two kinds of designs were developed: 1) potentiometric hydrogen sensors with proton conducting ceramics and 2) hydrogen permeation membrane sensors, using two different types of membranes (palladium and alpha-iron). Regarding the first ones, ceramics like SCZT85, BaC or SCZYb showed a deviation smaller than 100 mV between experimental data and theoretical calculations at 500°C, so those ceramics were considered promising for future experiments [San 13].

Concerning permeation membrane sensors, the alpha-iron sensor detected in all the experiments the hydrogen presence in the high-pressure compartment very fast, but it always needed a very long time to achieve the equilibrium pressure. The transition time can be minimized reducing the wall thickness membrane, decreasing the inner volume of the sensor and finally preventing possible oxidation of the iron membrane surface. In consequence, alpha-iron is considered a good candidate as membrane material in permeation sensors, although it is necessary to improve the design and the performance of this sensor for achieving shorter response times. The Pd sensor showed shorter transition times compared with the alpha-iron sensor ones, especially at high hydrogen pressures. However, they are still too long to follow fast changes in the hydrogen concentration in the high pressure compartment, so the sensor design must be improved for obtaining shorter response times [San 13].

Finally, UPV carried out some experiments to determine hydrogen transport properties – Sieverts' constant ( $K_s$ ) and diffusivity ( $D$ )- of liquid PbLi, using the absorption-desorption technique. The desorption results confirm the range of the absorption ones previously obtained, showing global consistence and confirming  $E_s$  of Reiter's tests (reference value in literature). The obtained  $K_s$  is high in comparison with the Reiter's one. This can be explained in terms of

PbLi QA (Li in excess). The derived D values are also high and can be explained by the effect of thermal convection in the crucible [Alb 10].

Some experiments were also carried out using the permeation technique. Samples of the RAFM steel ASTURFER developed within TecnoFus were characterized, as well as samples of the stainless steel 316L used to manufacture the permeator against vacuum mentioned above. A SiC sample provided by CEIT was mounted in the permeation facility but it lost its integrity during the mounting process, so the permeation technique was dismissed for this material [San 13]. On the other hand, the characterization of ASTURFER was not completely successful because of possible oxidation of the samples, different microstructure stabilization procedures, heat treatments, etc. [San 13]. The results of the tests with SS 316-L (200-550°C) confirmed the occurrence of diffusive transport regime and the obtained parameters are similar to those found in literature for SS 316-L [Sac 14]. However, the first experiments on gas extraction carried out in the PAV loop suggest the membrane material is less permeable than expected. For this reason, 6 samples were obtained from the PAV external surface filings and examined using a microscope. Examinations suggest the features of the PAV surface, obtained by the laser-cusing technique, are very different to the original material ones. Since surface limited transport model could occur, a new characterization of hydrogen transport parameters will be carried out at the UPV with SS 316L samples obtained by laser-cusing. If results show permeation is penalized by surface phenomena, it would imply the selected manufacturing technique is not appropriate [Fern 14].

#### **3.5.2.7. Environmental issues**

The CIEMAT-UPM-AEMET team worked in forecasting tritium transport in air as a consequence of an accidental release, taking Vandellós (site of a nuclear power plant) and Cadarache (site of the ITER Project) as reference scenarios. The objective was determining the position and characteristics of the HT effluents in real time, in order to delimit the affected interior or Mediterranean basin area, where the tritium clouds and the HT dry (or wet) deposition would be detected [San 13].

AEMET produced Lagrangian forecast by coupling ECMWF and FLEXPART. CIEMAT receipt the forecast and analysed the HT maximum concentrations and trajectories. Finally, UPM provided the specifications of the Gaussian plumes as initial input and documents with NORMTRI [San 13].

Key points for the development of HT clouds released from Cadarache were identified, suggesting that the North of Spain could be affected in some cases [San 13].

#### **3.5.2.8. DEMO specifications & systems codes**

UPC worked in the development of code modules which would enlarge the capabilities of the systems code AINA. In particular, implementation of QA tools, development of a new plasma-wall interaction model, review of loss of plasma control transients in ITER, analysis of the effect of two simultaneous perturbations during a loss of plasma and analysis of passive plasma shutdown during an ex-vessel LOCA in the ITER blanket [San 13].

On the other hand, different plasma oriented code modules were developed to be applied to the design of TecnoFus. Specifically, a fusion neutron source model and a systems analysis of the whole plant, including considerations of i.e. cost of electricity, RAMI and tritium self-sufficiency [San 13].

### **3.5.3. Power conversion system**

Within the task devoted to Plant Systems and Technologies (Sub-subsection 3.5.2.6), the University of Comillas and CIEMAT studied different He and S-CO<sub>2</sub> Brayton cycles for the power conversion system of a fusion reactor based on the TecnoFus DCLL breeding blanket design.

Both blanket coolants (eutectic PbLi and helium) and helium from the He-cooled divertor with two temperature levels (divertor bulk and target plate) were considered as thermal sources (Table 19). Besides the gas Brayton cycles investigated, the effect of coupling Rankine supplementary cycles was assessed [Lin 11]. In the case of the He-based Brayton cycles, Organic Rankine Cycles (ORC) were implemented in the configurations; whereas in the case of S-CO<sub>2</sub> steam Rankine cycles were considered. The low temperature of the helium coming from the blanket (BNK) is the key constraint when coupling the cycles. Therefore dual cycles were proposed and analysed as an alternative to overcome such shortcoming. They entail using the low quality thermal energy of BNK in an independent loop from the He-Brayton and S-CO<sub>2</sub> cycles [Lin 11].

A total of 6 layouts based on He Brayton cycles were investigated (Table 20) [Lin 11]. They consisted on different variations of the cycle shown in Fig. 28.

	Blanket helium (BNK)	Liquid metal (LM)	Low T divertor (LDIV)	High T divertor (HDIV)
Inlet temperature (°C)	300	480	566	700
Outlet temperature (°C)	400	700	700	800
Thermal power (MW)	793	1976	329	248
Thermal energy (MW)	413	1290	221	175

Table 19. Thermal sources [Lin 11].

The arrangement of the thermal sources shown in Fig. 28 was adopted in layouts from A to D. A and B are simple ones, with the latter including inter-cooling in between compression stages. In C, a second pre-cooler is situated before entering a heat recovery gas generator (HRGG) through which He residual heat is transferred to an organic fluid (iso-butane) flow that experiences a supercritical Rankine cycle. The configuration D adds intercooling in between compression stages removing both pre-coolers. By removing the BNK as a thermal energy source, the recuperation capability of He-Brayton cycles is retrieved and explored in configurations E and F (the latter includes inter compression cooling). In both cases, the thermal energy of the blanket is used for a steam Rankine cycle coupled in parallel to the He-Brayton one [Lin 11].

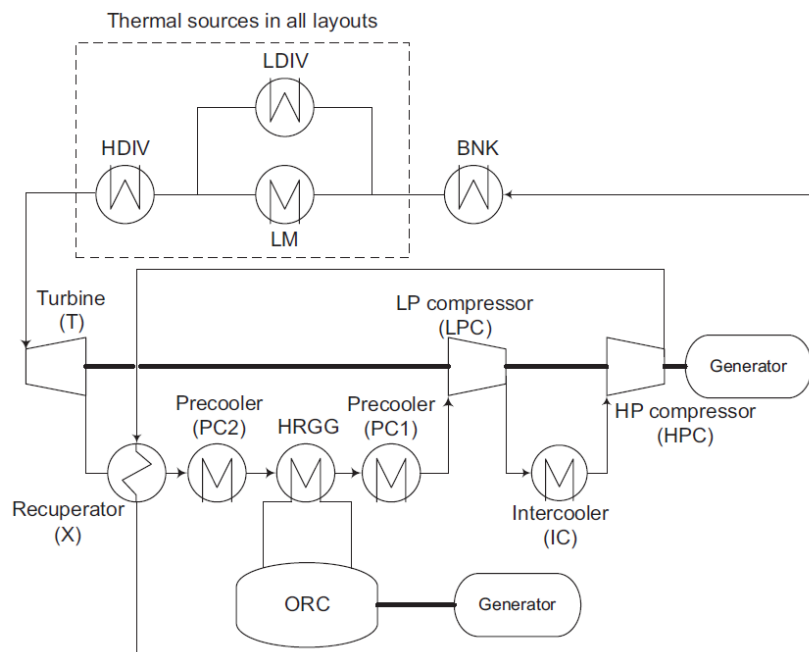


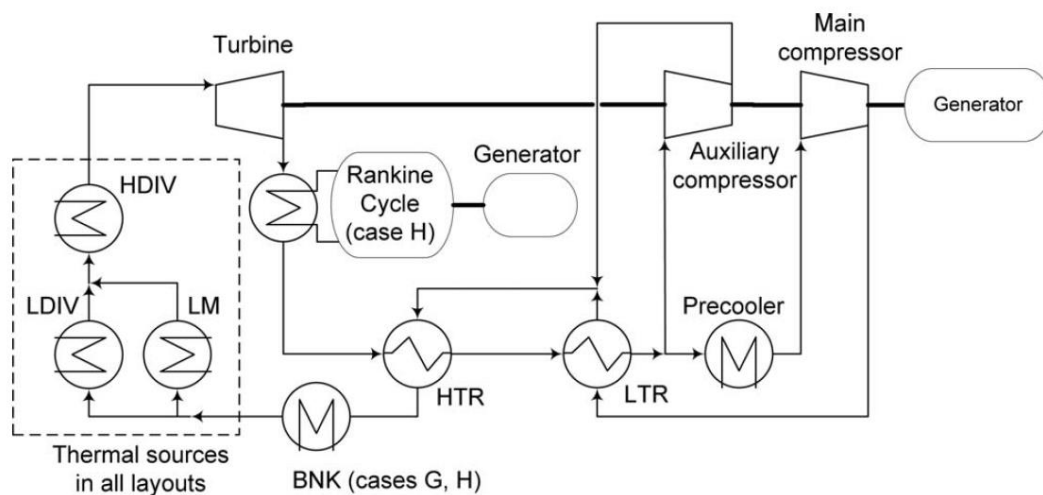
Fig. 28. He-based Brayton cycle showing all devices used analysed layouts [Lin 11].

	A	B	C	D	E	F
Inlet turbine (bar)	80	80	80	80	80	80
Inlet HP compressor (bar)	-	19.51	-	19.51	-	54.99
Inlet LP compressor (bar)	19.51	11.98	19.51	15.84	38.36	38.94
Thermal efficiency (%)	29.4	32.6	36.4	38.5	40.8	42.8
He power output (MW)	983.7	1089	919.1	1025	1087	1153
ORC power output (MW)	-	-	298.9	262.4	-	-
Rankine power output (MW)	-	-	-	-	277.6	277.6
Total power output (MW)	98.37	1089	1218	1287	1364	1430

Table 20. He-based Brayton cycles performances [Lin 11].

Regarding the S-CO<sub>2</sub> cycle (layout G), before implementing the option of printed circuit heat exchangers, already mentioned in Subsection 3.4.5 concerning S-CO<sub>2</sub> cycles for a HCLL-based near term DEMO, it was considered that the heat exchangers would achieve low effectiveness because of the BNK low temperature [Lin 11], affecting potential coupling with other supplementary cycles. For that reason, two potential solutions were studied [Lin 11]: coupling with a steam Rankine cycle downstream the turbine (Layout H), and implementing a dual cycle where BNK is dealt with as an independent heat source exploited by means of a steam Rankine cycle (layout I).

	G	H	I
Inlet turbine (bar)	201.8	201.8	190
Inlet main compressor (bar)	74	74	74
Thermal efficiency (%)	41.12	46.78	45.79
Rankine power output (MW)	-	783.8	277.6
CO <sub>2</sub> power output (MW)	1376	781.2	1254
Total power output (MW)	1376	1565	1532

Table 21. S-CO<sub>2</sub> cycles performances [Lin 11].Fig. 29. S-CO<sub>2</sub> cycle (coupling to a Rankine indicated) [Lin 11].

Results on He cycles show that, in spite of the significant improvement resulting from implementing an ORC, it is dual cycles (E and F) strategy that brings the He configurations to the highest thermal performances, reaching thermal efficiencies higher than 40% in both layouts. This gain, due to a good extent to the recuperator implementation in the layouts, means a thermal efficiency increase of 38.75% and 31.28% with respect to the plain He-Brayton

configurations (A and B). As a consequence, the power output is also enhanced to values more than 35% higher than in the plain configurations [Lin 11]. Obviously, these results are very far from the obtained for the specifications of a near term DEMO based on a helium-cooled blanket (EFDA WP12, Sub-subsection 3.4.2.2 ) [Har 12], where a maximum cycle efficiency of only 29% was achieved for He-Brayton cycles [Lat 12]. In spite of the similar temperature of the blanket helium, the major contribution of the blanket (liquid PbLi) and the He-cooled divertor as moderately high temperature sources results crucial to get so large differences with the TecnoFus case.

On the other hand, the S-CO<sub>2</sub> cycles reach high thermal efficiencies even in the plain configurations (classical re-compression cycle, layout G). Both the combined architecture (layout H) and the dual cycle one (layout I) entail improvements in the cycle thermal performance. The biggest enhancement is achieved through the case H, which yields a thermal efficiency close to 47% and would provide a moderate increase of power output too (about 14%). Nonetheless, concerning output power, the most outstanding impact is not the net power output but how it gets distributed: the steam Rankine cycle being responsible for more than 50% [Lin 11].

The dual cycle (layout I) thermal-hydraulics was afterwards modelled and simulated by Batet et al. [Bat 14] using the RELAP5-3D code. Several steady-state calculations were run to test the performance of the model. After designing some minimal control features and adjusting their parameters, a few transient calculations were also run in order to demonstrate the capabilities of the code.

In summary, He-Brayton based cycles need more complex layouts -by setting up dual cycles (40.8%), preferably with intercooling (42.8%)- to obtain similar performances as the plain configurations of the S-CO<sub>2</sub> cycles, which can achieve outstanding performances (~47%) when a combined cycle architecture is built [Lin 11]. Therefore, He-Brayton cycles were discarded for the TecnoFus power conversion system and S-CO<sub>2</sub> were further investigated.

Thus, a new layout was proposed by Serrano et al. [Ser 13] to avoid the need of the Rankine cycle. It includes a new recuperator, denoted as BBR (By-pass Blanket Recuperator). The BBR recovers the energy at the turbine outlet and heats a stream which by-passes the BNK. This arrangement allows increasing the turbine inlet temperature without increasing the temperature of the CO<sub>2</sub> stream entering into the low pressure side of the HTR. So, this is a more compact solution than that which uses a bottoming Rankine cycle as it adds only one heat exchanger and avoids the use of a second cycle.

Two layouts were proposed based on the use of this new recuperator: REC3 and REC2. The first uses three recuperators (HTR and LTR, as usual in any classical recompression S-CO<sub>2</sub> cycle, and the additional BBR), while in the second the HTR has been suppressed without loss in efficiency and using a lower inlet turbine pressure. So REC2 was proposed as the final design for TecnoFus, with efficiency close to 46.5% [Ser 14b].

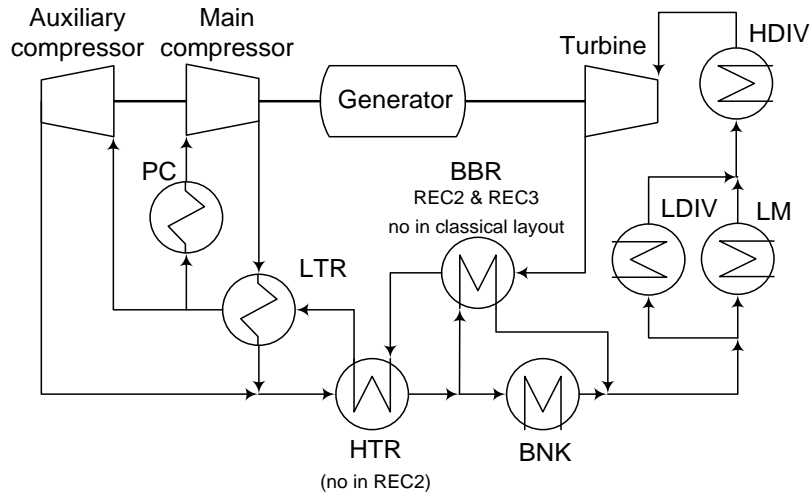


Fig. 30. REC2 and REC3 layouts [San 13].

On the other hand, the use of printed circuit heat exchangers was finally assumed, in the same way as the later study of S-CO<sub>2</sub> PCS in the framework of EFDA WP13 (Subsection 3.4.5), taking into account suggestions from literature, due to the highly compact design and robustness for the high pressures and temperatures required. First, a detailed analysis of the pre-cooler design was made in order to determine the influence on its behaviour of the closeness of its operation conditions to the critical point [Ser 12]. Then, all the heat exchangers were analysed and sized [Ser 14]. For most of them, the methodology was based on the discretization of the heat exchanger into sub-heat exchangers, as explained in Subsection 3.4.5. In the case of the more complex heat exchangers, the LTR and the pre-cooler, CFD simulations were made [Ser 14]. The proposed design of the liquid metal heat exchanger is also based in PCHE technology, but it presents a number of particularities and it was not studied in [Ser 14]. This design is described in Subsection 3.5.4.

### 3.5.4. Design of the lead-lithium/supercritical CO<sub>2</sub> heat exchanger

#### 3.5.4.1. Introduction

As said above, the specific design of this heat exchanger has been studied apart from the gas heat exchangers by Fernández and Sedano [Fern 12].

As referred in Subsections 3.4.5 and 3.5.3, Printed Circuit Heat Exchangers begin to be widely used in experimental loops and industry. They have been recommended in literature for S-CO<sub>2</sub> power conversion cycles because of their compactness, thermal effectiveness and high temperature and pressure capability. Adding corrosion resistance to these features, PCHEs appear as an interesting design option for fusion reactors based on Dual Coolant Breeding Blankets or even Self-Cooled Breeding Blankets.

At present, Heatic is the world's largest manufacturer of Printed Circuit Heat Exchangers. Heatic's PCHEs are made up by diffusion-bonded thin plates with chemically etched channels, with semi-circular cross section and zig-zag trajectories. The work described below starts from these designs and explores the optimization of the printed circuit to minimize pressure drops with low penalization in heat transfer area by means of introducing airfoil shaped fins [Cha 08]. The issue of tritium permeation from the primary to the secondary coolant is also assessed. Computer fluid-dynamics and tritium transport tools have been used for these purposes, and the LM heat exchanger of the basic S-CO<sub>2</sub> recompression cycle (layout G) in [Lin 11] has been taken as the case of study.

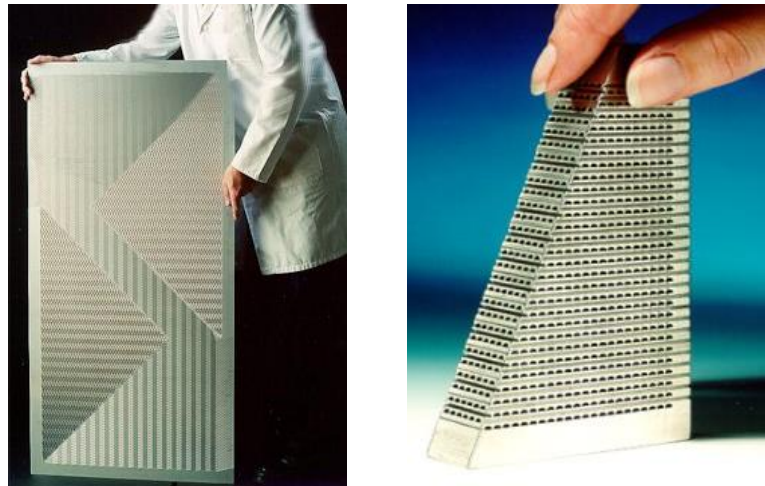


Fig. 31. Heatric PCHE plate (left) and set of diffusion-bonded plates (right).

#### 3.5.4.2. Design of the PCHE

##### Structural material selection

Silicon carbide ceramics and SiC<sub>f</sub>/SiC composites are among the most promising candidates as structural materials for fusion technology because of their potential application for high performance reactors and superior safety characteristics compared to metallic materials [Ric 04]. For a DEMO DCLL blanket, thermal applications require heat and pressure resistances at high operating temperatures, compatibility with the liquid metal breeder [Noz 09] and low tritium diffusivity and solubility. One important issue in this field is the development of SiC joining techniques, which include diffusion bonding using various active fillers, transient eutectic phase methods such as Nano-Infiltration and Transient Eutectic-phase (NITE), laser joining, selected area chemical vapour deposition, glass-ceramic joining, solid state displacement reactions and preceramic polymer routes [Sne 11]. NITE joining is believed to be the most promising option, since it is based on a joining zone having the same composition of NITE-SiC<sub>f</sub>/SiC composites matrix. A scaled module of a NITE-SiC<sub>f</sub>/SiC composite compact heat exchanger has been already built [Tak 10] and tested with notable performances from the point of view of heat transfer.

Silicon carbide is very resistant to chemical etching. However, chlorine-containing gas mixtures [Zin 04], hot potassium hydroxide (KOH) or reactive ion etching (RIE) are capable to etch the ceramic surface. They must be more developed, but they must be considered as candidate techniques to produce the printed circuit of the silicon carbide heat exchanger.

##### Geometric configuration

The characteristics of the thermal source in the blanket and the secondary side of the power conversion cycle determine several working parameters. Thus, PbLi and CO<sub>2</sub> mass flows ( $\dot{m}_{\text{PbLi}}=1.089 \cdot 10^4$  kg/s,  $\dot{m}_{\text{CO}_2}=2.875 \cdot 10^3$  kg/s) and inlet temperatures ( $T_{\text{in PbLi}}=700^\circ\text{C}$ ,  $T_{\text{in CO}_2}=391^\circ\text{C}$ ) are input data for the pre-sizing of the heat exchanger, as well as the inlet pressure for the CO<sub>2</sub> circuit ( $P_{\text{CO}_2}=200$  bar). The value of the PbLi inlet pressure is not relevant since the physical properties used here are not pressure-dependent.

	PbLi	CO <sub>2</sub>
Mass flow (kg/s)	10890	2875
Inlet temperature (°C)	700	391
Inlet pressure (MW)	-	200

Table 22. Hot and Cold streams inlet conditions.

The body of the PCHE is composed by a stack of plates which alternatively contain hot (PbLi) and cold ( $\text{CO}_2$ ) streams. The arrangement of the streams is in counterflow. The inlet and the outlet of the cold fluid occurs at the opposite faces of the longer sides of the plates due to the space needs of the manifolds, so two zones of cross flow are needed. However, for the purposes of this work, counterflow arrangement is considered along the whole length of the heat exchanger.

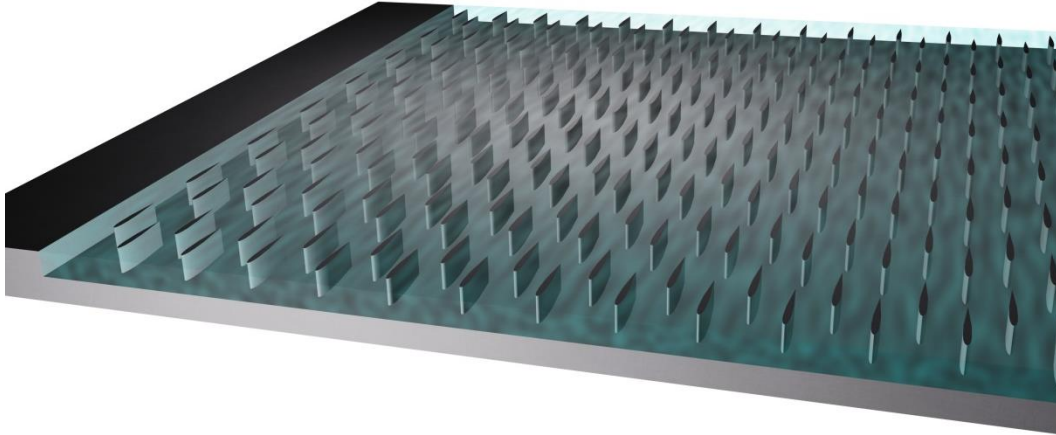


Fig. 32. Plate CAD model.

The dimensions of each plate are 820 mm (length) x 588 mm (width) x 1.5 mm (thickness). Each plate contains airfoil-shaped fins with 1.5 mm of height, whereas the end faces include a ledge to stiffen the joint between consecutive plates. The total number of plates for each fluid is 6000, which can be arranged in 10 modules of 1200 plates (total).

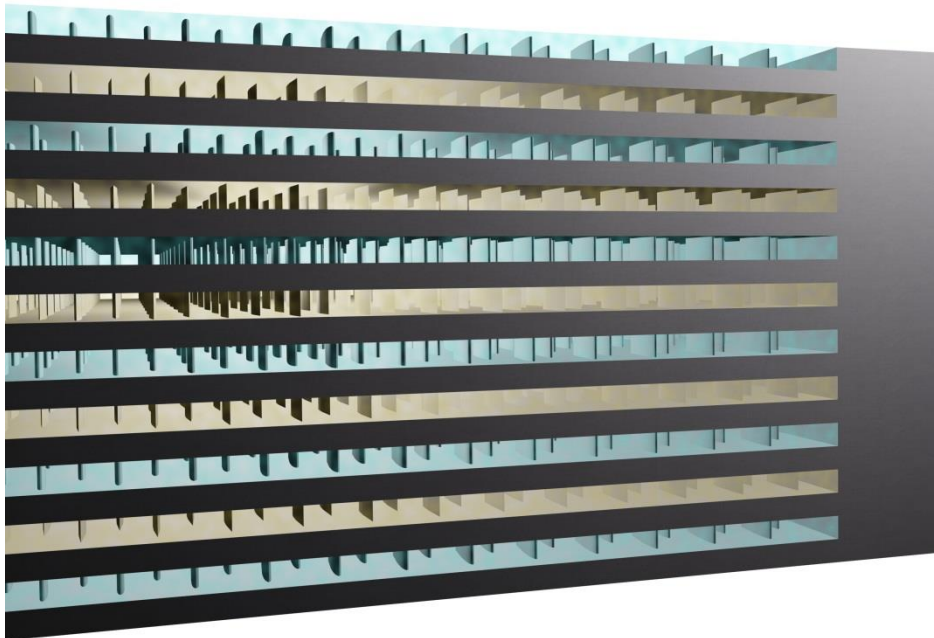


Fig. 33. Stack of hot and cold plates (CAD model).

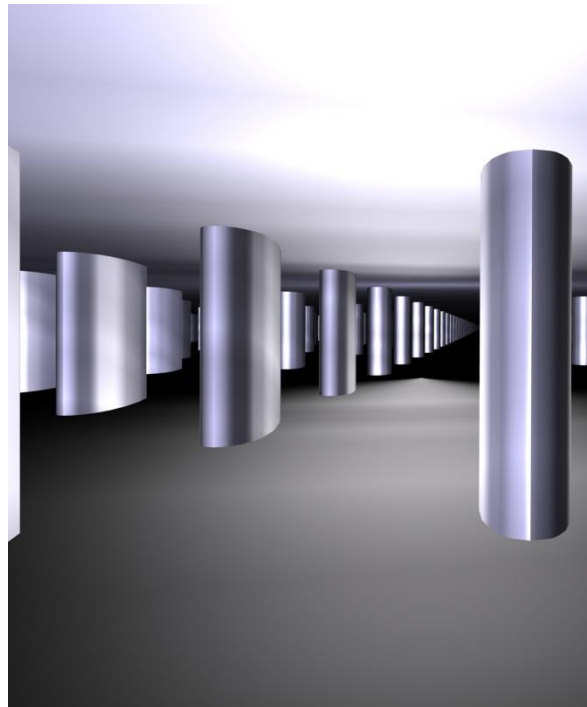
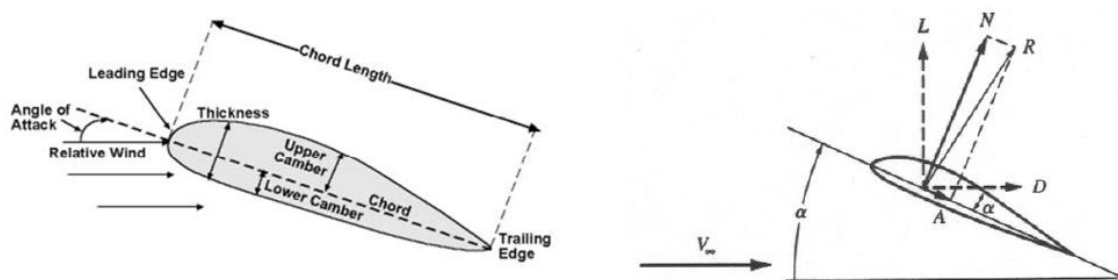


Fig. 34. Rendered view of the interior of a channel.

### Airfoils shape

Airfoil shapes used in aeronautics are designed to provide high lift values at low drag for given flow conditions. Each profile is defined by the set of parameters shown in Fig. 35. The chord is defined as the line connecting the leading edge and the trailing edge. Camber is defined as the maximum distance from the chord to either surface. Chord length, is the overall airfoil length. The angle of attack is the angle between the extended chord and the relative fluid flow direction (usually horizontal).

Fig. 35. Pressure distribution over an airfoil (L: lift force, D: drag force, R: resultant force, N: normal force, A: axial force,  $\alpha$ : angle of attack,  $v_\infty$ : velocity) [Mey 13].

Aerodynamics forces result from the pressure distribution over the surface. The total force which the pressure distribution exerts on a wing is:

$$\vec{F} = \oint - (P \cdot \vec{n}) dA \quad (8)$$

The decomposition of the resultant force into horizontal and vertical components (Fig. 35) allows recovering the aerodynamic forces of lift and drag:

$$L = F_y = \int -P(\cos(\alpha + \phi)) dA \quad (9)$$

$$D = F_x = \int -P(\sin(\alpha + \phi)) dA \quad (10)$$

Non-dimensional parameters based on the pressure coefficient are used in order to handle different flow conditions:

$$C_{p_x} = \frac{P_x - P_\infty}{\frac{1}{2} \rho_{air} U_\infty^2} = \frac{P_x - P_\infty}{q_\infty} \quad (11)$$

$C_p$  is the difference between local static pressure and free-stream static pressure, non-dimensionalised by the free-stream dynamic pressure. It is also common to represent lift and drag forces by means of non-dimensional coefficients:

$$C_L = \frac{L}{q_\infty S} \quad (12)$$

$$C_D = \frac{D}{q_\infty S} \quad (13)$$

Where  $S$  is the wing planform area which represents the viewed area of the wing from a top view.

In our case, the shape of the airfoil fins which define the printed circuit of each plate (Fig. 35) has been optimized to obtain a minimum resistance to the flow, by minimizing their drag coefficient ( $C_d$ ).

The study has been focused on NACA-4-digit series for aircraft wings, developed by the National Advisory Committee for Aeronautics (NACA). Each NACA-4 profile is named by a 4-digit code, where the first digit describes the maximum camber as percentage of the chord and the second digit describes the distance of the maximum camber from the airfoil leading edge in tens of percent of the chord, whereas the last two digits describe the maximum thickness of the airfoil as percent of the chord. Thus, e.g. NACA 4415 has a maximum camber of 4% of chord, a distance from the maximum camber to the leading edge of 40% of the chord, and a maximum thickness of 15% of the chord. In the case of asymmetric (cambered) airfoils, the geometry is defined by the following equations [Lad 96]:

$$y_t = 5tc \left[ \begin{array}{l} 0.2969 \cdot \left(\frac{x}{c}\right)^{1/2} - 0.126 \cdot \left(\frac{x}{c}\right) - 0.3537 \cdot \left(\frac{x}{c}\right)^2 + 0.2843 \cdot \left(\frac{x}{c}\right)^3 \\ -0.1015 \cdot \left(\frac{x}{c}\right)^4 \end{array} \right] \quad (14)$$

$$y_c = \begin{cases} m \frac{x}{p^3} \left(2p - \frac{x}{c}\right) & 0 \leq x \leq p \cdot c \\ m \frac{c-x}{(1-p)^2} \left(1 + \frac{x}{c} - 2p\right) & p \cdot c \leq x \leq c \end{cases} \quad (15)$$

$$x_u = x - y_t \cdot \sin \theta; \quad y_u = y_c + y_t \cdot \cos \theta \quad (16) \quad (17)$$

$$x_l = x + y_t \cdot \sin \theta; \quad y_l = y_c - y_t \cdot \cos \theta \quad (18) \quad (19)$$

$$\theta = \arctan\left(\frac{dy_c}{dx}\right) \quad (20)$$

$$\frac{dy_c}{dx} = \begin{cases} \frac{2m}{p^2} \left( p - \frac{x}{c} \right) & 0 \leq x \leq p \cdot c \\ \frac{2m}{(1-p)^2} \left( p - \frac{x}{c} \right) & p \cdot c \leq x \leq c \end{cases} \quad (21)$$

Where  $m$  is the first digit divided by 100,  $p$  is the second digit divided by 10,  $t$  is the combination of the third and the fourth digits divided by 100,  $c$  is the chord length,  $y_c$  is the  $y$ -coordinate of the camber line,  $y_t$  is the distance from either the upper surface or the lower one to the camber line,  $x$  is the distance to the leading edge along the chord,  $y_u$  is the  $y$ -coordinate of the upper surface and  $y_l$  is the  $y$ -coordinate of the lower surface.

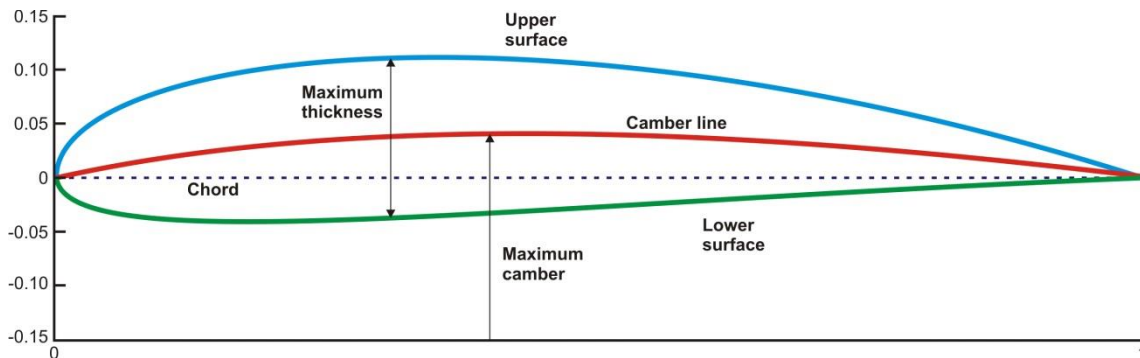


Fig. 36. NACA4415 profile.

There are also NACA-4-digit symmetrical airfoils, where there is no camber line and both upper and lower surfaces are symmetric with respect to the chord (NACA00XX). Their geometry is defined by the equation (14) and the following ones [Lad 96]:

$$x_u = x_l = x; \quad y_u = y_t; \quad y_l = -y_t \quad (22) \quad (23) \quad (24)$$

XFOIL is a code first developed in the 1980s at Massachusetts Institute of Technology. Despite its vintage (although the last version is from 2013), this code written in FORTRAN is still widely used for the design and analysis of subsonic isolated airfoils. Given the coordinates specifying the shape of a 2D airfoil, angle of attack, Reynolds and Mach numbers, XFOIL calculates the pressure distribution on the airfoil and hence lift and drag characteristics. It has been used here to select the optimum airfoil shape for the PCHE plates from the NACA-4-digit series.

An interface code has been programmed in MATLAB to automatically execute XFOIL and analyse every NACA-4 digit profile with thickness of 10% of the chord (in order to reduce the calculation time), for a range of angle of attack of 0-4°. The Reynolds and Mach numbers estimated for the CO<sub>2</sub> stream, where it is expected the larger pressure drop, have been utilized. The MATLAB code allows saving the profile name, the angle of attack and the values of the drag coefficient ( $C_d$ ) in a text file for an easy evaluation.

The results show the profile with the smallest  $C_d$  for the given conditions is NACA4110 with an angle of attack of 2.4°. However, this profile presents an asymmetry between its upper and lower surfaces, which is used to increase the lift coefficient of the airfoil in aeronautics. In our case, using a symmetric profile is preferable because no lift force is required. Thus, the selection has been restricted to profiles with 0% of camber and 0° as angle of attack. Within this group, the NACA0010 is the profile with the smallest  $C_d$ .

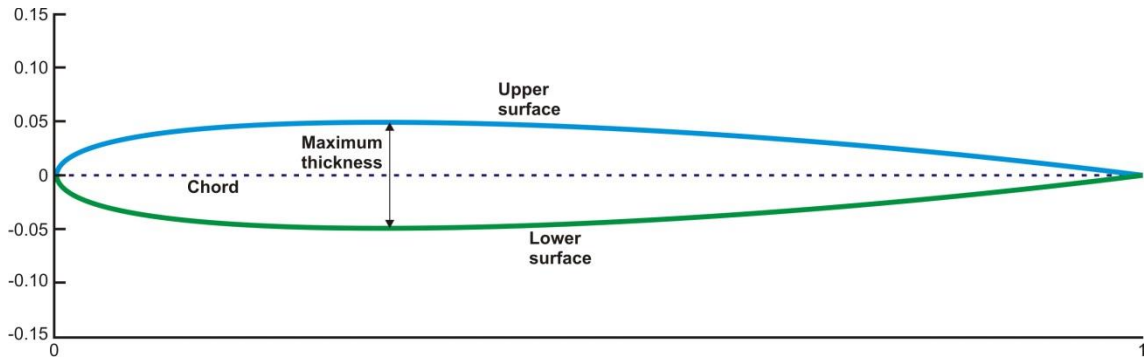


Fig. 37. NACA0010 profile.

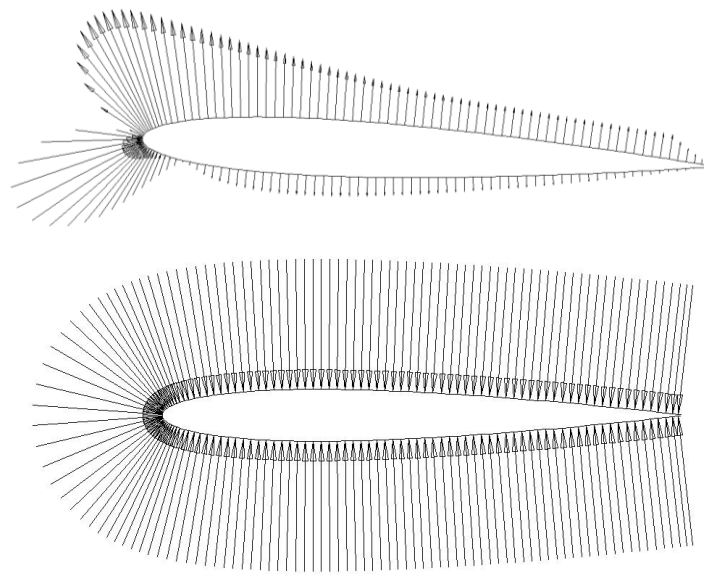


Fig. 38. Comparison of pressure distribution in NACA0010 with  $\alpha > 0$  (top) and  $\alpha = 0$  (bottom).

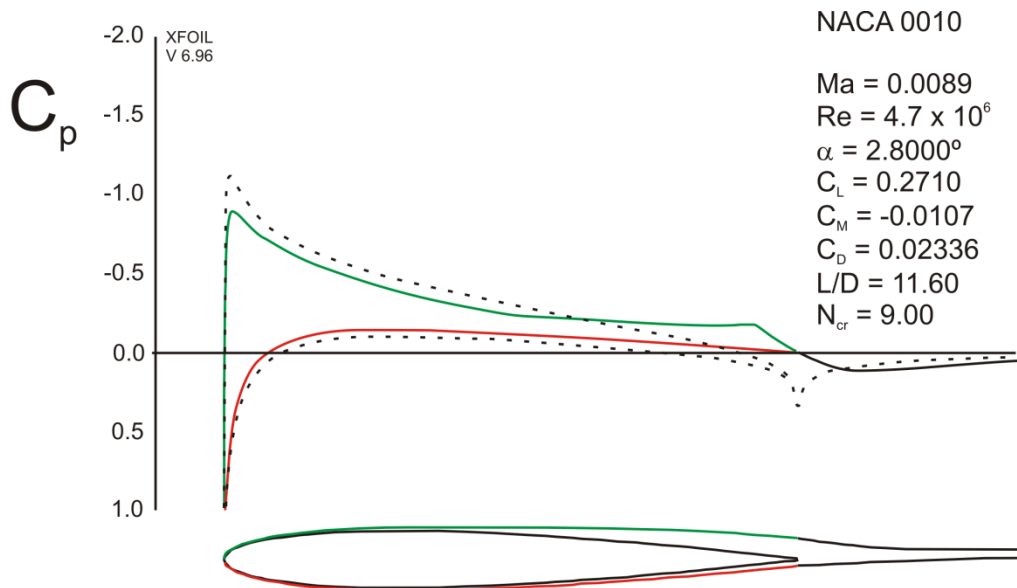


Fig. 39. Coefficient of pressure in the upper and lower surfaces of NACA0010 for  $\alpha = 2.8^\circ$ .

### 3.5.4.3. 1-D heat transfer model

A one-dimensional heat transfer model has been used to pre-size the PCHE by evaluating the temperature profiles along the channels for both hot and cold streams [Son 07].

The length of the PCHE is divided into a number of nodal segments. The temperature at a given node in each channel is considered as constant, as well as the specific heat, thermal conductivity, viscosity and density. The heat transferred from the hot side to each segment,  $q_n$ , can be expressed as:

$$q_n = \dot{m}_h \cdot C_{p_h} \cdot (T_{h_n} - T_{h_{n+1}}) \quad (25)$$

Where  $q$ ,  $\dot{m}$ ,  $C_p$  and  $T$  are the heat transfer rate, mass flow rate, specific heat and temperature, respectively. In a similar way, the heat transferred to the cold side can be calculated as follows:

$$q_n = \dot{m}_c \cdot C_{p_c} \cdot (T_{c_n} - T_{c_{n+1}}) \quad (26)$$

The Log Mean Temperature Difference (LMTD) method is applied to each segment of the PCHE:

$$q_n = U \cdot \frac{A}{n} \cdot \frac{(T_{h_n} - T_{c_n}) - (T_{h_{n+1}} - T_{c_{n+1}})}{\ln\left(\frac{T_{h_n} - T_{c_n}}{T_{h_{n+1}} - T_{c_{n+1}}}\right)} \quad (27)$$

Where  $U$  is the overall heat transfer coefficient,  $A$  is the heat transfer area and  $n$  is the number of nodes. So we have three equations for each segment of the PCHE and we can establish the following equalities: (25)=(26)=(27).

A MATLAB code has been created to write the nodal equations and numerically solve the non-linear system. A total number of 20 nodes have been used, but the result is practically invariant inside a close range of numbers of nodes.

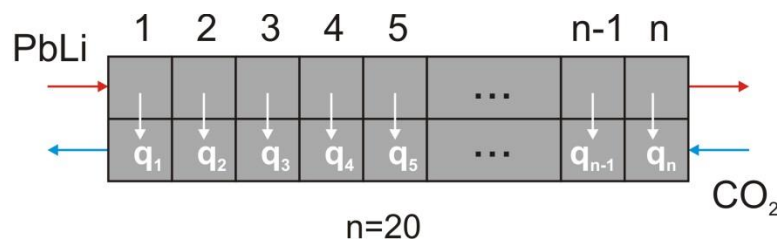


Fig. 40. Scheme of the 1-D heat transfer model.

The capability of this 1-D model to predict the temperature profiles strongly depends on the estimation of the overall heat transfer coefficient  $U$ :

$$U = \frac{1}{\frac{1}{h_h} + \frac{t}{k} + \frac{1}{hc}} \quad (28)$$

Where  $h$ ,  $t$ , and  $k$  refer to convection heat transfer coefficient, effective thickness of the wall and thermal conductivity of the wall material, respectively. The evaluation of the Nusselt numbers for the lead-lithium and the  $\text{CO}_2$  streams reveals strong differences between empirical correlations. Several correlations for forced convection heat transfer in pipes proposed by Gnielinski, Dittus-Boelter, Wang-Peng and Kottowski have been assessed. The results obtained by using Wang-Peng for the carbon dioxide and Kottowski for the lead-lithium are the most similar to the 3-D

CFD results. Wang and Peng correlation [Son 07] is a modification of the well-known Ditus-Boelter correlation for rectangular channels:

$$Nu = 0.00805 \cdot Re^{0.8} \cdot Pr^{0.8} \quad (29)$$

Kottowski proposed a suitable correlation for heat transfer in liquid metal fully developed turbulent flows through pipes with various geometrical shapes [Tak 10]:

$$Nu = \frac{2}{3} \cdot Nu_{sm} + 0.025 \cdot (Re \cdot Pr)^{0.8} \quad (30)$$

Where  $Nu_{sm}$  is the Nusselt number for slug flow. A value of 8.00 has been recommended [Tak 10].

The 1-D and CFD results are compared in the Sub-subsection 3.5.4.4.

#### 3.5.4.4. 3-D CFD model

##### Scaled model

Numerical analyses have been performed to optimize the airfoil fins arrangement in terms of pressure drop ( $\Delta P$ ) and integrated thermal flux ( $Q$ ) by varying the distance between the airfoils along the flow direction (pitch X) with a constant distance in the perpendicular direction (pitch Y) [Cha 08].

3-D scaled models (Fig. 41) have been designed in CATIA. The geometry of the NACA0010 airfoils has been created using a Visual Basic macro which parts from equations (14) and (22-24) and minimizes the number of points to be linked by splines.

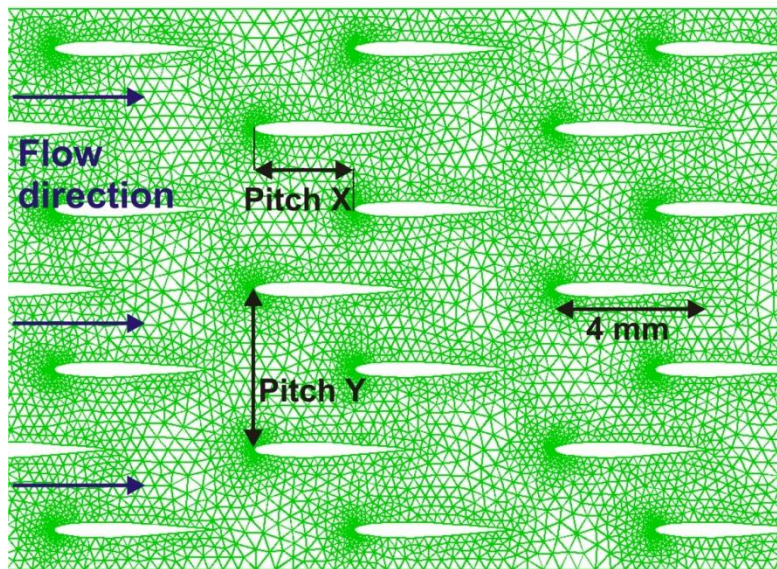


Fig. 41. Top view of the channel configuration (scaled model).

The scaled CAD model is composed by three reduced-size plates: two cold and a central hot. The size of the model is 25 mm (length) x 14 mm (width) x 9 mm (height).

The steady-state fluid dynamics model with conjugated heat transfer has been defined and solved with ANSYS FLUENT. The size of the meshes has been about 200000 elements. As in the case of the 1-D heat transfer model, the properties of the fluids have been maintained as constant [Mas 08] [Nist], since their variations in the considered ranges of temperature and pressure are not significant. For the thermal properties of silicon carbide, a low porosity NITE-

SiC has been taken as reference, due to its quite high thermal conductivity [Par 09], although the SiC wall only exerts a small influence on the overall heat transfer coefficient.

Velocity-inlet and pressure-outlet have been established as boundary conditions for both streams, and the k- $\epsilon$  turbulence model has been used. The inlet temperatures appearing in Table 22 have been also introduced.

The results show that the minimum relation  $\Delta P/Q$  occurs with the largest distance between airfoils (Table 23). Both variables exhibit high values because the inlet velocities ( $v_{\text{PbLi}}=2$  m/s;  $v_{\text{CO}_2}=28$  m/s) were calculated for a reduced number of plates (800).

Pitch X (mm)	Pitch Y (mm)	$\Delta P_h$ (Pa)	$\Delta P_c$ (Pa)	Q (W)
4	4	12247	26845	2046
2.5	4	13958	32285	2113
1	4	14967	41103	2188

Table 23. Comparison of results for different values of pitch X.

#### Entire length model

The entire length model is based on the same airfoil arrangement as the 4 mm (pitch X) x 4 mm (pitch Y) scaled model, but it includes the total length of the PCHE (820) mm. The model is composed by a hot and a cold plate, as well as the half of the upper and lower SiC plates, where periodic boundaries have been established to simulate the succession of plates (6000 for each fluid). The size of the mesh has been about 2900000 elements (hexahedra+tetrahedra). The inlet velocities for CO<sub>2</sub> and PbLi have been 3.60 m/s and 0.23 m/s, respectively. The rest of parameters have been the same that in the scaled models simulations except that, in this case, k- $\omega$  with Shear Stress Transport (SST), which is suitable for relatively low Reynolds flows, has been used as turbulence model.

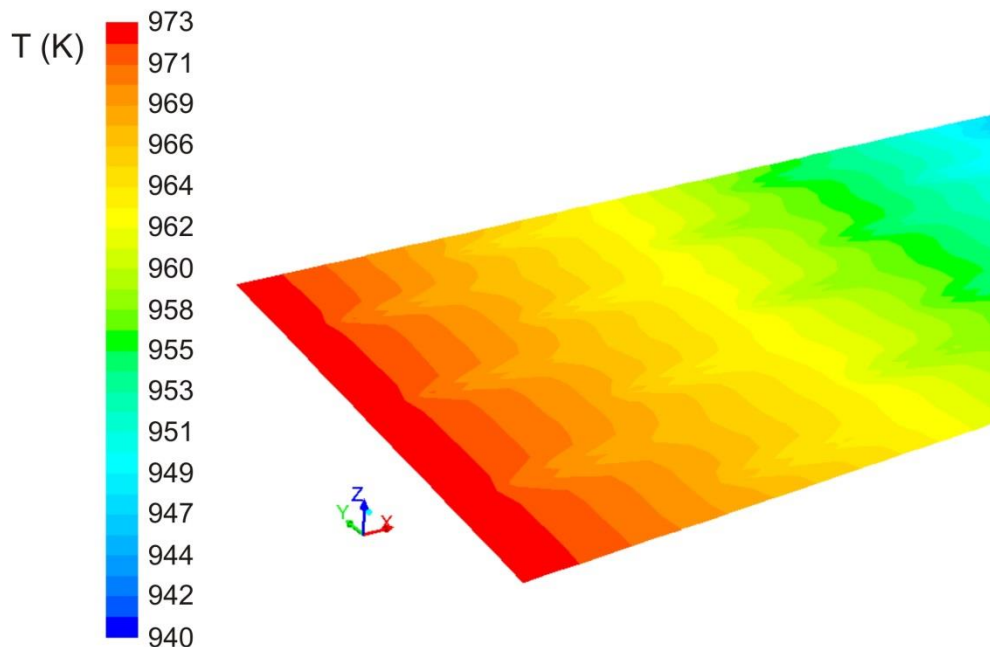


Fig. 42. Temperature distribution near inlet on an intermediate plane in the PbLi channel.

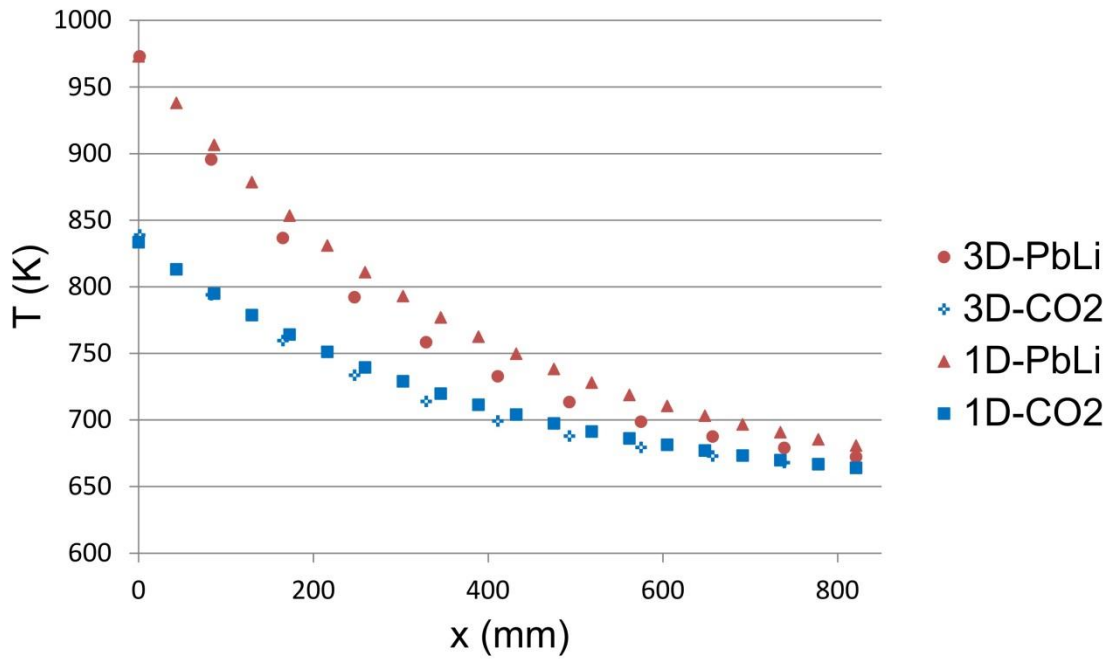


Fig. 43. Comparison of temperature profiles in both streams for 1-D and 3-D models.

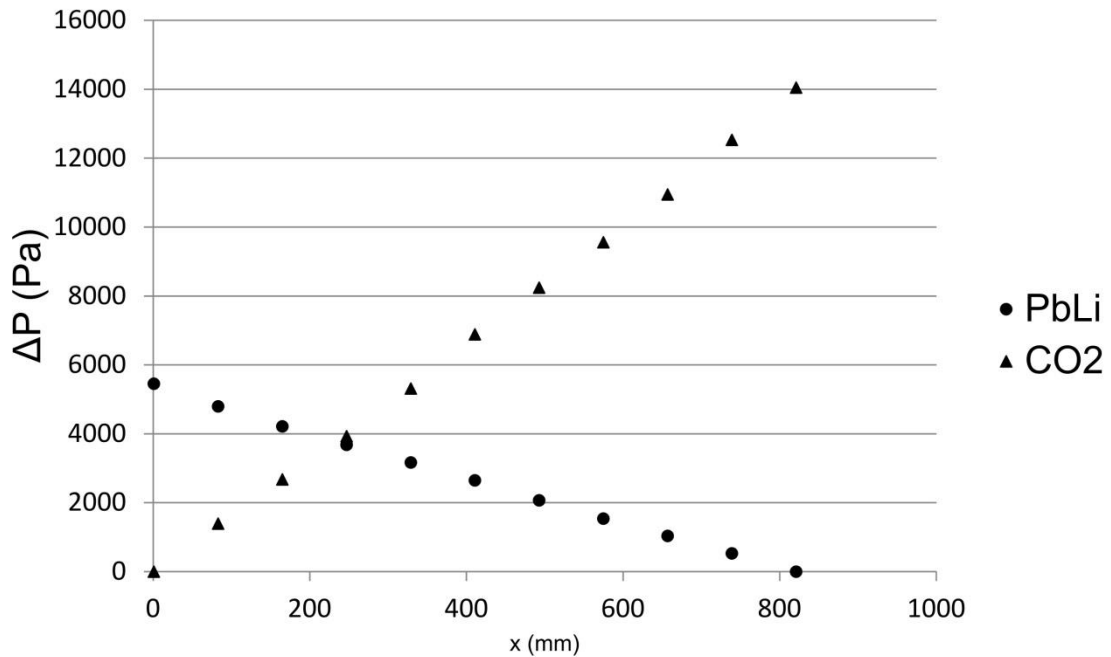


Fig. 44. Pressure drop in the hot and the cold streams.

Fig. 43 shows a good agreement between the temperature profiles obtained with the 1-D and the 3-D CFD model, although the chosen empirical correlations lead to slightly underestimate the overall heat transfer coefficient. The pressure drops are low for both hot and cold streams (Fig. 44). On the other hand, the total integrated flux of the PCHE, whose value is about 648 MW, is larger than the one expected for this exchanger and would allow reducing the CO<sub>2</sub> mass flow in this sector of the TecnoFus power conversion layout if necessary.

### 3.5.4.5. Tritium transport model

A tritium transport model has been developed in order to evaluate the permeation of dissolved tritium in the liquid metal breeder to the secondary CO<sub>2</sub> (Fig. 45).

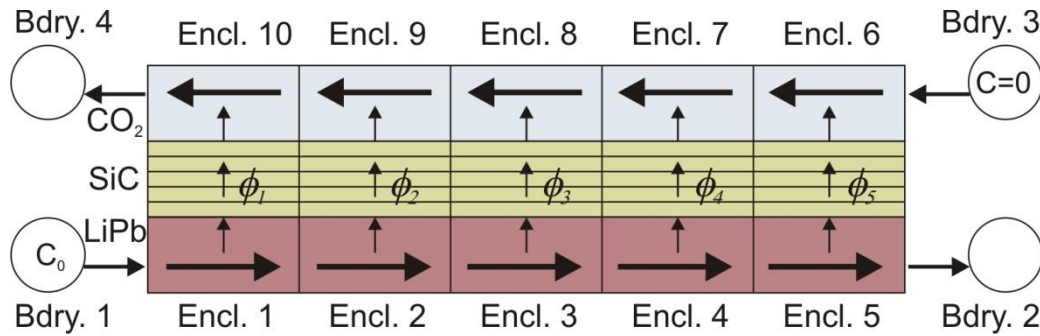


Fig. 45. Process flow diagram for tritium transport.

The model has been implemented in TMAP7, a 1-D code based on a finite difference method and written at Idaho National Laboratories. Neither trapping nor diffusion along the direction of flow is assumed. Besides, only T as diffusive specimen and T<sub>2</sub> as enclosure specimen are considered. The solid part is divided into five segments along the length of the PCHE, whereas each of them is discretized with 5 nodes along the thickness of the plate. On the other hand, the fluid channels are divided in 10 functional enclosures (5 for PbLi and 5 for CO<sub>2</sub>), whereas 4 boundary enclosures are disposed at the inlets and the outlets and are used as sources/sinks of tritium and volumetric flow.

The temperature of each functional enclosure and the segments is obtained from the CFD entire length model and fixed. The governing equations for the interfaces between functional enclosures and SiC segments are the following:

Concentration equilibrium at the interface PbLi-SiC:

$$\frac{C_{T,PbLi}}{K_{sT,PbLi}} = \frac{C_{T,SiC}}{K_{sT,SiC}} \quad (31)$$

Sieverts' law at the interface SiC-CO<sub>2</sub>:

$$C_{T,SiC} = K_{sT,SiC} \cdot \sqrt{P_{T_2,CO_2}} \quad (32)$$

Diffusion across SiC (Fick's law):

$$J_{T,SiC} = -D_{T,SiC} \cdot \frac{\partial C}{\partial x} \quad (33)$$

Where C, K<sub>s</sub>, P, J, D and x are concentration, Sieverts' constant, partial pressure, flux of dissolved tritium atoms, diffusivity and normal distance to the SiC surface, respectively.

The inlet tritium concentration for the liquid metal has been calculated from [Pal 12], assuming the most unfavourable scenario without tritium extracting system before the heat exchanger.

The calculations have been made for 4 types of SiC with very different diffusivity [Cau 93] [Est 02]. The solubility has been less widely studied in literature, so a unique value for a β-SiC has been used for all the calculations [Cau 93]. Concentration of T in SiC and PbLi, partial pressures of T<sub>2</sub> in CO<sub>2</sub>, diffusive flux to CO<sub>2</sub> channel and mobile inventory in SiC have been obtained.

Fig. 46 shows the practically null diffusive flux of tritium to  $\text{CO}_2$ , whereas the final partial pressure of  $\text{T}_2$  in the secondary is lower than the tolerance of the code, which demonstrates the efficacy of silicon carbide as tritium permeation barrier.

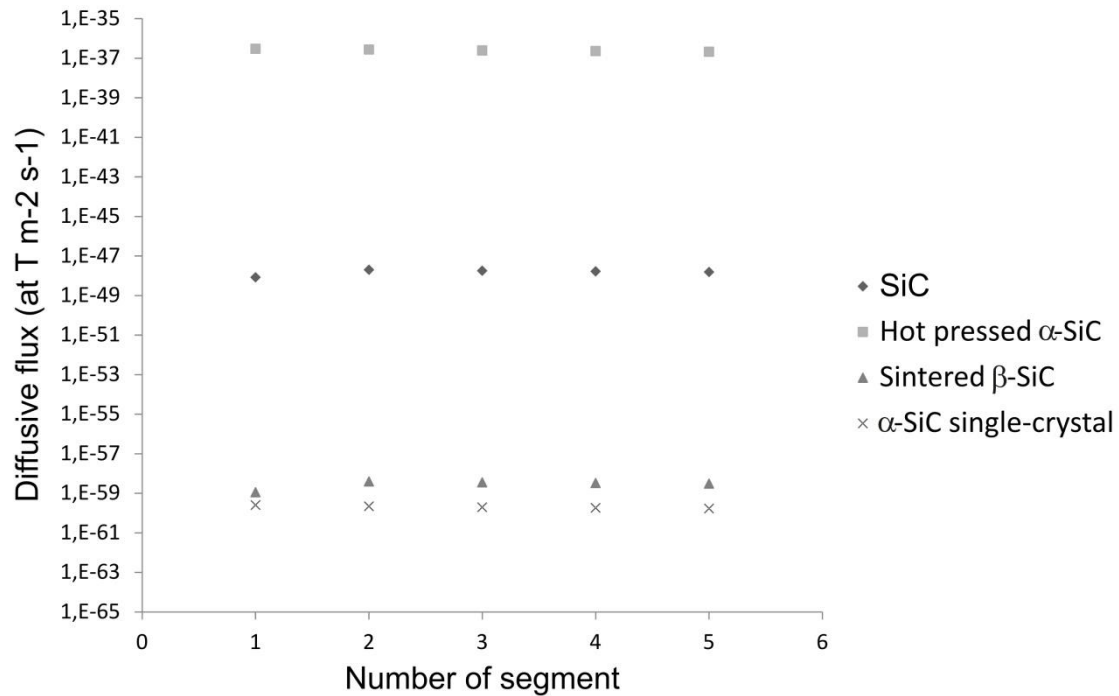


Fig. 46. Diffusive flux to the  $\text{CO}_2$  stream.

#### 3.5.4.6. The issue of blockage

Blockage has been reported by some authors as relatively usual in compact heat exchangers and specifically in PCHEs [Kimc 10] because of the use of microchannels. The liquid metal stream is particularly critical because of the presence of solid impurities and corrosion products. Regarding this, the choice of silicon carbide as structural material is an advantage because of its high resistance to flowing PbLi corrosion. However, particles coming from the rest of the PbLi loop can be transported and deposited inside the PCHE channels. In this sense, another important advantage of the present design is the fact that the wavy microchannels are replaced by wide channels with internal fins, which are less favourable to deposition. A stringent QA for the procurement of the PbLi and the development of efficient corrosion barriers for the breeding blanket and the rest of the loop, as well as PbLi purification methods, are key issues to avoid blockage in this kind of heat exchanger.

#### 3.5.4.7. Conclusions

A design of a lithium-lead/supercritical  $\text{CO}_2$  printed circuit heat exchanger which optimizes the pressure drop performance has been studied, and it has been pre-sized for its use in one of the power conversion cycles investigated for the TecnoFus Programme. Together with the use of silicon carbide as structural material, whose efficiency as tritium permeation barrier has been demonstrated, it supposes an interesting research line to be developed.

## 3.6. References

[Alb 10] G. Alberro, P.M. Martínez, E. Wirth, S. Moreau et al.,  $\text{H}_2/\text{D}_2$  Sieverts' solubility constant in LiPb eutectic from two independent Isovolumetric Desorption Tests, presentation for the International Workshop on Liquid Metal Breeder Blankets, CIEMAT, Madrid, 2010.

- [Aqu 07] D. Aquaro, M. Pieve, High temperature heat exchangers for power plants: performance of advanced metallic recuperators, *Applied Thermal Engineering* 27 (2007) 389-400.
- [Bah 12] J.S. Bahamonde-Noriega, Design Method for S-CO<sub>2</sub> Gas Turbine Power Plants, MSc dissertation, Delft University of Technology, 2012.
- [Bat 14] L. Batet, J.M. Álvarez-Fernández, E. Mas de les Valls, V. Martínez-Quiroga et al., Modelling of a supercritical CO<sub>2</sub> power cycle for nuclear fusion reactors using RELAP5-3D, *Fusion Engineering and Design* 89 (2014) 354-359.
- [Bub 13] E. Bubelis, W. Hering, Report on the results of BoP modelling for DEMO fusion power plant, final report for Task Agreement WP13-DAS08-T02, EFDA internal document (EFDA\_2M4RMC), 2013.
- [Cau 93] R.A. Causey, W.R. Wampler, J.R. Retelle, J.L. Kaae, Tritium migration in vapor-deposited  $\beta$ -silicon carbide, *Journal of Nuclear Materials* 203 (1993) 196-205.
- [Cha 08] J.E. Cha, T.H. Lee, J.H. Eoh, S.H. Seong et al., Supercritical CO<sub>2</sub> Brayton Cycle energy Conversion System Coupled with SFR, KAERI report TR-3680/2008, 2008.
- [Cha 09] J.E. Cha, T.H. Lee, J.H. Eoh, S.H. Seong et al., Development of supercritical CO<sub>2</sub> Brayton Energy conversion system coupled with a sodium cooled fast reactor, *Nuclear Engineering and Technology* 41 (2009) 1025-1044.
- [Chac 11] R. Chacartegui, J.M. Muñoz de Escalona, D. Sánchez, B. Monje, T. Sánchez, Alternative cycles based on carbon dioxide for central receiver solar power plants, *Applied Thermal Engineering* 31 (2011) 872-879.
- [Dos 04] V. Dostal, A Supercritical Carbon Dioxide Cycle for Next Generation Nuclear Reactors, Ph. D. Thesis, Massachusetts Institute of Technology, 2004.
- [Dos 09] V. Dostal, M. Kulhanek, Research on the supercritical carbon dioxide cycles in the Czech Republic, S-CO<sub>2</sub> Power Cycle Symposium 2009, RPI, Troy, USA, 2009.
- [Efd 11] EFDA Power Plant Physics and Technology (PPPT) Monitoring 2011, EFDA internal document (EFDA\_D\_2MJTU7), 2011.
- [Est 02] G.A. Esteban, A. Perujo, F. Legarda, L.A. Sedano, B. Riccardi, Deuterium transport in SiC<sub>f</sub>/SiC composites, *Journal of Nuclear Materials* 307-311 (2002) 1430-1435.
- [Fed 14] G. Federici, R. Kemp, D. Ward, C. Bachmann et al., Overview of EU DEMO design and R&D activities, *Fusion Engineering and Design* 89 (2014) 882-889.
- [Fern 12] I. Fernández, L. Sedano, Design analysis of a lead-lithium/supercritical CO<sub>2</sub> printed circuit heat exchanger for primary power recovery, *Fusion Engineering and Design* 88 (2013) 2427-2430.
- [Fern 14] I. Fernández, Summary of FUSKITE results on materials, modeling and data analysis, presentation for the 2<sup>nd</sup> EU-US DCLL Workshop, University of California, Los Angeles, 2014.
- [Flo 13] J. Floyd, N. Alpy, A. Moiseyev, D. Haubensack et al., A numerical investigation of the S-CO<sub>2</sub> recompression cycle off-design behavior, coupled to a sodium cooled fast reactor, for seasonal variation in the heat sink temperature, *Nuclear Engineering and Design* 260 (2013) 78-92.
- [Ful 12] R. Fuller, J. Noall, J. Preuss, Turbomachinery for supercritical CO<sub>2</sub> power cycles, GT2012, Proceedings of the ASME Turbo Expo 2012, Copenhagen, 2012.

- [Gez 04] K. Gezelius, Designs of Compact Intermediate Heat Exchangers for Gas Cooled Fast Reactors, MSc dissertation, Massachusetts Institute of Technology, 2004.
- [Gia 03] L. Giancarli, L. Bühler, U. Fischer, R. Enderle et al., In-vessel component designs for a self-cooled lithium-lead fusion reactor, *Fusion Engineering and Design* 69 (2003) 763-768.
- [Hal 12] B. Halimi, K.Y. Suh, Computational analysis of supercritical CO<sub>2</sub> Brayton cycle power conversion system for fusion reactor, *Energy Conversion and Management* 63 (2012) 38-43.
- [Han 09] W.E. Han, D. J. Ward, Revised assessments of the economics of fusion power, *Fusion Engineering and Design* 84 (2009) 895-898.
- [Har 12] J. Harman, Input parameters for balance of plant design assessment studies, technical note for the Task Agreement WP12-DAS08-T01, EFDA internal document (EFDA\_D\_2LEKX7), 2012.
- [Har 13] J. Harman, Technical Specification for WP13-DAS08: Primary Heat Transfer & Balance of Plant Systems, EFDA internal document (EFDA\_D\_2LJB2E), 2013.
- [Her 09] L.E. Herranz, J.I. Linares, B.Y. Moratilla, Power cycle assessment of nuclear high temperature gas-cooled reactors, *Applied Thermal Engineering* 29 (2009) 1759-1765.
- [Hes 01] J.E. Hesselgreaves, Compact Heat Exchangers. Selection, Design and Operation, Pergamon, Amsterdam, 2001.
- [Ish 08] S. Ishiyama, Y. Muto, Y. Kato, S. Nishio et al., Study of steam, helium and supercritical CO<sub>2</sub> turbine power generations in prototype fusion power reactor, *Progress in Nuclear Energy* 50 (2008) 325-332.
- [Ive 13] B.D. Iverson, T.M. Conboy, J.J. Pasch, A.M. Kruizenga, Supercritical CO<sub>2</sub> Brayton cycles for solar-thermal energy, *Applied Energy* 111 (2013) 957-970.
- [Jeo 13] W.S. Jeong, Y.H. Jeong, Performance of supercritical Brayton cycle using CO<sub>2</sub>- based binary mixture at varying critical pints for SFR applications, *Nuclear Engineering and Design* 262 (2013) 12-20.
- [Kal 14] C. Kalra, D. Hofer, E. Sevincer, J. Moore, K. Brun, Development of high efficiency hot gas turbo-expander for optimized CSP supercritical CO<sub>2</sub> power block operation, 4<sup>th</sup> International Symposium on Supercritical CO<sub>2</sub> Power Cycles, Pittsburgh, 2014.
- [Kimc 10] C.S. Kim, D-U. Seo, T-H. Yoo, S-D. Hong, Y.W. Kim, Operation Experiences of the Small Scale Nitrogen Loop with a Water-Cooling Printed Circuit Heat Exchanger, Transactions of the Korean Nuclear Society Autumn Meeting, Jeju, Korea, 2010.
- [Kimd 08] D.E. Kim, M.H. Kim, J.E. Cha, S.O. Kim, Numerical investigation on thermal-hydraulic performance of new printed circuit heat exchanger model, *Nuclear Engineering and Design* 238 (2008) 3269-3276.
- [Kimj 10] J.H. Kim, S. Baek, S. Jeong, J. Jung, Hydraulic performance of a microchannel PCHE, *Applied Thermal Engineering* 30 (2010) 2157-2162.
- [Kov 13] M. Kovari, J. Harman, WP13-DAS08 Balance of Plant: Suggestions for reporting plant power and efficiency, EFDA internal document (EFDA\_D\_2LJYCN), 2013.
- [Kov 13b] M. Kovari. C. Howorth, Molten salt energy storage for helium-cooled reactor, final report for Task Agreement WP13-DAS08-T03, EFDA internal document (EFDA\_D\_2MF92C), 2013.
- [Lad 96] C.L. Ladson, C.W. Brooks Jr., A.S. Hill, D.W. Sproles, Computer Program To Obtain Ordinates for NACA Airfoils, NASA technical memorandum 4741, 1996.

[Lat 12] H. Latham, P. Clarkson, Fusion Balance of Plant Assessment (under EFDA WP12-DAS08-BoP), EFDA internal document (EFDA\_D\_2LLNBX), 2012.

[Lat 13] H. Latham, J. Charlton, M. Kovari, C. Harrington et al., Definition of Steam Based Power Conversion System for Fusion DEMO reactor, final report for Task Agreement WP13-DAS08-T02, EFDA internal document (EFDA\_2M97B7), 2013.

[Lat 13b] H. Latham, Design assessment of pulsed power profiles in relation to balance of plant systems, final report for Task Agreement WP13-DAS08-T04, EFDA internal document (EFDA\_D\_2MJW5L), 2013.

[Lin 11] J.I. Linares, L.E. Herranz, B.Y. Moratilla, I.P. Serrano, Power conversion systems based on Brayton cycles for fusion reactors, *Fusion Engineering and Design* 86 (2011) 2735-2738.

[Lin 13] J.I. Linares, L.E. Herranz, I. Fernández, B.Y. Moratilla, A. Cantizano, Design, modelling and analysis of primary heat transfer and BoP options for integration with a DEMO fusion power plant: Final Report on supercritical CO<sub>2</sub> Brayton power cycles, final report for Task Agreement WP13-DAS08-T02, EFDA internal document (EFDA\_D\_2L58SM), 2013.

[Lin 15] J.I. Linares, L.E. Herranz, I. Fernández, A. Cantizano, B.Y. Moratilla, Supercritical CO<sub>2</sub> Brayton power cycles for DEMO fusion reactor based on Helium Cooled Lithium Lead blanket, *Applied Thermal Engineering* 76 (2015) 123-133.

[Ma 11] Z. Ma, C.S. Turchi, Advanced supercritical carbon dioxide power cycle configurations for use in concentrating solar power systems, *Supercritical CO<sub>2</sub> Power Cycle Symposium*, Boulder, NREL/CP- 5500-50787, 2011.

[Mai 05] D. Maisonnier, I. Cook, P. Sardain, R. Andreani et al., A Conceptual Study of Commercial Fusion Power Plants – final report of the European Fusion Power Plant Conceptual Study (PPCS), EFDA internal document (EFDA-RP-RE-5.0), 2005.

[Mal 99] S. Malang, Limitations on blanket performance, *Fusion Engineering and Design* 46 (1999) 193-206.

[Mar 14] F. Martín-Fuertes, I. Fernández, I. Palermo, D. Rapisarda, E. Mas de les Valls, DCLL CAD, Neutronic, Thermo-Hydraulic and Thermo-mechanical analysis – Contribution to DDD2014, WPBB-D-421-01, Eurofusion internal document (EFDA\_D\_2LLRQS), 2014.

[Marl 13] L. Martín, M. Martín, Optimal year-round operation of a concentrated solar energy plant in the south of Europe, *Applied Thermal Engineering* 59 (2013) 627-633.

[Mas 08] E. Mas de les Valls, L. Sedano, L. Batet, I. Rikapito et al., Lead-lithium eutectic material database for nuclear fusion technology, *Journal of Nuclear Materials* 376 (2008), 252-257.

[Mcd 14] C.F. McDonald, Power conversion system considerations for a high efficiency small modular nuclear gas turbine combined cycle power plant concept (NGTCC), *Applied Thermal Engineering* 73 (2014) 80-101.

[Med 07] M. Medrano, D. Puente, E. Arenaza, B. Herrazti et al., Power conversion cycles study for He-cooled reactor concepts for DEMO, *Fusion Engineering and Design* 82 (2007) 2689-2695.

[Mey 13] J.M. Meyers, D.G. Fletcher, Y. Dubief, Lift and Drag on an Airfoil, Thermo-Fluids Laboratory notes, University of Vermont, 2013.

[Mit 06] M. Mito, N. Yoshioka, Y. Ohkubo, N. Tsuzuki, Y. Kato, Fast reactor with indirect cycle system of supercritical CO<sub>2</sub> gas turbine plant, ICAPP 06, Reno, 2006.

- [Moi 09] A. Moiseyev, J.J. Sienicki, Investigation of alternative layouts for the supercritical carbon dioxide Brayton cycle for a sodium-cooled fast reactor, *Nuclear Engineering and Design* 239 (2009) 1362-1371.
- [Ngo 06] T.L. Ngo, Y. Kato, K. Nikitin, N. Tsuzuki, New printed circuit heat exchanger with S-shaped fins for hot water supplier, *Experimental Thermal and Fluid Science* 30 (2006) 811-819.
- [Nik 06] K. Nikitin, Y. Kato, L. Ngo, Printed circuit heat exchanger thermal-hydraulic performance in supercritical CO<sub>2</sub> experimental loop, *International Journal of Refrigeration* 29 (2006) 807-814.
- [Nist] NIST database (<http://webbook.nist.gov/chemistry/fluid>).
- [Noz 09] T. Nozawa, T. Hinoki, A. Hasegawa, A. Hokhyama et al., Recent advances and issues in development of silicon carbide composites for fusion applications, *Journal of Nuclear Materials* 386-388 (2009) 622-627.
- [Oh 08] C. Oh, E. Kim, Heat Exchanger Design Options and Tritium Transport Study for the VHTR System, Idaho National Laboratory report (INL/EXT- 08-14799), 2008.
- [Pal 12] I. Palermo, J.M. Gómez-Ros, G. Veredas, J. Sanz, L. Sedano, Neutronic design analyses for a dual-coolant blanket concept: Optimization for a fusion reactor DEMO, *Fusion Engineering and Design* 87 (2012) 1019-1024.
- [Pam 09] J. Pamela, A. Bécoulet, D. Borba, J.-L. Boutard et al., Efficiency and availability driven R&D issues for DEMO, *Fusion Engineering and Design* 84 (2009) 194-204.
- [Par 09] Y.H. Park, T. Hinoki, A. Kohyama, Development of multi-functional NITE-porous SiC for ceramic insulators, *Journal of Nuclear Materials* 386-388 (2009) 1014-1017.
- [Per 15] P. Pereslavtsev, General Issues affecting the tritium breeding performance, presentation for the WPBB Design Review Meeting, EUROfusion internal document, 2015.
- [Perp 12] G.D. Pérez-Pichel, J.I. Linares, L.E. Herranz, B.Y. Moratilla, Thermal analysis of supercritical CO<sub>2</sub> power cycles: assessment of their suitability to the forth-coming sodium fast reactors, *Nuclear Engineering and Design* 250 (2012) 23-24.
- [Por 12] M. Porton, V. Vizvary, H. Latham, P. Clarkson, Assessment of DEMO-relevant helium-cooled balance of plant technology, final report for Task Agreement WP12-DAS-08-T02, EFDA internal document (EFDA\_D\_2M4XFP), 2012.
- [Ric 04] B. Riccardi, L. Giancarli, A. Hasegawa, Y. Katoh et al., Issues and advances in SiC/SiC composites development for fusion reactors, *Journal of Nuclear Materials* 329-333 (2004) 56-65.
- [Sac 14] R. Sacristán, G. Veredas, I. Bonjoch, I. Peñalva et al., Fuskite® preliminary experimental tests based on permeation against vacuum for hydrogen recovery as a potential application in Pb15.7Li loop systems, *Fusion Engineering and Design* 89 (2014) 1551-1556.
- [Sak 14] Y. Sakamoto, M. Nakamura, K. Tobita, H. Utoh et al., Relationship between net electric power and radial build of DEMO based on ITER steady-state scenario parameters, *Fusion Engineering and Design* 89 (2014) 2440-2445.
- [San 13] J. Sánchez (coordinating researcher) et al., Consolider-Ingenio 2010 Programme: Scientific Closing Report for Project CSD2008\_079, 2013.
- [Sar 09] J. Sarkar, Second law analysis of supercritical CO<sub>2</sub> recompression Brayton cycle, *Energy* 34 (2009) 1172-1178.

- [Ser 12] I.P. Serrano, A. Cantizano, J.I. Linares, B.Y. Moratilla et al., Numerical modeling and design of supercritical CO<sub>2</sub> pre-cooler for fusion nuclear reactors, *Fusion Engineering and Design* 87 (2012) 1329-1332.
- [Ser 13] I.P. Serrano, J.I. Linares, A. Cantizano, B.Y. Moratilla, A novel supercritical CO<sub>2</sub> power cycle for energy conversion in fusion power plants, *Fusion Science and Technology* 64 (2013) 483-487.
- [Ser 14] I.P. Serrano, A. Cantizano, J.I. Linares, B.Y. Moratilla, Modelling and sizing of the heat exchangers of a new supercritical CO<sub>2</sub> Brayton power cycle for energy conversion for fusion reactors, *Fusion Engineering and Design* 89 (2014) 1905-1908.
- [Ser 14b] I.P. Serrano, J.I. Linares, A. Cantizano, B.Y. Moratilla, Enhanced arrangement for recuperators in supercritical CO<sub>2</sub> Brayton power cycle for energy conversion in fusion reactors, *Fusion Engineering and Design* 89 (2014) 1909-1912.
- [Sin 13] R. Singh, S.A. Miller, A.S. Rowlands, P.A. Jacobs, Dynamic characteristics of a direct-heated supercritical carbon-dioxide Brayton cycle in solar thermal power plant, *Energy* 50 (2013) 194-204.
- [Smo 08] S. Smolentsev, N.B. Morley, C. Wong, M. Abdou, MHD and heat transfer considerations for the US DCLL blanket for DEMO and ITER TBM, *Fusion Engineering and Design* 83 (2008) 1788-1791.
- [Sne 11] L.L. Snead, T. Nozawa, M. Ferraris, Y. Katoh et al., Silicon carbide composites as fusion power reactor structural materials, *Journal of Nuclear Materials* 417 (2011) 330-339.
- [Son 07] H. Song, Investigations of a Printed Circuit Heat Exchanger for Supercritical CO<sub>2</sub> and Water, MSc dissertation, Kansas State University, 2007.
- [Sto 14] D. Stork, P. Agostini, J.-L. Boutard, D. Buckthorpe et al., Materials R&D for a timely DEMO: Key findings and recommendations of the EU Roadmap Materials Assessment Group, *Fusion Engineering and Design* 89 (2014) 1586-1594.
- [Tak 10] Y. Takeuchi, C. Park, K. Noborio, Y. Yamamoto, S. Konishi, Heat transfer in SiC compact heat exchanger, *Fusion Engineering and Design* 85 (2010) 1266-1270.
- [Tsu 07] N. Tsuzuki, Y. Kato, T. Ishiduka, High performance printed circuit heat exchanger, *Applied Thermal Engineering* 27 (2007) 1702-1707.
- [Tur 13] C. Turchi, T. Held, J. Pasch, K. Gawlik, 10-MW Supercritical-CO<sub>2</sub> Turbine Test, SunShot Concentrating Solar Power Program Review 2013, Phoenix, 2013.
- [Ward 15] D. Ward, R. Kemp, The resilience of an operating point for a fusion power plant, *Fusion Engineering and Design*, in press-corrected proof.
- [Wei 11] P.S. Weitzel, Steam generator for advanced ultra-supercritical power plants 700 to 760C, ASME 2011 Power Conference, Denver, 2011.
- [Wri 10] S.A. Wright, R.F. Radel, M.E. Vermon, G.E. Rochau, P.S. Pickard, Operation and Analysis of a Supercritical CO<sub>2</sub> Brayton Cycle, Sandia National Laboratories report (SAND2010-0171), 2010.
- [Wri 10b] S.A. Wright, R.F. Radel, R. Fuller, Engineering performance of supercritical CO<sub>2</sub> Brayton cycles, ICAPP 10, San Diego, 2010.
- [Wri 11] S.A. Wright, T. Conboy, G. Rochau, Break-even Power Transients for two Simple Recuperated S-CO<sub>2</sub> Brayton Cycle Test Configurations, Supercritical CO<sub>2</sub> Power Cycle Symposium, Boulder, 2011.

[Xu 14] X. Xu, T. Ma, L. Li, M. Zeng et al., Optimization of fin arrangement and channel configuration in an airfoil fin PCHE for supercritical CO<sub>2</sub> cycle, *Applied Thermal Engineering* 70 (2014) 867-875.

[Yum 13] S.B. Yum, E.H. Lee, D.W. Lee, G.Ch Park, Model validation of GAMMA code with heat transfer experiment for KO TBM in ITER, *Fusion Engineering and Design* 88 (2013) 716-720.

[Zin 04] A.V. Zinovev, J.F. Moore, J. Hryn, O. Auciello et al., Chemical Etching of Silicon Carbide Ceramic Surface in Chlorine-Containing Gas Mixtures, *28<sup>th</sup> International Conference on Advanced Ceramics and Composites B: Ceramic Engineering & Science Proceedings* 25 (2004) 405-410.

[Zol 11] G. Zollino, G. Casini, D. Pierobon, V. Antoni et al., A comparison between a steady state and a pulsed fusion power plant, *Fusion Engineering and Design* 86 (2011) 2782-2790.

# **Chapter IV**

***The value of CAD & graphic design tools and virtual reality in the integration of complex systems***



## List of figures

Fig. 1. Set of geometric operations in the CATIA structured tree (left) .....	286
Fig. 2. 3DVia Composer interface (timeline located at the bottom) .....	287
Fig. 3. Pivot-type kinematics link between two pieces of the Hot Cell manipulator right clamp .....	287
Fig. 4. Extraction operation step 1 .....	289
Fig. 5. Extraction operation step 2 .....	289
Fig. 6. Extraction operation step 3 .....	289
Fig. 7. Extraction operation step 4 .....	290
Fig. 8. Extraction operation step 5 .....	290
Fig. 9. Extraction operation step 6 .....	291
Fig. 10. Split operation step 1 .....	292
Fig. 11. Split operation step 2 .....	292
Fig. 12. Split operation step 3 .....	293
Fig. 13. Split operation step 4 .....	293
Fig. 14. Split operation step 5 .....	294
Fig. 15. Split operation step 6 .....	294
Fig. 16. Split operation step 7 .....	295
Fig. 17. Split operation step 8 .....	295
Fig. 18. Split operation step 9 .....	296
Fig. 19. Split operation step 10 .....	296
Fig. 20. Split operation step 11 .....	297
Fig. 21. Split operation step 12 .....	297
Fig. 22. Split operation step 13 .....	298
Fig. 23. Insertion operation step 1 .....	299
Fig. 24. Insertion operation step 2 .....	299
Fig. 25. Insertion operation step 3 .....	300
Fig. 26. Insertion operation step 4 .....	300
Fig. 27. Insertion operation step 5 .....	301
Fig. 28. Insertion operation step 6 .....	301
Fig. 29. Insertion operation step 7 .....	302
Fig. 30. Insertion operation step 8 .....	302
Fig. 31. Insertion operation step 9 .....	303
Fig. 32. Insertion operation step 10 .....	303
Fig. 33. Pipe Forest & Bioshield Door assembly installation step 1 .....	305
Fig. 34. Pipe Forest & Bioshield Door assembly installation step 2 .....	305
Fig. 35. Pipe Forest & Bioshield Door assembly installation step 3 .....	306
Fig. 36. Pipe Forest & Bioshield Door assembly installation step 4 .....	306
Fig. 37. Pipe Forest & Bioshield Door assembly installation step 5 .....	307
Fig. 38. Pipe Forest & Bioshield Door assembly installation step 6 .....	307
Fig. 39. Pipe Forest & Bioshield Door assembly installation step 7 .....	308
Fig. 40. Pipe Forest & Bioshield Door assembly installation step 8 .....	308
Fig. 41. Pipe Forest & Bioshield Door assembly installation step 9 .....	309
Fig. 42. Pipe Forest & Bioshield Door assembly installation step 10 .....	309
Fig. 43. Pipe Forest & Bioshield Door assembly installation step 11 .....	310
Fig. 44. Pipe Forest & Bioshield Door assembly removal step 1 .....	310
Fig. 45. Pipe Forest & Bioshield Door assembly removal step 2 .....	311
Fig. 46. Pipe Forest & Bioshield Door assembly removal step 3 .....	311
Fig. 47. Pipe Forest & Bioshield Door assembly removal step 4 .....	312
Fig. 48. IF2a connection step 1 .....	313
Fig. 49. IF2a connection step 2 .....	313
Fig. 50. IF2a connection step 3 .....	314
Fig. 51. IF2a connection step 4 .....	314
Fig. 52. IF2a connection step 5 .....	314
Fig. 53. IF2a connection step 6 .....	315
Fig. 54. IF2a connection step 7 .....	315
Fig. 55. IF2a connection step 8 .....	315
Fig. 56. IF2a connection step 9 .....	316

Fig. 57. IF2a connection step 10. ....	316
Fig. 58. IF2a connection step 11. ....	316
Fig. 59. IF2a connection step 12. ....	317
Fig. 60. IF2a connection step 13. ....	317
Fig. 61. IF2a disconnection step 1. ....	317
Fig. 62. IF2a disconnection step 2. ....	318
Fig. 63. IF2a disconnection step 3. ....	318
Fig. 64. AEU installation step 1. ....	319
Fig. 65. AEU installation step 2. ....	320
Fig. 66. AEU installation step 3. ....	320
Fig. 67. AEU removal step 1. ....	321
Fig. 68. AEU removal step 2. ....	321
Fig. 69. Cross-section of the divertor area, divertor port ant transfer cask. RH equipment (in bold characters) is transporting a divertor cassette along the divertor RH port duct [F4E 11]. ....	322
Fig. 70. Cassette layout, supported by the vessel rails [F4E 11]. ....	323
Fig. 71. Cable guide reference design [Ass 13]. ....	323
Fig. 72. Cassette toroidal mover transporting a divertor cassette. The reference cable guide design is shown [F4E 11]. ....	324
Fig. 73. Side view of the reference design joint mock-up [Ass 13]. ....	324
Fig. 74. Telescopic and chain cable guide [Fern 13]. ....	325
Fig. 75. Electrical, optical and hydraulic interfaces [Fern 13]. ....	326
Fig. 76. Multi-pin connector [Fern 13]. ....	326
Fig. 77. Umbilical side socket [Fern 13]. ....	327
Fig. 78. Detail of the toroidal movement sequence kinematic model in Blender. 'Bones' and 'empty' elements are shown. ....	328
Fig. 79. Detail of the connector mating sequence kinematic model in Blender. ....	328
Fig. 80. Blender graphical interface: CTM, divertor system and vacuum vessel model. ....	329
Fig. 81. Toroidal movement step 1. ....	330
Fig. 82. Toroidal movement step 2. ....	331
Fig. 83. Toroidal movement step 3. ....	331
Fig. 84. Toroidal movement step 4. ....	332
Fig. 85. Toroidal movement step 5. ....	332
Fig. 86. Toroidal movement step 6. ....	333
Fig. 87. View from the camera mounted on the CTM (1). ....	333
Fig. 88. View from the camera mounted on the CTM (2). ....	334
Fig. 89. View from the zenithal camera (1). ....	334
Fig. 90. View from the zenithal camera (2). ....	335
Fig. 91. Multi-pin connector plugging step 1. ....	336
Fig. 92. Multi-pin connector plugging step 2. ....	336
Fig. 93. Multi-pin connector plugging step 3. ....	337
Fig. 94. Multi-pin connector plugging step 4. ....	337
Fig. 95. Multi-pin connector plugging step 5. ....	338
Fig. 96. Multi-pin connector plugging step 6. ....	338
Fig. 97. Identification of a problem related to the guidance system and the articulation position. ....	339

## 4.1. Introduction

Some reflexions on the role of CAD modelling and kinematics simulation in the integration of components and complex systems are made in this chapter. Part of the exposed ideas is applied to several practical cases regarding the remote maintenance of the Test Blanket System and the Divertor System in ITER.

## 4.2. CAD kinematics simulation and virtual reality

CAD combined with graphical design software and kinematics simulations are very useful to validate integration concepts and maintenance operations from the early design stages. They allow reducing the time and cost of development by reducing the number of physical mock-ups and avoiding deadlocks. Effectively, the construction of mock-ups is time consuming, expensive and only cost effective in a late phase in the design [Oos 14]. If the design does not comply or changes due to other reasons, the full design cycle has to be repeated.

If the digital models can be examined through an immersive virtual reality (VR) system, the user experiences the sensation of staying in a real environment scene where it is possible to interact with the numerical mock-up intuitively in real-time. This improves the exchange of information between designers or design teams discussing in front of the same model and makes much easier to identify possible issues. Even it is possible to recommend solutions to identified anomalies through the same software platform, so they can be corrected by the design office [Kel 13].

VR can be used from the conceptual design phase right into the operational phase with the digital environment increasing in complexity and realism as more data is known [Elz 09]. It results particularly useful in the case of remote handling (RH) integration assessments and design of remote maintenance operations, whose implication in the availability of fusion reactors has been discussed in Chapter 2. Animated sequences of assembly and maintenance operations can be created through CAD tools, whereas the required level of realism is achieved by means of graphical design tools (real-time rendering) or through functions included in the same CAD software. By examining these sequences, it is possible to check that no collision happens, and if assembly clearances and functional gaps are well considered and sufficient [Kel 13]. Instead of comparing only key positions (according to the classic method) the full paths can be followed continuously, taking advantage of collision/contact evaluation functions available in current software tools. VR also allows a better understanding of the restrictions of the remote maintenance process [Elz 09], which can influence the design of the handled/repared component.

Some examples of the application of virtual reality to the design of fusion technology components or the planning of RH operations can be given. CEA has built an immersive virtual reality platform which directly integrates the CAD software used in the institute (CATIA, 3DVia Composer, Solidworks, etc.). This tool enables the user to interact with the simulated environment and helps to imagine what will be the real environment and if maintenance and accessibility to critical components is feasible [Kel 13]. Takeda et al. developed a simulator for the remote maintenance system of the ITER blanket modules which provides some visual virtual information [Tak 08]. In the case of the ITER ECH (Electron Cyclotron Heating) system remote maintenance, the VR analysis of the replacement of a blanket shielding module carried out by Elzendoorn et al. resulted in the introduction of new RH tools and equipment as well as access plugs and hatches in the upper port launcher (UPL) design. Furthermore, during the analysis of the task sequence several additional tasks were identified. On the other hand, the logistics and the geometry of the UPL handover from the vessel to the cask and from the cask into the Hot Cell were identified as critical [Elz 09]. Ferlay et al. carried out a man-in-the-loop simulation of the critical remote handling steps for the RH maintenance of the ITER ICH&CD (Ion Cyclotron Heating & Current Drive) antenna in the Hot Cell [Ferl 13]. The simulations of the removal and installation of the straight plates with captive screws highlighted the need of a handle compatible with a robotic gripper and also a small gripper because of the tight space and the low visibility.

Apart from the design review of components, the integration of complex systems and the verification of remote handling equipment paths, one of the most interesting applications of CAD and virtual reality is the interactive simulation of operations with man-in-the-loop. Thus, modelling has become an important tool for both the planning of RH operation sequences and for providing an overview of operations during task execution [Ham 14], including estimation of mean time to repair (MTTR). Teleoperation has notably evolved in last years in relation to perception of the environment by the operator. Today, virtual reality and operator support systems are widely used to reduce the amount of mental and physical workload perceived by the operators and to make teleoperation tasks faster and safer.

In virtual reality systems, teleoperators are not guided by images captured by cameras installed in the operation area. They operate based on views of CAD models which are updated in order to reconstruct in real-time the positions of the RH equipment, the handled components and the environment from data transmitted from sensing instruments installed in motors and actuators (resolvers, LVDTs, etc.), as well as from other instruments like limit switches, inclinometers, etc. This presents important advantages over the real view operation, since in fusion devices, achieving good viewing of the remote environment during maintenance activities can be very challenging. Restricted camera locations, poor lighting, cluttered space, lack of contrast in objects, the hazardous environment for sensors, all contribute to making it difficult to gain an adequate level of viewing for carrying-out remote maintenance operations [Ham 14]. Augmented virtual reality (AVR) provides guidance support to operators during the execution of maintenance tasks. An AVR system can generate any view of the operation area, so the RH operators can always view the work area of particular interest to the current task with any zoom factor. In a system based solely on camera images for primary viewing, the views are limited to those where the cameras can physically go, both in terms of manipulator location as well as due to obstructions. Further, an obstruction in the desired viewing path is still not a problem as components can be drawn as wire frames allowing operators to see through them while still being aware of their location [Kin 09]. This could be particularly useful for insertion tasks where the area for insertion is often blocked from real world line of sight viewing by both the component itself and the manipulator being used in the task.

Another advantage of an AVR system is the consistent interface presented to those using the system independent of the sensor selection imposed by the hazardous environment. The benefits of operators having exactly the same experience when using the system offline in training with a physical simulation of the environment to that found in actual operations is clear. For example, when using cameras in an environment like the inside of a tokamak a combination of the lighting, the image quality available from radiation hardened cameras and the fact that most of the components end up a similar colour after plasma operations serves to remove many of the elements that aid human depth perception. Cameras also take away binocular and focal length cues [Kin 09]. However, An AVR system could artificially reintroduce colour and shading cues to the environment as displayed to the RH operators, simultaneously reducing the likelihood of mistakes caused by errors in depth judgement and increasing operator confidence, thus improving productivity [Kin 09].

Another interesting benefit of augmented virtual reality is the possibility of using visual assistances consisting in displaying the available actions in the environment. When a procedure step is selected by the operator, the system can display the interfaces which are compatible in the environment. Augmented reality is useful in this case to display relevant information in the field of view of the operator by overlaying the virtual reality visualization for instance. Objective of such assistances is thus to improve the operator situation awareness by relieving the workload for perception of relevant information in the environment and understanding of this information. In other words, virtual guides are used to restrain degrees of freedom in order to facilitate the achievement of actions [Zie 13]. The objective is to release the operator from the complete control of the motion. Indeed, a transparent representation simulating the object motion that is to be achieved with the virtual guide can be displayed in the virtual reality visualization to help the operator understand the assistance [Zie 13].

Nevertheless, standard virtual reality modelling is not enough for operations that interact with the environment and direct sensing of the changing environment becomes necessary. There are some methods which consist on constructing 3D models based on fusing live sensing of the

remote environment and existing model data [Ham 14], as well as on the presentation of 'synthetic' views to the operator. These views have demonstrated different advantages over direct viewing like providing ideal viewpoints, revealing occluded areas or implementing good lighting and colour contrast. Up to now, special markers have been used to help identifying and localizing environment objects in real-time, but it is expected that improvements in object recognition and localization algorithms and computing speed will make possible to do without them [Ham 14].

### **4.2.1. Dynamic effects**

Apart from visual virtual reality, haptic shared control systems –which suppose another form of augmented virtual reality- have demonstrated to improve teleoperation results significantly. The idea is to assist the operators during haptic bilateral teleoperation tasks by generating virtual forces based on virtual models of the teleoperation environment and sensor data from the slave manipulator [Vii 14]. These artificial assisting forces are combined with force feedback signals from the environment. The assisting forces make bilateral teleoperation more efficient and safer by guiding the operator to the point of interest in the teleoperation environment, and by damping motion when close to contact with protected areas of the teleoperation environment [Vii 14]. Until recent times, VR systems for teleoperation only used geometric models of the environment and the objects being handled as well as kinematic models of the manipulation systems based on real-time rigid body dynamics. However, dynamic effects are included in present VR simulations.

One example of important dynamic effects are forces due to contact transitions, that is, transitions from noncontact to contact states, which should be fast and stable with minimal impact forces and without bounce [Nel 95]. Other relevant dynamic effect is the bending of beams under heavy loads. In fusion reactors, the large loads being handled (many tons) can mean that the RH equipment will have significant deviation from the rigid body kinematics typically assumed in VR models. Saarinen et al. developed for ITER a methodology based on introducing additional coordinate frames at key locations along a mechanical structure to capture the deflections of the joining beams [Saa 13]. They used a general deflection model for the deflection transformations, whereas both structural analysis and real structure measurements were employed to calibrate the deflection model parameters. This approach was used on the Cassette Multifunctional Mover (CMM) prototype on the Divertor Test Platform (DTP2), with the VR model accuracy improving from 80 mm to 5 mm, even during the release/lift transitions of the 9 t divertor cassette load [Saa 13]. Heemskerk et al. investigated the addition of dynamic effects into the VR simulations of maintenance operations on the ITER ECH upper port launcher plug with the challenge of modelling jamming and wedging. They found it very promising, and they also concluded that force feedback in operations with 6 degrees of freedom (DOF) is indispensable [Hee 11].

### **4.2.2. Web-based virtual reality environments**

A kind of development which has received increasingly large amounts of attention is the implementation of web-based virtual reality environments. Kim et al. established a web-based (HTML5) interactive toolkit which allows users to dynamically create, interact and share with others, large sets of data generated by fusion experiments and simulations [Kim 12]. General Atomics developed a customizable scientific web-portal for the DIII-D nuclear fusion experiment which supported interactive collaborations and provided services such as real-time experiment status monitoring, diagnostic data access, interactive data analysis and visualization [Abla 10]. Iba et al. constructed the JT-60U remote research environment and confirmed the efficiency of developing such virtual experimental system [Iba 08]. Li et al. proposed an approach to establish the real-time virtual EAST physical experiment system for browsers to roam in the environment and get experimental information by interacting with the environment [Li 14]. They concluded that technologies such as VRML, Java 3D, JSP and HTML are able to help producing high interaction and good rendering performance.

One of the most significant examples of web-based VR environments is the case of JET. During the planning of the EP2 shutdown in JET, remote handling engineers started preparing their component strip-out and installation procedures when component designs were still evolving. Therefore changes to the VR models representing individual components were required to be remotely and globally updated on all the circulating versions. The use of a new VR code (VR4MAX) allowed structuring the JET Vessel VR model using externally referenced models. This enabled multiple engineers to have individually configurable VR models that at the same time could have their constituent parts remotely updated as the design of component parts evolved. This ensured the RH engineers were always rehearsing their tasks in the most up-to-date VR environment [Rob 09] [Wil 11].

### **4.2.3. Virtual reality for hands-on maintenance**

Regarding the maintenance of fusion devices, virtual reality is not only applied to harsh environments and remote handling systems, but also to assess hands-on operations. In fact, 3D CAD software with digital human models (DHM) technology is very useful to investigate human accessibility to environments with restricted space. For example, Tarallo et al. used the CATIA Human Builder module to support the design of a suitable arrangement for equipment and piping lines of the part of the ITER Test Blanket System located at the CVCS area (Chemical and Volumetric Control System), by checking the human accessibility and the maintenance postures [Tar 15]. In some cases, the simulations resulted in changes in the initial space reservations.

### **4.2.4. Reliability in remote handling software**

Software failures have passed hardware as the most common source for computer system outages in the last decades [Gray 90]. Plant subsystems like RH may have complex safety-related functionality which must be implemented with software. Examples of such conditions include stability of machines, anti-collision systems and reduced speed & restricted space for robots. Therefore, software failures present a major threat for the reliability of remote handling systems.

Safety critical subsystems include [Alh 13]:

- RH input device and computer assisted teleoperation (CAT) which are used for control in manual control.
- Virtual reality which provides information for CAT.
- Command and control which is used for executing commands in automatic operations.

Any software feature identified as a potential hazard should be designated as safety-critical to ensure that future changes and verification processes can take them into consideration [NASA 04]. Candidates for safety-critical items list can be identified through failure mode and effects analysis (FMEA).

Software development is usually guided by dependability requirements instead of strict safety standards, as risks are economical ones. Cost-efficient development needs to take into account that different subsystems therefore need different levels of reliability (e.g. diagnostics is not as critical as command & control). Systematically developed requirements can be used to form a dependability case for the system under development, where requirements, architectural solutions, verification etc. are provided to give sufficient confidence in the reliability of software [Alh 13].

### **4.3. Application case 1: ITER Test Blanket System RH system**

CAD modelling and kinematics simulation with rendering has been widely used during the development of the ITER TBM Remote Handling Test Facility conceptual design studies carried out by CIEMAT and IBERDROLA and described in Chapter 2. The objective of these simulations has been identifying those design features which involve potential issues for the integration of the EU Test Blanket System and its maintainability by remote handling equipment, as well as checking the planned remote maintenance sequences to avoid interferences or inaccessible locations.

The main simulation activities have been carried out during the 2010-2011 campaigns, which have been focused on the detailed study of several RH operations to be performed in the ITER Hot Cell and all the RH operations to be performed in the Port Cell and the Interspace, as mentioned in Chapter 2. A description of such simulations and the used tools is shown in the following Subsections.

#### **4.3.1. Tools and methodology**

CAD models of the whole equipment (both those specifically designed for the Facility and those adapted from reference components and systems), structures and auxiliary systems involved in the studied RH operations have been created and/or integrated in a global CAD model, as anticipated in Chapter 2. Design features and sizes of non-specific equipment, as well as some CAD models, have been obtained from literature available in on-line databases (e.g. ITER Document Management System –IDM-) or directly from the designers involved in the definition of the EU TBS through EFDA or the European Domestic Agency for ITER (Fusion for Energy, F4E) activities.

CATIA V5 has been the selected CAD tool, since it has been the reference tool for ITER, EFDA and EUROfusion during last years. CATIA, already mentioned in several chapters of this thesis, is a CAD-CAM-CAE integrated tool developed by Dassault Systèmes. Its mechanical engineering modules allow the generation of 3D parts from 2D sketches, advanced surface generation tools, molded, forged or tooling parts, etc., and part assemblies. Among others, CATIA also includes several modules to make easier the design of electronic, electrical, and distributed systems such as fluid and HVAC systems, as well as the production of documentation for manufacturing (drafting, functional tolerancing & annotation, etc.).

Like other CAD-CAM-CAE tools as SolidWorks, ProEngineer or NX, the procedure to design 3D parts and assemblies is based on a structured tree where operations which add new features to the model are arranged. This has the advantage of allowing easy and fast modifications, since the model can be automatically updated by the successive updating of the features situated in the tree under the modified operation.

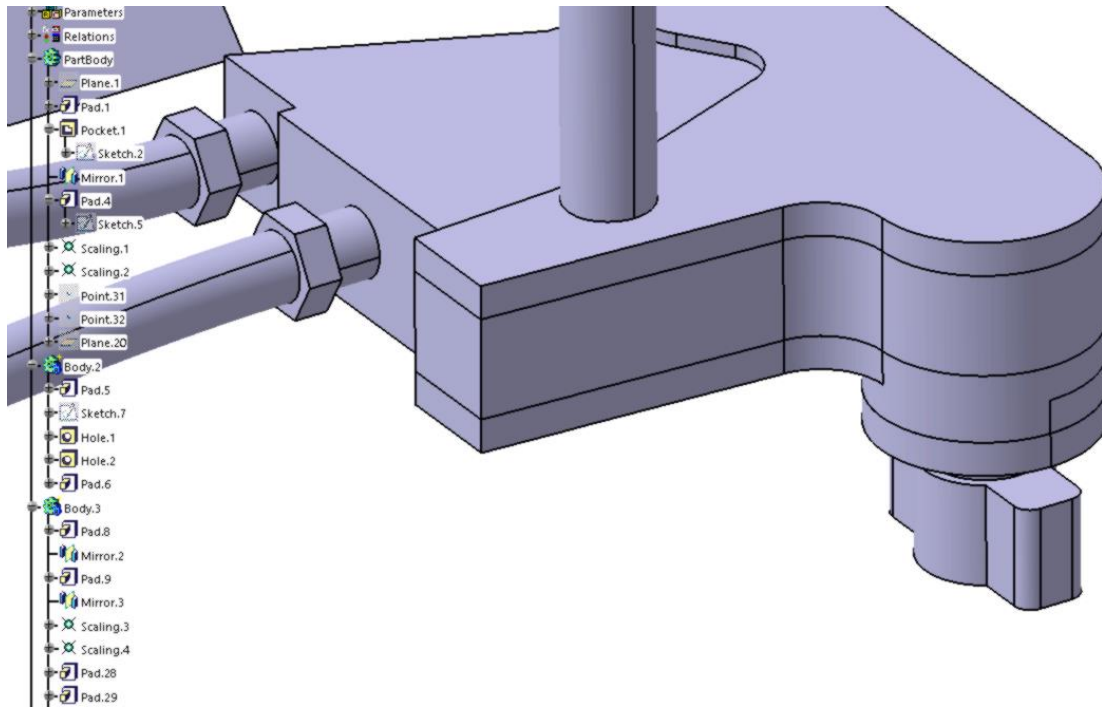


Fig. 1. Set of geometric operations in the CATIA structured tree (left).

Within its Digital Mock-Up (DMU) set of modules, CATIA includes some tools for creating assemblies motion sequences and performing space analysis. DMU Fitting allows simulating part movements for assembly and maintainability issues. It can be used to manipulate models from the definition of tracks. The sequences can be displayed on the screen and then exported into video formats. Distance dynamic measurement and detection of interferences are also possible.

On the other hand, DMU Kinematics allows simulating several kinds of mechanisms (kinematics joints) established between different parts of an assembly, which can be controlled by commands. As in the case of DMU Fitting, recording or exportation of simulations into other formats is also possible.

In spite of the good performance of the kinematics modules and the availability of a Real Time Rendering tool, CATIA is not particularly aimed at high quality rendering and video simulations. For this reason, a more specific tool as 3DVia Composer has been selected to define the animated sequences, render the scenes and produce video files with different formats.

3DVia Composer is a graphic tool also developed by Dassaul Systèmes which, among other functionalities, allows generating fairly good quality rendered images from 3D models provided in different formats. CATIA native files are especially suitable. 3DVia Composer also simplifies the creation of mechanical joints and the definition of kinematics paths by interpolating the position of the model objects at critical points. Such points are reflected in a timeline where it is also possible to set objects appearance & hiding and opacity/transparency grade, as well as camera positions, while it is the software which manages the transitions between them – although it is possible to customize camera tracks-. Once defined the movements, clearance checking and interactive collision detection tools can be used to help analysing the sequence.

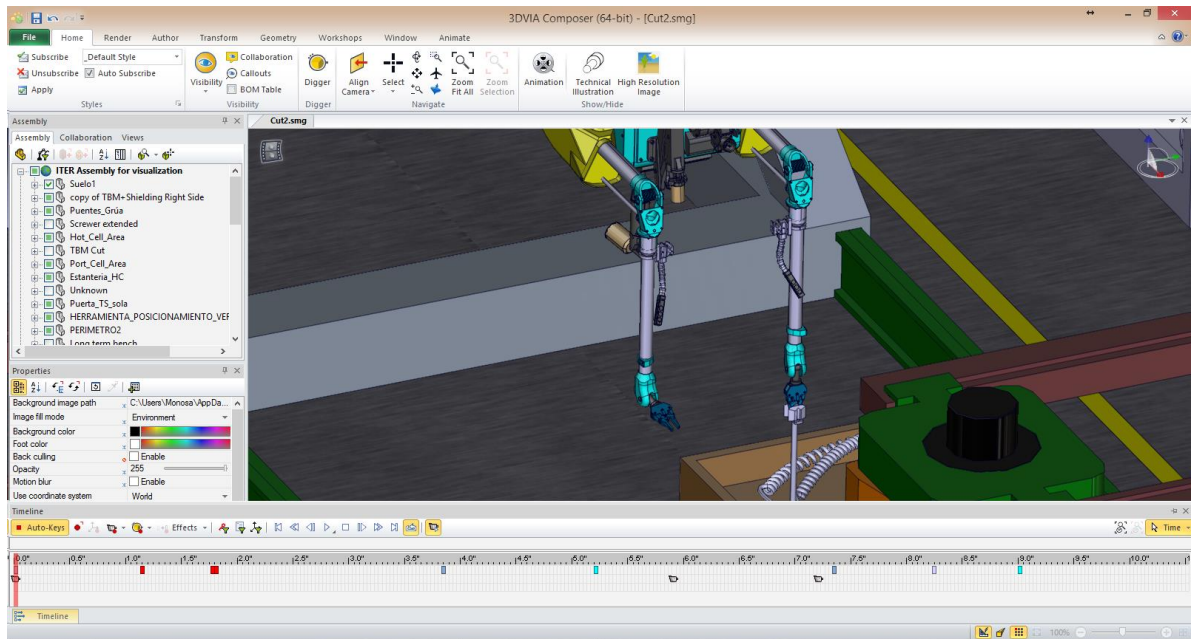


Fig. 2. 3DVIA Composer interface (timeline located at the bottom).

Kinematic joints (or links, according to the 3DVIA nomenclature) are established from parent-son relations between parts of the model (Fig. 3). One disadvantage of 3DVIA Composer in comparison with CATIA DMU Kinematics is that each 'son' part can only establish one link with one 'parent' part, which complicates achieving the desired movements in more complex mechanisms as the manipulator clamp ones.

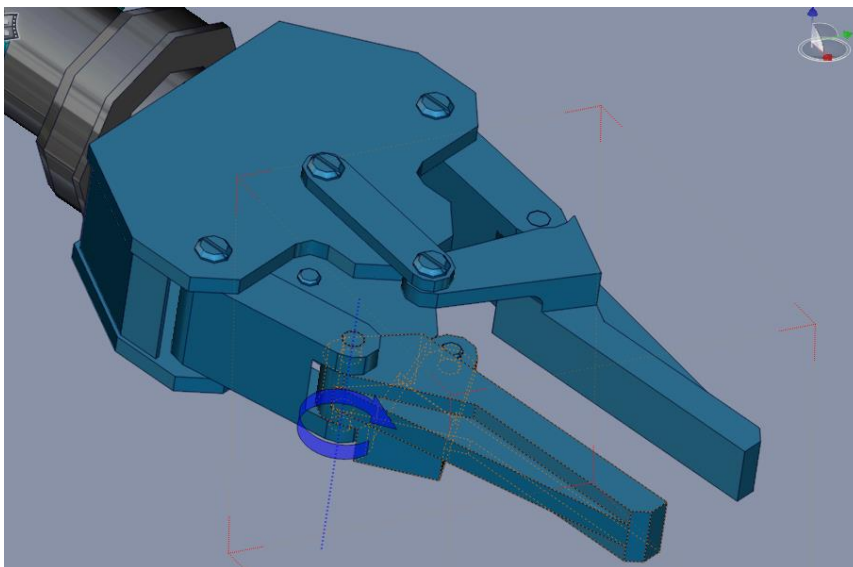


Fig. 3. Pivot-type kinematics link between two pieces of the Hot Cell manipulator right clamp.

As 3 animated sequences have been developed in the environment of the Hot Cell operations area, and another 3 have been developed in the environment of the Port Cell & Interspace operations area, both the kinematic links of all the involved equipment and the graphical features for rendering (colours, textures, etc.) have been previously established in a general 3D model for each of the environments. Afterwards, the specific paths and movements, camera positions, etc. of each operation have been defined in separate 3DVIA files. Finally, the animated sequences have been rendered with the selected video format and then exported to AVI or WMV file format.

On the other hand, some of the resulting video files have included post-production to add some visual effects like laser light or welding sparks, in order to improve the realism and to help understanding some sequences. Adobe After Effects, a digital visual effects, motion graphics, and compositing application developed by Adobe Systems has been used. Another application developed by Adobe (Premiere) has been also used in some cases to compress the files produced by 3DVia Composer.

As commented in Chapter 2, the process described in the ITER Maintenance Management Systems (IMMS) has been followed to design these operations. First, Plant definition forms (PDF) describing the characteristics of the whole involved equipment have been produced. Then Task Definition Forms (TDS) have been created to give a detailed list of the steps composing each RH operation. The TDS have been used to generate the Operations Sequence Descriptions (OSD), detailed scripts of the RH processes which have been followed to create the simulations. In some cases, several iterations of the whole process have been necessary, because of the identification and solution of issues regarding components design or features of the RH operations.

The RH operations which compose the 6 simulations, extracted from their respective OSDs, are described in the following Subsection:

### **4.3.2. Description of the sequences and influence on the design**

#### **4.3.2.1. Extraction of a TBM & shield assembly from the port plug**

##### Description

The TBM & shield assembly must be extracted from the port plug (PP) after removing the sealing and joining features between both (operations #5 and 6 from Chapter 2).

##### Task objective

The objectives of the task are: 1) to remove the sealing and joining features between the TBM & shield assembly and the port plug; 2) to extract the TBM & shield assembly from the port plug, 3) to place the TBM & shield assembly in the separation bench.

##### Assumptions

- Vacuum seal integrated in the shield flange.
- Using of a hydraulically driven screwer.
- Lifting tool features.
- Using of a bench to disassembly the shield from the TBM.

##### Start conditions

The TBM & shield assembly are joined to the port plug frame, which is inserted into the vertical positioning tool.

##### End conditions

The TBM & shield assembly is placed in the separation bench

##### Remote operations sequence

- 1) The manipulator grips the hydraulically driven screwer from the storage shelves and places it on each screw of the shield flange.

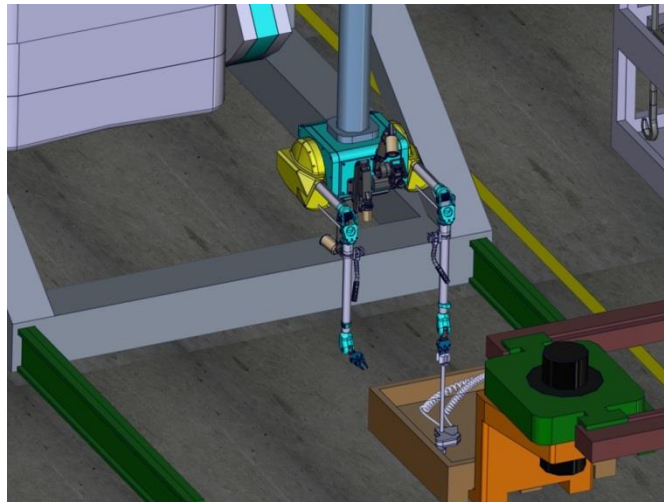


Fig. 4. Extraction operation step 1.

2) The screwer unbolts the captive bolts.

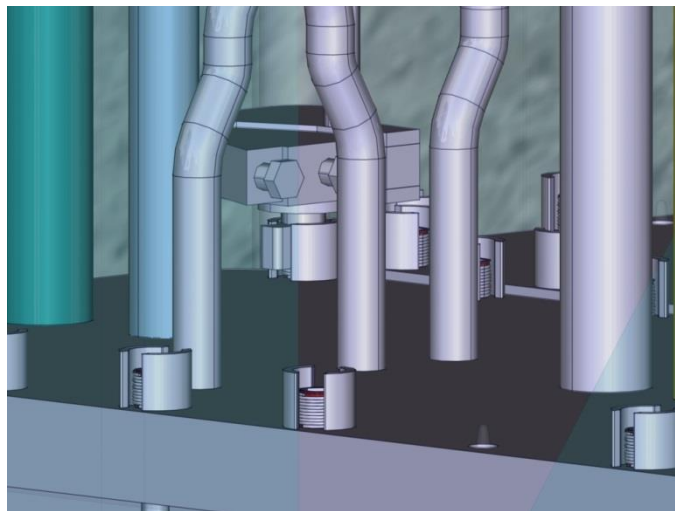


Fig. 5. Extraction operation step 2.

3) The manipulator leaves the screwer in the pallet.

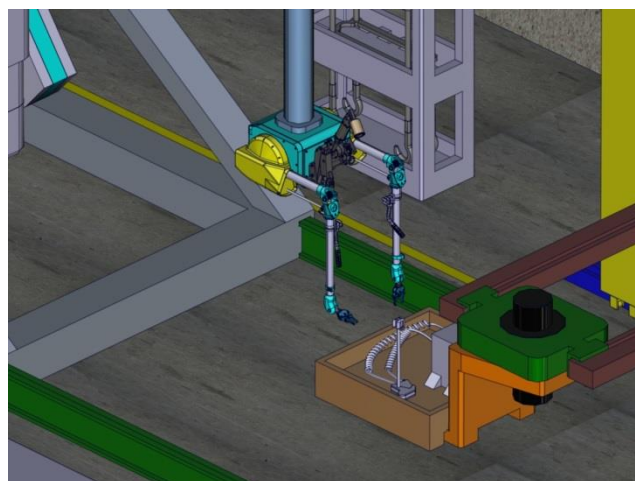


Fig. 6. Extraction operation step 3.

- 4) The coupling tool gets the lifting tool from its container.

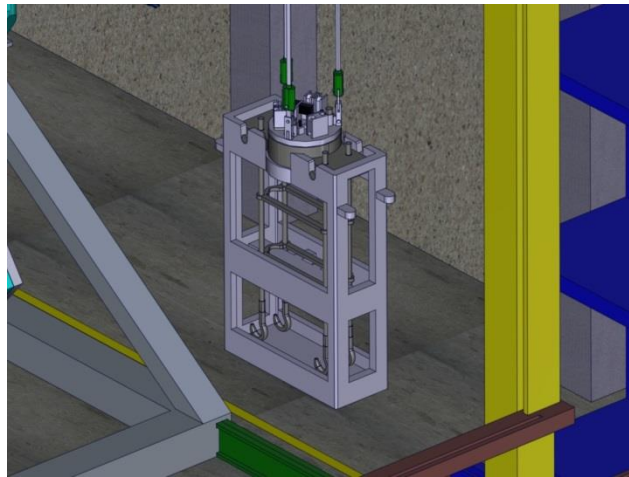


Fig. 7. Extraction operation step 4.

- 5) The lifting tools couples to the shield handling features.

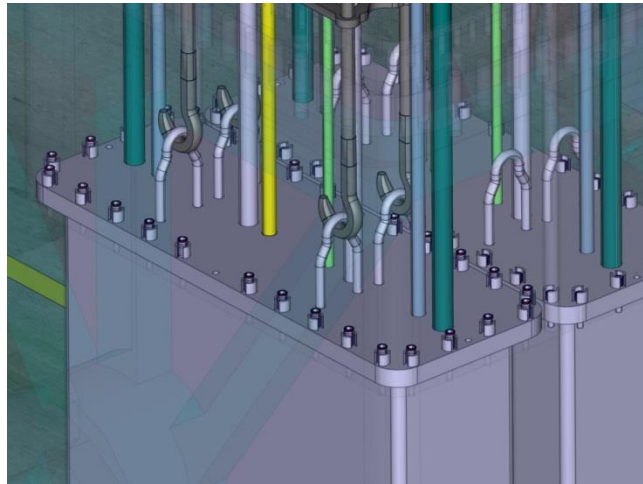


Fig. 8. Extraction operation step 5.

- 6) The lifting tool lifts the TBM & shield assembly and places it on the separation bench.

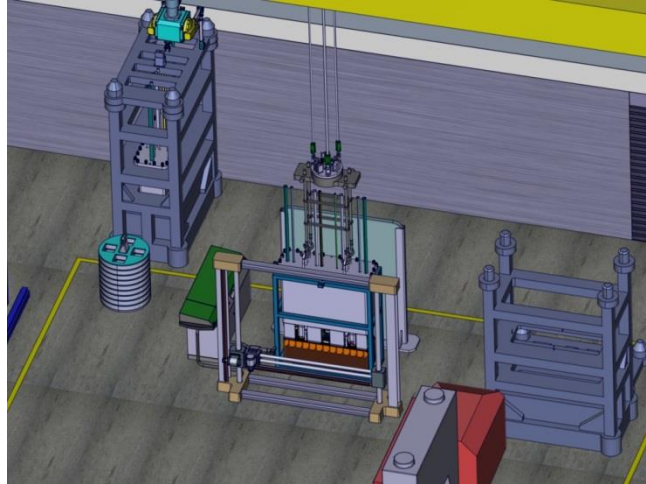


Fig. 9. Extraction operation step 6.

#### 4.3.2.2. Split of the TBM & shield

##### Description

This task consists in cutting the connection between the TBM and its shield, transporting the shield to the long term storage bench, and finally transporting the TBM to the cutting machine (operation #8 from Chapter 2).

##### Task objective

To separate the TBM from the shield in order to: 1) place the shield in a storage bench; and 2) place the TBM on the cutting machine.

##### Assumptions

- Two sweeps of laser are necessary to cut the TBM-shield interface.
- It is not necessary to cut the pipes located in the rear part of the shield.

##### Start conditions

The TBM & shield assembly is inside the cutting bench, ready to be cut. The lifting tool is above the shielding, the laser cutting tool is in front of the bench and the laser shielding structure is behind the bench.

##### End conditions

The shield is located inside the long term storage bench and the TBM is located in the cutting machine.

##### Remote operations sequence

- 1) At the beginning the TBM & shield assembly is inside the cutting bench, the lifting tool is above the shield, the laser cutting tool is in front of the bench and the laser shielding structure is behind the bench.

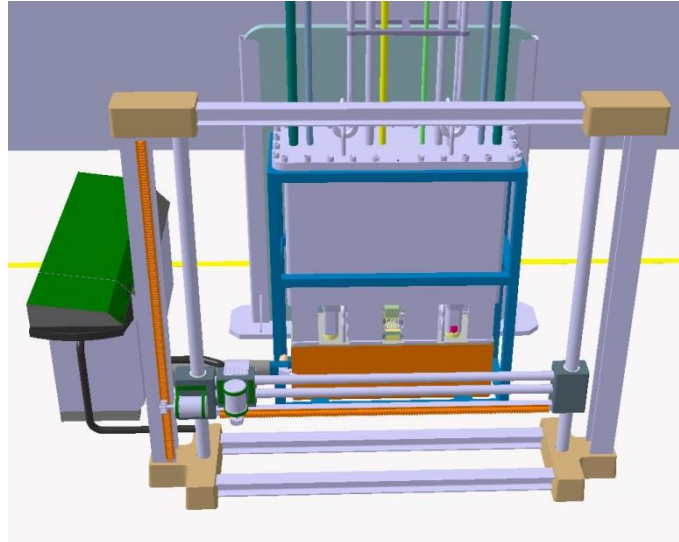


Fig. 10. Split operation step 1.

- 2) The laser cutting tool is activated and makes a first horizontal sweep to cut the first row of union plates and the interface piping. The laser must cut neither the lifting washers nor the shear keys.

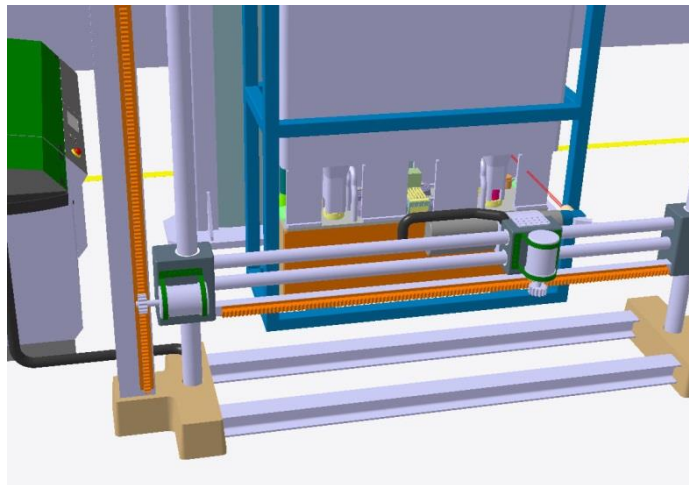


Fig. 11. Split operation step 2.

- 3) The laser cutting tool makes a second horizontal sweep to cut the second row of union plates. The laser must cut neither the lifting washers nor the shear keys.

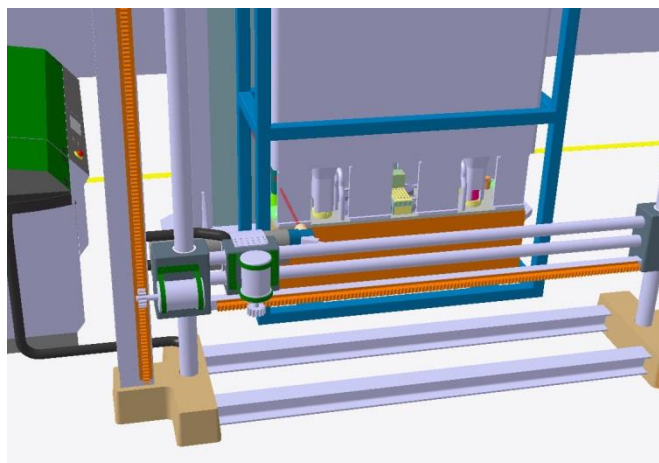


Fig. 12. Split operation step 3.

- 4) The four hooks of the lifting tool attach the shield through its four lifting washers. The lifting tool is coupled to the 20 t crane.

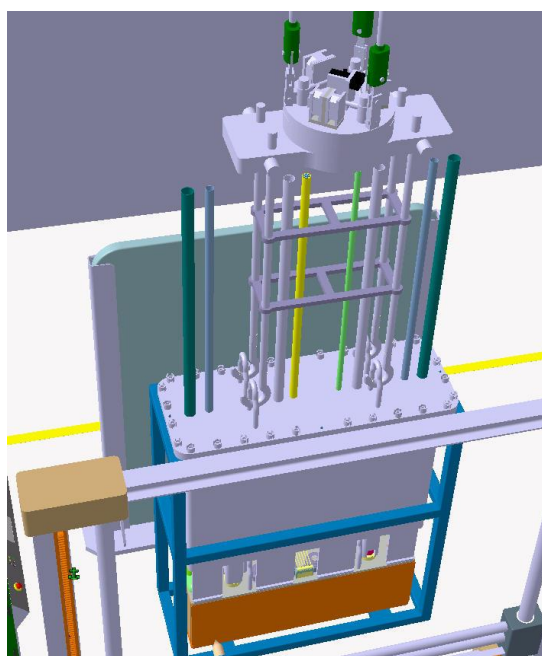


Fig. 13. Split operation step 4.

- 5) The lifting tool is lifted up, extracting the shield from the bench. The shield must be lifted above the height of the long term storage container.

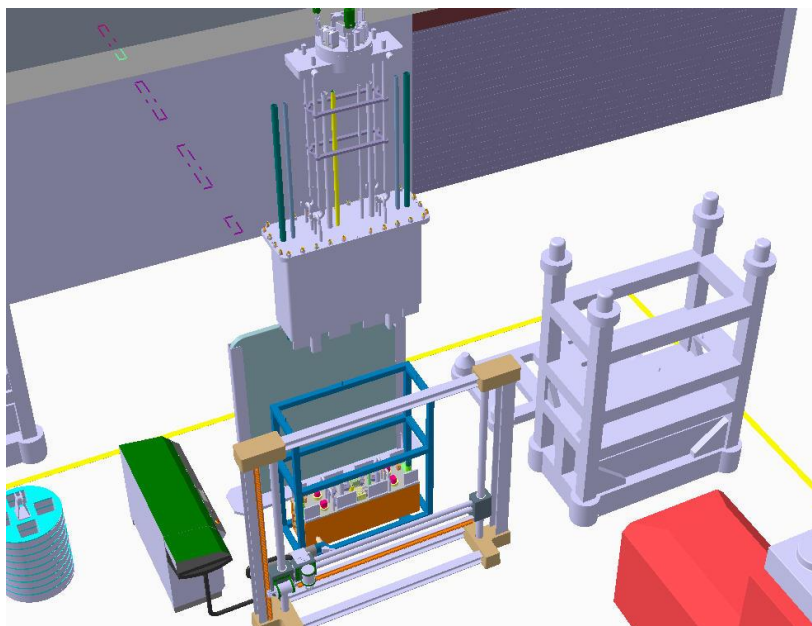


Fig. 14. Split operation step 5.

- 6) The shield is transported horizontally by the 20 t crane to the long term storage container.

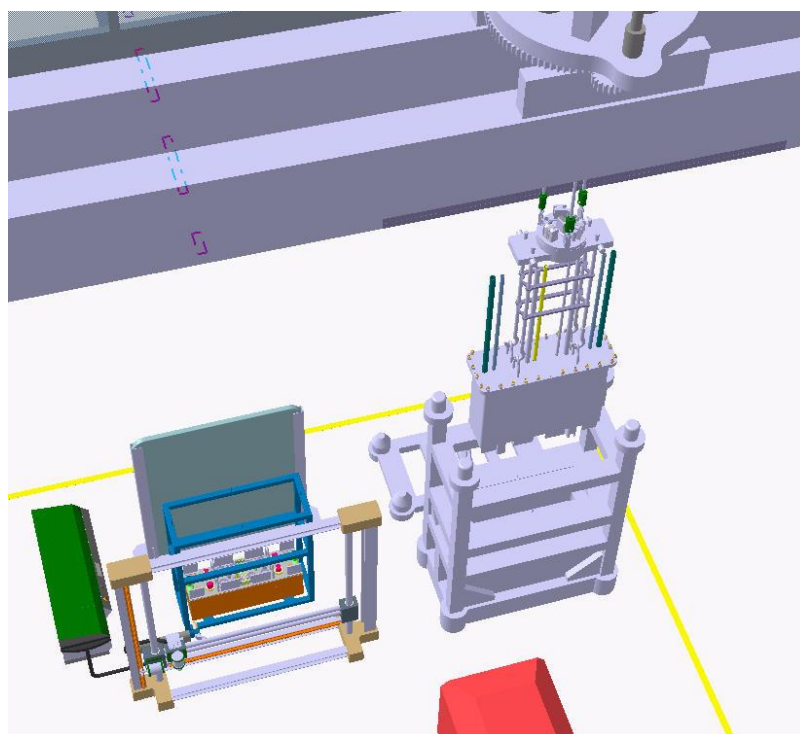


Fig. 15. Split operation step 6.

- 7) The lifting tool goes down inserting the shield into the long term storage container.

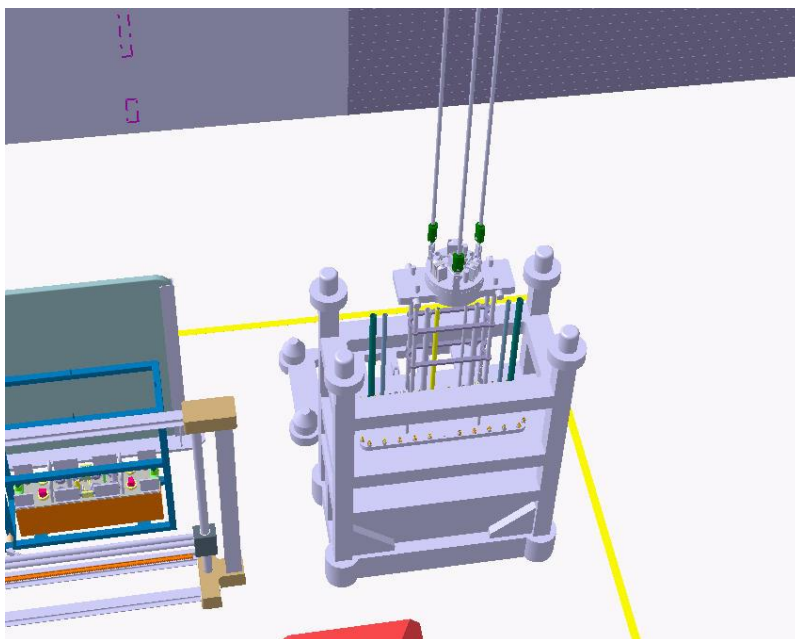


Fig. 16. Split operation step 7.

- 8) The lifting tool is disengaged from the shield; then it is lifted up again and moved back to the cutting bench.

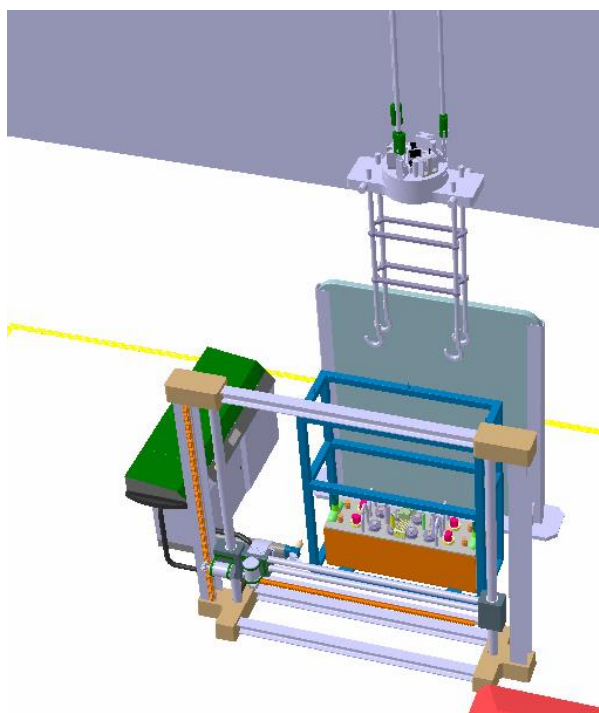


Fig. 17. Split operation step 8.

- 9) The four hooks of the lifting tool attach the TBM through its four lifting washers.

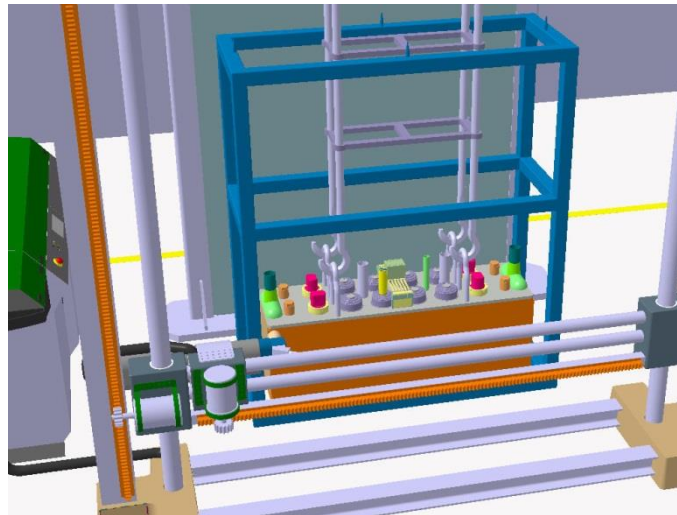


Fig. 18. Split operation step 9.

- 10) The lifting tool is elevated, extracting the TBM from the bench. The TBM must be lifted above the height of the laser cutting structure.

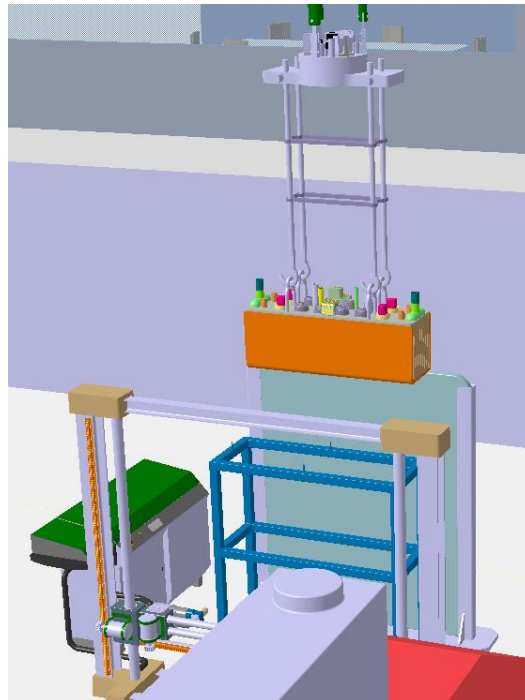


Fig. 19. Split operation step 10.

- 11) The TBM is transported horizontally by the 20 t crane to the cutting machine.

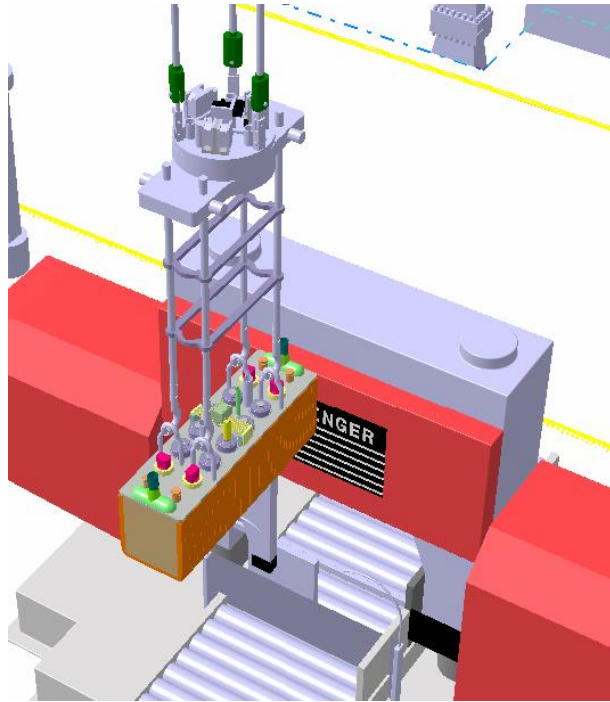


Fig. 20. Split operation step 11.

12) The lifting tool goes down leaving the TBM on the cutting machine.

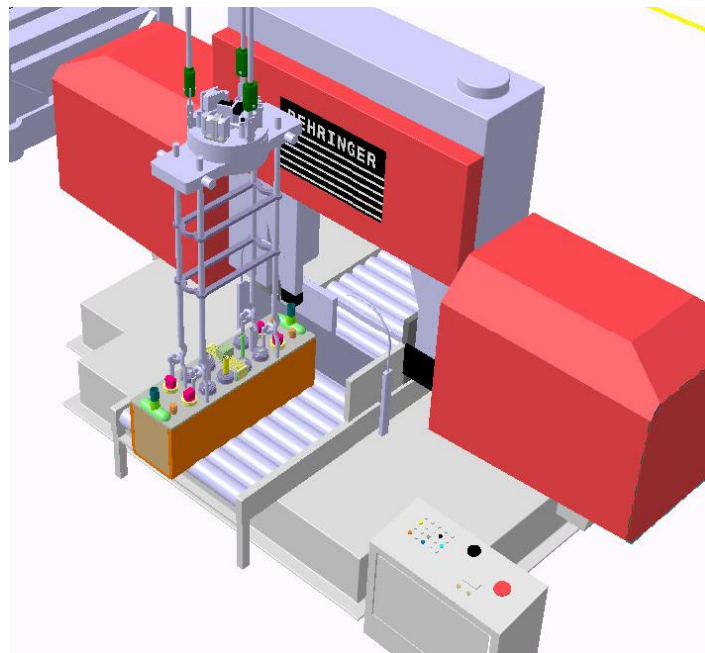


Fig. 21. Split operation step 12.

13) The lifting tool is disengaged from the TBM and it is lifted up again.

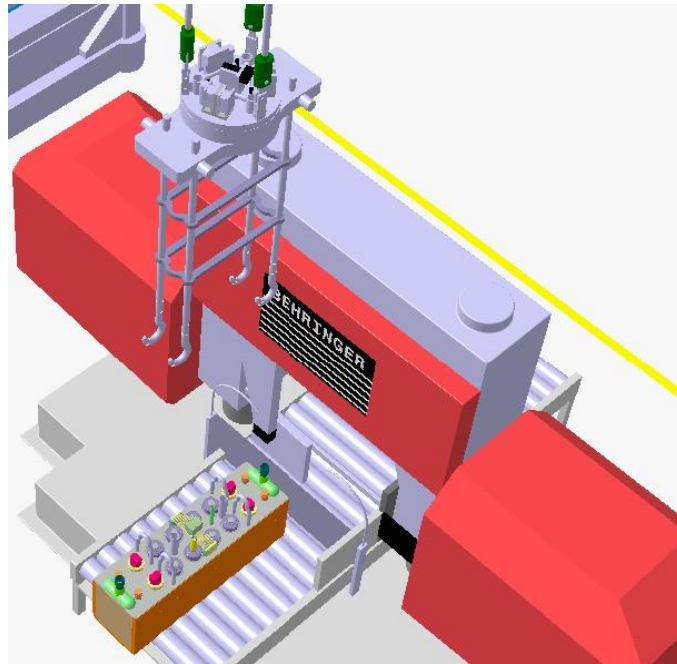


Fig. 22. Split operation step 13.

#### 4.3.2.3. Insertion of the TBM & shield assembly inside the port plug

##### Description

Any possible rests of the two gaskets (O-rings) left on the port plug flange after the extraction of the TBM & shield assembly from the port plug must be cleaned. Then, a new TBM & shield assembly must be inserted into the port plug (operations #10 and 11 from Chapter 2).

##### Task objective

To bolt the new TBM & shield assembly to the port plug flange ensuring the vacuum sealing.

##### Assumptions

- The new TBM & shield assembly comes from factory inside a bench.
- This shipping bench will be placed in the Hot Cell area.
- The bench is the same as the one used for the shield long term storage.

##### Start conditions

The port plug is inserted into the vertical positioning tool. It contains some rests of the O-rings from the previous TBM & shield assembly.

##### End conditions

The port plug frame is cleaned and a new TBM & shield assembly is inserted and bolted to the port plug.

##### Remote operations sequence

- 1) The palletizing system places the polisher and its transfer box near the vertical positioning tool.

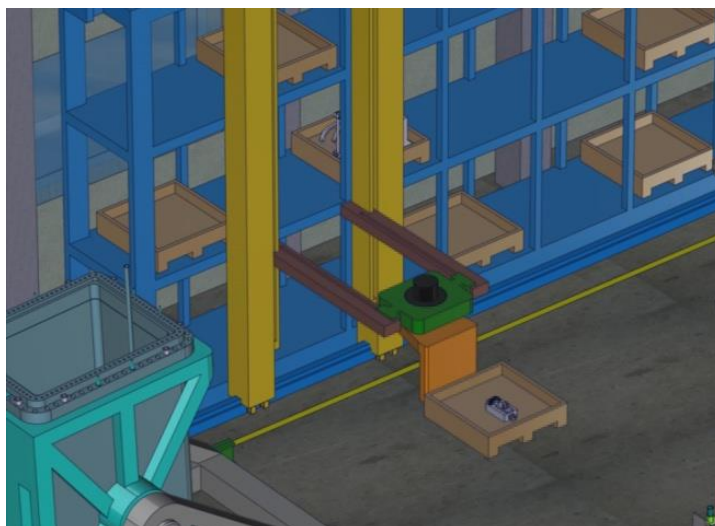


Fig. 23. Insertion operation step 1.

- 2) The robotic manipulator grips the polisher and moves to the interior of the PP. The polisher is positioned in the PP and it is ready to start the operation.

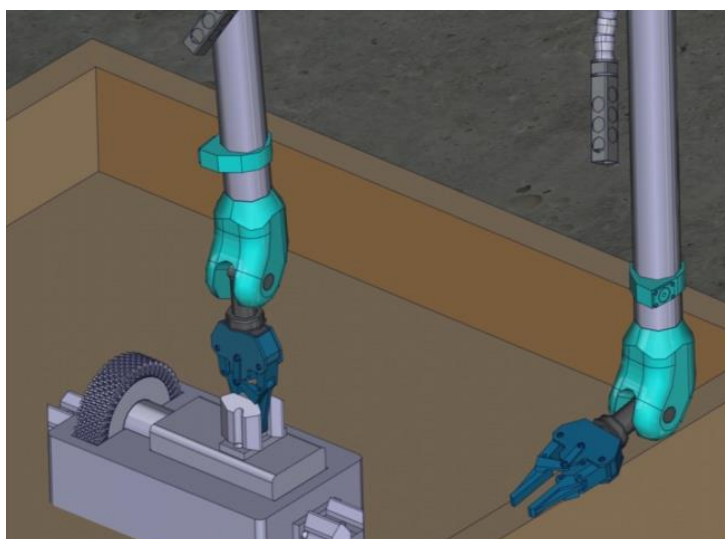


Fig. 24. Insertion operation step 2.

- 3) The robotic manipulator moves the polisher along the PP frame and removes the remains of the previous O-rings.

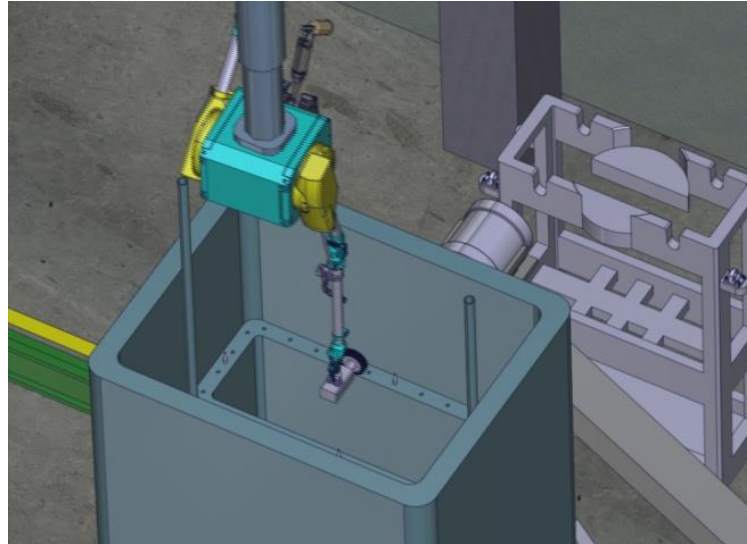


Fig. 25. Insertion operation step 3.

- 4) The robotic manipulator moves outside of the PP and leaves the polisher in its transfer box.

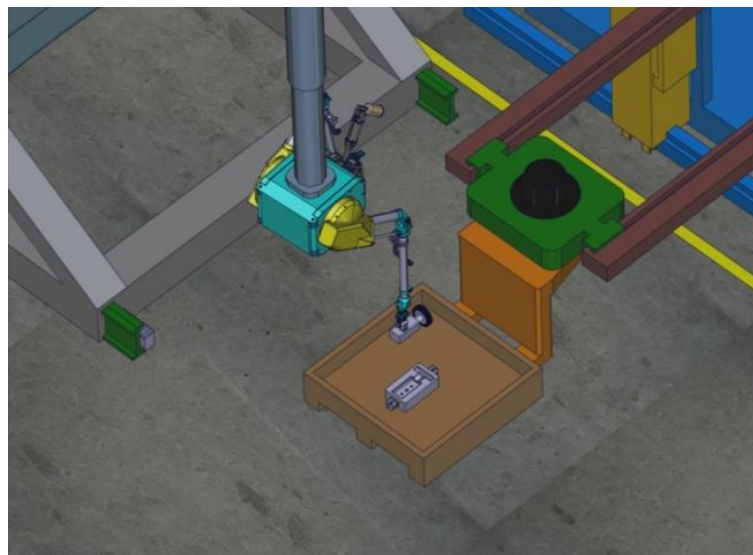


Fig. 26. Insertion operation step 4.

- 5) The palletizing system places the transfer box of the polisher in the storage shelves and picks the pallet which houses the screwdriver. It leaves it near the vertical positioning tool.



Fig. 27. Insertion operation step 5.

- 6) The TBM & shield assembly lifting tool moves towards the location of the new TBM & shield shipping bench and picks up the assembly.

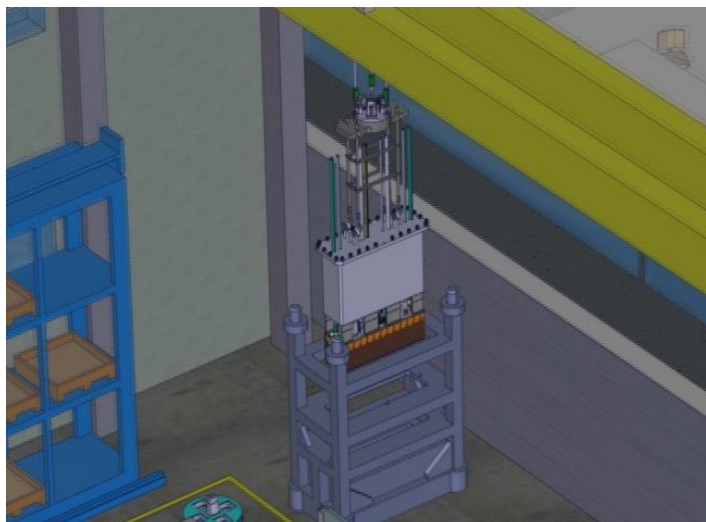


Fig. 28. Insertion operation step 6.

- 7) The lifting tool places the TBM & shield assembly in the port plug frame.

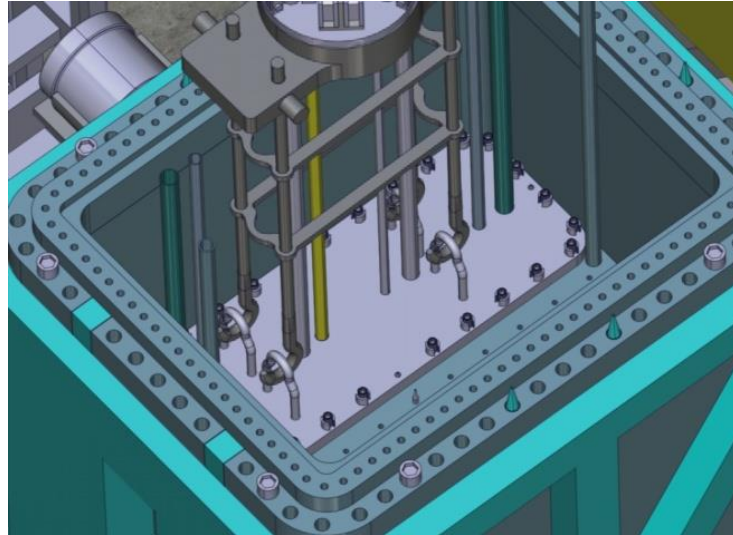


Fig. 29. Insertion operation step 7.

- 8) The lifting tool hooks are uncoupled from the shield lifting washers. The tool moves out of the port plug.

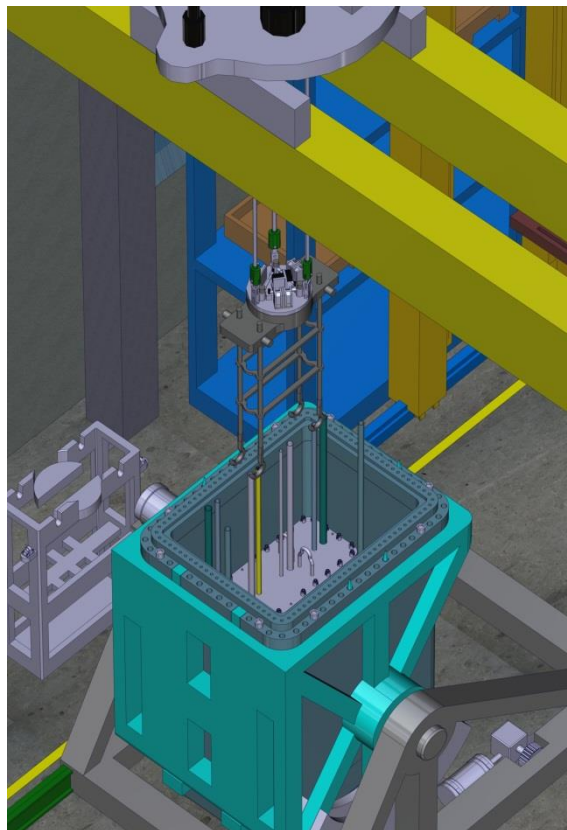


Fig. 30. Insertion operation step 8.

- 9) The robotic manipulator takes the screwer from the pallet and moves inside the port plug.

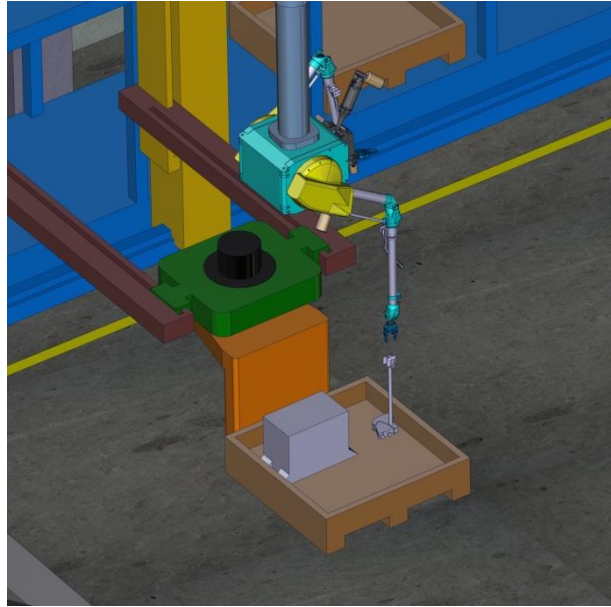


Fig. 31. Insertion operation step 9.

- 10) The robotic manipulator screws all the captive bolts. Finally the robotic manipulator moves out of the PP and leaves the tool in its transfer box.

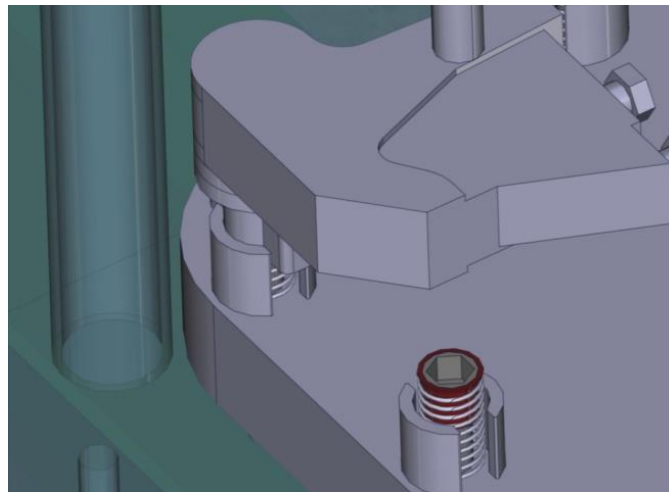


Fig. 32. Insertion operation step 10.

#### 4.3.2.4. Consequences of the simulation process

Partial simulations and 'manual drag' kinematics analysis previous to the final video sequences have allowed identifying and correcting design issues which were critical for some of the most important TBS RH operations in the Hot Cell. These procedures have been useful for the following issues, among others:

- Checking of the accessibility of the Hot Cell manipulator and the lifting tool to the rear part of the port plug.
- The design of the mechanical joints and the handling features at the IF1 has been adapted to the characteristics of the laser cutting tool.
- The design of some pipes (TBM, shield, port plug) has been slightly modified (location, length...).

- The design of the RH features (dowels and holes) in the interface between the port plug and the shield has been modified to improve the alignment of captive bolts during the insertion of the TBM & shield assembly.
- The design of the RH features in the benches to support the alignment and insertion operations has been modified.

#### 4.3.2.5. Installation and removal of the Pipe Forest & Bioshield Door assembly

##### Description

The Pipe Forest & Bioshield Door assembly must be carried from the Storage Area and installed in the Interspace/Port Cell. Then it must be removed from the Port Cell and placed in the Storage Area (operations #15 and 16 from Chapter 2).

##### Task objective

###### *First part: installation*

1) To carry the Pipe Forest & Bioshield Door assembly from the Storage Area to the Port Cell Area; 2) to insert the assembly into the Interspace; 3) To connect the diagnostics/electric supply pipes at IF2a; 4) to join the Bioshield Door to the Bioshield Wall.

###### *Second part: removal*

5) To disjoin the Bioshield Door from the Bioshield wall; 6) To disconnect the diagnostics/electric supply pipes; 7) to extract the assembly from the Interspace; 8) to carry the assembly from the Port Cell to the Storage Area.

##### Assumptions

- The Pipe Forest & Bioshield Door assembly is transported from the Storage Area to the Port Cell by means of the Air Transfer System.
- The Pipe Forest is inserted in the Interspace by means of a 6-wheel system. Some of the wheels are motor-driven, which are located behind the Bioshield Door.
- The wheels are guided by rails located on both the air transfer system (ATS) and the port structures, without interfering with the bellows.
- The two front wheels are placed at a higher level than the four rear ones, avoiding height discontinuity between the ATS base and the Port base, in such a way that before the Pipe Forest arrives to the port, it is supported only by the rear wheels.
- The intermediate wheels are collapsible, so that when they reach the height of the Bioshield Door they fold back and remain in that position by means of small hydraulic cylinders.
- At this point, the front wheels are already supported by the port structures rails so the Pipe Forest can continue to its final position.
- To ensure the piping alignment of the Pipe Forest with both TBMs (HCPB and HCLL) on the Interface 2a, the Pipe Forest has an alignment system based on two plates joined together by rigid joints. The first plate has circular holes in which are inserted the pipes of the Pipe Forest. The second plate, which is located nearer the port plug, has tapered holes to achieve the correct coupling of the TBM pipes.
- Some elements with the same taper as in the previous plate are installed in each TBM pipe, providing the self-alignment of the TBM pipes with those of the Pipe Forest.
- The gap between the first and second plate on the alignment system is enough to allow the robotic arm to gain access to all the pipes and perform the IF2a maintenance operations.

##### Start conditions

###### *First part: installation*

The Pipe Forest & Bioshield Door assembly is located in the Storage Area.

*Second part: removal*

The Pipe Forest & Bioshield Door assembly is located in the Interspace/Port Cell. The Pipe Forest is joined to the Port Extension and the Bioshield Door is joined to the Bioshield Wall.

End conditions*First part: installation*

The Pipe Forest & Bioshield Door assembly is located in the Interspace/Port Cell. The Pipe Forest is joined to the port extension and the Bioshield Door is joined to the Bioshield Wall.

*Second part: removal*

The Pipe Forest & Bioshield Door assembly is located in the Storage Area.

Remote operations sequence

- 1) The Pipe Forest & Bioshield Door assembly is transferred from the Storage Area by means of Air Transfer System.

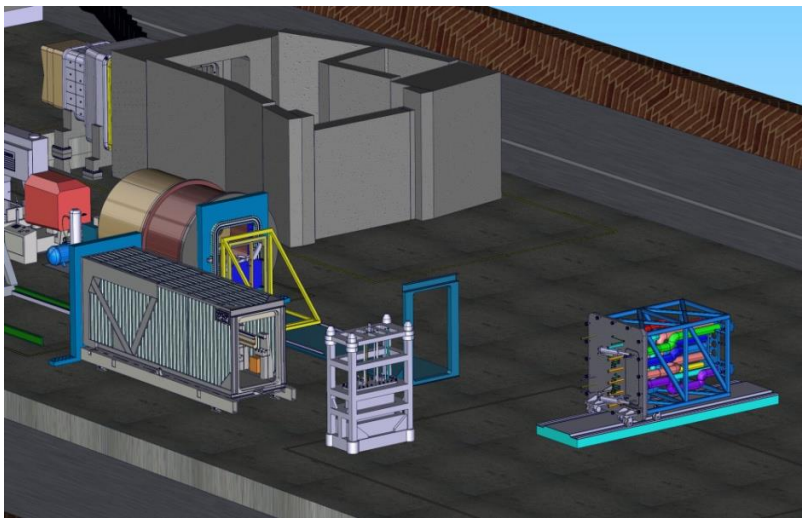


Fig. 33. Pipe Forest & Bioshield Door assembly installation step 1.

- 2) The assembly is located in front of the Port Cell door.

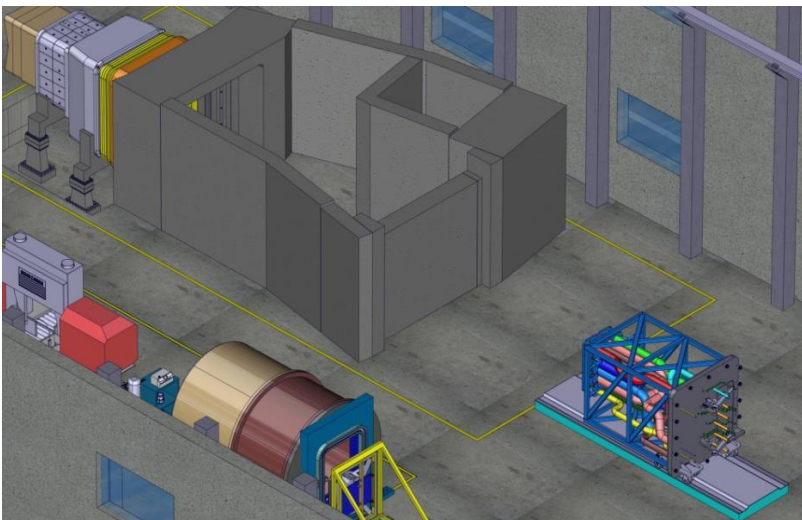


Fig. 34. Pipe Forest & Bioshield Door assembly installation step 2.

- 3) The Port Cell door is opened.

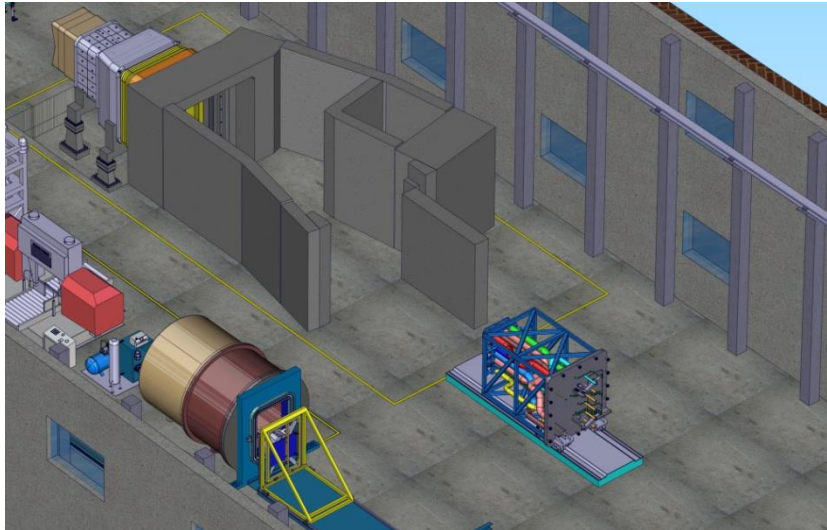


Fig. 35. Pipe Forest & Bioshield Door assembly installation step 3.

- 4) The Pipe Forest enters into the Port Cell and is positioned.

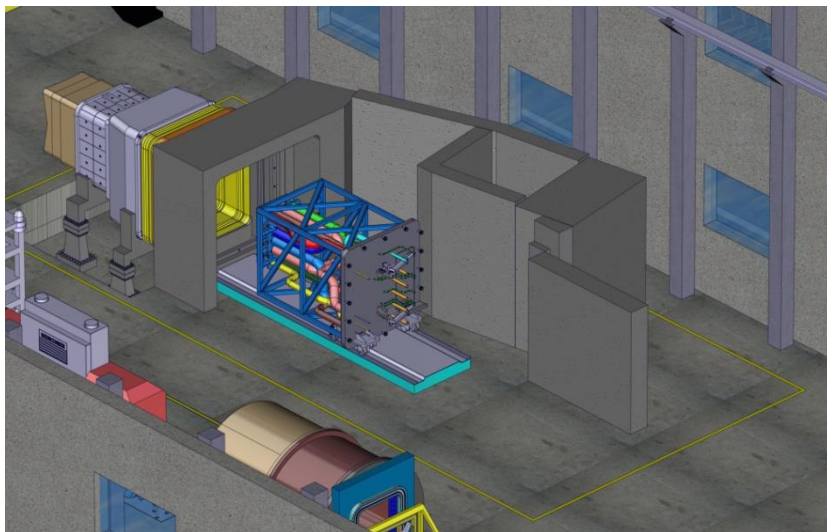


Fig. 36. Pipe Forest & Bioshield Door assembly installation step 4.

- 5) The assembly moves on the ATS rails by means of its rear wheels.

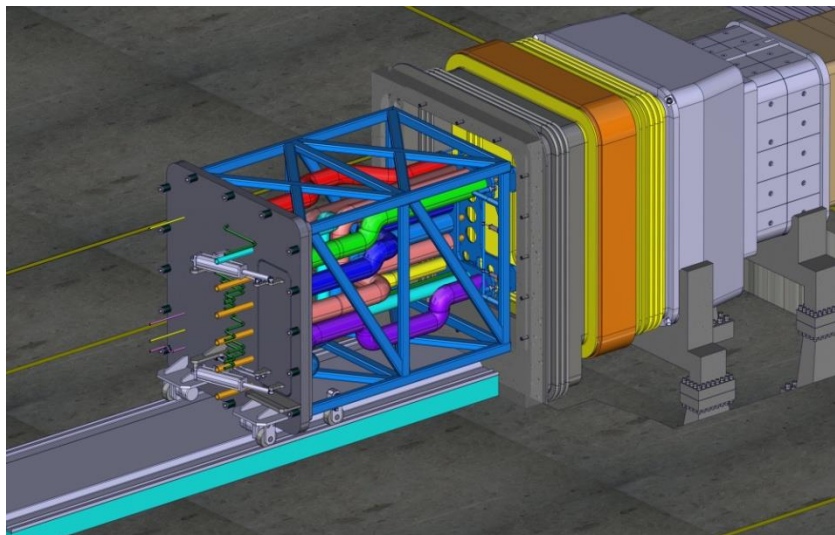


Fig. 37. Pipe Forest & Bioshield Door assembly installation step 5.

- 6) The front wheels of the Pipe Forest assembly rest in the Connecting Duct rails.

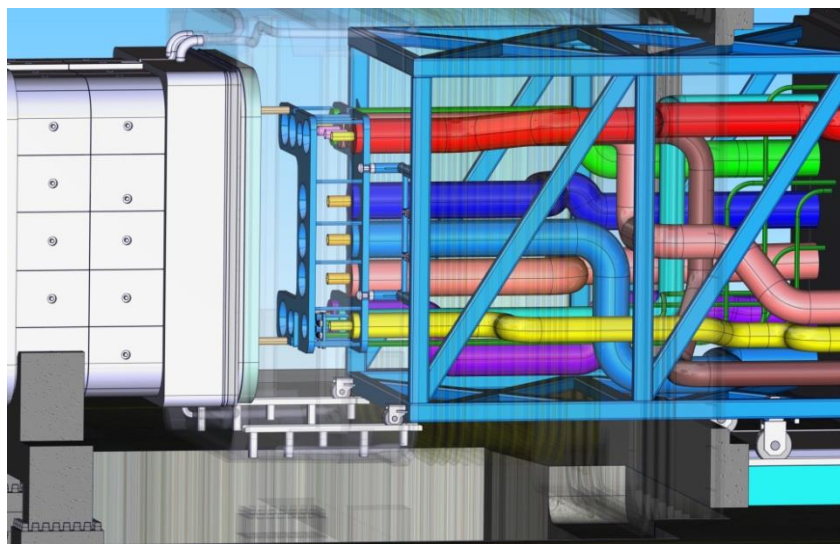


Fig. 38. Pipe Forest & Bioshield Door assembly installation step 6.

- 7) The intermediate wheels of the Pipe Forest assembly are folded when the Bioshield doorstep is reached.

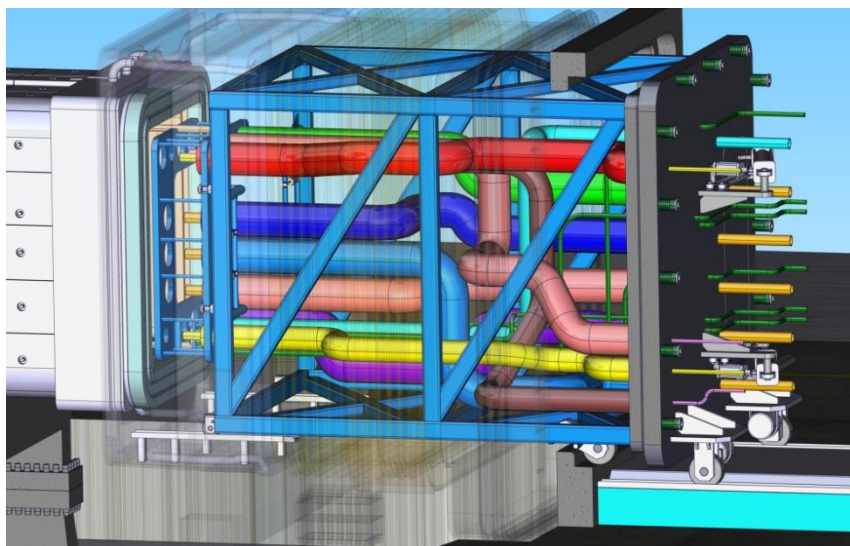


Fig. 39. Pipe Forest & Bioshield Door assembly installation step 7.

- 8) The Bioshield Door fits in the Bioshield Wall and the diagnostics/electric supply pipes are connected.

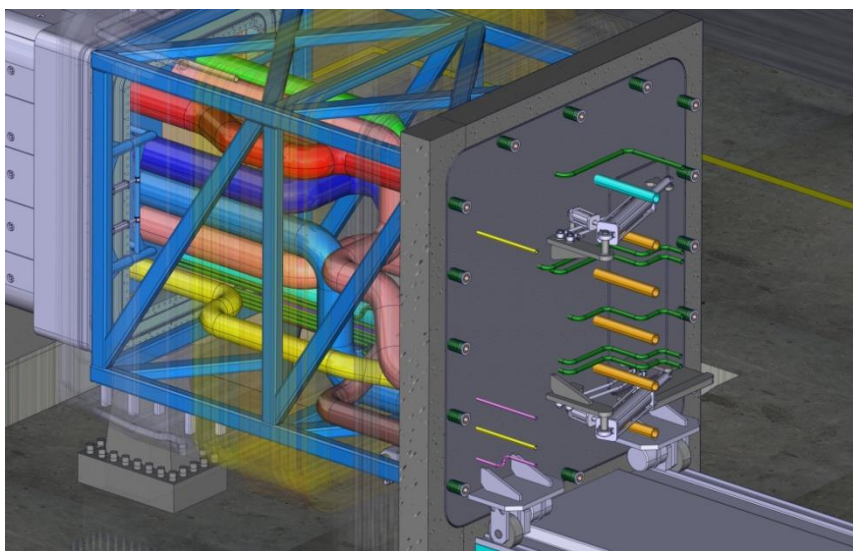


Fig. 40. Pipe Forest & Bioshield Door assembly installation step 8.

- 9) The pipes are aligned by the alignment system at IF2a.

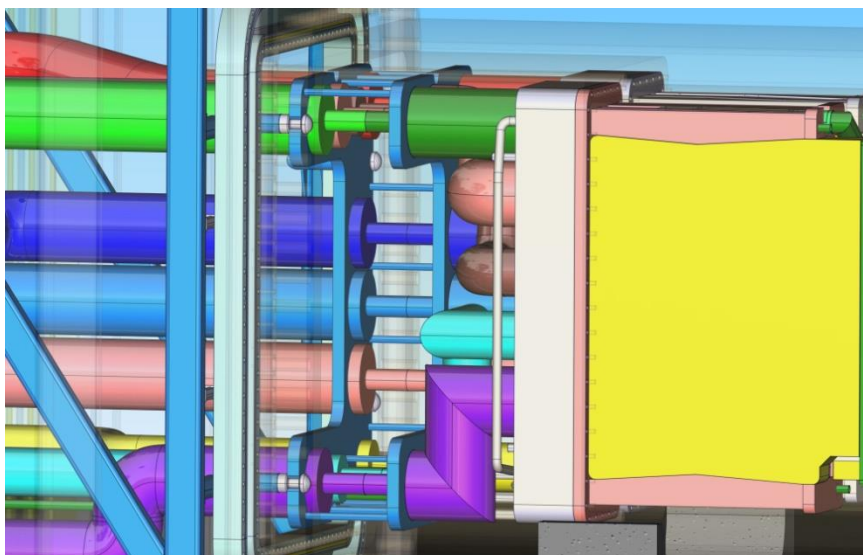


Fig. 41. Pipe Forest & Bioshield Door assembly installation step 9.

10) The Bioshield Door is joined to the Bioshield wall by means of captive bolts.

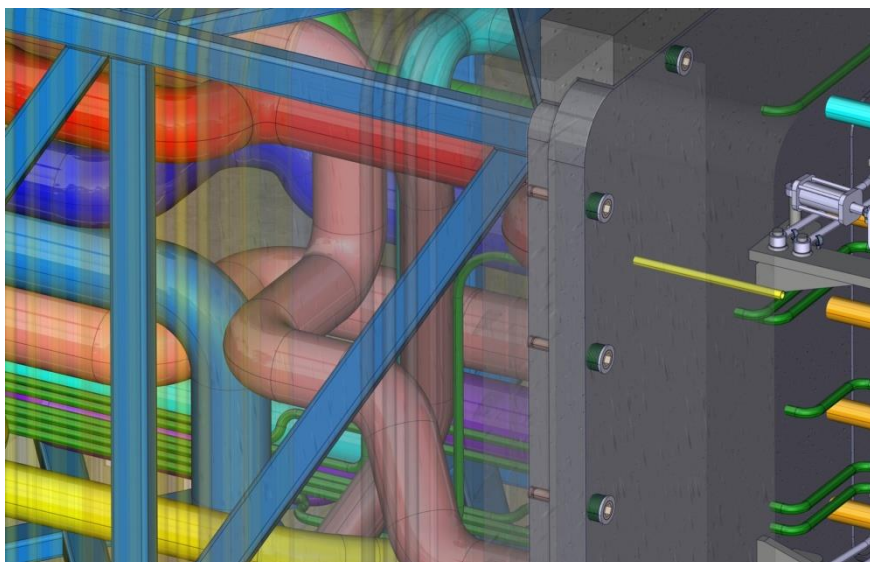


Fig. 42. Pipe Forest & Bioshield Door assembly installation step 10.

11) The ATS leaves the assembly and goes back to the Storage Area.

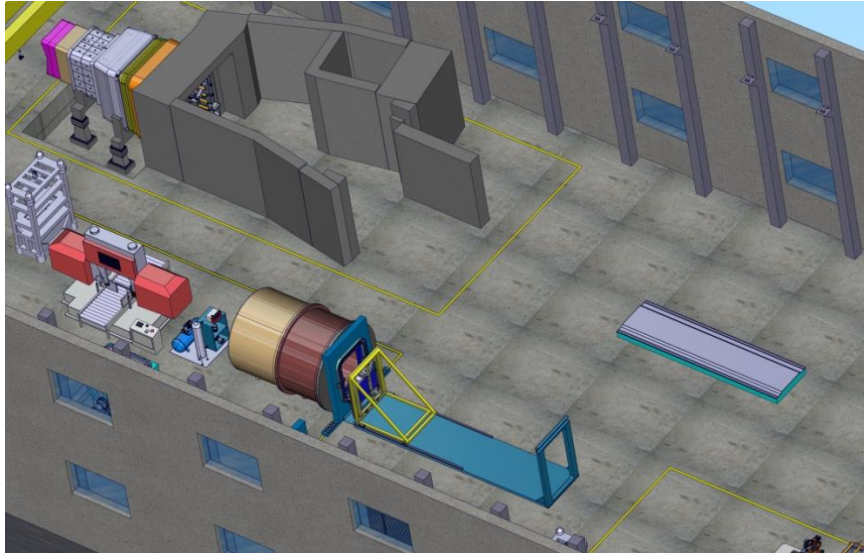


Fig. 43. Pipe Forest & Bioshield Door assembly installation step 11.

**Second part: Removal**

- 1) The captive bolts are unscrewed to disjoin the Pipe Forest & Bioshield Door assembly from the Bioshield wall. The ATS entries into the Port Cell and is positioned next to the Bioshield Door.

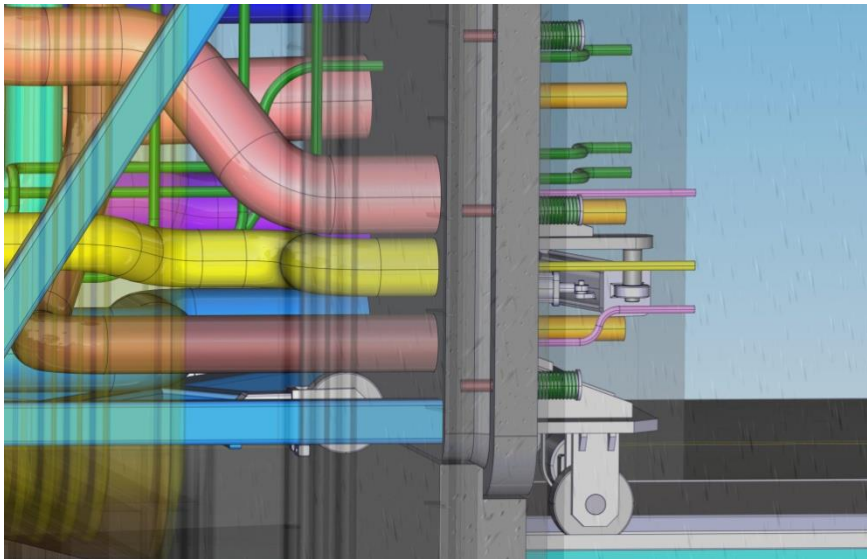


Fig. 44. Pipe Forest & Bioshield Door assembly removal step 1.

- 2) The ATS removes the Pipe Forest & Bioshield Door assembly from the Port Cell.

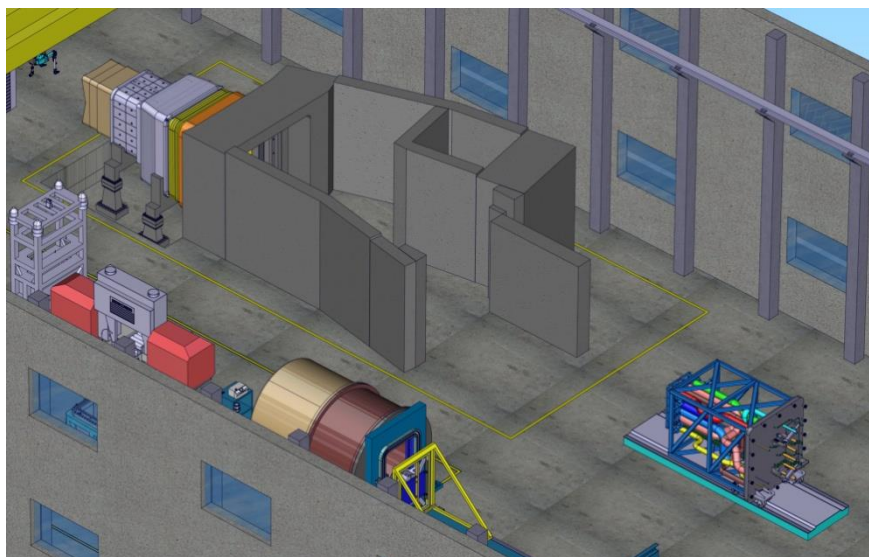


Fig. 45. Pipe Forest & Bioshield Door assembly removal step 2.

- 3) The Port Cell door is closed.

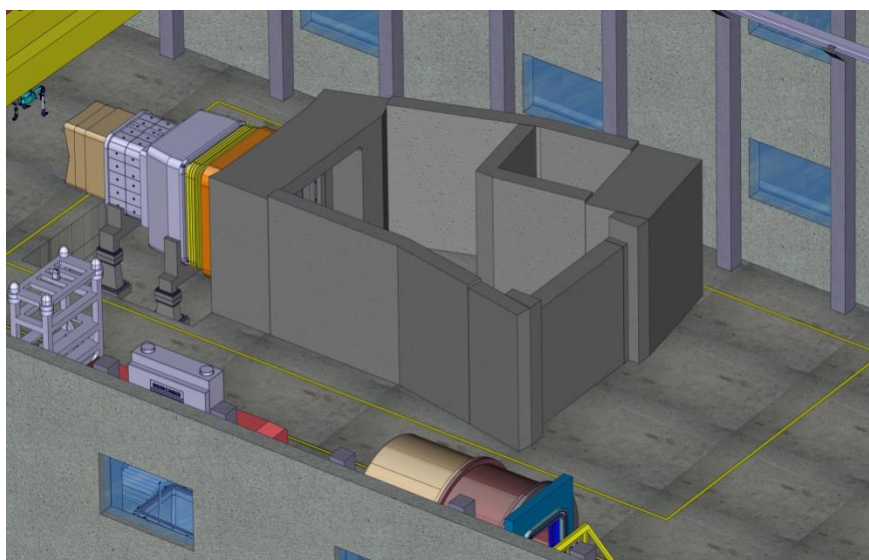


Fig. 46. Pipe Forest & Bioshield Door assembly removal step 3.

- 4) The ATS leaves the assembly in the Storage Area.

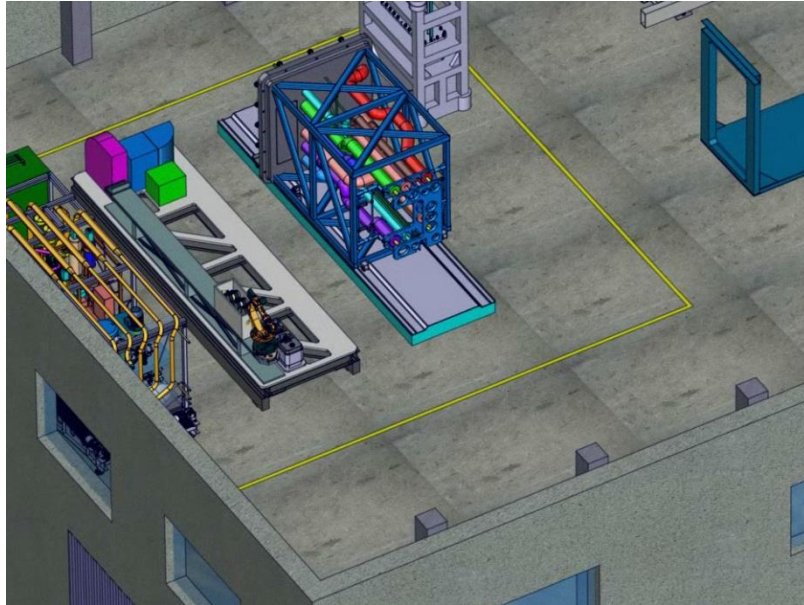


Fig. 47. Pipe Forest & Bioshield Door assembly removal step 4.

#### 4.3.2.6. Connection and disconnection of pipes at Interface 2a

##### Description

The Pipe Forest pipes must be connected/disconnected to/from the TBM pipes at Interface 2a. This operation includes pipe welding, inspection and cutting, as well as installation/removal of thermal insulating modules (operations #17, 18, 19, 20, 21 and 22 from Chapter 2).

##### Task objective

###### *First part: connection*

1) To place the RH Platform Unit in the Port Cell by means of the ATS; 2) to put the robotic arm –mounted on the deployable carrier- in the Interspace through the Bioshield Window; 3) to weld the pipes at IF2a and to check the weld beads; 4) to install the thermal insulating modules.

###### *Second part: disconnection*

5) To remove the insulating modules; 6) to cut the pipes at IF2a; 7) to take out the robotic arm from the Interspace through the Bioshield Window; 8) to place the RH Platform Unit in the Storage Area.

##### Assumptions

- The RH Platform Unit is transported between the Storage Area and the Port Cell by means of the Air Transfer System.
- There is a system to constrict/unconstrict the pipes at IF2a to allow the remote maintenance operations.
- The conceptual design of the end effectors is taken from [Bed 07].

##### Start conditions

###### *First part: connection*

The RH Platform Unit is located in the Storage Area. The pipes at IF2 are disconnected.

###### *Second part: disconnection*

The RH Platform Unit is located in the Port Cell. The pipes at IF2 are connected.

End conditions*First part: connection*

The RH Platform Unit is located in the Port Cell. The pipes at IF2 are connected.

*Second part: disconnection*

The RH Platform Unit is located in the Storage Area. The pipes at IF2 are disconnected.

Remote operations sequence

- 1) The RH Platform Unit enters into the Port Cell by means of the ATS.

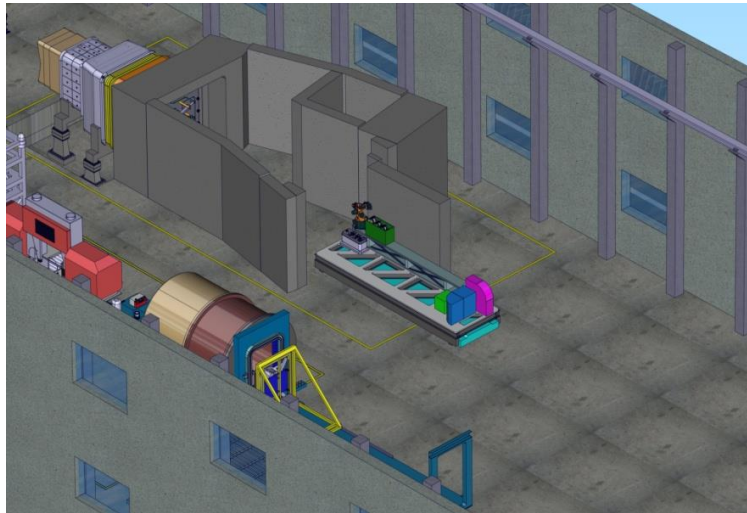


Fig. 48. IF2a connection step 1.

- 2) The RH Platform Unit is positioned next to the Bioshield Door by means of the ATS.

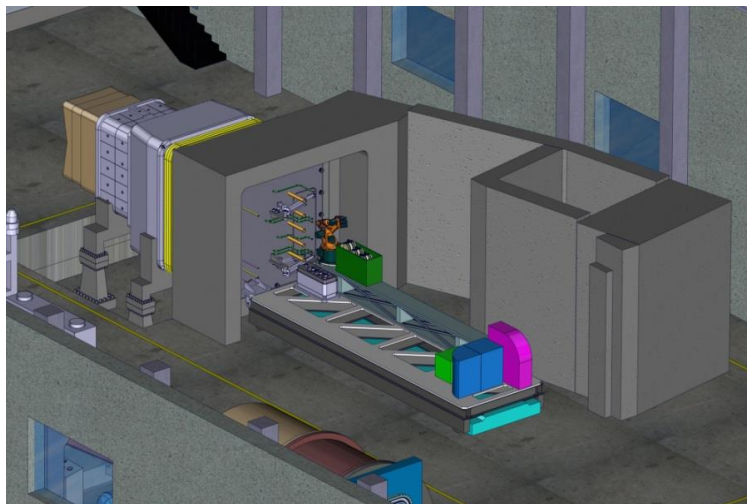


Fig. 49. IF2a connection step 2.

- 3) The Bioshield window is opened.

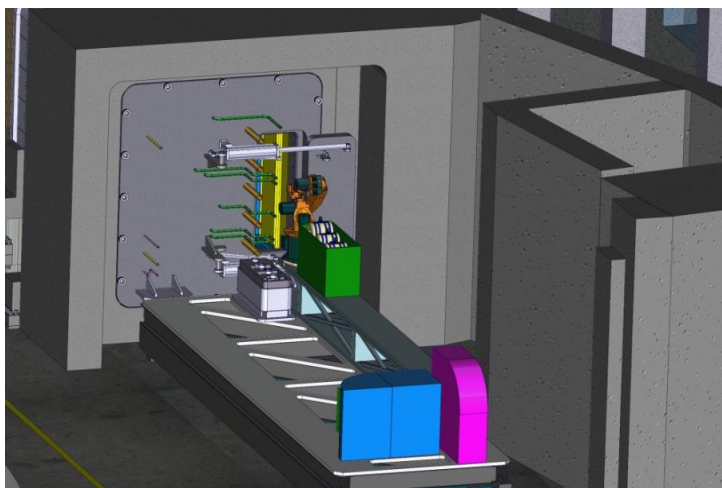


Fig. 50. IF2a connection step 3.

- 4) The welding tool is taken by the robotic arm.

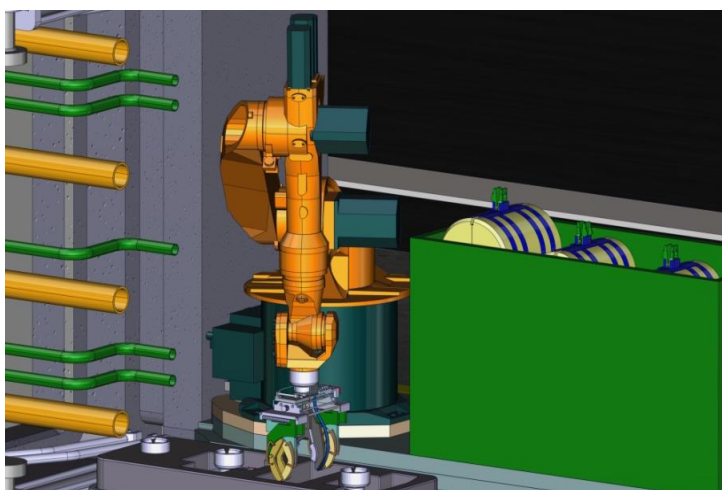


Fig. 51. IF2a connection step 4.

- 5) The robotic arm is positioned at IF2a.

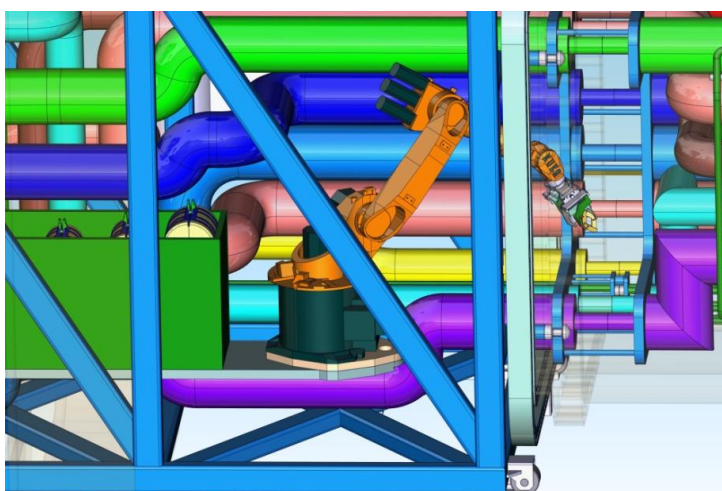


Fig. 52. IF2a connection step 5.

- 6) The pipes are welded at IF2a.

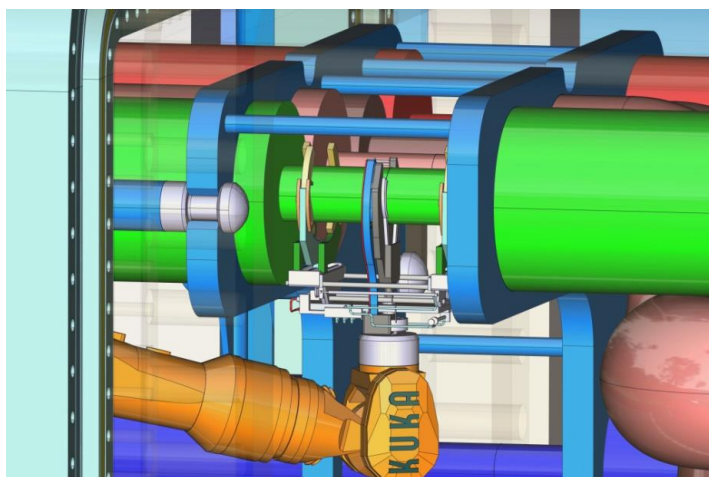


Fig. 53. IF2a connection step 6.

- 7) The welding inspection tool is taken by the robotic arm.

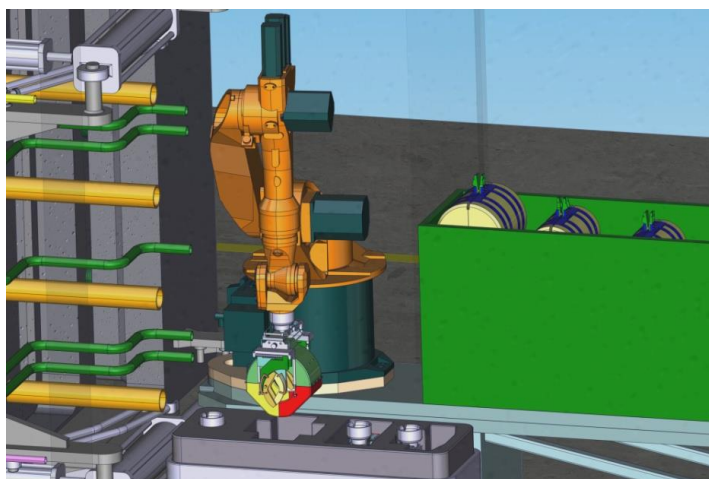


Fig. 54. IF2a connection step 7.

- 8) The welds are inspected at IF2a.

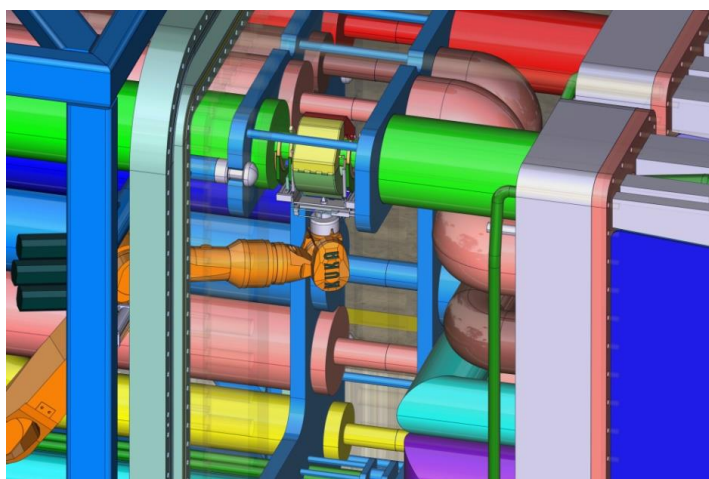


Fig. 55. IF2a connection step 8.

- 9) The clamp is taken by the robotic arm.

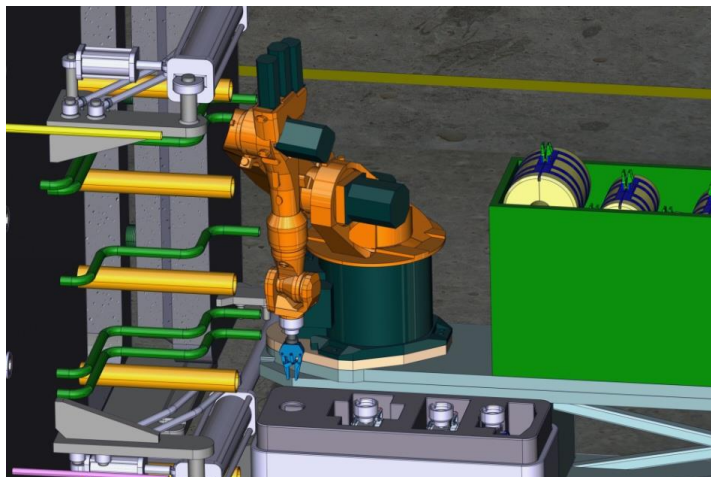


Fig. 56. IF2a connection step 9.

- 10) The insulation modules are installed at IF2a.

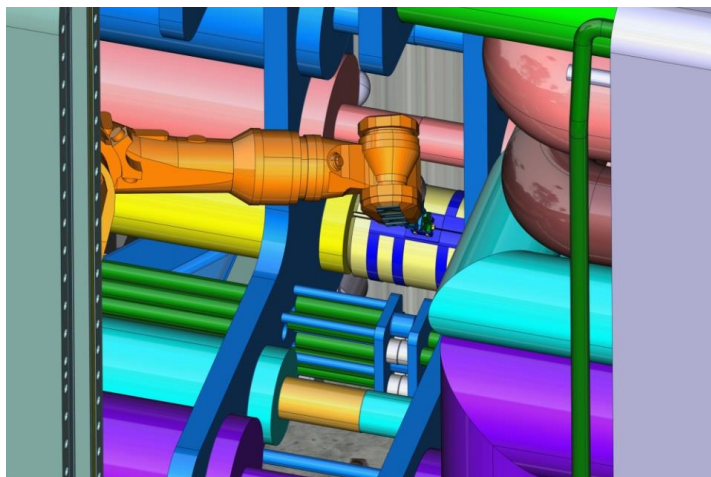


Fig. 57. IF2a connection step 10.

- 11) The pipes are unstricted at IF2a.

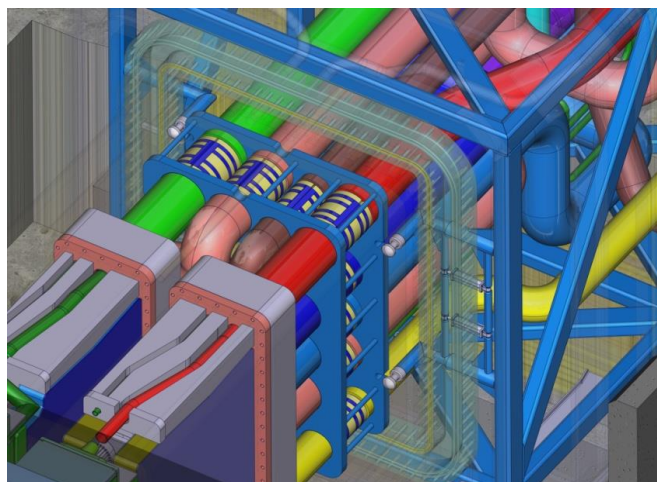


Fig. 58. IF2a connection step 11.

12) The Bioshield window is closed.

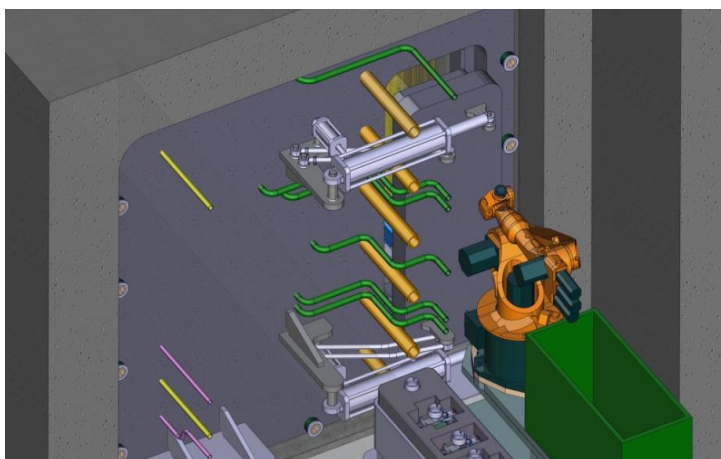


Fig. 59. IF2a connection step 12.

13) The RH Platform Unit leaves the Port Cell.



Fig. 60. IF2a connection step 13.

### Second part: disconnection

1) The pipes are constricted at IF2a.

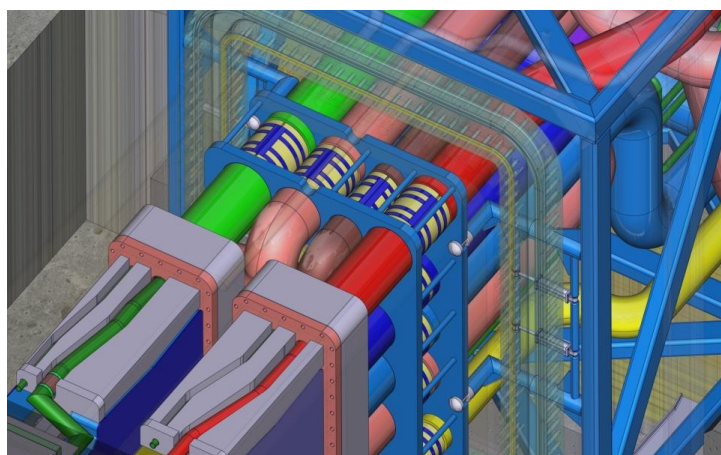


Fig. 61. IF2a disconnection step 1.

- 2) The ATS carries the RH Platform Unit to the Port Cell. The robotic arm gains access to the IF2a and removes the insulation modules.

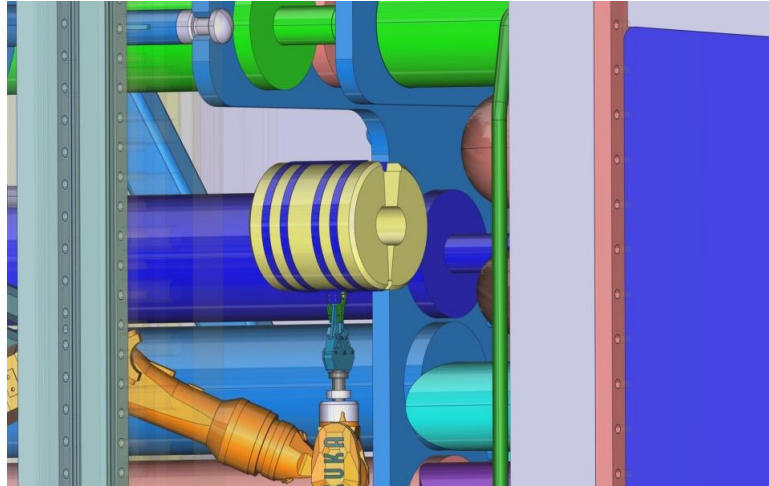


Fig. 62. IF2a disconnection step 2.

- 3) The robotic arm takes the cutting tool and cuts the pipes at IF2a.

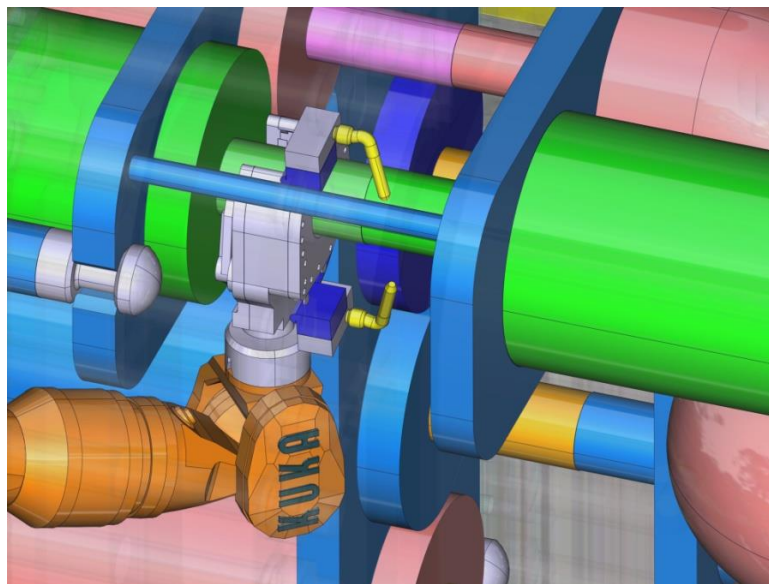


Fig. 63. IF2a disconnection step 3.

#### 4.3.2.7. Installation and removal of the Ancillary Equipment Unit

##### Description

The Ancillary Equipment Unit (AEU) is carried from the Storage Area to the Port Cell. The it is positioned to be joined by hands-on to the pipes coming from the Pipe Forest and the Port Cell walls. Then it must be taken back to the Storage Area (operation #23 from Chapter 2).

##### Task objective

1) To put the AEU in the Port Cell; 2) to accurately place the AEU in order to align the pipes with the Interfaces 2b and 3 pipes; 3) to remove the AEU and transport it to the Storage Area.

### Assumptions

- The ATS must be able to align the AEU pipes to the Port Cell pipes with enough accuracy to allow carrying out the pipe maintenance operations by hands-on.
- There is no Interface 3 pipes mock up in the Test Facility.

### Start conditions

#### *First part: installation*

The AEU is located in the Storage Area.

#### *Second part: removal*

The AEU is installed in the Port Cell.

### End conditions

#### *First part: installation*

The AEU is installed in the Port Cell.

#### *Second part: removal*

The AEU is located in the Storage Area.

### Remote operations sequence

- 1) The AEU enters into the Port Cell by means of the Air Transfer System.

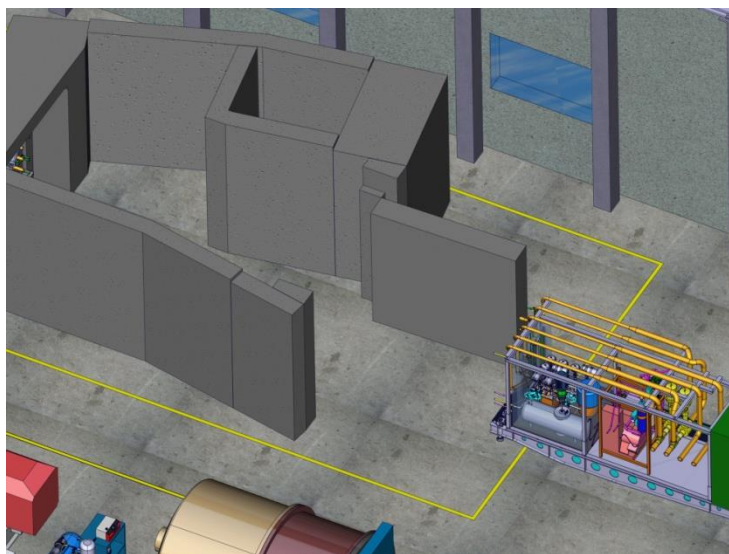


Fig. 64. AEU installation step 1.

- 2) The AEU is positioned.

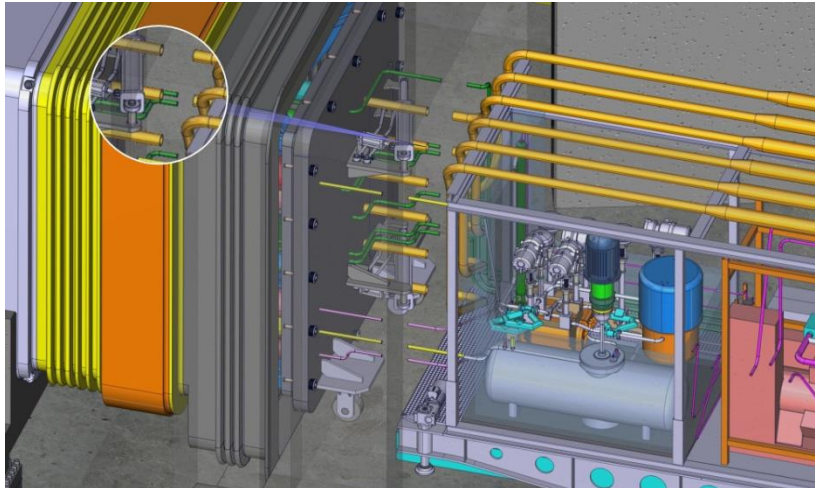


Fig. 65. AEU installation step 2.

- 3) The pipes are welded at Interfaces 2b and 3 (hands-on) (assessment of hands-on operations is not an objective of the task).

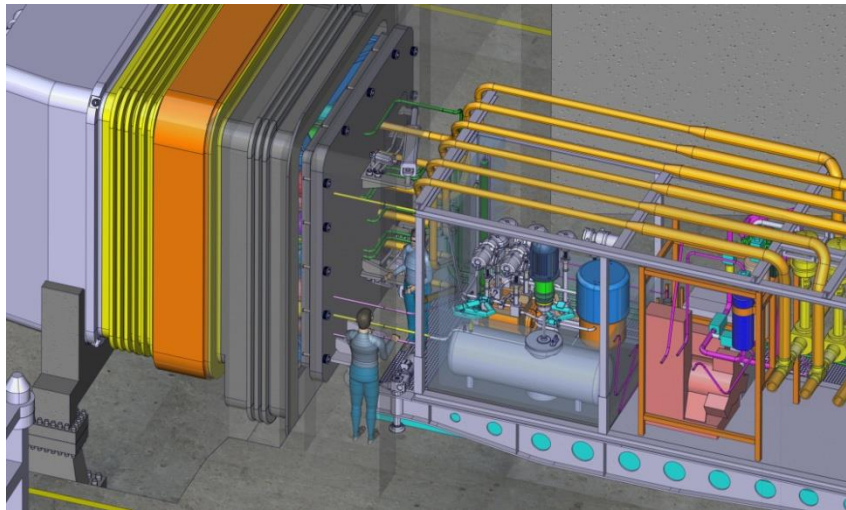


Fig. 66. AEU installation step 3.

## Second part: removal

- 1) The pipes are cut at Interfaces 2b and 3 (hands-on) (as in the case of the installation last step, this is not an objective of the task).

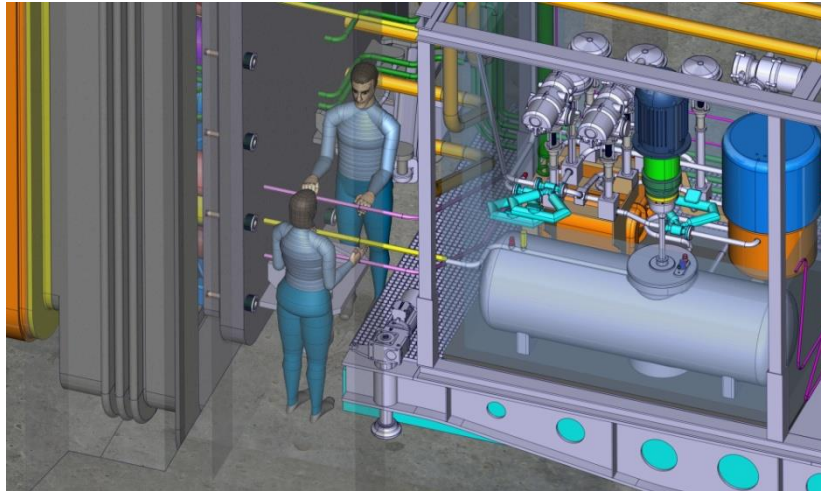


Fig. 67. AEU removal step 1.

- 2) The ATS carries the AEU from the Port Cell to the Storage Area.

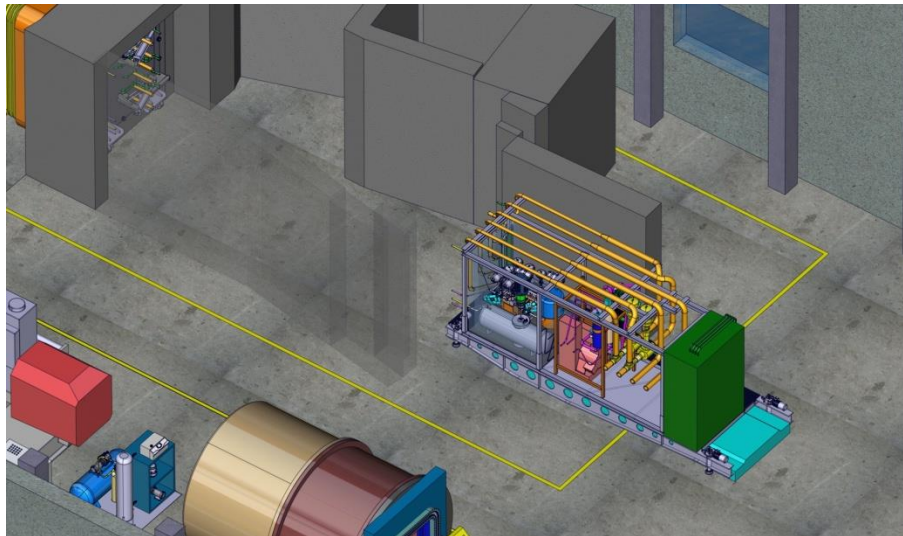


Fig. 68. AEU removal step 2.

### 4.3.2.8. Consequences of the simulation process

The integration process from models and simulations previous to the final video sequences has produced a number of consequences on the design of the equipment and RH operations. Among others, the following issues can be highlighted:

- Modification of the position and size of the Pipe Forest & Bioshield Door assembly collapsible wheels.
- Modification of the Connecting Duct rails position.
- Modification of the Bioshield Door shape to improve the alignment of the captive bolts.
- Modification of the Bioshield window mechanism.
- Modification of paths in some Pipe Forest pipes to allow the robotic arm reaching all the needed positions at IF2a.

## 4.4. Application case 2: ITER Divertor RH system

### 4.4.1. Introduction

Fusion for Energy (F4E), the European Domestic Agency for ITER, launched in November 2011 a “Call for Interest” (F4E-OMF-340) concerning Multiple Framework Contracts in cascade for Remote Handling Systems in ITER: Divertor RH System, Cask & Plug RH System and Neutral Beam Cell RH System. The scope of the Multiple Framework Contracts comprises the design, manufacturing, delivery, on-site integration, commissioning and final acceptance tests of components and systems to be delivered in-kind to ITER.

Regarding the Lot 1 (Divertor RH System), several candidates were pre-selected to participate in a competitive dialogue procedure. CIEMAT was involved as subcontractor within the consortium STAR, led by Telstar Technologies and composed of a number of private companies and research organisms (Tecnomare, Ansaldo Nucleare, Tecnatom, Procon Systems, ENEA, VTT and UPM).

An engineering study focused on the nuclearisation of the Cassette Toroidal Mover (CTM) was proposed by F4E to assess the design, nuclear engineering and project management skills of the candidates invited to tender [F4E 12].

The functions of the Cassette Toroidal Mover are transporting and installing/removing the divertor cassettes in/from the vacuum vessel. The CTM is equipped with inboard and outboard drive units allowing it to be driven along the toroidal rails. The CTM is also equipped with two lifting devices (with hook-type interfaces) that when fitted into the divertor cassette slots are capable of lifting the cassettes from the divertor rails. The cassettes need to be lifted and held by the CTM in a cantilever manner in order to transport them along the vessel (toroidally) [F4E 11]. It must be noted that the CTM systems must withstand gamma dose rates about 200-500 Gy/h and temperatures around 50°C during 2000 hours at least.

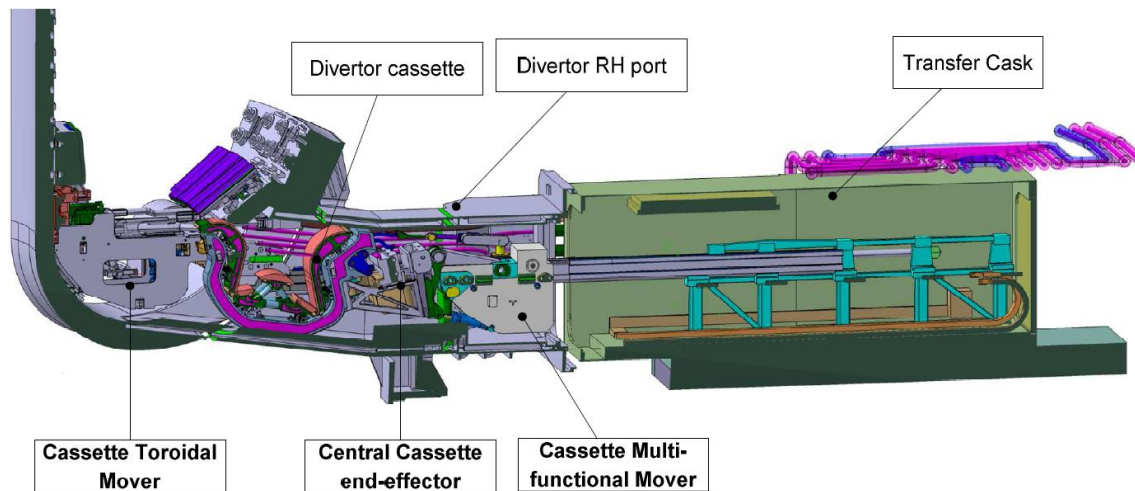


Fig. 69. Cross-section of the divertor area, divertor port and transfer cask. RH equipment (in bold characters) is transporting a divertor cassette along the divertor RH port duct [F4E 11].

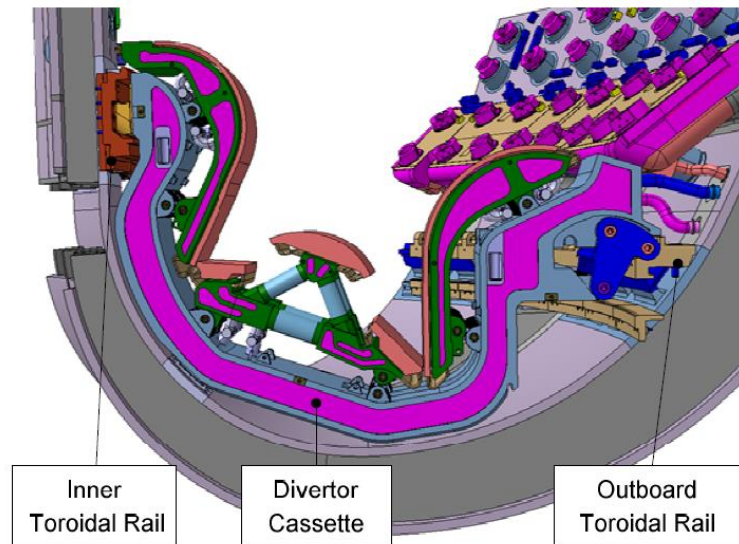


Fig. 70. Cassette layout, supported by the vessel rails [F4E 11].

Control, power and other services are provided to the CTM through a special cable guide connected to an umbilical feed-through which is fixed at the RH port duct before the deployment of the CTM [F4E 11].

Task #2 of the F4E-OMF-340 Business Case consisted on the design of the cable guide feeding the CTM, as well as on the study of rescue procedures. Besides the evaluation of all the signals & services for the CTM and the conceptual design of the instrumentation (Subtask #2.1), CIEMAT was the responsible of creating 3D animations to demonstrate connector matting and cable guide articulation during CTM movements, as part of Subtask #2.3 (design of the CTM cable guide).

#### 4.4.2. Design of the CTM cable guide

According to [Fern 13b], the cable guide should carry a total number of 38 cables (279 electric signals) with a specific weight of 3.51 kg/m, and 6 hydraulic hoses (diameter 21 mm). The analysis of the reference CTM cable guide design showed some problematic features [Ass 13]: 1) it has 4 rotational joints (each joint has an axis that interferes with the cables); 2) cables must withstand twisting and bending with this kind of articulations; 3) it is difficult to respect the cables minimum bending radius; 4) the cable guide position in every moment is unknown; 5) the model cannot be used in either direction (it needs mechanical stops in the joints to have some control of the movement) and 6) some problems regarding the decontamination or the maintenance process could occur because of the placement of the cables in the tubes.

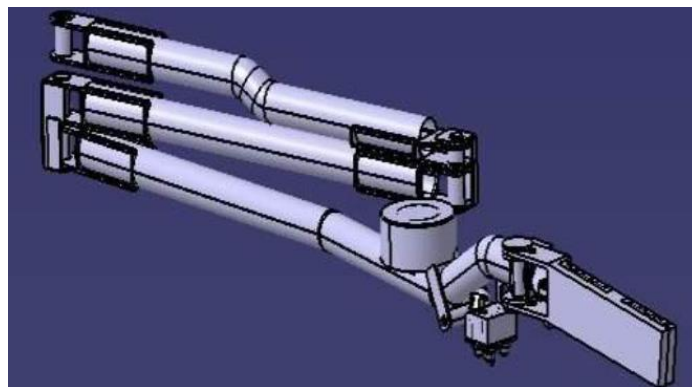


Fig. 71. Cable guide reference design [Ass 13].

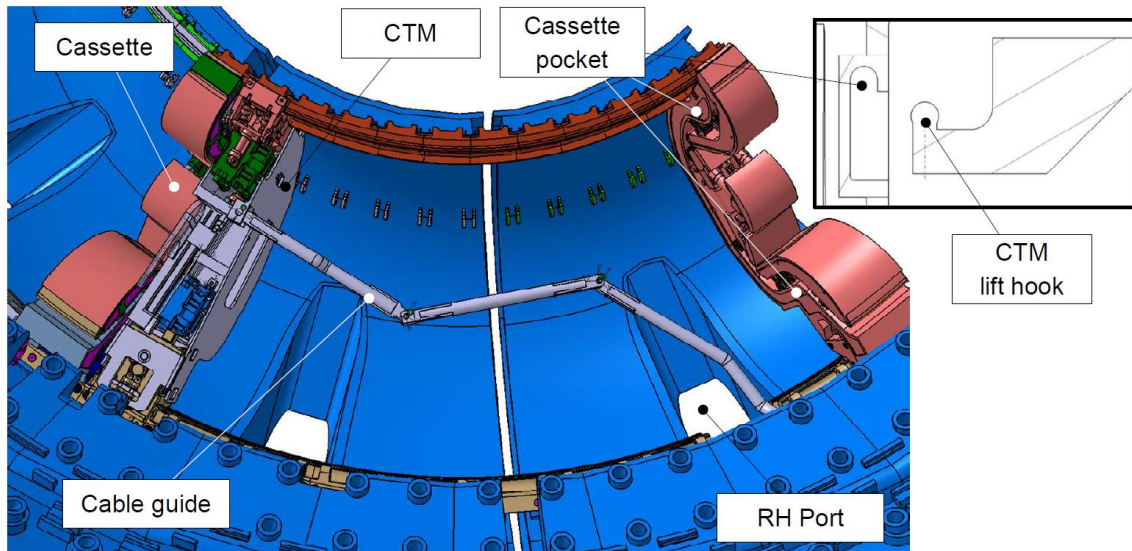


Fig. 72. Cassette toroidal mover transporting a divertor cassette. The reference cable guide design is shown [F4E 11].

Furthermore, a representative mock-up of one joint of the reference configuration was constructed and tested by Tecnatom in order to better evaluate the reference design considering the cable passage and to study possible modifications to obtain symmetric functionality (capability to move both left and right). A representative bundle of electrical cables and hydraulic lines was mounted on the mock-up. Deployment tests permitted to set the adequate length for the bundle of cables over the joint in order to avoid excessive deformation of the cables. The results showed that protruding bundles of cables were feasible to be accommodated at each joint without interference with other parts or components mounted on the CTM [Ass 13].



Fig. 73. Side view of the reference design joint mock-up [Ass 13].

On the other hand, two solutions were proposed to accommodate the cable guide reference design for both left and right movements [Ass 13]: 1) to eliminate the hard stop (although the need for actuators to control the configuration would remain as an issue; and 2) to change the configuration of the joint retracting axis position. Another mock-up representative of the second solution was constructed in order to check for cable configuration and overall envelope. Results showed the solution was not feasible, in spite of its simplicity. Assuming the cable guide envelope volume at stowage configuration in the CTM, each arm should be shortened 300 mm

at each joint end. In such case, the total extension length shown in Fig. 72 could not be reached by the new configuration [Ass 13].

In consequence, after reviewing the state-of-the-art of industrial applications to deploy and manage bundles of cables, four new designs for the CTM cable guide were proposed:

- Pantograph model.
- Pendant model.
- Telescopic model.
- Telescopic and chain model.

The telescopic and chain model, consisting in several slides and a cable chain which adapt to the toroidal movement of the CTM, avoiding torsion in cables, was selected as the best option. Among its advantages, the following ones must be underlined [Ass 13]: 1) ability to work in either direction; 2) autonomy; 3) thinness; 4) best ratio rigidity/weight; 5) adaptation to the parking position; 6) articulated lower arm to avoid interferences with the master/slave robotic arm (MAM) mounted on the CTM. The main advantages could be 1) weight (although it can be made of structural aluminium); 2) rescue-ability; 3) decontamination.

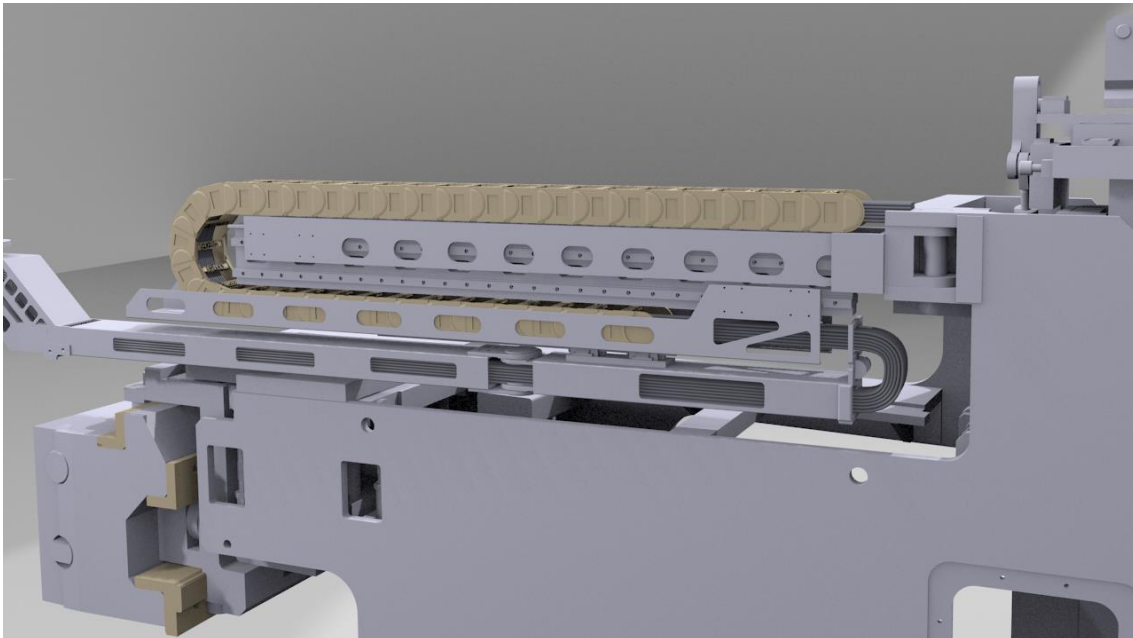


Fig. 74. Telescopic and chain cable guide [Fern 13].

Cables and hydraulic lines coming from the CTM trough the cable guide are connected to the umbilical ones by means of a multi-pin connector and a corresponding socket located in the umbilical side (Fig. 75). The design of the multi-pin connector must be reliable and robust enough to allow plugging the cable guide to the umbilical cable by means of a RH manipulator and to withstand the mechanical stresses due to the CTM operations which are transmitted through the cable guide. The ODU MAC Modular Connection System was selected for the electric & optic signals male and female connectors. This system consists of a variety of rugged, customizable frames, plastic insulation bodies and removable crimp contacts for power, signal, coax, air couplings and optic fibre connections. On the other hand, quick-change clamping modules were proposed for the socket block, in order to make easier the connection by the manipulator. The selected system was VERO-S NSE mini 90 (Schunk) [Fern 13].

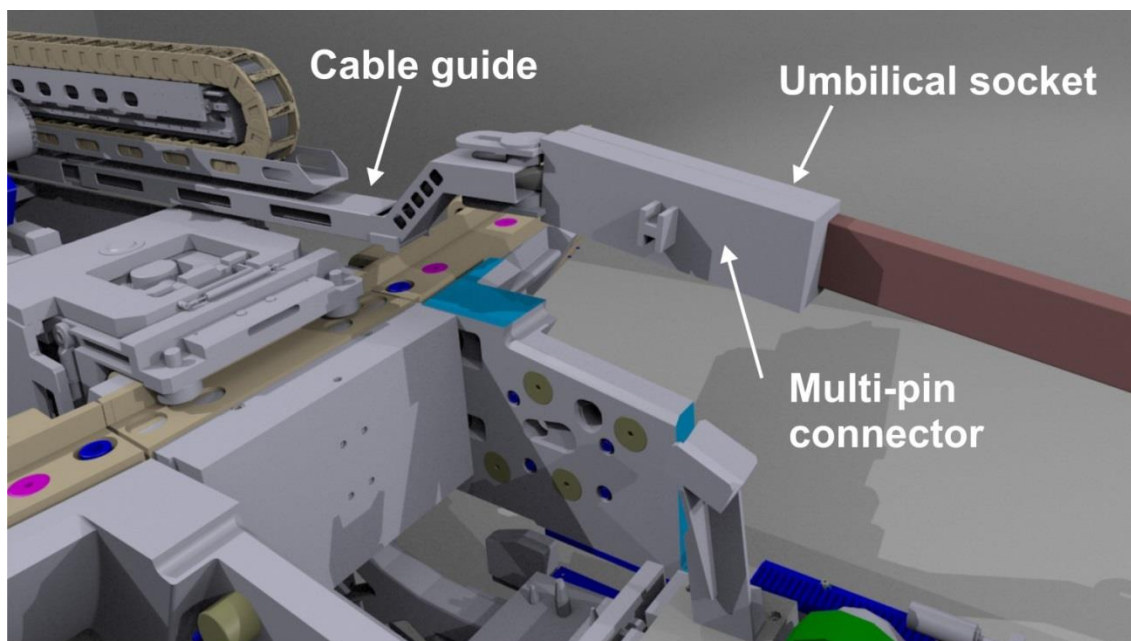


Fig. 75. Electrical, optical and hydraulic interfaces [Fern 13].

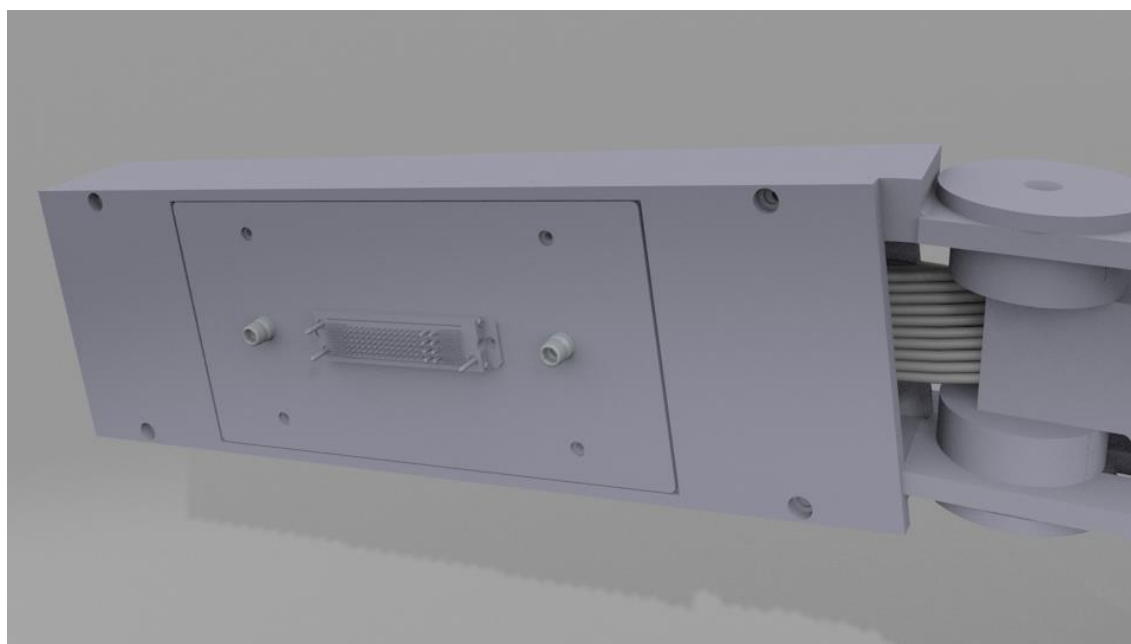


Fig. 76. Multi-pin connector [Fern 13].

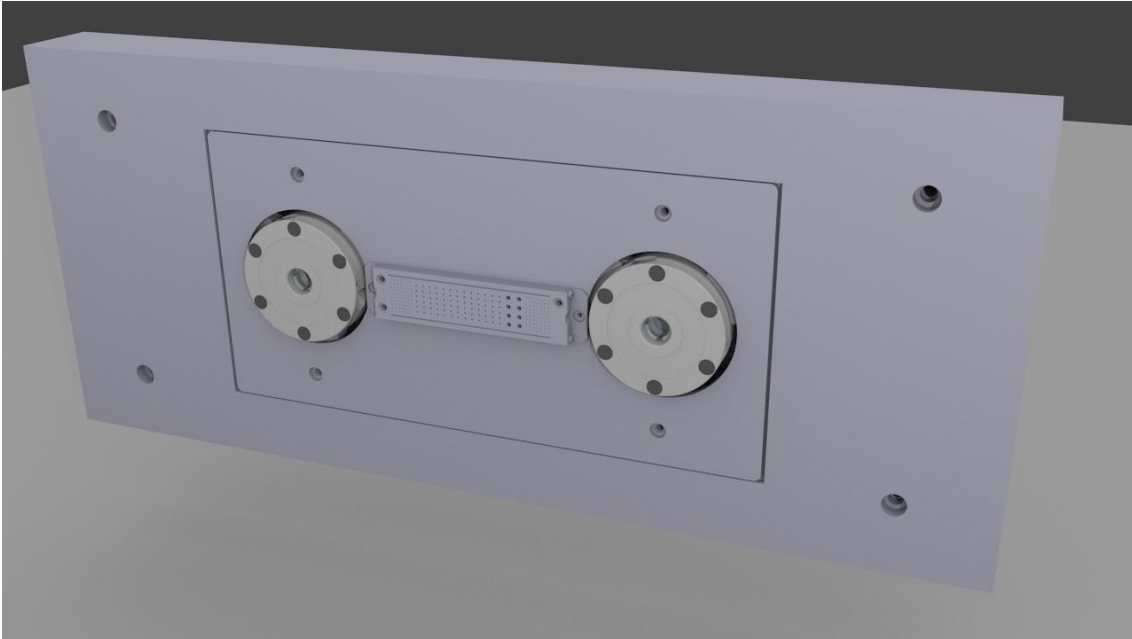


Fig. 77. Umbilical side socket [Fern 13].

### 4.4.3. Tools and methodology

The need of analysing the behaviour of flexible elements like the chain and the cables by means of 3D animations forces to discard rigid body kinematics tools like CATIA or 3DVia Composer. In consequence, a different tool named Blender has been used to produce the animated sequences required by the Business Case Subtask #2.3.

Blender is a free and open source software which provides a broad spectrum of modelling, texturing, lighting, animation and video post-processing functionalities in one package.

Blender allows adding 'modifiers' to objects, which work by changing how an object is displayed and rendered, but not the actual object geometry. Other modifiers can be employed to enable physics simulations like collisions between objects, fluid flows, particle systems, etc. One of the most interesting modifiers for our application is the 'armature', which is used for building skeletal systems for animating the poses of characters and anything else which needs to be posed, like a robotic manipulator or the slides of a telescopic mechanism ('rigging' process). Armature bones can be also deformable.

Another interesting characteristic for this case is the possibility of applying constraints to the joints between objects. Thus, constraints are a way of connecting transform properties (position, rotation and scale) between objects. They can be considered the object counterpart of the modifiers, which work on the object data (i.e. meshes, curves, etc.). They can be very useful to limit/control the degrees of freedom of an object e.g. in relation to another objects. For example, it is possible to control a chain of bones by specifying the endpoint target (inverse kinematics), to limit the distance between mobile objects, to force an object to have the same location as its target or to apply rotations to an object, so that it always points a given axis towards its target. It is also possible to apply constraints to each bone of an armature, which behaves like a standard object. Together with the mentioned deformability of bones, this is the most important rigging feature in Blender which can be exploited to accurately simulate the behaviour of the cable guide elements during its manipulation.

Although Blender includes powerful modelling tools, the graphical objects used in the simulations have been designed in CATIA. Objects composing the geometric environment (vacuum vessel, ports, blanket system, divertor rails, umbilical, etc.) as well as the CTM, the Cassette Multifunctional Mover (CMM) which provides radial transport of in-vessel components

(divertor cassettes) and RH equipment through the divertor RH ports [F4E 11], the MAMs mounted in both the CTM and the CMM, and one of the divertor cassettes which must be manipulated have been provided by F4E as part of the Business Case Technical Specification. The cable guide CATIA model has been created and provided by Tecnatom, although some modifications have been made in CIEMAT.

Blender does not read CATIA native files or compatible formats like STEP, so the models have had to be previously converted to 3D Studio file format (\*.3ds) through 3DVia Composer and then imported into Blender. Afterwards, the complex rigging process starts, comprising operations like: assignation of deformable/non-deformable multiple-bones armatures, use of 'empty' elements associated with objects to define different kinds of constraints between them like inverse kinematics, 'limit distance' or 'follow paths', use of modifiers like 'hooks' or curve deformations, etc. In this sense, an important advantage of Blender over e.g. 3DVia Composer is that there are not many restrictions to combine a number of constraints and modifiers, so that very complex kinematics/dynamics mechanisms can be simulated.

Once established the mechanisms, the animated sequence is defined in a similar way to the one explained for 3DVia Composer (use of a timeline) in Subsection 4.3.1. The next step is to specify materials, textures (if any), lighting, cameras, graphical performances, etc. In this case, no special material or textures have been added, and most of the original colours have been kept.

Finally, the sequence is rendered and exported to video format (MP4, AVI, WMV, etc.), which can be later post-processed using video edition tools (e.g. to apply compression).

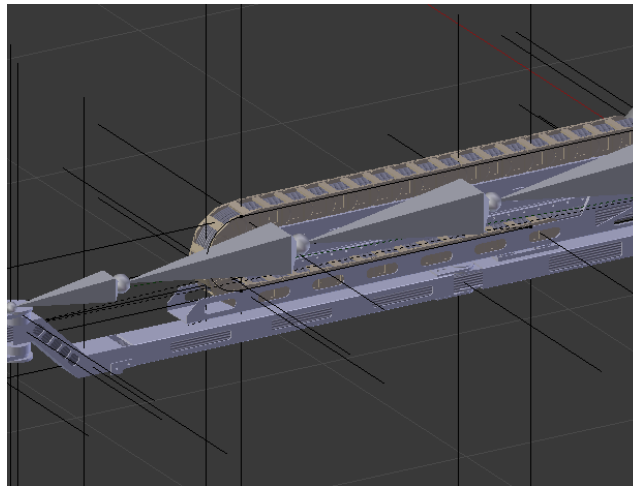


Fig. 78. Detail of the toroidal movement sequence kinematic model in Blender. 'Bones' and 'empty' elements are shown.

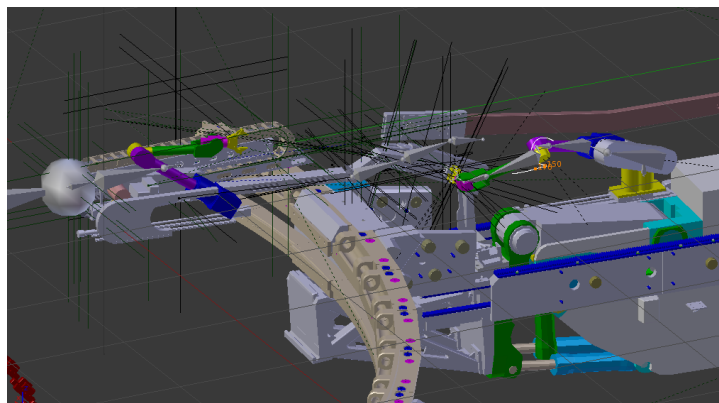


Fig. 79. Detail of the connector mating sequence kinematic model in Blender.

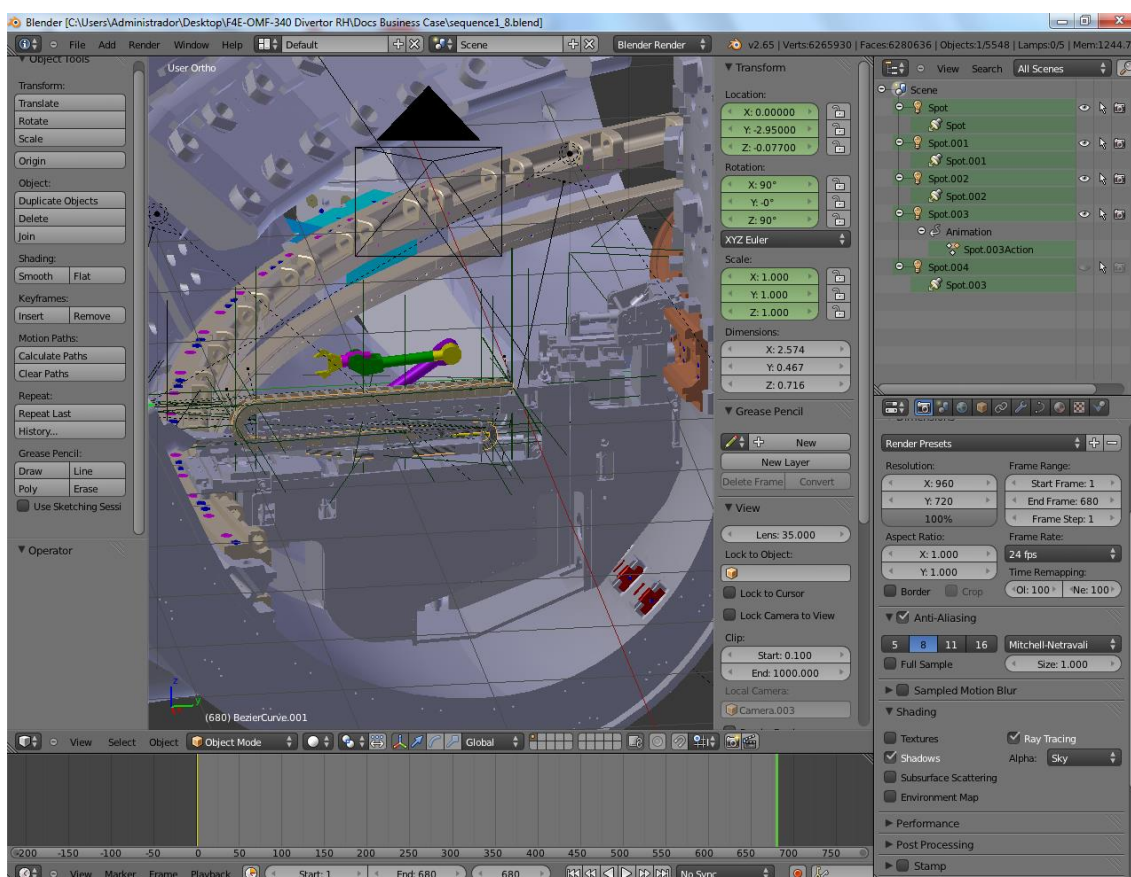


Fig. 80. Blender graphical interface: CTM, divertor system and vacuum vessel model.

Unlike the Test Blanket System (TBS) animations described in Subsection 4.3.2, none of the Divertor RH System animations have been planned according to the ITER Maintenance Management System. Therefore, not PDFs, TDFs and OSDs have been generated. Nevertheless, the same template used for the TBS animations is followed in the next Subsection to describe the Divertor RH System sequences.

#### 4.4.4. Description of the sequences and influence on the design

##### 4.4.4.1. Performance of the cable guide during the toroidal movement of the CTM

###### Description

The Cassette Toroidal Mover (CTM) moves toroidally to reach the divertor cassette which is located farther away from the vacuum vessel lower port. It handles the cassette and moves toroidally to position the cassette in front of the port to be subsequently extracted.

###### Task objective

1) To move the CTM toroidally to be close to the divertor cassette; 2) to place accurately the CTM next to the divertor, allowing the CTM lifting system to handle the cassette; 3) to move the CTM toroidally (in the opposite direction) to position the cassette in front of the lower port.

###### Assumptions

- The use of the telescopic and chain cable guide design is assumed.

Start conditions

The CTM is located in front of the lower port.

End conditions

The divertor cassette transported by the CTM is located in front of the lower port.

Remote operations sequence

- 1) The CTM is located in front of the vacuum vessel lower port.

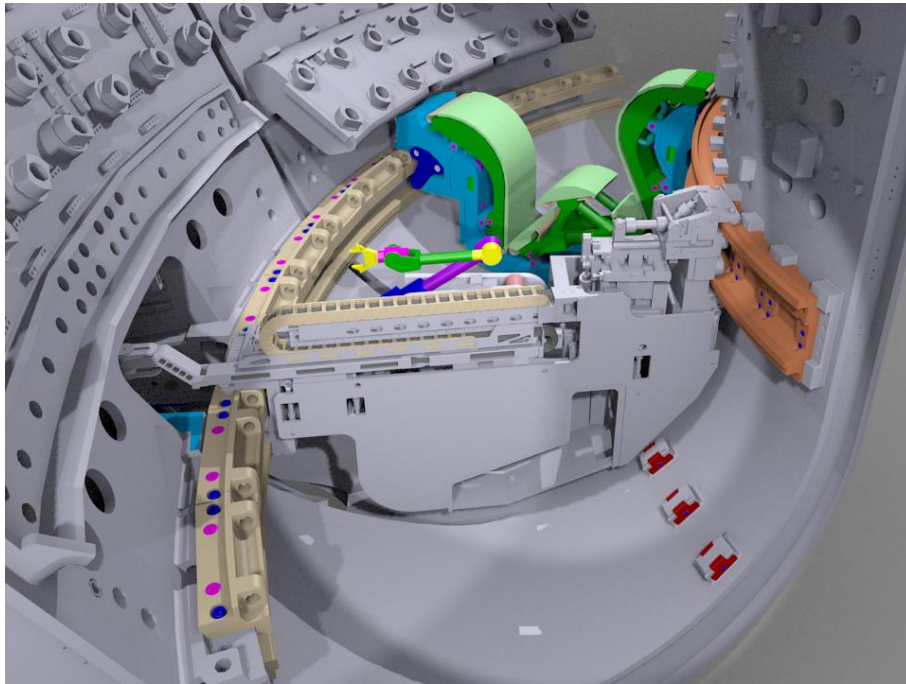


Fig. 81. Toroidal movement step 1.

- 2) The Outboard and Inboard Driving Systems move the CTM in toroidal direction towards the cassette position. The cable guide slides are sequentially deployed while the chain continuously adapts to the new configuration of the slides to reach the maximum length.

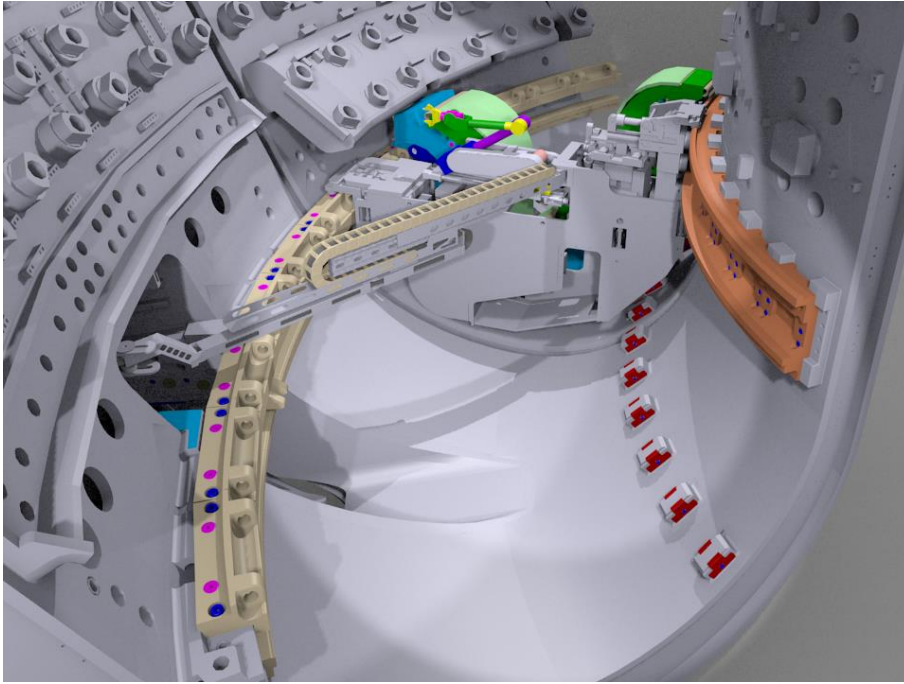


Fig. 82. Toroidal movement step 2.

- 3) Once the cable guide is fully deployed, the revolute joint which is located close to the umbilical moves along the slot and the maximum distance between the CTM and the port is reached.

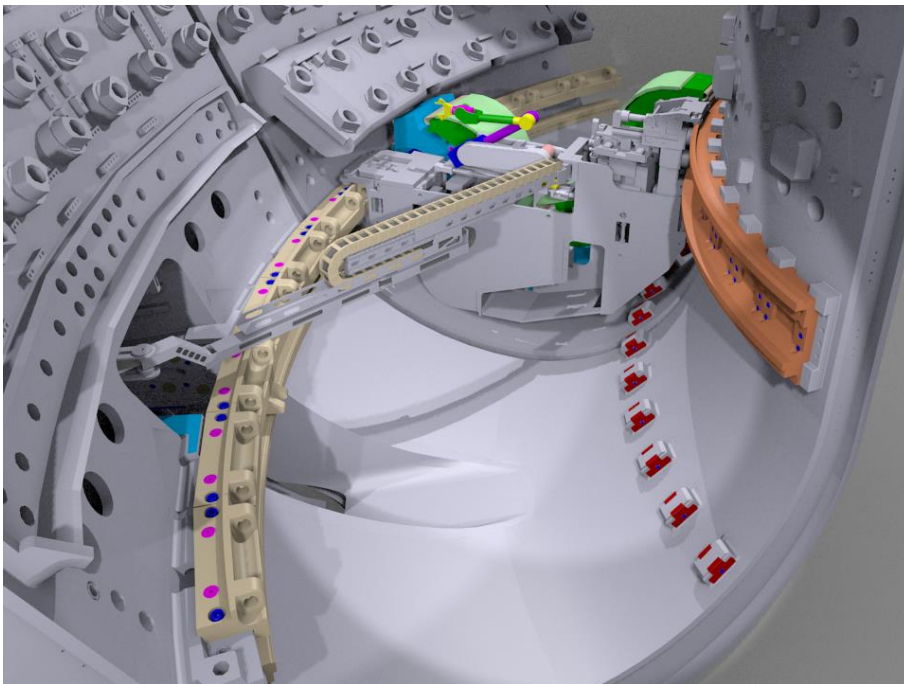


Fig. 83. Toroidal movement step 3.

- 4) The CTM lifting systems handles the cassette and lifts it.

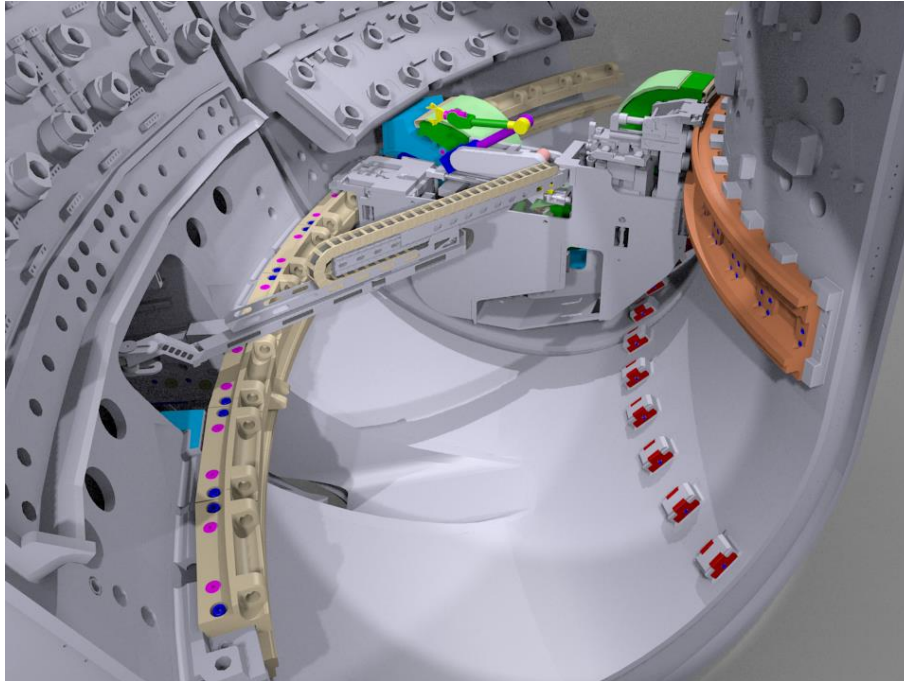


Fig. 84. Toroidal movement step 4.

- 5) The CTM moves back in toroidal direction to the initial position.

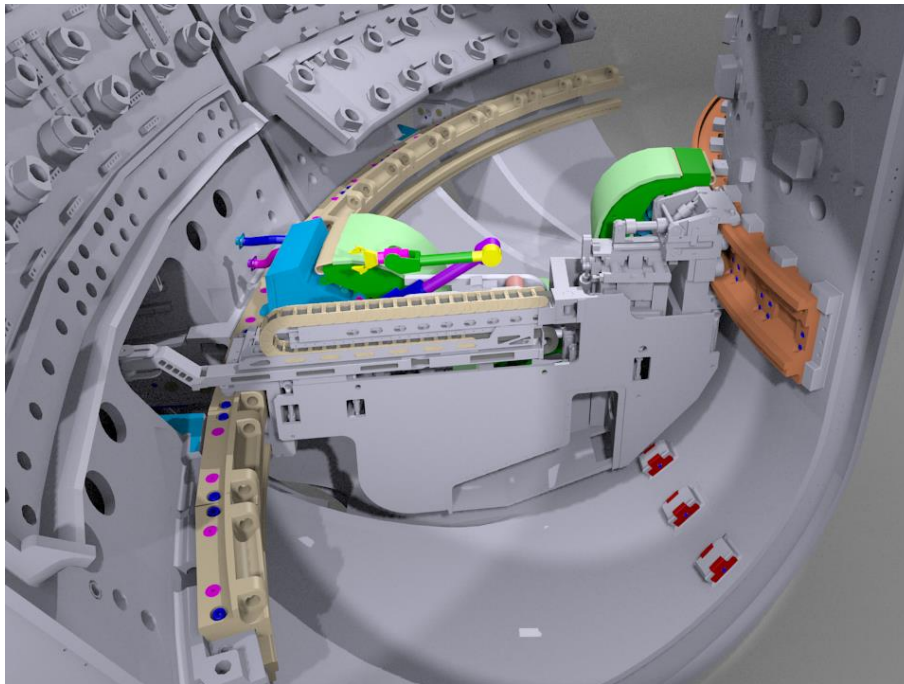


Fig. 85. Toroidal movement step 5.

- 6) The CTM stops and then continues its movement while an actuator bends the cable guide lower slide at its intermediate revolute joint, whereby the divertor cassette can be positioned in front of the lower port.

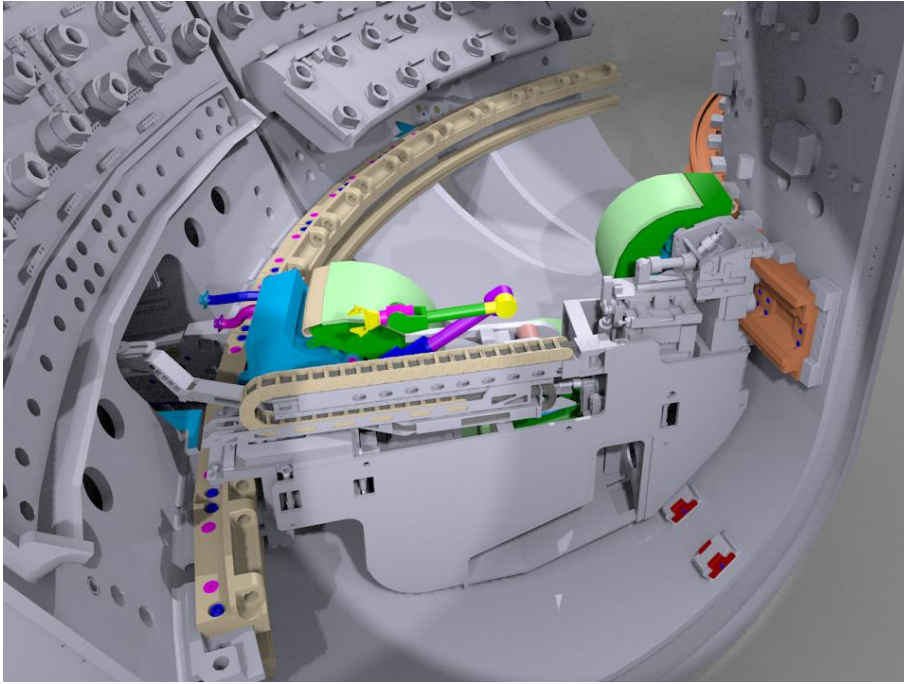


Fig. 86. Toroidal movement step 6.

This animation shows the sequence from three different cameras in order to better control the cable guide mechanisms and to ensure there is not any interference between the objects. The first camera, used to capture the previous frames, has been located near the equatorial plane of the vacuum vessel.

The second camera has been mounted on the CTM, so it moves accordingly:

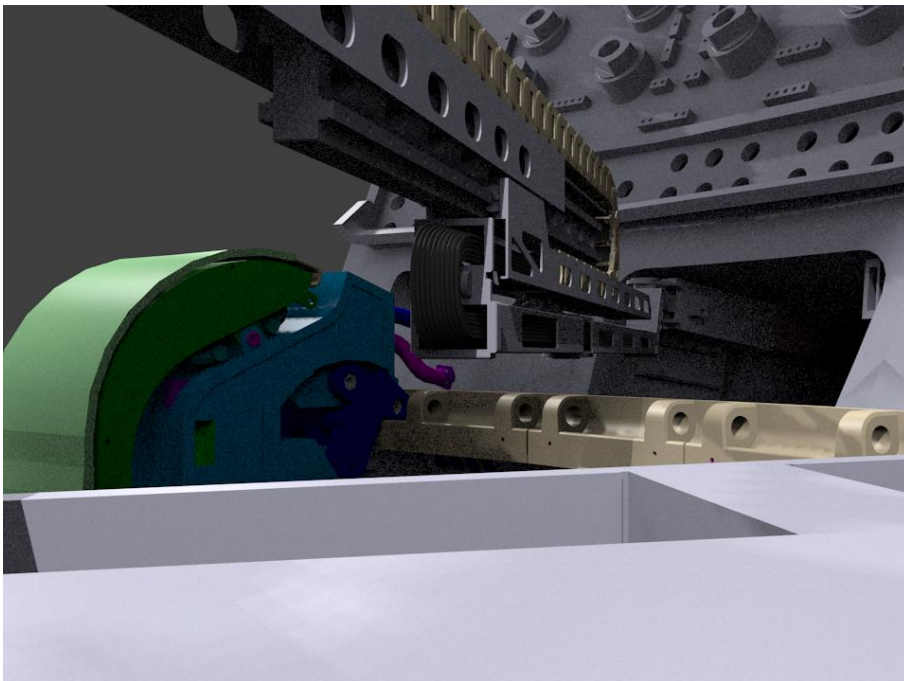


Fig. 87. View from the camera mounted on the CTM (1).

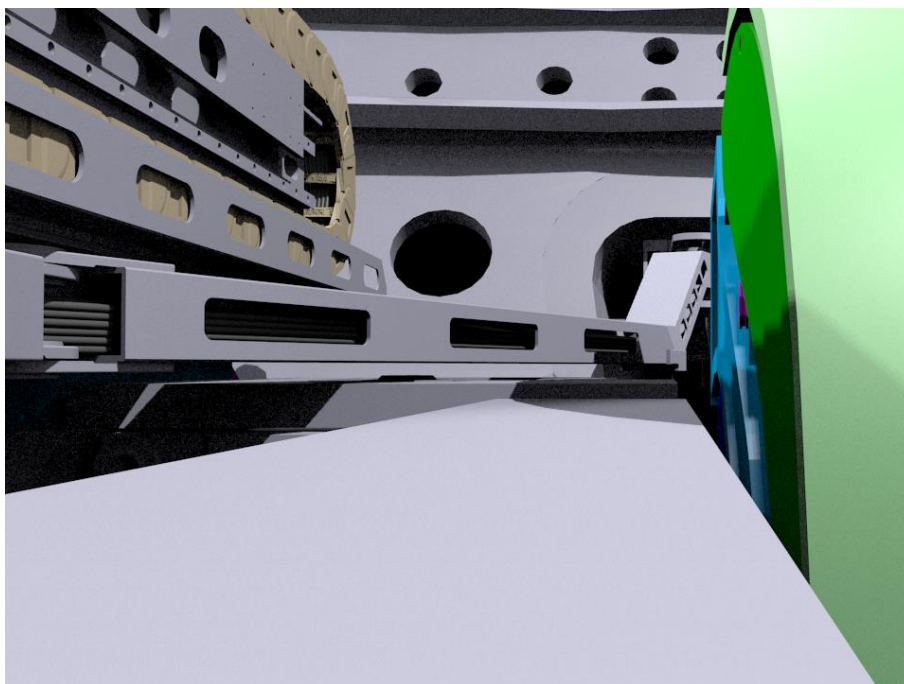


Fig. 88. View from the camera mounted on the CTM (2).

Finally, a third camera has been installed near the top of the vacuum vessel to capture zenithal views:

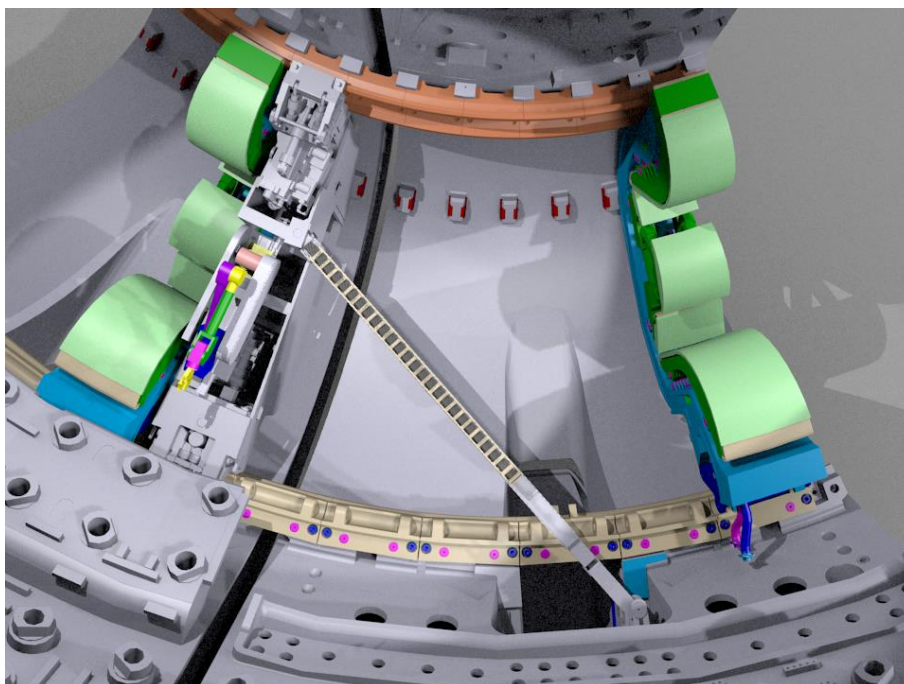


Fig. 89. View from the zenithal camera (1).

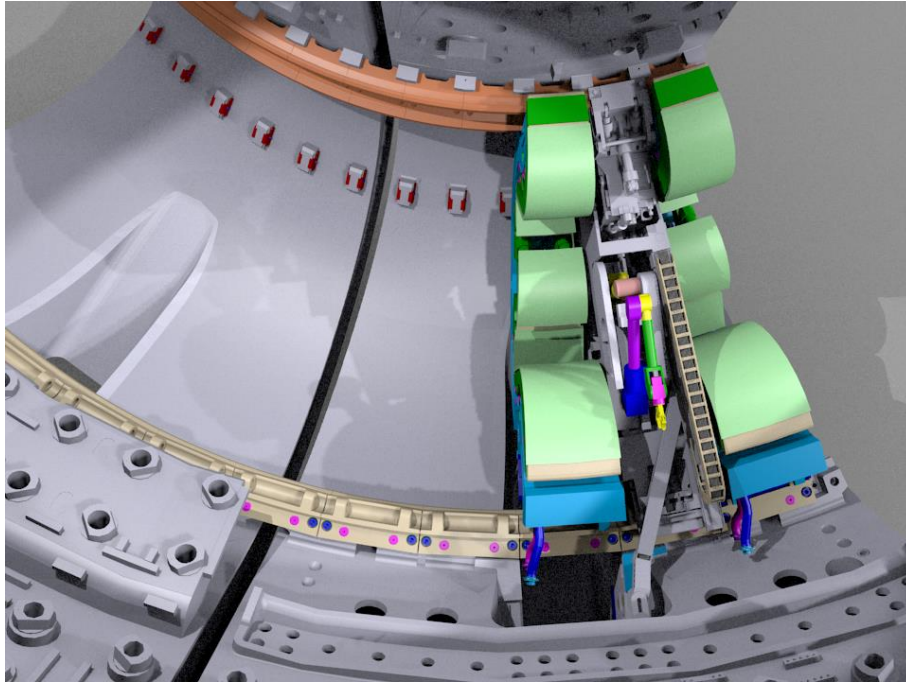


Fig. 90. View from the zenithal camera (2).

#### 4.4.4.2. Plugging of the multi-pin connector by the CMM MAM

##### Description

The robotic manipulator (MAM) which is mounted on the Cassette Multifunctional Mover handles the cable guide multi-pin connector and plugs it in the umbilical side socket. The whole cable guide adapts to the multi-pin connector movements.

##### Task objective

1) The MAM clamp handles the RH compatible feature installed on the multi-pin connector; 2) The MAM moves the multi-pin connector towards the umbilical side socket and plugs it in; 3) the MAM clamp releases the multi-pin connector.

##### Assumptions

- The use of the telescopic and chain cable guide design is assumed.
- The MAM payload in its deployed position is compatible with the weight of the multi-pin connector, the Z-shape cable guide piece and the corresponding cables section. Additionally, the MAM is capable to overcome the coupling-decoupling resistance force.

##### Start conditions

The CTM is placed in front of the vacuum vessel lower port. The last section of the cable guide (Z-shape piece) and the multi-pin connectors are supported by a base mounted on the CTM.

##### End conditions

The CTM remains in the same position. The multi-pin connector is plugged in the umbilical side socket.

Remote operations sequence

- 1) The MAM clamp approaches to the multi-pin connector handle.

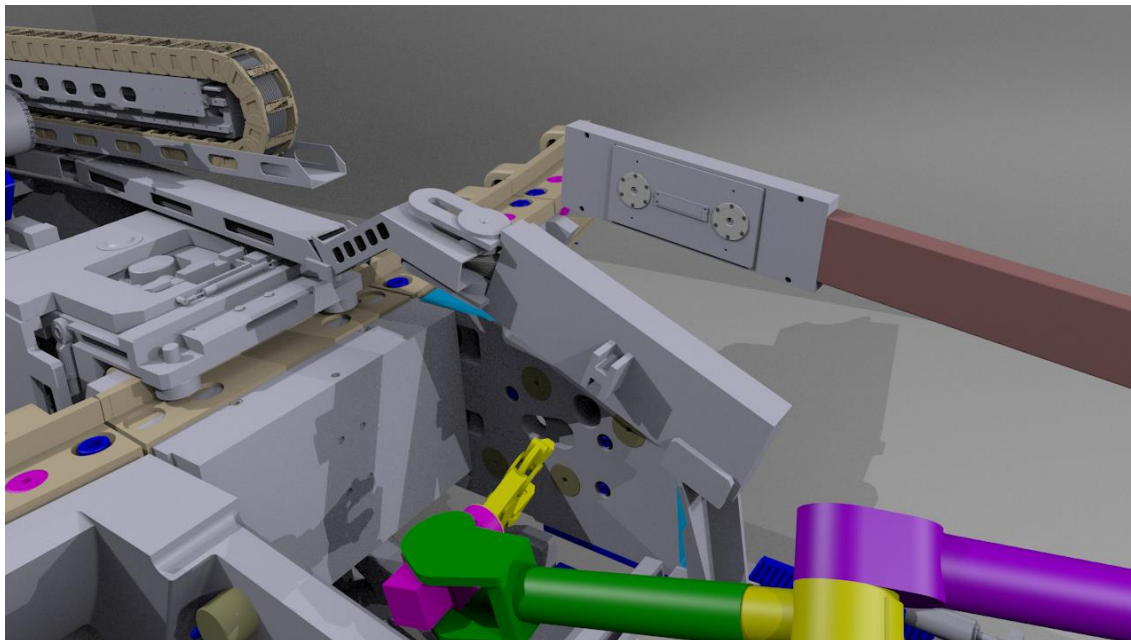


Fig. 91. Multi-pin connector plugging step 1.

- 2) The clamp handles the multi-pin connector.

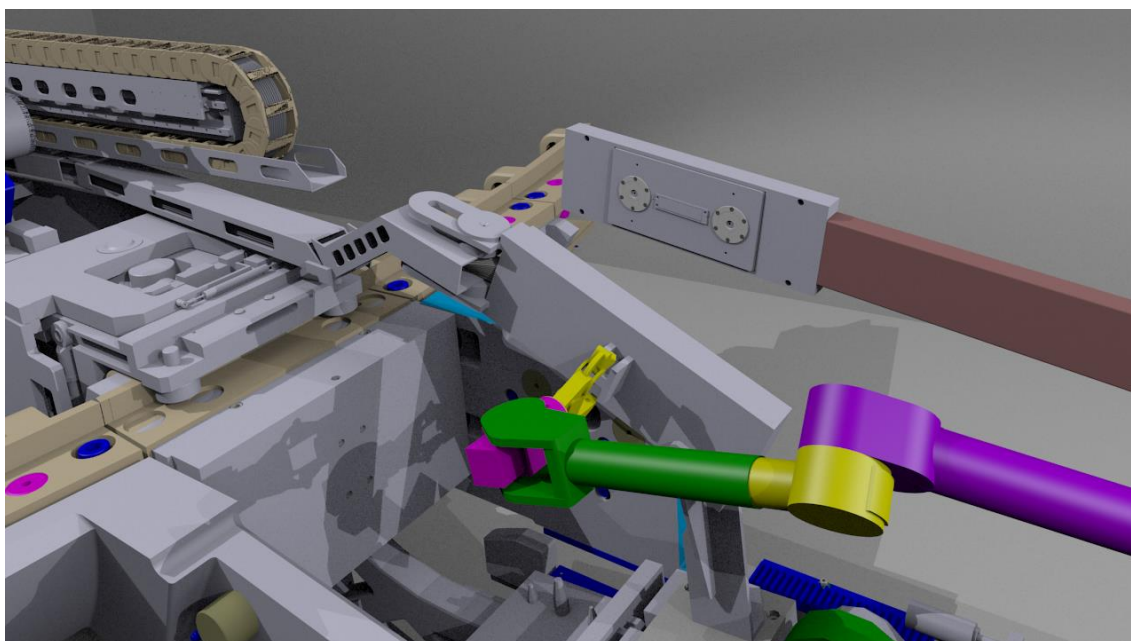


Fig. 92. Multi-pin connector plugging step 2.

- 3) The MAM lifts the multi-pin connector and the cable guide segment and moves them towards the umbilical side socket.

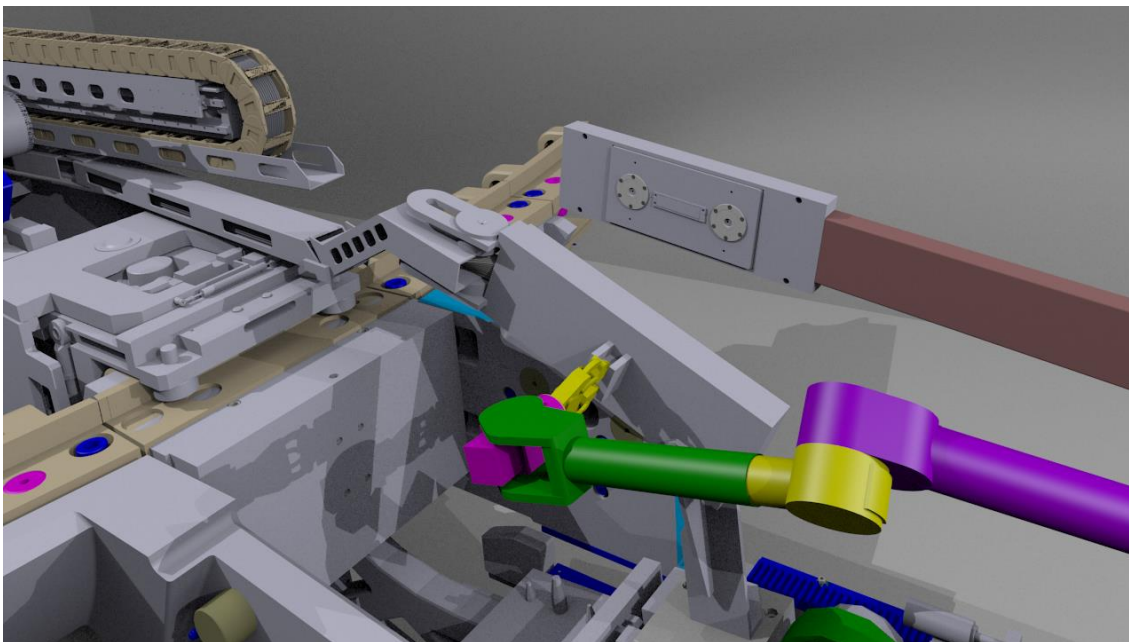


Fig. 93. Multi-pin connector plugging step 3.

- 4) The multi-pin connector approaches the umbilical side socket.

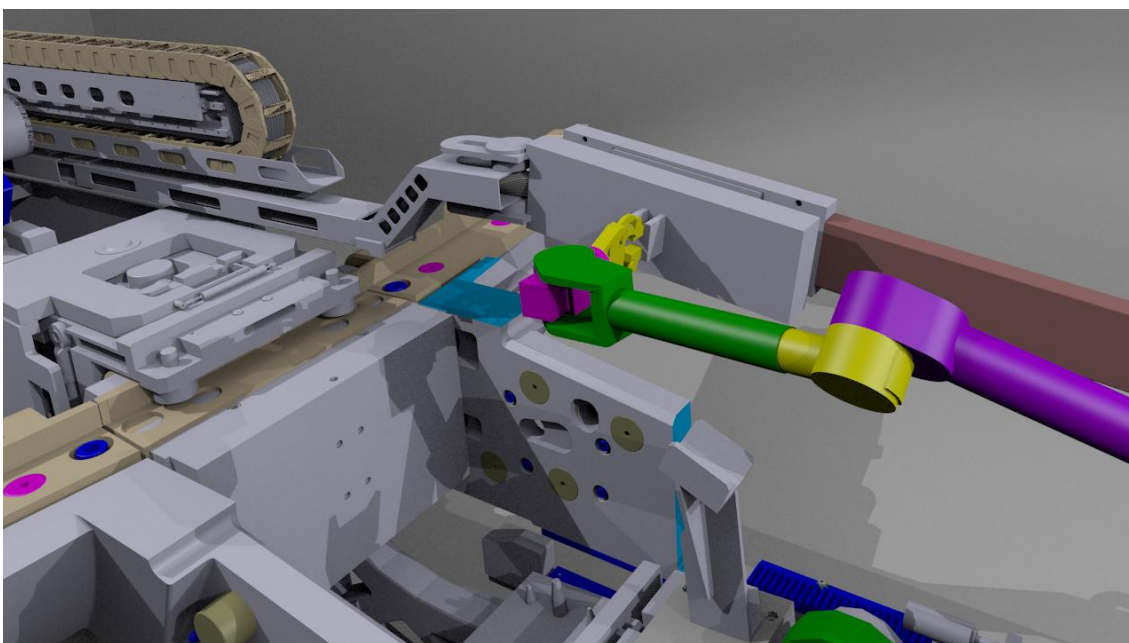


Fig. 94. Multi-pin connector plugging step 4.

- 5) The MAM plugs the multi-pin connector in the umbilical side socket. The clamp opens and releases the handle.

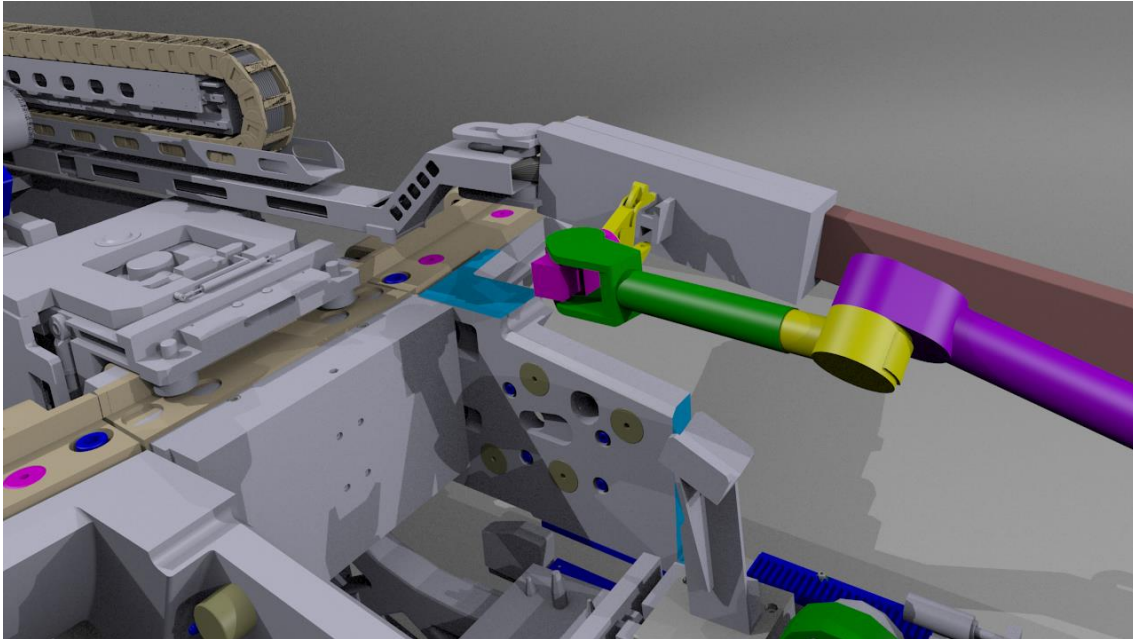


Fig. 95. Multi-pin connector plugging step 5.

- 6) The MAM gets away from the umbilical side socket.

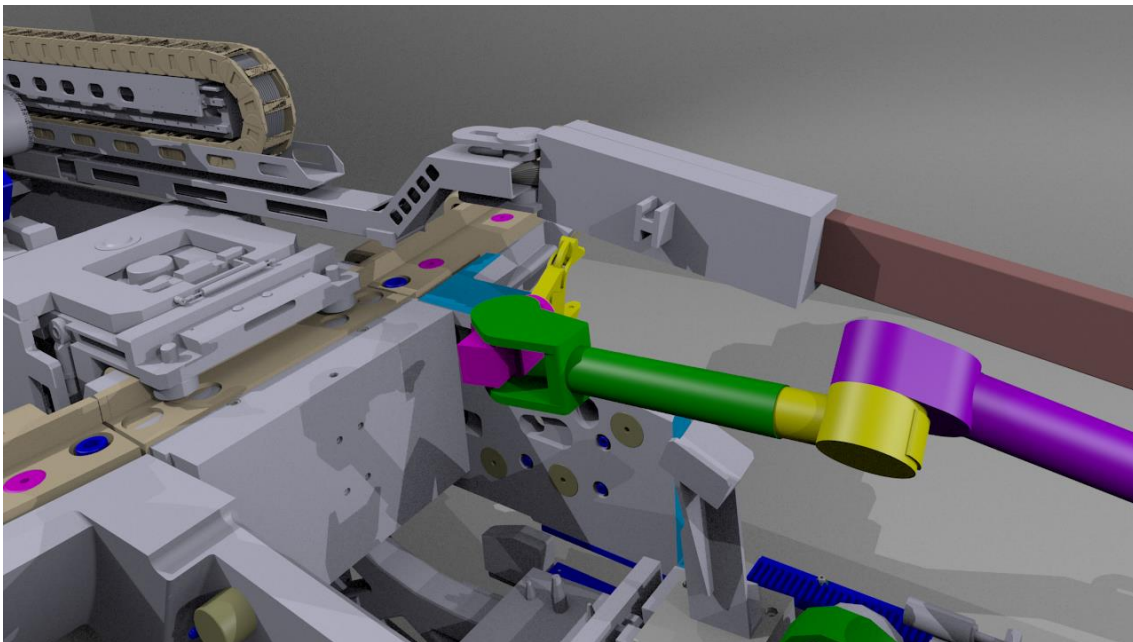


Fig. 96. Multi-pin connector plugging step 6.

#### 4.4.4.3. Consequences of the simulation process

Apart from fulfilling the F4E-OMF-340 Business Case requirements, these animations have been very useful to help the whole design group understanding the cable guide functioning and its compatibility with the reference design of the umbilical and the CMM MAM. Moreover, it was also valuable to identify different design issues. In particular:

- Modification of the articulation position in the lower slide to avoid the carriage (ball monorail guidance system) leaving the guide (Fig. 97).

- Modification of the Z-shape piece located in the cable guide zone closer to the multi-pin connector.
- Modification of the available space for the cables inside the multi-pin connector.
- Modification of the CMM MAM base position.
- Modification of the multi-pin connector RH handle position.

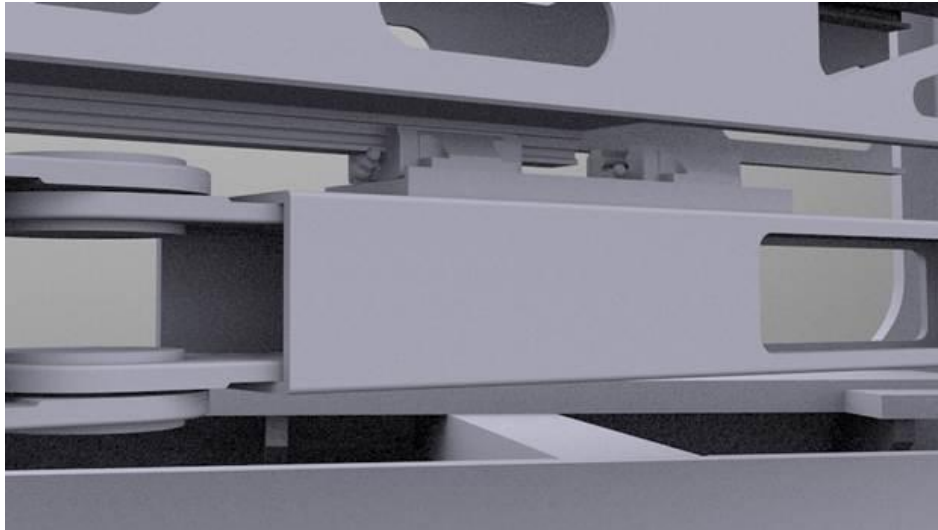


Fig. 97. Identification of a problem related to the guidance system and the articulation position.

## 4.5. References

[Abla 10] G Abla, E.N. Kim, D.P. Schissel, S.M. Flanagan, Customizable scientific web portal for fusion research, *Fusion Engineering and Design* 85 (2010) 603-607.

[Alh 13] P. Alho, J. Mattila, Breaking down the requirements: Reliability in remote handling software, *Fusion Engineering and Design* 88 (2013) 1912-1915.

[Ass 13] A. Ruiz de Assín, C. Fernández, Design justification note of the CTM cable guide and associated connectors, technical report for the Business Case of F4E-OMF-340 Lot 1 (Deliverable 13), Consortium led by Telstar Technologies S.L.U., 2013

[Bed 07] O. Bede, I. G. Kiss, A. Piros, J. Recski, Detailed analysis of the HCPB TBM maintenance sequence at interface 2 and 3, report of EFDA Subtask TW6-TTBB-001-D4, ITER internal document (ITER\_D\_27T6BS\_v1.0), 2007.

[Elz 09] B. Elzendoorn, M. de Baar, R. Chavan, T. Goodman et al., Analysis of the ITER ECH Upper Port Launcher remote maintenance using virtual reality, *Fusion Engineering and Design* 84 (2009) 733-735.

[F4E 11] Fusion for Energy, Technical Description Document of Lot 1 (Divertor Remote Handling System), F4E internal document (F4E\_D\_244X63), 2011.

[F4E 12] Fusion for Energy, Technical Specification for the Business Case of F4E-OMF-340 Lot 1, Annex 12 to Tender Specifications, F4E internal document (F4E\_D\_24CM4J), 2012.

[Ferl 13] F. Ferlay, J.M. Bernard, C. Dechelle, L. Doceul et al., First analysis of remote handling maintenance procedure in the hot cell for the ITER ICH&CD antenna – RVTL replacement, *Fusion Engineering and Design* 88 (2013) 1924-1928.

- [Fern 13] I. Fernández, Conceptual design of the CTM instrumentation, technical report for the Business Case of F4E-OMF-340 Lot 1 (Deliverable 10), Consortium led by Telstar Technologies S.L.U., 2013.
- [Fern 13b] I. Fernández, D. Marchante, B. Plana, R. Campaci, Evaluation of all signals & services for CTM, technical report for the Business Case of F4E-OMF-340 Lot 1 (Deliverable 9), Consortium led by Telstar Technologies S.L.U., 2013.
- [Gray 90] J. Gray, A census of Tandem system availability between 1985 and 1990, Tandem Computers Technical Report 90.1 (Part Number 33579), 1990.
- [Ham 14] D.T. Hamilton, A. Tesini, R. Ranz, H. Kozaka, Progress in standardization for ITER Remote Handling control system, *Fusion Engineering and Design* 89 (2014) 2409-2414.
- [Hee 11] C.J.M. Heemskerk, M.R. de Baar, H. Boessenkool, B. Graafland et al., Extending Virtual Reality simulation of ITER maintenance operations with dynamic effects, *Fusion Engineering and Design* 86 (2011) 2082-2086.
- [Iba 08] K. Iba, T. Ozeki, T. Totsuka, Y. Suzuki et al., Development and verification of remote research environment based on "Fusion research grid", *Fusion Engineering and Design* 83 (2008) 495-497.
- [Kel 13] D. Keller, L. Doceul, F. Ferlay, G. Jiolat et al., ITER design, integration and assembly studies assisted by virtual reality, *Fusion Engineering and Design* 88 (2013) 1951-1954.
- [Kim 12] E.N. Kim, D.P. Schissel, G. Abla, S. Flanagan, X. Lee, Web-based (HTML5) interactive graphics for fusion research and collaboration, *Fusion Engineering and Design* 87 (2012) 2045-2051.
- [Kin 09] R. King, D. Hamilton, Augmented virtualised reality-Applications and benefits in remote handling for fusion, *Fusion Engineering and Design* 84 (2009) 1055-1057.
- [Li 14] D. Li, B.J. Xiao, J.Y. Xia, F. Yang, Real-time virtual EAST physical experiment system, *Fusion Engineering and Design* 89 (2014) 736-740.
- [NASA 04] National Aeronautics Space Administration (NASA), *Software Safety Guidebook*, 2004.
- [Nel 95] B.J. Nelson, J.D. Morrow, P.K. Khosla, Fast stable contact transitions with a stiff manipulator using force and vision feedback, *Proceedings of the IEEE/RSJ International Conference on Human Robot Interaction and Cooperative Robots (volume 2)*, Pittsburgh, 1995.
- [Oos 14] J. van Oosterhout, C.J.M. Heemskerk, J.F. Koning, D.M.S. Ronden, M. de Baar, Interactive virtual mock-ups for Remote Handling compatibility assessment of heavy components, *Fusion Engineering and Design* 89 (2014) 2294-2298.
- [Rob 09] E. Robbins, S. Sanders, A. Williams, P. Allan, The use of virtual reality and intelligent database systems for procedure planning, visualisation, and real-time component tracking in remote handling operations, *Fusion Engineering and Design* 84 (2009) 1628-1632.
- [Saa 13] H. Saarinen, V. Hämäläinen, J. Karjalainen, T. Määttä et al., Simulating and visualizing deflections of a remote handling mechanism, *Fusion Engineering and Design* 88 (2013) 2025-2028.
- [Tak 08] N. Takeda, S. Kakudate, M. Nakahira, K. Shibanuma, A. Tesini, Development of a virtual reality simulator for the ITER blanket remote handling system, *Fusion Engineering and Design* 83 (2008) 1837-1840.

[Tar 15] A. Tarallo, R. Mozzillo, G. Di Gironimo, A. Aiello et al., Preliminary piping layout and integration of European test blanket modules subsystems in ITER CVCS area, *Fusion Engineering and Design* 93 (2015) 24-29.

[Vii 14] M. Viinikainen, J. Tuominen, P. Alho, J. Mattila, Improving the performance of DTP2 bilateral teleoperation control system with haptic augmentation, *Fusion Engineering and Design* 89 (2014) 2278-2282.

[Wil 11] A. Williams, S. Sanders, G. Weder, R. Bastow et al., Evolving the JET virtual reality system for delivering the JET EP2 shutdown remote handling tasks, *Fusion Engineering and Design* 86 (2011) 1898-1902.

[Zie 13] S. Zieba, F-X Russotto, M. Da Silva Simoes, Y. Measson, Assistance tools for generic definition of ITER maintenance tasks and scenarios in advanced supervisory control systems, *Fusion Engineering and Design* 88 (2013) 2067-2072.



# **Chapter V**

***Alternative piping connection systems for DEMO and non-destructive testing technologies***



## List of figures

Fig. 1. Technetics-Garlock gaskets characteristics [Garlock]..	347
Fig. 2. Helicoflex gasket components: inner lining, spring and jacket.....	347
Fig. 3. General view of the assembly and the RH equipment. ....	348
Fig. 4. RH equipment for the flange jacket connector. ....	349
Fig. 5. Lower pipe with alignment pins for the gasket. ....	349
Fig. 6. HNR-229 (double Helicoflex gasket joined by means of an intermediate tongue).....	350
Fig. 7. Classification and configuration of the gasket [Garlock]. ....	351
Fig. 8. Load versus deflection curve [Garlock].....	351
Fig. 9. Comparison between HN and NHR typical load versus deflection curves [Garlock]. ....	352
Fig. 10. Pressure and temperature chart for Helicoflex gaskets [Garlock].....	353
Fig. 11. Groove dimension for double HNR-229. ....	354
Fig. 12. V-clamp. ....	356
Fig. 13. V-clamp key parameters. ....	357
Fig. 14. Examples of Class 500 (left) and 1000 (right) v-clamps [Garlock b].....	358
Fig. 15. High temperature QDS (650°C) [Garlock c]. ....	358
Fig. 16. V-clamp in open position [Garlock c].....	359
Fig. 17. Support and alignment for QDS [Garlock c].....	359
Fig. 18. Reinforcement of the fastener in a QDS [Garlock c].....	360
Fig. 19. General view of the brazing connector (including bolted union). ....	370
Fig. 20. Longitudinal section of the brazing connector (including bolted union). ....	370
Fig. 21. SS-316 lower body. ....	371
Fig. 22. Ni-200 lower body. Integration into the SS-316 lower body.....	371
Fig. 23. SS-316 upper body. ....	372
Fig. 24. Ni-200 upper body. Integration into the SS-316 upper body.....	372
Fig. 25. Vertical and horizontal arrangements. ....	373
Fig. 26. Interior of a vacuum brazing furnace.....	374
Fig. 27. Holes in the Ni-200 upper body for the brazing atmosphere supply and leak testing system.....	375
Fig. 28. Multi-function plug. ....	375
Fig. 29. Induction heating coil.....	376
Fig. 30. Equipotential lines of magnetic flux near the BAu-4 ring. ....	377
Fig. 31. Temperature (K) in the connector during induction heating (t=25 s). ....	378
Fig. 32. Temperature evolution in the BAu-4 filler metal ring. ....	378
Fig. 33. Effect of Curie point in the evolution of temperature (°C) in a node belonging to the filler metal. ....	379
Fig. 34. Temperature (K) in the connector at the later stages of the heating process (t=1540 s). ....	380
Fig. 35. 2D geometry and mechanical boundary conditions for the thermomechanical analyses.....	381
Fig. 36. Equivalent plastic strain at the beginning of the cooling process.....	381
Fig. 37. Schematic showing the relationship between contact angle and surface tension: a) wetting system; b) non-wetting system [ASM 93].....	382
Fig. 38. Position of the BAu-4/He interface after $1.316 \cdot 10^{-3}$ s .....	385
Fig. 39. Advance of the interface between BAu-4 and helium .....	385
Fig. 40. Mesh tally distribution of the total neutron flux density [ $\text{cm}^{-2} \text{s}^{-1}$ ] in the upper and the divertor port areas [Fis 12]. ....	386
Fig. 41. Surface gamma dose rate in the components of the brazing connector. ....	387
Fig. 42. Specific activity in the components of the brazing connector. ....	387
Fig. 43. Flow process diagram implemented in TMAP7.....	389
Fig. 44. Tritium integrated diffusive flow to the environment.....	390
Fig. 45. RH aligner. 1) plate; 2) guides; 3) upper clamp; 4) lower clamp.....	391
Fig. 46. Interfacing elements for the installation/removal of the brazing connector.....	391
Fig. 47. Modification of the Hanford Purex clamp. RH equipment and interface. ....	394
Fig. 48. Pockets in the rear face of the lower SS316 body to insert the jaws. ....	395
Fig. 49. Releasing sequence of the clamp based on the Hanford Purex concept. ....	395

Fig. 50. RH device.....	396
Fig. 51. Flexible hose connected to the rigid multi-function plug (left). Guide pins to align the upper and the lower parts of the connector (center). Guide rail for the RH equipment (right). .....	396
Fig. 52. Interface between the RH device and the clamp. ....	396
Fig. 53. Quick geared triple hook concept.....	398
Fig. 54. Movements in the clamp. ....	398
Fig. 55. Dependence of dark current on image sensor temperature and exposure time (data for a QSI 516 thermoelectrically cooled CCD camera) [QSI].....	402
Fig. 56. Location of points for absorbed radiation calculations. ....	403
Fig. 57. Front view of a Spectral Instruments Inc. Model 1050 camera showing the CMOSIS CMV4000 sensor.....	404
Fig. 58. Basic operation of the CID pixel [Bha 08]. ....	405
Fig. 59. Performance under radiation (300 Gy/h) of a CCD sensor versus a passive pixel CID sensor [Bha 08]......	405
Fig. 60. Sketch of an actively cooled casing for CID8825D. ....	406
Fig. 61. Fundamental physical principles exploited by an EMAT [Rib 11]. ....	407
Fig. 62. Meander coil configuration [Rib 11].....	409
Fig. 63. Olympus magnetostrictive EMAT [OLYM].....	409
Fig. 64. Sketch of laser ultrasonic detection of internal defects [Che 13]. ....	410
Fig. 65. Laser-Ultrasonic inspection System for Aerospace components (LUIS) [Tecnar].....	411

## List of tables

Table 1. Lead-lithium circuit parameters (HCLL, WCLL) evaluated at the maximum temperature (500°C). ....	345
Table 2. Helium circuit parameters (HCLL) evaluated at the maximum temperature (500°C). ....	345
Table 3. Water circuit parameters (WCLL) evaluated at the maximum temperature (325°C). ....	345
Table 4. General inputs for the selection of the metallic seal. ....	346
Table 5. Table of characteristics values for standard Helicoflex HN gaskets with axial compression and stainless steel, Inconel or titanium as jacket material for T=400°C [Garlock]. ....	353
Table 6. Recommended roughness depending on the sealing material for use on turned surfaces [Garlock].....	354
Table 7. Gasket characteristics for PbLi pipes.....	355
Table 8. Gasket characteristics for helium pipes. ....	355
Table 9. Gasket characteristics for H <sub>2</sub> O pipes. ....	356
Table 10. Calculated values of minimum seating forces and flange groove dimensions. ....	356
Table 11. Seal-clamp compatibility [Garlock b]. ....	357
Table 12. Mechanical calculations and selection of v-clamps for the different circuits.....	358
Table 13. Chemical composition requirements for BAu-4 [ASME 07]. ....	368
Table 14. Chemical composition requirements for BNi-5 [ASME 07]. ....	368
Table 15. Solidus and liquidus temperatures for the selected filler metals [ASME 07].....	369
Table 16. Recommended joint clearance for the selected filler metals at their brazing temperatures [ASM 93]. ....	383
Table 17. Surface gamma dose rate in the components of the brazing connector. ....	386
Table 18. Specific activity in the components of the brazing connector. ....	387
Table 19. List of isotopes with the largest contribution to the total specific activity. ....	388
Table 20. Neutron fluence in the modified Hanford Purex clamp spring. ....	397

## 5.1. Introduction

One key issue affecting the availability of future fusion reactors is the time consumed by operations concerning the pipe systems which feed the breeding blanket and the divertor. The use of RH-adapted conventional welding techniques using individual heads –like in the case of the ITER Test Blanket System- penalizes excessively the duration of maintenance tasks because of the large number of pipes and the time needed to cut, weld –including the application of heat treatment- and inspect the pipe joints. Thus, the development of feasible quick pipe connectors -adapted to the novel maintenance concepts which are being developed and must be validated for DEMO- for the connection/disconnection of critical in-vessel components is crucial.

This chapter is focused on the design of pipe joining systems for DEMO as alternative to the reference cutting & welding methods. The characteristics of a flange & gasket connector and a brazing connector designed in the framework of EFDA WP12 and WP13 Remote Maintenance activity are presented, as well as an overview of several non-destructive inspection techniques for pipe systems and particularly welded unions.

## 5.2. General piping assumptions

The designs presented in this Chapter are particularized for the dimensions of the HCLL and the WCLL breeding blanket service connections, which have been provided by EFDA as input data [Har 12b]. The pipe parameters for the different working fluids (eutectic lead-lithium, helium and water) and their properties are gathered in Table 1, Table 2 and Table 3, considering the operating conditions of each fluid, most of which have been taken from [Boc 11].

Fluid	Site	ID (mm)	OD (mm)	t (mm)	P (MPa)	T <sub>max</sub> (°C)	ρ (kg/m <sup>3</sup> )	μ (Pa·s)	Re	v <sub>max</sub> (m/s)	Q <sub>max</sub> (kg/s)
PbLi	IB	75	85	5	1	500	9601	1.14·10 <sup>-3</sup>	5·10 <sup>4</sup>	0.079	3.35
	OB	75	85	5	1	500	9601	1.14·10 <sup>-3</sup>	5·10 <sup>4</sup>	0.079	3.35

Table 1. Lead-lithium circuit parameters (HCLL, WCLL) evaluated at the maximum temperature (500°C). ID is internal diameter, OD is external diameter, t is pipe thickness, T is temperature, ρ is density, μ is dynamic viscosity, Re is Reynolds number, v is velocity and Q is mass flow.

Fluid	Site	ID (mm)	OD (mm)	t (mm)	P (MPa)	T <sub>max</sub> (°C)	ρ (kg/m <sup>3</sup> )	μ (Pa·s)	v <sub>max</sub> (m/s)	Q <sub>max</sub> (kg/s)
He	IB	270	300	15	8	500	4.9215	3.856·10 <sup>-3</sup>	50	14
	OB	345	375	15	8	500	4.9215	3.856·10 <sup>-3</sup>	50	23

Table 2. Helium circuit parameters (HCLL) evaluated at the maximum temperature (500°C).

Fluid	Site	ID (mm)	OD (mm)	t (mm)	P (MPa)	T <sub>max</sub> (°C)	ρ (kg/m <sup>3</sup> )	μ (Pa·s)	v <sub>max</sub> (m/s)	Q <sub>max</sub> (kg/s)
H <sub>2</sub> O	IB	95	125	15	15.5	325	666.51	7.838·10 <sup>-5</sup>	20	94.5
	OB	120	155	15	15.5	325	666.51	7.838·10 <sup>-5</sup>	20	150.8

Table 3. Water circuit parameters (WCLL) evaluated at the maximum temperature (325°C).

The PbLi velocity in HCLL/WCLL pipes has been calculated from a representative value of the Reynolds number according to corrosion tests in the PICOLO loop [Kra 07].

Helium and water physical properties at the working conditions (temperature and pressure) have been taken from [Nist]. PbLi properties have been taken from [Mas 08] and [Kra 07]. In

addition to this, 316L(N)-IG austenitic stainless steel has been selected as reference material for pipes. Nevertheless, apart from other considerations, it is not advisable for lead-lithium pipes due to corrosion issues. The possibility of using RAFM steels like EUROFER is also pointed out.

### **5.3. Design of a QDS-compatible flange jacket for DEMO blanket pipes**

This section proposes a conceptual design of a generic 'flange jacket' to be used together with a bolted quick disconnection system (QDS) as mechanical connector for DEMO blanket pipes. The concept has been developed starting from the following statements concerning flanges and metallic seals:

- a) The flange for pipe joining should include a built-in captive seal which allows remote maintenance.
- b) Compared to polymer O-rings, metallic seals exhibit reasonable leak rates and relatively low tritium permeability, and their comparative rigidity makes them easier to be remotely handled [Min 12].
- c) A v-clamp can be used to achieve the necessary seating load for the seal.
- d) In the case of lead-lithium pipes, it is necessary to heat the connector in order to re-melt the solidified layer of PbLi in the interface between both halves of the flange. Thus, when the pipe line is drained and the temperature falls below the eutectic temperature, both flange parts can be separated, preventing the re-assembly of the connector.
- e) It is possible to evaluate the seal performance against gas leakage by monitoring the seal interspace.

Different kinds of metallic seals (Helicoflex<sup>®</sup>, Delta<sup>®</sup>, VATSEAL and VAT CF) have been preliminarily assessed. Taking into consideration the inputs from Table 4, information from catalogues (e.g. Fig. 1) and recommendations from Technetics-Garlock (Helicoflex and Delta manufacturer), the Helicoflex gaskets have been selected for further studies, due to their capability to operate at high temperature and both low and high pressure, as well as to fulfil the required leak rate. Furthermore, they are compatible with QDS and they show good spring back behaviour with a special design, so that a gasket can be reused after several cycles of seating load application with the same sealing features.

Parameters	Average value	Comments
<b>Cumulative radiation</b>	1-5 dpa (40 years)	High radiation environment (cumulative 1-5 dpa can be assumed at the location of the flange after 40 years of irradiation) [Que 12]. Assessed gaskets have not been tested under representative radiation conditions.
<b>Maximum leak rate</b>	$< 10^{-9}$ mbar l s <sup>-1</sup>	The leak rate taken from [Min 12] is assumed to be a DEMO requirement.
<b>Range of pressure</b>	0.1-15.5 MPa	Range of pressure considered in Section 5.2.
<b>Range of temperature</b>	325-500 °C	Range of temperature considered in Section 5.2.
<b>Materials (soft metal)</b>	Ag/Al	Aluminium has good behaviour against corrosion, but there are other materials with good corrosion resistance and higher service temperature (around 200°C) [Que 12].
<b>Flange surface roughness</b>	0.4 µm	Flange surface roughness is a manufacturer's requirement [Min 12].

Table 4. General inputs for the selection of the metallic seal.

Application Information	SEAL TYPE					
						
	Helicoflex®	Delta®	O-Flex™	C-Flex™	E-Flex™ U-Flex™*	Machined Seal*
Ultra High Vacuum	●	▲▲	■	■	■	▲
Low Pressure	▲▲	●	▲	▲	▲	▲
High Pressure	▲▲	■	▲	▲▲	●	▲
Cryogenic Temperature	▲▲	▲	●	●	●	■
High Temperature	▲▲	▲	▲	▲	▲	■
Spring Back	●	●	●	▲	▲▲	■
Shaped Seals	▲	▲	▲	●	■	■
Axial Sealing	▲	■	●	▲	■	■
QDS Compatible	▲	▲	■	■	■	■
Seating Load	High	Moderate	High Moderate	Moderate Low	Low	High Moderate
Leak Rate Approximation	Helium	Ultra-Helium	Helium Bubble	Helium Bubble	Low Bubble	Helium

Fig. 1. Technetics-Garlock gaskets characteristics [Garlock]. Application legend: excellent (▲▲), good (▲), optional-special design (●), not recommended (■). Leak legend: ultra-helium ( $\leq 10^{-11}$  std.cm<sup>3</sup>/s He), helium ( $\leq 10^{-9}$  std.cm<sup>3</sup>/s He), bubble ( $\leq 10^{-4}$  std.cm<sup>3</sup>/s He), low bubble ( $\leq 25$  cm<sup>3</sup>/s at 0.345 MPa nitrogen per 25.4 mm of diameter).

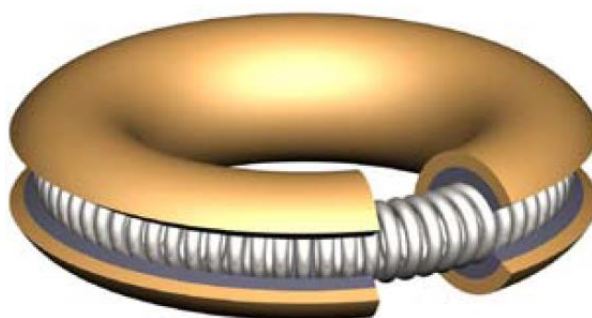


Fig. 2. Helicoflex gasket components: inner lining, spring and jacket.

### 5.3.1. Description of the design

The proposed design concept is based on using a Helicoflex double gasket as sealing method and a chain v-clamp with a screwed fastener to provide the necessary seating load. The design has been fit to the vertical section of blanket pipes (Vertical Maintenance Scheme requirement), although it could be adapted for horizontal pipes.

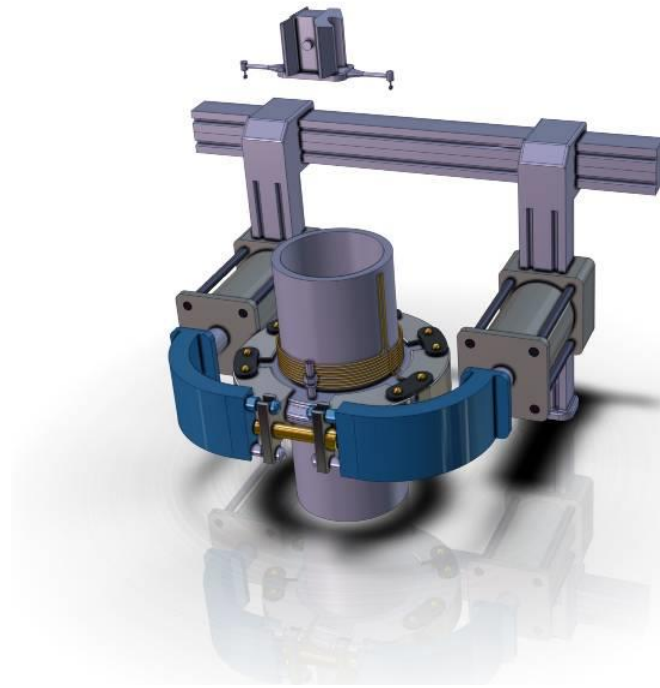


Fig. 3. General view of the assembly and the RH equipment.

The assembly shown in Fig. 3 is composed by the following elements:

#### Flange

The flange, together with the gasket, provides pipe joint sealing. It also protects the gasket against thermal loads and radiation. Its design is adapted to the features of the selected commercial gasket and v-clamp.

#### Gasket

A double Helicoflex gasket is placed inside the flange to ensure sealing. Moreover, it allows monitoring the sealing performance.

#### V-clamp

The proposed design consists on a v-shaped segmented clamp like the shown in Fig. 12. Its function is to apply the required tightening load on the flange and hence on the gasket, so that the double Helicoflex gets 'viscoplastic-elastic' behaviour under the pipes working conditions.

#### RH equipment

Since the gasket and the v-clamp must be installed/uninstalled by remote handling techniques, two RH tools have been designed to transport and install/remove both components: the so-called 'gasket manipulator' and 'v-clamp manipulator', respectively.

The v-clamp manipulator consists of:

- A frame that supports and transfers the RH components from the maintenance area to the upper port where the connector is placed. This structure is composed by screw driven sliders. It allows two linear movements (horizontal and vertical).
- Two arms with pins and a bolting tool placed at the end of the arms. The upper pins are aligned with the v-clamp tightening features, so that the lower pins can turn and grip the v-clamp. The arms are supported by the frame through two hydraulic cylinders with radial movement. The bolting tool is hidden into the arm (retractile) until the pins are positioned.

On the other hand, the gasket manipulator is composed by two twist-locks which interact with the pins situated on the lower part of the flange and the holes of the gasket tongue to allow transporting, positioning, aligning, fixing and removing the double gasket. The manipulator can rotate around itself and move in three directions. It also includes a standard interface for a robotic arm.

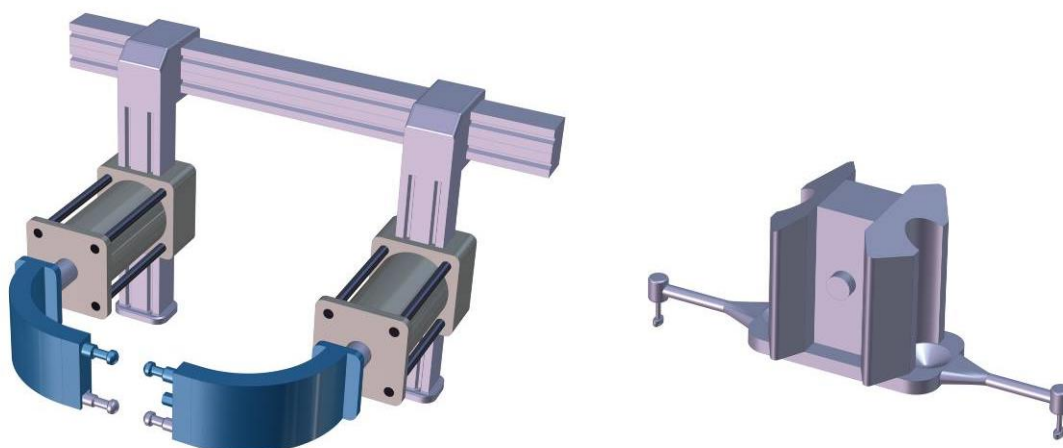


Fig. 4. RH equipment for the flange jacket connector.

Further details about the design of the flange, the gasket and the clamp are shown in the next Sub-subsections.

#### 5.3.1.1. Flange

The lower part of the flange has a groove to board the gasket and two pins to align and fix the gasket. The upper part is equipped with a connector that links the vacuum system with the groove to carry out helium leak testing. The flange external profile is adapted to the geometry of the v-clamp segments.

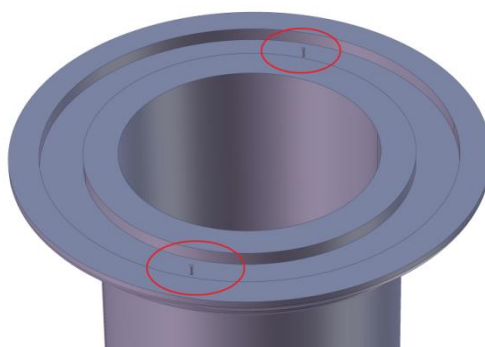


Fig. 5. Lower pipe with alignment pins for the gasket.

Also, a resistive heating system (mineral insulated wire) is included near the interface between both parts of the flange for baking purposes, as well as for re-melting the solidified layer of PbLi ( $T_{\text{eutectic}} \approx 236^{\circ}\text{C}$ ) in the interface between both parts of the flange (in the case of PbLi pipes).

#### 5.3.1.2. Gasket (Helicoflex HNR-229)

The selected gasket is composed by two Helicoflex rings (HNR-229 type) joined through a tongue with three kinds of holes, whose functions are:

- a) To position and fix the gasket into the groove cavity of the flange lower part.
- b) To improve the pumping performance during leak testing (the double seal arrangement allows helium leak testing to monitor the sealing conditions).
- c) To allow RH operations (extraction/insertion of the seal from/into the groove).

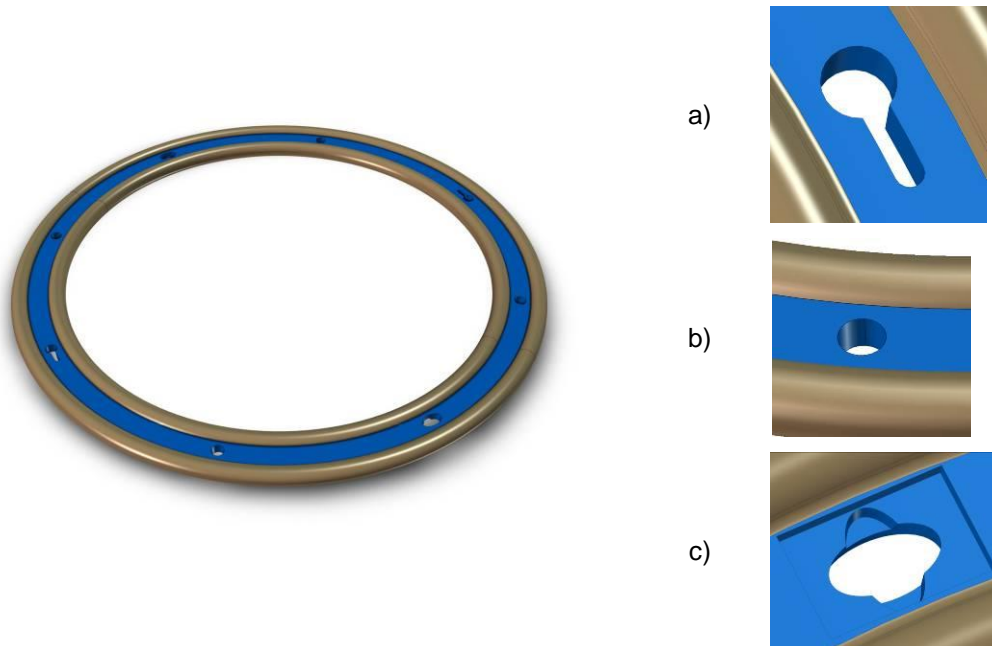


Fig. 6. HNR-229 (double Helicoflex gasket joined by means of an intermediate tongue).

The geometry of both rings forming the double seal arrangement has been defined according to the cross-section types and mechanical parameters provided by the Helicoflex manufacturer and shown in Fig. 7, Fig. 8 and Fig. 9.

The HNR cross-section type uses the so-called 'Helicoflex  $\beta$ ' sealing principle, which provides a better distribution of the spring reaction on the seal lining [Garlock]. Thus, the value of the linear load to reach the seating point and the metal to metal contact is theoretically 30% lower than in the case of HN cross-section type (Fig. 9).

According to the manufacturer's catalogue [Garlock], the digits defining each HNR-XYZ cross-section make reference to the existence of an inner lining (X), the jacket orientation (Y) and the section orientation (Z) (Fig. 7).

Thus, the selected design (HNR-229) includes an inner lining besides the jacket. The lining is viscoplastically deformed by the compression of the helicoidal spring and improves the sealing quality. In addition, the double seal is oriented to better support internal/external pressures: the inner seal gives resistance to the internal pressure (0: jacket orientation) and the outer seal gives resistance to the external pressure (2: jacket orientation). A detailed view can be found in Fig. 11. However, each ring separately faces the pressure like external pressure.

It must be highlighted that numerical analyses carried out by CEA and the Helicoflex manufacturer showed that DN65 and DN150 flange designs, optimized its overall dimensions and combined with HNR-229 seals, were acceptable for loading conditions related as operational requirements specified by ITER Organization [Led 12].

Cross Section Type	HN HNR HNV HND HNDE	single section ground spring for precise load control (Beta Spring) low load (Delta Seal) tandem Helicoflex seals tandem Helicoflex and elastomer seals note: "L" indicates internal limiter (ex: HLDE)
Jacket/Lining	1 = jacket only	2 = jacket with inner lining
Jacket Orientation	0  1  2  3  4  5  6  7  8  9 	
Section Orientation	0  1  2  3  4  5  6  7  8  9 	

Fig. 7. Classification and configuration of the gasket [Garlock].

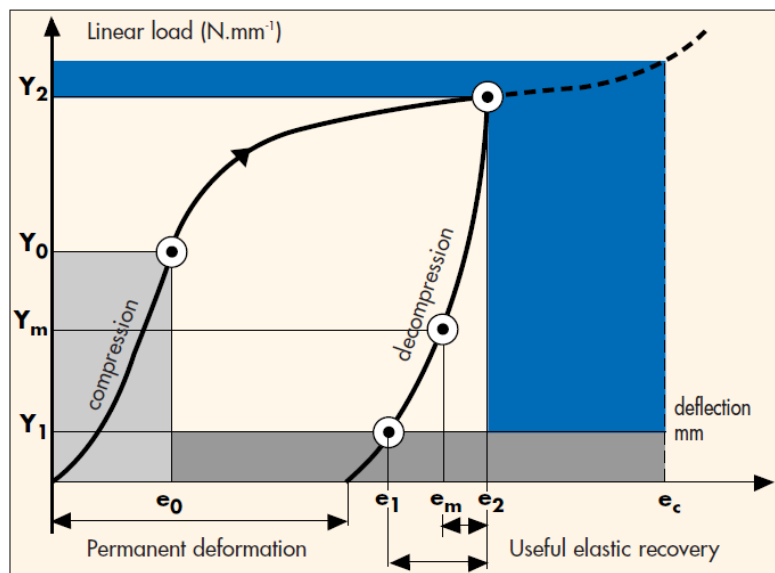


Fig. 8. Load versus deflection curve [Garlock].  $Y_0$  is the linear load from where the required sealing level is obtained,  $Y_2$  is the linear load needed to reach the seating point and the metal to metal contact,  $e_2$  is the compression value to get the metal to metal contact (it is related to the linear load  $Y_2$  and determines the groove depth),  $e_c$  is the critical compression value beyond which the sealing level could deteriorate,  $Y_m$  is the minimum linear load to maintain sealing in service (it varies according to the pressure and the temperature) and  $e_m$  is the compression value related to  $Y_m$  below which the sealing level is lost ( $f(P,T)$ ).

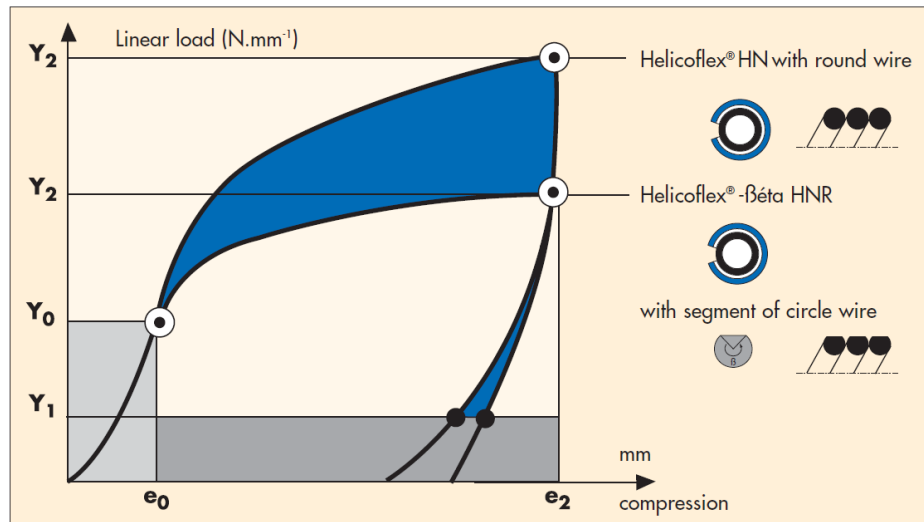


Fig. 9. Comparison between HN and NHR typical load versus deflection curves [Garlock].

### 5.3.1.3. Materials

The selection of the materials for the different parts of the gasket is clearly related to the pressure and temperature conditions. The Helicoflex manufacturer proposes a method to help selecting such materials [Garlock], which is based on the following key points.

- The service temperature of Helicoflex must be close to the working temperature of the fluid flowing inside the pipe.
- This temperature is given by  $Pu_{\theta}$ , which indicates the maximum pressure at the service temperature ( $\theta$ ) which the seal has been designed for. As the T-P curve is not linear (Fig. 10),  $\theta$  must be close to the pipes working temperature, since the increasing working temperature decreases the maximum pressure which the seal can bear without leakages.
- The maximum temperature ( $\theta_{max}$ ) must be higher than the working temperature.
- It must accomplish with the 'helium sealing' requirement ( $He$  leak flux  $<10^{-9}$  mbar l s $^{-1}$ ) for this application.

For example, in the previously mentioned study carried out by CEA and Technetics, the use of silver/aluminium for the jacket, Inconel 600 for the inner lining and Nimonic 90 for the spring was proposed [Toc 11]. For such study, a working temperature of 200°C was considered, and this is the same service temperature than the manufacturer's catalogue recommends for the aluminium lining.

In our case, the working temperature in the PbLi and He pipes reaches 500°C, whereas the manufacturer only categorizes values up to 400 °C. This means that the gasket would withstand a pressure lower than the reference one ( $Pu_{400^{\circ}C}$ ) at the service temperature, according to Fig. 10. The foreseen jacket materials for  $T=400^{\circ}C$  are stainless steel, Inconel and titanium. Materials like Inconel are resistant to corrosion and high heat loads [MegaMex] [SMetal]. However, it should not be used as jacket material for gaskets installed in PbLi pipes, since materials with high nickel content are easily corroded by lead-lithium (nickel dissolution mechanism). Anyway, as can be observed in Fig. 11, it is not probable that flowing PbLi contacts the gasket jacket, so the real risk would be very limited. On the other hand, titanium does not seem adequate because its high tritium permeability. Therefore, stainless steel can be proposed as jacket material for the PbLi and He pipes gaskets, although Inconel can be also effective for the last ones.

Regarding H<sub>2</sub>O pipes, taking into account their lower working temperature, nickel, Monel and tantalum are recommended by the manufacturer. As in the case of titanium, tantalum is not suitable because of its high tritium permeability, so nickel and Monel are preferable.

In any case, aluminium and silver are softer than materials like Inconel or stainless steel; therefore the seating load for these materials must be higher.

Inconel and Nimonic can be selected as materials for the inner lining and the spring, respectively, in all the circuits.

CS (mm)	$e_2$ (mm)	$e_c$ (mm)	$Y_2$ (N/mm)	$Y_1$ (N/mm)	$Pu_{20^\circ C}$ (MPa)	$Pu_{400^\circ C}$ (MPa)
1.60	0.40	0.50	350	100	90	25
1.90	0.50	0.60	400	100	91	27
2.20	0.50	0.70	450	110	92	29
2.50	0.60	0.80	500	120	97	32
3.00	0.60	0.90	575	130	100	36
3.50	0.60	0.90	660	150	104	39
4.00	0.70	1.00	750	170	107	42
4.50	0.70	1.00	825	220	110	45
5.00	0.70	1.10	n/a	n/a	n/a	n/a
5.50	0.70	1.30	n/a	n/a	n/a	n/a
6.00	0.80	1.60	n/a	n/a	n/a	n/a
7.00	0.80	1.80	n/a	n/a	n/a	n/a
8.00	0.80	2.10	n/a	n/a	n/a	n/a

Table 5. Table of characteristics values for standard Helicoflex HN gaskets with axial compression and stainless steel, Inconel or titanium as jacket material for  $T=400^\circ C$  [Garlock].

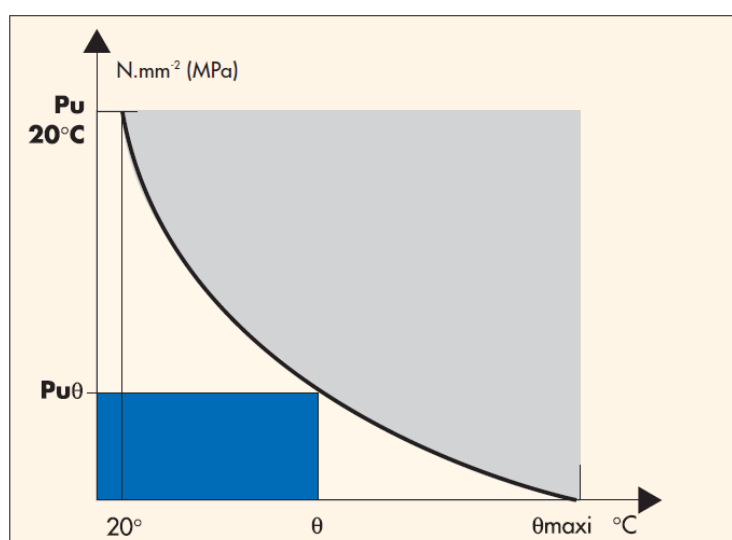


Fig. 10. Pressure and temperature chart for Helicoflex gaskets [Garlock].  $Pu$  is the maximum pressure that the seal can withstand at certain temperature,  $Pu_{20^\circ}$  is the maximum pressure at room temperature ( $20^\circ C$ ),  $Pu_\theta$  is the maximum pressure at service temperature and  $\theta_{max}$  is the temperature where  $Pu_\theta$  is nearly zero (it allows calculating  $Y_m$ ).

#### 5.3.1.4. Surface finish

The performance of the Helicoflex gasket is closely related to the quality of the sealing areas surface finish. For that reason, the manufacturer recommends the most suitable values of roughness in the flange, depending on the material type and the process used (turning, milling, reaming, etc.).

For the selected jacket materials, a maximum roughness of 0.8-1.6  $\mu m$  is recommended [Garlock]. These values are higher than the one provided by Mindham [Min 12], which was also

obtained from the Helicoflex manufacturer. So it seems the manufacturer's requirement has evolved in last years.

The surface condition must be checked during the blanket maintenance activities, so that it must be maintained within the recommended range. If it is found out from such range, the connector shall be carried to the maintenance area to apply some of the available techniques which can obtain this grade of surface finish (boring, grinding, turning, etc.).

Ra ( $\mu\text{m}$ )	12.5	6.3	3.2	1.6	0.8	0.4	0.2
Rt (in $\mu\text{m}$ )	50	37	21	11	6.2	3.4	1.9
Plating (Pb, Sn, In) PTFE-FEP	N	N	N	A	R	R	A
Aluminium	A	A	R	R	A	A	A
Silver, cooper, iron	N	A	R	R	A	A	N
Nickel, stainless steel	N	A	A	R	R	A	A

Table 6. Recommended roughness depending on the sealing material for use on turned surfaces [Garlock]. N: non-recommended; A: acceptable; R: recommended.

### 5.3.1.5. Calculation of the minimum seating load and the flange groove dimensions

A code has been written in MATLAB in order to calculate the minimum force applied by the QDS to preserve sealing in service, according to the manufacturer's recommendations ([Garlock]). The inputs are based on the selected Helicoflex type features (e.g. gasket cross section) and the pipe working pressure. The mathematical model assumes the double ring gasket is like two springs connected in parallel.

Another MATLAB code calculates the rough dimensions of the flange groove according to the geometry and mechanical characteristics of the gasket and the internal and external pressures.

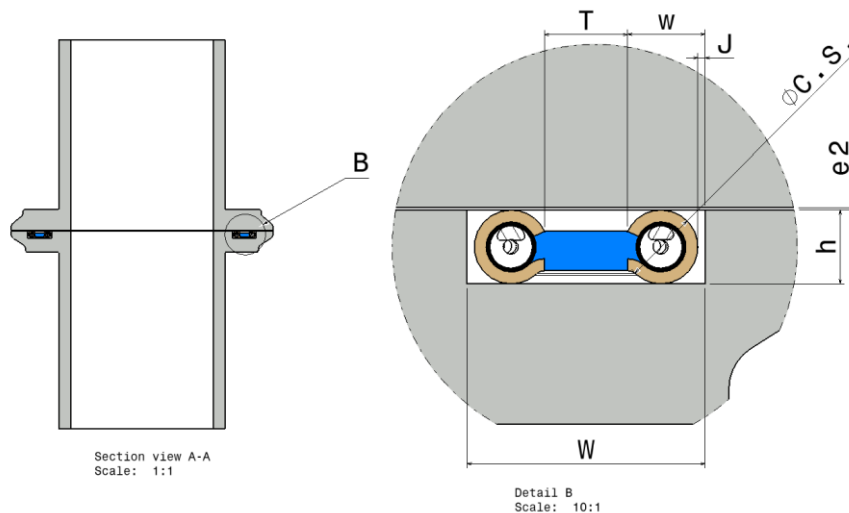


Fig. 11. Groove dimension for double HNR-229.

Both codes are based on the following assumptions:

- The mean diameter of the seal is taken from the pipes outer diameter.
- An external pressure of 0.1 MPa is assumed.
- The width of the tongue between both rings is assumed to be 10 mm to allow the gasket remote manipulation.

Table 7, Table 8 and Table 9 show the input data to calculate  $F_{\min}$  and the flange groove dimensions, whose results for the different analysed cases are presented in Table 10.

Fluid	PbLi
Seal type	HNR-229
Jacket material	Stainless steel/Inconel/titanium
Maximum allowed He leak	$10^{-9}$ mbar l s <sup>-1</sup>
Surface finish	0.8-1.6 $\mu$ m
Range of temperatura	300-500°C
Gasket maximum temperature	600°C
Cross section (CS)	4 mm
$e_2$ (compression)	0.7 mm
$e_c$ (compression)	1 mm
$Y_2$	750 N/mm
$Y_1$	170 N/mm
Pu 20°C	107 MPa
Pu <sub>0</sub> 400°C	42 MPa

Table 7. Gasket characteristics for PbLi pipes.

Fluid	He
Seal type	HNR-229
Jacket material	Stainless steel/Inconel/titanium
Maximum allowed He leak	$10^{-9}$ mbar l s <sup>-1</sup>
Surface finish	0.8-1.6 $\mu$ m
Range of temperature	300-500°C
Gasket maximum temperature	600°C
Cross section (CS)	4 mm
$e_2$ (compression)	0.7 mm
$e_c$ (compression)	1 mm
$Y_2$	750 N/mm
$Y_1$	170 N/mm
Pu 20°	107 MPa
Pu <sub>0</sub> 400°	42 MPa

Table 8. Gasket characteristics for helium pipes.

Fluid	H <sub>2</sub> O
Seal type	HNR-229
Lining material	Stainless steel/Inconel/titanium
Maximum allowed He leak	$10^{-9}$ mbar l s <sup>-1</sup>
Surface finish	0.8-1.6 $\mu$ m
Range of temperature	285-325°C
Gasket maximum temperature	420°C
Cross section (CS)	2.2 mm
$e_2$ (compression)	0.5 mm

$e_c$ (compression)	0.7 mm
$Y_2$	390 N/mm
$Y_1$	90 N/mm
$P_u 20^\circ$	76 MPa
$P_{u_0} 400^\circ$	21 MPa

Table 9. Gasket characteristics for H<sub>2</sub>O pipes.

Fluid	Place	D (mm)	T (°C)	P (MPa)	$F_{min}$ (N)	h (mm)	w (mm)
<b>PbLi</b>	IB/OB	85	500	1	$1.02 \cdot 10^5$	3.5	22.2
<b>He</b>	IB	300	500	8	$1.45 \cdot 10^6$	3.5	22.8
	OB	375	500	8	$2.17 \cdot 10^6$	3.5	22.8
<b>H<sub>2</sub>O</b>	IB	125	325	15.5	$5.39 \cdot 10^5$	1.9	18.4
	OB	150	325	15.5	$7.38 \cdot 10^5$	1.9	18.4

Table 10. Calculated values of minimum seating forces and flange groove dimensions. IB is inboard, OB is outboard, D is the gasket mean diameter, T is temperature, P is pressure,  $F_{min}$  is the minimum force which must be applied in service to maintain sealing, h is the groove height and w is the groove width.

### 5.3.1.6. Design of the Quick Disconnect System (v-clamp)

The selection of the QDS for the present connector design starts from the v-shaped segmented clamp concept (Fig. 12). A v-clamp is composed of:

- V-shape segments that distribute the tightening load on the seal.
- Plates. The segments are linked through two plates (upper/lower). The chain of segments and plates allow the turning movement on the rivets. Thus the v-clamp is flexible in the radial plane and quite rigid in the axial plane.
- Fastener screw. It is used to close and tighten the v-clamp around the flange pipes.

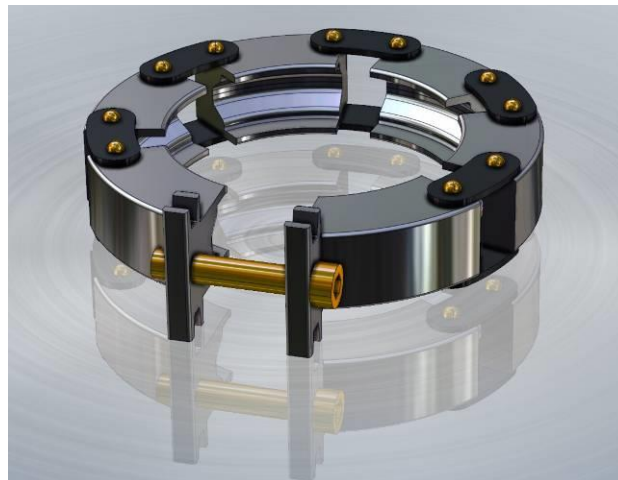


Fig. 12. V-clamp.

Since the clamp must be compatible with the gasket, the QDS catalogue from the Helicoflex manufacturer has been taken as reference [Garlock b]. The catalogue proposes a selection method based on:

- Calculation of the minimum force which must be applied on the gasket in service to maintain sealing ( $F_{min}$ ) (previous Sub-subsection).
- Calculation of the minimum axial clamping load ( $F_b$ ).

A MATLAB code has been written to obtain the minimum axial clamping load using an approach referred by Shoghi et al. [Sho 04]. The calculation is based on the minimum tightening force needed by the gasket ( $F_{min}$ ), a friction coefficient which takes into account the friction between the internal clamp surface and the external flange surface, and the geometry of the clamp cross section ( $\Phi$  and  $\beta$  angles). The relation between these parameters is shown in Fig. 13.

After the calculation of the distributed axial clamping load on the flange, which is referred as the minimum clamp load per diameter (CL, considering the values of the outer diameter for each circuit,  $D_j$ , employed in the previous Sub-subsection), a QDS from the catalogue can be selected taking into account:

- The maximum clamping load of the QDS must be higher than the calculated CL.
- The material compatibility between the Helicoflex gasket and the clamp (Table 11).
- The working temperature in each circuit.

Furthermore, the screw diameter must be estimated in order to know the tightening torque that shall be provided by the RH screwer. The screw must withstand the axial clamping load ( $F_b$ ), which is similar to a traction force. Therefore, considering the ultimate tensile strength of the material (e.g. duplex stainless steel) the minimum section of the screw can be calculated.

The diameter of the screw ( $d_b$ ) is then selected according to the standard ISO BS 3643-1:1981 [BS3643], as proposed by the ITER Remote Handling Code of Practice [Raj 09]. Finally, a standard thread size (M8, M10, M12, M16 and M20) is chosen. The results of these calculations are shown in Table 12.

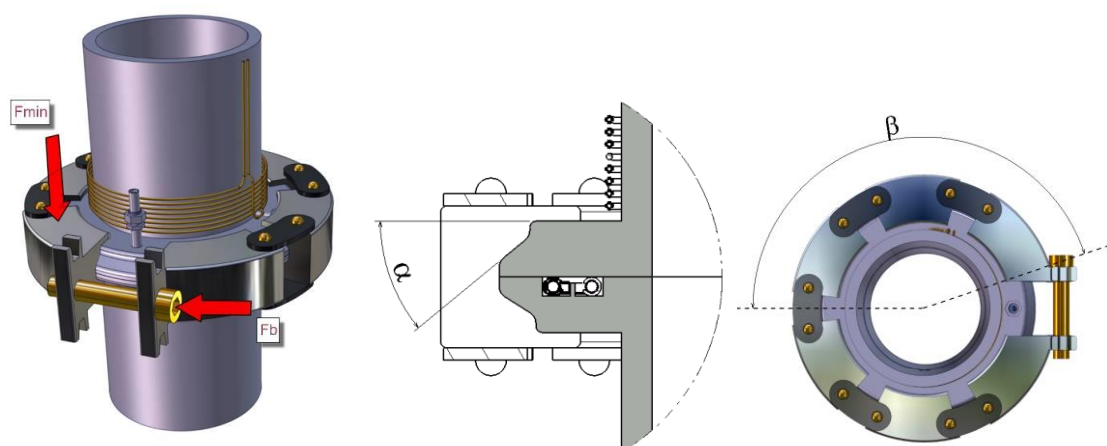


Fig. 13. V-clamp key parameters.

Jacket material	Class 150	Class 300	Class 500	Class 1000
Aluminium	O	O	O	O
Silver	X	O	O	O
Copper	X	X	O	O
Nickel	X	X	O	O
Stainless steel	X	X	O	O

Table 11. Seal-clamp compatibility [Garlock b].

Fluid	Place	Fb (N)	CL (N/mm)	Thread size	Torque (N·m)	Pre-selected clamp class [Garlock b]
PbLi	IB/OB	$1.093 \cdot 10^4$	128.6	M8	18	Class 1000
He	IB	$1.554 \cdot 10^5$	517.9	M16	160	Class 1000
	OB	$2.320 \cdot 10^5$	618.7	M20	300	Class 1000
H <sub>2</sub> O	IB	$5.766 \cdot 10^4$	461.3	M10	37	Class 500
	OB	$7.897 \cdot 10^4$	526.46	M12	60	Class 1000

Table 12. Mechanical calculations and selection of v-clamps for the different circuits.



Fig. 14. Examples of Class 500 (left) and 1000 (right) v-clamps [Garlock b].

The simpler Class 300 could be valid for PbLi pipes in terms of minimum load per diameter, but the expected temperature is much higher than the allowed by this Class (300°C). Moreover, it is not compatible with the relatively hard materials selected for the gasket jacket, according to manufacturer's recommendations. For these reasons, the Class 1000, which is made of high carbon steel (clamp section and side plates) and high grade stainless steel (screws), has been selected. Although a maximum working temperature of 400°C is advised [Garlock b], which is lower than the maximum temperature expected in PbLi and He pipes, some real applications of Technetics-Garlock QDS overcome these restrictions. For example, Figure 45 shows the use of one of these QDS in a pipe heated up to 1200°C, where the estimated clamp temperature is 650°C. Consequently, the possibility of using these v-clamps in PbLi and He pipes seems to be feasible. In the case of H<sub>2</sub>O inboard pipes, Class 500 has been selected (stainless steel for links and side plates, carbon steel or stainless steel for the screws).



Fig. 15. High temperature QDS (650°C) [Garlock c].

On the other hand, the proper operation of the proposed RH equipment (Subsection 5.3.2) depends on the clamp rigidity in the axial plane. In this sense, Fig. 16 shows an open clamp on a table without any support; that is, it is supported on the table by itself, so it seems to have the necessary rigidity.



Fig. 16. V-clamp in open position [Garlock c].

Depending on the clamp weight, a support to align and rest the clamp could be necessary. Fig. 17 shows a support with grooves to manage the clamping movement through pivots and one rail to address the fastener when it is open/closed.



Fig. 17. Support and alignment for QDS [Garlock c].

Finally, it is possible to use reinforcements in the clamp fastener (Figure 12). They provide a better distribution of the load in the v-clamp section. Furthermore, they allow reducing the bolts diameters.



Fig. 18. Reinforcement of the fastener in a QDS [Garlock c].

### **5.3.2. Remote handling operations to install/uninstall the flange connector**

This Subsection describes a sequence of RH operations to carry out the disconnection/connection of the mechanical connector based on the flange and gasket designs presented in the previous Subsection. These processes could occur during both the blanket scheduled and non-scheduled maintenance.

The same template used in Chapter 4 for the ITER Test Blanket System and Divertor System animations is followed here to describe the sequence:

#### Description

##### *Uninstallation*

The v-clamp manipulator uninstalls and removes the clamp. In the case of PbLi pipes, the heater re-melts the PbLi solidified layer between both parts of the pipe previously to their separation (non-specified RH equipment). After, the gasket manipulator removes the gasket from the flange groove and transfers it to the maintenance area.

##### *Installation*

It is essentially identical to the uninstallation process. Once finalized, a helium leak test is carried out to evaluate the sealing performance.

#### Task objective

##### *Uninstallation*

1) To uninstall the v-clamp; 2) to re-melt the liquid metal solidified layer between both parts of the pipe in order to allow their separation (PbLi pipes case); 3) to remove the gasket.

##### *Installation*

1) To install the gasket in the flange; 2) to install the v-clamp (placement and tightening); 3) to perform helium leak testing.

#### Assumptions

- There is enough space for the operation of the v-clamp manipulator.

- The gasket manipulator includes an interface to be handled by a robotic arm. However, it could be handled by a much simpler RH system including rotation and translation along the pipe axis as DOF to avoid the issues linked to a robotic arm (radiation resistance, required space for operation, operation time and complexity, cost, etc.).
- There is a generic RH system (to be defined) –which could be the same to handle the gasket manipulator and even the v-clamp manipulator- to separate the upper part of the pipe from the blanket-side pipe.

### Start conditions

#### *Uninstallation*

The connector is installed (the gasket is placed in the flange groove and tightened by the v-clamp).

#### *Installation*

The v-clamp and the gasket are uninstalled. They are brought by the v-clamp manipulator and the gasket manipulator, respectively.

### End conditions

#### *Uninstallation*

The connector is installed (the gasket is placed in the flange groove and tightened by the v-clamp). A helium leak test has been performed.

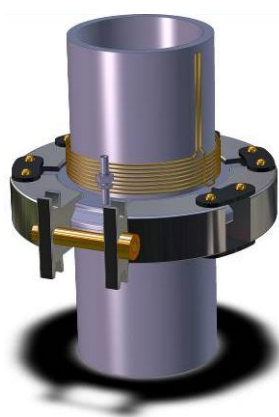
#### *Installation*

The v-clamp and the gasket have been removed.

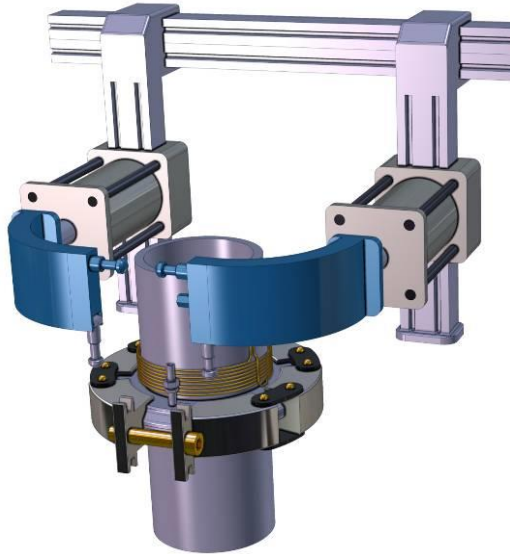
### Remote operations sequence

#### *Uninstallation*

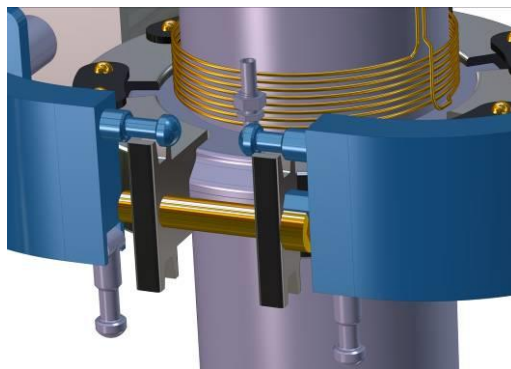
- 1) The pipe line is drained. The connector must be removed for the extraction of the blanket segment or for the replacement of the metallic seal (in the case of the sealing requirements are not fulfilled).



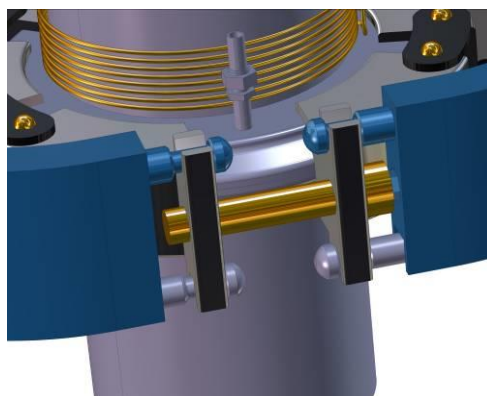
- 2) The v-clamp manipulator approaches to the slots of the clamp segment to start the fastener unscrewing. The manipulator arms have 3 translation DOF that allow positioning their upper pivots on the slots. The lower pivots are in vertical position to avoid the clash between them and the clamp.



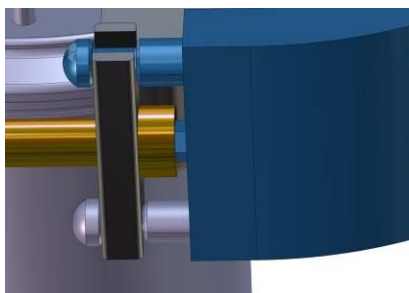
- 3) The arms go down towards the slots. The slots are composed by conical shapes forming sloping planes that allow correcting the possible misalignment between the arms pivots and the clamp slots.



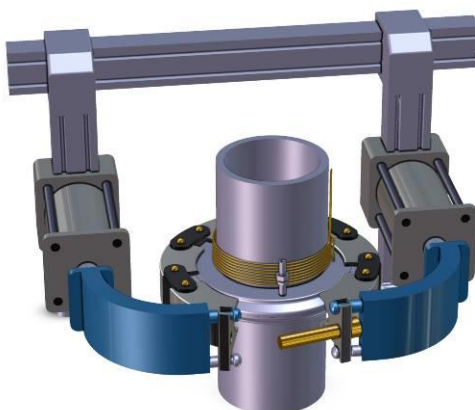
- 4) When the upper pins (pivots) are positioned, the lower pivots turn and grip the clamp lower slots. These slots are also conical-shaped to correct possible misalignments.



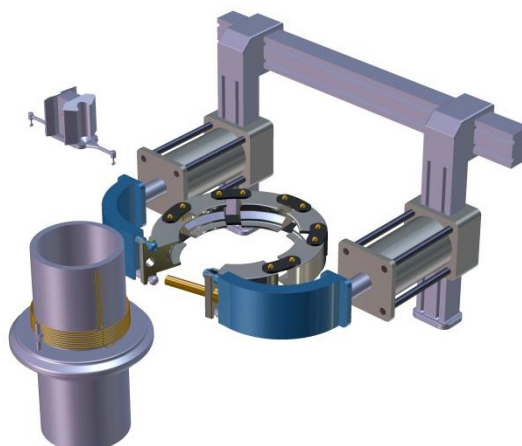
- 5) The retractile bolting tool unbolts the screw. The bolting tool is located inside the arm until the lower pivots are positioned.



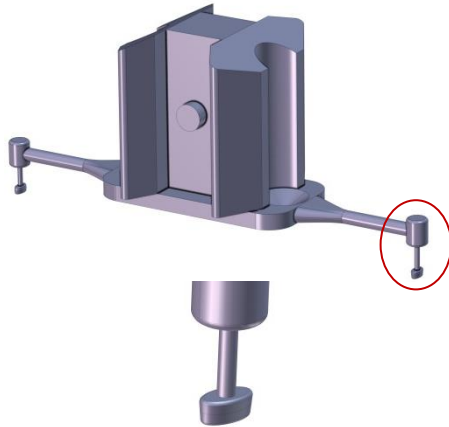
- 6) Both arms move away in order to release the v-clamp from the pipe flange.



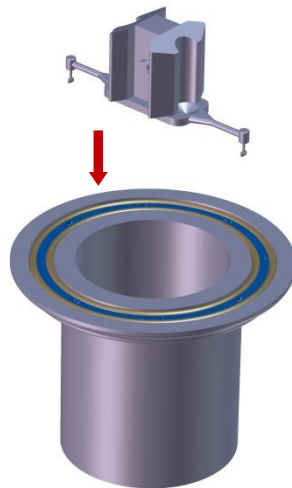
- 7) The v-clamp moves the v-clamp away from the pipe. In the case of PbLi pipes, the RH equipment (TBD) in charge of extracting the upper side of the pipe approaches while the heater raises the temperature of the flange over the eutectic temperature, so that the re-melting of the PbLi solidified layer is achieved. Then the upper side of the pipe is extracted.



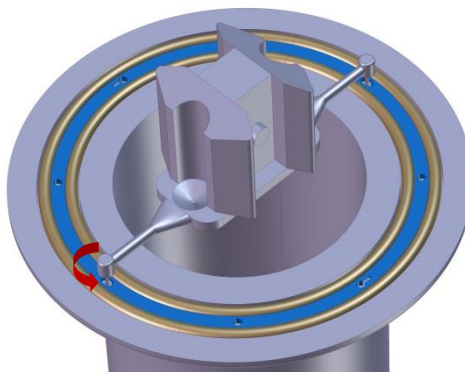
- 8) The manipulator for installing/removing the double Helicoflex gasket approaches to the lower pipe. The gasket manipulator is composed by two twist-locks.



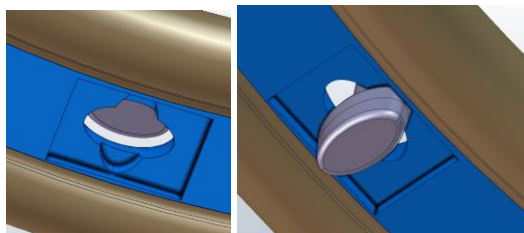
- 9) The gasket manipulator is positioned over the lower pipe and is aligned with the gasket holes that have been foreseen to contain the twist-locks. The manipulator approaches to the gasket.



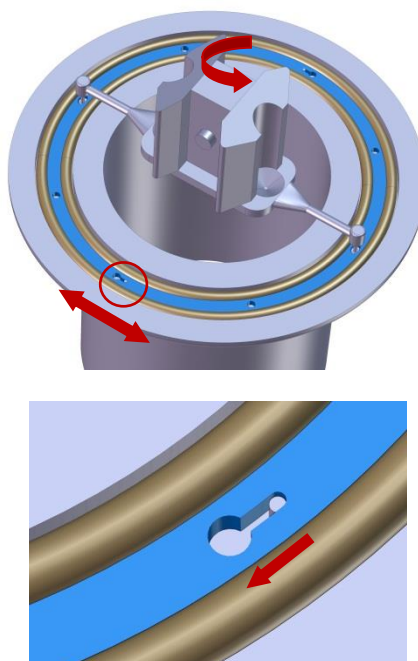
- 10) The twist-locks turn 90° when they are inserted into the gasket holes.



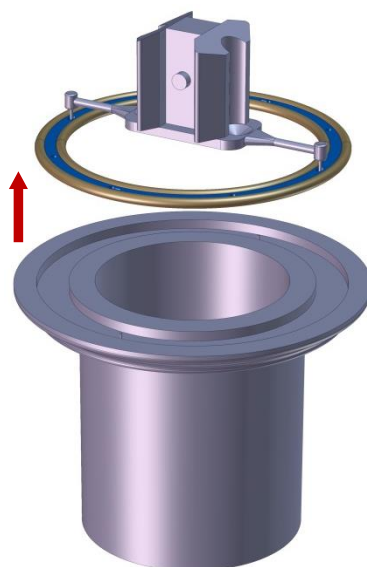
- 11) The gasket holes are designed with sloping surfaces to align the twist-locks with the two available positions (open/closed). Open: twist-lock moves into/out from the hole. Closed: the gasket is moved into/out from the flange groove.



- 12) Once the gasket is gripped, the manipulator turns around the pipe axis to extract the pins from the holes. The pins are used to fix the gasket into the flange groove. The holes are progressively narrowed to correct the possible misalignment.

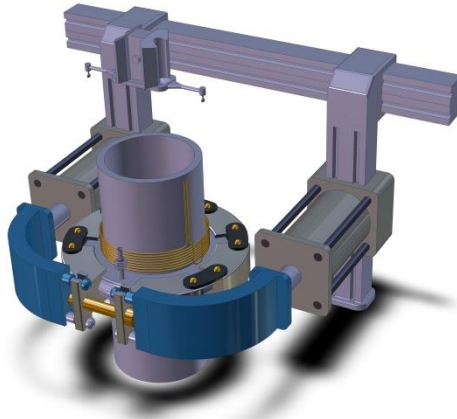


- 13) The manipulator extracts the gasket. The gasket is transferred to the maintenance area.

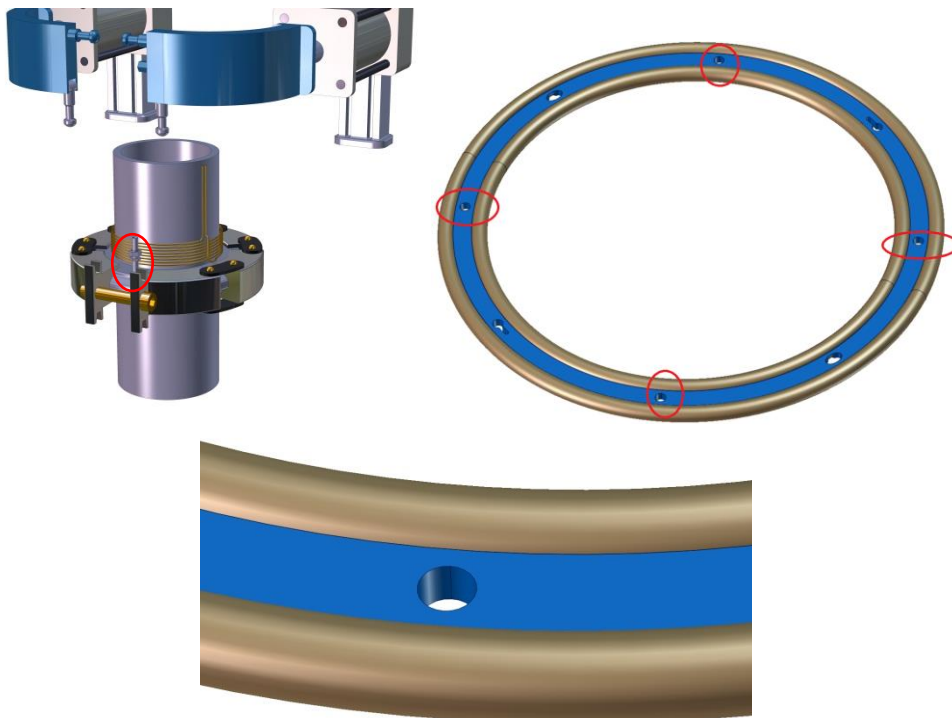


#### *Installation*

- 1) The connection sequence is approximately the reverse of the disconnection sequence.



- 2) Leak testing is required after installing the connector to evaluate the gasket sealing performance. The flange groove is connected to a vacuum auxiliary system by means of a pipe which goes through the flange. Several holes are placed in the gasket tongue to improve the pumping performance in both sides of the gasket (up/down). The pumping system provides vacuum conditions in the groove and then helium flows through the pipe. A helium leak detector connected to the pumping system measures the flow of He across the seal. The leak rate must be lower than  $10^{-9}$  mbar l s<sup>-1</sup> to approve the installation procedure.



### **5.3.3. Summary of results and conclusions**

A design concept of a generic flange to be used together with quick disconnection systems has been proposed. The sealing requirements can be fulfilled by using Helicoflex metallic gaskets. Specifically, the double seal configuration of the selected gasket -HNR229 (Helicoflex)-, which accomplishes with ITER requirements for UHV applications, also allows leak testing.

The maximum working temperature of the gasket (600°C) makes it suitable for the different pipes of DEMO blankets, although more developments should be needed if primary coolants

temperatures are raised to optimize the power conversion cycle efficiency. However, no evidences about the performance of Helicoflex gaskets under the considerably high 14-MeV neutron flux expected in the vacuum vessel upper ports during operation have been found in literature. Helicoflex are extensively used to seal pressure vessels in PWR, BWR and gas-cooled reactors but not in fast fission reactors, with a neutron spectrum more similar to the fusion one. Nor it is known the behaviour of this sealing method against loads coming from plasma events like disruptions, mainly because there are still too many uncertainties about such phenomena in DEMO.

On the other hand, several v-clamp designs from the gasket manufacturer are able to keep the seal seating load requirements (minimum axial clamping load and minimum tightening load).

Both the v-clamp and the gasket can be installed/removed in/from the flange by remote handling. A v-clamp manipulator allows transport and placing of V-clamp, as well as screwing/unscrewing of the fastener. Besides, the gasket manipulator allows transporting, positioning, aligning, fixing and removing the double seal gasket.

Considering the RH systems can be adapted to the available space in the upper ports, the main disadvantage of this proposal is the difficulty of using only a RH system to install a number of connectors in parallel, so that operation times can be excessively penalized if the procedure is sequential.

## **5.4. Design of a brazing connector for DEMO blanket pipes**

In the final report of the EFDA Task Agreement WP11-DAS-RH-04, Queral recommended the development of 'innovative, simple and reliable solutions for a robust bolted connector sealed by internal brazed surfaces. [...] Then the brazed surface would act only as a sealing method and the bolts only as a strength mechanism', after concluding that 'according to ITER research and report, regulations do not exist for diffusion brazed components in nuclear plants. However if all the standards, regulations and tests are performed then diffusion brazed connectors could be used in nuclear plants' [Que 12].

Following this recommendation, and together with in-bore welding methods and mechanical connections like the described in Section 5.3, a brazing connector conceptual design was produced in the framework of EFDA WP12 [Fern 14] and further developed in WP13 [Fern 14b].

This work takes as reference a concept for a remote handling compatible pipe jointing system [Shu 09], based on an in-situ reversible brazing technique developed by Sandia National Laboratories (SNL) for closing radioactive material transport packages made of stainless steel [Pie 95]. The result is a remote handling compatible design which includes an induction heating system, a brazing atmosphere supply system, an inspection system (helium leak testing) and a positioning and alignment system. A bolted/clamped union can be added if necessary to provide stiffness against off-normal conditions.

### **5.4.1. Preliminary selection of materials**

Brazing is a group of joining processes that produces the coalescence of materials by heating them to the so-called brazing temperature in the presence of a filler metal having a liquidus temperature above 450°C and below the solidus temperature of the base metal [ASME 07]. The filler metal is distributed into or held in the closely fitted faying surfaces of the joint by capillary action, whereas a protective atmosphere is used to protect the metal surfaces from oxidation during heating and to provide good wetting and capillarity. As result, a properly designed joint has essentially the same strength as the parent metal [Pie 95], with excellent stress distribution, little distortion and minimum oxidation. Sealing capability and no need of thermal treatment are other well-known advantages of brazing over mechanical connections and welding, respectively.

The previously mentioned research carried out by Sandia National Laboratories demonstrated the feasibility of brazing and debrazing piece parts in a helium atmosphere for as many as twenty times without the need to perform any special joint preparation [Pie 95]. This may be used for sealing the interface between two independent pieces (helium leak rate  $< 10^{-9}$  mbar l s<sup>-1</sup>) and unsealing/separating them later.

Metallographic analyses determined that stainless steel tends to chromia formation at high temperature in helium atmosphere. Furthermore, base metal dissolution problems and grain growth were found to be significant problems when two pieces of stainless steel 304 are repeatedly brazed together. In addition, the braze alloy would change in composition due to dissolution of elements from the stainless steel and therefore the liquidus temperature would also change. Nickel alloys offer better performance in this sense [Pie 95].

For this reason, SNL developed a procedure which includes two brazed joints, each one of which implies a specific filler metal and atmosphere. The first is a previous ex-situ permanent brazing of austenitic stainless steel and Ni-200 and the second uses in-situ brazing/debrazing cycles of two pieces of Ni-200.

It must be noted that high nickel content alloys like Ni-200 cannot be used as pipe material for PbLi because of the high corrosion rate, so this material selection is only valid for helium and water pipes. Another possible issue coming from the use of Ni alloys is neutron-induced swelling, but it is not clear enough. Some experiments show swelling can be partial or totally prevented by adding solutes like 1% Si or 0.5% Al to pure nickel [Por 13]. Density of dislocations and defects previous to cold-work as well as dpa rate are critical for the achieved swelling level.

Anyway, the following subsections are based on the selected combination of base metals and filler metals. Alternative materials for PbLi pipes but also for He and H<sub>2</sub>O pipes are discussed in Subsection 5.4.8.

#### 5.4.1.1. Filler metals

Gold-nickel alloys are mostly used for brazing iron, nickel and cobalt base metals when high ductility or high resistance to oxidation and corrosion is required. The braze alloy best suited for rebrazing Ni-200 pieces appears to be the 82Au-18Ni alloy, which is also identified as the AWS BAu-4 alloy as specified in AWS-A5.8 [Pie 95].

AWS Classification	Composition, weight percent		
	Au	Ni	Other elements, total
BAu-4	81.5-82.5	Remainder	0.15

Table 13. Chemical composition requirements for BAu-4 [ASME 07].

In the case of the brazing between Ni-200 and stainless steel parts, BNi-5 was identified as the most appropriate filler metal in terms of re-brazeability [Pie 95].

AWS Classif.	Composition, weight percent												
	Ni	Cr	B	Si	C	P	S	Al	Ti	Zr	Co	Se	Other
BNi-5	Rem.	18.5	0.03	9.75	0.06	0.02	0.02	0.05	0.05	0.05	0.10	0.005	0.50
		-		-									
		19.5		10.5									

Table 14. Chemical composition requirements for BNi-5 [ASME 07].

The liquidus temperature of the filler metal for brazing/debrazing cycles must be adequately lower than the solidus temperature of the SS/Ni-200 permanent joint. A difference of 130°C

between the BAu-4 liquidus temperature and the BNi-5 solidus temperature is enough for the expected temperature field during brazing.

Joint	AWS Class.	T solidus (°C)	T liquidus (°C)	Range of brazing T (°C)
SS/Ni-200	BNi-5	1079	1135	1149-1204
Ni-200/Ni-200	BAu-4	949	949	949-1004

Table 15. Solidus and liquidus temperatures for the selected filler metals [ASME 07].

Although BAu-4 has also high Ni content, the previously referred issue of corrosion under PbLi flow cannot be considered a significant problem here; since it is improbable flowing PbLi comes into contact with the filler metal. Nonetheless, since it has been specifically selected for Ni-200 parts brazing, in the case of PbLi pipes it may be substituted by other filler metal more suitable for alternative base metals.

#### 5.4.1.2. Protective atmospheres

Mixtures of gases containing hydrogen provide better wettability than pure helium for BAu-4. SNL proved this concept with pure helium atmosphere, since the presence of hydrogen could suppose an issue for the application for which the method was developed, but in our case a mixture of helium and hydrogen (10%) can be convenient to improve the filler metal wettability [Pie 95].

In the case of BNi-5, good results were achieved with vacuum instead of protective atmosphere [Pie 95].

#### 5.4.1.3. The case of EUROFER

As mentioned at the beginning of this Chapter, SS-316 has been taken as reference material for DEMO pipes in EFDA Work Programmes technical specifications. However, RAFM steel is clearly more adequate to manufacture in-vessel components pipes. There are no references of brazed joints between EUROFER (or any other reduced activation ferritic-martensitic steels) and nickel alloys. Only some works about brazing between EUROFER and tungsten have been carried out to date [Mun 11].

Sandia National Laboratories studied the brazing process between SS304 and Ni-200 coupons because the waste containers were made of such type of stainless steel. We can extrapolate its results to SS-316/Ni-200 brazing because filler metals generally wet type 316 stainless steel better than type 304. The improved wettability of braze filler metals on type 316 stainless steel is believed to be due to the presence of molybdenum in the surface oxide [ASM 93]. SS316 contains 2.30-2.70% of Mo.

In EUROFER molybdenum is substituted by vanadium and tungsten, which avoid the grain growth during heating and suppose 0.15-0.25% and 1.0-1.2% of the weight composition, respectively, although whether these metals are related to the wettability of the filler metal is unknown. In general, the particular chemical composition of EUROFER results in a very specific microstructure (e.g. large carbide precipitation) which confers it really good mechanical properties, but complicates any kind of joint (welding, diffusion bonding, etc.). In this sense, we could expect more difficulties for brazing EUROFER and Ni-200 than in the case of 316 and Ni-200.

### 5.4.2. Design description

#### 5.4.2.1. Main design features

The connector is divided in two parts, each one of which includes two main bodies: one internal made of Ni-200 and one concentric external made of stainless steel. The interface between Ni-

Ni-200 bodies is cyclically brazed to achieve the sealing of the pipe, as well as the interfaces between the Ni-200 and SS bodies, although these joints are permanent.

The first design of the connector included a bolted union at the interface between the SS bodies to ensure the stiffness of the assembly against disruptions and other major loads, according to [Que 12] recommendations.

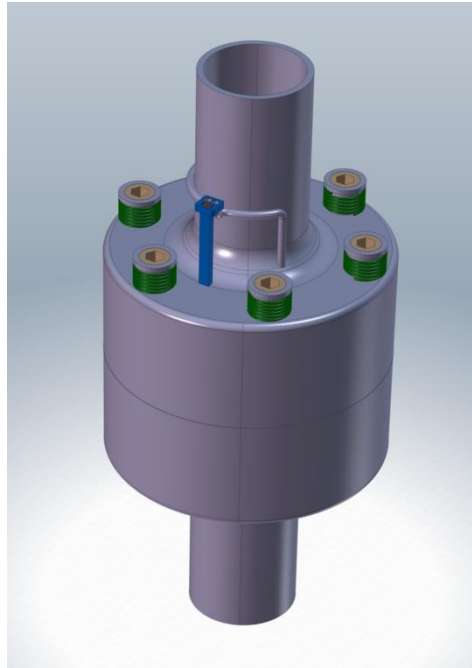


Fig. 19. General view of the brazing connector (including bolted union).

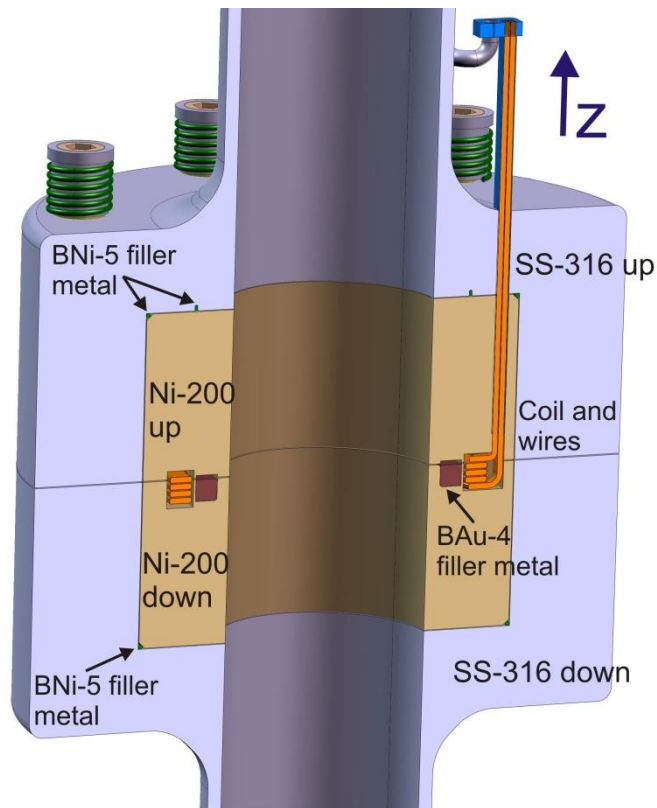


Fig. 20. Longitudinal section of the brazing connector (including bolted union).

The design of the SS-316 lower body is very simple and shows revolution symmetry. It only includes an external crown for the bolted union and a pocket to introduce the Ni-200 body (with a small gap).

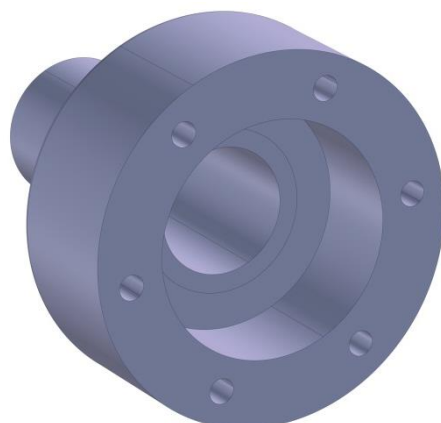


Fig. 21. SS-316 lower body.

The Ni-200 lower body includes an internal groove for placing the filler metal BAu-4 and another external for placing the heating coil. The back edge is also prepared for placing the external ring of filler metal BNi-5.

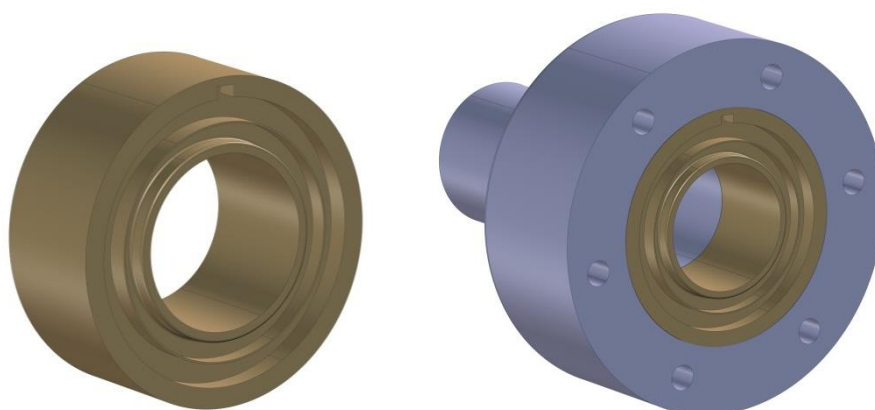


Fig. 22. Ni-200 lower body. Integration into the SS-316 lower body.

The SS-316 upper body is similar to the lower one, but includes a groove to place the internal filler metal BNi-5, a pocket to connect the heating coil with the supply and control system, and two holes to allow pumping, blowing and leak testing.

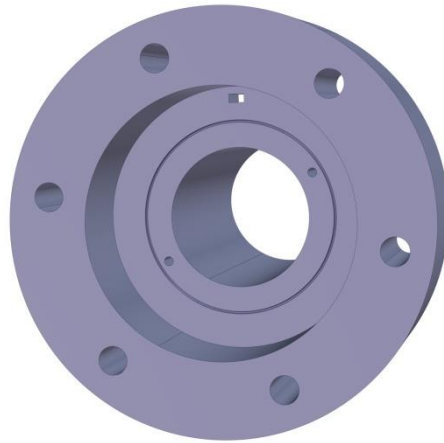


Fig. 23. SS-316 upper body.

Like the SS316 upper body, the Ni-200 upper body contains a pocket for the heating system and two holes to communicate the BAu-4 groove with the protective atmosphere auxiliary systems. It includes also a groove for BAu-4, but, unlike the Ni-200 lower body, this groove does not contain the filler metal ring in the beginning, but it receives part of the filler metal when it spreads during the brazing process.

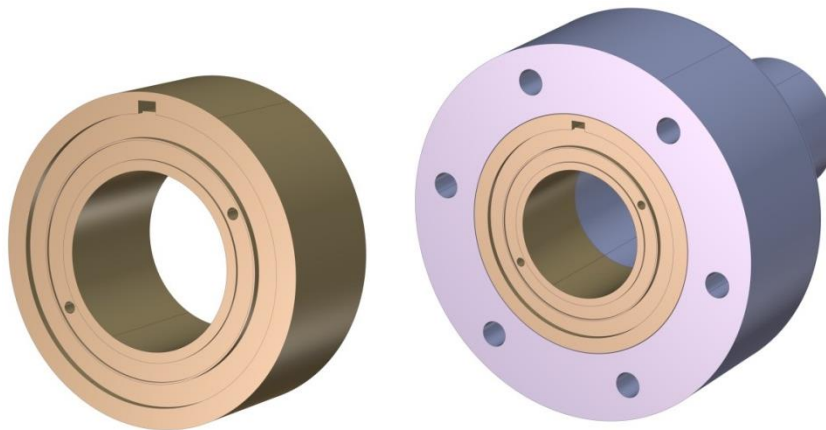


Fig. 24. Ni-200 upper body. Integration into the SS-316 upper body.

#### 5.4.2.2. Filler metals pre-placement

The filler metals are provided in form of pre-placed rings with different sections, in accordance with their position, the features of the brazing techniques used for each joint and the characteristics of wettability and spreadability of the different alloys. There are a total of three rings: the first is made of BAu-4 and must provide a sealed and resistant joint between the Ni-200 bodies. The other two are made of BNi-5; the function of the external ring is similar to the BAu-4 one, although here the produced joint is permanent instead of cyclic. On the other hand, the internal ring must provide sealing of the holes for the heating and protective atmosphere systems. Considering that the shape of the filler metal preforms and grooves affects the filler metal flow (sharp or smooth edges), as well as the placement of the filler metal (faces, corners, etc.), the designs of the filler metal rings profile and the grooves in base materials are adapted to improve the filler metal spreadability. Thus, the internal edges of the BAu-4 ring and its groove in the Ni-200 lower body have been rounded, whereas the external edges are sharp to define a preferential way of filler metal spread during the brazing process and to avoid its movements towards the heating coil groove. The BNi-5 rings profiles as well as their placement in the base metals have been also designed according to spread and joint strength requirements (chamfered/rounded edges in Ni-200 and SS3-16 bodies). It may be necessary to apply a 'stop-off agent' to prevent the flow of filler metals outside the area of interest (e.g. boron

nitride) [Gros 06]. It can aid to restrict the spread towards the interior of the pipe and the coil groove.

#### 5.4.2.3. Adaptability to flow direction

As in the case of the QDS-compatible jacket flange (Section 5.3), the brazing connector has been designed to be used in vertical pipes, but it can be adapted for horizontal pipes. Only the design of the interfaces between both Ni-200 parts, as well as the design of the heating coil and the filler metal BAu-4 groove must be modified. A comparison between the original design and a possible sketch for horizontal pipes can be found in Fig. 25.

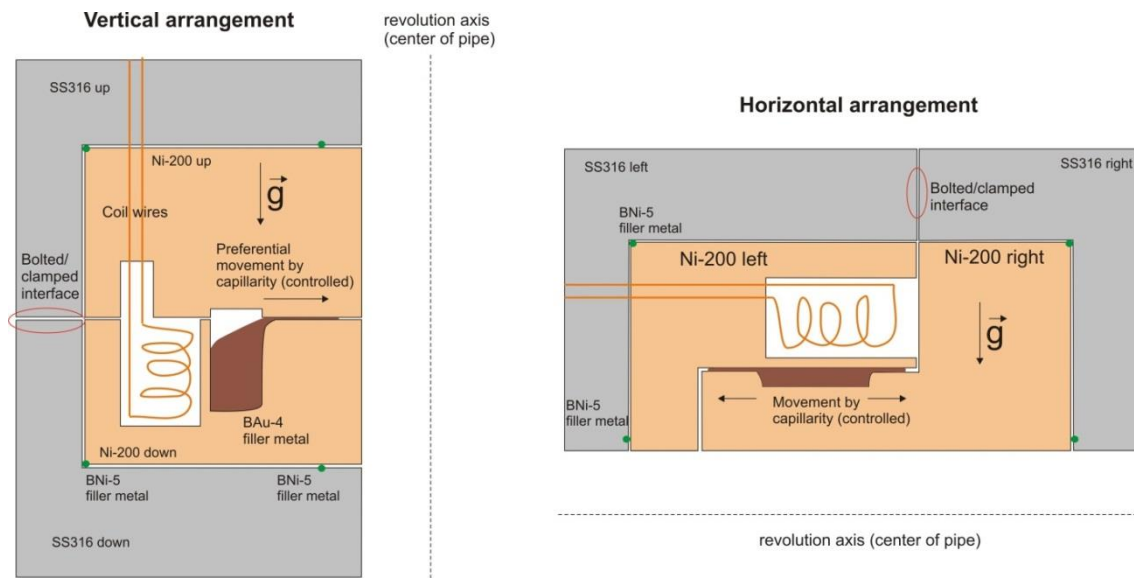


Fig. 25. Vertical and horizontal arrangements.

#### 5.4.2.4. Brazing processes

The SS-316/Ni-200 permanent brazing is proposed to be carried out in an external furnace with vacuum conditions. Furnace brazing is widely applied in a variety of industries. For example, it is the most common system used in the production of jet engine components [ASM 93].

In the furnace brazing process, cleaned parts and brazing filler metal are assembled, placed in a furnace and heated to the brazing temperature. Heating is slow and this results in total floor-to-floor cycle times in the range of 2-10 hours [EN14324]. The method shows several advantages for this application [ASM 93]:

- It is a method in which many variables can be easily controlled to ensure repeatability of the process and guarantee a high-quality joint. Brazing temperature and process duration, as well as heating and cooling rates, can be controlled and monitored.
- The absence of flux entrapment allows more flexibility in joint design.
- Because a whole assembly is heated, distortion of the parts can be minimized or eliminated. In some cases, heat treatment of parent materials can be simultaneously performed.
- More than one joint per work piece can be brazed in a brazing cycle. Several different assemblies requiring the same brazing conditions can also be brazed simultaneously.

As main limitation, we can mention the initial investment in furnace brazing equipment, which is relatively high. Furthermore, the maintenance of the equipment is critical and can be more expensive than other brazing techniques. In addition, since the whole assembly is heated, the cost of heating exceeds that of other brazing operations.



Fig. 26. Interior of a vacuum brazing furnace.

On the other hand, the use of induction heating in a mixture of helium and hydrogen atmosphere is proposed for the cycled brazing between the Ni-200 parts.

Induction brazing is used where relatively high-strength heat-resistant joints are required between components parts. Induction brazing has been used extensively in the production of consumer and industrial products, structural assemblies, electric and electronic products, mining equipment, machine and hand tools, military and ordnance equipment, and aerospace components. Some advantages of this method for our case are the following [ASM 93]:

- a) Induction brazing features rapid heating that produces joints in seconds because each joint area is exposed to the electromagnetic field of the specific coil involved.
- b) Induction brazing provides control of the heat pattern and rapid heating, which serve to localize the heated zone, thereby preventing or minimizing deterioration of properties in previously heat-treated or cold-worked materials.
- c) Induction brazing uses predetermined amounts of brazing alloys in the form of rings, strip, or powder; thus, the possibility of excessive material use is avoided, lowering joining alloy costs.
- d) Rapid heating minimizes oxidation in most instances.

Limitations of induction brazing include need for relatively uniform clearance between components, the initial cost of equipment and the complexity of the system.

#### 5.4.2.5. Brazing atmosphere and inspection system

Two pipes for blowing and extracting the mixture of gases communicate the BAu-4 groove with the auxiliary systems. This allows implementing an inspection system to check the sealing quality of the brazed joint by using a leak detector or measuring the pressure evolution after vacuum pumping.

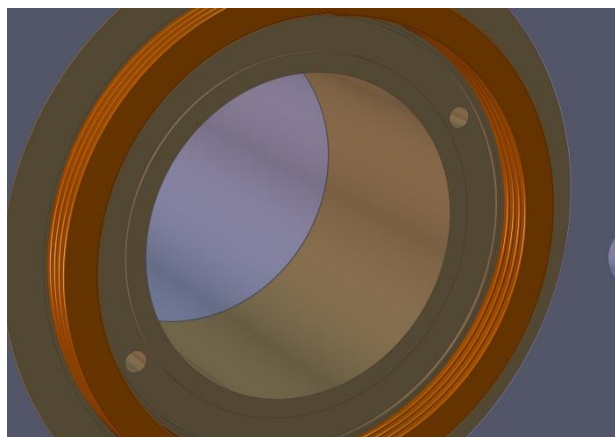


Fig. 27. Holes in the Ni-200 upper body for the brazing atmosphere supply and leak testing system.

The coil power and cooling supplies as well as the atmosphere supply/inspection system are disposed in a common plug with RH plugging features which is placed in the rear part of the upper half of the connector.

On the other hand, some of the auxiliary systems (pumps, valves, gas volumes, etc.) could be placed in a robot running around the vacuum vessel upper ports on a rail system.

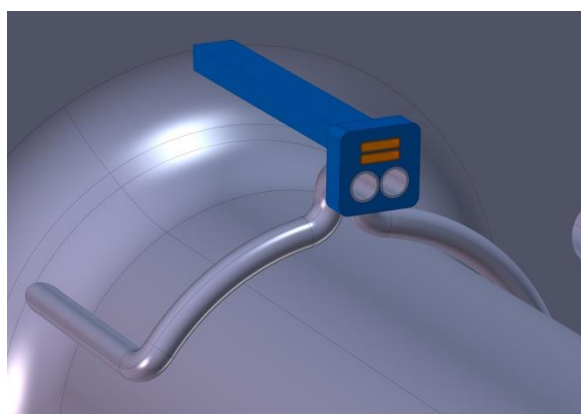


Fig. 28. Multi-function plug.

### **5.4.3. Induction heating assessment**

The main component of the induction heating system is a specifically designed cooper coil which is inserted in a groove between the lower and upper part of the connector. The coil, which is internally cooled by water, is fixed to the upper part of the connector and is connected with the supply and control system through the SS-316 and Ni-200 bodies. Commercially available power sources based on solid-state technology, which allows reducing the size of electronic equipment and increasing its reliability, can be used for this application.

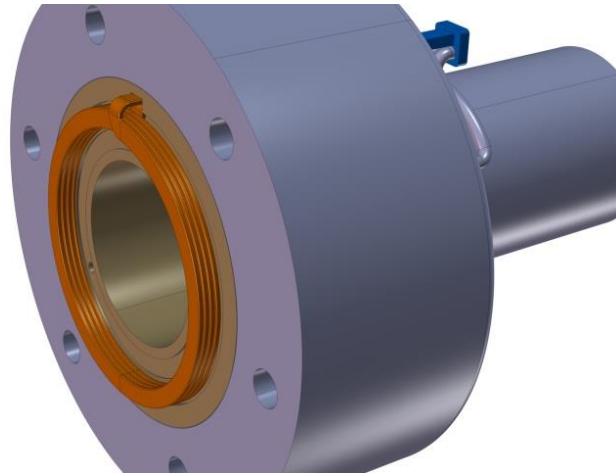


Fig. 29. Induction heating coil.

FEM analyses with the code ANSYS APDL have been done in order to evaluate the capabilities of the induction heating system and to pre-size its main parameters and geometries (coil shape, filler metal and coil grooves shape and position, current intensity and frequency, and power source). Electromagnetic-thermal axisymmetric analyses have been carried out, considering the connector design adapted to pipes with an inner diameter of 75 mm and a thickness of 5 mm. Furthermore, the filler metal groove has been placed in the upper part of the connector.

In first time, a harmonic analysis has been carried out considering the following parameters:

- Number of coil turns: 4;  $I=200$  A/turn;  $f=30$  kHz.

where  $I$  is the current intensity per coil turn and  $f$  is the current frequency. Following, from Joule heating load due to eddy currents calculated in the magnetic analysis, a transient thermal analysis has been carried out. Radiation between Ni parts and the coil, as well as convection and radiation in external nodes have been included. Some of the parameters considered in the calculation were the following:

- $T_{\text{water}}=323$  K;  $T_{\infty}=298$  K;  $h=100$  W m<sup>-2</sup> K<sup>-1</sup>;  $\epsilon_{\text{Ni-200 surface}}=0.5$

where  $T_{\text{water}}$  and  $T_{\infty}$  are respectively the temperatures of the coil cooling water and the convective environment,  $h$  is the convection heat transfer coefficient and  $\epsilon_{\text{Ni-200 surface}}$  is the surface emissivity of Ni-200.

The results show the use of high frequency current allows concentrating magnetic flux contour lines in the external surface of the filler metal ring and focusing the generation of heat, as can be seen in Fig. 30. However, simulations show that the larger magnetic permeability of Ni-200 with respect to BAu-4 causes the density of magnetic flux lines is even higher in the Ni-200 wall between the filler metal and the coil grooves. This hinders the filler metal heating process.

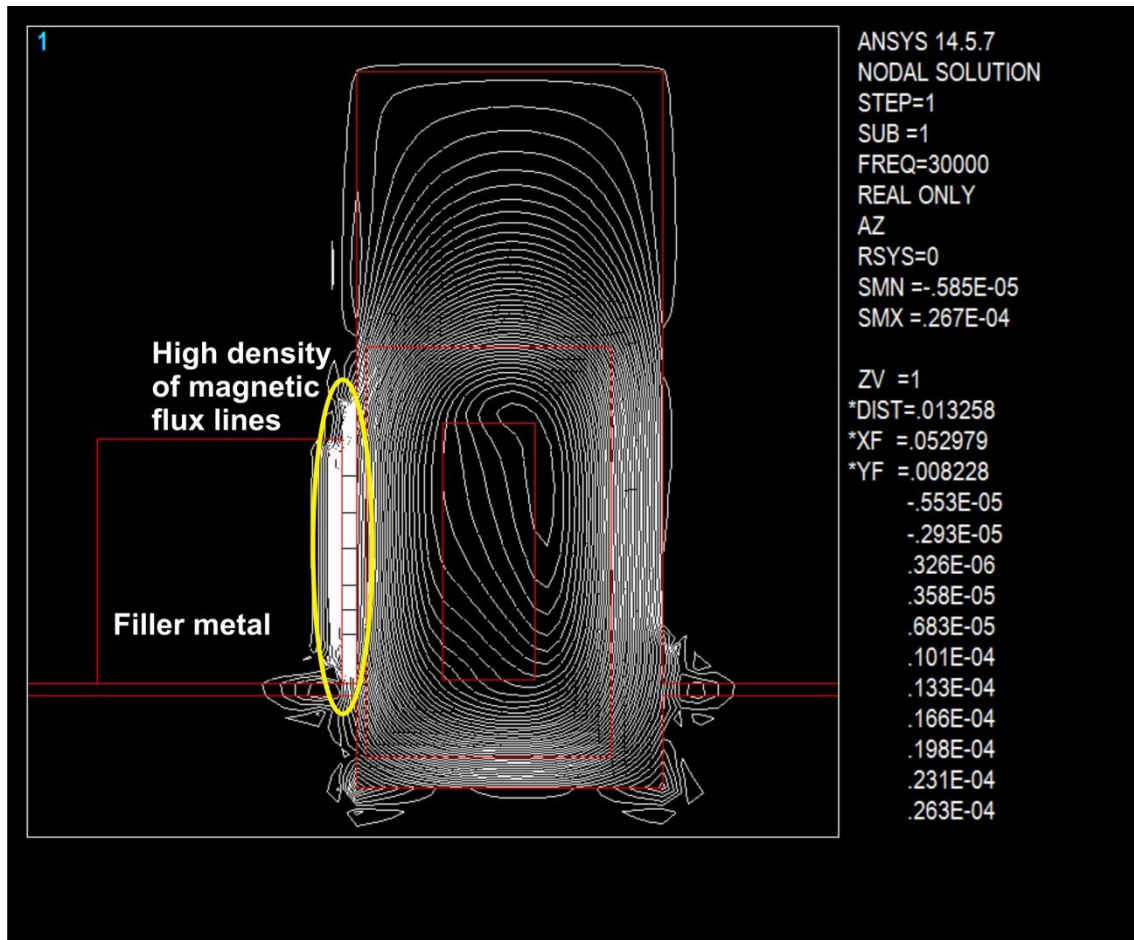


Fig. 30. Equipotential lines of magnetic flux near the BAu-4 ring.

In spite of that, the much higher melting temperature of Ni-200 compared with the filler metal one provides a large margin for the heating of the Ni-200 bodies up to the point that the filler metal reaches its liquidus temperature. On the other side of the Ni-200 wall, the water cooling is enough to maintain the coil temperature in a suitable range (Fig. 31). Anyhow, Fig. 32 shows the heating process of the filler metal is very fast and located. As can be seen, after 20 s the whole filler metal ring has reached the BAu-4 solidus temperature and the brazing process occurs. In these analyses, the magnetic permeability of the different materials has been considered constant (Curie temperatures over the operation range have been assumed).

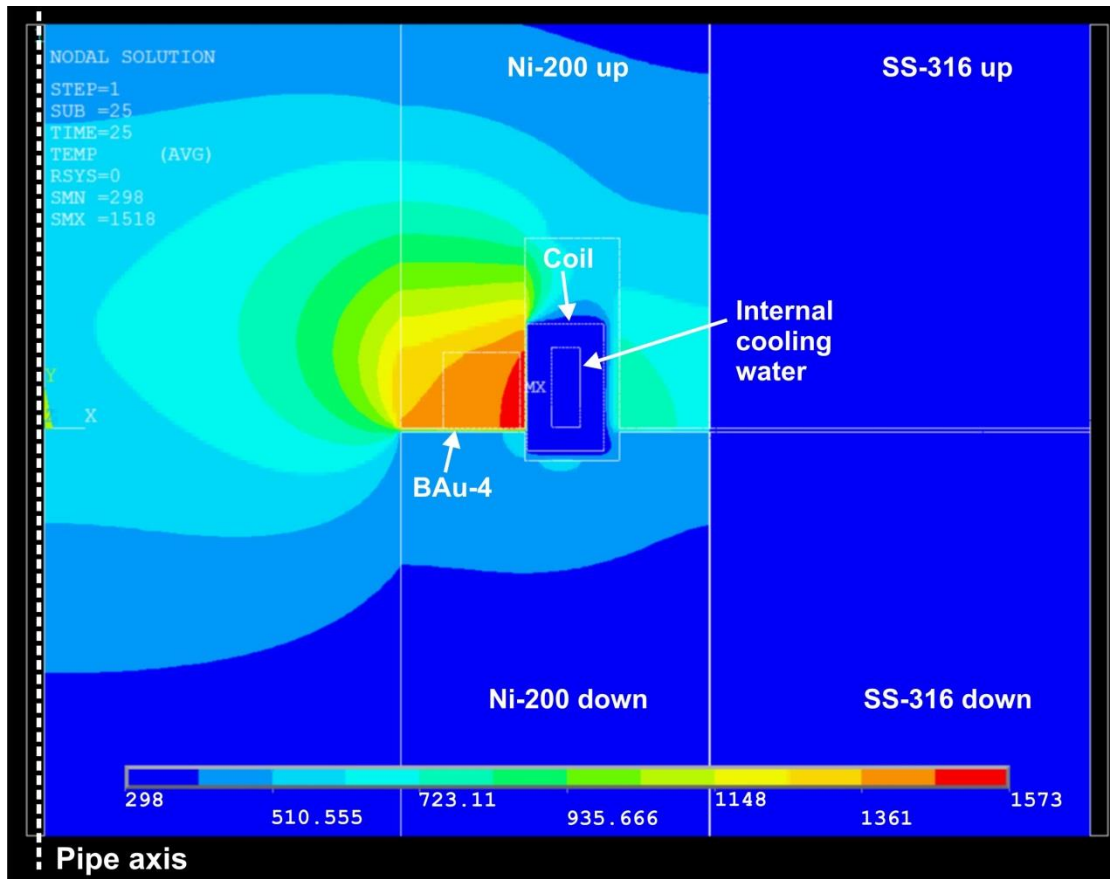


Fig. 31. Temperature (K) in the connector during induction heating (t=25 s).

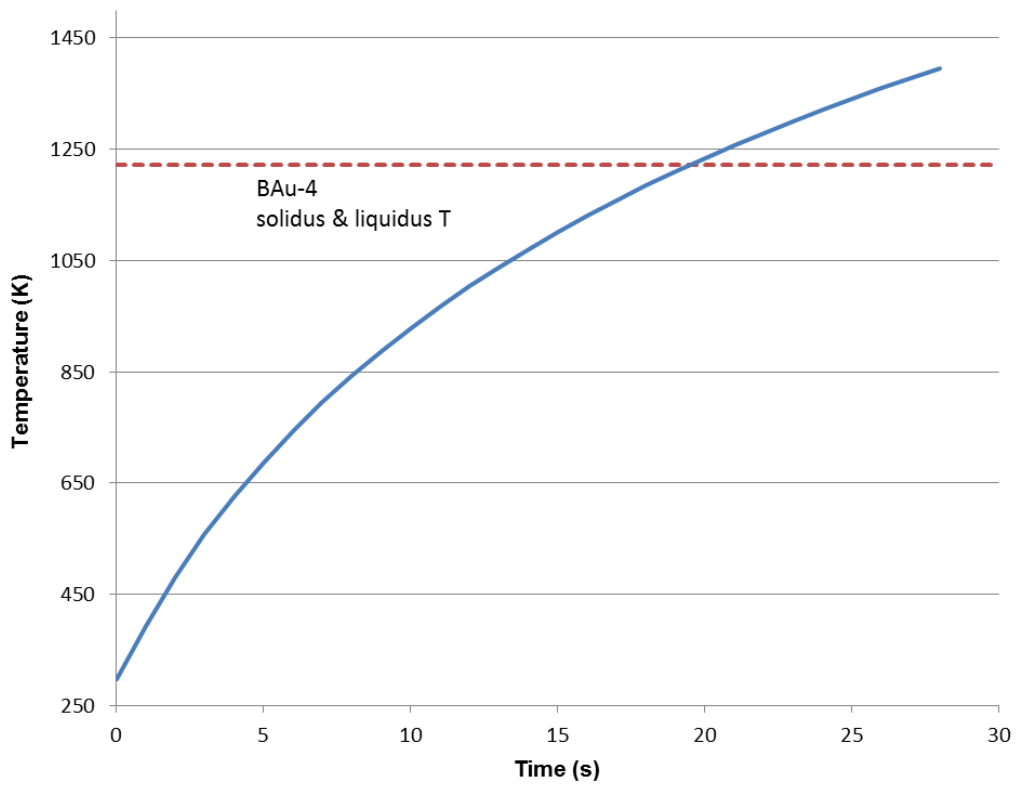


Fig. 32. Temperature evolution in the BAu-4 filler metal ring.

### 5.4.3.1. New electromagnetic-thermal analysis

The previous results show the induction heating can be very fast and localized. However, the brazing process requires uniform temperature near the interface between the base metal and the filler metal to obtain suitable mechanical properties. Thus, the electromagnetic-thermal analysis has been repeated modifying the coil and its groove geometries, as well as the operational parameters of the induction heating system (number of coil turns: 4;  $I=600$  A/turn;  $f=10$  kHz), to achieve a more uniform heating in the gap between the Ni-200 parts. For example, a lower current frequency allows reducing the skin effect and therefore increasing the depth of heating. Besides, the new APDL input code includes the definition of Curie point (temperature where a ferromagnetic material becomes paramagnetic) at  $360^{\circ}\text{C}$  for both Ni-200 and BAu-4. No values of Curie point for these materials have been found in literature, so that the nickel one (main constituent) has been taken. Thus, the input code performs successively electromagnetic and thermal calculations; when the temperature in a Ni-200 or BAu-4 node reaches the Curie point, the relative magnetic permeability changes and the calculation continues. On the other hand, the filler metal has been placed definitively in the lower part of the connector.

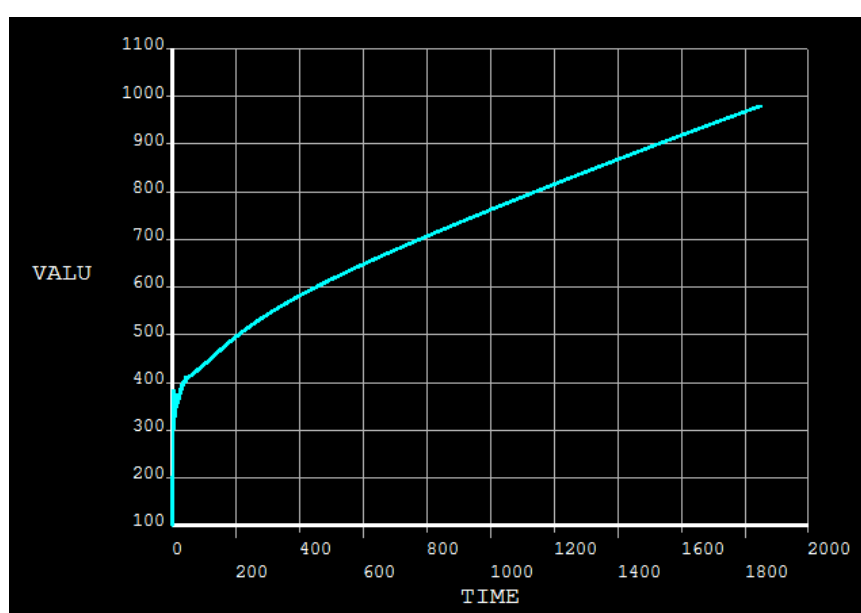


Fig. 33. Effect of Curie point in the evolution of temperature ( $^{\circ}\text{C}$ ) in a node belonging to the filler metal.

Fig. 33 shows the strong impact of assuming this Curie point value on the heating curve. With these conditions, the time needed to reach the BAu-4 liquidus temperature ( $949^{\circ}\text{C}$ ) is around 30 minutes. But even so, this time is much shorter than the one consumed by heat treatment in the case of in-bore welded joints in EUROFER pipes ( $\sim 2$  hours) [Keo 13]. Anyway, it must be noted that this is just a rough estimation, taking into account the number of assumptions on the properties of the considered materials.

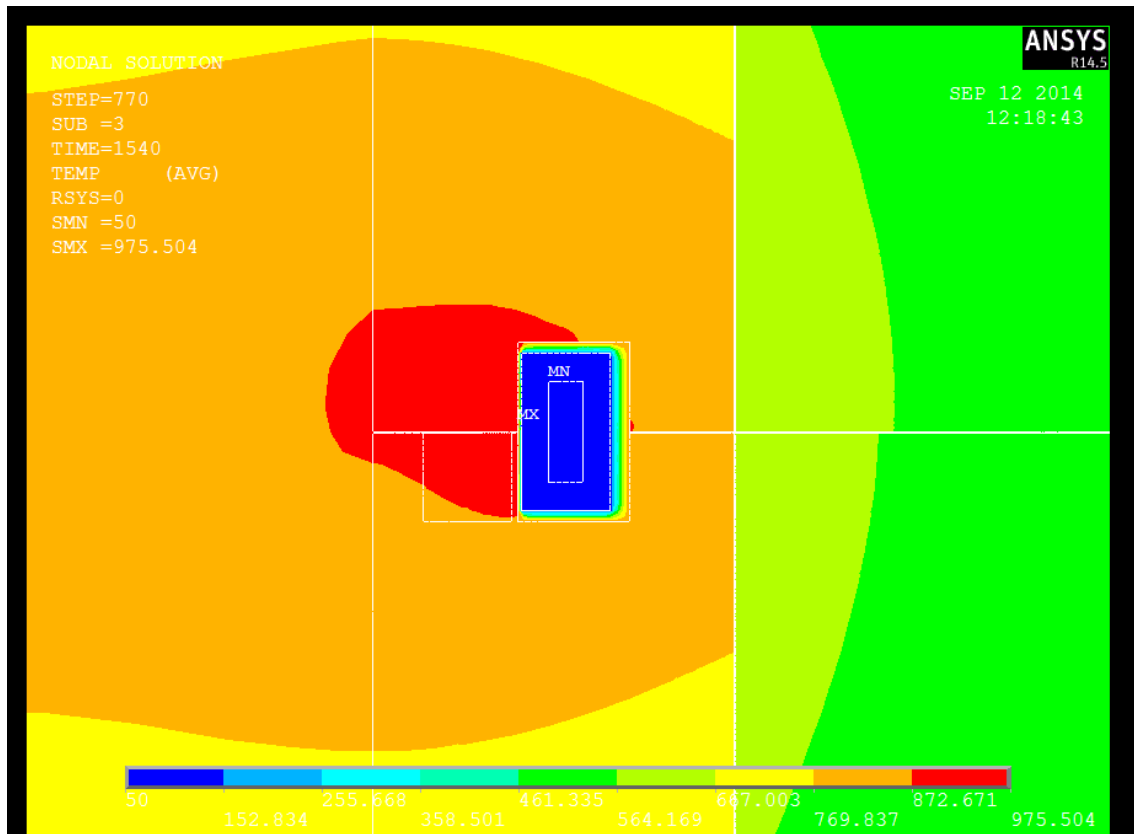


Fig. 34. Temperature (K) in the connector at the later stages of the heating process ( $t=1540$  s).

#### 5.4.3.2. Thermomechanical analyses

Despite the more uniform heating (Fig. 34) with respect to the previous results, the thermal stresses produced during the heating process could originate plastic deformation and residual stresses. These phenomena could also occur during cooling processes. For this reason, the mechanical behaviour of the joint between the Ni-200 parts through the BAu-4 filler metal has been characterized during a cooling scenario through 2D axisymmetric thermomechanical analyses with ANSYS Workbench. The model is focused on a sample of 15 mm (height) of Ni-200 in the lower and upper parts of the connector and it includes the BAu-4 filler metal (spread shape).

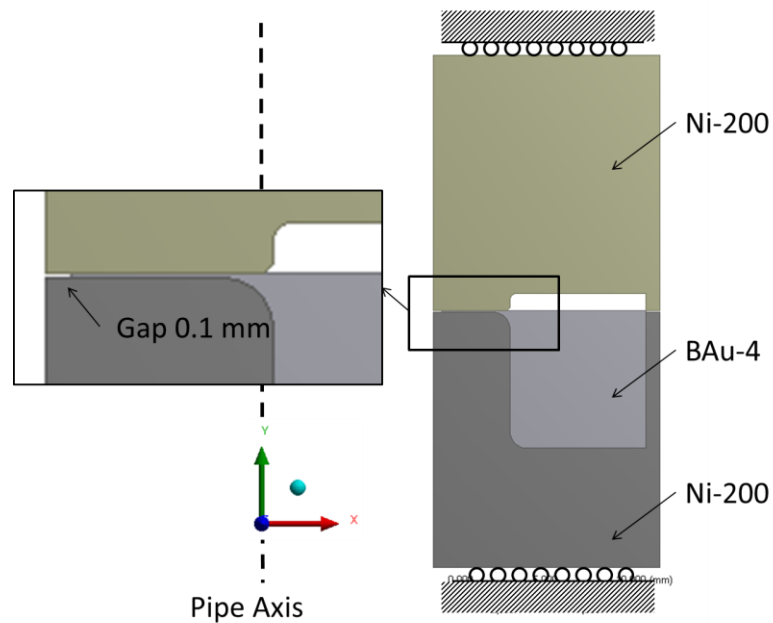


Fig. 35. 2D geometry and mechanical boundary conditions for the thermomechanical analyses.

The initial temperature map has been obtained from the electromagnetic-thermal analysis at the time when the whole filler metal is under its liquidus temperature. Additional temperature maps at 25 s and 120 s after the start of the cooling process have been obtained from a thermal transient analysis, for which a heat flux has been estimated and imposed at the upper and lower edges of the Ni-200 parts.

The three temperature maps have been used as input in static structural analyses, assuming elastoplastic behaviour for both materials (Ni-200 and BAu-4), which is defined by bilinear stress-strain curves. Null displacements along the longitudinal axis at the upper and lower edges of the Ni-200 parts have been imposed as boundary conditions (conservative assumption), whereas the BAu-4 part has been set as bonded to the Ni-200 parts.



Fig. 36. Equivalent plastic strain at the beginning of the cooling process.

As expected, the results show the initial temperature map is the most unfavourable scenario, due the higher temperature gradients. Small plastic strain mainly occurs in the Ni-200 upper part (Fig. 36), but it can be minimized by modifying the shape of the filler metal groove.

#### 5.4.4. Modelling of capillary flow

One key issue affecting the mechanical behaviour of the brazed joint between the Ni-200 parts is the spreading process of the filler metal when its liquidus temperature is reached during the induction heating. This phenomenon is mainly governed by capillary forces, where wetting plays a principal role. Thus, the objective of this assessment is to develop a methodology for modelling the filler metal flow along the gap, in order to optimize the spreading of the filler metal by means of modifying the filler metal groove and gap geometries.

Wetting is a surface phenomenon related to the balance of the solid-liquid surface tension,  $\gamma_{SL}$ , the solid-vapour surface tension,  $\gamma_{SV}$ , and the liquid-vapour surface tension,  $\gamma_{LV}$ . The contact angle,  $\theta$ , between the solid and the liquid is defined in equilibrium conditions as the angle between the vectors that represents the liquid-vapour surface tension and the solid-liquid surface tension. The relationship between the contact angle and the surface tensions is given by the Young-Dupré equation [ASM 93]:

$$\gamma_{LV} \cdot \cos\theta = \gamma_{SV} - \gamma_{SL} \quad (1)$$

A liquid is said to wet a solid when the contact angle is less than  $90^\circ$ . In this case, for constant  $\gamma_{LV}$  the solid-vapour surface tension is greater than the solid-liquid surface tension. On the other hand, if the solid-vapour surface tension is lower than the solid-liquid surface tension, the contact angle is greater than  $90^\circ$  and the liquid will not wet the solid. Fig. 37 shows a wetting and a non-wetting system in a joint. In neither case did a reaction layer form between the solid and the liquid.

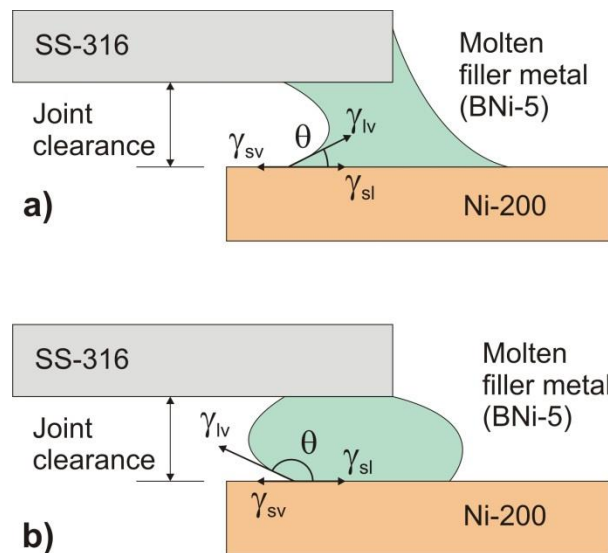


Fig. 37. Schematic showing the relationship between contact angle and surface tension: a) wetting system; b) non-wetting system [ASM 93].

Spreading is a dynamic process related to the contact angle  $\theta$  and can be described as an increase in the liquid surface and the interfacial area,  $\Delta A$ , with time. Thus, a liquid is said to completely spread over a solid surface when the contact angle tends to  $0^\circ$ . Alternatively, spreading is considered to proceed when the liquid surface area increases to a maximum, even if  $\theta$  is greater than  $0^\circ$ . The rate of spreading can be inhibited by the liquid inertia and/or the liquid viscosity [ASM 93].

As can be deduced from these facts, joint clearance is an important factor in the brazeability of a joint. The American Welding Society (AWS) recommends the following values for the joint clearance of the selected filler metals at their brazing temperatures:

AWS filler metal	Joint clearance (mm)
<b>BAu-4</b>	0.05-0.12
<b>BNi-5</b>	0.05-0.12

Table 16. Recommended joint clearance for the selected filler metals at their brazing temperatures [ASM 93].

A CFD approach can be used to model the spreading problem as a biphasic flow with one liquid phase (BAu-4) and one gaseous phase (helium). The selected approach is based on the Eulerian-Eulerian multiphase model.

Specifically, the Volume of Fluid (VOF) model is a surface-tracking technique applied to a fixed Eulerian mesh, where the tracking of the interfaces between the phases is accomplished by the solution of a continuity equation for the volume fraction of the phases. A single momentum equation is solved throughout the domain, and the resulting velocity field is shared among the phases, as well as the energy equation [FLUENT].

These equations are implemented and solved in ANSYS FLUENT. The model also includes the effects of surface tension along the interface between the phases. The continuum surface force (CSF) model has been used here such that the addition of surface tension to the VOF calculation results in a source term ( $\vec{F}$ ) in the momentum equation. The contact angles between the phases and the walls are also specified.

#### 5.4.4.1. Governing equations:

Continuity equation for the volume fraction of the phases:

$$\frac{1}{\rho_q} \left[ \frac{\partial}{\partial t} (\alpha_q \rho_q) + \nabla \cdot (\alpha_q \rho_q \vec{v}_q) \right] = S_{\alpha_q} + \sum_{p=1}^n (\dot{m}_{pq} - \dot{m}_{qp}) \quad (2)$$

$$\sum_{q=1}^n \alpha_q = 1 \quad (3)$$

Where  $\alpha_q$  is the volume fraction of the phase q in a given cell (if  $\alpha_q=0$  the cell is empty of the phase q, if  $\alpha_q=1$ , the cell is full of the phase q and if  $0 < \alpha_q < 1$  the cell contains the interface between the phase q and one or more phases –the other phase in this case-),  $\rho$  is the density of the phase q,  $\dot{m}_{qp}$  is the mass transfer from phase q to phase p,  $\dot{m}_{pq}$  is the mass transfer from phase p to phase q and  $S_{\alpha_q}$  is the source term.

Momentum equation (dependent on the volume fractions of all phases through the properties  $\rho$  and  $\mu$  –dynamic viscosity-):

$$\frac{\partial}{\partial t} (\rho \vec{v}) + \nabla \cdot (\rho \vec{v} \vec{v}) = -\nabla p + \nabla \cdot [\mu (\nabla \vec{v} + \nabla \vec{v}^T)] + \rho \vec{g} + \vec{F} \quad (4)$$

Energy equation:

$$\frac{\partial}{\partial t} (\rho v E) + \nabla \cdot (\vec{v} (\rho E + p)) = \nabla \cdot (k_{eff} \nabla T) + S_h \quad (5)$$

Where energy, E, and temperature, T, are treated as mass-averaged variables:

$$E = \frac{\sum_{q=1}^n \alpha_q \rho_q E_q}{\sum_{q=1}^n \alpha_q \rho_q} \quad (6)$$

$E_q$  for each phase is based on the specific heat of that phase and the shared temperature. The properties  $\rho$  and  $k_{\text{eff}}$  (effective thermal conductivity) are shared by the phases. The source term,  $S_h$ , contains contributions from radiation, as well as any other volumetric heat sources.

Surface tension:

$$F_{\text{vol}} = \sum_{\text{pairs } ij, i < j} \sigma_{ij} \frac{\alpha_i \rho_i \kappa_j \nabla \alpha_j + \alpha_j \rho_j \kappa_i \nabla \alpha_i}{\frac{1}{2}(\rho_i + \rho_j)} \quad (7)$$

The contact angle between the fluid and the wall is used to adjust the surface normal in cells near the wall, instead of imposing this boundary condition at the wall itself:

$$\hat{n} = \hat{n}_w \cos \theta_w + \hat{t}_w \sin \theta_w \quad (8)$$

Where  $\hat{n}_w$  and  $\hat{t}_w$  are the unit vectors normal and tangential to the wall, respectively.

#### 5.4.4.2. Simulation results

A preliminary 2D transient analysis has been made focusing the geometry on the gap between the upper and the lower Ni-200 parts (a clearance of 0.1 mm has been chosen).

As previously mentioned, although 10% of the brazing atmosphere is hydrogen, the problem has been simplified to a biphasic flow:

- Phase 1: Helium ( $\rho = 0.1625 \text{ kg/m}^3$ ;  $\mu = 1.99 \cdot 10^{-5} \text{ Pa}\cdot\text{s}$ ).
- Phase 2: BAu-4 ( $\rho = 8330 \text{ kg/m}^3$ ;  $\mu = 5.3 \cdot 10^{-3} \text{ Pa}\cdot\text{s}$ ).

Since viscosity values for the filler metal have not been found in literature, the viscosity used here has been obtained from Au and Ni data [Are 04]. Regarding the liquid-vapour surface tension coefficient ( $\gamma_{lv} = 1.1019 \text{ N/m}$ ), it has been obtained from BAu-4 constituents using Guggenheim's equation [Are 04]. The contact angle has been taken from experiments with Inconel 625 as base metal (61% Ni vs 99% for Ni-200 alloy) in a furnace with argon as protective atmosphere [Rok 11].

The resulting advance of the interface between both phases which simulates the spreading of the filler metal can be compared (Fig. 39) with the obtained from the flow equation for horizontal brazing gaps (9) [ASM 93], which is derived from Washburn's equation, in order to validate the numerical method.

$$\frac{dh}{dt} = \frac{1}{2} \cdot \sqrt{\frac{\gamma_{lv} \cdot d \cdot \cos \theta}{\mu \cdot t}} \quad (9)$$

Where  $h$  is the filler metal penetration in the joint (m),  $t$  is the brazing time (s),  $d$  is the joint clearance (m),  $\theta$  is the contact angle,  $\gamma_{lv}$  is the liquid-vapor surface tension (N/m) and  $\mu$  is the molten filler metal viscosity (Pa s).

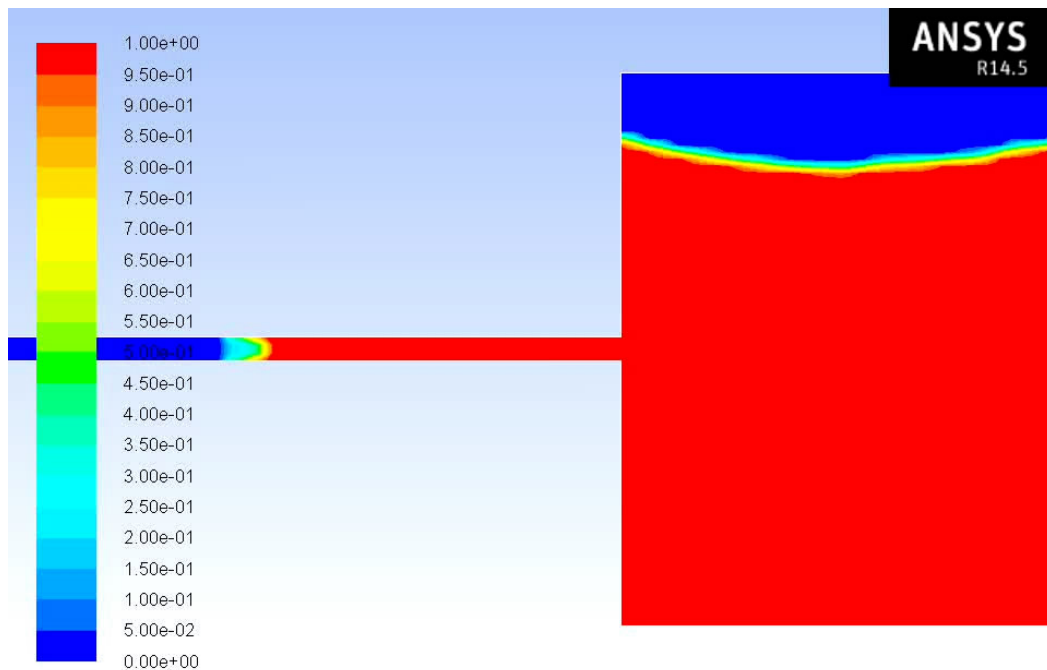


Fig. 38. Position of the BAu-4/He interface after  $1.316 \cdot 10^{-3}$  s (legend: volume fraction of phase BAu-4).

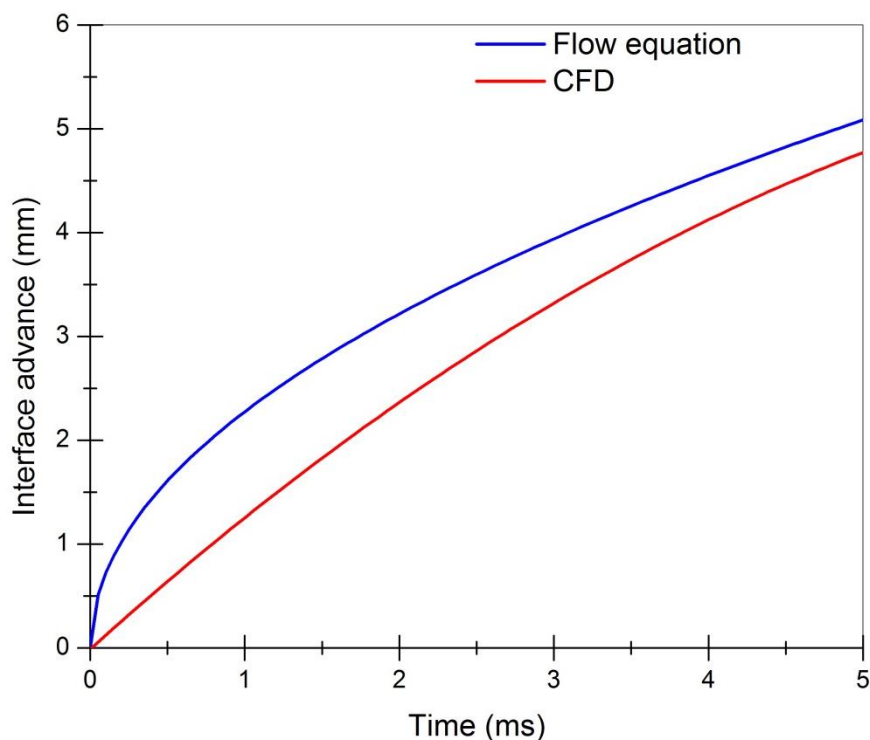


Fig. 39. Advance of the interface between BAu-4 and helium.

Fig. 39 shows the interface advance is quite similar in both cases, mainly taking into account that these results have been obtained for a short time, due to the very small time step ( $10^{-6}$  s) used for solution stability, and the fact of Washburn's equation shows a good agreement with experimental data for long-time predictions, since the capillary penetration has started to stabilize and the quasi-steady state assumption becomes more appropriate [Xu 04]. Beyond the validation of the model, this result confirms the flow due to capillary forces is very fast at the

beginning, which involves the need of an accurate control system for the heating process, as well as a careful design of the gap, the filler metal ring and its groove.

### 5.4.5. Transmutation assessment

In [Que 12] the possibility of producing long half-life transmutation isotopes from the brazing materials, particularly from Ag, was mentioned. This design proposal does not include Ag based filler-metals; however, an assessment of transmutation phenomenon has been done.

The activation code ACAB has been used for the calculations [Sanz 00]. The composition and density of the different materials have been taken from [Bar 03], [Matweb] and [TBraze], whereas the volumes of the components have been taken from the design adapted for pipes of 75 mm diameter and 5 mm thickness. In the same way, austenitic steel 316-LN(IG) has been chosen for these evaluations, so the activation results would be more favourable in the case of using a RAFM steel like EUROFER.

The reference irradiation scenario and the neutron flux has been taken from [Fis 12], considering the placement of the connector in the upper port of the vacuum vessel without any extra shield, as service connector for the breeding blanket modules. A conservative neutron flux density of  $2 \cdot 10^{12} \text{ n cm}^{-2} \text{ s}^{-1}$  has been considered.

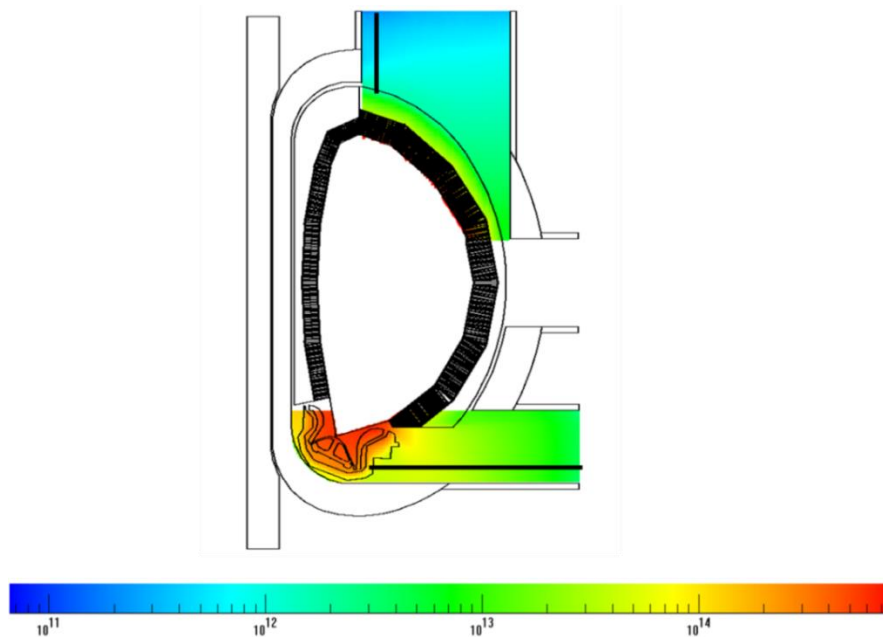


Fig. 40. Mesh tally distribution of the total neutron flux density [ $\text{cm}^{-2} \text{ s}^{-1}$ ] in the upper and the divertor port areas [Fis 12].

Surface gamma dose rate and specific activity have been obtained for the main components of the brazed connector (structural bodies, filler metals and coil; bolts have not been considered) at shutdown and 5 days, 12 days and 1 year after it.

Surface gamma dose rate ( $\text{Sv h}^{-1} \text{ cm}^{-3}$ )					
time (sec)	Ni-200	SS-316LN(IG)	BAu-4	BNi-5	Cu
<b>1 (shutdown)</b>	32.57	15.44	27.71	31.22	27.78
<b>4.24E+05 (5 days)</b>	28.15	4.853	11.27	20.08	2.391
<b>1.05E+06 (12 days)</b>	26.2	4.553	5.497	18.67	2.373
<b>3.15E+07 (1 year)</b>	3.735	1.006	0.547	2.638	2.09

Table 17. Surface gamma dose rate in the components of the brazing connector.

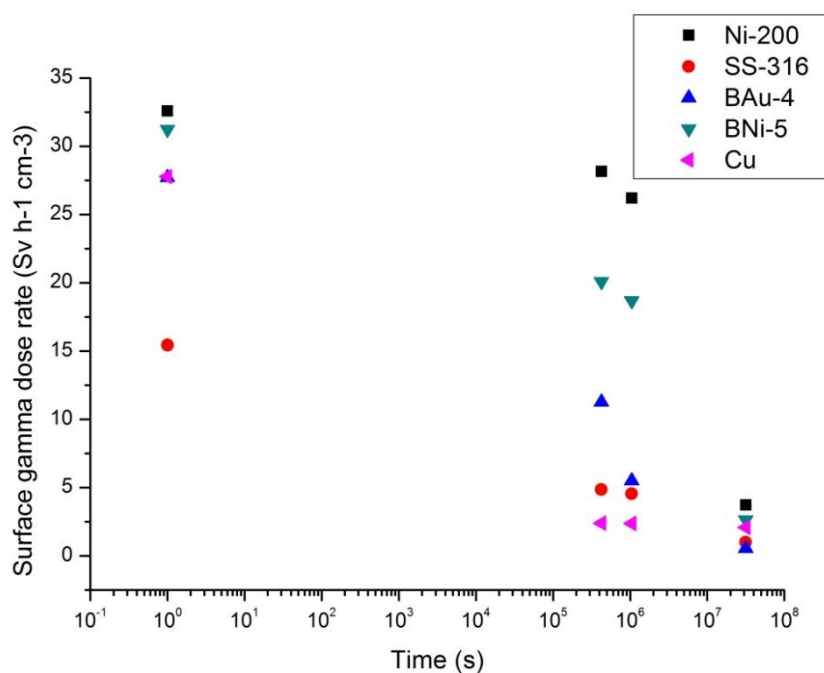


Fig. 41. Surface gamma dose rate in the components of the brazing connector.

Specific Activity ( $\text{Bq cm}^{-3}$ )					
time (sec)	Ni-200	SS-316LN(IG)	BAu-4	BNi-5	Cu
<b>1 (shutdown)</b>	2.504E+09	1,069E+09	6.490E+09	1.774E+09	2.570E+09
<b>4,24E+05 (5 days)</b>	1.935E+09	7,938E+08	1.787E+09	1.295E+09	3.840E+07
<b>1,05E+06 (12 days)</b>	1.853E+09	7,574E+08	7.122E+08	1.227E+09	3.582E+07
<b>3,15E+07 (1 year)</b>	5.131E+08	4,004E+08	8.723E+07	3.148E+08	3.225E+07

Table 18. Specific activity in the components of the brazing connector.

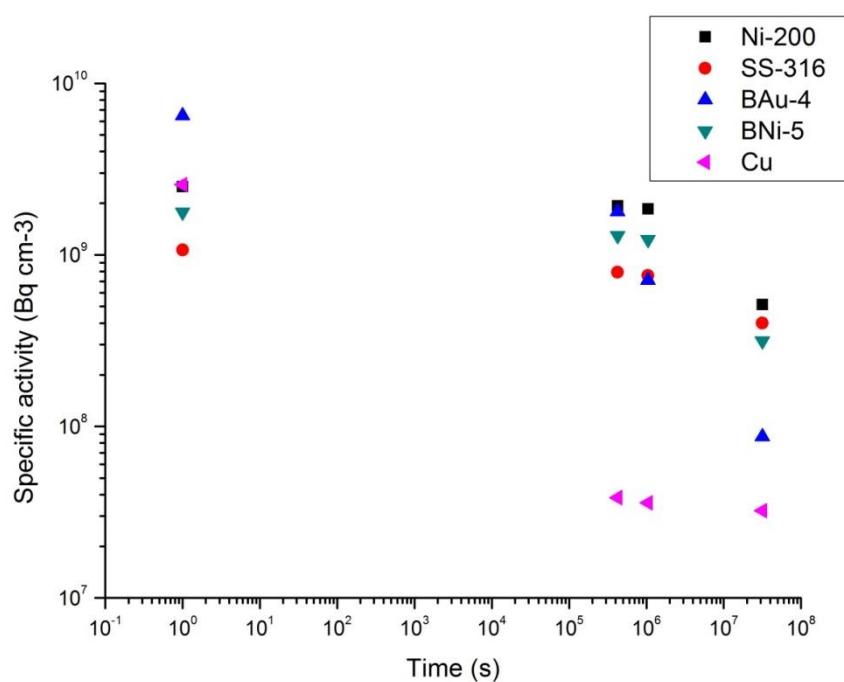


Fig. 42. Specific activity in the components of the brazing connector.

The results show the specific activity is not high, and decays very fast in the case of Cu, and quite fast in the case of Ni-200, BAu-4 and BNi-5 (Table 17, Table 18, Fig. 41, Fig. 42). Taking into account the standard values of surface gamma dose rate to be able to use conventional ( $<0.01 \text{ Sv h}^{-1}$ ) or advanced ( $<10000 \text{ Sv h}^{-1}$ ) RH equipment [EI-G 07], the obtained values for scheduled maintenance ( $<30 \text{ Sv h}^{-1}$ ) does not allow using conventional RH equipment but the grade of radiation hardening of the RH components should not be too high.

In addition to this, Table 19 shows the list of isotopes which contribute most to the total specific activity and their half-life.

Ni-200		SS-316		BAu-4		BNi-5		Cu	
<b>Specific activity <math>&gt; 10^9 \text{ Bq cm}^{-3}</math> after shutdown</b>									
Isotope	Half-life	Isotope	Half-life	Isotope	Half-life	Isotope	Half life	Isotope	Half-life
Fe55	2.7 y	Cr51	27.7 d	Au196	6.2 d	Cr51	27.7 d	Cu62	9.7 min
Co57	270.9 d	Mn56	2.6 h	Au197m	7.7 s	Co57	270.9 d	Cu66	5.1 min
Co58	70.8 d	Fe55	2.7 y	Au198	2.7 d	Co58	70.8 d		
Co58m	9 h					Co58m	9 h		
<b>Specific activity <math>&gt; 10^8 \text{ Bq cm}^{-3}</math> after shutdown</b>									
Isotope	Half-life	Isotope	Half-life	Isotope	Half-life	Isotope	Half life	Isotope	Half-life
Co60	5.27 y	V52	3.7 min	Co57	270.9 d	Al28	2.2 min	Co60	5.27 y
Co60m	10.5 min	Mn54	312.5 d	Co58	70.8 d	V52	3.7 min	Co60m	10.5 min
Ni57	35.6 h	Co57	270.9 d	Au196m	8.1 s	Fe55	2.7 y	Ni65	2.5 h
		Co58	70.8 d			Co60	5.27 y		
		Co58m	9 h			Co60m	10.5 min		
		Mo99	66 h			Ni57	35.6 h		
		Tc99m	6 h						
<b>Specific activity <math>&gt; 10^7 \text{ Bq cm}^{-3}</math> after shutdown</b>									
Isotope	Half-life	Isotope	Half-life	Isotope	Half-life	Isotope	Half life	Isotope	Half-life
				Fe55	2.7 y				
				Co58m	9 h				

Table 19. List of isotopes with the largest contribution to the total specific activity.

Most of these isotopes have short half-life. Only  $\text{Co}^{60}$  (5.27 y) and  $\text{Fe}^{55}$  (2.7 y) have medium half-life. They both come from the nickel alloys (Ni-200 and BNi-5), from the copper coil ( $\text{Co}^{60}$ ) and from the austenitic steel ( $\text{Fe}^{55}$ ), but only the contribution of  $\text{Fe}^{55}$  coming from Ni-200 to the total specific activity is significant.

The production of some of these isotopes can be reduced or avoided by making stricter the requirements for the materials chemical composition, as well as by using reduced activation steel as piping material. Anyway, transmutation in the current materials does not seem to be an issue, since the reduction of mass for the main elements of the different components is very low.

#### 5.4.6. Tritium permeation assessment

A key requirement for pipe joining systems is to avoid tritium permeation from the fluid circulating inside the pipe to the environment. Thus, a model of the connector for 75 mm diameter pipes has been created and implemented in the 1-D code TMAP7. Although Ni-200 is not compatible with flowing PbLi, the calculation has been conservatively made assuming PbLi

is flowing inside at 500°C with a volumetric flow of  $3.4454 \cdot 10^{-4} \text{ m}^3/\text{s}$  and a tritium partial pressure of 100 Pa (upper limit for HCLL PbLi pipes).

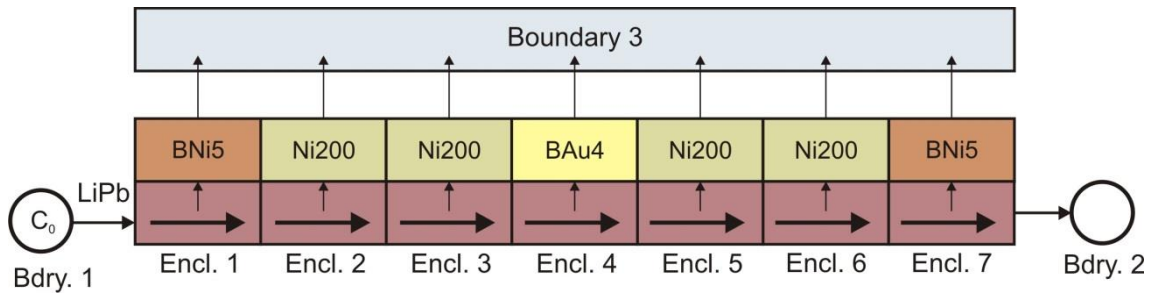


Fig. 43. Flow process diagram implemented in TMAP7.

Like in the case of the TMAP7 model developed in Chapter 3, we assume the occurrence of the diffusion limited transport model, neither trapping nor Soret effect are included, and only T is considered as diffusive specimen and  $T_2$  as enclosure specimen. The model is focused in the central part of the connector, without considering tritium diffusion across the SS-316 parts, which is expected to be negligible. Furthermore, the internal BNI-5 ring located in the upper side has been conservatively removed.

The governing equations for the different solid segments and interfaces between functional enclosures, boundaries and solid segments are the following:

Concentration equilibrium at the interfaces PbLi-solid segments:

$$\frac{C_{T,LiPb}}{K_{S_{T,LiPb}}} = \frac{C_{T,mat}}{K_{S_{T,mat}}} \quad (10)$$

Sieverts' law at the interface PbLi-Boundary 3:

$$C_{T,mat} = K_{S_{T,mat}} \cdot \sqrt{P_{T_2,gas}} \quad (11)$$

Diffusion across solid segments (Fick's law):

$$J_{T,mat} = -D_{T,mat} \cdot \frac{\partial C}{\partial x} \quad (12)$$

No data have been found in literature about the tritium transport properties of BAu-4, BNI-5 and Ni-200 (99%Ni), so their diffusivity and solubility have been taken from their main constituents. In the case of gold tritium solubility, the copper one has been conservatively used.

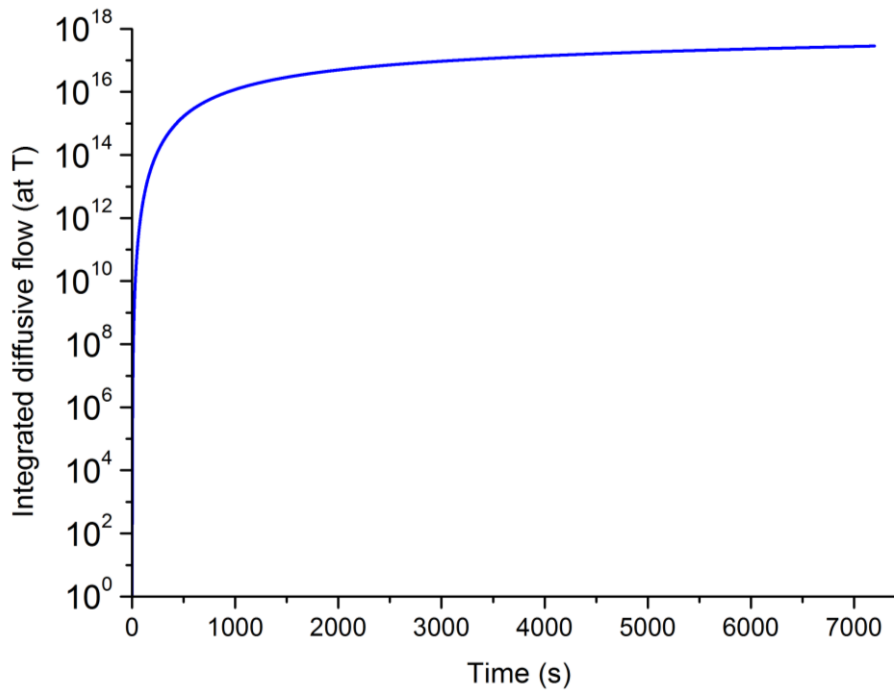


Fig. 44. Tritium integrated diffusive flow to the environment.

The results show the permeation of tritium to the environment through the connector is certainly low ( $4.7 \cdot 10^{-7}$  g/pulse), as well as the mobile inventory in the material segments after one pulse ( $5.29 \cdot 10^{22}$  at T; 0.088 g T). Taking into account the conservative assumptions, these results are promising for helium and water pipes connectors –although more complex phenomena could be expected in the last case-. On the other hand, the model should be adapted and analysed for the alternative base and filler metals selected for PbLi pipes.

### **5.4.7. Remote handling implementation**

#### **5.4.7.1. Positioning and alignment system. Disconnection sequence (bolted union option)**

The positioning and alignment of the two halves of the connector are provided by a component called RH aligner (Fig. 45). The RH aligner grips the pipe arising from the blanket module which includes the lower part of the brazed connector. The vertical position of the aligner is fixed by a block (Fig. 46 right), whereas the pipes ledges fit in the aligner guides. On the other hand, the incoming upper part is fixed by a clamp with a hinge mechanism. The vertical positioning is achieved by means of a spindle, while a concave cylindrical bearing together with a rail-slot concept correct the movement.

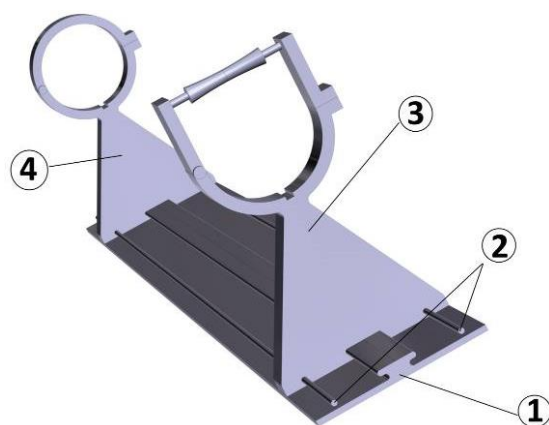


Fig. 45. RH aligner. 1) plate; 2) guides; 3) upper clamp; 4) lower clamp.

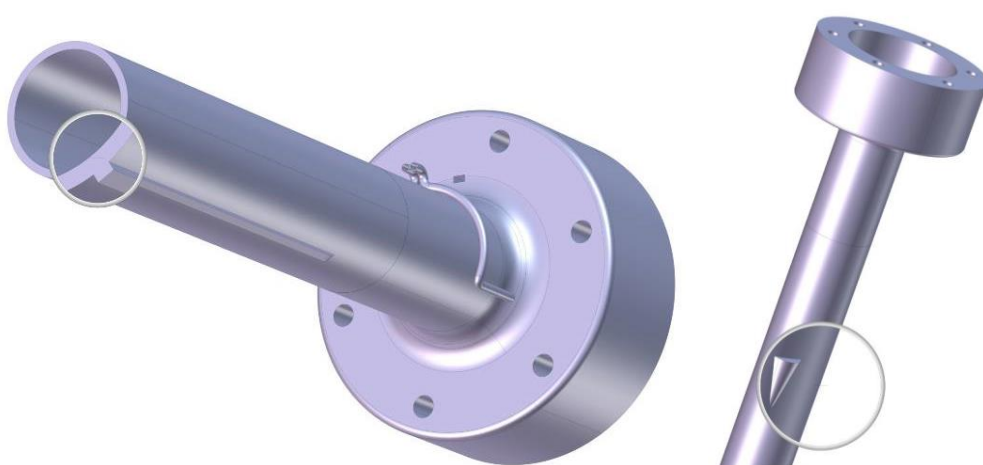


Fig. 46. Interfacing elements for the installation/removal of the brazing connector.

Captive bolts are used to stiffen the connector, which allows screwing/unscrewing by a manipulator. Additionally, a pin is used to correct misalignments due to the tolerance of the aligner guides.

The brazing connector disconnection sequence is described by the following pictures. The assembly sequence is approximately the reverse of the connection sequence.

- 1) The pipes are drained. The removal of the brazing connector starts.



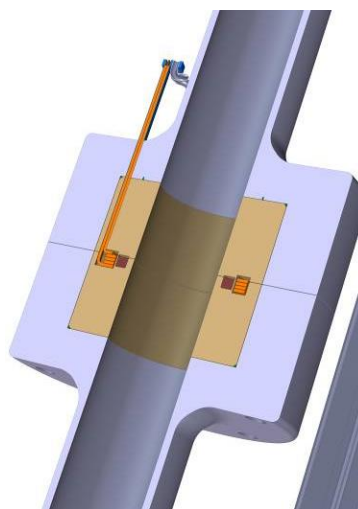
- 2) The captive bolts are unbolted. The procedure of unbolting is diametrically opposite to the bolting sequence. Depending on the required torque, it may be repeated in several stages.



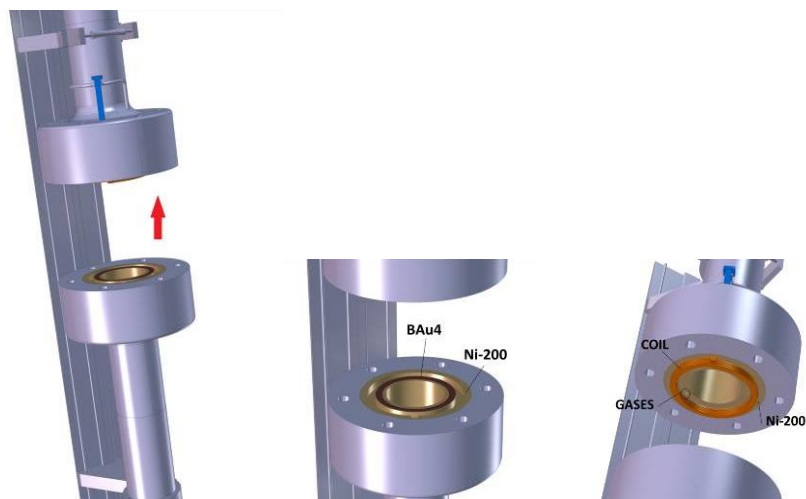
- 3) The multi-function plug (coil power and cooling supplies, atmosphere supply/inspection system) is unplugged.



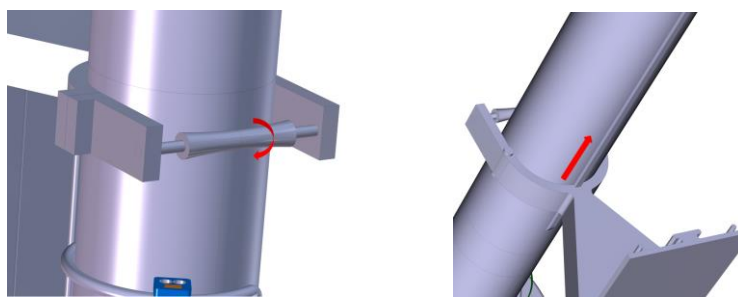
- 4) The induction system heats the BAu-4 filler metal to debraze the Ni-200 parts joint.



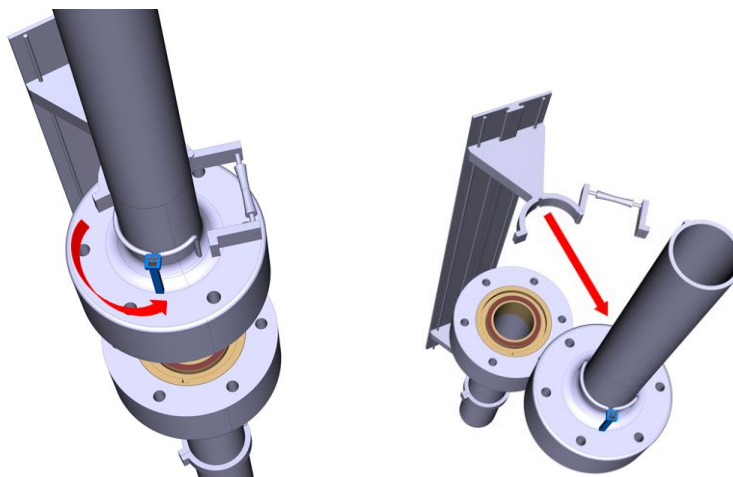
- 5) When the BAu-4 reaches the liquidus temperature, the heating stops and the upper half of the connector is separated from the lower one by means of the RH aligner.



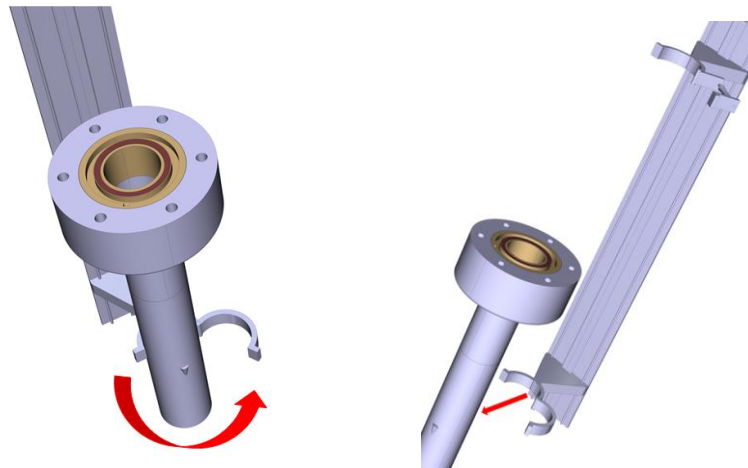
- 6) The upper pipe slides into the upper clamp to get away from the lower pipe. The concave cylindrical bearing and the rain-slot concept correct the upper pipe vertical movement.



- 7) The upper clamp is opened and the upper pipe is extracted.



- 8) The lower clamp opens and releases the lower pipe. Then the RH aligner can be removed.



#### 5.4.7.2. Hanford Purex clamping concept

A bolted union is not a feasible option since the bolting/unbolting processes slow down the maintenance operations. Furthermore, as commented in Subsection 5.3.2 regarding the installation/removal of the jacket flange connector, a simpler RH bolting tool should be used in order to avoid the issues linked to robotic manipulators (radiation, space, operation time, complexity, etc.). In consequence, the possibility of combining the brazing connector and other concepts of quick mechanical connections to provide stiffness has been proposed. Specifically, the combination of the brazed connector and the so-called Hanford Purex (H-P) clamp has been assessed.

The Purex clamp is originally conceived to be mounted in elbows, so it can be adapted to linear connections and its tightening mechanism can be simplified. The solution which is shown in Fig. 47 and Fig. 48 consists on a central ring with gear profile, and three jaws placed at 120°. There is also a spring which provides the force which ensures the strength of the assembly.

The idea is to provide a rotation movement of the jaws for placing/removing them in/from the neighbourhood of the pockets in the lower SS-316 part of the brazed connector, and a translation movement along the axis of the pipe for releasing/inserting the jaws from/into the pockets (Fig. 48).

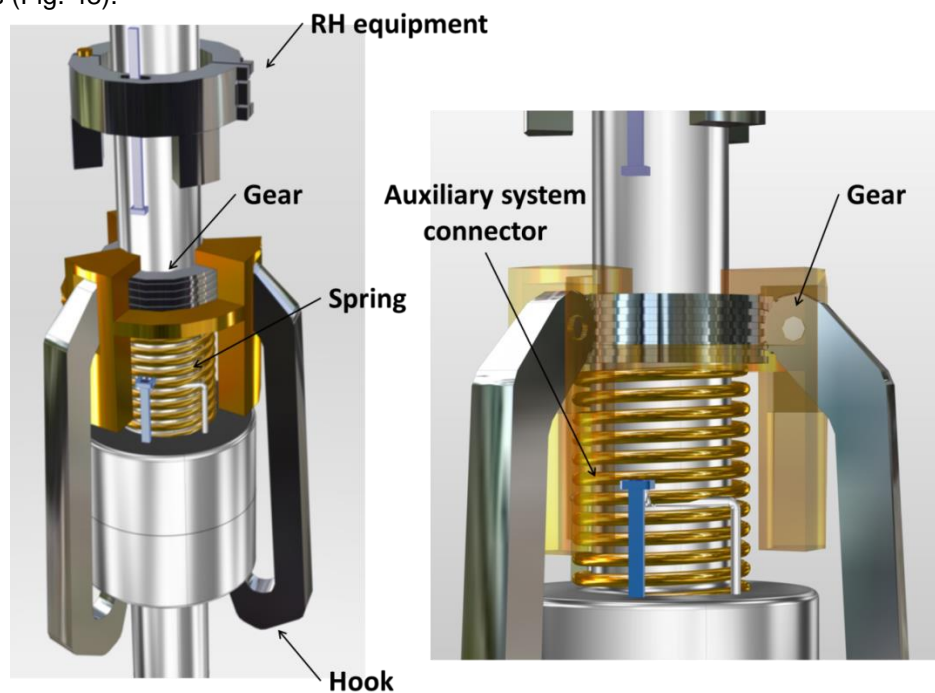


Fig. 47. Modification of the Hanford Purex clamp. RH equipment and interface.

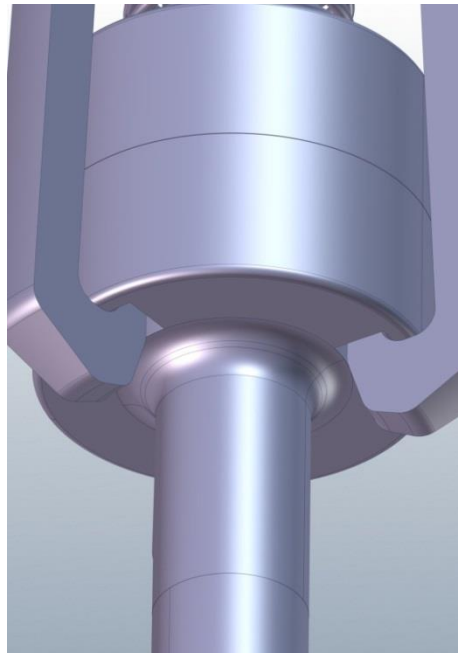


Fig. 48. Pockets in the rear face of the lower SS316 body to insert the jaws.

A RH device has been designed to connect the auxiliary systems (electric supply, coil cooling system and atmosphere & inspection system) for brazing/debrazing operations, as well as to install/uninstall the external clamp (Fig. 50 and Fig. 51). It consists on a ring which hugs the pipe by means of a hinge and a quick fastener. It moves along the pipe axis on bearings.

This RH device pushes down the central ring and compresses the spring. Then the upper heads of the jaws engage the central ring, so the jaws open. Once the assembly is pushed down and aligned by two pins and holes placed in the brazed connector SS-316 bodies, the compressing force ends and the jaws fit in the pockets of the bottom of the lower SS316 body. To uninstall the assembly a new compression of the spring is needed to allow the jaws leaving the pockets.

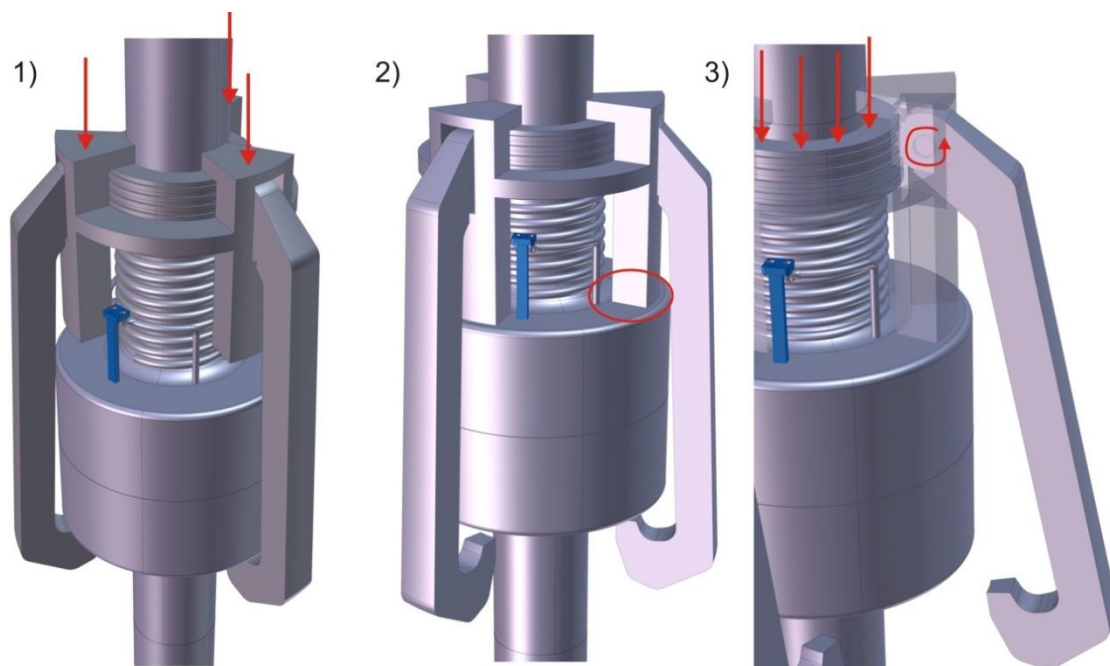


Fig. 49. Releasing sequence of the clamp based on the Hanford Purex concept.

Fig. 49 shows the releasing sequence. In the initial situation, the jaws are inserted in the pockets placed in the lower part of the connector. 1) Then the 'jaws ring' is pushed down until (2) it reaches the SS-316 upper surface and the jaws abandon the pockets. 3) The "jaws ring" is kept in this position (not defined here) while the central ring with rear profile is pushed down, which allows the jaws rotating and leaving the lower part of the connector.

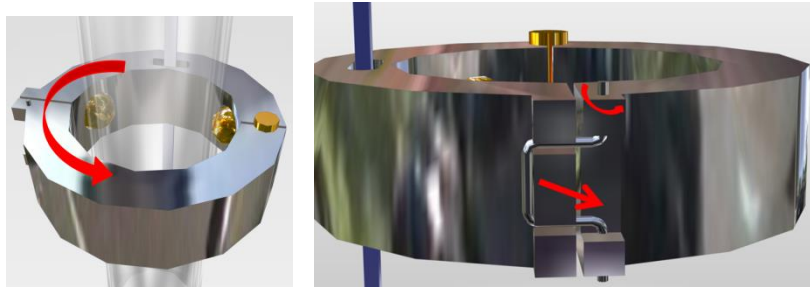


Fig. 50. RH device.

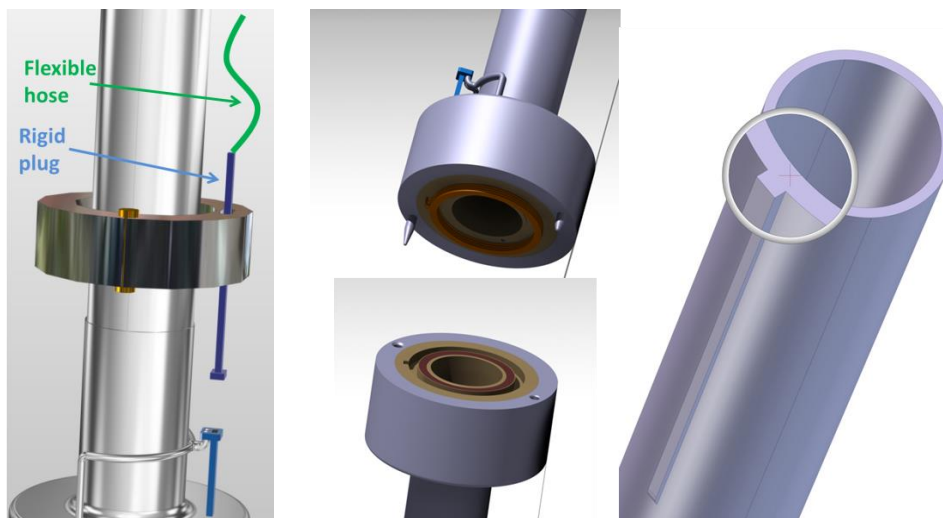


Fig. 51. Flexible hose connected to the rigid multi-function plug (left). Guide pins to align the upper and the lower parts of the connector (center). Guide rail for the RH equipment (right).

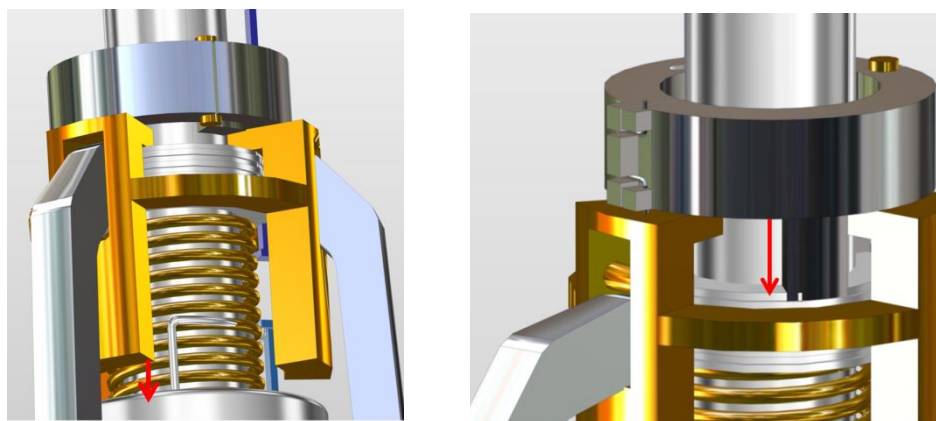


Fig. 52. Interface between the RH device and the clamp.

This simple design with few components improves the reliability of the clamp. Furthermore, the movement of the three hooks is synchronized, and the spring keeps the hooks closed at rest position, which avoids the accidental disconnection of the clamp.

A potential issue related to the use of a spring could be the degradation of this component due to the harsh environmental conditions (high temperature and neutron irradiation) expected in the vacuum vessel upper ports, which would involve a modification in its elastic behaviour.

The neutron flux in the upper ports decreases from  $2 \cdot 10^{12} \text{ n cm}^{-2} \text{ s}^{-1}$  to  $2 \cdot 10^{11} \text{ n cm}^{-2} \text{ s}^{-1}$  if a shield of 0.2 m is used. From these values, the fluence in the connector location has been calculated considering the replacement of a “starter” blanket ( $\leq 20 \text{ dpa}$ ) would be necessary after  $\sim 2 \text{ fpy}$  or  $\sim 5 \text{ fpy}$  in the case of a second blanket with a neutron damage capability of  $\sim 50 \text{ dpa}$  (Table 20).

Neutron flux ( $\text{n cm}^{-2} \text{ s}^{-1}$ )	Full power years (fpy)	Neutron fluence ( $\text{n cm}^{-2}$ )
$2 \cdot 10^{11}$	2	$1.26 \cdot 10^{19}$
$2 \cdot 10^{11}$	5	$3.16 \cdot 10^{19}$
$2 \cdot 10^{12}$	2	$1.26 \cdot 10^{20}$
$2 \cdot 10^{12}$	5	$3.26 \cdot 10^{20}$

Table 20. Neutron fluence in the modified Hanford Purex clamp spring.

According to [MRP 07], springs exposed to a fluence screening value of  $1.3 \cdot 10^{20} \text{ n cm}^{-2}$  are potentially susceptible to irradiation-enhanced stress relaxation and irradiation creep. Therefore, only in the case of a blanket without extra shield of 0.2 m and replaced each 5 fpy this issue is relevant.

On the other hand, several materials like Inconel or XC 80 steel (AISI 1074-SAE) could be used to avoid the spring relaxation at the maximum temperature in the connector for PbLi pipes ( $\sim 500^\circ\text{C}$ ).

In summary, both requirements (neutron fluence and temperature) seem to be separately fulfilled, although the possibility of synergic effects makes the spring performance under real conditions remains uncertain.

#### 5.4.7.3. Quick geared triple hook concept

This concept has been designed as an alternative to the H-P clamp. As in the case of the H-P clamp, the design includes an interface with the proposed RH equipment.

The relative movement between the mechanical part of the connector and the pipe is achieved through a geared part in the pipe and gears in the head of the hooks that transfer the movement from the cover to the pipe. The heads of the hooks allow free turn without turning the hook.



Fig. 53. Quick geared triple hook concept.

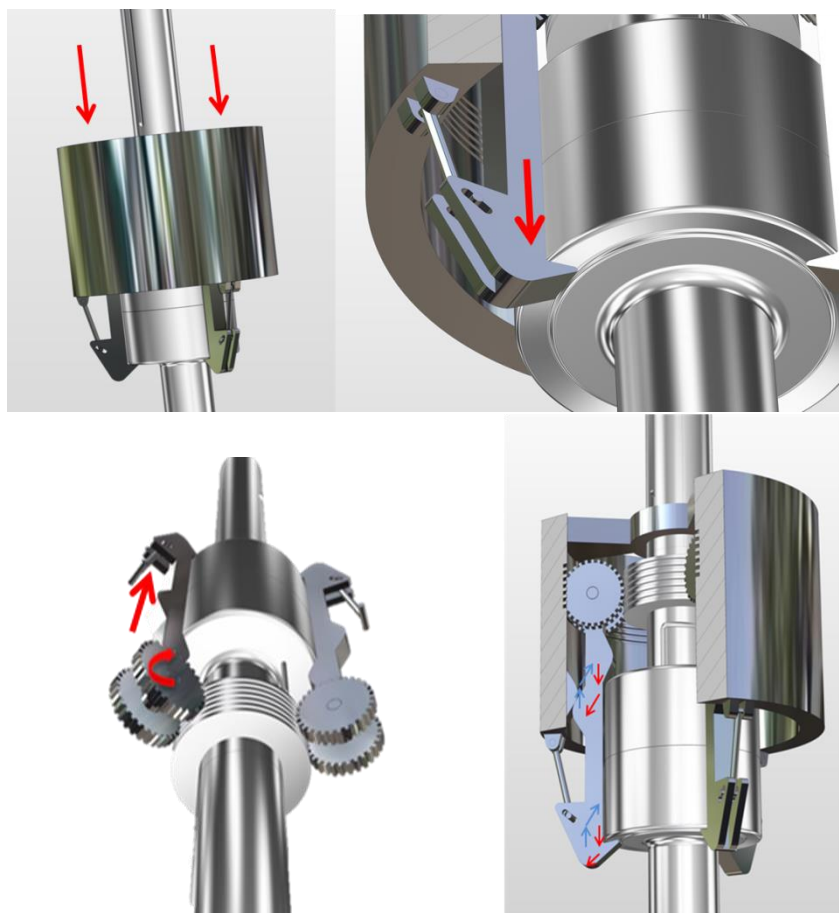


Fig. 54. Movements in the clamp.

The main advantage with respect to the previous concept is that there is not any spring, so the risk of failure by degradation of the mechanical properties is reduced. However, the complexity of the design with a larger number of geared components increases the possibility of jamming. A RAMI analysis would be necessary to compare the reliability of this design and the modified H-P clamp one.

#### **5.4.8. Mechanical properties of the brazed joint and alternative filler metals**

A number of variables like process atmosphere, brazing temperature and time, clearance and condition of surface affect the capillary flow of the filler metal during brazing and, consequently, the mechanical strength of the joint. Although theoretical or modelling approaches can be followed, experiments are by far the best way to optimize these features, showing that the type of filler metal is a more important factor affecting the mechanical strength of the joint than the clearance and the brazing time [Nis 98]. Regarding this, previous experimental works show brazed joints using BAu-4 and BNi-5 as filler metals nearly keep the yield strength of the base metal, and joint failures are produced in the base metal [Nis 98] [Lug 79] [Pie 95]. This is a very important fact, since it can make possible to do without the external clamp. This would ensure much better integrability of the connector with the environment and compatibility with the current blanket maintenance schemes. Pipes maintenance time would be drastically reduced since the brazing technique could be adapted for joining a set of pipes with only one device.

On the other hand, taking into account that BAu-4 contains 82% of gold, which is expensive, it is advisable to test alternative filler metals like Ni-Pd-Cr-Fe-B-Si alloys, considering the mechanical properties of brazed joints made with some of them are comparable to those of BAu-4 joints at high temperature. The shear strength at 538°C of joints using Ni-Pd-Cr alloys was found equal or superior to those of BAu-4 [Bos 83]. In addition, the joint ductility at room temperature and the corrosion susceptibility of such alloys is similar to those of BAu-4 [Bos 83].

Another issue to be assessed is the possibility of suppressing the internal Ni-200 parts to directly braze the stainless steel parts. As already mentioned, stainless steel tends to form a chromia scale in a helium atmosphere at elevated temperatures [Pie 95], but it would be interesting to know the influence of this fact in the re-brazeability and general behaviour of the joint for this specific application, taking into account the number of brazing/debrazing cycles should be very limited. This could be convenient in order to adapt the connector design to PbLi pipes, although austenitic-steel is not recommended from the point of view of corrosion (unless corrosion barriers like coatings are used) and activation. As mentioned in Sub-subsection 5.4.1.3, the study of the application of this method for joining RAFM steel pipes is recommended.

### **5.5. State of the art of non-destructive testing technologies**

#### **5.5.1. Introduction**

As complement to the description of the flange & QDS connector and the brazing connector designs given in Sections 5.3 and 5.4, the state of the art of three selected non-destructive testing technologies for welded joints in pipes, which can be also used to inspect any mechanical component, is summarized here.

Inspection methods are needed to detect all the discontinuities and defects in weld joints and to ensure their quality. In first place, it is important to distinguish between 'discontinuity' and 'defect'. Discontinuity refers to 'an interruption of the typical structure of a material, such as a lack of homogeneity in its mechanical, metallurgical or physical characteristics; a discontinuity is not necessarily a defect'. On the other hand, a defect refers to 'a condition or conditions that render a part unable to meet applicable minimum acceptance standards or specifications'. All

defects are discontinuities, but not all discontinuities are defects. A defect can be considered an unacceptable discontinuity. Considering discontinuities in general, the list includes cracks, inclusions, incomplete fusion, incomplete joint penetration, overlap, porosity, undercut and poor fillet weld profiles [AWS 04].

Visual inspection is a very effective inspection method which is included in most of effective Quality Control Programmes as the primary weld inspection method. It has been shown repeatedly that visual inspection, conducted by properly trained inspectors, results in the discovery of the vast majority of those defects which would only be discovered later by some more expensive non-destructive testing methods. While visual inspection is limited to materials' surface-only examination, it often detects the most damaging defects.

When human visual inspection is not possible due to the need of operating in severe environments (e.g. high temperature and radiation), the use of cameras is a very valuable alternative. Moreover, the present development of digital cameras and sophisticated imaging process software allows automatizing the inspection procedures and thus increasing their productivity.

On the other hand, the dominant technology at present for transducers in the field of ultrasonic non-destructive testing is piezoelectric. However, some industrially important applications, like the inspection of components operating at high temperature or while in motion, are difficult tasks for standard piezoelectric probes since mechanical contact is required. In these cases, contactless NDT techniques can be an attractive alternative. Among the available options, Electromagnetic Acoustic Transducers (EMATs) can generate and detect ultrasonic waves without the need for a physical contact between the probe and the test object, as their operation relies on electromagnetic, rather than mechanical coupling. Since EMATs do not require any coupling liquid, the experimental procedures for inspection set-up are simplified and a source of uncertainty is eliminated, yielding highly reproducible tests that make EMATs suitable to be used as calibration probes for other ultrasonic tests. A further advantage of EMATs is the possibility of exciting several wave-modes by appropriate design of the transducer. Unfortunately, EMATs are also characterized by a relatively low signal-to-noise ratio and by a complex operation relying on different transduction mechanisms that make their performance dependent on the material properties of the test piece [Rib 11].

Besides this, laser ultrasonic techniques use high-energy laser pulses to produce ultrasound and interferometric techniques to detect the surface vibrations of the return signals. Certainly, the generation of ultrasonic waves was one of the first applications of lasers. However, the detection of these waves posed the biggest challenge for its adoption in industrial applications. In the early 1980's, Krautkramer, now a part of GE Measurement and Control Solutions, began the development of laser ultrasonics for industrial applications. They were unsuccessful as the technology had not advanced, yet, to a level that could permit practical cost effective solutions. However, Krautkramer can be credited with being the first company to venture into the commercialization of laser ultrasonics, which until then, remained a research topic in universities and R&D centres. The actual commercialization of laser ultrasonics started in the 1990's, with several companies attempting to gain a foothold in a market that was still considered nascent and the technology still immature. In the late 1990's, Tecnar Automation licensed its laser ultrasonic technology for wall thickness measurement of seamless steel tubes from NRC, which was developed in collaboration with Timken Steel. This solution for wall thickness measurement of seamless steel tubes is considered to be the single biggest success of laser ultrasonics. Tecnar Automation is the sole licensee of this technology and sells this system to steel tube mills globally, with considerable success.

Despite cost challenge and slow acceptance of this technology, several experts strongly believe that it has the potential to become the standard NDT technology in certain applications.

## **5.5.2. Peltier cooled cameras for visual inspection**

The possibility of converting an optical image into an electronic signal by means of an image sensor and subsequently performing image numeric processing is very valuable for remote visual inspection. Most currently used image sensors are digital charge-coupled device (CCD) and complementary metal-oxide-semiconductor (CMOS) active pixel sensors. The main difference between both technologies is that CCD sensors convert charge accumulated on a pixel to voltage on the printed circuit board, whereas CMOS sensors do the conversion at the pixel level [Stemmer].

CCD's dynamic range (ratio of saturation level to signal threshold) is about twice that of a CMOS sensor. This is also related to the noise advantage that CCDs have over CMOS sensors. It means that generally if an application needs a high dynamic range (also known as bit depth or colour depth), CCDs are likely to give better results. By contrast, CMOS sensors are marginally more responsive to light.

The sensors in CMOS cameras have lower power consumption than CCD sensors; however, other circuits in the camera may require more power than CCD cameras. Low-end CMOS devices generally have lower power requirements, but high-speed CMOS designs generally have higher power requirements than CCD cameras.

In general, CMOS sensors are noisier than CCD sensors and these traditionally have a better uniformity of response to a given light level (hot pixels, warm pixels, dead pixels). CCDs have a single amplifier for all pixels whereas CMOS sensors have an amplifier per pixel. Differences in the pixel-to-pixel amplification lead to non-uniformity. However, post-processing (flat-field correction) can be used to correct for this.

CMOS sensors have an advantage over CCD sensors when it comes to speed. This is partly because more components are integrated within the chip, helping to give lower inductance, capacitance and propagation delays. There are also major differences when only part of the sensor's area is required for read-out. CCD sensors are limited to a vertical partial scan (entire rows have to be read-out). In order to see speed advantages, the partial scan on a CCD needs to be centred on the middle row of the sensor. By contrast, CMOS sensors allow any region of the sensor to be read-out with a speed increase based on the number of pixels. Some CMOS sensor designs also allow multiple regions to be read off the sensor.

A further difference between CCD and CMOS sensors is the way they deal with over-exposure. CCD sensors can suffer from 'smearing' around over-exposed pixels. Smearing is caused by charge in overexposed pixels overflowing into the shift register. This has the effect of a bright column of pixels extending above and below the offending pixel. CMOS sensors have an immunity to smear as they have no shift registers. For CCD sensors specific solutions have to be designed.

### **5.5.2.1. Thermoelectric cooling**

Some undesirable electrons which are not the result of light photons hitting the sensor surface will be stored in any pixel. Some of these electrons result from thermal noise, a random effect due to the interaction of heat with the CCD/CMOS chip material. The electric charge of these unwanted electrons (electrons that would exist in the pixel even if there were no light coming in contact with the chip) is called dark current.

The effect of dark current is to limit the practical length of a CCD/CMOS exposure time: ultimately, dark-current electrons saturate the pixels so that no additional photon-induced electrons can be generated. Thus, the lower the dark current, the longer a CCD/CMOS exposure can be and image quality improves. This is particularly useful when the ambient light intensity is low, like in the interior of the DEMO vacuum vessel during visual inspection.

Dark current can be very significantly reduced by lowering the sensor temperature, which allows extending the exposure time. Thermoelectric cooling is the most common method of image sensor cooling. It is based on the phenomenon of heat absorption at the junction of two rods of

metal or semiconductor when a current is made to pass through them (Peltier effect). Due to this effect, the cooler acts as a heat pump, pulling heat from the CCD/CMOS detector onto the Peltier cooling device, and dissipates the heat via radiating fins. Some cameras employ a two-stage Peltier cooler to improve the effectiveness of the device.

Peltier coolers incorporate a regulating system in an effort to keep the CCD detector at the desired constant temperature. In reality, however, these devices do not function precisely, and the temperature may vary slightly with time.

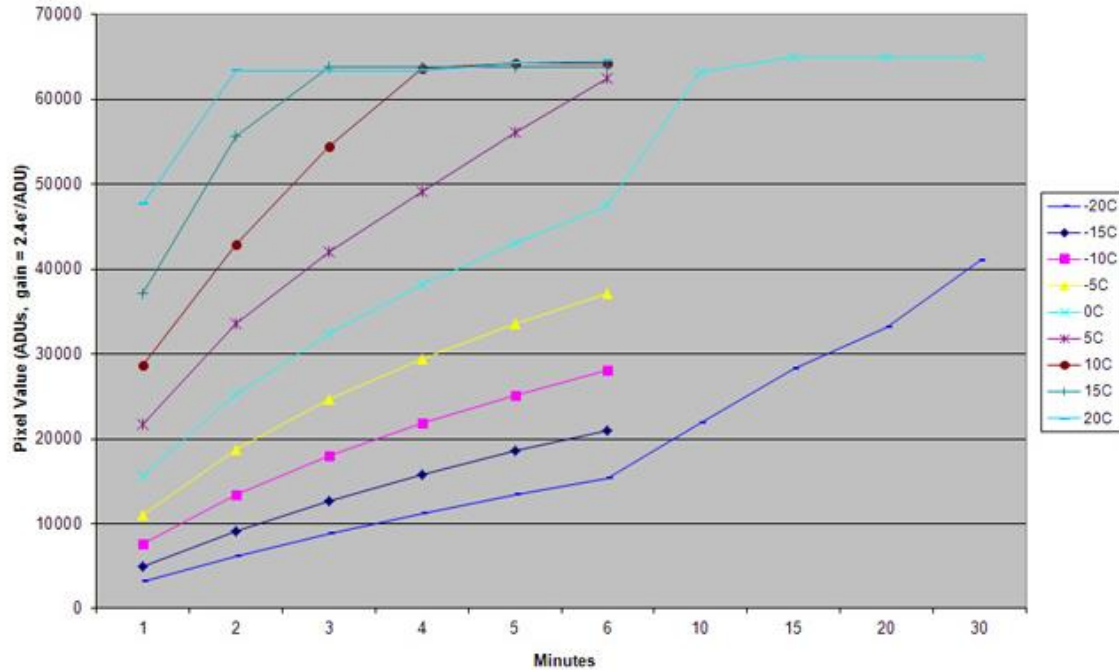


Fig. 55. Dependence of dark current on image sensor temperature and exposure time (data for a QSI 516 thermoelectrically cooled CCD camera) [QSI].

#### 5.5.2.2. CCD/CMOS cameras in DEMO radiation environment

One important limitation for the use of CCD/CMOS cameras in the inspection of welds inside the vacuum vessel of DEMO is the high radiation hardness requirement.

Although it is true that Peltier cooling, besides the improvement of the signal-to-noise ratio, increases the useful lifetime of CCD/CMOS cameras under radiation conditions [Fra 04], the performance of CCD/CMOS cameras is permanently degraded by total ionizing dose and displacement damage effects. Total ionizing dose produces threshold voltage shifts on the CCD/CMOS gates and displacement damage reduces the charge transfer efficiencies, increases the dark current, produces dark current non-uniformities and creates random telegraph noise in individual pixels [Mars 03].

To evaluate CCD/CMOS capability of operating in this environment, results from an assessment on in-vessel and ex-vessel radiation conditions during shutdown periods have been used [Sanz 13]. Absorbed gamma dose rates have been calculated for RH equipment materials in several points of interest without shielding. The considered irradiation scenario has been the same as for the brazed connector transmutation assessment: an average neutron wall loading of  $1.27 \text{ MW/m}^2$  and an irradiation time of 1.57 full power years (fpy) for the blanket and divertor, and 6 fpy for the vacuum vessel and TF coils.

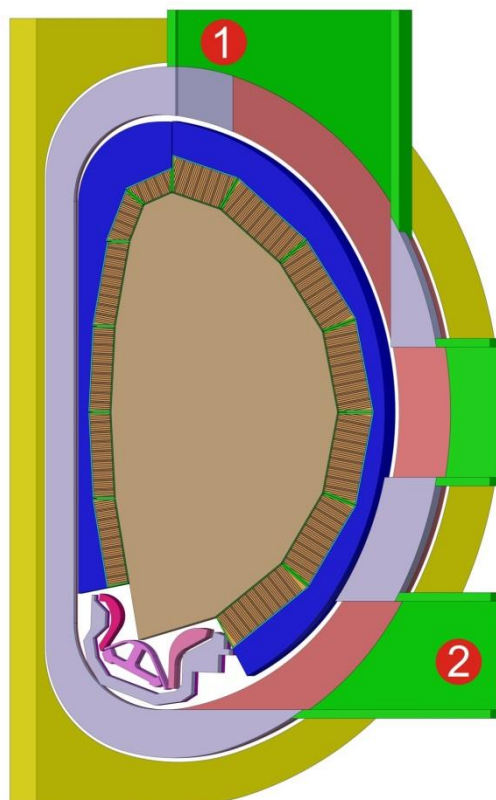


Fig. 56. Location of points for absorbed radiation calculations.

For the upper port (point 1), the gamma dose rate levels for most of the materials are around 4 Gy/h for 1 week after shutdown, with a maximum value for Viton of 5 Gy/h, that we can adopt as conservative reference value for this zone.

For the lower port (point 2), the dose rate levels for most of the materials are around 90 Gy/h (1 week after shutdown) and the maximum value corresponds to Viton (109 Gy/h), that we can adopt as conservative reference value for this zone.

The National Ignition Facility (NIF) uses x-ray streak cameras and gated x-ray cameras to provide spatial and time resolved images of the inertial confinement fusion implosion. Common to both diagnostics is the use of a gated micro-channel plate and phosphor, coupled by a fibre optic to either a scientific grade megapixel CCD camera developed by Spectral Instruments Inc. Recently, the 1000 Series CCD cameras have been substituted by 1050 CMOS-based cameras, which include a 2K x 2K CMV4000 sensor from CMOSIS Inc. [Kimb 12].

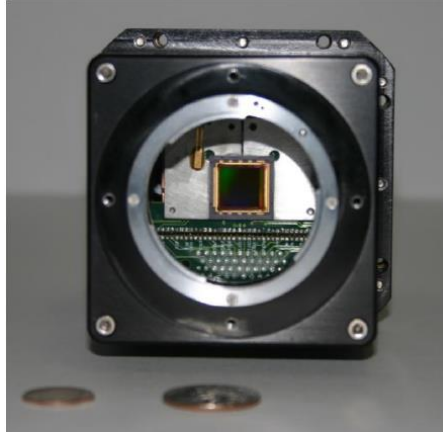


Fig. 57. Front view of a Spectral Instruments Inc. Model 1050 camera showing the CMOSIS CMV4000 sensor.

Depending upon the distance from the implosion capsule, the earliest arrival time of the 14 MeV neutrons is 24 ns after the x-rays. The 14 MeV neutrons produced by the capsule interact with the material creating protons, alpha particles, and gamma radiation. Radiation tests at the Omega laser at the Laboratory for Laser Energetics (LLE) with a Kodak 16800 CCD gave an operational limit of  $10^8 \text{ n cm}^{-2}$  due to the increasing background noise.

These cameras have an optical trigger, the ability to read out an image in  $\approx 250 \text{ ms}$  over fibre optics, and operate in a thermoelectrically cooled mode down to  $-40^\circ\text{C}$ , which allows to withstand an estimated total dose of 100 Gy (Si). Control and readout of the sensor is through an Actel RT3PE600L Field Programmable Gate Array (FPGA) 6 with 600000 gates. This FPGA which is part of the radiation-tolerant RT ProASIC family experiences a 10% increase in propagation delay between 150 and 250 Gy (Si). The program is stored in a 3D Plus radiation-tolerant memory which is good to 150 Gy (Si) [Kimb 12]. Nevertheless, information about the tolerated dose rate is not provided, although a total dose of 100 Gy would only allow using the camera for 20 hours with the expected dose rate of 5 Gy/h in the upper port, or for 0.91 hours if it would operate inside the lower port (109 Gy/h).

### 5.5.2.3. CID cameras

The CID (Charge Injection Device) sensors offer a class of semiconductor imaging devices as an alternative to CCD and CMOS. Similar to a CCD, the CID is monolithic metal oxide semiconductor (MOS) silicon charge transfer device. The pixels are configured in a one-dimensional or a two-dimensional array. Incident photons are converted to a proportional amount of electrical charge, which is stored in the MOS capacitors of each pixel.

The traditional CID pixel has two principle photogates: 'Storage' and 'Sense.' The basic mode of operation for a CID pixel is illustrated in Fig. 58.

Integration is the collection of photon generated charge (A). Typically, the accumulated charge is collected under the Storage photogate. However, depending on the electrode biasing, Sense may also be used for collecting the charge. The photon-generated charge is determined by measuring the voltage change induced by transferring the charge between the two photogates (B and C). This process is non-destructive of the photon-generated charge. The photon generated charge may be cleared by collapsing the potential wells under both the Storage and Sense photogates (D) there by injecting the charge into the underlying substrate [Bha 08].

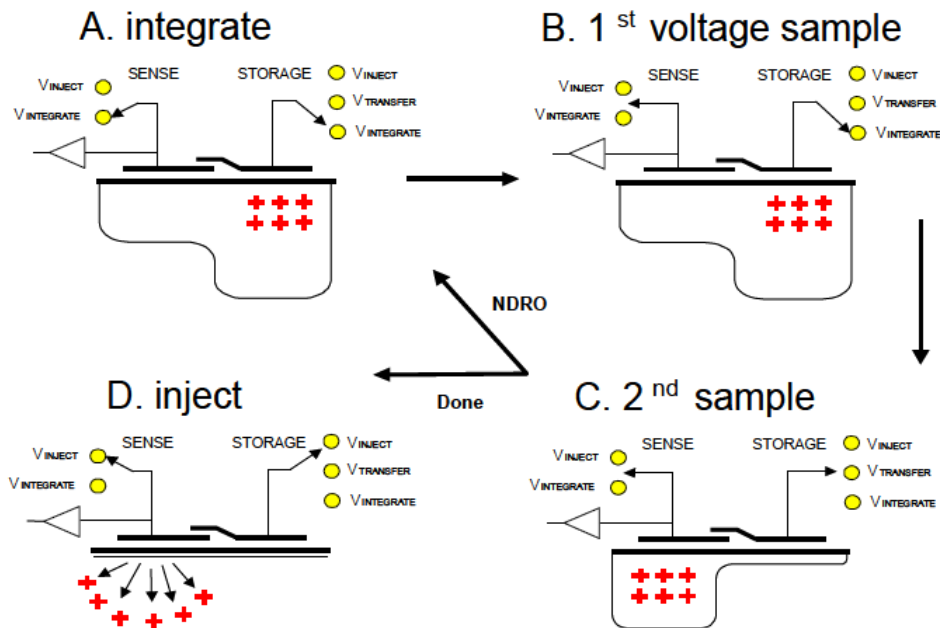


Fig. 58. Basic operation of the CID pixel [Bha 08].

The main advantages of CIDs include UV sensitivity due to relatively high fill factor, superior anti-blooming performance and radiation hardness. Depending on the specific design, CIDs may also be capable of true random-access pixel addressing for non-destructive or destructive read-out and charge clear. These capabilities allow obtaining images with extreme high dynamic range.

There are two primary approaches used for CID image sensors: passive pixel and active pixel. Traditionally, CID designs employed passive pixel architecture. The active pixel, or preamplifier-per-pixel (PPP), was developed for applications requiring higher dynamic range. The read noise of active pixel CIDs is really low, but the architecture makes it somewhat complicated and sensitive to transient noise effects when exposed to gamma radiation.

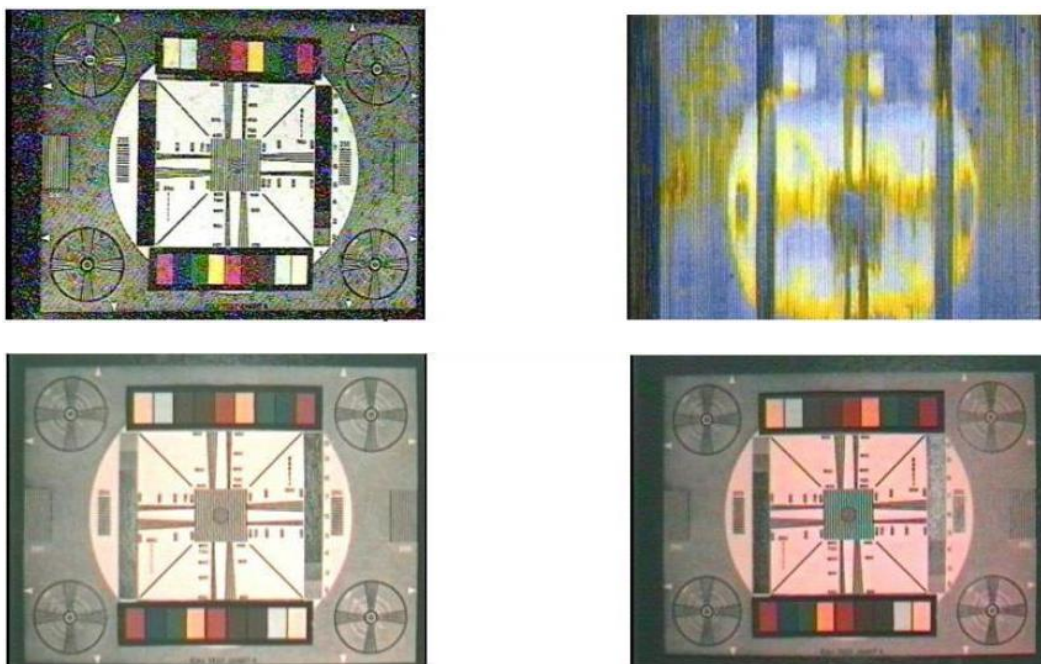


Fig. 59. Performance under radiation (300 Gy/h) of a CCD sensor versus a passive pixel CID sensor [Bha 08]. Top: CCD sensor (after 0 h and 1 h). Bottom: CID sensor (after 0 h and 45 h).

Thermo Scientific 3MegaRAD line of cameras uses a thermoelectric cooler. They are available in both monochrome and colour version systems. These cameras are used both in JET and General Atomics for monitoring areas such as the divertor rail.

The CID8825D is the only radiation hardened solid-state camera capable of colour imaging in high radiation environments. This camera features a small detachable remote head with radiation tolerance to at least  $3 \cdot 10^4$  Gy (total dose) [ThermoS] and low noise operation in flux rates up to  $10^3$  rad/h, which is about 200 times the expected gamma dose rate in the vacuum vessel upper ports one week after shutdown, and 10 times the expected dose rate in the divertor ports. The integrated dose limit would allow operating for 6000 hours in the upper ports, but only about 275 hours in the lower ports.

Video output is standard NTSC format via the Camera Control Unit (CCU) BNC connector, RGB connectors, or digitally via the USB 2.0 port. The image format is 730 x 512, whereas the pixel size is  $18.6 \times 16.4 \mu\text{m}$ . This series of cameras include CID8825DX6 for operation up to 50 meters remote distance between the radiation-hardened head and CCU, or CID8825DX7, which offers remote operation up to 150 meters.

There is also an equivalent model in monochrome (CID8725D), with similar features in image resolution and radiation hardness. But the most interesting monochrome proposal is the CID8710D1 MX1 model. The resolution is higher than colour model CID8825D,  $768 \times 612$ , with  $11.5 \mu\text{m}$  square pixels [ThermoS]. Furthermore, this model supports a dose rate of  $7 \cdot 10^3$  Gy/h (gamma, neutron, high energy electrons, and proton radiation), although the integrated total dose is a little lower ( $10^4$  Gy). Other advantages are the wide spectral response (400-1100 nm) and the possibility of using coatings for x-ray, deep UV, and IR, which reveals very interesting for combining the direct visual inspection with subsequent or real-time advanced image analysis.

Nevertheless, these cameras are limited in terms of temperature hardness. 8825D and 8725D can operate with a room temperature lower than  $55^\circ\text{C}$ , and this value is reduced to  $30^\circ\text{C}$  in the case of 8710D1 MX1. According to [Min 12], temperatures of  $70^\circ\text{C}$  could be expected in the upper ports of the vacuum vessel during maintenance processes. For this reason, the use of an actively cooled casing for controlling the temperature of the camera is proposed and should be further investigated.

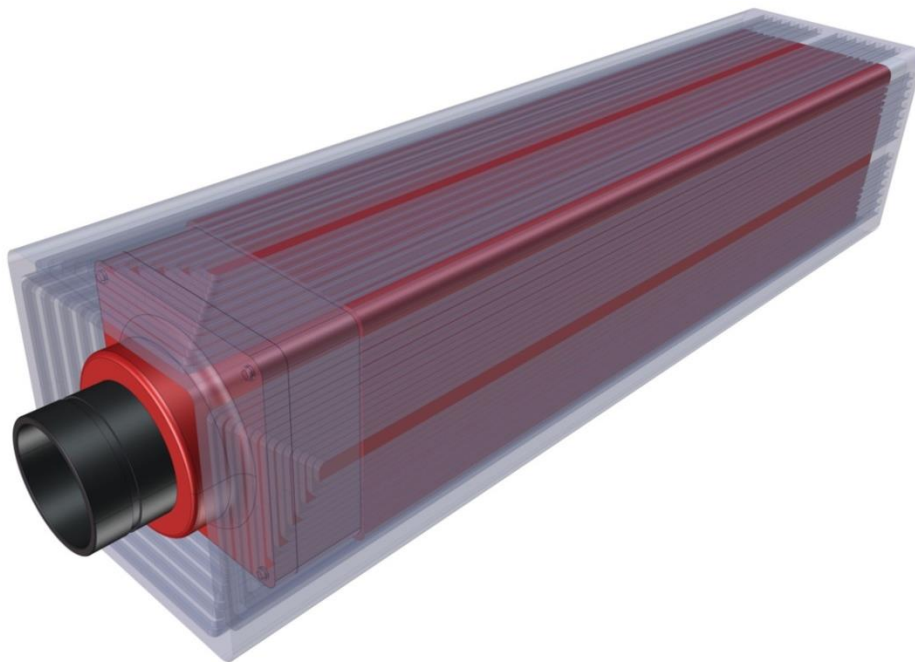


Fig. 60. Sketch of an actively cooled casing for CID8825D.

### 5.5.3. Electromagnetic-acoustic transducers

Electromagnetic-acoustic transducers are essentially made of a coil fed by a large dynamic current (pulse or tone burst are commonly used) and a magnet or electromagnet providing a static magnetic field. When the sensor is close to a metallic sample, an eddy current density  $J_e$  is induced in it; the interaction of this current density with the bias magnetic flux density  $B$  results in a net body force on the sample, according to the Lorentz equation:

$$f = J_e \times B \quad (13)$$

This force causes the generation of ultrasonic waves in the solid, which can be exploited for NDT purposes.

The Lorentz force effect takes place in any conducting metal; if the sample is ferromagnetic a further principle contributes to the generation of elastic waves: the so-called magnetostriction [Rib 11]. There are two different types of magnetostriction: spontaneous magnetostriction and field induced magnetostriction. The first takes place when a ferromagnet is cooled through its Curie temperature.

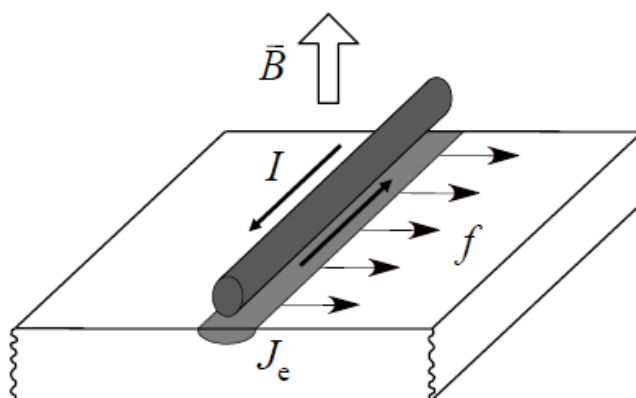


Fig. 61. Fundamental physical principles exploited by an EMAT: (a) Lorentz force. A driving current  $I$  induces eddy current density  $J_e$ ; the interaction with a static magnetic flux density  $B$  generates volume force density  $f$  [Rib 11].

EMATs can exploit field induced magnetostriction: a dynamic field superposed on a bias field results in dynamic total magnetic field that causes dynamic stresses in the material, that propagate in the form of elastic waves. Thanks to reciprocity, these physical principles also work in the inverse sense, allowing the detection of ultrasonic waves. A mechanical wave travelling in a conductive medium causes dynamic currents that combined with a static magnetic field induce an electric field in a coil, proportional to the speed of the metal particles in the material (inverse Lorentz mechanism). An inverse magnetostriction phenomenon also takes place when the deformation of a ferromagnetic body produces a magnetic flux density variation that can be detected by the coil.

#### 5.5.3.1. Advantages and limitations of EMATs

The previously outlined principles exploit electromagnetic induction; hence, operation without any contact is possible. Actually, the efficiency of the transduction decays exponentially with the distance between the sensor and the sample, limiting the practical separation to a few millimetres. However, this tiny gap is enough to give a big advantage over piezoelectric transducers in some applications: high temperature testing is made possible as well as operation on moving samples. Since no contact is needed, coupling fluids do not have to be used, which simplifies the operation and minimizes the need for surface preparation; moreover, highly reproducible measurements can be achieved because variability due to the couplant is eliminated [Rib 11].

EMATs have been successfully employed in different industrial applications for several decades. For instance, high temperature ( $> 1000^{\circ}\text{C}$ ) thickness gaging of seamless steel pipes have been achieved during manufacturing processes using water-cooled permanent magnets (or electromagnets).

Another example of EMAT application is steel sheet production, where the rolling process causes preferred orientations in the microstructure of the samples, resulting in anisotropy in the elastic and electromagnetic properties. A pair of EMATs separated by a known distance can be used to measure the speed of sound at different angles from the rolling direction, yielding important information on the formability of the metal sheets. Here the lack of couplant between the transducer and the sample is the key factor to obtain a fast scan of the plate in several directions.

Another main advantage of EMATs is the large variety of ultrasonic modes that can be generated. A careful design of the geometry of the coil and the magnet and their relative position allows the excitation and detection of complex wave patterns. EMATs have been used to generate and detect bulk longitudinal and shear waves, Lamb and Shear Horizontal waves in plate-like structures as well as torsional, flexural and longitudinal modes in pipes and wires.

However, the contactless nature of EMATs comes at a price of some disadvantages: first of all, these transducers are inefficient when compared to traditional sensors. The signal-to-noise ratio is rather poor if the transducer is not carefully designed and special electronics are not employed [Rib 11] [She 03] [Mass 08]. Another major problem is that the principles on which EMATs rely to generate and detect ultrasonic waves imply that only good electrical conductors can be tested. The use of austenitic stainless steel 316 for DEMO pipes would give low-quality signals compared with a lower electrical resistivity material like RAFM steel (e.g. EUROFER). If necessary, EMAT can be applied to the inspection of non-conducting materials as composites by adhering a removable aluminium foil tape on the part surface [Hsu 99]. Ultrasonic waves generated in the aluminium layer by the EMAT readily propagate into the non-conducting composite, whereas the reversed process is used in the reception of ultrasonic waves by EMAT.

### 5.5.3.2. EMATs for weld inspection in DEMO pipes

As previously stated, one of the most attractive features of EMATs is their capability of generating a wide range of ultrasonic wave-modes, by careful design of their geometric configuration, including shear horizontal (SH) waves in plate-like structures or torsional waves in pipe-like components.

For several types of defects the use of shear waves has advantages compared to the use of longitudinal waves. The fundamental shear horizontal and torsional waves are of practical importance in guided wave inspection due to their non-dispersive character, e.g. their group and phase velocities are not frequency-dependent, simplifying the interpretation of signals.

In practice, shear waves can detect surface defects or vertical defects that do not reflect ultrasound, but rather scatter the energy of shear (transverse) waves [Ege 06]. This fact is used in the inspection of plates, but it can be extended for pipe inspection due to the similarities between the shear horizontal waves and torsional waves. Thus, the main options available regarding EMAT configurations for SH waves are Periodic Permanent Magnet (PPM) EMATs and Magnetostrictive EMATs.

In 2003, EMATs were proposed for inspection of waste package closure system in Yucca Mountain Project [She 03], due to their capability for operating at high surface temperatures (contactless). The expected temperatures were  $93\text{--}500^{\circ}\text{C}$ , whereas the transducers would be subjected to a radiation environment of 160 R/h, which is equivalent to 1.4-1.6 Gy/h. This requirement is 3-3.5 times lower than the reference gamma dose rate in the upper ports for 1 week after shutdown.

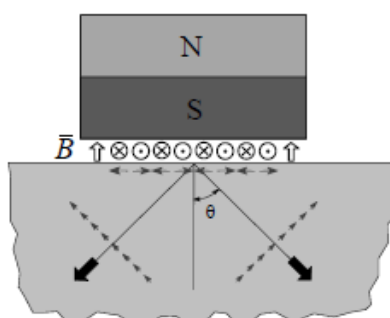


Fig. 62. Meander coil configuration [Rib 11].

EMATs have been adopted for inspection of shielding blanket cooling pipes in ITER. The ITER Remote Handling Manual includes a tool catalogue where several types of electromagnetic-acoustic transducers can be found. One of them is an EMAT referenced by JAERI for inspecting 100 mm diameter pipes with a really high radiation tolerance of  $3 \cdot 10^4$  Gy/h [Spe 05].

Present EMATs can be combined with high sensitivity flaw detectors which provide advanced wave analysis software, as well as with thickness gages, which allows evaluating corrosion in pipe walls with resolutions up to  $10^{-3}$  mm.



Fig. 63. Olympus magnetostrictive EMAT [OLYM].

#### 5.5.4. Laser ultrasonic transducers

In the same way that there are electromagnetic methods for producing and measuring ultrasonic waves in materials, lasers can be used for generating and detecting ultrasonic waves (optical methods).

Laser generation of ultrasonic waves can be recognized as exciting the waves with an optical hammer. When a high energy pulsed laser beam (YAG are the most usual lasers for this application) is irradiated onto a specimen surface, an interaction of the laser beam with the specimen occurs in one or both of two distinct processes, thermoelastic and ablative. By controlling the laser irradiation conditions, it is possible to generate any types of ultrasonic waves such as longitudinal, shear and guided waves at a desired frequency.

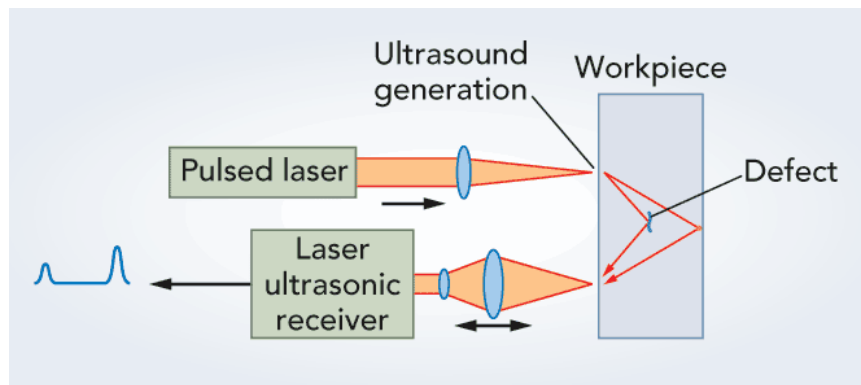


Fig. 64. Sketch of laser ultrasonic detection of internal defects [Che 13].

To detect ultrasonic waves, a laser beam is illuminated onto the specimen surface during enough time to capture the ultrasonic signal of interest. Ultrasonic waves are then detected by measuring surface displacements caused by ultrasonic disturbance, using a laser-assisted interferometer or other device. Mickelson, Confocal Fabry-Perot or Photorefractive Two-wave Mixing interferometers are often utilized [Iha 08]. The ability of laser-ultrasonic devices to operate at large standoff distances provides big advantages in industrial applications such as materials process monitoring at high temperatures. Some years ago, laser based UT testing technologies were less developed than other techniques and suffer from low detection efficiency, sensitivity to surface conditions, and complexity. It was also more difficult to control beam focusing and directionality [She 03]. However, today there is no other technology available for some applications as specific as the measurement of paper bending stiffness on-line, during manufacturing [IndInn].

Laser UT method is also used for on-line seamless steel tubing process control [Jes 04]. The accuracy of the system in contactless measurement of pipe thickness variation was verified by selecting several tubes and measuring them at room temperature with a conventional ultrasonic gauging system. The results obtained at high and room temperatures were found in very close agreement (within  $\pm 0.5\%$ ). The performance for austenitic grain size measurements was also tested by comparing the laser UT data with metallographic measurements. With estimated metallographic grain size accuracy between 0.5 and 1 ASTM, a statistical analysis showed that the laser-ultrasonic grain sizes determined online had at least the same accuracy.

Following with industrial applications, Tecnar has developed a system called LUIS, which is a complete and functional laser-ultrasonic inspection system for aircraft components, ready to be put into operation for production use [Tecnar]. The flexibility of the LUIS allows inspection of both small components, containing acute angle geometry, and large components. No contact is needed between the inspected component and the inspection system. The LUIS can detect a wide range of defects within composites and composites bonded with honeycomb structure. With the LUIS, each point of acquisition on the surface of the inspected component is identified by the scanner angular coordinates and the distance of the target acquisition point to the centre of the scanner mirror (measured by a ranging system included). With this information, the position of each acquisition point with respect to the part reference point is calculated and used to map the resulting ultrasonic images. The LUIS uses a single scanning mirror to inspect a component. Since the mechanical motions involved in the scanning procedure consists only in the tilt and roll of the scanner mirror, and since laser-ultrasonic has a relaxed normalcy requirements, complex-shaped composite components can be inspected with a speed and flexibility not available with conventional pulse-echo ultrasonic inspection systems.



Fig. 65. Laser-Ultrasonic inspection System for Aerospace components (LUIS) [Tecnar].

Intelligent Optical Systems has researched the automated weld inspection market and developed a system for this application, which seems to work particularly well with laser welds [Intopsys]. Laser UT is also used for inspection of MIG welds in automotive industry [Blo 08]. One of the major challenges which laser ultrasonic technology faces is price. Industrial laser ultrasonic systems range from 400000 to 1500000 €, although R&D systems are less expensive. On the other hand, although laser ultrasonic is considered a promising technique for inspection in radiation environments [Chi 06], it is difficult to find references of real applications. For example, in 2006, a vibration mode of an Inconel hollow capped cylinder was measured by Laser Resonant Ultrasound Spectroscopy (LRUS) throughout a period of 170 hours with gamma dose rate of  $10^4$  Gy/h. The vibration mode frequency was observed to change in a manner consistent with the temperature dependence of the elastic stiffness coefficients of the material. The results illustrated the efficacy of the laser approach for real-time resonant ultrasound measurements in this severely hostile nuclear environment [Tel 06].

## 5.6. References

[Are 04] M.F. Arenas, V.L. Acoff, R.G. Reddy, Physical properties of selected brazing filler metals, *Science and Technology of Welding and Joining* 9 (2004), 423-429.

[ASM 93] ASM Handbook, Volume 6: Welding, Brazing and Soldering and Volume 18: Friction, Lubrication and Wear Technology, ASM International, 1993.

[ASME 07] ASME Boiler & Pressure Vessel Code, Section II, part C: Specifications for Welding Rods, Electrodes and Filler metals, 2007.

[AWS 04] American Welding Society (AWS), *The Everyday Pocket Handbook for Visual Inspection and Weld Discontinuities. Causes and Remedies*, 2004.

[Bar 03] V. Barabash, Material Specification for the supply of 316L(N)-IG austenitic stainless steel forgings, ITER internal document (ITER\_22F6AJ), 2003.

[Bha 08] S. Bhaskaran, T. Chapman, M. Pilon, S. VanGorden, Performance based CID imaging: past, present and future, *Proceedings of SPIE (international society for optics and photonics) Meeting*, 2008.

[Blo 08] A. Blouin, S. Kruger, J. Monchalin, Applications of laser-ultrasonics to the automotive industry, *Proceedings of the 17<sup>th</sup> World Conference on Non-Destructive Testing (WCNDT)*, 2008.

[Boc 11] L.V. Boccaccini, Requirements of the hydraulic connection for blanket and divertor systems, technical note for the Task Agreement WP11-DAS-RH-04, EFDA internal document (EFDA\_D\_2HER55), 2011.

[Bos 83] D. Bose, A. Datta, A. Rabinkin N. J. de Cristofaro, High strength nickel-palladium-chromium brazing alloys, 14th International AWS-WRC Brazing and Soldering Conference, Philadelphia, 1983.

[BS3643] British Standard BS-3643-1:1981, Specification for ISO metric screw threads.

[Che 13] Y. Cheng, Y. Deng, J. Cao, X. Xiong et al., Multi-Wave and Hybrid Imaging Techniques: A New Direction for Nondestructive Testing and Structural Health Monitoring, *Sensors* 13 (2013) 16146-16190.

[Chi 06] P. Chivavibul, S. Lin, H. Fukutomi, S. Higuchi, T. Ogata et al., Development of a multi-beam laser ultrasonic inspection system and its application on flaw sizing, Central Research Institute of Electric Power Industry (CRIEPI) report Q05024, 2006.

[Ege 06] M. Ege J. Schröder A. Kirikov, Ultrasonic testing of hot plates using EMAT technology, *Proceedings of the European Conference on Non-Destructive Testing (ECNDT)*, 2006.

[EI-G 07] L.A. El-Guebaly, V. Massaut, K. Tobita, L. Cadwallader, Environmental aspects of recent trend in managing fusion radwaste recycling and clearance, avoiding disposal, *Proceedings of the 2<sup>nd</sup> IAEA Technical Meeting of First Generation of Fusion Power Plants: Design and Technology*, 2007.

[EN14324] European Standard EN 14324:2004, Brazing. Guidance on the application of brazed joints.

[Fern 14] I. Fernández, E. Rosa, I. Palermo, Design of a brazing connector for DEMO in-vessel components, *Fusion Engineering and Design* 89 (2014) 2363-2367.

[Fern 14b] I. Fernández, E. Rosa, A. Ibarra, Progress on the design of a brazing connector for DEMO in-vessel components, *Proceedings of 28<sup>th</sup> Symposium on Fusion Technology*, San Sebastián, 2014.

[Fis 12] U. Fisher, J. Sanz, J.P. Catalán, R. Juárez, Definition of Radiation Map in DEMO, final report for the Task Agreement WP11-DAS-RH-07, EFDA internal document (EFDA\_D\_2LMBPU), 2012.

[FLUENT] ANSYS FLUENT v.14.5 Theory guide.

[Fra 04] E.M. Franken, J.C. de Boer, J.C. Barnhoorn, B.J. Heijmen, Characteristics relevant to portal dosimetry of a cooled CCD camera-based EPID, *Medical Physics* 31 (2004) 2549-2551.

[Garlock] Garlock Sealing Technologies Cefilac catalogue: High performance sealing Helicoflex (ET512E0130).

[Garlock b] Garlock Sealing Technologies Cefilac catalogue: Quick disconnect system for conical flanges, Class 150, 300 & 500 (ET5127FE9930).

[Garlock c] Garlock Sealing Technologies, Quick disconnect system presentation.

[Gros 06] R.A. Gross Gourley, I.L.W. Wilson, D.W. Pratt, J.A. Lewis, Vacuum brazing of CA6NM components, *Heat Treating 2005: Proceedings of the 23<sup>rd</sup> Heat Treating Society Conference* (2005) 66-69, 2006.

[Har 12b] J. Harman, Dimensions of blanket service connections, technical note for the Task Agreement WP12-DAS06-T06, EFDA internal document (EFDA\_D\_2GDGLD), 2012.

[Hsu 99] D.K. Hsu, K-H Im, I-Y Yang, Applications of electromagnetic acoustic transducers in the NDE of non-conducting composite materials, *KSME International Journal* 13 (1999) 403-413.

[Iha 08] I. Ihara, Ultrasonic sensing fundamentals and its applications to non-destructive evaluation, *Lecture Notes Electrical Engineering* 21 (2008) 287-305.

[IndInn] Industrial Innovations (<http://sensors.lbl.gov>).

[Intopsys] Intelligent Optical Systems Inc. (<http://www.intopsys.com>).

- [Jes 04] G. Jeskey, R. Kolarik II, E. Damm, J-P Monchalin et al., Laser ultrasonic sensor for on-line seamless steel tubing process control, Proceedings of the 16<sup>th</sup> World Conference on Non-Destructive Testing (WCNDT), 2004.
- [Keo 13] K. Keogh, Assessment of the feasibility of in-bore cutting, welding and testing for DEMO Blanket service pipes, Final Report for Task Agreement WP13-DAS07-T09, EFDA internal document (EFDA\_D\_2LF5TM), 2013.
- [Kimb 12] J.R. Kimbrough, J.D. Moody, P.M. Bell, Design and testing of a mega pixel CMOS charge dump and read camera, Proceedings of SPIE (international society for optics and photonics) Meeting, 2012.
- [Kra 07] W. Krauss, J. Konys, H. Steiner, J. Novotny et al., Development of modelling tools to describe the corrosion behaviour of uncoated EUROFER in flowing Pb-17Li and their validation by performing of corrosion tests at T up to 550°C, FzK internal document (FZKA 7295), 2007.
- [Led 12] F. Ledrappier, Numerical analysis of optimized bolted flange design for ITER, technical note, CEA internal document (DTEC/SDTC/2012/03, 2012.
- [Lug 79] E. Lugscheider, K. Klöhn, R. Lison, Strength of high temperature brazed joints – influence of brazing parameters, 10<sup>th</sup> International AWS-WRC Brazing Conference, Detroit, 1979.
- [Mars 03] C.J. Marshall, P.W. Marshall, CCD radiation effects and test issues for satellite designers, report for NASA-GSFC Multi-Engineering Disciplinary Support Contract Task 1058, 2003.
- [Mas 08] E. Mas de les Valls, L. Sedano, L. Batet, I. Rikapito et al., Lead-lithium eutectic material database for nuclear fusion technology, Journal of Nuclear Materials 376 (2008), 252-257.
- [Mass 08] M.E. Massie, Device to transmit critical information from the interior of a spent fuel cask, University of Tennessee Honors Thesis Projects, 2008.
- [Matweb] Specifications of Ni-200 and Cu (UNS C15710) (<http://www.matweb.com>).
- [MegaMex] MegaMex catalogue (<http://www.megamex.com>).
- [Min 12] T. Mindham, Feasibility assessment of in-vessel components connections for remote handling, final report for Task Agreement WP11-DAS-RH-04, EFDA internal document (EFDA\_D\_2HEE3W), 2012.
- [MRP 07] MRP Responses to U.S. Nuclear Regulatory Commission Comments on MRP-175 Materials Reliability Program: PWR Internals Aging Degradation Mechanism Screening and Threshold Values, ML071500469, 2007.
- [Mun 11] C.J. Munez, M.A. Garrido, J. Rams, A. Ureña, Experimental study of W-EUROFER laser brazing for divertor application, Journal of Nuclear Materials 418 (2011) 239–248.
- [Nis 98] H. Nishi, K. Kikuchi, Influence of brazing conditions on the strength of brazed joints of alumina dispersion-strengthened copper to 316 stainless steel, Journal of Nuclear Materials 258-263 (1998) 281-288.
- [Nist] NIST database (<http://webbook.nist.gov/chemistry/fluid/>).
- [OLYM] Olympus inspection & measurement systems (<http://www.olympus-ims.com/>).
- [Pie 95] J.D. Pierce, J.J. Stephens, C.A. Walker, F.M. Hosking, R.M. Curlee, Development of a re-brazeable containment system for special nuclear material storage & transport, Sandia National Laboratories internal document (SAND95-0206C), 1995.

[Por 13] S.I. Porollo, A.M. Dvoriashin, Y.V. Konobeev, F.A. Garner, Microstructure and swelling of neutron irradiated nickel and binary nickel alloys, *Journal of Nuclear Materials* 442 (2013) 5809-5812.

[QSI] QSI Imaging (<http://www.qsimaging.com>).

[Que 12] V. Queral, Feasibility assessment of in-vessel components connections for remote handling, final report for the Task Agreement WP11-DAS-RH-04-04, EFDA internal document (EFDA\_D\_2LM5NS), 2012.

[Raj 09] S. Rajendran, J. Palmer, ITER Remote Handling Code of Practice, ITER internal document (ITER\_D\_2E7BC5), 2009.

[Rib 11] R. Ribichini, Modelling of electromagnetic acoustic transducers, PhD Thesis, Imperial College London, 2011.

[Rok 11] M. Rokvam, Caractérisation de microstructures de joints brasés avec les alliages BCu-1, BAg-13a, BAu-4, BAu4-6, BNi-1a, BNi-2, BNi-3 et Palnico 36M ayant pour métal de base un superalliage base nickel, Master thesis, University of Québec, 2011.

[Sanz 00] J. Sanz, ACAB activation code for fusion applications: user's manual v5.0, Lawrence Livermore National Laboratory internal document (UCRL-MA-143238), 2000.

[Sanz 13] J. Sanz, Summary of top-level conclusions for the Task Agreement WP12-DAS06-T03, EFDA internal note, 2013.

[She 03] C.V. Shelton-Davis, S. Michael Berry, R.J. Bitsoi, K.M. Croft et al., Vendor assessment for the waste package closure system (Yucca Mountain Project), Idaho National Engineering and Environmental Laboratory, report for DOE Contract DE-AC07-99ID13727, 2003.

[Sho 04] K. Shoghi, S.M. Barrans, H.V. Rao, Stress in v-section band clamps, *Proceedings of the Institute of Mechanical Engineering Part C, Journal of Mechanical Engineering Science* 218 (2004) 251-261.

[Shu 09] R. Shuff, S. Mills, A study of pipe jointing technology with reference to ITER requirements, *Fusion Engineering and Design* 84 (2009) 1767-1769.

[SMetal] Special Metals catalogue (<http://www.specialmetals.com>).

[Spe 05] B. Spears, ITER Remote Handling Manual, ITER internal document (ITER\_D\_229CW2), 2005.

[Stemmer] Stemmer Imaging (<http://www.stemmer-imaging.de>).

[TBraze] Properties of filler metals BAu-4 and BNi-5 (<http://www.turbobraze.com>).

[Tecnar] Tecnar (<http://www.tecnar.com>).

[Tel 06] K. Telschow, R. Schley, D. Cottle Real-time in-situ measurement of material elastic properties in a high gamma irradiation environment, *Proceedings of EPRI 5<sup>th</sup> International Conference on NDE*, 2006.

[ThermoS] Thermoscientific (CID cameras) (<http://www.thermoscientific.com>).

[Toc 11] G. Tocheport, O. Constant, Calculation of sheet flanges DN65 and DN150, ITER internal document (ITER\_D\_7A4A7F), 2011.

[Xu 04] H. Xu, C. Guetari, The use of CFD to simulate capillary rise and comparison to experimental data, *International ANSYS Conference*, Pittsburgh, 2004.

# Chapter VI

*General conclusions and  
proposals for further  
development*



## **6.1. Introduction**

Different approaches can be adopted in the design of components and systems for fusion technology in order to maximize the availability of future devices like commercial power plants. This will be critical in the final cost of electricity generated by fusion. Some studies have demonstrated achieving high values of reactor availability (near 80%) will be necessary for the economic feasibility of fusion. This is most due to the fact of fusion electricity cost, in contrast to other energy technologies, will not be fundamentally conditioned by operating costs (e.g. fuel cost), but by capital construction costs. The design of key components will be based on novel and insufficiently demonstrated technologies, like the ones used for the self-sufficient fuel cycle or power exhaust systems, whose reliability is not well-known. There is also enormous lack of awareness on plasma transient phenomena like disruptions or ELMs, which could affect the overall plant reliability.

In-vessel components and particularly plasma-facing components will be subject to very high 14-MeV neutron fluence, causing damage rates  $\sim 10$  dpa/fpy in the case of DEMO and 20-30 dpa/fpy for a FPP. Their necessary replacement each 2-5 fpy by remote handling techniques increases inexorably the plant unavailability to critical limits. It is envisaged the duration of scheduled maintenance for in-vessel components using a single RH system is about 22 months. Doubling the number of systems operating in parallel almost halves the maintenance duration so that four systems could complete the maintenance in about 6 months.

R&D activities can help improving components intrinsic reliability, e.g. by developing new materials with higher fluence resistance. But it is also the configuration/arrangement of basic components which can improve systems reliability (e.g. redundancy, derating, etc.) and mainly systems availability through maintainability and inspectability (e.g. assuming principles of preventive maintenance).

In consequence, the RAMI approach must be part of design procedures from the early conceptual phases to detailed engineering. They must be firmly supported by failure mode, effects and criticality analysis (FMECA). Design codes like RCC-MR or ASME, codes of practices and standards libraries must feature RAMI concepts and channel design activities in the form of standardized procedures. They must be adapted to the design approach currently adopted in most of international fusion programmes: starting from a set of initial hypothesis and requirements and address global physics and technology issues in 0-D systems codes before further more detailed analysis in unidimensional or multidimensional codes.

An overview of the main conclusions achieved in the previous Chapters is provided in the following Sections, together with some proposals for the further development of the work presented in this thesis.

## **6.2. ITER Test Blanket System integration studies. Conceptual design of a remote handling test facility**

The availability of components test facilities between ITER and DEMO will be limited. Only the construction of neutron sources for testing materials (IFMIF or less demanding options like DONES or ENS) and small facilities like gas or liquid metal loops can be forecast at present.

In consequence, it is possible many key technologies for a fusion power plant will not be able to be tested in representative operating conditions before the construction of DEMO, so the proposed technology shall be based on extrapolations from the upper limits of ITER operation.

In spite of this poor perspective, the development of remote handling techniques can be benefited from the requirement of ITER Organization of physical demonstration of the remote handling systems before their installation in the ITER site. One of the most relevant transversal research programmes in ITER is the TBM (Test Blanket System). It will allow evaluating

breeding blanket concepts by means of reduced-scaled prototypes in a representative fusion environment. Together with their auxiliary systems, the maintenance and replacement of TBMs along the Programme will be carried out by RH techniques. Therefore, ITER will require a TBM remote handling test facility.

A conceptual design of a remote handling test facility for the EU TBMs (HCLL and HCPB) has been produced. The objectives of such facility are to demonstrate the feasibility of the remote handling operations involving TBMs in ITER, confirm design choices for TBM RH equipment and systems (manipulators, tools, viewing, virtual reality, actuators, controllers, software, etc.), validate and optimize operating procedures, examine consequences of system failures and confirm pre-planned rescue procedures, allow long term endurance testing to assess availability/reliability of the RH systems and provide a training platform for RH systems designers and operators.

The work started from an intense bibliographic research to identify requirements from ITER and the TBM designers. Then, the facility has been designed considering all the requirements. This comprises the conceptual design of equipment and systems, as well as the layout of equipment and systems in the facility.

Graphic design has been extensively used. Around 350 assemblies with a total number of ~1200 parts have been designed and/or integrated in the 3-D CAD model. The graphic design has been combined with kinematic simulations, especially for some of the most important operations in the Hot Cell, as well as the installation/removal of the Test Blanket System components in the Port Cell 16. These operations have been studied with a higher level of detail. This process has allowed gaining specific experience in remote handling systems and specific design tools (like the described in Chapter IV) which have been afterwards utilized in other research projects.

Some of the solutions adopted later by ITER show a notable agreement with the ones proposed in this thesis.

At present, there is not any initiative to construct the testing facility in Spain. However, the interest of going ahead towards a detailed design continues because the possibility of adapting the scope of the facility beyond the European TBMs, with the aim of selling testing services to the rest of ITER Domestic Agencies involved in the TBM programme. This would be also important because there are some concepts linked to the TBS remote handling which can be relevant for DEMO. Their influence on fusion components reliability databases and R&D activities for DEMO is undeniable.

### **6.3. Power conversion systems for DEMO**

The Brayton cycle is a very attractive solution for DEMO power conversion system (PCS) due to its relative simplicity and compactness. However, the use of a very light gas as helium taxes thermal efficiency because of the necessary compression before absorbing heat from the thermal source. This might be partially compensated by using thermal recuperation and by reaching very high temperatures. But there are limitations derived from the use of reduced activation ferritic-martensitic steels like EUROFER as structural material for the breeding blanket, e.g. ductile-brittle transition temperature, creep phenomenon at moderate temperature, etc. Such compression work involves high consumption in pumping power, which penalizes excessively the plant net electric power and efficiency, especially in the case of near-term fusion reactors ( $\sim 2 \text{ GW}_{\text{th}}$ ). The power loss due to the current low-efficiency heating and current drive systems must be considered. Besides, there are reasonable doubts about the future availability of helium in the indispensable amount to operate a net of fusion power plants. Indeed, these facts constraint severely the possibility to compensate the issue of achieving high plant availability and its influence on the cost of electricity by means of optimizing the balance of plant.

The balance of plant of a near term DEMO reactor based on a helium-cooled blanket (specifically a HCLL) using **supercritical carbon dioxide Brayton cycles** (S-CO<sub>2</sub>) for the secondary side has been studied here.

A survey of open literature on the matter to identify advantages and potential issues of S-CO<sub>2</sub> has been made.

Several cycle layouts using high thermal sources (blanket; 1835 MW) and low ones (divertor and vacuum vessel; 149 and 34.56 MW, respectively) integrated in a S-CO<sub>2</sub> power cycle have been proposed and analysed through a conventional methodology based on the First and Second Laws of Thermodynamics and with a number of approximations and hypotheses made. The main objective has been maximizing the electricity production. Four alternatives to a basic re-compression cycle in which the blanket is the only thermal source have been proposed and investigated.

The so-called layout C shows the best electrical performance (684 MW<sub>e</sub>;  $\epsilon=33.89\%$ , with net electric efficiency of 24.72%).

The assessment has been completed by a sensitivity study on key cycle variables and by the optimization of the heat exchangers, whose design is based on printed circuit heat exchangers technology (PCHE). The sensitivity study has identified the turbine inlet pressure and the main compressor inlet temperature as the key variables in the performance of the plant. Regarding the heat exchangers the pinch point at the low temperature recuperator and the overall pressure drop are the most influential variables. Their increase, according to their influence on electricity production, means a reduction of 1/3 of the overall volume of the heat exchangers. The turbine inlet pressure has been increased 20 bar to maintain the power losses below 1%.

The reliability of the components of the power conversion system is a key point in the availability of fusion reactors. It could be needed to match the maintenance of the PCS secondary side with the scheduled maintenance periods of in-vessel components like the breeding blanket or the divertor (main constituents of the Primary Heat Transfer System), so that it is necessary to reduce unplanned outages as far as possible. This principle has been applied to the design of a **lead-lithium/supercritical CO<sub>2</sub> printed circuit heat exchanger** for a 3.35 GW<sub>th</sub> fusion reactor based on the dual-coolant lead-lithium (DCLL) breeding blanket concept proposed within the Spanish National Programme Consolider TecnoFus.

Silicon carbide has been selected as structural material because of its heat and pressure resistance at high operating temperatures, compatibility with flowing lead–lithium, low tritium diffusivity and solubility and superior safety characteristics compared to metallic materials. Different techniques have been proposed to join the plates composing the heat exchanger. Additionally, some compounds have been proposed to produce the printed circuit by chemical etching of the ceramic surface.

The commercial printed circuit pattern based on semi-circular cross section channels with zig-zag trajectories has been substituted here by an arrangement of airfoil shaped fins. This allows minimizing the pressure drop with low penalization in the heat transfer area. A code for the design and viscous (or inviscid) analysis of subsonic isolated airfoils has been used to optimize the airfoil shape by minimizing its drag coefficient. The aerodynamic profile NACA0010 belonging to the NACA-4-digit series for aircraft wings has been selected for both hot and cold streams.

A one-dimensional heat transfer model has been used to pre-size the PCHE by evaluating the temperature profiles along the channels for both hot and cold streams. Besides, CFD analyses with scaled models have been performed to optimize the airfoil fins arrangement in terms of pressure drop and integrated thermal flux by varying the distance between the airfoils along the flow direction. An entire length model has been then used. The results show close results for the temperature profiles between the 1-D and the CFD model, although the chosen empirical correlations lead to slightly underestimate the overall heat transfer coefficient. The pressure drops are low for both hot and cold streams. On the other hand, the total integrated flux is larger than the one initially expected for this heat exchanger from the cycle design.

Finally, a transport model has been developed in order to evaluate the permeation of dissolved tritium in the liquid metal breeder to the secondary CO<sub>2</sub>. The 1-D code TMAP7 has been used. It can be inferred from the results that the diffusive flux of tritium to the CO<sub>2</sub> is practically null, whereas the final partial pressure of T<sub>2</sub> in the secondary is lower than the tolerance of the code. This demonstrates the efficacy of silicon carbide as tritium permeation barrier.

As a proposal to continue this development, the design could be adapted for a near-term reactor (e.g. the so-called DEMO1 assessed under the EU Programme). Besides, further analyses should be performed (e.g. characterization of the thermomechanical behaviour in terms of response to thermal transients, off-normal operation, etc.). Above all, it would be very valuable to construct and test a prototype.

#### **6.4. The value of CAD & graphic design tools and virtual reality in the integration of complex systems**

The use of CAD combined with graphical design tools, including kinematics simulation and augmented virtual reality (e.g. force feedback in haptic devices) has revealed as very useful to validate integration concepts and maintenance operations from the early design stages. They allow reducing the time and cost of development by reducing the number of physical mock-ups and avoiding deadlocks.

The possibility of evaluating possible collision paths, assembly clearances, design incompatibilities, etc., as well as estimating operating times is remarkably improved by modern geometry analysis tools and rendering engines.

This is particularly valuable in the design of remote maintenance procedures in very harsh environments like inside the vacuum vessel of a fusion reactor (high temperature and radiation dose rate, limited space, poor visibility, absence of colour contrast, etc.) since it can help teleoperators in an extraordinary manner. This fact can increase the reliability of remote procedures and the operating time can be reduced; in consequence, the unavailability related to maintenance downtimes is also reduced, for both planned and unplanned outages.

The use of this kind of tools is described in this thesis. They have been used during part of the design activities developed in Chapter 2 for the demonstration of the remote handling procedures related to the Test Blanket System in ITER. The used tools have been very useful to identify and correct design issues.

An improved methodology has been used to assess the behaviour and improve the design of the cable guide carrying the control & power cables to the Cassette Toroidal Mover, a component belonging to the ITER Divertor Remote Handling System.

As mentioned in Section 6.2, these methodologies can be used in any other engineering development with saving in time, efforts and cost.

#### **6.5. Alternative piping connection systems for DEMO and non-destructive testing technologies**

A significant factor affecting the time needed for planned and unplanned maintenance of in-vessel components like the breeding blanket and the divertor is the connection/disconnection of fluid circuits feeding such components (coolants, breeders and tritium carriers). It is estimated cutting and welding involve 51% of the total process time in the upper ports (39% for the lower ports) for scheduled maintenance. Current RH procedures based on conventional welding, cutting and inspection are intrinsically slow and usually need the intervention of robotic manipulators. Thus, the development of quick feasible pipe connectors is mandatory.

A design concept of a generic **jacket flange including leak testing and tightened by a quick disconnection system** (QDS) has been proposed here. Indeed, it has been demonstrated that current commercial gaskets (Helicoflex HNR229) and QDS can fulfil the sealing requirements foreseen for DEMO pipes. For example, this specific kind of gasket could be used for ultra-high vacuum applications in ITER.

The maximum working temperature of the double seal gasket HNR229 (600°C) makes it suitable for using in the different pipes of DEMO in-vessel components, although more developments should be needed if the temperature of primary coolants is raised to improve the power conversion cycle efficiency. On the other hand, no evidences about the performance of Helicoflex gaskets under the considerably high 14-MeV neutron flux expected in the vacuum vessel upper ports during operation have been found in literature. Helicoflex gaskets are extensively used to seal pressure vessels in PWR, BWR and gas-cooled fission reactors but not in fast reactors, with a neutron spectrum more similar to the fusion one. Nor it is known the behaviour of this sealing method against loads coming from plasma transient events like disruptions, mainly because there are still too many uncertainties about such phenomena in DEMO.

Several v-clamp designs from the gasket manufacturer have been found to fulfil the gasket seating load requirements in terms of minimum axial clamping load and minimum tightening load.

Both the v-clamp and the gasket can be installed/removed in/from the flange by remote handling. A v-clamp manipulator has been designed to transport and place the v-clamp, as well as to screw/unscrew the fastener. Besides, another tool has been designed to allow transporting, positioning, aligning, fixing and removing the double seal gasket.

Considering the design of the RH equipment can be adapted to the available space in the upper ports, the main disadvantage of this proposal is the difficulty of using only a RH system to install a number of connectors in parallel, so that operation times can be excessively penalized if the procedure is sequential.

Besides the jacket flange connector, **a conceptual design of a RH compatible pipe connection system for DEMO breeding blanket pipes based on brazing** has been produced. Brazing is a widely used joining technique which produces leak-proof high strength joints, with excellent stress distribution, little distortion and minimum oxidation.

The design is based on a selection of materials proposed by Sandia National Laboratories to seal radioactive material transport packages made of stainless steel by brazing in a helium atmosphere, so that such combination of materials achieves the best wetting behaviour. Although it is possible to provide alternatives to one of the indicated filler metals (BAu-4) -mainly composed by gold (82%)-. For example, Ni-Pd-Cr alloys are cheaper and their mechanical performance is similar or even superior. On the other hand, the use of internal parts made of a nickel alloy (Ni-200) excludes its utilization under flowing PbLi because of high corrosion rate, but it is suitable for helium and water pipes.

The design includes an induction heating system, a brazing atmosphere supply, an inspection system (helium leak testing) and a positioning and alignment system.

The initial design also included a bolted union to provide stiffness against disruptions and thermal loads because it had been recommended by a previous work. Since screwing/unscrewing of captive bolts excessively slows down the maintenance procedure, two different designs of quicker clamped unions have been created, as well as a remote handling device to install/uninstall them. However, several references found in literature suggest the possibility of suppressing the external clamp, which would significantly improve the integrability of the connector.

Electromagnetic-thermal transient analyses with the FEM code ANSYS APDL have demonstrated that the induction heating system can provide a really fast way to ensure the sealing of pipes by means of a proper design of the geometry and the coil operation

parameters, which allows concentrating the heat in a very small volume. However, the heating velocity strongly depends on the Curie temperature of the selected filler metal and base metal. Furthermore, the brazing process requires uniform temperature near the interface between the base metal and the filler metal to obtain suitable mechanical properties, which means longer heating times. Assuming low values of Curie temperature for both materials involves increasing the heating time from 25 s to 30 minutes, approximately. But even so, this time is shorter than the one consumed by heat treatment in the case of in-bore welded joints (EUROFER pipes).

Thermomechanical analysis with the FEM code ANSYS Workbench have been made in order to study the possibility of originating plastic deformation and residual stresses near the joint between the Ni-200 parts due to thermal gradients during cooling after the end of the brazing process. Results show small plastic strain occurs in the Ni-200 upper part, but it can be minimized by modifying the shape of the filler metal groove.

The capillary flow of the BAu-4 filler metal during the brazing process has been modelled using a CFD approach (FVM code ANSYS FLUENT). The objective has been to develop a methodology for predicting the filler metal flow along the gap, in order to optimize its spreading by means of modifying the filler metal groove and gap geometries. The results show a fairly good agreement with the analytical model ones. Beyond the validation of the numerical model, this result confirms the flow due to capillary forces is very fast at the beginning, which involves the need of an accurate control system for the heating process, as well as a careful design of the mentioned elements of the connector.

The possibility of producing long half-life transmutation isotopes from the connector materials has been assessed using the activation code ACAB. Surface gamma dose rate and specific activity have been obtained for the main components of the brazing connector at shutdown and 5 days, 12 days and 1 year after it. According to the results, the grade of radiation hardening of the RH equipment should not be too high. On the other hand, although the production of activation products can be reduced or avoided by making stricter the requirements for the chemical composition of the materials, as well as by using RAFM steel as piping material, it can be seen that transmutation in these materials is not an issue, since the reduction of mass for the main elements of the different components is very low.

The tritium permeation phenomenon through the connector has been also studied in a preliminary way with the 1-D code TMAP7, showing the amount of tritium permeated to the environment is certainly low, as well as the mobile inventory in the material segments after one pulse. These results are promising for helium and water pipes connection –although more complex phenomena are expected in the last case-. On the other hand, the model should be adapted and analysed for the alternative base and filler metals selected for PbLi pipes.

Different works in literature show there is a number of variables like process atmosphere, brazing temperature and time, clearance and condition of surface affecting the capillary flow of the filler metal during brazing and, consequently, the mechanical strength of the joint. Although theoretical or modelling approaches can be followed, experiments are by far the best way to optimize these features, showing that the type of filler metal is a more important factor affecting the mechanical strength of the joint than the clearance and the brazing time. In consequence, it is recommendable to guide the following steps towards manufacturing and testing a mock-up of the connector. Specifically, it is advisable to study the application of the method for joining RAFM steel pipes and the suppression of the internal Ni-200 parts to directly braze the pipe material. The use of the connector in PbLi pipes would be benefited from it.

As complementary to the development of the previously commented design of pipe connectors, the state of the art of three **non-destructive testing technologies** for welded joints in pipes, which can be also used to inspect any mechanical component, has been assessed.

The possibility of converting an optical image into an electronic signal by means of an image sensor and subsequently performing image numeric processing is very valuable for remote visual inspection. The use of **thermoelectric cooling** (based on Peltier's effect) allows reducing the image sensors dark current, which turns into an increase of the exposure time and hence allows extending the useful life of the device.

Cameras based on CCD and CMOS image sensors are not suitable to operate in high radiation environments as the expected during DEMO in-vessel components maintenance.

CID cameras are the unique solid-state cameras capable of operating in high radiation environments. Some models of these cameras can operate with low noise level in environments with 200 times the expected gamma dose rate in the upper ports of DEMO vacuum vessel one week after shutdown, and with 10 times the expected dose rate in the lower ports.

Furthermore, these kinds of cameras offer the possibility of using coatings for x-ray, deep ultra-violet and infrared, which is very interesting for combining direct visual inspection with subsequent or real-time advanced image analysis.

Nevertheless, the maximum working temperature of CID cameras is lower than ones expected in upper ports during maintenance of in-vessel components. This issue could be overcome by using and actively cooled casing for controlling the temperature of the camera.

**Electromagnetic-acoustic transducers (EMAT)** are very suitable for high temperature applications since they do not require contact. The capability of generating a wide range of ultrasonic wave-modes by different configuration of transducers is very appropriate for the inspection of a wide variety of weld defects. Specifically, torsional and flexural waves are the most suitable for the inspection of pipe-like components.

Furthermore, EMAT can be applied to the inspection of paramagnetic and relatively low electric conductivity materials like austenitic stainless steels, even in the case of composites.

Present EMATs can be combined with high sensitivity flaw detectors which provide advanced wave analysis software, as well as with thickness gages, which allows evaluating corrosion in pipe walls with high resolution. As referenced by the ITER Remote Handling Manual (this kind of transducers are going to be used for the inspection of the shielding blanket cooling pipes in ITER), they are also radiation hardened and are capable of operating in the conditions existing during DEMO in-vessel components maintenance.

Finally, **Laser ultrasonic transducers** are widely used for industrial applications like on-line seamless steel tubing process control, automated weld inspection in automotive industry, or the inspection of aircraft components, where speed and flexibility of this technique are not available with conventional pulse-echo ultrasonic inspection systems. As its relative EMAT, it has the advantage of contactless for high temperature applications.

The major disadvantage of this method is probably price. Industrial laser ultrasonic systems range from 400000 to 1500000 €, although R&D systems are less expensive.

Although laser ultrasonic is considered a promising technique for inspection in radiation environments, it is difficult to find references of real applications in these conditions. At least a reference of the efficacy of the laser approach for real-time resonant ultrasound measurements in a severe radiation environment has been found.

At present, EMAT and Laser UT are being further studied in the framework of the EUROfusion Remote Maintenance Project in order to develop an integrated tool based on in-bore welding, cutting and NDT. A mock-up is expected to be constructed and tested within the current programme (2014-2018).



# **Annexes**



# Objetivos

El principal objetivo de esta tesis es demostrar la necesidad de aplicar los principios del RAMI al diseño de componentes y sistemas nucleares para tecnología de fusión.

Esto se aborda a través de varios objetivos técnicos que pueden resumirse en los siguientes puntos:

- Propuesta de un diseño conceptual de una instalación de demostración de manipulación remota del ITER Test Blanket System. Esta instalación, complementaria a otras instalaciones de evaluación de componentes que serán requeridas en los próximos años, debe proporcionar soluciones para validar conceptos de diseño, para estudiar la fiabilidad del equipamiento –ciertamente valioso para aumentar y mejorar las bases de datos que se usarán en el diseño de dispositivos posteriores- y para entrenar a futuros operadores de sistemas de manipulación remota.
- Desarrollo de metodologías para validar conceptos de integración y operaciones de mantenimiento mediante el uso de combinaciones de herramientas de CAD y de diseño gráfico. Estas metodologías, que se revelan muy útiles para minimizar el tiempo, el esfuerzo y el coste de desarrollo de tecnología, se aplican al estudio de varias operaciones de mantenimiento remoto del Test Blanket System y el Divertor System de ITER.
- La dificultad de alcanzar una alta disponibilidad global de planta en las futuras centrales eléctricas de fusión y su influencia en el coste de la electricidad pueden contrarrestarse parcialmente mediante la optimización del balance de planta. Esto se afronta aquí a través del diseño de un ciclo de conversión de potencia compacto, eficiente, fiable y adaptable a perfiles de generación pulsada, basado en dióxido de carbono, para un reactor de demostración a corto plazo.
- El diseño de componentes primeros en su especie encaminados a maximizar la fiabilidad y la disponibilidad de los sistemas de los que formarán parte y, al mismo tiempo, optimizar su rendimiento funcional (ej. eficiencia térmica, nivel de sellado, etc.). Esto comprende el diseño de: a) un novedoso intercambiador de calor de metal líquido para el sistema de conversión de potencia de un DEMO a medio plazo; y b) Sistemas rápidos de conexión y desconexión de tuberías: fiables, inspeccionables y compatibles con manipulación remota, que incrementan la disponibilidad de los componentes internos de la cámara de vacío, los cuales representan los elementos más críticos en una central eléctrica de fusión.



## **6.1. Introducción**

En el diseño de componentes y sistemas para tecnología de fusión pueden seguirse distintas estrategias para maximizar la disponibilidad de futuros dispositivos como es el caso de las centrales eléctricas comerciales. Esto será crítico en el coste final de la electricidad generada por fusión. Diversos estudios han demostrado que será necesario alcanzar valores de disponibilidad elevados (cerca del 80%) para garantizar la viabilidad económica de la fusión. Esto es debido en la mayor parte al hecho de que el coste de la electricidad generada por fusión, en contraste con la obtenida mediante otras tecnologías energéticas, no estará condicionado fundamentalmente por los costes de operación (ej. coste del combustible), sino por el capital de inversión en construcción. El diseño de componentes clave estará basado en tecnologías novedosas y no suficientemente demostradas, como las usadas para el ciclo de combustible autosuficiente o los sistemas de disipación de calor, cuya fiabilidad es poco conocida. También hay enormes lagunas en el conocimiento de fenómenos transitorios del plasma como interrupciones o ELMs, que podrían afectar a la fiabilidad global de la planta.

Los componentes del interior de la cámara de vacío, y en particular los componentes situados de cara al plasma estarán sometidos a una fluencia muy elevada de neutrones de 14 MeV, que provocará tasas de daño de  $\sim 10$  dpa/año (a plena potencia) en el caso de DEMO; y 20-30 dpa/año (a plena potencia) en el caso de una central eléctrica. El necesario replazo de estos componentes cada 2-5 años (plena potencia) mediante técnicas de manipulación remota incrementa inexorablemente la indisponibilidad de la planta hasta límites críticos. Se prevé que la duración del mantenimiento planificado de los componentes del interior de la cámara de vacío sea de unos 22 meses. Si se dobla el número de sistemas que operan en paralelo la duración del mantenimiento se reduciría a casi la mitad, de modo que cuatro sistemas podrían completar el mantenimiento en unos 6 meses.

Las actividades de I+D pueden ayudar a mejorar la fiabilidad intrínseca de los componentes, por ejemplo mediante el desarrollo de nuevos materiales con mayor resistencia a la fluencia. Pero es la configuración/disposición de los componentes básicos lo que puede mejorar la fiabilidad de los sistemas (ej. redundancia, reducción de carga, etc.) a principalmente su disponibilidad, a través de la mantenibilidad y la inspeccionabilidad (ej. asumiendo principios de mantenimiento preventivo).

En consecuencia, la estrategia del RAMI debe formar parte de los procedimientos de diseño desde las primeras fases conceptuales hasta las fases de ingeniería de detalle. Todas ellas deben estar firmemente apoyadas por el análisis modal de fallos, efectos y criticidades (FMECA). Los códigos de diseño como RCC-MR o ASME, los códigos de prácticas y las librerías de estándares deben presentar los conceptos del RAMI y canalizar las actividades de diseño en la forma de procedimientos estandarizados. Deben adaptarse a las estrategias de diseño adoptadas actualmente en la mayoría de los programas internacionales de fusión: comienzo desde un conjunto de hipótesis y requisitos iniciales y tratamiento global de los problemas físicos y tecnológicos en códigos de sistemas 0-D, antes de pasar a análisis más detallados en códigos unidimensionales o multidimensionales.

En las siguientes Secciones se presenta una visión general de las principales conclusiones alcanzadas en los Capítulos anteriores, junto con algunas propuestas para un desarrollo posterior del trabajo presentado en esta tesis.

## **6.2. Estudios de integración del Test Blanket System en ITER. Diseño conceptual de una instalación de demostración de manipulación remota**

La disponibilidad de instalaciones de evaluación de componentes entre ITER y DEMO será limitada. Actualmente, sólo puede preverse la construcción de fuentes de neutrones para el ensayo de materiales (IFMIF o variantes simplificadas como DONES o ENS) y pequeñas instalaciones como lazos de gas o metal líquido.

En consecuencia, es posible que muchas de las tecnologías claves para una central de fusión no puedan probarse en condiciones de operación representativas antes de la construcción de DEMO, de modo que la tecnología propuesta deberá basarse en extrapolaciones de los límites superiores de la operación de ITER.

A pesar de esta pobre perspectiva, el desarrollo de técnicas de manipulación remota puede beneficiarse del requisito de la Organización ITER de demostrar físicamente la operación de los sistemas de manipulación remota antes de su instalación en el edificio del reactor y en el resto de edificios implicados. Uno de los programas de investigación transversales más importantes en ITER es el Programa TBM (Test Blanket Modules, módulos de ensayo de la envoltura regeneradora). Permitirá ensayar conceptos de envoltura regeneradora en un entorno de fusión representativo a través de prototipos construidos a escala reducida. Al igual que sus sistemas auxiliares, el mantenimiento y remplazo de los TBMs a lo largo del Programa se llevará a cabo mediante técnicas de manipulación remota. Por lo tanto, ITER requerirá una instalación de demostración de la manipulación remota de los TBM.

Se ha producido un diseño conceptual de una instalación de demostración de la manipulación remota de los TBMs europeos (HCLL y HCPB). Los objetivos de dicha instalación son demostrar la viabilidad de las operaciones de manipulación remota relacionadas con los TBMs en ITER, confirmar opciones de diseño para los equipos y sistemas de manipulación remota (manipuladores, herramientas, sistemas de visualización, realidad virtual, actuadores, controladores, software, etc.), validar y optimizar procedimientos de operación, examinar las consecuencias de fallos de los sistemas y confirmar procedimientos de rescate pre-establecidos, permitir ensayos de resistencia a largo plazo para estudiar la disponibilidad/fiabilidad de los sistemas de manipulación remota y proporcionar una plataforma de entrenamiento para diseñadores y operadores de sistemas de manipulación remota.

El trabajo comenzó con una intensa investigación bibliográfica para identificar los requisitos impuestos por ITER y por los diseñadores de los TBMs. Posteriormente, se ha diseñado la instalación considerando todos los requisitos identificados. Esto comprende el diseño conceptual de equipos y sistemas y su disposición en la instalación.

Se ha usado extensivamente el diseño gráfico. Se han diseñado y/o integrado en el modelo CAD 3-D alrededor de 350 ensamblajes con un número total de ~1200 partes. Se ha combinado el diseño gráfico con simulaciones cinemáticas, especialmente para analizar algunas de las operaciones más importantes de la Hot Cell, así como para las operaciones de instalación/desinstalación de los componentes del Test Blanket System en la Port Cell número 16. Estas operaciones se han estudiado con un nivel de detalle superior. Este proceso ha permitido adquirir experiencia específica en sistemas de manipulación remota y en herramientas de diseño específicas (como las descritas en el Capítulo 4), que se han utilizado posteriormente en otros proyectos de investigación.

Algunas de las soluciones adoptadas posteriormente por ITER son notablemente semejantes a las propuestas en esta tesis.

Actualmente no hay ninguna iniciativa para construir la instalación de demostración en España. Sin embargo, aún persiste el interés de continuar hacia el diseño de detalle por la posibilidad de adaptar el alcance de la instalación más allá de los TBMs europeos, con el objetivo de vender servicios de demostración al resto de Agencias Domésticas involucradas en el Programa TBM. Esto también sería importante porque algunos conceptos ligados a la manipulación remota del TBS pueden ser relevantes para DEMO. Su influencia en las bases de datos de fiabilidad de componentes de fusión y en las actividades de I+D para DEMO es innegable.

### **6.3. Sistemas de conversión de potencia para DEMO**

El ciclo de Brayton es una solución muy atractiva para el sistema de conversión de potencia de DEMO debido a su relativa simplicidad y compacidad. Sin embargo, el uso de un gas muy ligero como el helio penaliza la eficiencia térmica debido a la necesaria compresión antes de la

absorción de calor de la fuente térmica. Esto podría compensarse parcialmente usando recuperación térmica y alcanzando temperaturas muy elevadas. Pero existen limitaciones derivadas del uso de aceros ferrítico-martensíticos de baja activación como el EUROFER como material estructural para la envoltura regeneradora, por ejemplo: temperatura de transición dúctil-frágil, fenómeno de fluencia a temperatura moderada, etc. Semejante trabajo de compresión implica un consumo muy alto en potencia de bombeo, lo cual penaliza excesivamente la potencia y la eficiencia eléctricas netas de la planta, especialmente en el caso de reactores de fusión a corto plazo ( $\sim 2 \text{ GW}_t$ ). Debe considerarse la pérdida de potencia debida a la baja eficiencia de los sistemas actuales de calentamiento y generación de la corriente del plasma. Además, existen dudas razonables sobre la disponibilidad futura de helio en la cantidad indispensable para operar una red de centrales eléctricas de fusión. Ciertamente, estos hechos restringen severamente la posibilidad de compensar el problema de alcanzar valores elevados de disponibilidad de la planta y su influencia en el coste de la electricidad mediante la optimización del balance de planta.

Aquí se ha estudiado el balance de planta de un reactor DEMO a corto plazo basado en una envoltura regeneradora refrigerada por helio (específicamente de tipo HCLL) y en el uso de **ciclos Brayton de dióxido de carbono supercrítico (S-CO<sub>2</sub>)** en el secundario.

Se ha analizado la literatura existente sobre esta materia para identificar las ventajas y los problemas potenciales del S-CO<sub>2</sub>.

Se han propuesto y analizado varias configuraciones de ciclo con fuentes de alta energía (envoltura regeneradora; 1835 MW) y de baja energía (divertor y cámara de vacío; 149 y 34,56 MW, respectivamente) integradas en un ciclo de potencia S-CO<sub>2</sub>, mediante una metodología convencional basada en la Primera y en la Segunda Ley de la Termodinámica, teniendo en cuenta varias aproximaciones e hipótesis. El principal objetivo ha sido maximizar la producción de electricidad. Se han propuesto e investigado cuatro propuestas a un ciclo básico de recompresión en el cual la envoltura regeneradora es la única fuente térmica.

La llamada Configuración 3 muestra el mejor rendimiento eléctrico ( $684 \text{ MW}_e$ ;  $\epsilon=33,89\%$ , con una eficiencia eléctrica neta del  $24,72\%$ ).

El trabajo se ha completado con un estudio de sensibilidad a variables claves del ciclo y con la optimización de los intercambiadores de calor, cuyo diseño está basado en la tecnología de intercambiadores de calor de circuito impreso (PCHE). El estudio de sensibilidad ha identificado la presión de entrada a la turbina y la temperatura de entrada al compresor principal como las variables claves en el rendimiento de la planta. Respecto a los intercambiadores de calor, las variables más influyentes son el punto pinch en el recuperador de baja temperatura y la caída de presión total. Su incremento, de acuerdo con su influencia en la producción de electricidad, significa una reducción de  $1/3$  en el volumen total de los intercambiadores de calor. La presión de entrada a la turbina se ha incrementado 20 bar para mantener las pérdidas de potencia por debajo del  $1\%$ .

La fiabilidad de los componentes del sistema de conversión de potencia es un punto clave en la disponibilidad de los reactores de fusión. Podría ser necesario hacer coincidir el mantenimiento de la parte secundaria del sistema de conversión de potencia con los periodos de mantenimiento planificado de los componentes internos de la cámara de vacío, como la envoltura regeneradora y el divertor (principales constituyentes del Sistema de Transferencia de Calor Primario), de modo que es imprescindible reducir las paradas no planificadas al máximo posible. Este principio se ha aplicado al diseño de **un intercambiador de calor de circuito impreso de plomo-litio/CO<sub>2</sub> supercrítico** para un reactor de fusión de  $3,35 \text{ GW}_t$  basado en el concepto de envoltura regeneradora a doble refrigerante –plomo-litio y helio- (DCLL) propuesto en el Programa Nacional Consolider TecnoFus.

Se ha seleccionado el carburo de silicio como material estructural por su resistencia a la presión y al calor bajo altas temperaturas de operación, su compatibilidad con flujos de plomo-litio, bajas difusividad y solubilidad de tritio y características de seguridad superiores a las de los materiales metálicos.

Se han sustituido los patrones de circuitos impresos comerciales basados en canales con sección semi-circular y trayectorias en zig-zag por una disposición de aletas con forma de perfil aerodinámico. Esto permite minimizar la caída de presión con una baja penalización en el área de transferencia de calor. Se ha usado un código para el diseño y el análisis viscoso (o no viscoso) de perfiles aerodinámicos subsónicos aislados para optimizar la forma de los perfiles mediante la minimización de su coeficiente de arrastre. Se ha seleccionado el perfil NACA0010, que pertenece a las series NACA-4-dígitos para alas de aviones, tanto para la corriente caliente como para la fría.

Se ha usado un modelo de transferencia de calor unidimensional para pre-dimensionar el intercambiador mediante la evaluación de los perfiles de temperatura a lo largo de los canales de ambas corrientes. Además, se han llevado a cabo análisis CFD con modelos a escala para optimizar la configuración de las aletas en términos de caída de presión y flujo térmico integrado, mediante la variación de la distancia entre las aletas según la dirección de flujo. A continuación se ha utilizado un modelo con la longitud total. Los resultados muestran resultados muy parecidos entre los perfiles de temperatura obtenidos con el modelo 1-D y el modelo CFD, aunque las correlaciones empíricas seleccionadas conducen a una ligera subestimación del coeficiente global de transferencia de calor. Las caídas de presión son bajas tanto para la corriente caliente como para la fría. Por otra parte, el flujo integrado total es mayor que el inicialmente esperado para este intercambiador a partir del diseño del ciclo.

Finalmente, se ha desarrollado un modelo de transporte para evaluar la permeación del tritio disuelto en el metal líquido regenerador al  $\text{CO}_2$  secundario. Se ha usado el código 1-D TMAP7. Puede deducirse de los resultados que el flujo difusivo de tritio al  $\text{CO}_2$  es prácticamente nulo, mientras que la presión parcial final de  $\text{T}_2$  en el secundario es menor que la tolerancia del código. Esto demuestra la eficacia del carburo de silicio como barrera de permeación de tritio.

Como propuesta para continuar este desarrollo, podría adaptarse el diseño para un reactor a corto plazo (ej. el llamado DEMO1, estudiado en el Programa Europeo). Además, deberían realizarse nuevos análisis (ej. caracterización del comportamiento termomecánico en términos de respuesta a transitorios térmicos, operación en condiciones anormales, etc.). Por encima de todo, sería muy valioso construir y ensayar un prototipo.

## **6.4. La importancia del CAD y de las herramientas de diseño gráfico en la integración de sistemas complejos**

El uso de CAD combinado con herramientas de diseño gráfico, incluyendo simulación cinemática y realidad virtual aumentada (ej. reflexión de fuerzas en dispositivos hápticos) se ha revelado muy útil para validar conceptos de integración y operaciones de mantenimiento desde las primeras fases de diseño. Permiten reducir el tiempo y el coste de desarrollo mediante la reducción del número de prototipos o maquetas físicas y la eliminación de puntos muertos.

Las modernas herramientas de análisis geométrico y los motores de renderización mejoran extraordinariamente la posibilidad de evaluar posibles trayectorias de colisión, holguras en ensamblajes, incompatibilidades de diseño, etc., así como de estimar tiempos de operación.

Esto es particularmente útil en el diseño de procedimientos de mantenimiento remoto in ambientes muy severos como el del interior de la cámara de vacío de un reactor de fusión (alta temperatura y tasa de dosis de radiación, espacio limitado, visibilidad pobre, ausencia de contrastes de color, etc.) dado que puede ayudar a los teleoperadores de manera notable. Este hecho puede incrementar la fiabilidad de los procedimientos remotos y reducir el tiempo de operación; en consecuencia, puede reducirse la indisponibilidad relacionada con las paradas de mantenimiento, tanto planificadas como no planificadas.

El uso de este tipo de herramientas se describe en esta tesis. Se han utilizado durante parte de las actividades de diseño desarrolladas en el Capítulo 2 para la demostración de los procesos

de manipulación remota relacionados con el Test Blanket System en ITER. Las herramientas empleadas han sido muy útiles para identificar y corregir problemas de diseño.

Se ha utilizado una metodología mejorada para estudiar el comportamiento y mejorar el diseño de la guía de cables que conduce los cables de control y potencia al Cassette Toroidal Mover (CTM), un componente del Sistema de Manipulación Remota del Divertor en ITER.

Como se ha mencionado en la Sección 6.2, estas metodologías pueden utilizarse en cualquier otro desarrollo de ingeniería con ahorro de tiempo, esfuerzo y coste.

## **6.5. Sistemas alternativos de conexión de tuberías para DEMO y tecnologías de inspección no destructiva**

Un factor que afecta significativamente al tiempo necesario para el mantenimiento tanto planificado como no planificado de componentes del interior de la cámara de vacío como la envoltura regeneradora y el divertor es la conexión y desconexión de los circuitos de fluidos que alimentan a dichos componentes (refrigerantes, regeneradores y portadores de tritio). Se estima que el corte y la soldadura de las tuberías suponen el 51% del tiempo total de proceso en los puertos superiores (39% para los inferiores) para mantenimiento planificado. Los procedimientos actuales de manipulación remota basados en soldadura convencional, corte e inspección son intrínsecamente lentos y suelen necesitar la intervención de manipuladores robóticos. Así, es imprescindible desarrollar conectores rápidos viables para tuberías.

Aquí se ha propuesto un concepto de diseño de una **brida genérica que incluye evaluación de fugas y que se asegura mediante un sistema de desconexión rápida** (QDS). Ciertamente, puede demostrarse que los sellos (Helicoflex HNR229) y QDS comerciales actuales pueden cumplir los requisitos de sellado previstos para las tuberías de DEMO. Por ejemplo, este tipo específico de sello podría usarse para aplicaciones de ultra-alto vacío en ITER.

La máxima temperatura de operación del doble sello HNR229 (600°C) hace que sea adecuado para usarse en las diferentes tuberías de los componentes internos de DEMO, aunque sería necesario un mayor desarrollo si se incrementara la temperatura de los refrigerantes primarios para optimizar la eficiencia del ciclo de conversión de potencia. Por otra parte, en la literatura no se han encontrado evidencias del rendimiento de los sellos Helicoflex bajo el flujo considerablemente alto de neutrones de 14 MeV que se espera en los puertos superiores de la cámara de vacío. Los sellos Helicoflex se utilizan ampliamente para sellar las vasijas de presión de reactores de fisión PWR, BWR y refrigerados con gas, pero no en reactores rápidos, cuyo espectro neutrónico es más similar al de fusión. Tampoco se conoce el comportamiento de este método de sellado frente a cargas provocadas por transitorios del plasma como es el caso de las interrupciones, principalmente porque aún hay demasiadas incertidumbres sobre tales fenómenos en DEMO.

Se ha visto que diversos diseños de abrazaderas con perfil V del mismo fabricante que el sello seleccionado cumplen los requisitos de carga de sellado en términos de mínima carga de ajuste axial y mínima carga de apriete.

Tanto la abrazadera con perfil V como el sello pueden instalarse/desinstalarse en/de la brida mediante manipulación remota. Se ha diseñado un manipulador para transportar y colocar la abrazadera, así como para atornillar/desatornillar el elemento de apriete. Además se ha diseñado otra herramienta para transportar, colocar, alinear, fijar y quitar el doble sello.

Considerando que el diseño del equipamiento de manipulación remota puede adaptarse al espacio disponible en los puertos superiores, la principal desventaja de esta propuesta es la dificultad de usar sólo un sistema para instalar varios conectores en paralelo, de modo que los tiempos de operación pueden verse excesivamente penalizados si el procedimiento es secuencial.

Junto al conector de brida, se ha producido un **diseño conceptual de un sistema de conexión compatible con manipulación remota para tuberías de la envoltura regeneradora de DEMO, basado en brazing**. El brazing es una técnica de unión muy extendida que produce uniones de alta resistencia, a prueba de fugas, con excelente distribución de tensiones, pequeña distorsión y mínima oxidación.

El diseño está basado en una selección de materiales propuesto por Sandia National Laboratories para sellar contenedores de transporte de material radiactivo mediante brazing en una atmósfera de helio, de modo que tal combinación de materiales consigue el mejor comportamiento en términos de mojabilidad. Aunque es posible proporcionar alternativas para uno de los metales de relleno indicados (BAu-4, fundamentalmente compuesto por oro (82%)). Por ejemplo, las aleaciones de Ni-Pd-Cr son más baratas y su comportamiento mecánico es similar o incluso superior. Por otra parte, el uso de partes internas fabricadas en una aleación de níquel (Ni-200) excluye su uso en tuberías de PbLi debido a la alta tasa de corrosión, pero resulta adecuado para tuberías de helio y agua.

El diseño incluye un sistema de calentamiento por inducción, un sistema de suministro de atmósfera, un sistema de inspección (test de fugas) y un sistema de posicionamiento y alineación.

El diseño inicial también incluía una unión atornillada para proporcionar mayor solidez frente a disrupciones y cargas térmicas porque un trabajo previo lo había recomendado. Teniendo en cuenta que el atornillado/desatornillado de los tornillos cautivos retarda excesivamente el proceso de mantenimiento, se han creado dos diseños diferentes de uniones más rápidas basadas en conectores mecánicos, así como un dispositivo para instalarlas/desinstalarlas de forma remota. Sin embargo, varias referencias encontradas en la literatura sugieren la posibilidad de suprimir la unión externa, lo cual mejoraría significativamente la integridad del conector.

Análisis electromagnéticos-térmicos transitorios con el código de elementos finitos ANSYS APDL han demostrado que el sistema de calentamiento por inducción puede conseguir el sellado de las tuberías de una forma realmente rápida, por medio de un diseño adecuado de la geometría y de los parámetros de operación de la bobina, que permite concentrar el calor en un volumen muy pequeño. Sin embargo, la velocidad de calentamiento depende considerablemente de la temperatura Curie del metal de relleno y del metal base seleccionados. Además, el proceso de brazing requiere una temperatura uniforme cerca de la interfaz entre el metal base y el metal de relleno para obtener unas propiedades mecánicas adecuadas, lo cual significa tiempos de calentamiento más largos. Si se asumen valores bajos de la temperatura Curie para ambos materiales, el tiempo de calentamiento se incrementa desde 25 segundos a 30 minutos, aproximadamente. Pero incluso así, resulta una duración menor que la necesaria para el tratamiento térmico en el caso de uniones soldadas por métodos in-bore (tuberías de EUROFER).

Se han hecho análisis termomecánicos con el código de elementos finitos ANSYS Workbench para estudiar la posibilidad de que se originen deformación plástica y esfuerzos residuales cerca de la unión entre las partes de Ni-200 debido a los gradientes térmicos durante el enfriamiento posterior al proceso de brazing. Los resultados muestran que se produce una pequeña deformación plástica en la parte superior de Ni-200, pero puede minimizarse modificando la forma de la ranura del metal de relleno.

Se ha modelado el flujo capilar del metal de relleno BAu-4 durante el proceso de brazing utilizando un enfoque de CFD (código de volúmenes finitos ANSYS FLUENT). El objetivo ha sido desarrollar una metodología para predecir el flujo del metal de relleno a lo largo del espacio entre las piezas de metal base, de modo que se pueda optimizar su propagación mediante la modificación de la geometría de la ranura y del espacio entre las piezas. Los resultados concuerdan bastante bien con los obtenidos con el modelo analítico. Más allá de la validación del modelo numérico, este resultado confirma que el flujo debido a las fuerzas capilares es muy rápido al principio, lo cual implica la necesidad de un sistema de control preciso para el proceso de calentamiento, así como de un diseño cuidadoso de los mencionados elementos del conector.

Se ha utilizado el código ACAB para estudiar la posibilidad de producir isótopos de larga vida media por transmutación de los materiales del conector. Se han obtenido tasas de dosis gamma superficiales y actividades específicas para los principales componentes del conector en el momento de la parada del reactor y 5 días, 12 días y 1 año después. De acuerdo con los resultados, el grado de resistencia/protección frente a la radiación del equipamiento de manipulación remota no debería ser alto. Por otra parte, aunque la producción de productos de activación puede reducirse o evitarse haciendo que los requisitos de composición química de los materiales sean más estrictos, así como usando aceros ferrítico-martensíticos de baja activación para fabricar las tuberías, puede verse que en estos materiales la transmutación no supone un problema, ya que la reducción de masa en los principales elementos de los diferentes componentes es muy baja.

También se ha estudiado preliminarmente el fenómeno de la permeación de tritio a través del conector mediante el código 1-D TMAP7, observándose que la cantidad de tritio que ha permeado al ambiente es ciertamente baja, así como el inventario móvil en los segmentos de material tras la duración de un pulso. Estos resultados son prometedores para la conexión de tuberías de helio y agua –aunque se esperan fenómenos más complejos en el último caso-. Por otra parte, el modelo debería adaptarse y analizarse para los metales base y de relleno seleccionados para las tuberías de PbLi.

Diferentes trabajos en la literatura muestran que hay toda una serie de variables, como la atmósfera del proceso, la temperatura y el tiempo de brazing, la holgura entre piezas de metal base y las condiciones superficiales, que afecta al flujo capilar del metal de relleno durante el brazing y, consecuentemente, a la resistencia mecánica de la unión. Aunque puede recurrirse a aproximaciones teóricas o a modelización, los experimentos son de lejos el mejor modo de optimizar dichas variables, y muestran que el tipo de metal de relleno es un factor más importante que afecta a la resistencia de la unión que la holgura y el tiempo de brazing. En consecuencia, se recomienda guiar los próximos pasos hacia la fabricación y la evaluación de un prototipo del conector. Específicamente, es aconsejable estudiar la aplicación del método a la unión de tuberías de aceros ferrítico-martensíticos de baja activación y la supresión de las piezas internas de Ni-200 para realizar directamente el brazing del material de la tubería. De ello se beneficiaría el uso del conector en tuberías de plomo-litio.

Como complemento al desarrollo de los diseños de conectores de tuberías previamente comentados, se ha analizado el estado del arte de **tecnologías de inspección no destructiva para uniones soldadas en tuberías**, que también pueden usarse para inspeccionar cualquier tipo de componente mecánico.

La posibilidad de convertir una imagen óptica en una señal electrónica por medio de un sensor de imagen y posteriormente llevar a cabo el procesamiento numérico de la imagen es muy valiosa para inspección visual remota. El uso de **refrigeración termoeléctrica** (basada en el efecto Peltier) permite reducir la corriente de oscuridad de los sensores de imagen, lo cual deviene en un incremento del tiempo de exposición y por tanto permite extender la vida útil del dispositivo.

Las cámaras basadas en sensores de imagen CCD y CMOS no son adecuadas para operar en entornos de alta radiación como el previsto durante el mantenimiento de los componentes del interior de la cámara de vacío en DEMO.

Las cámaras CID son las únicas cámaras de estado sólido capaces de operar en entornos de alta radiación. Algunos modelos de este tipo pueden operar con bajo nivel de ruido en entornos con tasas de dosis gamma de hasta 200 veces la esperada en los puertos superiores de la cámara de vacío de DEMO una semana después de la parada del reactor, y de hasta 10 veces la tasa esperada en los puertos inferiores.

Además, este tipo de cámaras ofrece la posibilidad de usar recubrimientos para rayos-x, ultravioleta profundo e infrarrojo, lo cual es muy interesante para combinar inspección visual directa con análisis avanzado de imagen en tiempo real.

No obstante, la máxima temperatura de operación de las cámaras CiD es menor que las temperaturas previstas en los puertos superiores durante el mantenimiento de los componentes internos. Este problema podría solucionarse usando carcasas con refrigeración activa para controlar la temperatura de la cámara.

Los **transductores electromagnéticos-acústicos (EMAT)** son muy adecuados para aplicaciones de alta temperatura, dado que no requieren contacto. La capacidad de generar un extenso rango de modos de onda ultrasónicos mediante la diferente configuración de los transductores resulta muy apropiada para la inspección de una amplia variedad de defectos en soldaduras. Específicamente, las ondas torsionales y de flexión son las más adecuadas para la inspección de componentes como tuberías.

Además, los EMAT pueden aplicarse a la inspección de materiales paramagnéticos y con conductividad eléctrica relativamente baja como los aceros inoxidable austeníticos, incluso en el caso de composites.

Los EMAT actuales pueden combinarse con detectores de defectos que proporcionan software avanzado de análisis de ondas, así como con medidores de espesor, lo cual permite evaluar con alta resolución la corrosión en las paredes de las tuberías. Como se referencia en el Manual de Manipulación Remota de ITER (este tipo de transductores va a utilizarse para la inspección de las tuberías de refrigeración del blanket de ITER), son resistentes a radiación y son capaces de operar en las condiciones existentes durante el mantenimiento de los componentes internos de DEMO.

Finalmente, los **transductores ultrasónicos por láser** se usan ampliamente en aplicaciones industriales como el control en línea del proceso de fabricación de tubos de acero sin soldaduras, la inspección automática de soldaduras en la industria automovilística o la inspección de componentes de aviación, para los cuales la rapidez y flexibilidad de esta técnica no tienen correspondencia en los sistemas convencionales de inspección ultrasónica de pulso-eco. Como su relativo EMAT, tiene la ventaja de no necesitar contacto en aplicaciones de alta temperatura.

La principal desventaja de este método es probablemente su precio. Los sistemas ultrasónicos por láser industriales cuestan entre 400000 y 1500000 €, aunque los sistemas de I+D son más baratos.

Aunque se considera que la técnica de ultrasonidos por láser es prometedora para la inspección en ambientes radiactivos, es difícil encontrar referencias de aplicaciones reales en tales condiciones. Al menos se ha encontrado una referencia de la eficacia de esta técnica para medidas de ultrasonidos resonantes en tiempo real en un ambiente de radiación severa.

Actualmente, las técnicas EMAT y UT láser están siendo estudiadas con mayor profundidad en el marco del Proyecto de Mantenimiento Remoto de EUROfusion, con el objetivo de desarrollar una herramienta integrada basada en soldadura in-bore, corte e inspección no destructiva. Se espera que se fabrique y evalúe un prototipo dentro del programa en curso (2014-2018).

# Related publications

## Publications in International Journals

J.I. Linares, L.E. Herranz, I. Fernández, A. Cantizano, B.Y. Moratilla, Supercritical CO<sub>2</sub> Brayton power cycles for DEMO fusion reactor, *Applied Thermal Engineering* 76 (2015) 123-133.

I. Fernández, E. Rosa, I. Palermo, Design of a brazed connector for DEMO in-vessel components, *Fusion Engineering and Design* 89, Issues 9–10 (2014) 2363-2367

I. Fernández, L.A. Sedano, Design analysis of a lead-lithium/supercritical CO<sub>2</sub> printed circuit heat exchanger for primary power recovery, *Fusion Engineering and Design* 88, Issues 9-10 (2013) 2427-2430.

I. Serrano, A. Cantizano, J.I. Linares, B.Y. Moratilla, I. Fernandez, L.A. Sedano, Numerical modelling and design of supercritical CO<sub>2</sub> pre-cooler for fusion nuclear reactors, *Fusion Engineering and Design* 87, Issues 7–8 (2012) 1329-1332.

## Communications in Conferences

I. Fernández, E. Rosa, A. Ibarra, Progress on the design of a brazing connector for DEMO in-vessel components, proceedings of the 28<sup>th</sup> Symposium on Fusion Technology, San Sebastián (Spain), September 2014. Paper under review for publishing in *Fusion Engineering and Design*.

I. Fernández, E. Rosa, I. Palermo, Design of a brazed connector for DEMO in-vessel components, proceedings of the 11<sup>th</sup> International Symposium on Fusion Nuclear Technology, Barcelona (Spain), September 2013.

I. Fernández, L.A. Sedano, Design analysis of a lead-lithium/supercritical CO<sub>2</sub> printed circuit heat exchanger for primary power recovery, proceedings of the 27<sup>th</sup> Symposium on Fusion Technology, Liège (Belgium), September 2012.

A. Marqueta, J. Sanz, I. García, A. Gómez, A. García, I. Fernández, L. Ríos, L.A. Sedano, Diseño conceptual de la instalación de demostración de los dispositivos de manipulación remota para los módulos de ensayo de envoltura regeneradora de ITER, oral presentation in the 37<sup>th</sup> Annual Meeting of the Spanish Nuclear Society (Best presentation award in fusion area), Burgos (Spain), September 2012.

I. Fernández, G. Veredas, I. Serrano, A. Cantizano, J.I. Linares, B.Y. Moratilla, J. Fradera, L.A. Sedano, Design analyses of a lead-lithium/supercritical CO<sub>2</sub> printed circuit heat exchanger at DEMO power conversion ranges, proceedings of the 10<sup>th</sup> International Symposium on Fusion Nuclear Technology, Portland (USA), September 2011.

I. Fernández, L. Ríos, L.A. Sedano, Diseño conceptual de una instalación de demostración de la capacidad de manipulación remota del Test Blanket System en ITER, oral presentation and proceedings of the 36<sup>th</sup> Annual Meeting of the Spanish Nuclear Society, Santiago de Compostela (Spain), October 2010.

I. Fernández, J. Juanas, R. Rodríguez, L. Ríos, P. Vázquez, A. Bayón, J.I. Díaz, J. Alonso, L.A. Sedano, Estudio de detalle de varios procesos de manipulación remota de TBM en ITER, oral presentation and proceedings of the 35<sup>th</sup> Annual Meeting of the Spanish Nuclear Society, Sevilla (Spain), October 2009.

S. Terrón, I. Fernández, L. Ríos, J.M. Juanes, A. Bayón, J.I. Díaz, J. Alonso, L.A. Sedano, Estudios de integración de los Módulos de Ensayo de Envoltura en ITER. Revisión de especificaciones de los sistemas de manipulación integral remota para el diseño conceptual de una instalación de demostración, oral presentation in the 34<sup>th</sup> Annual Meeting of the Spanish Nuclear Society, Murcia (Spain), October 2008.

# Abbreviations

AC	Alternating Current
AEMET	Agencia Estatal de Meteorología
AEU	Ancillary Equipment Unit
AGHS	Activated Gas Handling System
AMF	Active Maintenance Facility
ANL	Argonne National Laboratory
ASM	American Society for Metals
ASME	American Society of Mechanical Engineers
ASTM	American Society for Testing and Materials
ATS	Air Transfer System
AVR	Augmented Virtual Reality
AWS	American Welding Society
BB	Breeding Blanket
BBR	By-Pass Blanket Recuperator
BIT	Built in Test
BM	Back Manifolds
BNK	Blanket
BPVC	Boiler and Pressure Vessel Code
BSM	Blanket Shielding Module
BWR	Boiling Water Reactor
BZ	Breeding Zone
CAD	Computer Aided Design
CAE	Computer Aided Engineering
CAM	Computer Aided Manufacturing
CAT	Computer Assisted Teleoperation
CC	Cooling Circuit
CCD	Charge-Coupled Device
CCFE	Culham Centre for Fusion Energy
CCU	Camera Control Unit
CCWS	Component Cooling Water System
CEA	Commissariat à l'énergie atomique et aux énergies
CED	Committed Effective Dose
CEIT	Centro de Estudios e Investigaciones Técnicas de Guipúzcoa
CFC	Carbon Fibre-reinforced carbon Composite
CFD	Computational Fluid Dynamics
CHWS	Chilled Water System
CID	Charge Injection Device
CIEMAT	Centro de Investigaciones Energéticas, Medioambientales y Tecnológicas
CIMNE	International Center for Numerical Methods in Engineering
CL	Clamp Load
CMM	Cassette Multifunctional Mover
CMOS	Complementary Metal-Oxide Semiconductor
CMT	Crane Mounted Transporter
CNC	Computer Numeric Control
CODAC	Control and Data Acquisition
CoE	Cost of Electricity
CoG	Centre of Gravity
CPRHS	Cask and Plug Remote Handling System
CPS	Coolant Purification System
CSF	Continuum Surface Force
CSP	Concentrated Solar Plants
CTM	Cassette Toroidal Mover
CVCS	Chemical and Volumetric Control System
CVD	Chemical Vapor Deposition
DBTT	Ductile-Brittle Transition Temperature
DCLL	Dual Coolant Lithium Lead

DEMO	Demonstration reactor
DHT	Digital Human Models
DIV	Divertor
DMU	Digital Mock-Up
DOF	Degrees of Freedom
DSC	Differential Scanning Calorimetric
DTP	Divertor Test Platform
EA	Empresarios Agrupados
EAM	Embedded Atom Method
ECRH	Electron Cyclotron Resonance Heating
ECTS	Equatorial Cask Transport System
EFDA	European Fusion Development Agreement
ELM	Edge Localized Modes
EM	Electromagnetic
EMAT	Electromagnetic-Acoustic Transducer
ENEA	Ente per le nuove tecnologie, l'energia e l'ambiente
EU	European Union
EURATOM	European Atomic Energy Community
F4E	Fusion for Energy
FCI	Flow Channel Inserts
FEM	Finite Element Method
FEP	Fluorinated Ethylene Propylene
FMEA	Failure Mode and Effects Analysis
FMECA	Failure Modes, Effects and Criticalities Analysis
FPGA	Field Programmable Gate Array
FPP	Fusion Power Plant
FRDB	Failure Rate Database
FW	First Wall
GE	General Electric
GUI	Graphical User Interface
H&CD	Heating and Current Drive
HC	Hot Cell
HCCB	Helium Cooled Ceramic Breeder
HCCR	Helium Cooled Ceramic Reflector
HCF	Hot Cell Facility
HCLL	Helium Cooled Lithium Lead
HCML	Helium Cooled Molten Lithium
HCPB	Helium Cooled Pebble Bed
HCS	Helium Cooling System
HEX	Heat Exchanger
HLCS	High Level Control System
HMI	Human Machine Interface
HP	High Pressure
HRGG	Heat Recovery Gas Generator
HRS	Heat Rejection System
HT FM	High-Temperature Ferritic-Martensitic
HTR	High Temperature Recuperator
HTS	High Temperature Superconductor
HTS	High Temperature Shield
HVAC	Heating, Ventilating and Air Conditioning
IAEA	International Atomic Energy Agency
IB	Inboard
ICRH	Ion Cyclotron Resonance Heating
IDM	ITER Document Management System
IEC	International Electrotechnical Commission
IFERC	Fusion Energy Research Centre
IFMIF	International Fusion Materials Irradiation Facility
ILW	ITER Like Wall
IMMS	ITER Maintenance Management System
IO	ITER Organization

IQS	Institut Químic de Sarrià
IR	Infrared
IRMS	ITER Remote Maintenance System
ISHM	Integrated System Health Management
ITB	Internal Transport Barrier
ITER	International Thermonuclear Experimental Reactor
ITMA	Instituto Tecnológico de Materiales de Asturias
IVM	In-Vessel Mover
IVT	In-Vessel Transporter
IVVS	In-Vessel Viewing System
JAERI	Japan Atomic Energy Research Institute
JET	Joint European Torus
KAERI	Korea Atomic Energy Research Institute
KIT	Karlsruhe Institute of Technology
LAC	Local Air Coolers
LLCB	Lithium Lead Ceramic Breeder
LLE	Laboratory for Laser Energetics
LM	Liquid Metal
LMTD	Log Mean Temperature Difference
LOCA	Loss of Coolant Accident
LP	Low Pressure
LRUS	Laser Resonant Ultrasound Spectroscopy
LTR	Low Temperature Recuperator
LTS	Low Temperature Shield
LWR	Light Water Reactor
MAM	Master/Slave Robotic Arm
MDT	Mean Down Time
MDTNS	Mean Down Time Non-Scheduled
MDTS	Mean Down Time Scheduled
MHD	Magnetohydrodynamics
MIG	Metal Inert Gas
MMS	Multi-Module Segment
MOS	Metal-Oxide Semiconductor
MPD	Multi-Purpose Deployer
MTBF	Mean Time Between Failures
MTTF	Mean Time to Failure
MTTR	Mean Time To Repair
MUT	Mean Unavailability Time
NACA	National Advisory Committee for Aeronautics
NB	Neutral Beam
NBI	Neutral Beam Injector
NDT	Non-Destructive Testing
NET	Next European Torus
NIF	National Ignition Facility
NITE	Nano-Infiltration and Transient Eutectic-phase
OB	Outboard
ODS	Oxide Dispersion-Strengthened
ORC	Organic Rankine Cycles
OSD	Operations Sequence Description
OWT	Orbital Welding Technology
PAV	Permeator Against Vacuum
PC	Port Cell
PCHE	Printed Circuit Heat Exchanger
PCS	Power Conversion System
PDF	Plant Definition Form
PF	Pipe Forest
PF	Poloidal Field
PFCT	Plasma-Facing Components Transporter
PHTS	Primary Heat Transfer System
PP	Port Plug

PPCS	Power Plant Conceptual Studies
PPM	Periodic Permanent Magnet
PPP	Preamplifier-Per-Pixel
PPPT	Power Plant Physics and Technology
PTFE	Polytetrafluoroethylene
PWR	Pressurized Water Reactor
QA	Quality Assurance
QDS	Quick Disconnection System
RAFM	Reduced Activation Ferritic-Martensitic
RAMI	Reliability, Availability, Maintainability, Inspectability
RCC-MR	Règles de Conception et de Construction des Matériels mécaniques des îlots nucléaires RNR
RCM	Reliability Centred Maintenance
RH	Remote handling
RHCS	Remote Handling Control System
RIE	Reactive Ion Etching
SC	Supercritical
SCLL	Self-Cooled Lithium Lead
SEM/EBSD	Scanning Electron Microscope / Electron Backscatter Diffraction
SFR	Sodium Fast Reactors
SH	Shear Horizontal
SNL	Sandia National Laboratories
SS	Stainless Steel
SSC	Systems, Structures and Components
SST	Shear Stress Transport
STP	Satellite Tokamak Program
SW	Side Wall
TBM	Test Blanket Module
TBR	Tritium Breeding Ratio
TBS	Test Blanket System
TC	Transfer Cask
TCWS	Tokamak Cooling Water System
TDF	Task Definition Form
TEM	Transmission Electron Microscopy
TES	Tritium Extraction System
TF	Toroidal Field
TFTR	Tokamak Fusion Test Reactor
TIG	Tungsten Inert Gas
TMT	Thermomechanical Treatment
UHV	Ultra-High Vacuum
UPC	Universidad Politécnica de Cataluña
UPL	Upper Port Launcher
UPM	Universidad Politécnica de Madrid
UPS	Uninterrupted Power Supply
UPV	Universidad del País Vasco
UT	Ultrasonic
UV	Ultraviolet
VHTR	Very High Temperature Reactor
VMC	Vertical Maintenance Crane
VOF	Volume Of Fluid
VR	Virtual Reality
VSD	Variable Speed Drive
VTT	Technical Research Centre of Finland
VV	Vacuum Vessel
WCCB	Water Cooled Ceramic Breeder
WCLL	Water Cooled Lithium Lead
WPRM	Work Programme Remote Maintenance
WRF	Waste Recycling Facility
YAG	Yttrium Aluminium Garnet